# Synthesis of Chiral Donor-Acceptor Dyes to Study Charge Transfer Dynamics in a Chiral Environment

**Dissertation**

der Mathematisch-Naturwissenschaftlichen Fakultät
der Eberhard Karls Universität Tübingen
zur Erlangung des Grades eines
Doktors der Naturwissenschaften
(Dr. rer. nat.)

vorgelegt von
M. Sc. Marc Jens Junge
aus Bad Urach

Tübingen
2021

Gedruckt mit Genehmigung der Mathematisch-Naturwissenschaftlichen Fakultät der Eberhard Karls Universität Tübingen.

| | |
|---|---|
| Tag der mündlichen Qualifikation: | 28.10.2021 |
| Dekan: | Prof. Dr. Thilo Stehle |
| 1. Berichterstatterin: | Ass. Prof. Dr. Erin T. Chernick |
| 2. Berichterstatter: | Prof. Dr. Holger F. Bettinger |

# Preface

The work presented here has been carried out from November 2017 to November 2020 under the supervision of Jun. Prof. Dr. Erin T. Chernick and co-supervision of Prof. Dr. Holger F. Bettinger at the Eberhard Karls University of Tübingen.

Following parts of the synthetic work were done by students within internships and thesis.

Rita S. Stauder (Masterthesis; Oct. 2018): Synthesis of asymmetric BINOL derivatives based on 3,3'-(dibromo)-2,2'-(dimethoxy)-1,1'binapthalene

Blagoje Blagojevic (Internship; Nov. – Dez. 2018): Repeating the synthesis of **4a**.

Albert Schwarz (Internship; Feb. – Mar. 2019): Optimization of the synthesis of **24(*S*)**.

Mike A. Kordan (Internship; Jul. – Aug. 2019): First synthesis of **15b**.

The thesis is based on results which are already published in the following paper:

Synthesis of Chiral Donor−Acceptor Dyes to Study Electron Transfer Across a Chiral Bridge

Marc J. Junge, Mike A. Kordan, Erin T. Chernick

*J. Org. Chem.* **2020**, *85*, (21), 13793−13807

Content of this work was already presented as a poster during the following scientific conferences:

Gordon Research Conference on Photochemistry

14. – 19. July 2019 Stonehill College Easton, MA, United States

Gordon Research Seminar on Photochemistry

13. – 14. July 2019 Stonehill College Easton, MA, United States

5$^{th}$ International Symposium on Synthetic Carbon Allotropes – SFB 953 "Synthetic Carbon Allotropes"

29. September – 02. October 2019 Friedrich-Alexander Universität Erlangen-Nürnberg, Germany

## Summary

In this work the synthesis and characterization of chiral charge transfer dyes is presented. The dyes consist of a carbazole donor (D), a thiophene *π*-conjugated spacer (S), a benzothiadiazole primary acceptor (A1), BINOL as a chiral bridge (B) and a cyanacrylic ester as a secondary acceptor (A2), or a TEMPO stable free radical (SFR). The modular synthetic approach to synthesize these dyes is primarily based on Stille and Sonogashira cross-coupling reactions. This approach allows for the modular assembly of the molecular building blocks.

In the synthesized dyes, photoinduced intramolecular charge transfer (CT) of an electron from the electron rich donor moiety to the electron withdrawing acceptor part takes place. During this process, the electron moves through a chiral bridge. Therefore, the presented dyes allow the study of intramolecular chiral induced spin selectivity (CISS) effects. The CISS effect describes a phenomenon where electrons moving through a chiral environment are filtered according to their electron spin. CISS effects has received increasing attention in the research field of spintronics, which uses the quantized nature of the electron spin for digital data storage and manipulation. Further progress in the field of CISS facilitate spintronics to be used in versatile real-life applications. The research field of quantum information science (QIS) goes one step beyond spintronics and uses systems of multiple spins to manipulate and transport information in the form of the magnetic exchange between interacting electron spins. Appending a SFR to a chiral dye allows for the study of the interaction between a stable unpaired spin of a radical, and the charge-separated exited state of the charge-transfer system. Knowledge off these interactions can help to design functional systems for QIS applications.

Two series of dyes varying in the spatial arrangement of D, B and A1 were synthesized. In series I dyes D and A1 are on the same side of B resulting in a D-S-A1-B-A2/SFR arrangement. The charge transfer in series I dyes takes place between D and A1, but does not pass through the chiral bridge to A2 or the SFR group. Substitution of the D, with electron donating *n*-butoxy groups, facilitates the CT process but does not allow CT to A2. In series II dyes D and A1 are separated by the chiral bridge to enforce CT over or through the chiral moiety. Therefore, molecules in series II dyes have a D-S-B-A1-S-A2/SFR arrangement.

Computational results support the experimental evidence, that a CT across B requires the separation of D and A1. These molecules were sent to international collaborators to study intramolecular CISS effects and the interaction of the SFR and the charge transfer system.

# Zusammenfassung

Die im Folgenden beschriebene Arbeit behandelt die Synthese und Charakterisierung von chiralen Ladungstransfer-Farbstoffen. Die Farbstoffe bestehen aus einem Carbazol Donor (D), einem $\pi$-konjugierten Thiophin als Spacer (S), einem Benzothiadiazole als ersten Akzeptor, Binol als chirale Brücke (B) und einem Cyanacrylsäureester als zweiten Akzeptor (A2), welcher wahlweise mit einem TEMPO stabilen freien Radikal (SFR) ersetzt werden kann. Der modulare Syntheseplan basiert hauptsächlich auf Stille und Sonogashira Kreuzkupplungen. Dadurch ist es möglich die Abfolge der Bausteine zu verändern oder einzelne Bausteine gänzlich durch zu ersetzen.

In den synthetisierten Ladungs-Transfer Farbstoffen findet ein lichtinduzierter intramolekularer Elektronentransfer vom elektronenreichen Donor zum elektronenarmen Akzeptor statt. Während dieses Prozesses bewegt sich das Elektron in einer chiralen Umgebung. Daher ermöglichen diese Farbstoffe die Untersuchung des intramolekularen Chiral Induced Spin Selectivity (CISS) Effekts. Der CISS Effekt beschreibt ein Phänomen bei welchem Elektronen, die sich in einem chiral Umfeld bewegen, entsprechend ihres Elektronenspins angereichert werden. CISS erfährt große Aufmerksamkeit im Forschungsfeld der Spintronic. In der Spintronic versuchen Forscher die Quantelung des Elektronenspins zur Speicherung und Verarbeitung digitaler Daten zu verwenden. Weitere Forschung in diesem Feld könnte den vielseitigen Einsatz von Spintronic basierten Anwendungen ermöglichen. Die Forschung im Bereich der Quantum Information Science (QIS) geht sogar noch einen Schritt weiter als die Spintronic und verwendet magnetische Austauschinterakationen von Multi-Spin-Systeme zur Verarbeitung und zum Transport von Informationen. Die SFR substituierten Derivate der chiralen Farbstoffe ermöglichen es die Wechselwirkungen zwischen dem stabilen ungepaarten Spin des Radikals und dem angeregten Ladungs-Separierten Zustand des Farbstoffes zu untersuchen. Die hierbei erlangten Erkenntnisse können dabei helfen Moleküle für QIS Anwendungen zu entwerfen.

Zwei Serien von Farbstoffen wurden synthetisiert. Die Serien variieren in der Abfolge von D, B und A1. In Serie I sind D und A1 auf derselben Seite der chiralen Brücke. Diese Farbstoffe haben den Aufbau D-S-A1-B-A2/SFR. Der

Ladungs-Transfer in Farbstoffen der Serie I findet zwischen D und A1 statt. Die Ladung erreicht dabei nicht A2 oder SFR und passiert den chiralen Teil nicht. Eine Substitution des Donors mit elektronenreichen *n*-Butoxy Gruppen senkt die energetischen Anforderungen des Ladungstransfers ermöglicht aber keinen Transfer zu A2. In Farbstoffen der Serie II sind D und A1 durch B voneinander separiert, um einen Ladungstransfer über oder durch die chirale Brücke zu erzwingen. Die Moleküle der Serie II haben den Aufbau D-S-B-A1-S-A2/SFR. Die Ergebnisse von Computersimulationen der Moleküle stimmen mit den experimentell beobachteten Ergebnissen insofern überein, dass ein Ladungstransfer über die chirale Brücke eine Separierung von D und A1 benötigt. Die synthetisierten Moleküle wurden an internationale Kollaborationspartner verschickt. Diese Partner analysieren die Moleküle nun hinsichtlich des intramolekularen CISS Effekts und der Wechselwirkung zwischen dem SFR und dem Ladungstransfer Systems.

# Acknowledgements / Danksagung

Meine Familie und Freunde teilen mit mir alle Zeiten mögen sie fröhlich und leicht oder stressig und schwer sein. Darum möchte ich allen voran diesen Menschen für Ihre Unterstützung, in der wohl bisher intensivsten Zeit meines Lebens danken. Im Besonderen möchte ich hier meiner Frau Ann-Kathrin und meinen Freunden Jessica, Norbert und Rita danken. Ihr musstet so manches mal meine schlechten Launen und meinen Frust wegen schiefgegangener Experimente, nerviger Säulen oder einfach nur dem selbst gemachten Stress ertragen. Die innere Ruhe und die anderen Gedanken, die Ihr mir gabt, sei es bei der täglichen Autofahrt, beim genüsslichen Tee trinken, bei entspannten Spieleabenden oder einfach so zwischendurch, haben mir unglaublich gutgetan und mich davor bewahrt durchzudrehen. Ich möchte mich hier aber nicht nur für die schwierigen Zeiten bedanken. Vielmehr noch will ich euch für die fröhlichen, die lustigen und die außergewöhnlichen Zeiten danken. Diese machen das Leben doch erst so richtig lebenswert. Außerdem will ich an dieser Stelle meiner Familie dafür danken, dass Sie immer an mich geglaubt haben und mir die Möglichkeit gaben all das zu schaffen. But I think now it is better to switch to English.

I want to thank my supervisor Jun. Prof. Dr. Erin T. Chernick for the possibility to do my thesis and all the support she gave me during this intensive time. It was not just the great project and the possibility to work with a lot of freedom but also the atmosphere in the group helping me giving my very best with a huge amount of motivation. During the time working in the group, I have learned a lot. I have not only got experience in chemistry, but I also learned a lot about myself.

I want to thank my co-supervisor Prof. Dr. Holger F. Bettinger for his support, his time and all the possibilities he opened up for me. Also thank you for a lot of interesting scientific discussions and the perfect cooperation between the groups.

I want to thank the working group of Prof. Dr. Chernick, Prof. Dr. Bettinger, Prof. Dr. Maier and Dr. J. P. Wagner for all the help. It doesn't matter if I needed help with my chemistry, with task to in the lab or with organizational task I always found friendly people helping me. Herein also a special thanks to Maria, Magdalena, Mrs. Friedrichs.

I want to thank the Eberhard-Karls University of Tübingen and especially the Facutly of science for the possibility to do my thesis.

I want to thank the NMR and the MS department at the University of Tübingen for all their work with my sometimes very stubborn molecules.

I want to thank the group of Prof. Dr. H.-J. Meyer and Dr. Jochen Glaser for supporting me with the SQUID measurements.

And last but not least I want to thank all the other people helping and supporting me during the last years at the university. There are so many nice people that I do not have the space here to name all of you. But all of you have helped my conquering the difficulties of chemistry and finishing up this thesis.

Ich denke jeder der mich kennt weiß das ich kein Freund der großen Worte bin. Daher will ich nun ohne weiter Umschweife zum Ende kommen und den eigentlich wichtigen Teil dieser Arbeit beginnen.

# Table of Contents

# List of Figures

# List of Abbrevations

| | |
|---|---|
| 9-PCz | 9-Phenyl-9*H*-carbazole |
| *Δ*E | Energy-Gap |
| *ε* | Molar Extinction Coefficient |
| *λ* | Wavelength |
| *Φ* | Fluorescence Quantum Yield |
| A | Acceptor |
| Å | Angströme |
| A1 | Acceptor 1 |
| A2 | Acceptor 2 |
| AFM | Atomic Force Microscopy |
| APCI | Atmospheric Pressure Chemical Ionization |
| B | Chiral Bridge |
| BINAP | 2,2'-Bis(diphenylphosphino)-1,1'-binapthyl |
| BINOL | (1,1'-Binaphthalene)-2,2'diol |
| BTDA | 2,1,3-Benzothiadiazole |
| CISS | Chiral Induced Spin Selectivity |
| CT | Charge Transfer |
| CTS | Charge Transfer State |
| CW-EPR | Continuous-Wave Electron Paramagnetic Resonance |
| D | Donor |
| DCM | Dichloromethane |
| DFT | Density Functional Theory |
| DMABN | 4-*N*,*N*'-Dimethylaminobenzonitrile |
| DMF | *N*,*N*'-dimethylformamide |
| DMSO | Dimethylsulfoxide |
| DSSC | Dye Sensitized Solar Cell |
| E | Energy |
| EA | Electron Accepting |

| | |
|---|---|
| $E_A$ | Activation Energy |
| ED | Electron Donating |
| ESI | Electron Spray Ionization |
| EtOAc | Ethyl Acetate |
| FML | Ferromagnetic Layer |
| FPP | Fluorazene Phenylpryrrole |
| GMR | Giant Magnetoresistance Effect |
| GS | Ground State |
| $h\upsilon$ | Energy of a Photon |
| HCl | Hydrochloric Acid |
| HOMO | Highest Occupied Molecular Orbital |
| HPLC | High Pressure Liquid Chromatography |
| IR | Infrared |
| L | Ligand |
| LEPET | Low-Energy Photoelectron Transmission |
| LES | Locally Exited State |
| LUMO | Lowest Unoccupied Molecular Orbital |
| MALDI | Matrix-Assisted Laser Desorption / Ionization |
| mc-AFM | Magnetic-Conductive Atomic Force Microscopy |
| MIN | 1-Methyl-5-cyanoindoline |
| NML | Nonmagnetic Layer |
| NMP | *N*-Methyl-2-pyrrolidone |
| NMR | Nuclear Magnetic Resonance |
| NR | No Reaction |
| OAc | Acetate |
| OP | Oxidation Potential |
| PICT | Planar Intramolecular Charge Transfer |
| PP | Phenylpyrrole |

| | |
|---|---|
| pTICT | Partially Twisted Intramolecular Charge Transfer |
| QIS | Quantum Information Science |
| RICT | Rehybridized Intramolecular Charge Transfer |
| S | π-Spacer |
| SAM | Self-Assembled Monolayer |
| SCE | Saturated Calomel Electrode |
| SFR | Stable Free Radical |
| $S_{N2}$ | Nucleophilic Substitution of Second Order |
| SQUID | Superconducting Quantum Interference Device |
| SXCC | Size Exclusion Column Chromatography |
| TBAF | Tetrabutylammonium Fluoride |
| TCNQ | Tetra-*p*-quiodimethan |
| TEMPO | (2,2,6,6-Tetramethylpiperid-1-yl)oxyl |
| THF | Tetrahydrofuran |
| TICT | Twisted Intramolecular Charge Transfer |
| TIPS | Tri-*iso*-propylsilyl |
| TLC | Thin Layer Chromatography |
| TMABN | Tetramethylaminobenzonitrile |
| TMEDA | *N,N,N',*N'-Tetramethylethylen-1,2-diamine |
| TMS | Trimethylsilyl |
| TPA | Triphenylamine |
| TTF | Tetrathiofulvalene |
| UC | Unknown Compound |
| UV | Ultra-Violet |
| Vis | Visible |

# List of Used Compounds

| | |
|---|---|
| **1** | 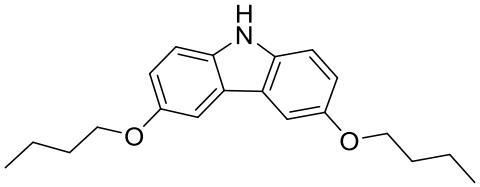 |
| **2a** | 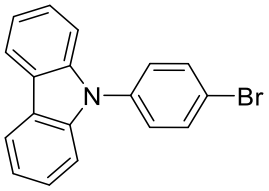 |
| **2b** | 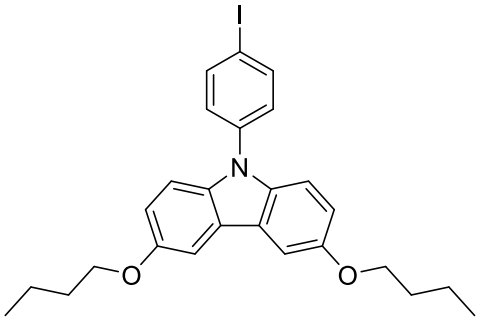 |
| **3** | 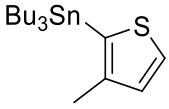 |
| **4a** | 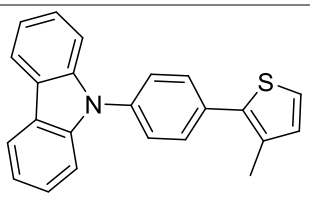 |
| **4b** | 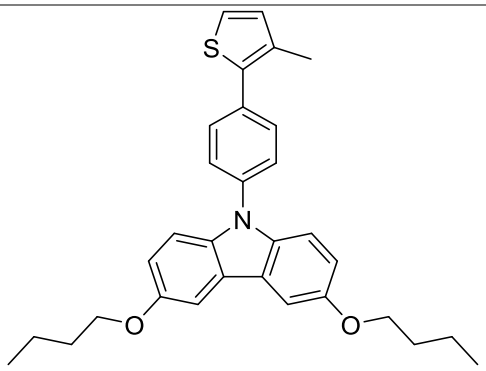 |
| **5a** | 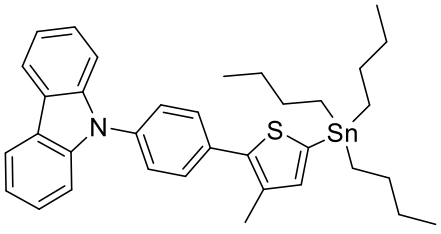 |

| | |
|---|---|
| **5b** | 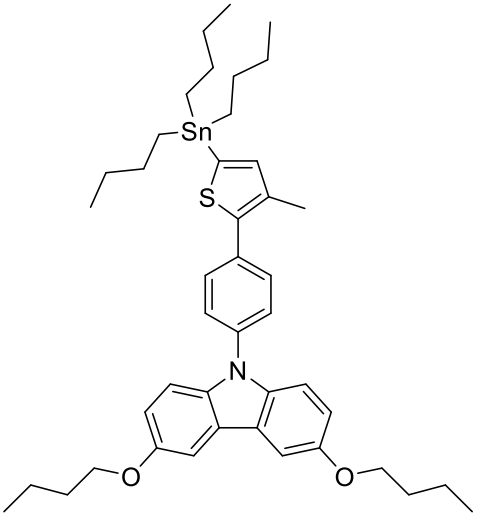 |
| **6** | 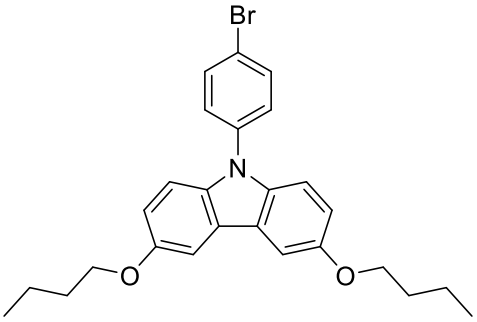 |
| **7** | 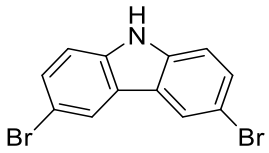 |
| **8** | 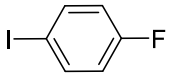 |
| **9** | 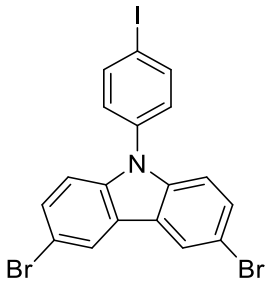 |
| **10** | 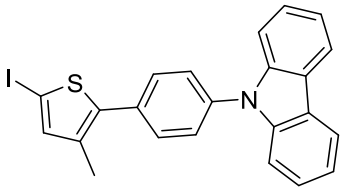 |

| | |
|---|---|
| **11** | 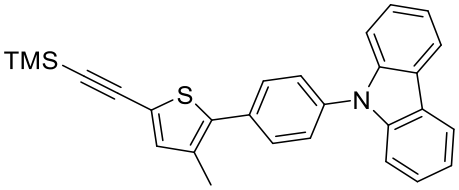 |
| **12** | 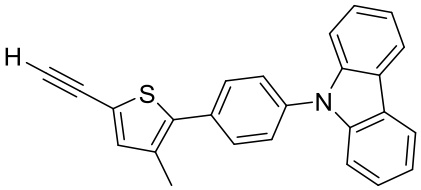 |
| **13** | 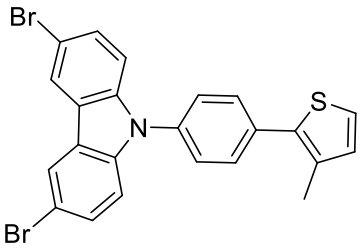 |
| **14** | 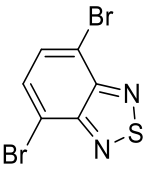 |
| **15a** | 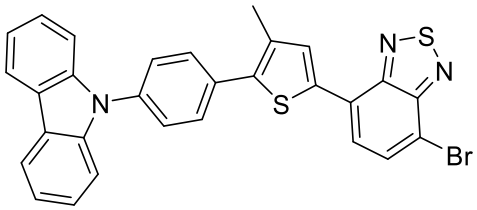 |
| **15b** | 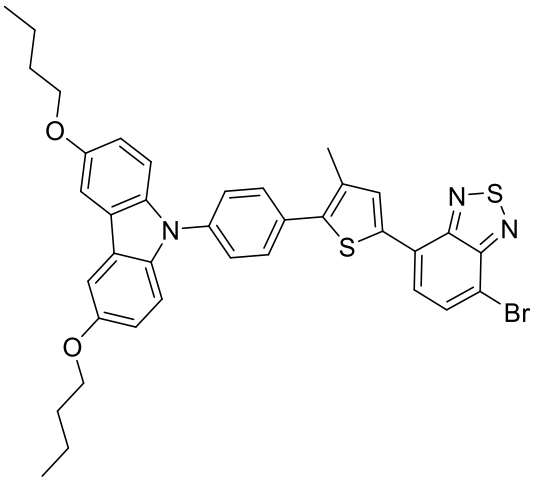 |

| | |
|---|---|
| **16** | 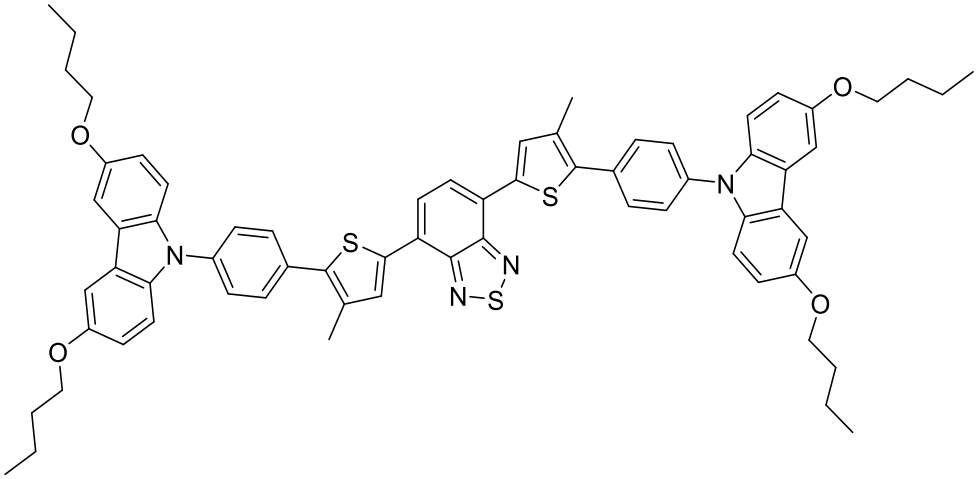 |
| **17** | 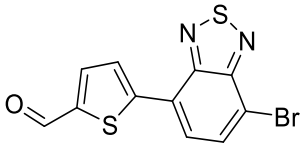 |
| **18** | 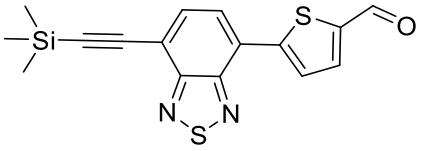 |
| **19(*S*)** | 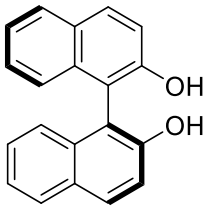 |
| **20(*S*)** | 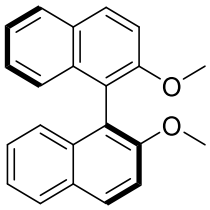 |
| **21(*S*)** | 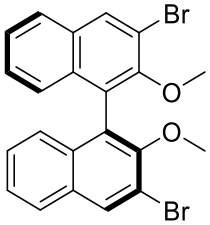 |
| **22(*S*)** | 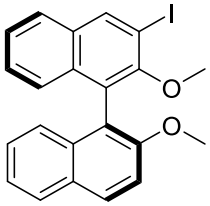 |

| | |
|---|---|
| **23(*S*)** | 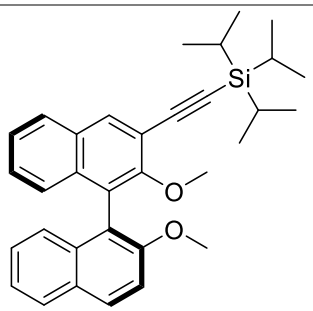 |
| **24(*S*)** | 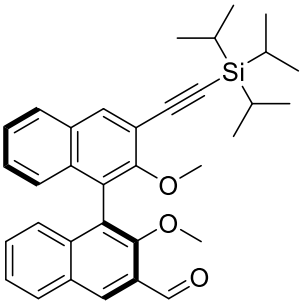 |
| **25(*S*)** | 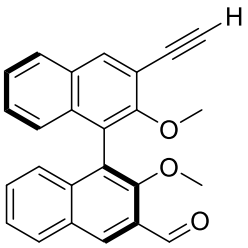 |
| **26(*S*)** | 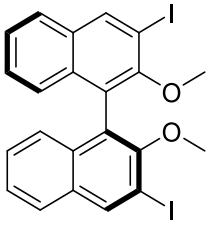 |
| **27(*S*)** | 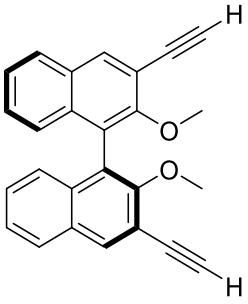 |
| **28(*S*)a** | 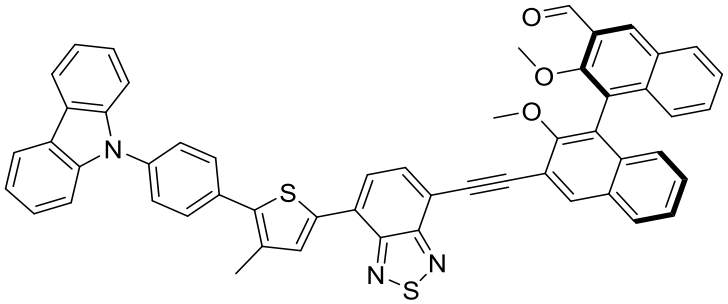 |

| | |
|---|---|
| **28(*S*)b** | 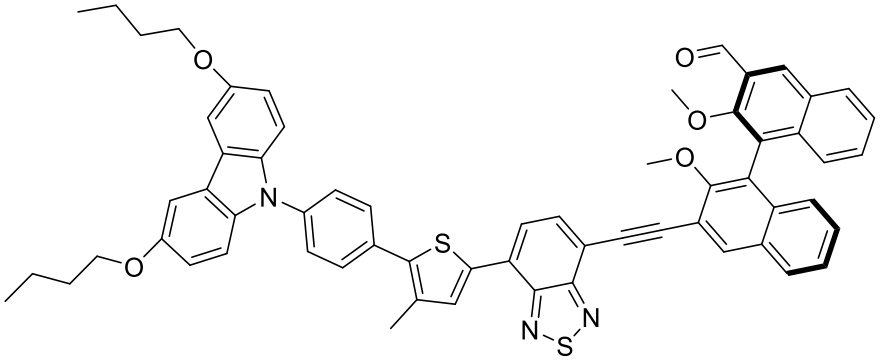 |
| **29(*S*)a** | 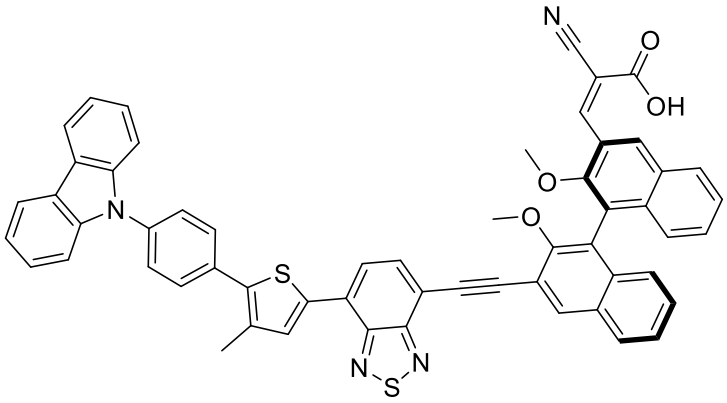 |
| **30(*S*)a** | 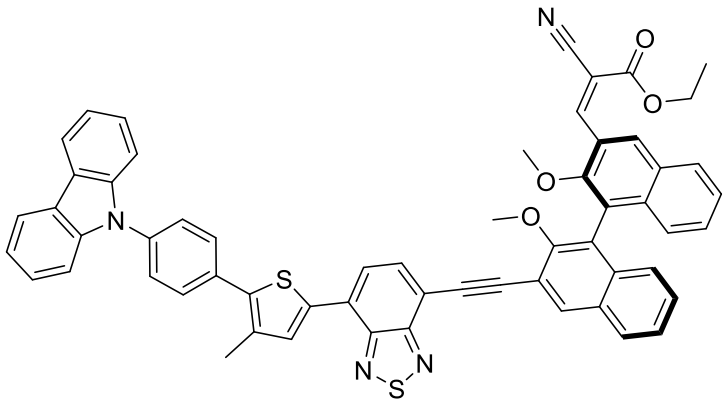 |
| **30(*S*)b** | 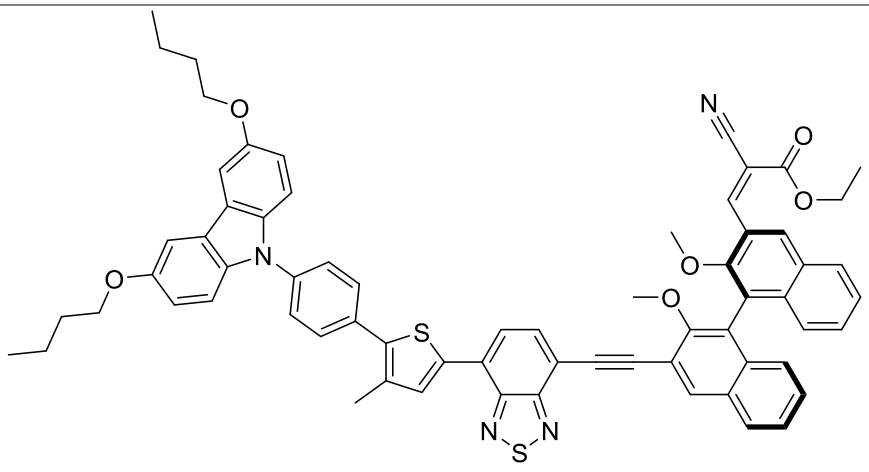 |

| | |
|---|---|
| **31(*S*)a** | 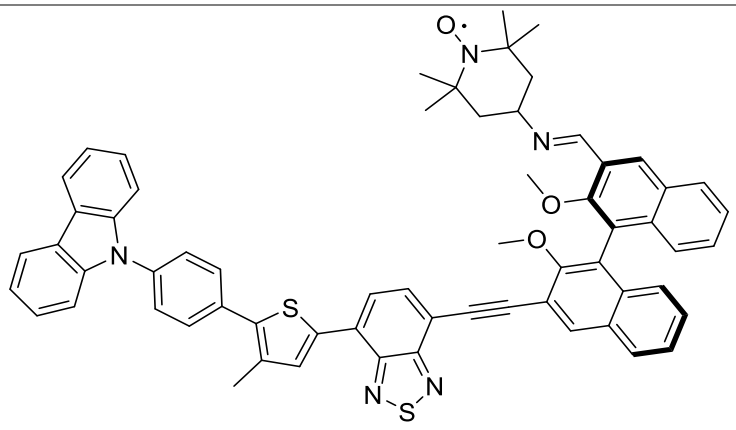 |
| **31(*S*)b** | 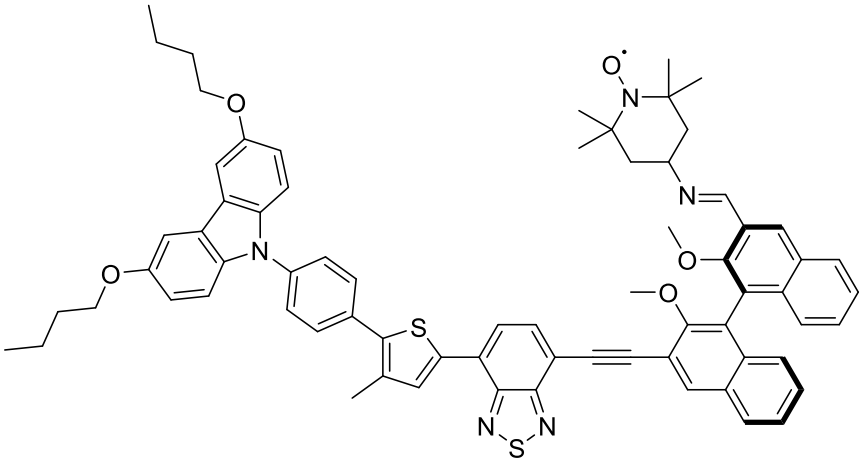 |
| **32(*S*)** | 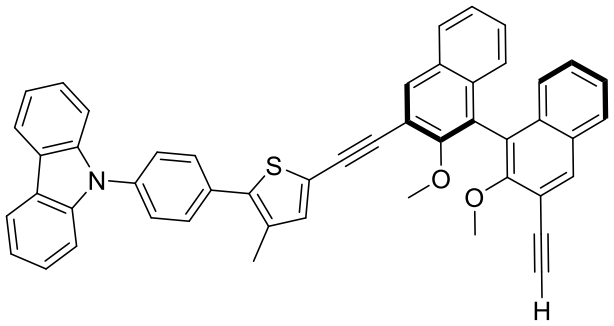 |
| **33(*S*)** | 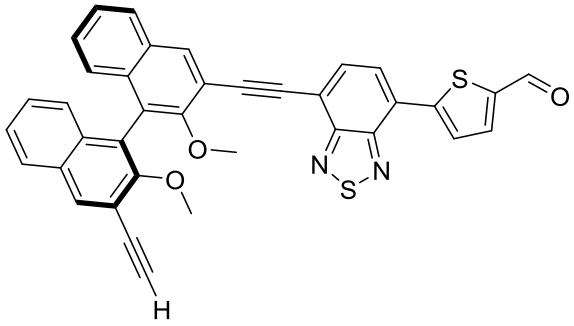 |

| | |
|---|---|
| **34(*S*)** | 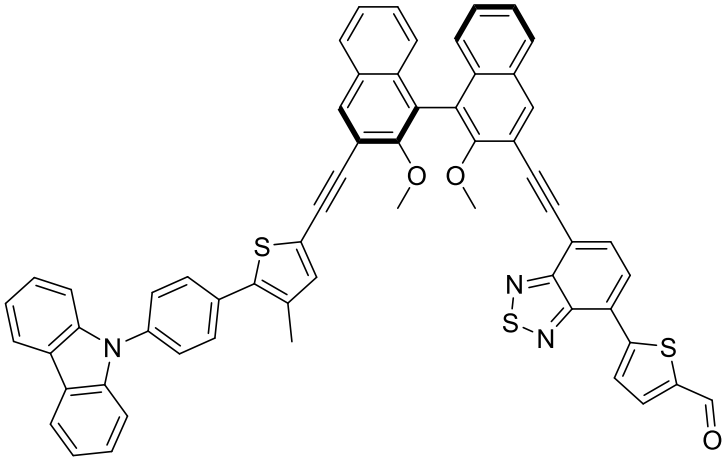 |
| **35(*S*)** | 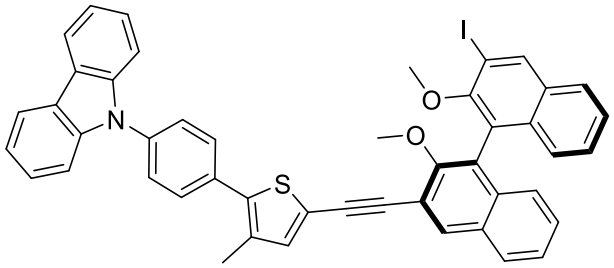 |
| **36(*S*)** | 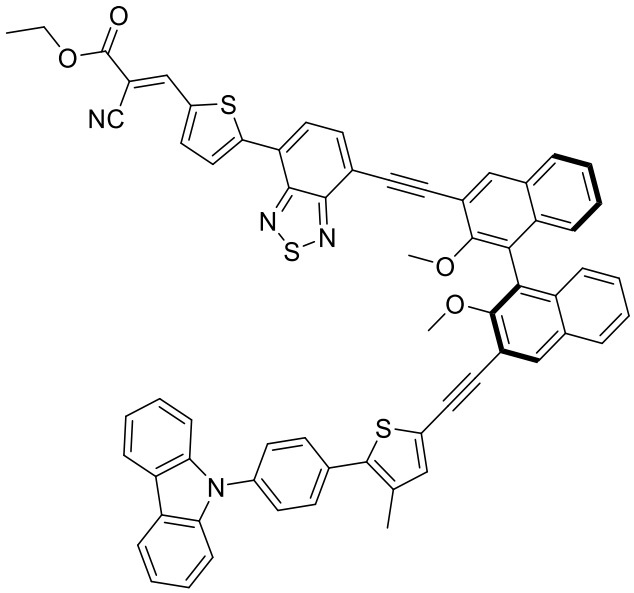 |

| | |
|---|---|
| **37(*S*)** | 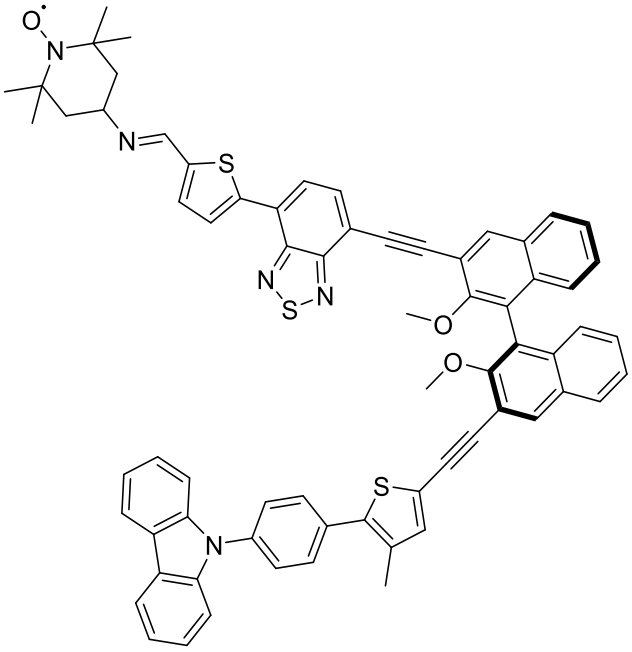 |

# 1. Introduction

## 1.1. Spintronics and Quantum Information Science

In the field of quantum information science (QIS) qubits are used to store and manipulate data, similar to bits in classical computers.[1] Qubits can be single molecules, complexes or clusters of atoms, like diamonds with nitrogen vacancies.[1] A qubit has access to different distinguished quantum states as for example the spin of an electron or the optical excitation level of a molecule. In contrast to a classical bit, qubits can have more than two states and these states can be in superposition. Hence, qubit-based systems can potentially compute faster than classical systems.

One of the most basic forms of a qubit is the electron. Therefore, the two electron spin states represent two quantum states. In the research field of spintronics, the spin of an electron is used to store and manipulate digital data.[1a, 2] A spin valve is an example for a spintronic device using the giant magnetoresistance effect (GMR) to create a high resistance, non-conductive (0) and a low resistance, conductive (1) state.[2c, 3] Since the 1990's, the reading heads of hard drive discs using the GMR effect to enabled the extraction of data from the magnetized surface of the disc. A spin valve device consists of two ferromagnetic layers (FML) separated by a nonmagnetic layer (NML) as shown in Figure 1. One of the FMLs (FML 1) carries magnetization in one direction. The magnetization of FML 2 can be changed between parallel and antiparallel to the magnetization of FML 1 by an external magnetic field. Based on the GMR the resistance for an electric current from FML 1 to FML 2 can be changed by between a high and a low resistance state by arranging the magnetization of FML 2 antiparallel or parallel to the magnetization of FML 1, respectively.

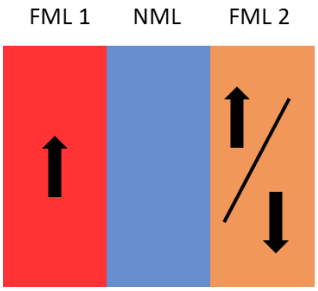


**Figure 1:** Scheme of a spin valve. Black arrows describe the magnetic polarization of the FM layers 1 and 2.

The high and low resistance states of a spin valve can be understood as the non-conductive and conductive state of a classic transistor, respectively. Therefore, spin valves can replace classic transistors in digital applications. In comparison to a classical transistor requiring an electric current to change their conductivity state, a spin valve requires an external magnetic field to change the state. The energy necessary to change the conductivity of a spin valve is lower than for a classical transistor and spin valves do not need to be recharged. While the performance of classic transistors decreases reaching a size smaller than tens of nanometers, spin valves can be minimized further. So, the use of spin valves becomes an efficient choice in data transfer, storage and manipulation.[2a, 2c, 2d, 4]

Electron spin filter effects were observed during electron transmission measurements of polarized photoelectrons through an ordered film of chiral organic molecules.[5] The effect is called chiral induced spin selectivity effect (CISS).[6] The first evidence of this phenomena was found during low-energy photoelectron transmission (LEPET) experiments through a self-assembled monolayer (SAM) of L- and D- stearoyl lysine on an Au surface as shown in Figure 2. Using circular polarized light to eject spin-polarized photoelectrons showed varying yields relative to the polarization of the light and the chirality of the molecules on the Au surface.[7]

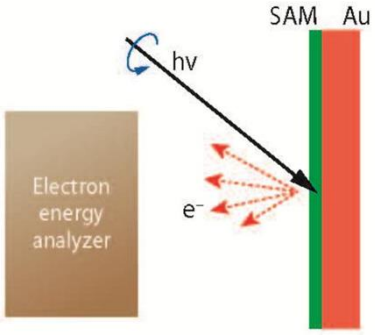


**Figure 2:** Scheme of the LEPET experiment to detect CISS.
Reprinted with permission from Naaman, R.; Waldeck, D. H., Chiral-Induced Spin Selectivity Effect. *J. Phys. Chem. Lett.* **2012,** *3* (16), 2178-2187. Copyright 2012 American Chemical Society.[6c]

A molecule has an electric field based on the distribution of electrons and nuclei. In chiral molecules these electric fields are also chiral. A moving charge, in an electric field, generates a magnetic field. If the electric field is chiral, the generated magnetic field is chiral, too. This chiral magnetic field interacts differently with either spins polarized up or down. Hence, one polarized electron spin will be favored, and passes through the field faster than the other. Therefore, the favored spin is enriched in the electrons that have passed the chiral system (Figure 3).[6c, 8] It has turned out that the CISS effect of oligopeptides and double-stranded DNA increases linearly with the length of the systems.[9]

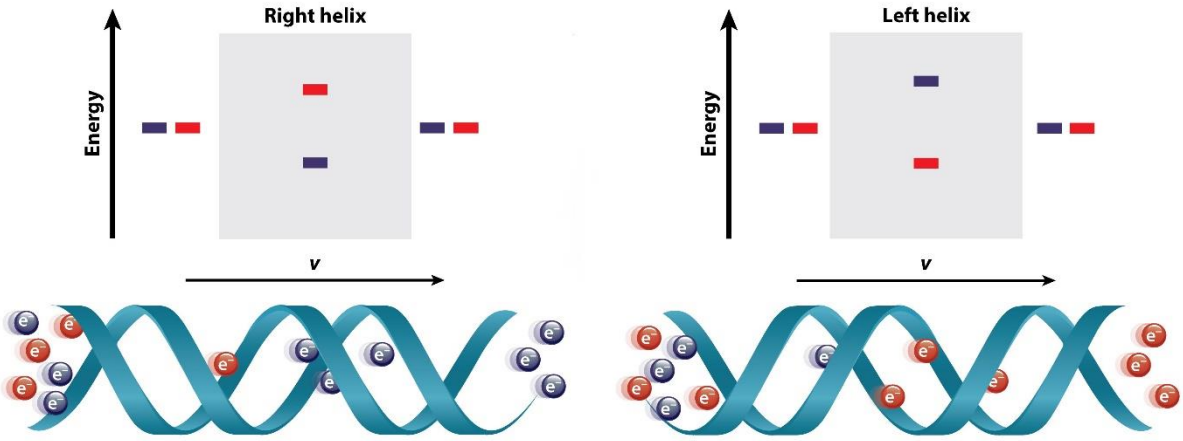


**Figure 3:** Schematic representation of CISS. Red colored spheres and energy levels refer to spin up electrons; Blue colored spheres and energy levels refer to spin down electrons.
Republished with permission of Annual Reviews, Inc., from Naaman, R.; Waldeck, D. H., Spintronics and Chirality: Spin Selectivity in Electron Transport Through Chiral Molecules. *Annu. Rev. Phys. Chem.* **2015,** *66* (1), 263-281; permission conveyed through Copyright Clearance Center, Inc[8]

Different scientific methodologies can be used to observe the CISS effect. One possibility is the magnetic-conductive atomic force microscopy (mc-AFM), which is a modification of the atomic force microscopy (AFM).[10]

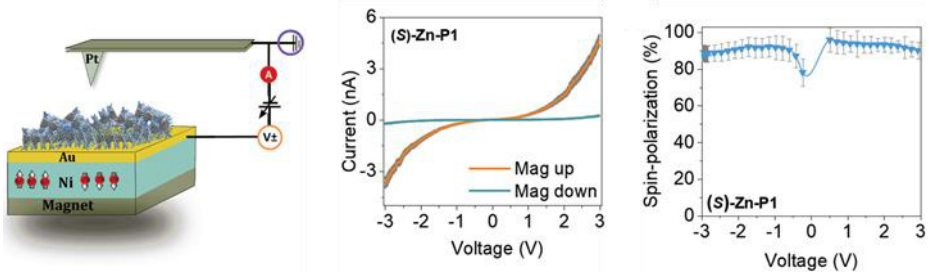


**Figure 4:** Scheme of a mc-AFM experiment and examples for the results. Reprinted with permission from Kulkarni, C.; Mondal, A. K.; Das, T. K.; Grinbom, G.; Tassinari, F.; Mabesoone, M. F. J.; Meijer, E. W.; Naaman, R., Highly Efficient and Tunable Filtering of Electrons' Spin by Supramolecular Chirality of Nanofiber-Based Materials. *Adv. Mater.* **2020,** *32* (7), 1904965. Copyright 2020 John Wiley & Sons, Inc. [10]

In this experiment a Ni surface coated with Au is layered with chiral molecules. In this setup the Ni substrate can be magnetized perpendicular to the Au-coated surface, with the north pole either pointing up or down.[10] An AFM tip is placed above the layer of chiral molecules and a potential is applied between the Au layer and the AFM tip (Figure 4). If the CISS effect is taking place, the current circulating between the AFM tip and the Au layer is influenced not only by the applied voltage, but also by the magnetization of the Ni substrate. The amount of spin polarization can be determined by $\frac{I_{up}- I_{down}}{I_{up}+ I_{down}} * 100$, with $I_{\mathrm{up}}$ and $I_{\mathrm{down}}$ representing the measured current when the Ni substrate is magnetized with the north pole pointing up and down, respectively.[10]

Another possibility to observe CISS is based on measuring the potential between a magnetized Ni and an Ag layer separated by an insulating $AlO_x$ barrier.[11] For example, self-assembled monolayer of double stranded DNA, derivatized with a donor-acceptor dye, was placed on the Ag surface as shown in Figure 5. Illumination of the SAM creates electron holes in the dye. These electron holes are filled with electrons from the Ag layer. Due to the chiral DNA molecule between the Ag surface and the dye, the electrons moving through the DNA are spin polarized. Hence, the electron holes in the silver layer are spin polarized. Electron holes in the Ag layer result in a measurable photo-potential between the Ni and the Ag layer. Electrons tunneling between Ni and Ag reduce the detectable photo-potential. In the case magnetization of the Ni layer is antiparallel to the spin polarization of the electron holes in the Ag layer, electron tunneling is inhibited and a higher photo-potential is observed.[8, 11]

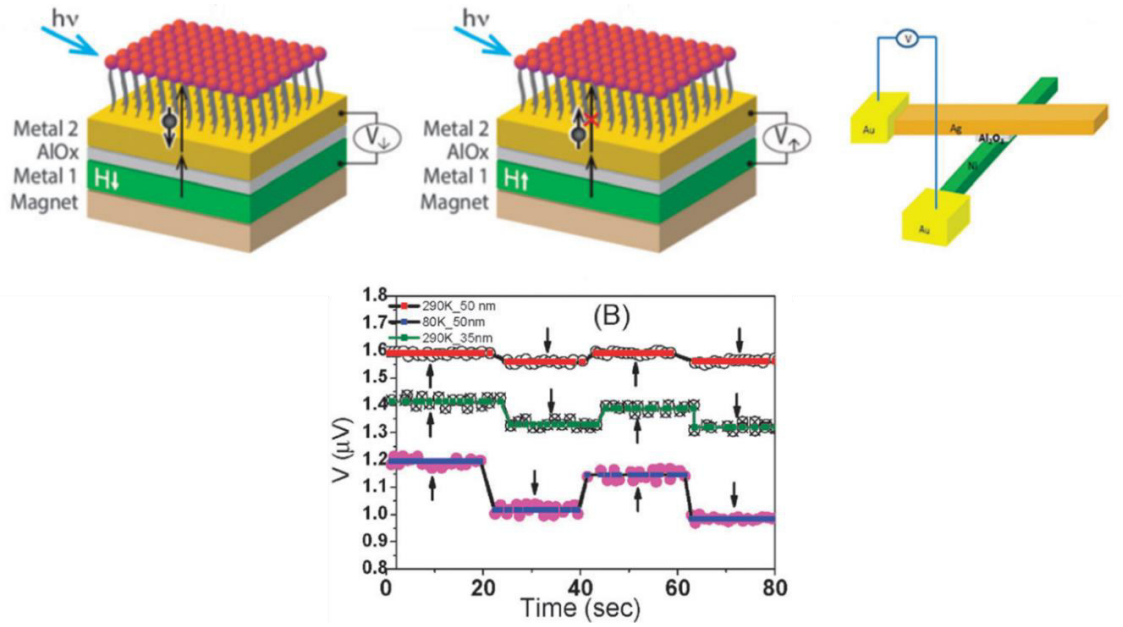


**Figure 5:** Scheme of experimental setup to measure CISS dependent photo-potential and related experimental data for 40 base pairs long double-stranded DNA equipped with Cy3 dye at various temperatures and various thickness of the silver layer.
Republished with permission of Royal Society of Chemistry, from Senthil Kumar, K.; Kantor-Uriel, N.; Mathew, S. P.; Guliamov, R.; Naaman, R., A Device for Measuring Spin Selectivity in Electron Transfer. *Phys. Chem. Chem. Phys.* **2013,** *15* (42), 18357-18362; permission conveyed through Copyright Clearance Center, Inc.[11]

In 2014 Mathew and coworkers reported a spin valve device were one of the ferromagnetic layer of the spin valve is replaced by a self-assembled monolayer of chiral molecules on an Au surface as shown in Figure 6.[12] To assemble this device, an $Al_2O_3$ film was grown via atomic layer deposition on the SAM of chiral molecules. The $Al_2O_3$ film, acts as the NML, and adapts a chiral structure, induced by the underlying chiral monolayer.[13] Measuring the electrical resistance between the Au surface and the second FML, in this case a Ni layer, shows dependency to the magnetic field applied at the FML.

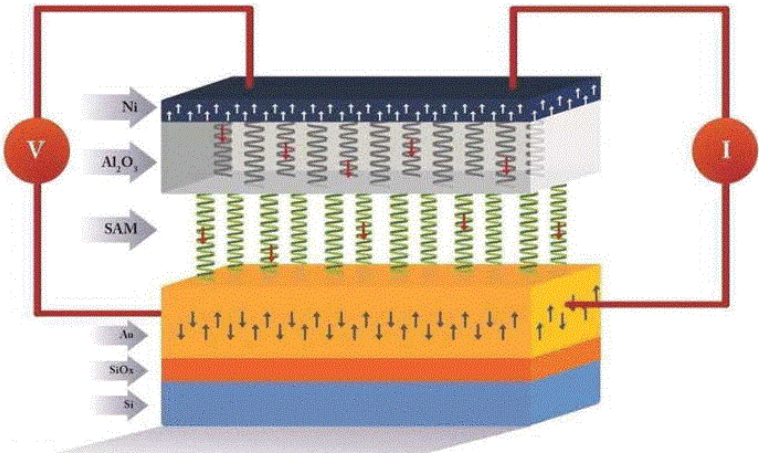


**Figure 6:** Scheme of the device produced by Mathew and coworkers. Reprinted from Mathew, S. P.; Mondal, P. C.; Moshe, H.; Mastai, Y.; Naaman, R., Non-Magnetic Organic/Inorganic Spin Injector at Room Temperature. *Appl. Phys. Lett.* **2014,** *105* (24), 242408, with permission of AIP Publishing.[12]

Further development and research in the field of CISS can lead to effective spintronic devices based on chiral organic molecules. For example, spin valves based on the CISS effect could be used for data storage and manipulation and replace classical transistors. Replacing classical transistors comprised of rare and expensive metals with spin valves consisting of organic molecules reduces production costs and makes data storage more ecological friendly.

Spintronics uses electrons, which can populate two different quantum states, as qubits. In the superior field of quantum information science, the nature of qubits can be different and therefore qubits can also be able to populate more than two quantum states. An example of a qubit is a molecular system comprising multiple unpaired spins. The system has the possibility to change between more than two states.[1a, 1d, 2b, 2c, 14] The photoexcitation of a charge transfer (CT) dye for example can create a diradical charge transfer state (CTS) as shown in Figure 7.[3b, 15]

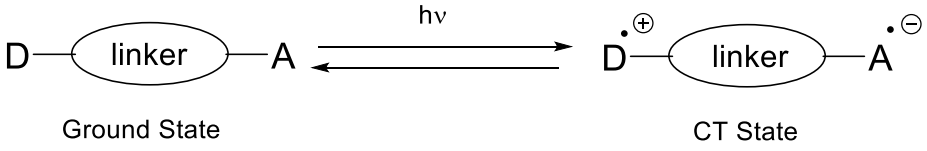


**Figure 7:** Scheme of a CT dye creating a CTS by photoexcitation. D is an electron donating group; A is an electron accepting group.

The coherence time of a qubit describes the timeframe an initiated pure quantum state exists until it changes due to spontaneous interaction with the environment. One of the many goals in actual QIS research is to elongate the coherence time of qubits.[1, 2b, 2c, 14] For example, the major decay pathway of CTS, and therefore also the major limiting factor for the coherence time of this system, is the charge recombination. Covalently linking a stable free radical (SFR) to a CT dye has shown to increase the lifetime of the photoinduced CTS.[16]

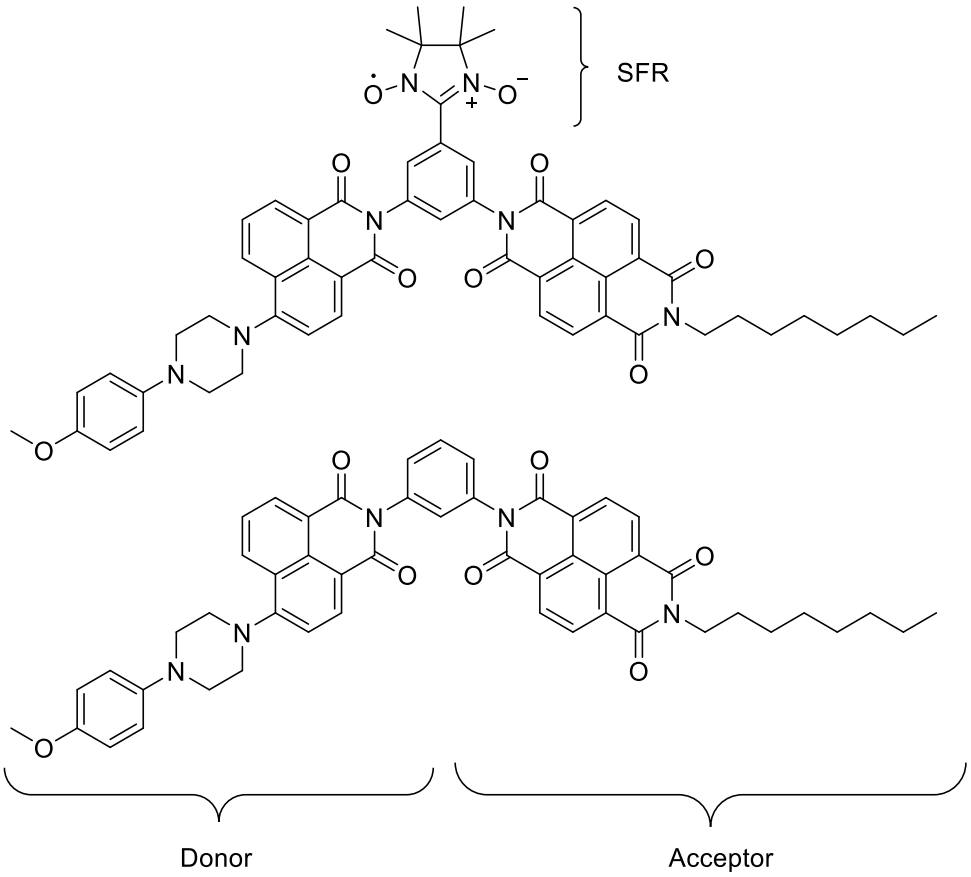


**Figure 8:** CTD used by Chernick et al. to study the effect of a SFR on a CTS.[16a]

Chernick and coworkers have studied a CT dye comprise of a *p*-methoxyaniline substituted 4-(*N*-piperidinyl)naphthalene-1,8-dicarboximide as a donor and a *n*-hexyl substituted naphthalene-1,8:4,5-bis(dicarboximide) as an acceptor. Donor and acceptor were bridged by a phenyl ring, which was either unsubstituted or substituted by a nitronyl nitroxide stable free radical as shown in Figure 8.The group carried out time resolved transient absorption and time resolved continuous wave electron paramagnetic resonance spectroscopy to study the dynamics within the system after photoexcitation. They have observed a slower

charge recombination of the CTS in the presence of the SFR. Additionally they were able to observe a net spin polarization of the SFR during the decay of the CTS.[16a]

Further knowledge of the dynamics in CTS and their interaction with SFRs can help to control spin states of molecular systems. For example, a longer coherence time of the qubit result in a longer time data can be stored and manipulated in the qubit. More precise methods to creation, control, and analysis distinguished spin states improve applications like quantum computing and can help to make these powerful technologies available for everyone.[1a, 1b, 1d, 2b]

## 1.2. Charge Transfer

Charge transfer (CT) is a process where a charge or a partial charge is transferred from an electron rich donor (D) to an electron poor acceptor (A). Charge transfer processes occur in nature; for example, the photosynthesis of plants is based on a light induced CT between chlorophyl a and pheophytin as a primary step for the splitting of water into oxygen and protons.[17] While CT in the photosynthesis process takes place intermolecular between two molecules in close proximity to each other, CT can also take place intramolecular between the metal and a ligand of an complex.

The color of metal complexes can be explained by a CT state between the metal and ligand.[18] In 1952 Mulliken introduced the idea of CT to described UV-Vis absorptions of complexes; for example $I_2$ and benzene, which cannot be attributed to the individual components of the complex.[15a, 19] When the energy $h\upsilon$ of a photon is equal or higher than the energy gap $\Delta E$ between the highest occupied (HOMO) and lowest unoccupied (LUMO) molecular orbital of a molecule, the photon can be absorbed. White light is a superposition of photons with all visible wavelengths. In the case a molecule absorbs a visible photon, the residual light is colored complementary to the color of the absorbed photon. When an electron donating (ED) group with a high energy HOMO, and an electron accepting (EA) group with a lower energy LUMO are combined in a molecule or complex, CT is possible. In these molecules or complexes, the $\Delta E$ decreases in comparison to the energy gaps ($\Delta E_{ED}$ and $\Delta E_{EA}$) of the individual ED or EA groups (Figure 9). D-A molecules can possess physical properties where $\Delta E$ lies within the visible energy range. Hence, these molecules absorb visible photons and appear colored.

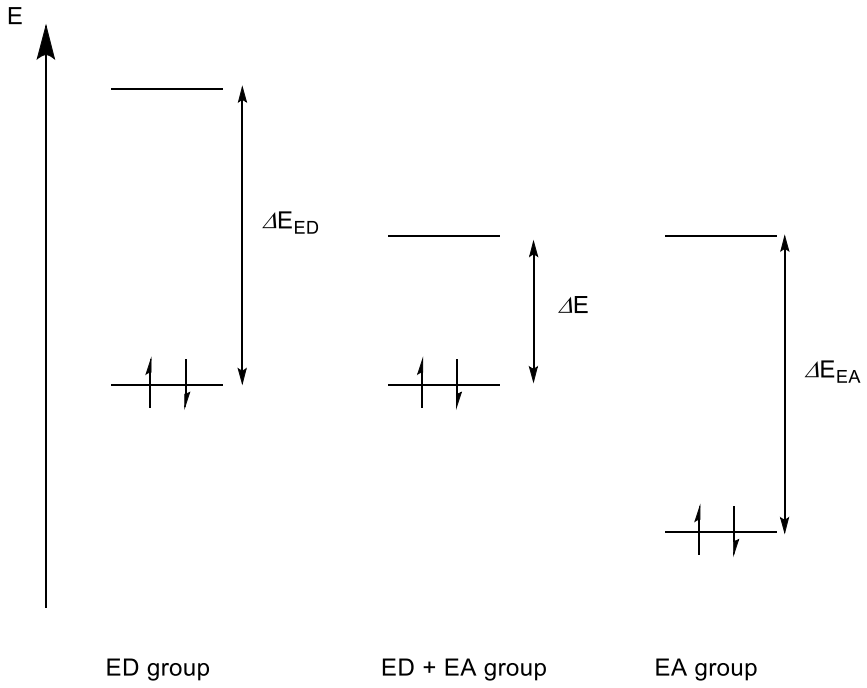


**Figure 9**: Different HOMO-LUMO gaps; ED: electron donating; EA: electron accepting.

Charge transfer processes can take place in an intermolecular or intramolecular manner.[15c, 20] Intermolecular CT is observed in CT-complexes, such as the tetrathiofulvalene/tetracyano-*p*-quinodimethane (TTF/TCNQ) complex shown in Figure 10.[21]

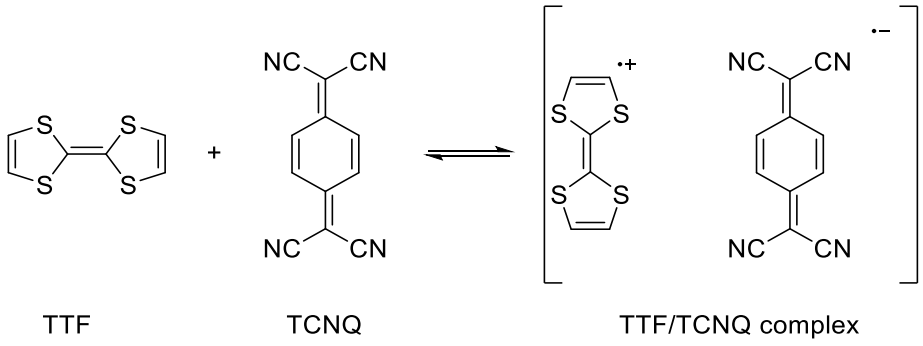


**Figure 10:** Tetrathiofulvalene (TTF) and tetracyano-*p*-quinodimethane (TCNQ).

Intramolecular CT occurs in molecules consisting of a D and an A. If D and A are connected by an unconjugated linker CT takes place through space or by tunneling. Tunneling or through space CT can be observed for example when D and A are bound to an amino acid or polymer backbone holding them in spatial proximity.[22] In the case D and A are linked by a conjugated system, the CT can

take place through bond. Many small CT molecules, like 4-*N*,*N*'-dimethylaminobenzonitrile (DMABN), consist of a phenyl ring substituted in *para* arrangment by a D and an A.[20a, 23]

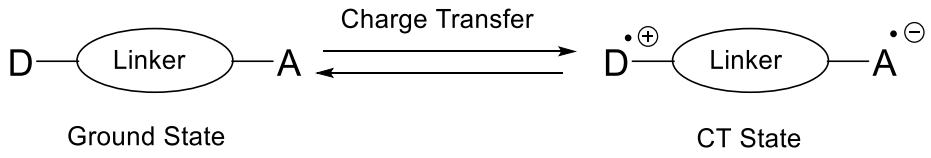


**Figure 11:** Ground and CT state of a D-A-molecule.

Shown in Figure 11, is a schematic demonstrating intramolecular CT, which produces a positive charge on the D and a negative charge on the A. In the case where the zwitterionic situation is not stable, the CT state (CTS) will relax back to the ground state (GS) through different mechanisms.

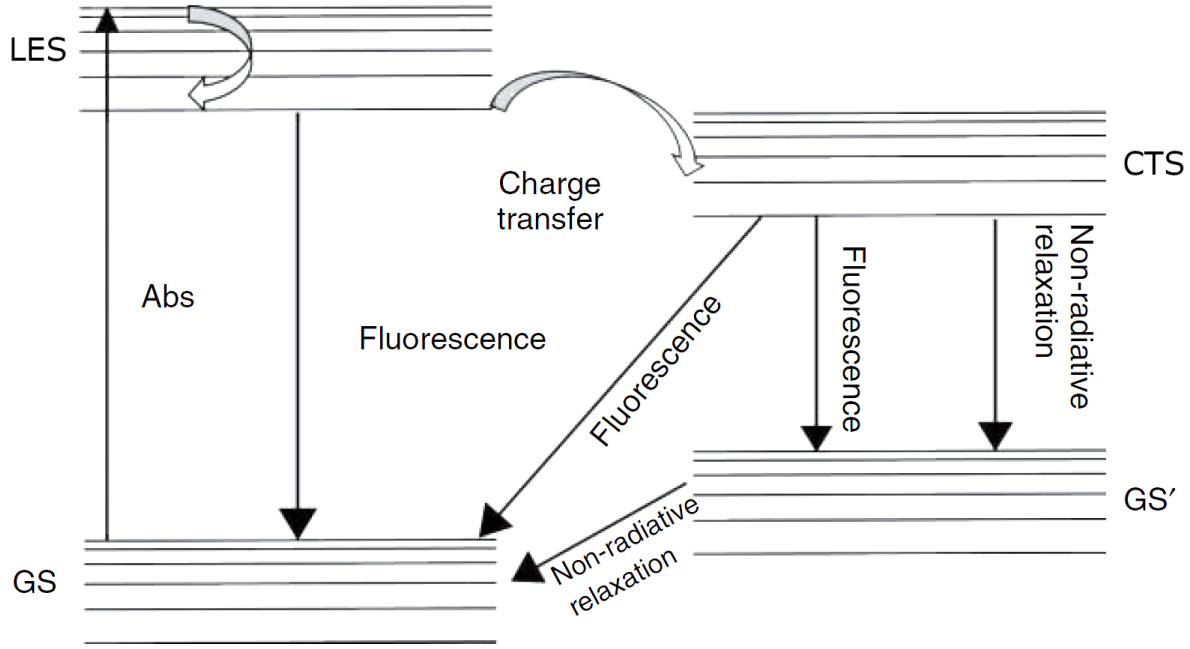


**Figure 12**: Jablonski-diagram of the excitation of a charge transfer dye. GS is the electronic ground state of the molecule. LES is the locally exited state of the molecule. CTS is the charge transfer state, an exited state with separated charges and a geometry unequal to the geometry of the ground state. GS' is an electronic ground state with the geometry of the CTS.

Figure 12 shows a Jablonski-diagram representing processes taking place in charge transfer dye. Upon absorption of a photon, a molecule will be exited from the GS to a vibrational level of the locally exited state (LES).[25] The relaxation of vibrational levels takes place by a process called internal conversion.[26] The exited molecule in the LES can relax back into the GS by different non-radiative pathways or fluorescence, which takes place typically within nanoseconds.[27] Apart from these processes, CT can take place resulting in the formation of the zwitterionic CTS.[20a, 28]

Conversion of the LES into the CTS consist of the movement of an electron within tens of picoseconds in polar solvents.[29] The zwitterionic CTS has an increased dipole moment in comparison to the LES. The increased dipole moment and the new charge distribution leads to a rearrangement of the surrounding solvent molecules. In addition to the rearrangement of the solvent molecules, the changes in the electron distribution of the molecule during the CT process requires structural changes. Molecules in the CTS can relax back to the GS similar to the LES by non-radiative relaxation or by fluorescence. Due to the structural changes that have taken place in CTS the relaxation leads to GS' a ground state with distorted geometry. Further non-radiative relaxation, including structural changes, are necessary to achieve GS with the lowest potential energy.[15c]

As shown in Figure 12 excited CT molecules can show fluorescence from either the LES or the CTS. The potential energy of the LES and the CTS are different. Therefore, the photons emitted from these states have different energies and wavelengths. The phenomenon of two fluorescence emission maxima is called dual fluorescence. Dual fluorescence of DMABN was first described by Lippert and coworkers (Figure 13).[30] Since then, dual fluorescence, and the mechanism responsible for this process has become a widely studied topic in the research field of charge transfer molecules.

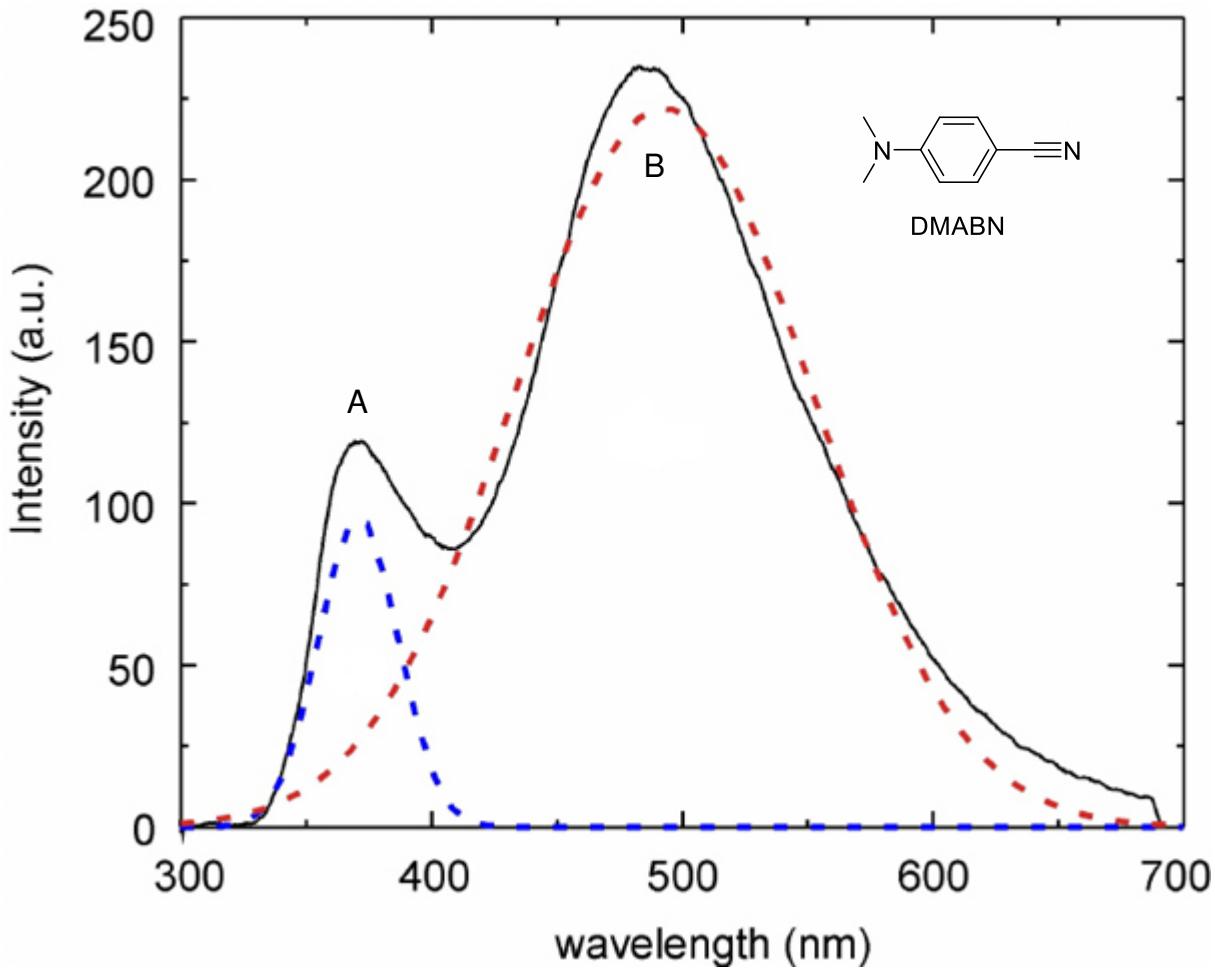


**Figure 13**: Fluorescence spectra and the structure of DMABN.[31]

DMABN shows fluorescence emission at two wavelengths. The intensity ratio of these emissions depends on the solvent polarity and temperature. In non-polar solvents, the shortest wavelength emission (A) is observed. In polar solvents and with increasing temperature, a second emission (B) with a longer wavelength appears. The increasing intensity of B corresponds with a decrease in the intensity of A. The wavelength of A is minimally affected by the solvent polarity; however, the wavelength of B shows a strong solvatochromic response with a shift to longer wavelengths with increasing solvent polarity. As shown in Figure 12, fluorescence of a CT molecule can take place either from the LES or from the CTS. Emission A can be attributed to fluorescence out of the LES, while emission B can be attributed to the fluorescence out of the CTS. The zwitterionic CTS shows an increased dipole moment in the molecule, compared to the LES.[32] Polar solvents can stabilize a dipole moment by electrostatic interactions. Hence, the potential energy of CTS is lower in polar solvents compared to non-polar solvents and

fluorescence out of CTS shows strong solvent dependency. The transition from LES to CTS requires activation energy ($E_A$). The activation barrier depends strongly on the potential energy of the CTS and therefore on the polarity of the solvent as shown in Figure 14. A polar solvent will result in a more stable CTS and a lower $E_A$. Following the Arrhenius equation a reduced $E_A$ leads to an increased transition rate and hence, to an increased fluorescence out of the CTS.[33]

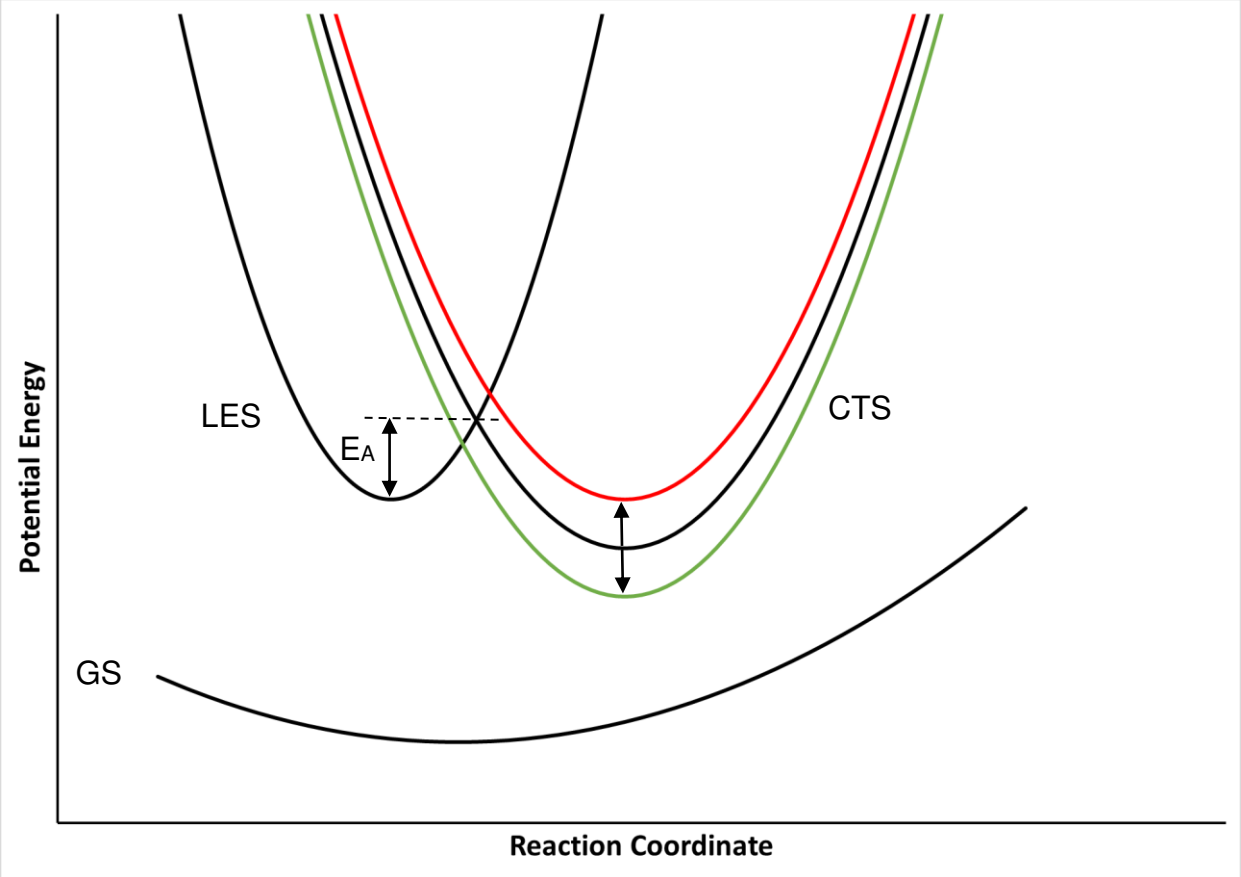


**Figure 14**: Potential energy curves of GS, LES, and CTS.
Shown in green and red are the energy curves of CTS in solvents of higher (green) and lower (red) polarity, respectively. $E_A$ gives the activation energy necessary for the transition from LES to CTS.

The conformation of the molecule in the CTS is a controversial topic.[20a, 24, 34] The proposed models for the CTS of DMABN are shown in Figure 15. The model of planar intramolecular charge transfer (PICT) proposes increased conjugation in the CTS in comparison to the GS, due to maximized orbital overlap. A model of rehybridized intramolecular charge transfer (RICT), involves rehybridization within the molecule to achieve the CTS.[35] The twisted intramolecular charge

transfer (TICT) mechanism, proposes a twist of a single bound between the D and the A. Thereby, the separated charges become electronically decoupled, preventing them from fast recombination.[20a, 36] Ab-initio calculations predict a partial twist of a single bond, known as partially twisted intramolecular charge transfer (pTICT).[23b, 34b, 37]

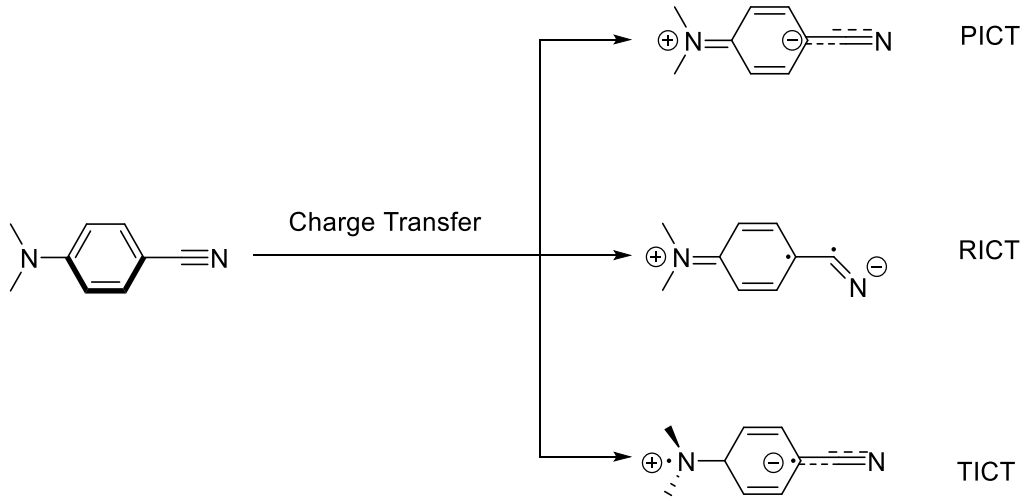


**Figure 15:** PICT, TICT and RICT in DMABN molecule during charge transfer.[15c, 20a, 23b, 34b, 35]

The TICT model, proposed by Grabowski and co-workers, can support the explanation of fluorescence in many DMABN derivatives.[20a, 36a] In the case of 1-methyl-5-cyanoindoline (MIN) (Figure 16), only short wavelength fluorescence out of the LES is observable. This result can be explained by the indoline substructure, which prohibits rotation of the amine group. Hence, the CTS cannot be formed and fluorescence out of CTS is not observed. Tetramethylaminobenzonitrile (TMABN), with two methyl groups appended in the *ortho* position to the amine does not show fluorescence out of the LES in non-polar solvents. In TMABN, the amine group is pre-deposed to a twisted arrangement in the ground state, due to stearic hinderance from the methyl groups in ortho position proximal to the amine. Therefore, the activation barrier to form the TICT state is lowered, and the CTS is preferred and formed faster than fluorescence emission from LES can take place.[20a]

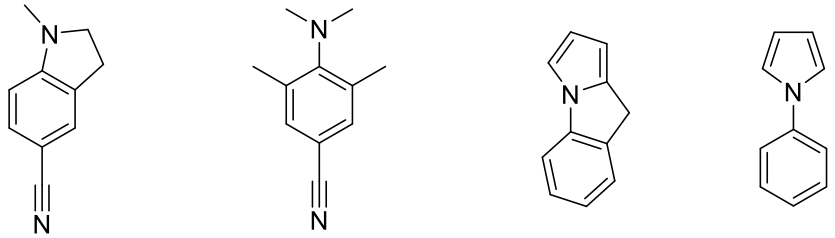


**Figure 16:** Structure of MIN, TMABN, FPP and PP.

The TICT model is not able to explain the fast formation of the CTS of fluorazene phenylpyrrole (FPP). Zachariasse and coworkers have shown that the rate of formation of the CTS in FPP and phenylpyrrole (PP) is comparable.[38] Both molecules consist of a phenyl ring connected to a pyrrole by a single bond (Figure 16). In PP, free rotation of this bond is possible, whereas for FPP the rotation is hindered sterically by a covalently bound unsaturated $CH_2$ group bridging the phenyl and the pyrrole subunit. Progressing research is demonstrating molecules can follow different conformational/structural changes upon CT, including the TICT or the PICT mechanism.[23a, 24, 34a, 39] Computational studies, for example done by Zhong, can help to predict whether a molecule forms a PICT or a TICT state. [40]

Apart from computations, additional experimental techniques can be used to study intramolecular CT processes. With time resolved infrared, and resonance Raman spectroscopy the bond strength between atoms in the exited states can be determined. Monitoring atom bond strength can clarify if a PICT or a TICT state is formed.[29d, 41] Transient absorption measurements are a method to determine the changes in the UV/Vis spectra of a molecule after excitation under ultrafast (ps-ns-ms) detection conditions. For example, the rise and the decay of the spectroscopic signature in the UV-Vis of an oxidized D can be used to determine the formation and decay rates in exited CT molecules.[29a, 42]

A variety of CT molecules constitute of covalently bound aromatic systems. These aromatic systems can be synthesized for example by palladium catalyzed cross-coupling reaction.

## 1.3. Palladium Catalyzed Cross-Couplings

Transition metals, such as Nickel (Ni), Ruthenium (Ru), Platinum (Pt), and Palladium have played a predominant role in the field of organometallic catalysis. Pd is used to catalyze reductions, oxidations, and C-C bond formations. Important applications include the Lindlar catalyst; Pd on charcoal; the Wacker process, and the cross-coupling reactions, later are discussed in this chapter.[43]

Metal mediated C-C bond formation reactions were explored near the end of the 19th century. Alkali and earth-alkali metal mediated reactions, such as the Wurtz reaction (1855), the Fittig reaction (1891), and the Grignard reaction (1900) have been reported.[44] Furthermore, Copper mediated C-C bond formations such as the Glaser coupling (1869), and the Ullman reaction (1901), have been published.[45] In 1968, Richard Heck published the first palladium catalyzed cross-coupling between an aromatic organomercury compound and alkenes.[46] For example, the cross-coupling between phenylmercury chloride (**I**) and methyl acrylic ester (**II**) with $Li_2PdCl_4$ under ambient conditions leads to methyl cinnamate(**III**) (Figure 17).

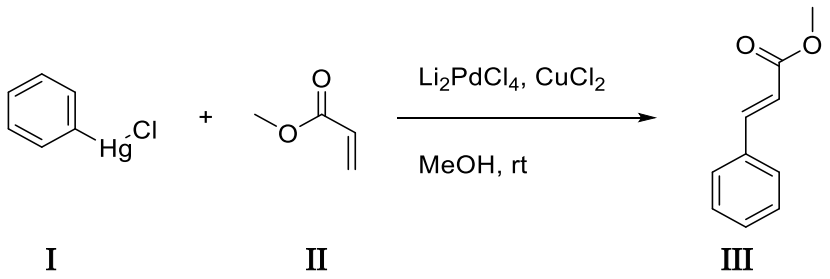


**Figure 17:** Example for Heck reaction published 1968 by Heck.[46a]

Taking into account the toxicity of organomercury compounds, alternative synthetic methods were developed to substitute the mercaptyl subunit by a halide.[47] In the following years, the catalytic use of Pd in C-C bond formation reactions evolved. The research results lead to a variety of developments, including different synthetic procedures; for example, the Sonogashira reaction, the Stille reaction, the Negishi reaction, and the Suzuki-Miyaura reaction.[45a, 45b, 48] In the year of 2010, Richard Heck, Ei-ichi Negishi, and Akira Suzuki received the

Nobel prize in Chemistry for their work on palladium catalyzed cross-coupling reactions in organic synthesis.[49]

Palladium catalyzed cross-couplings follow similar catalytic cycles, consisting of an oxidative addition, a transmetalation, and a reductive elimination step.[50]

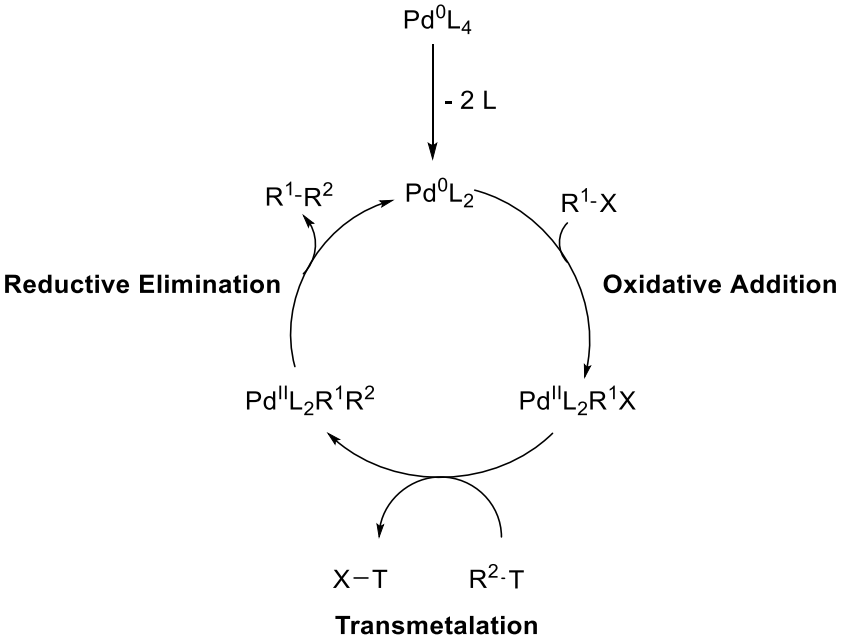


**Figure 18:** Catalytic cycle of a $Pd^0$ catalyzed cross-coupling.

A catalytic cycle for a $Pd^0$ species with two ligands (L) is shown in Figure 18. A reactive 14 valence electron $Pd^0L_2$ complex is initially formed by the dissociation of two L from the $Pd^0L_4$ complex. The $Pd^0L_2$ complex has a lack of valence electrons. The lack of electrons is compensated by oxidative addition of a substrate $R^1X$ to the $Pd^0L_2$ species, leading to a $Pd^{II}L_2R^1X$ complex.[51] The most common X groups are iodine, bromine or a triflate group (examples given in Figure 19).

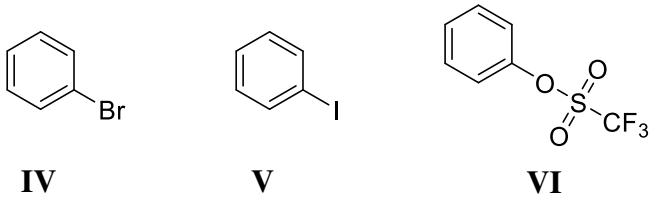


**Figure 19:** Benzene substituted with bromine (**IV**), iodine (**V**), and triflate (**VI**) as a X group.

The bond between these X groups and the carbon atom of $R^1$ is weak and allows for an efficient insertion of the palladium complex. In addition, halides and the triflate anion are good leaving groups and can therefore be eliminated in the transmetalation step.[51-52] A *β*-hydride elimination is a typical reaction in transition metal alkane complexes. To prevent the complex from undergoing this side reaction, the $R^1$ is chosen to be an aryl-group, which has no *β*-hydrogen atom, or a vinyl group.

The next step of the catalytic cycle is the transmetalation, whereby, X is exchanged by a $R^2$ group to form $Pd^{II}L_2R^1R^2$. The major difference between the different Pd catalyzed cross-couplings reactions is the source of the $R^2$ group ($TR^2$).[45a, 45b, 48a, 48e, 50a, 53] During the step where the bond between T and $R^2$ is cleaved, a bond between $Pd^{II}$ and $R^2$ is formed. Therefore, a weak T-$R^2$ bond (for example 238 kJ/mol for Sn-C)[54] enables a fast transmetalation process. A different approach involves activation of the $R^2$-T bond in-situ. The $R^2$-$B(OR)_2$ bond in a boronic acid or ester in a Suzuki coupling reaction, has a dissociation energy higher than a C-C bond (448 kJ/mol for B-C and 368 kJ/mol for $H_3C$-$CH_3$)[54]. The in-situ addition of a base, like sodium hydroxide or sodium acetate, to the boron atom forms a $NaR^2BOH(OR)_2$ complex, which activates the $R^2$-B bond for transmetalation.[45a, 45b, 48e, 55] This process will be discussed in detail, later in this chapter.

The final step in the catalytic cycle is the reductive elimination of $R^1R^2$ from $Pd^{II}L_2R^1R^2$ and the reformation of the active $Pd^0L_2$ species. The driving force for this step is the formation of the stable C-C bond.[51a, 56] The reductive elimination step requires a *cis* conformation related to $R^1$ and $R^2$ groups, which gives spatial proximity between both groups. In a *cis* conformation the bond angle $R^1$-Pd-$R^2$ is approximately 90°, based on a square planer complex geometry. Therefore, $R^1$ and $R^2$ are closer to each other in comparison to a *trans* conformation with a bond angle of 180°.

Various cross-coupling reactions, for example Sonogashira and Stille reactions, require additional isomerization step within the catalytic cycle as shown in Figure 20.

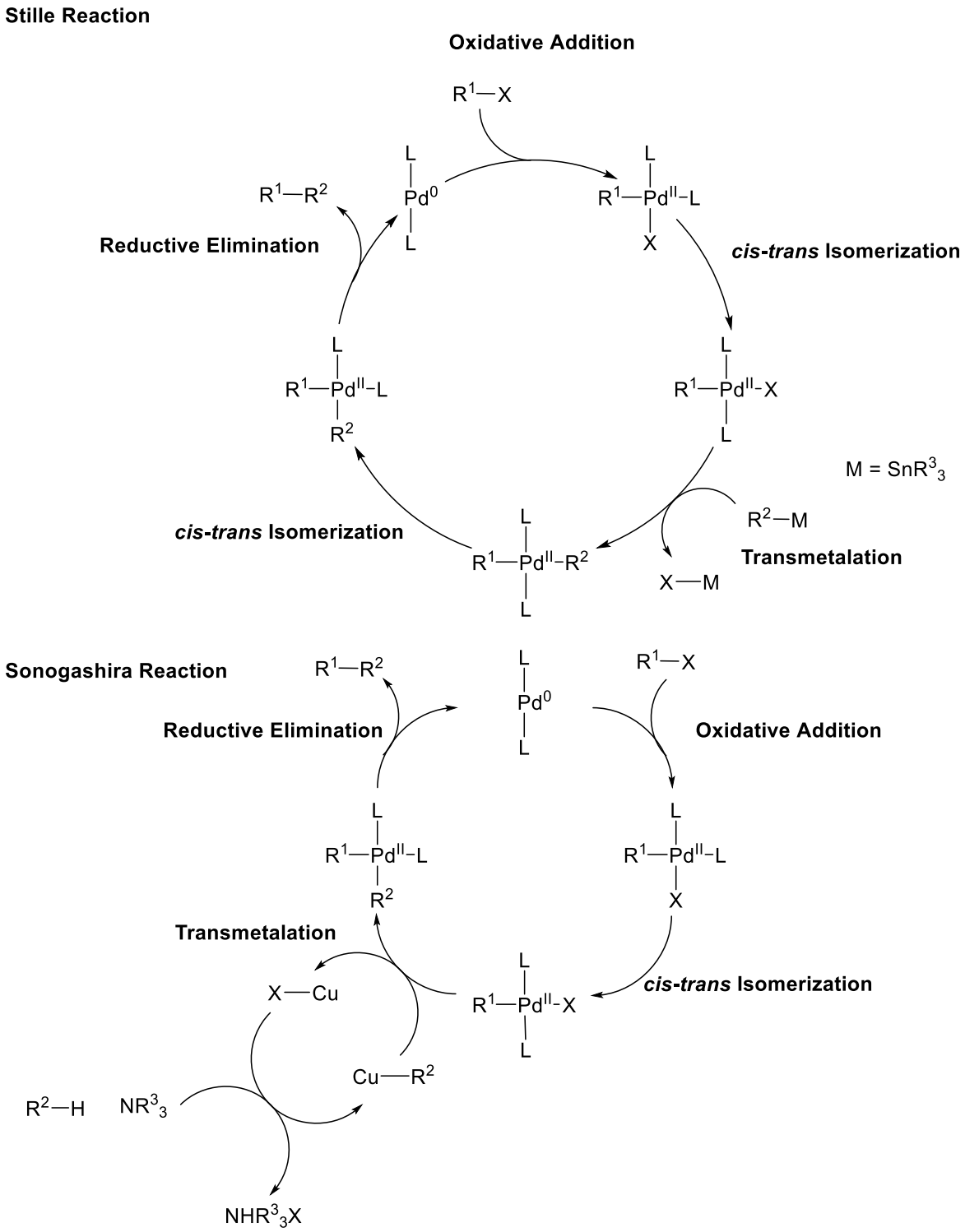


**Figure 20:** Reaction mechanisms of Stille and Sonogashira coupling.[48a, 57]

The oxidative addition and the reductive elimination steps are well established in the research field of transition metal complexes.[51a, 52a, 58] However, there is ongoing research to better understand the transmetalation process.[55, 59] In many palladium catalyzed cross-coupling reactions, the transmetalation step is

the slowest, and thereby the rate determining step of the reaction.[55] Most cross-coupling reactions use aryl halides, or aryl triflates as a transfer group ($R^1$) in the oxidative addition step. The different types of cross-coupling reactions vary in the functional group used to transfer $R^2$ during the transmetalation. Therefore, the transmetalation step of different cross-coupling reactions needs to be optimized individually.

Solvents play a role in the transmetalation step. For example, the Suzuki reaction is minimally affected by the solvent. The transmetalation process for other cross-coupling reactions can be strongly influenced by the solvent. In the Stille coupling reaction, polar aprotic amine solvents, such as *N,N'*-dimethylformamide (DMF), results in an increased transmetalation reaction rate in comparison to tetrahydrofuran (THF); or non-polar solvents such as toluene.[48b, 55, 60] This solvent dependence was explored by Mee et al.[48b] The Mee group studied the yield of a Stille cross-coupling reaction between *p*-iodotoluene (**VII**) and 4-(tri-*n*-butyltin)nitrobenzene (**VIII**) after a reaction time of 2 h with varying solvents, as shown in Figure 21.

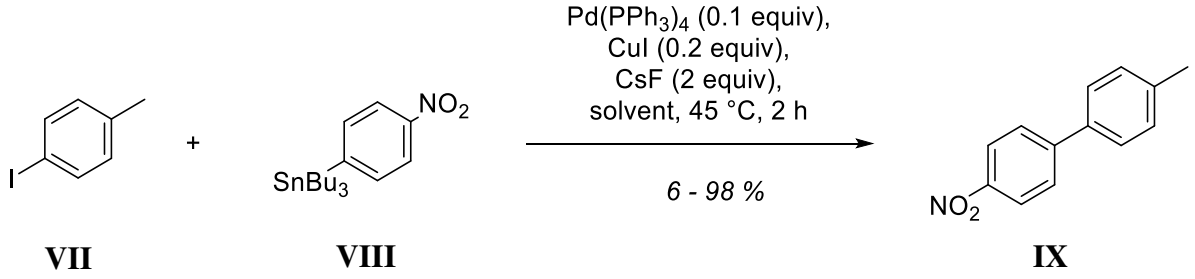


**Figure 21:** Stille cross-coupling reaction between **VII** and **VIII** as investigated by Mee et al.[48b]

In this study, carrying out the reaction in toluene resulted in only 6 % yield. However, the use of cyclic ethers as solvents, like THF or 1,4-dioxane improves the yield to 45 % and 48 %, respectively. The best yields were achieved by the use of DMF, dimethyl sulfoxide (DMSO) or *N*-methyl-2-pyrrolidone (NMP) which, lead to a maximum conversion of 98 %.

Beside variations of the solvent, improvement of the transmetalation process can be accomplished by adding co-catalysts. For example, the Sonogashira reaction, is supported by $Cu^I$ insertion into the C-H bond of a terminal

acetylene. The copper-acetylide complex formed transfers the acetylide to $Pd^{II}$, which is then coupled with aryl or alkenyl halides (Figure 20, bottom circle). Insertion of $Pd^{II}$ into the C-H bond of an acetylene is slow, and energetically unfavorable. Therefore, using $Cu^{I}$ as a co-catalyst in the Sonogashira reaction increases the conversion rate, and lowers the activation energy of the reaction.[48d, 50a, 61]

Dieck and Heck have published the synthesis of diphenylacetylene (**XI**). The reaction is a Pd catalyzed cross-coupling between **V** and phenylacetylene (**X**) (Figure 22).[62] Dieck and Heck carried out this reaction without CuI at 100 °C and achieved a yield of 57 %. However, Sonogashira used CuI as a co-catalyst in the reaction and was able to isolate **XI**, after 3 h at rt, in 90 % yield.

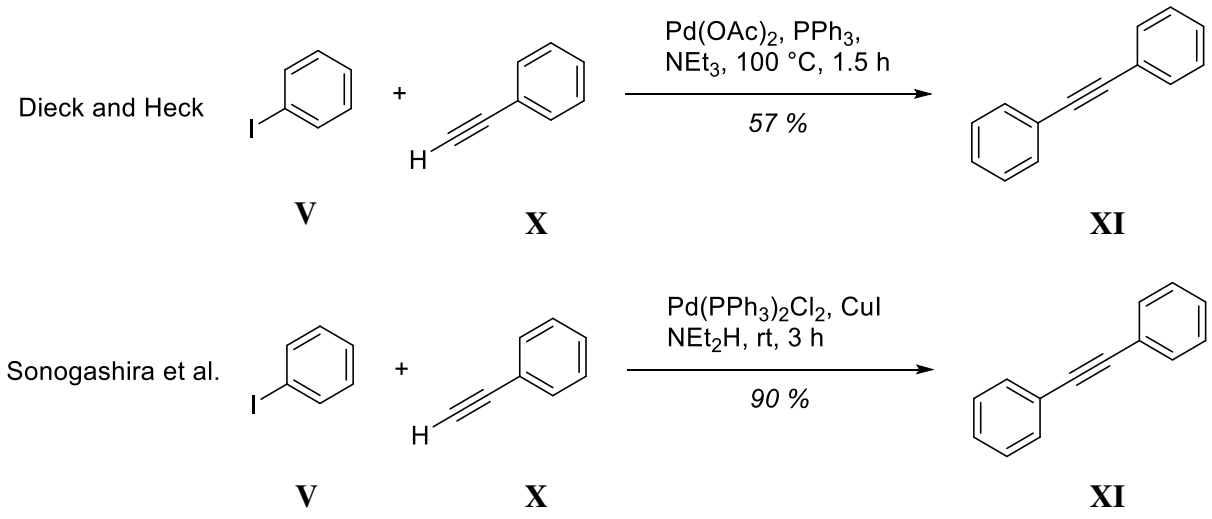


**Figure 22:** Sonogashira cross-coupling reaction between **V** and **X** under different conditions published either by Dieck and Heck or by Sonogashira.[62]

Figure 23 shows the hypothesized catalytic cycle of $Cu^{I}$ in a Sonogashira cross-coupling reaction.[50a] To date, the role of copper-ligand interactions is still not clear.[63]

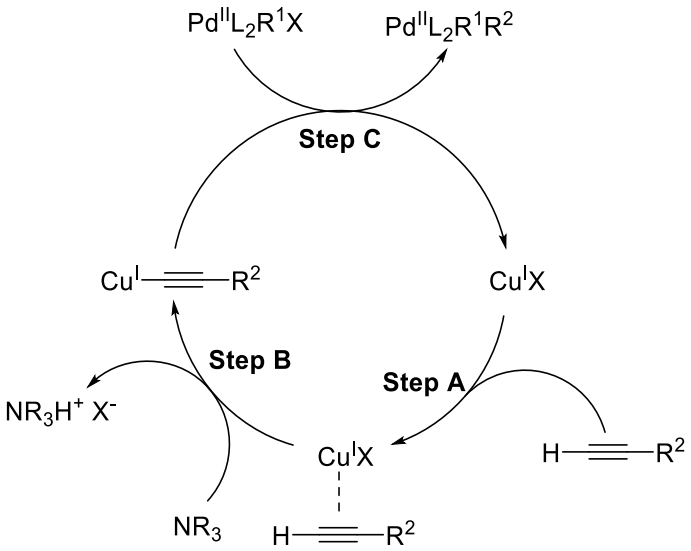


**Figure 23:** Supposed catalytic cycle of $Cu^I$ in the Sonogashira cross-coupling reaction.[50a]

In the catalytic cycle, Step B is supported by a base (shown in Figure 23). The base increases the rate of addition of the terminal acetylene to the $Cu^I$, by forming an ionic complex (for example $NR_3H^+X^-$) with the leaving HX group. Amine bases were chosen in the first Sonagashira cross-coupling reactions and are still frequently used in this type of reaction.[48d, 50a, 62b]

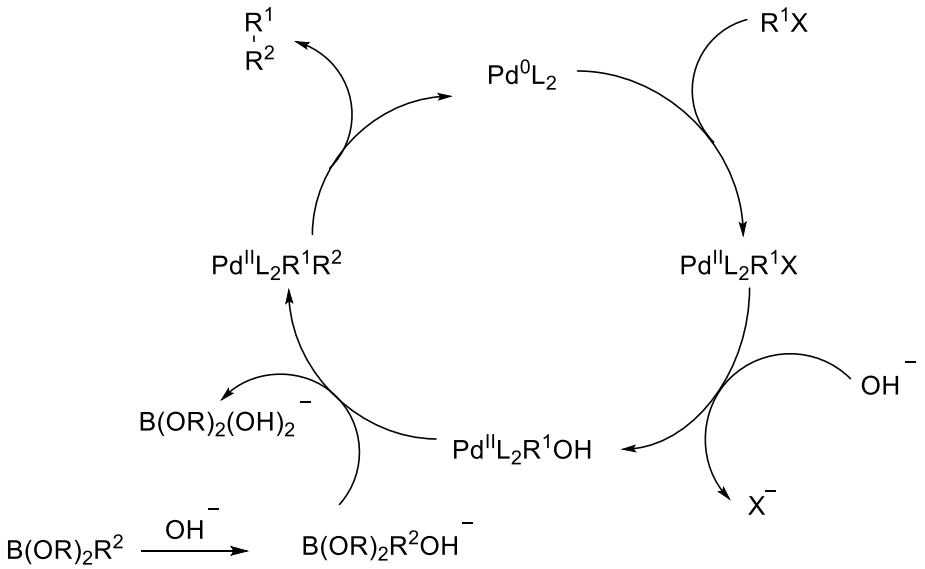


**Figure 24:** Mechanism of a Suzuki cross-coupling reaction.[48e]

The use of anionic bases, such as hydroxides or acetates, increases the rate of the transmetalation step in Suzuki cross-coupling reactions. A hydroxide base imparts two effects, shown in Figure 8. The X group of the $Pd^{II}L_2R^1X$ complex can be exchanged by the base to form the $Pd^{II}L_2R^1OH$ complex. The $Pd^{II}$-OH bond is more polar than a $Pd^{II}$-X bond, due to a higher electronegativity of oxygen in comparison to a halide. Transmetalation between a Pd complex and boron coupling partner requires the cleavage of the $Pd^{II}$-OH or $Pd^{II}$-X bond, and reformation of a new bond between the metal and the boron substrate. The process is faster with a more polarized $Pd^{II}$-OH bond versus a $Pd^{II}$-X.

The Suzuki cross-coupling reaction between 4-iodonitrobenzene (**XII**) with phenylboronic acid (**XIII**) under different pH conditions (Figure 25), has been investigated by Wallow and Novak.[64]

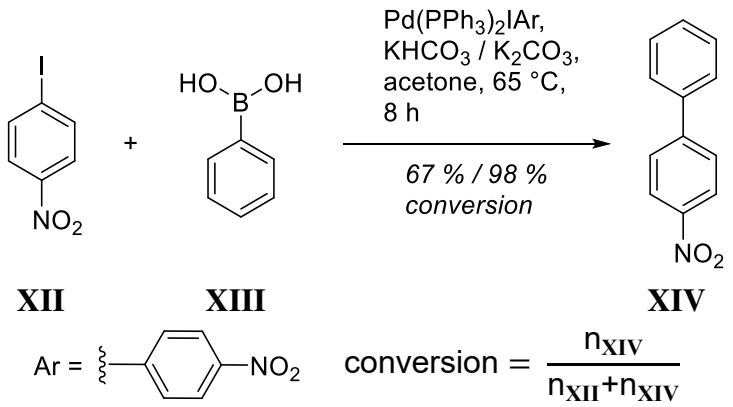


**Figure 25:** Suzuki cross-coupling between **XII** and **XIII** with different base used.[64]

The group used $KHCO_3$ or $K_2CO_3$ as a base in the reaction to achieve pH values of 7 – 8.5 and 9.5 – 11, respectively. The reaction shown in Figure 25 was carried out at 65 °C using both aforementioned pH range values. The reaction at pH 7 – 8.5 demonstrated 67 % conversion of **XII** to **XIV** while the reaction at pH 9.5 – 11 led to 98 % conversion. The formation of an anionic boronate complex $B(OR)_2R^2OH^-$ (**XVI**) out of $B(OR)_2R^2$ (**XV**) and a base at pH values between 11 and 12 were observed by Norrild and Eggert (Figure 26).[65]

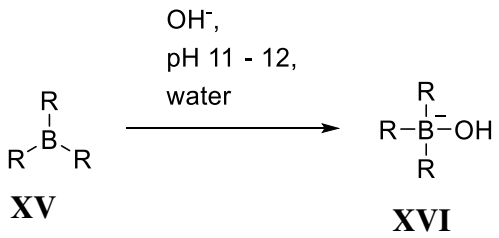


**Figure 26:** Formation of a anionic boronate complex at pH values of 11 – 12 observed from Norrild and Eggert.[65]

The formation of an anionic boronate complex at pH 11 – 12, could explain the increased conversion in the Suzuki reaction at pH values of 9.5 – 11 observed by Wallow and Novak.[48e, 64, 66]

The transmetalation step of different cross-coupling reactions vary and require different reaction conditions and co-catalysts. These parameters need to be optimized for each type of cross-coupling reaction and can also change by varying substrates within one type of coupling reaction. As previously mentioned,

many cross-coupling reactions, as for example the Stille and Sonogashira reactions, require a *cis-trans* isomerization within the catalytic cycle (Figure 20). Optimizing the reaction parameters for these additional steps can also improve the outcome of the reaction.

Despite all the difference between various types of cross-coupling reactions all of them require a $Pd^0L_2$ complex to proceed. Figure 27 represents the pathways to form the required $Pd^0L_2$ species. $Pd^0L_4$ is a frequently used source for $Pd^0$ in cross-coupling reactions, where the dissociation of two L leads to $Pd^0L_2$. $Pd^0L_2$ can also be obtained from $Pd^0{}_2dba_3$ in which two $Pd^0$ atoms are complexed by three dibenzylidenacetone ligands (dba). The ligand (L) is introduced into to the $Pd^0{}_2dba_3$ reaction cycle without metal complexation and competes with dba for the palladium metal. The affinity of L towards $Pd^0$ in comparison to the affinity of dba influences the amount of active $Pd^0L_2$ species in solution. $Pd^{II}$ in form of $Pd^{II}Cl_2$ or $Pd^{II}(OAc)_2$ can also be used to achieve an active $Pd^0L_2$ complex.[53c, 67] $Pd^0$ sources require a ligand dissociation ($Pd^0L_4$) or a ligand exchange ($Pd^0{}_2dba_3$) process. $Pd^{II}$ however, must be reduced to enter the catalytic cycle. The addition of two ligands to $Pd^{II}X_2$ forms a $Pd^{II}L_2X_2$ complex, where X can be, for example Cl or OAc. The $Pd^{II}L_2X_2$ complex undergoes two transmetalation processes with two R-T species (T is the transmetalation reagent). The formed $Pd^{II}R_2L_2$ complex then reductively eliminates the homocoupled side product R-R and releases the active $Pd^0L_2$ species.[68]

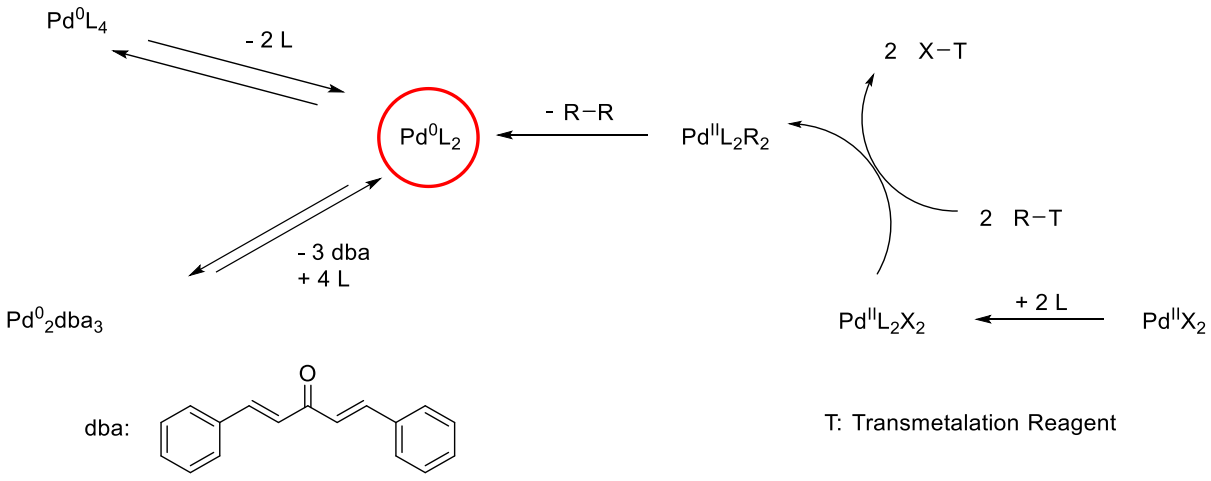


**Figure 27:** Processes towards the catalytic active $Pd^0L_2$ complex.

The aforementioned work by Mee et al. involved research on an optimized source of active $Pd^0L_2$ for the Stille reaction between 4-bromoanisole (**XVII**) and **VIII** (Figure 28). The procedure uses $Pd_2dba_3$, $Pd(OAc)_2$, and $PdCl_2$ as a source for palladium and P*t*-$Bu_3$ as a ligand, and yields were determined after 15 h at 45 °C. When $Pd_2dba_3$ was used as the the $Pd^0$ source, a yield of 64 % was recorded. The yield was increased by using $Pd(OAc)_2$ and $PdCl_2$, yielding 89 % and 97 %, respectively.[48b]

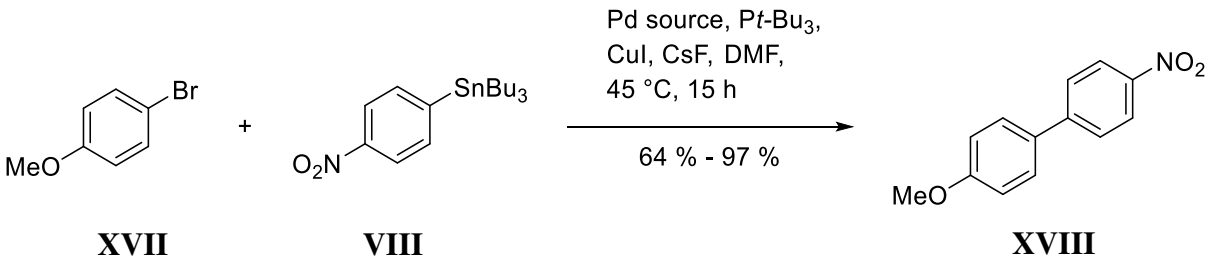


**XVII** **VIII** **XVIII**

**Figure 28:** Stille cross-coupling between **XVII** and **VIII** with varying $Pd^0L_2$ sources carried out by Mee et al.[48b]

In addition to the source of $Pd^0$, the choice of the ligand plays a major role on the outcome of a cross-coupling.[48b] The dissociation of $Pd^0L_4$, a complex with a preferred 18 valence electron configuration, towards the active $Pd^0L_2$ complex is favored with bulky ligands.[51a, 61, 69] The oxidative addition step is supported by a strong donor ligand, such as a phosphine group.[70] Each reactive metal-ligand complex differs slightly in the rate limiting step. In order to positively influence this step by implementing a L group for highest reaction yields, different L groups need to be tested. A commonly used ligand, with a good stability against oxygen, is triphenylphosphine ($PPh_3$), shown in Figure 29. If a higher reactivity is necessary for the reaction to proceed, tri-*t*-butyl phosphine (P*t*-$Bu_3$) can be used. P*t*-$Bu_3$ is a bulky and electron rich Ligand and therefore able to enhance transmetalation and oxidative addition within the catalytic cycle. [48a, 48b, 50a, 53c, 67]

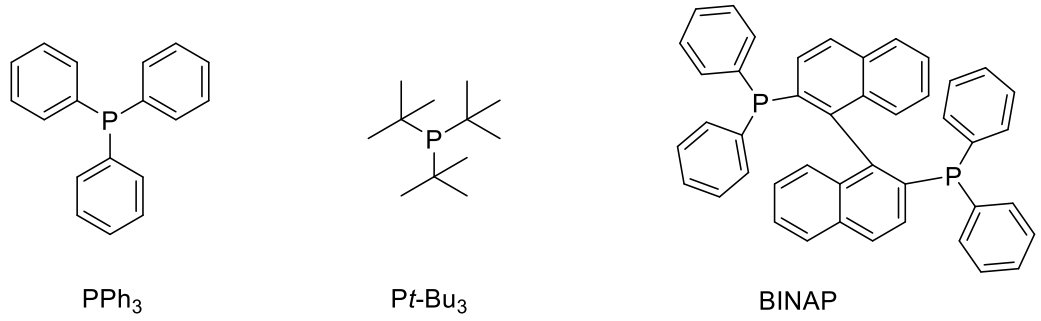


**Figure 29:** Ligands used for palladium catalyzed cross-coupling reactions.

Cross-coupling reactions of inactivated aryl or vinyl chlorides often show low yields or no conversion when triphenylphosphine is used as a ligand.[69b, 71] Using the more reactive P*t*-Bu$_3$ L can improve the outcome of these reactions. The group of Fu has studied the use of P*t*-Bu$_3$ in a variety of Stille and Suzuki reactions.[69, 71a, 71b, 72] For example, a Suzuki cross-coupling reaction between 4-chlorotoluene (**XIX**) and **XIII** with different phosphine ligands was investigated (Figure 30).[71a, 71b]

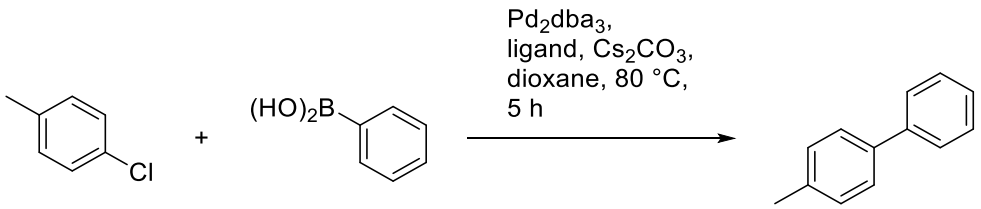


**XIX** **XIII** **XX**

**Figure 30:** Suzuki cross-coupling between **XIX** and **XIII** with different phosphine ligands done by Littke and Fu.[71a, 71b]

The group determined yields after 5 h of reaction at 80 °C, by gas chromatography. They have observed no reaction at all by the use of different tri-aryl phosphine ligands, comprising PPh$_3$ and BINAP. However, tri-alkane phosphine ligands such as tricyclohexyl phosphine, and P*t*-Bu$_3$ has led to 75 % and 86 % yield, respectively.[71a, 71b]

Computational chemistry can support the understanding of the mechanism of cross-coupling reactions.[52a, 57, 58b, 59] Detailed knowledge of the reaction mechanism helps to define requirements for an optimal ligand. Mechanistic studies of the transmetalation step involved in the Stille coupling have proposed two different pathways, as shown in Figure 31.[59, 73]

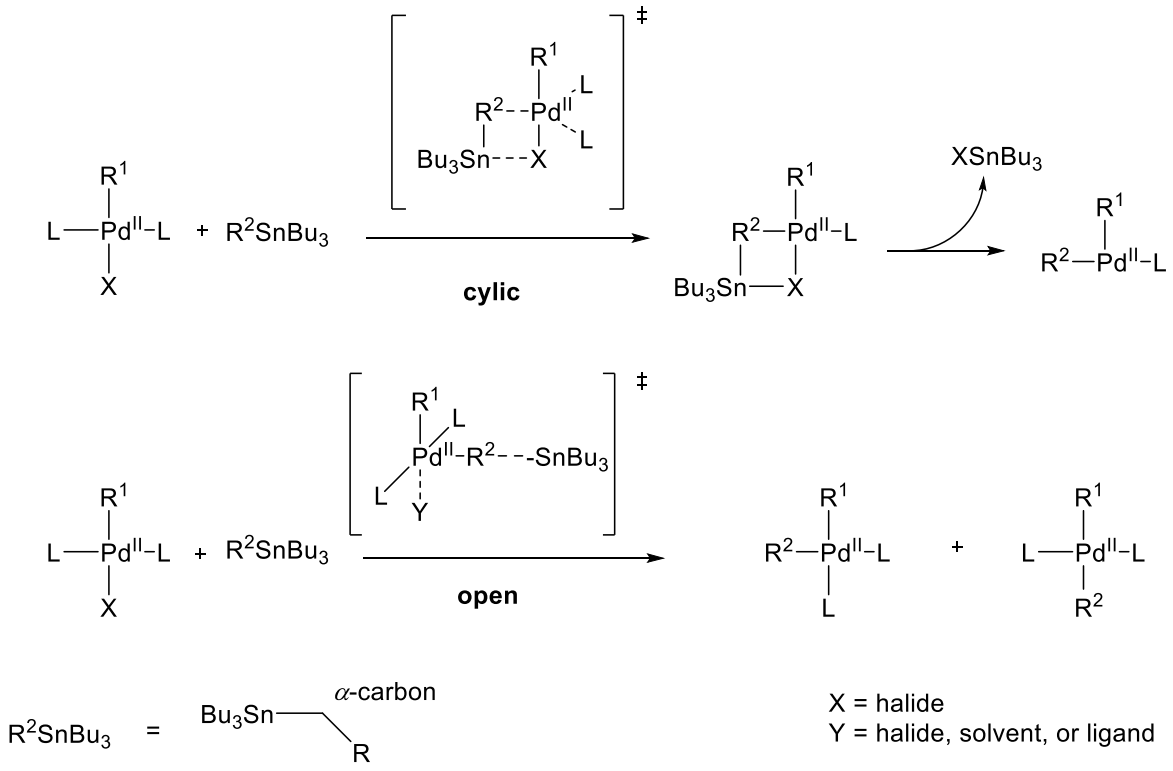


**Figure 31:** Different mechanisms for transmetalation in Stille cross-coupling.[59]

The first pathway includes a cyclic four membered ring intermediate, and can explain the retention of stereochemical configuration observed in some Stille coupling reactions.[73b] The second pathway forms an open, $S_N2$ transition state, leading to an inversion of the stereochemistry at the *α*-carbon shown in Figure 31. Reactions undergoing the cyclic pathway require the dissociation of a ligand, hence, they occur faster with a weak bond between L and $Pd^{II}$, such as for triphenyl arsine ($AsPh_3$).[48a, 59, 73a]

The formation of new C-C bonds by metal mediated cross-coupling reactions can lead to chiral molecules, which have a carbon center with four different substituents. The use of a chiral L, such as a BINAP derivative (Figure 29) in a Heck reaction, leads to an asymmetric Pd complex.[74] Cross-coupling reactions with these asymmetric complexes are enantioselective, and can produce an enantiomeric excess of more than 90%.[53a, 53b, 67, 74a] Tschoerner and Pregosin have studied enantioselective Heck reactions.[75] They coupled a triflate substituted phenylacetate (**XXI**) with dihydrofuran (**XXII**) to form product (**XXIII**) in 76 % yield, as shown in Figure 32. They found an enantiomeric excess of 99 of the *S* enantiomer over the *R* enantiomer.

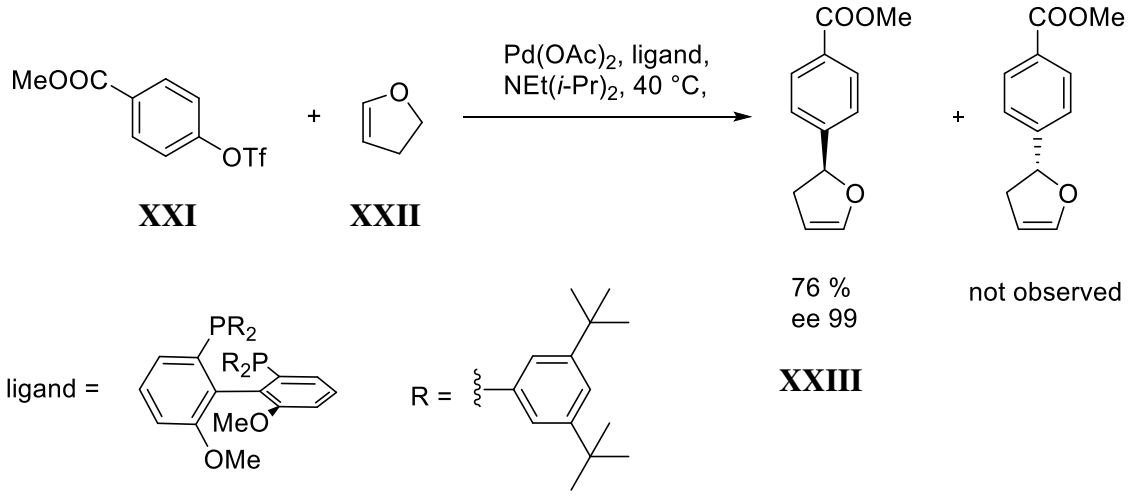


**Figure 32:** Enantioselective Heck reaction between a **XXI** and **XXII**.[75]

# 2. Chiral Charge Transfer Dyes

## 2.1. Design of Chiral Charge Transfer Dyes

The chiral dyes synthesized in this project are comprised of a donor (D), *π*-conjugated spacer (S), primary acceptor (A1), chiral bridge (B), and a secondary acceptor (A2), or stable free radical (SFR). Based on these building blocks two series of CT dyes have been synthesized. The two series of dyes vary in the proximity of donor and acceptor as shown in Figure 33.

The chiral induced spin selectivity effect (CISS) is a motivation for the synthesis of these dyes. CISS describes an electron spin filter effect. When an electron beam passes a chiral environment, like DNA molecules, one electron spin is favored and passes the system faster than the other. Therefore, the faster electron spin is enriched after passing the chiral environment. During the CT process in the synthesized dyes the electron moves within a chiral environment from the D to the A. Hence, CISS effects should be observable.

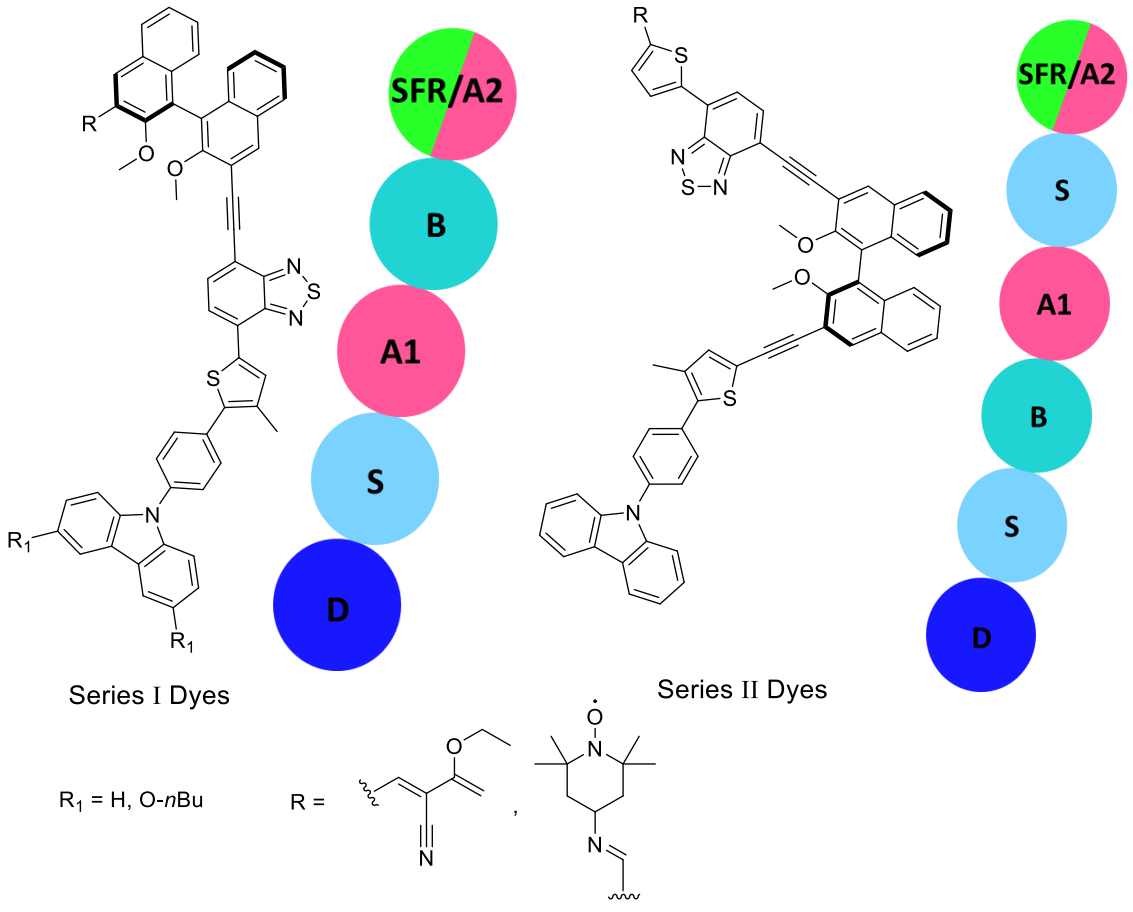


**Figure 33:** Molecular structure of Series I and II dyes.

Series I dyes are constructed in a D-S-A1-B-A2 fashion, where D and A1 are connected by the thiophene spacer S. In series II dyes the chiral bridge separates D and A1, resulting in a D-S-B-A1-S-A2 construction. Series I dyes were synthesized with either a proton or a *n*-butoxy substituent in the $R_1$ position of the carbazole donor moiety. Both series were substituted with a SFR and A2 in the R position. $Sp^2$ and sp hybridized spacers were used to incorporate the chiral bridge into the molecule to achieve sufficient conjugation.

The synthetic approach for the dyes reported in this thesis is constructed in a modular fashion. Stille and Sonogashira cross-coupling reactions, as well as imine condensation and Knoevenagel reactions are used to build up the dyes and form connections between the individual subunits.[48a, 48b, 48d, 50a, 57, 73b, 76] The modular synthetic approach provides the option to exchange building blocks within the dye and to vary the spatial and covalent bond arrangements. Therefore, the bonds between the donor and acceptor groups can be changed with respect to the extent of electronic communication. For example, the position of the chiral bridge, a building block with a small unconjugated gap, can be varied.

The characterization of series I dyes, indicated that the CT process only takes place between D and A1. Therefore, electron donating *n*-butoxy groups were appended to the donor unit to increase the electron density of the D to facilitate charge transfer to the secondary acceptor. Basic computational studies demonstrated an increased electron density of the donor, which predicted a lower HOMO-LUMO gap. However, the experimental result indicated the electron-donating capability to be not sufficient enough, to achieve an electron transfer to the final acceptor A2. A second series of dyes (series II) was synthesized in order to ensure the electron would transverse through the chiral bridge to the final A2 acceptor. In this series, the primary acceptor A1 is positioned after the chiral bridge B.

Studying CISS effects in the synthesized molecules allow insight on the effect of chiral systems to intramolecular CT processes. In series I dyes the CT process from D to A1 takes place in close approximation to a chiral system but does not transverse the chiral bridge to A2. In series 2 dyes the electron needs to

pass the chiral bridge during the CT process, either by a hopping or tunneling mechanism.[77]

Additionally, in both series of dyes, the A2 functional group can be replaced with a stable free radical (SFR) moiety. The motivation for this structural modification of the dye hinges upon the goal that an unpaired spin is interacting with a chiral CT system. Results from Chernick and coworkers has shown that an unpaired spin can slow down charge recombination processes.[16a] In the synthesized dyes the distance dependence of these effects can be studied. In addition, the system allows to study the influence of the spin polarized CT system to the electronically decoupled unpaired spin of the SFR. The interaction between the unpaired spin of the SFR and the CT state opens the possibility to populate multiple different quantum states of the system. Therefore, the system could potentially be used as a qubit in quantum information science research.

The donor moiety of the dye is 9-phenyl-9H-carbazole; a derivative of triphenylamine (TPA), as shown in Figure 34. TPA is a widely used D in the field of organic solar cells that operates upon utilizing the CT that occurs in these molecules.[78] The 5 membered ring formed by connecting adjacent phenyl rings of TPA in 9-phenyl-9H-carbazole leads to planarization and increased conjugation within the D moiety. The planarity of the carbazole facilitates electron communication through the $\pi$-network.

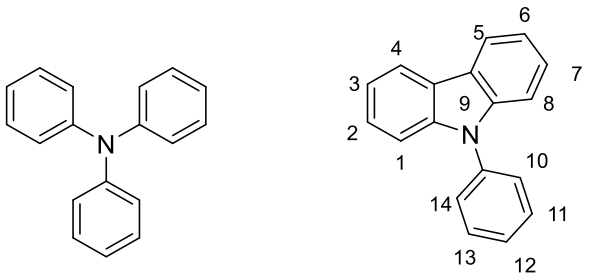


**Figure 34:** Chemical structure of triphenylamine (left) and 9-phenyl-9H-carbazole (right).

The 12-position of 9-phenyl-9H-carbazole is the connection point to build up the dye. Substitution of the 3 and 6 position on the carbazole with alkyl chains can improve the solubility of the dye. Substituting these positions with electron donating or withdrawing groups can also finetune the electronic properties of the donor.

Modification of the electron density influences the HOMO-LUMO gap of the molecule by raising the energy of the HOMO. The energies of HOMO and LUMO can be investigated by electrochemical measurements. The comparison of oxidation potentials (OP) of different carbazole derivatives allows the comparison of the HOMO energy levels. The oxidation potential of carbazole determined by electrochemistry is 1.16 V vs. the standard saturated calomel electrode (SCE). The OP of 9-phenyl-9H-carbazole is minimally influenced by the phenyl ring and has been reported to be 1.21 V vs. SCE.[79] The substitution of the 3 and 6 position of the carbazole with an electron donating methoxy group lowers the OP from 1.16 to 0.78 V vs. SCE.[79b, 80] In this project, one series of dyes was synthesized with a *n*-butoxy substituted donor moiety. The substituents were appended to the 3 and 6 position of the carbazole to serve as electron donating groups with ability to increase the solubility of the chromophore.


**Figure 35:** CT system with either a phenyl or an acetylene π-spacer.

*π*-Spacers in CT molecules enhance the interaction between D and A, due to a more planer conjugated system. Enhanced interaction between D and A decreases the HOMO-LUMO gap and lowers the amount of light energy needed to enable the CT process of the dye. Molecular subunits are connected by unsaturated $sp^2$/sp alkene/alkyne bonds. Connections via $sp^2$ hybridized phenyl rings can reduce the electronical coupling of D and A group due to the orthogonal arrangement between neighboring *π*-systems. When the $sp^2$ system is replaced by a sp hybridized triple bond, the electronic communication is enhanced due to a more planar, conjugated system with maximum orbital overlap as shown in Figure 35.

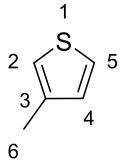


**Figure 36:** Chemical structure of 3-methylthiophene.

Beside heteroatom free spacers like phenyl, alkenyl or alkynyl units, heteroaromatic spacers like thiophene are commonly used in CT molecules for photovoltaic application. In this work the 3-methyl derivative of thiophene (Figure **36**) is used as the *π*-spacer (S). Heteroatom free spacers like phenyl, alkynyl or alkenyl spacer raise the energy of the HOMO to reduce the HOMO-LUMO gap, while heteroaromatic spacers lower the energy of the LUMO.[81] The use of heteroaromatic *π*-spacers in CT dyes has several advantages. Molecules comprised of a heteroaromatic *π*-spacer show chemical and thermal stability and due to their polarizability, demonstrate good solubility.[81b, 81c, 82] Substitution in 3 position of the thiophene with alkyl chains further improves the solubility of the molecules und reduces their reactivity. In this work, the 3 position of thiophene was substituted with a methyl group.

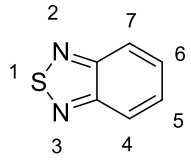


**Figure 37:** Chemical structure of BTDA.

The primary acceptor A1 is 2,1,3-benzothiadiazole (BTDA), as shown in Figure 37. BTDA is frequently used in organic CT dyes.[45i, 83] BTDA is stable under ambient conditions and is commercially available as the 4,7-dibromo-2,1,3-benzothiadiazole derivative. The bromine groups act as synthetic handles for further cross-coupling reactions. The electrochemically determined reduction potential of BTDA is –1.56 V vs. SCE.[84]

The chiral bridge B is derived from a 2,2'-dimethoxy-1,1'-binaphthalene unit, which is a derivative of 1,1'-binaphthalene-2,2'-diol (BINOL) (Figure 38). The 3 and 3' position of the bridge are the connection points for further reactions to build up the dye infrastructure. BINOL is a beneficial chiral element and is well documented in literature.[85] The chemistry of BINOL is well understood, and many of its physical properties are reported.[86]


**Figure 38:** Chemical structure of BINOL (left) and 2,2'-dimethoxy-1,1'-binaphthalene (right).

Furthermore, BINOL derivates are stable under a variety of synthetic conditions and used in many applications, including the prominent research field of chiral catalysis.[86a-c, 87] BINOL possesses structural axial chirality[88] in which the axis of symmetry can be found in one or more chemical bond(s) (Figure 39; A and B) or within an imaginary axis (Figure 39; C).

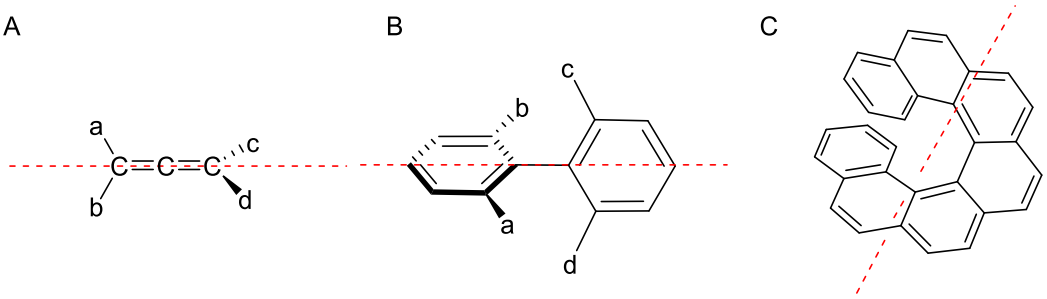


**Figure 39:** Different molecules with axial chirality. Shown in red is the chiral axis.

For molecules where the chiral axis lies along a chemical bond, the rotation around this bond leads to the transition from one enantiomer to the other. The stability of enantiomeric species directly influences the applicability in methodology where enantiomerical purity is required. Under these premises, it needs to be considered the racemization of 1,1'-binaphthyl takes places under standard reaction conditions. For example the half-life time ($t_{1/2}$) of enantiomeric pure 1,1'-binaphthyl is 14.5 min at 50°C in DMF.[89] The steric hindrance of the two hydroxyl groups in the 2 and 2' position of BINOL prevents rotation upon the bond between C1 and C1'. Therefore, racemization under standard reaction conditions is hindered. Patel and coworkers have measured a $t_{1/2}$ of 20 d for BINOL at 180°C in diphenylether.[86d]

To circumvent further reactivity of the BINOL moiety, the alcohols were methylated, which prevents deprotonation in further reactions involving for example

organo-lithium reagents. Methylation also improves the solubility of BINOL in non or weakly polar solvents such as hexane or dichloromethane (DCM). Additionally, the exchange of the alcohol proton to a methyl group increases the steric hinderance, further preventing racemization.

The substitution of protons in the 6 and 6' position of BINOL is well reported in literature.[86a, 90] Substituents in the 6 and 6' position can act as synthetic handles for functionalization that will influence the solubility, and/or finetune the electron density on the chiral bridge by using electron donating or accepting groups. For the synthetic results presented in this thesis, the 6 and 6' position remain unsubstituted.

The BINOL derivative is used as the chiral bridge in this research for a number of reasons, including providing a chiral environment while sustaining electronic coupling distance between the D and A components of the dyes. Close proximity between the two conjugated systems can lend to faster the CT from one side of the molecule to the other. The distance between the two decoupled $\pi$-systems in 2,2'-dimethoxy-1,1'-binaphthyl is approximately 1.49 Å.[91] An electron can transverse this distance by the mechanism of electron tunneling or hopping.[77]

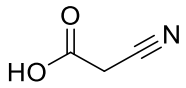


**Figure 40:** Chemical structure of 2-cyanoacetic acid.

The second acceptor A2 is 2-cyanoacetic acid (Figure 40). Dyes comprised with multiple acceptors, like the structure D-A1-S-A2, demonstrate increased photostability and a stronger CT character in comparison to D-S-A dyes.[83c, 92] The 2-cyanoactic acid moiety provides the ability to combine the chemical properties of an electron accepting group with the ability to attach to an electrode in dye sensitized solar cells (DSSC).[83e, 93] In *n*-type, DSSCs $TiO_2$ is a typically used surface material for electrodes.[93d, 93e, 94] The carboxylic acid functional groups can possess multiple modes to bind to the electrode surface, as shown in Figure 41.[93c, 93e, 93f]

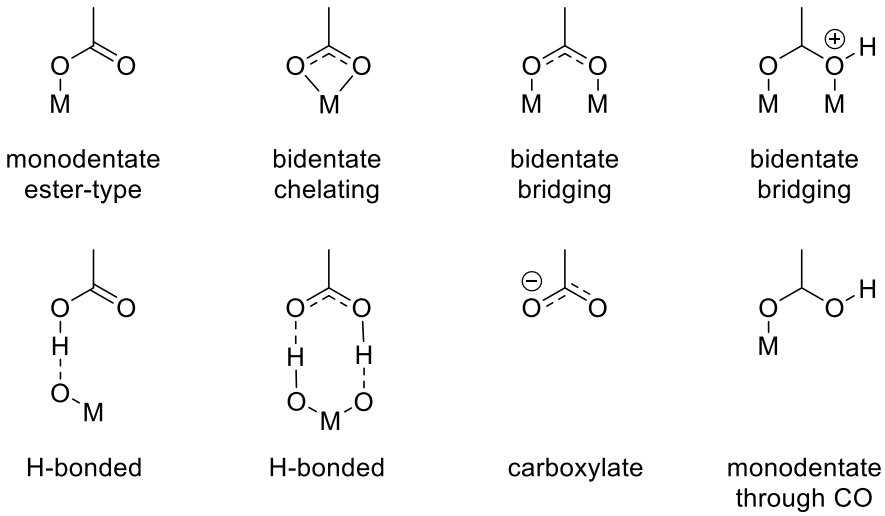


**Figure 41:** Binding modes of carboxylic acids to metal oxide surfaces.[93f]

The cyanide group is a strong electron withdrawing group, making it a strong acceptor for intramolecular CT processes. The cyanoacrylic acid group can be incorporated into organic molecules bearing an aldehyde moiety by the Knoevenagel reaction.[76b, 76c] In this reaction, polymerization side reactions can occur, hence, in this project ethyl cyanoacetate was used as the secondary acceptor (Figure 42).

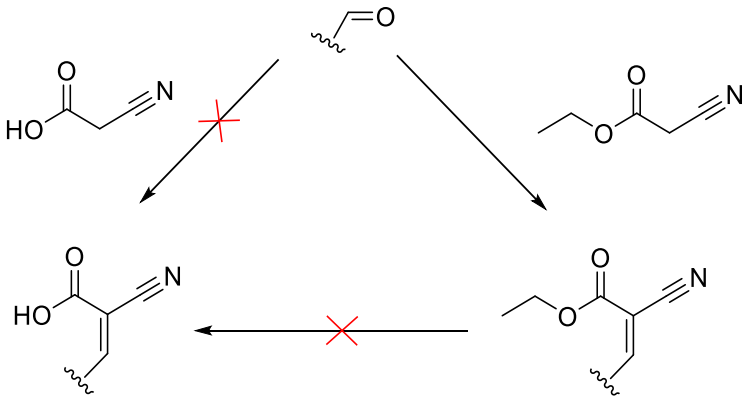

**Figure 42:** Synthetic efforts towards 2-cyanoacetic acid as A2.

The Knoevenagel reaction to form the cyanoacrylic ester can be carried out under ambient conditions, yielding the ester in good yields. However, hydrolysis to form the corresponding acid failed under different acidic and basic conditions. Hence, no further attempts were made to prepare the unprotected acid. The electron accepting property of A2, in form of ethyl cyanoacetate, only varies slightly from that of the acid.

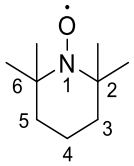


**Figure 43:** Chemical structure of TEMPO.

The SFR for this synthetic project is (2,2,6,6-tetramethylpiperidin-1-yl)oxyl (TEMPO), shown in Figure 43. TEMPO is an organic radical, that is stabilized by steric protection by adjacent methyl groups, preventing reactivity. TEMPO is a multifunctional SFR and is used in multiple applications such as oxidation reactions and radical polymerizations.[95] Commercially available 4-amino-TEMPO can be reacted with an aldehyde to form an imine bond.[96] The unpaired spin of the TEMPO radical is localized on the nitroxide atom and subsides in an $sp^3$ hybridized carbon network; hence the radical cannot delocalize onto a neighboring molecular system through bond interactions. Therefore, the interaction between the oxyl radical and another unpaired spin can take place only through space.

## 2.2. Synthesis of Chiral Charge Transfer Dyes

According to modular synthetic strategy, mentioned in the Design of the Dyes section, the formation of the subunits and the combination to the final dyes can be considered section wise.

### 2.2.1. Synthesis of the Donor-Spacer Subunit

The synthesis of the D-S subunit for series I dyes, with a tri-*n*-butyl tin group attached at the thiophene, is shown in Figure 44.

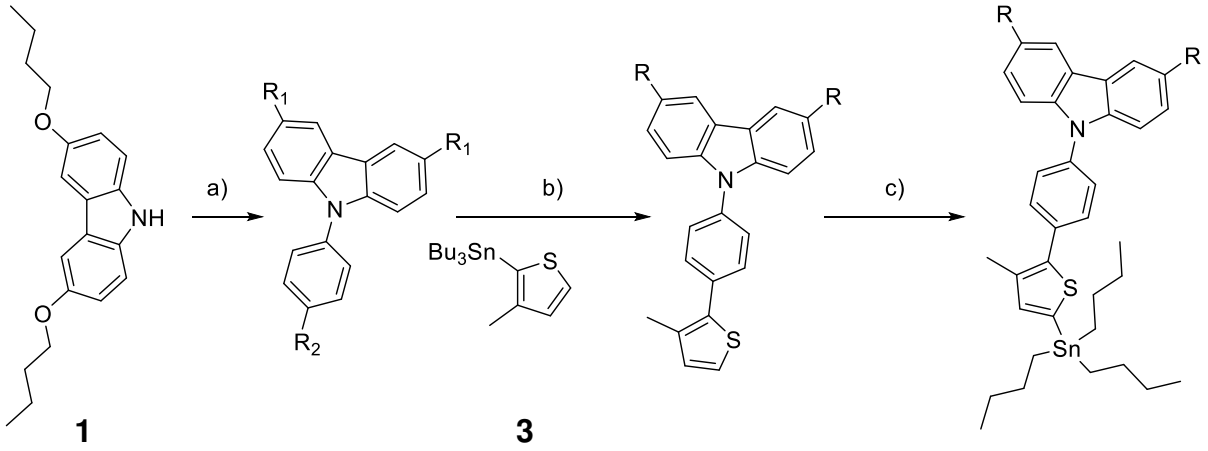


**Figure 44:** Synthesis of of D-S subunit of series I dyes with tri-*n*-butyl tin groups for further cross-coupling reactions.
a) 1-Fluoro-4-iodobenzene, $Cs_2CO_3$, DMF, 150 °C, 24 h. b(i)) $PdCl_2$, P(*t*-Bu)$_3$, CuI, CsF, DMF, 100 °C, 16 h. b(ii)) $Pd(PPh_3)_4$, CuI, CsF, DMF, rt, overnight. c) (1) *n*-BuLi, tetrahydrofuran (THF), – 78 °C; (2) $SnBu_3Cl$.

Donors **2a** and **2b** vary in the substituent in the $R_1$ and the $R_2$ position. **2a** has bromine in the $R_1$ position, while for **2b** these protons are replaced by electron donating *n*-butoxy groups. The $R_2$ position is either substituted with a bromine or with an iodine atom. The halogen atoms in $R_2$ position of compounds **2a** and **2b** are necessary for the Stille cross-coupling with thiophene derivative **3** leading to molecule **4a** and **4b**.

The Stille cross-coupling between molecule **6** and **3** at 120 °C over 12 h, shown in Figure 45, was tested but has led only to traces of **4b**. This observation can be explained by the reduced reactivity of electron rich aryl halides in oxidative addition reactions.[97] To overcome this problem the more reactive iodine substituted carbazole derivative **2b** was used.

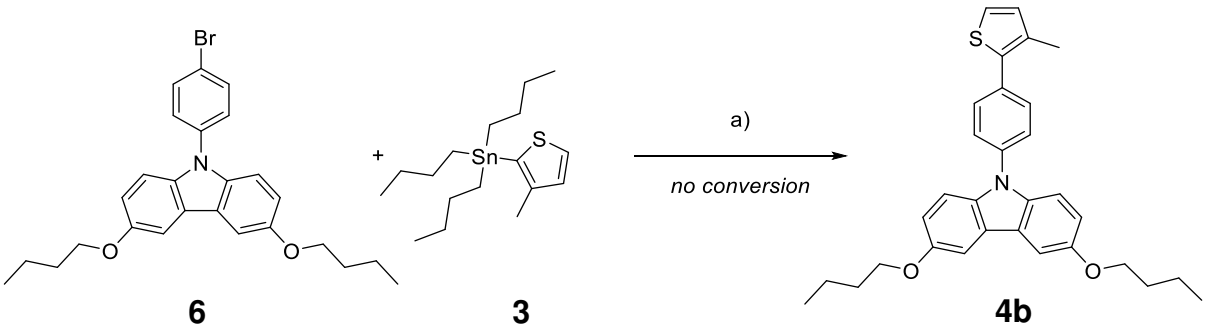


**6** **3** **4b**

**Figure 45:** Attempt of the synthesis of **4b** using **6**.
a) $Pd(PPh_3)_4$, CuI, DMF, 120 °C, 12 h.

While donor **2a** is commercially available, donor **2b** needs to be synthesized similar to an established procedure for the *N*-substitution of different carbazoles from Wang et al.[98] Therefore, literature known 3,6-di-*n*-butoxycarbazole **1** was *N*-substituted under metal free conditions with 1-fluoro-4-iodobenzene.[99] In the publication of Wang et al. the *N*-substitution of 3,6-dibromocarbazole (**7**) with 1-Fluoro-4-iodobenzene (**8**) shown in Figure 46 gave good yields of compound **9**.[98] By adapting the procedure of Wang et al. for the synthesis of **2b** the yield dropped from 81 % for **9** to 61 %. During the synthetic process it turned out that the temperature is crucial for the reaction.

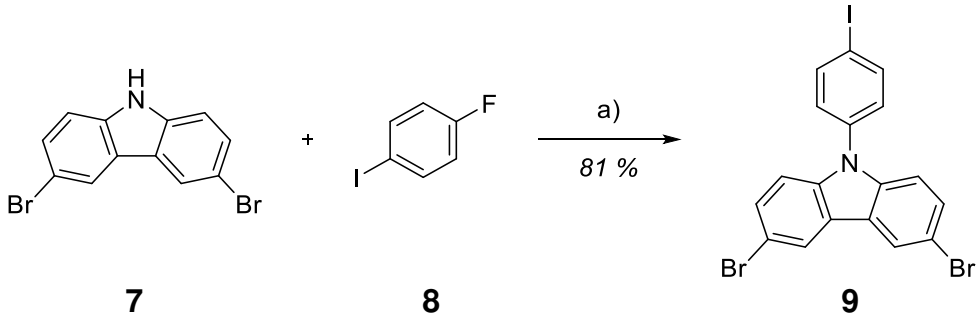


**7** **8** **9**

**Figure 46:** Synthesis of compound **9** published form Wang et al.[98]
a) $CsCO_3$, DMF, 150 °C.

Molecules **4a** and **4b** were prepared for further cross-coupling with A1 by lithiation of the thiophene moiety with *n*-butyl lithium, followed by a nucleophilic substitution with tributyltin(0)chloride, forming molecules **5a** and **5b**, respectively. Column chromatography of these organotin compounds on either silica or aluminum oxide leads to almost quantitative loss of the tributyltin substituent. Therefore **5a** and **5b** were not further purified.

In the synthesis of series II dyes the Donor-Spacer subunit as well as the A1-S-A2 subunit will be coupled to the chiral bridge by a Sonogashira cross-coupling. This cross-coupling requires an unprotected acetylene on one coupling partner and an aryl or vinyl halide on the other. The D-S subunit **4a** was therefore substituted with an iodine atom at the 5 position of the thiophene ring forming molecule **10** shown in Figure 47. **10** was cross-coupled with trimethylsilyl (TMS) protected acetylene to achieve **11**, which is then deprotected with $K_2CO_3$. The unprotected acetylene **12** is used to couple to the chiral bridge in the following synthesis of series II dyes.

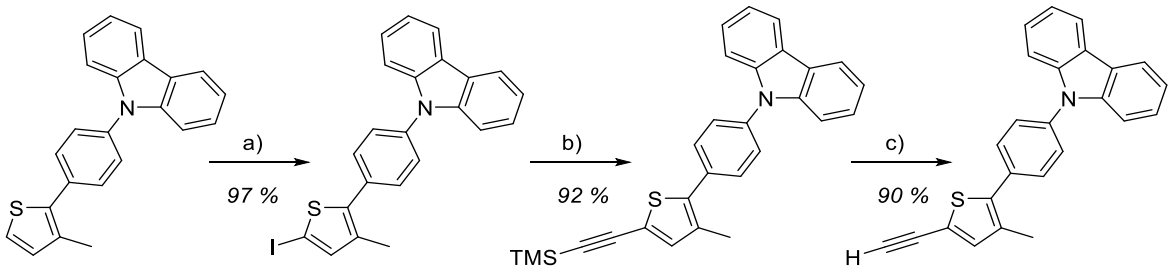


**4a** **10** **11** **12**

**Figure 47:** Synthesis of D-S subunit of series II dyes with a free acetylene for further Sonogashira coupling reactions.
a) (1) *n*-BuLi, tetrahydrofuran (THF), – 78 °C; (2) $I_2$. b) TMS-acetylene, $Pd(PPh_3)_4$, CuI, $NEt_3$, THF, rt, 5 h. c) $K_2CO_3$, THF, MeOH, rt, 1 h.

Further progress of the project can require the change of the carbazole substitution from *n*-butoxy groups to a substituent with better or worse electron donating ability. Molecule **9** can be used as a precursor for different substituted carbazoles. An iodine selective Stille cross-couplings of **9** with thiophene derivate **3** has been tested. The reaction, shown in Figure 48, formed molecule **13** selectively in good yields. In **13** the carbazole moiety can be derivatized in the 3 and 6 position by cross-coupling reactions at the bromine atoms.

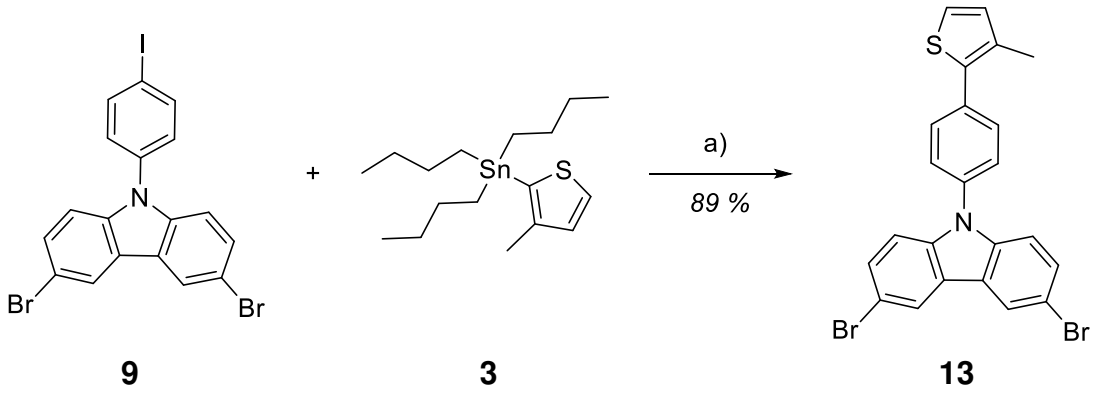


**9** **3** **13**

**Figure 48:** Synthesis of molecule **13**.
a) $Pd(PPh_3)_4$, CuI, CsF, DMF, rt, 3 h.

## 2.2.2. Synthesis of the Donor-Spacer-Acceptor1/Acceptor1-Spacer Subunit

In the synthesis of series I dyes the D-S subunits **5a** and **5b** were directly coupled with the commercially available 4,7-dibromobenzo[c]-1,2,5-thiadiazol **14** as shown in Figure 49.

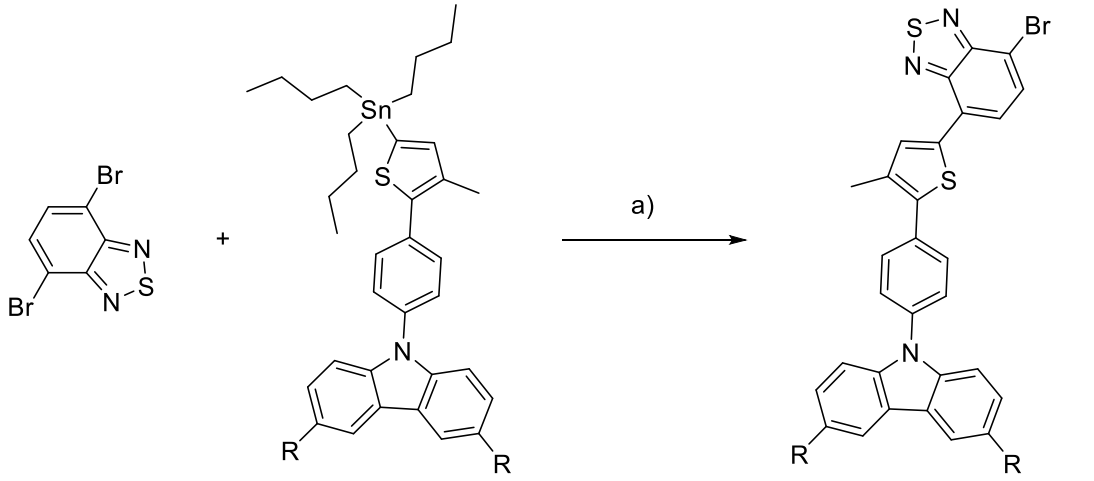


**14** **5a** R = H **15a** R = H *50% a(i)*

**5b** R = O-*n*Bu **15b** R = O-*n*Bu *29% a(ii)*

**Figure 49:** Synthesis of D-S-A1 subunit for series I dyes.
a(i)) $Pd(PPh_3)_4$, CuI, toluene, 80 °C, 16 h. a(ii)) $Pd(PPh_3)_4$, CuI, toluene, 50 °C, 4 h.

The molecules **15a** and **15b** varying in the substituent of the carbazole were isolated in 50 % and 29 % yield, respectively. The difference in yield can be explained by the increased electron density of **15b** in comparison to **15a**, due to the electron donating *n*-butoxy groups. An increased electron density of the organotin compound increases the reactivity in Stille cross-couplings.[100] The dibromo compound **14** can undergo two Stille cross-coupling reactions. Therefore, the increased reactivity of **5b** does not lead to an increased yield for **15b** because of the augmented formation of D-S-A1-S-D side product **16**.

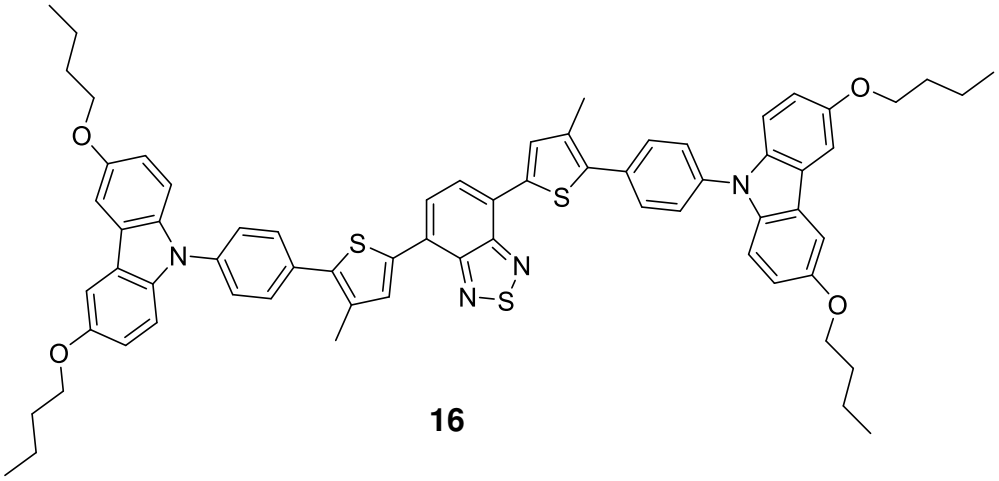

**16**

**Figure 50:** Product of Stille coupling between **5b** and **15b**.

In the synthesis of series II dyes, A1 was coupled with a spacer subunit to attach A2 or SFR on one side and with an acetylene moiety to connect to the chiral bridge on the other side (Figure 51). Following a literature known procedure from Dall'Agnese et al. **14** can be directly substituted by 2-thiophenecarboxaldehyde on one bromine to form the A1-S subunit **17**.[101] This subunit was further prepared for connecting to the chiral bridge by a Sonogashira cross-coupling reaction with TMS-acetylene, forming **18** in a good yield of 83 %. The TMS protected acetylene **18** was in situ deprotected in the cross-coupling reaction with the chiral bridge. If the TMS group is removed prior, removing the solvent leads to decomposition of the compound.

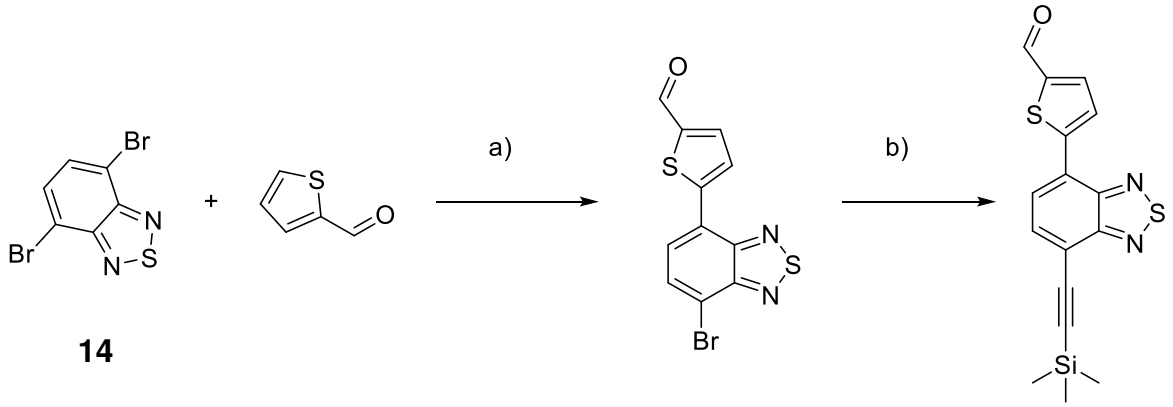


**14** **17** **18**

**Figure 51:** Synthesis of A1-S subunit for series II dyes.
a) $Pd(OAc)_2$, KOAc, DMAc, 105 °C, 72 h.[101] b) TMS-acetylene, $Pd(PPh_3)_4$, CuI, $NEt_3$, THF, 60 °C, 5 h.

## 2.2.3. Synthesis of the Chiral Bridge Subunit

The whole synthetic procedure for the chiral dyes was done on the *S* enantiomer of BINOL. The synthetic procedure does not comprise of any reaction step that typically prefer one enantiomer against the other. So, the racemate and the *R* enantiomer as well should also be achievable by the shown procedure in similar yields. The commercially available *S*-BINOL (**19(*S*)**) was methylated in the first step following a literature known procedure of Wipf and Jung giving **20(*S*)** in almost quantitative yields.[102]

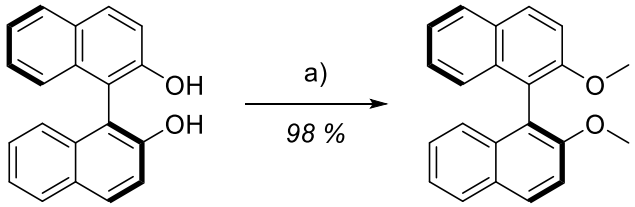


**19(*S*)** **20(*S*)**

**Figure 52:** Methylation of **19(*S*)**.[102]
a) $CH_3I$, $K_2CO_3$, acetone, reflux, 24 h.

In the first attempts **20(*S*)** was substituted in the 3 and 3' position with bromine forming molecule **21(*S*)** shown in Figure 53, also following the procedures of Wipf and Jung[102]. The substitution of one or both bromine atoms in **21(*S*)** with tri-*iso*-propylsilyl (TIPS) acetylene in a Sonogashira cross-coupling reaction has not worked under a variety of conditions.

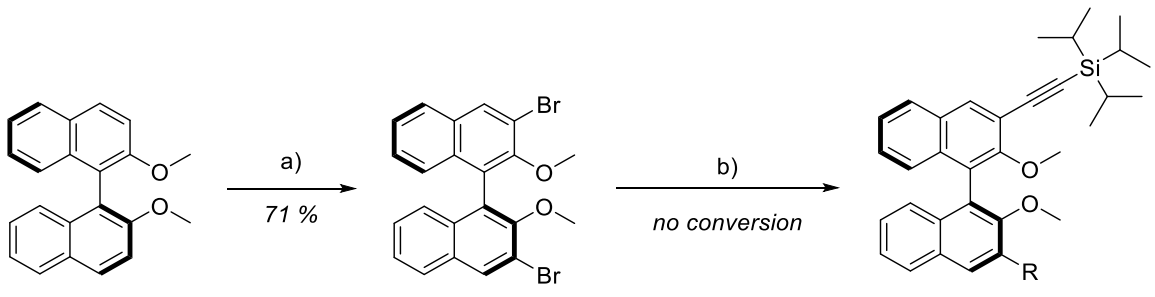


**20(*S*)** **21(*S*)** R = Br, TIPS acetlyene

**Figure 53:** Synthesis approach towards TIPS-Acetylene substituted *S*-binol.[102]
a) (1) *n*-BuLi, THF, – 78 °C;(2) $Br_2$. b) $Pd(PPh_3)_4$, CuI, $NEt_3$, TIPS-acetylene, THF.

To overcome this problem **20(*S*)** was substituted with the more reactive iodine atom. For series I dyes only on one side of the BINOL the proton was replaced by an iodine giving molecule **22(*S*)** shown in Figure 54. Therefore, the procedure of Mosca et al. was adapted and improved to a yield of 50 %.[103] In the next step the halogen atom of **22(*S*)** was replaced by a TIPS acetylene, in a cross-coupling reaction, leading to molecule **23(*S*)**.

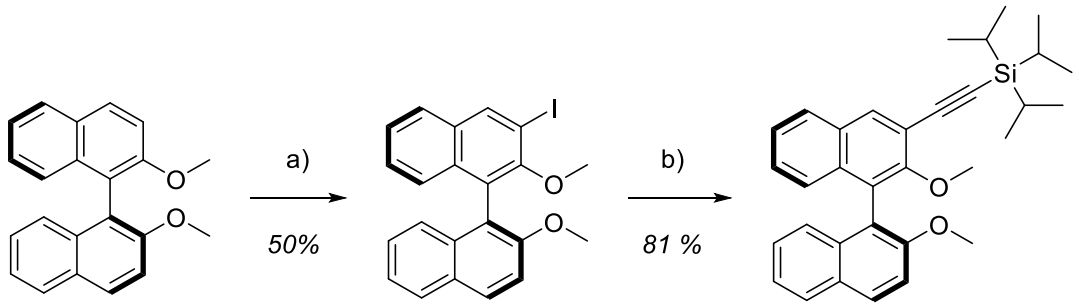


**20(*S*)** **22(*S*)** **23(*S*)**

**Figure 54:** Synthesis of molecule **23(*S*)** for series I dyes.
a) (1) *n*-BuLi, THF, 0 °C; (2) $I_2$, – 78° C.[103] b) TIPS-acetylene, $Pd(PPh_3)_4$, CuI, $NEt_3$, THF, 50 °C, 8 h.

After lithiation of the unsubstituted 3' position in **23(*S*)**, the addition of DMF and acidic workup with HCl lead to aldehyde **24(*S*)** (Figure 55). Deprotecting the acetylene moiety of **24(*S*)** with tetrabutylammonium fluoride (TBAF) provided **25(*S*)** with no residual starting material visible on the TLC of the reaction mixture. According to the high reactivity of both the aldehyde and the free acetylene moiety as well in **25(*S*)** the molecule was not purified and directly used for cross-coupling reactions with the D-S-A1 subunits of series I dyes.

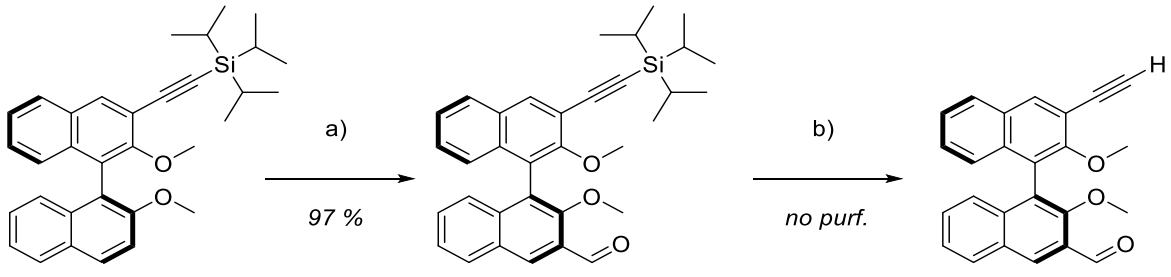


**23(*S*)** **24(*S*)** **25(*S*)**

**Figure 55:** Synthesis of B for series I dyes.
a) (1) *n*-BuLi, tetramethylethylendiamine (TMEDA), THF, rt; (2) DMF; (3) HCl. b) TBAF, THF, 0 °C.

In series II dyes a similar approach was tested. Thereby **20(*S*)** was substituted at the 3 and 3' position with iodine leading to molecule **26(*S*)** as shown in Figure 56.The reaction was done following a literature known procedure of Brenet et al.[87a]

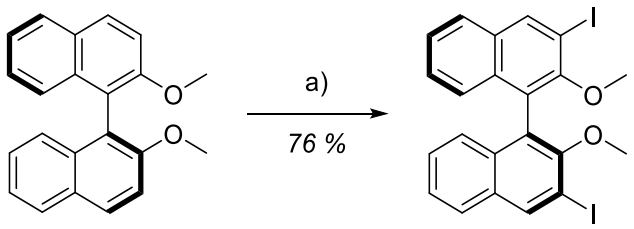


**20(*S*)** **26(*S*)**

**Figure 56:** Synthesis of **26(*S*)** following a procedure of Brenet et al.[87a]
a) (1) *n*-BuLi, TMEDA, $Et_2O$, rt, 20 min; (2) $I_2$, – 90 °C.

Different ways of exchanging the iodine atoms by TIPS/TMS acetylene on one side and an unprotected acetylene on the other side turned out to work in yields of up to 50 %. Different combinations of TIPS acetylene, TMS acetylene, free acetylene and iodine substituents on the BINOL scaffold show very similar $R_f$ values. Therefore, the purification of these compounds via column chromatography is limited to about 50 mg batches by using columns normally used for a 1 – 2 gram batch.

A further attempt to combine the different subunits of series II dyes is the substitution of both iodine atoms of **26(*S*)** with TMS acetylene followed by removing both TMS groups with $K_2CO_3$, forming molecule **27(*S*)** (Figure 57). In this reaction sequence the di(trimethylsilylacetylene) substituted intermediate was not purified. Therefore, the yield over two steps is 91 %.

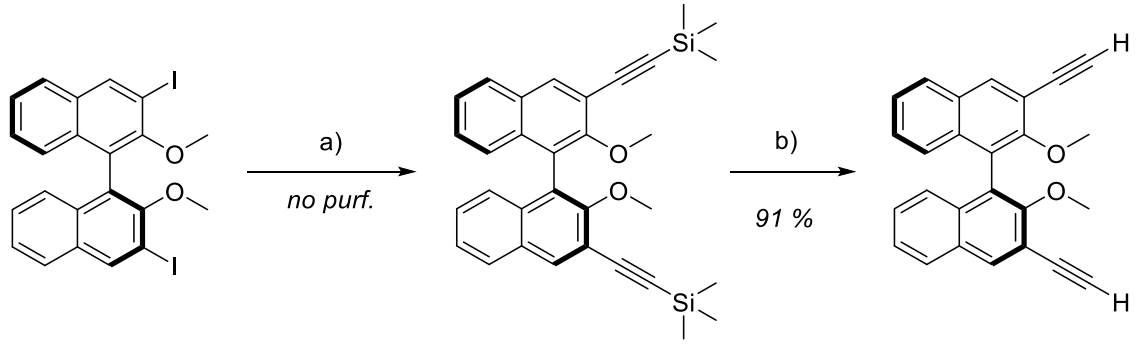


**26(*S*)** **27(*S*)**

**Figure 57:** Synthesis of **27(*S*)** as a B building block.
a) TMS-acetylene, $Pd(PPh_3)_4$, $NEt_3$, CuI, THF, 60 °C, 20 h. b) TBAF, THF rt, 10 min.

## 2.2.4. Combination of Subunits for Series I Dyes

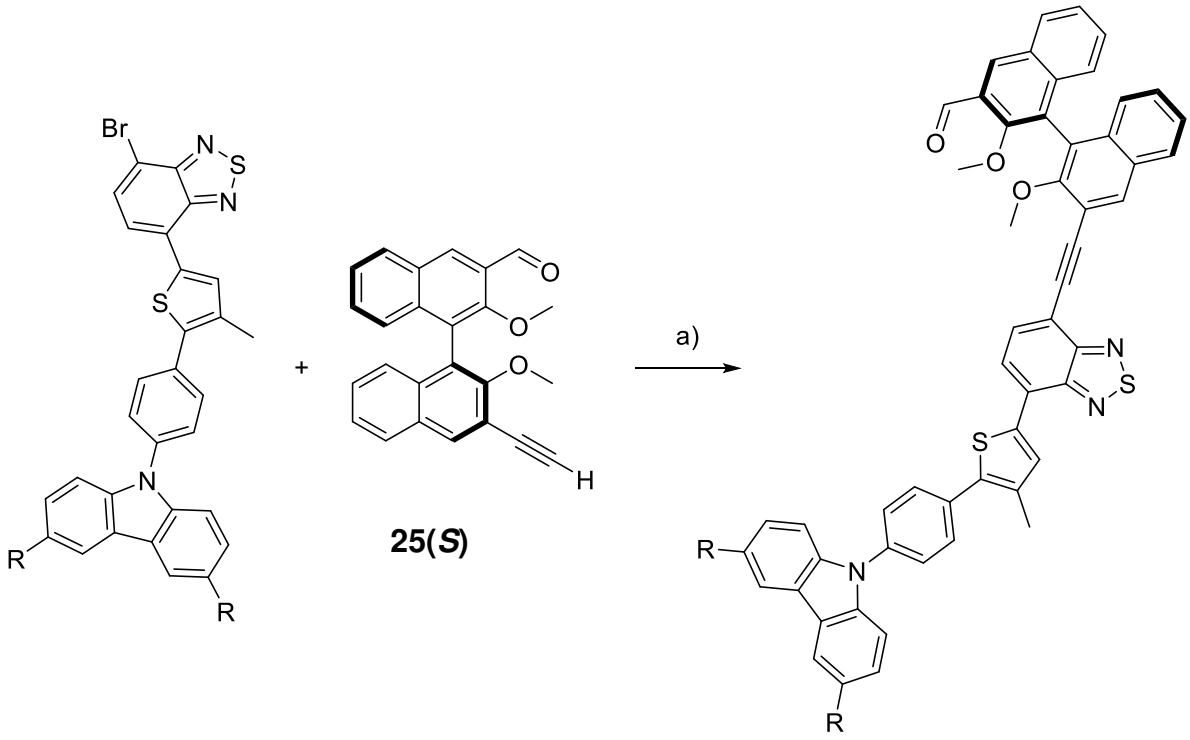


**15a** R = H
**15b** R = O-*n*Bu

**28(*S*)a** R = H *75 %*
**28(*S*)b** R = O-*n*Bu *90 %*

**Figure 58:** Cross-coupling between D-S-A1 and B subunits of series I dyes.
a) $Pd(PPh_3)_4$, CuI, $NEt_3$, THF, 60 °C, 16 h.

The combination of series I dyes was achieved by Sonogashira cross-coupling of the bromine substituted position of the D-S-A1 subunits **15a** or **15b** and the free acetylene of the B subunit **25(*S*)**. The reaction formed products **28(*S*)a** and **28(*S*)b** in good yields as shown in Figure 58. **28(*S*)b**, the compound with the *n*-butoxy groups on the carbazole, has shown 15 % higher yield, although the increased electron density on the aryl halide component should reduce the reactivity during the oxidative addition step of the cross-coupling reaction.[97] The aldehyde moieties of compounds **28(*S*)a** and **28(*S*)b** are used as a synthetic handle for either a Knoevenagel reaction with ethyl cyanoacetate A2 or an imine bond formation with TEMPO-amine SFR.

## 2.2.5. Synthesis of Series I Dyes with Acceptor 2

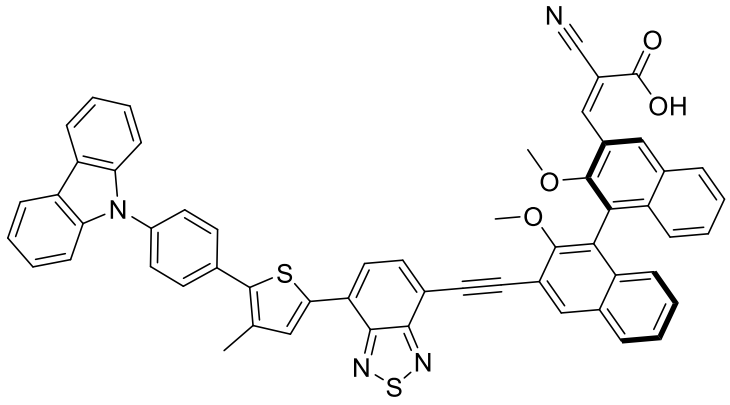


**29(*S*)a**

**Figure 59:** Series I dye with cyanoacrylic acid as A2.

The synthesis of the priorly aimed cyanoacrylic acid is challenging and was not successful yet. Several reaction procedures summarized in Table 1 for the Knoevenagel reaction of cyanoacetic acid and the aldehydes **28(*S*)a** where tested but have not lead to the formation of the desired products **29(*S*)a** (Figure 59). Therefore, the more CH-reactive and OH protected ethyl cyanoacetate was used in the Knoevenagel reaction forming the D-S-A1-B-A2 molecules **30(*S*)a** and **30(*S*)b** in good yields as shown in Figure 60.

**Table 1:** Procedures for the formation of **29(*S*)a**. NR = no reaction.

| Start material | Conditions | Temperature | Result |
|---|---|---|---|
| **28(*S*)a** | cyanoacetic acid, piperidine, DCM | rt | NR |
| **28(*S*)a** | cyanoacetic acid, piperidine, THF | 60 °C | NR |
| **28(*S*)a** | cyanoacetic acid, $NH_4Ac$, acetic acid | rt | NR |
| **28(*S*)a** | cyanoacetic acid, $NH_4Ac$, acetic acid | 120 °C | NR |

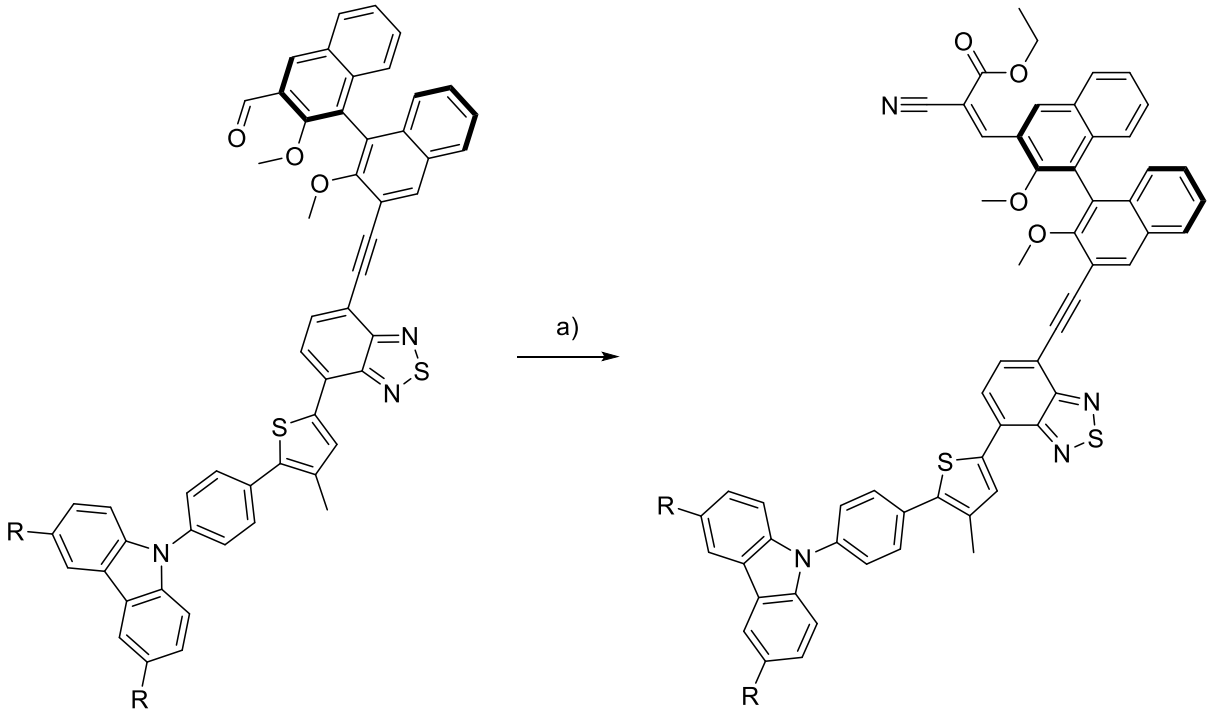


**28(*S*)a** R = H
**28(*S*)b** R = O-*n*Bu

**30(*S*)a** R = H *86 %*
**30(*S*)b** R = O-*n*Bu *93 %*

**Figure 60:** Knoevenagel reaction of series I dyes.
a) Ethyl cyanoacetate, piperidine, DCM, rt, 20 h.

To achieve the cyanoacrylic acid derivatives different protocols for acidic hydrolysis and saponification of **30(*S*)a** were tested and summarized in Table 2. None of these reaction conditions allowed the isolation of **29(*S*)a**. The reactions of mineral acids, trifluoroacetic acid and bases showed no reaction at rt. When the reactions were heated up to 60 °C TLC tests showed a decrease of **30(*S*)a** and the formation of a more polar compound with the same color.

**Table 2:** Procedures for the formation of **29(*S*)a**. NR = no reaction, UC = unknown compound.

| | | | |
|---|---|---|---|
| **30(*S*)a** | KOH, THF, water | rt | NR |
| **30(*S*)a** | KOH, THF, water | 60 °C | UC |
| **30(*S*)a** | LiOH, THF, water | rt | NR |
| **30(*S*)a** | LiOH, THF, water | 60 °C | UC |
| **30(*S*)a** | HCl, THF, water | rt | NR |
| **30(*S*)a** | HCl, THF, water | 60°C | UC |
| **30(*S*)a** | HBr, THF, water | rt | NR |
| **30(*S*)a** | (1) TFA, THF; (2) water | rt | NR |

The more polar compound was isolated and analyzed with NMR and mass spectrometric methods. The compound showed broad unresolved $^1$H-NMR signals which could not be used to solve or verify a structure. Mass spectrometric analysis with either electron spray ionization (ESI) or atmospheric pressure chemical ionization (APCI) of this compound does not give any evidence for **29(*S*)a**. A possible explanation could be the polymerization of cyanoacrylates which is initiated by the addition of a nucleophile (Figure 61).[104]

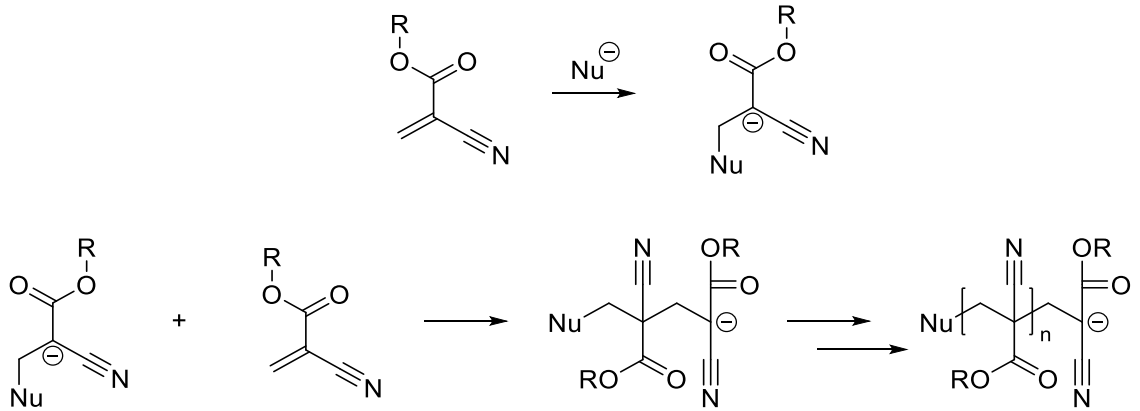


R = Alkyl

**Figure 61:** Polymerization of cyanoacrylates.[104]

**30(*S*)a** shows stability against nucleophiles under ambient conditions. The elevated temperature necessary for the cleavage of the ester could force a

nucleophile induced polymerization. Methods for characterizing polymers, like matrix-assisted laser desorption/ionization (MALDI) mass spectrometry, can be used to analyze the unknown compound and check this theory. To achieve the chiral dyes with a cyanoacrylic acid as A2 further synthetic strategies can be followed. One possibility would be the use of methyl or *t*-butyl cyanoacetate for the Knoevenagel reaction. Thereby, the cleavage of the formed methyl or *t*-butyl cyanoacrylic esters should be possible under milder conditions than the cleavage of the ethyl ester.[105] Another possibility would be the use of silyl- or thioesters, which can also be cleaved under very mild conditions.[106]

## 2.2.6. Synthesis of Series I Dyes with the Stable Free Radical

The formation of an imine bond between the aldehyde moiety of **28(*S*)a** and **28(*S*)b** and the amine functional group of TEMPO-amine lead to **31(*S*)a** and **31(*S*)b**, respectively. The procedure used in this synthesis was adapted from Chernick et al., where it was used to couple a TEMPO SFR and a pentacene substituted with an benzaldehyde.[96]

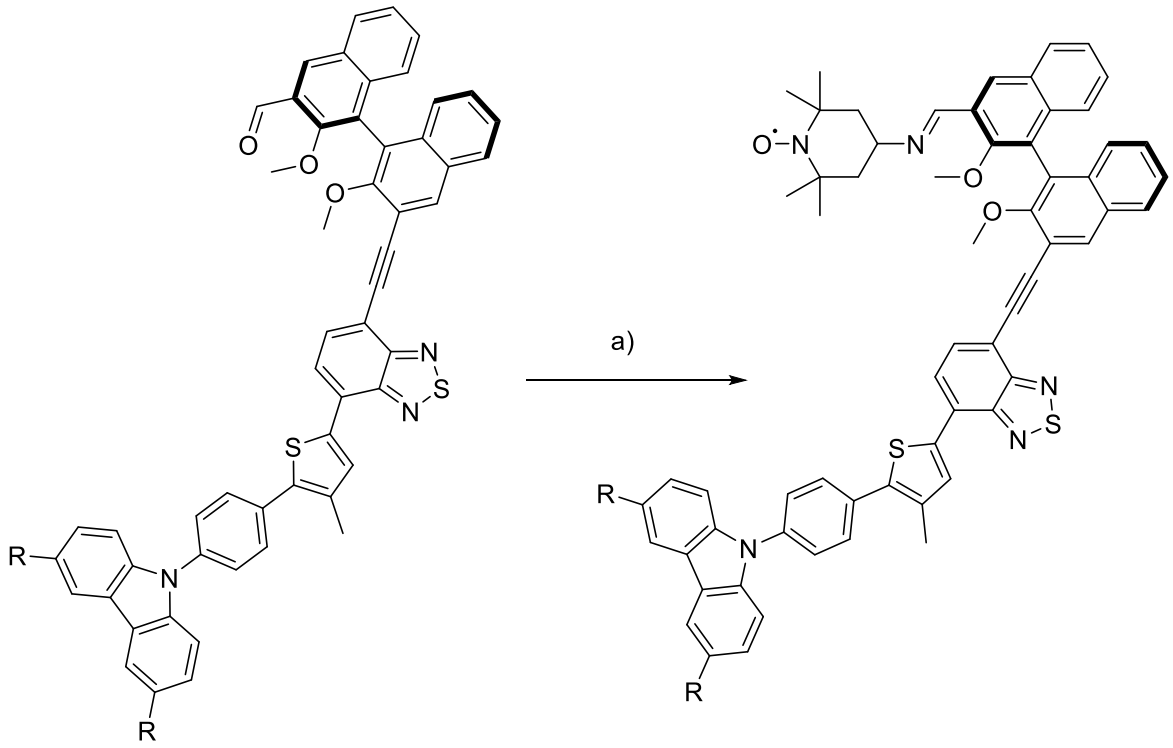


**28(*S*)a** R = H
**28(*S*)b** R = O-*n*Bu

**31(*S*)a** R = H *97 %*
**31(*S*)b** R = O-*n*Bu *92 %*

**Figure 62:** Synthesis of **31(*S*)a** and **31(*S*)b**.
a) TEMPO-amine, $Al_2O_3$, DCM, sonication, 2 h.[96]

The imine bound in molecules **31(*S*)a** and **31(*S*)b** combining the SFR and the chiral bridge is not stable towards hydrolysis. Therefore, purification by column chromatography on silica or alumina was not possible. The excess of TEMPO-amine simplifying the purification problem by leading to a full conversion of the used aldehyde compound. While Chernick et al. where able to separate their product from TEMPO-amine by crystallization, this procedure has not worked for our dyes. Taking the difference in size between the dyes and TEMPO-amine into account the size exclusion column chromatography technique can be used to

separate **31(*S*)a** or **31(*S*)b** from the crude products. In size exclusion column chromatography (SXCC), a solid phase based on a polymer is used to separate molecules based on their size and velocity cross section. Small molecules can enter cavities within the solid polymer. Thereby these molecules are slowed down in comparison to the solvent flow. The bigger the molecules are the less they can enter cavities and the faster they are released from the column. A typical application of SXCC is the separation of proteins and other biomolecules like nucleotides in aqueous solutions. The use of certain polymers, like polystyrenes, allows applications with organic non to medium polar solvents like toluene or DCM. A setup of styrene/divinylbenzene based solid phase combined with toluene as an eluent was used in this project to separate the products of the imine condensation reactions from the excess of TEMPO-amine. In this setup the hydrolysis of the imine bond is prevented and the difference in size by almost 800 g/mol allows good separation of the compounds.

Finally determining the purity of the samples after chromatography can not be done by NMR-spectroscopy due to the unpaired electron spin of the radical. Therefore, techniques like elemental analysis, quantitative electron paramagnetic resonance (EPR) spectroscopy or superconducting quantum interference device (SQUID) magnetometer measurements have to be used. Comparing these techniques elemental analysis has the benefit of being very accurate and not requiring a big amount of compound. The main disadvantage of the elemental analysis is that the required amount of compound is destroyed during the measurement. In the quantitative EPR spectroscopy the signal intensities of standard samples with known concentration are used to determine a linear intensity-concentration relation. This relation is used to calculate the concentration of an unknown sample by his signal intensity. To achieve accurate results the unknown radical should be similar to the radical used as a standard. While the used compound is not destroyed during these measurements the quantitative EPR method is susceptible towards errors during the preparation of the samples with known concentrations including the initial weight, the dilution, and the purity of the standard.[107] Using SQUID magnetometer measurements the temperature depended magnetic susceptibility of a probe can be measured. Using the Curie-Weiss law an experimental Bohr magneton can be calculated. With the spin-only

formula and the experimental Bohr magneton the number of unpaired spins per molecule and therefore the purity of the compound can be determined.[108] Apart from the initial weight of the probe and a diamagnetic correction factor for the probe container the SQUID method only uses pre-determined constants to calculate the purity of the samples, reducing the sources for errors. The measurement requires about 100 mg of sample, which can be fully recovered. Given all these facts the SQUID measurement was chosen to check the purity of the dyes substituted with the SFR. The purity of **31(*S*)a** was determined to be 104.5 % which is within the error range of the experimental equipment and technique.[108-109] Molecule **31(*S*)b** was not achieved in high enough quantity to do a SQUID measurement. On account of the similarity between the starting materials **28(*S*)a** and **28(*S*)b** for the imine condensation towards **31(*S*)a** and **31(*S*)b**, respectively, and the same reaction and purification procedure for both compounds, the purity of **31(*S*)b** can be expected to be comparable to the purity of **31(*S*)a**.

### 2.2.7. Combination of series II dye and the Substitution with SFR and A2

In Sonogashira cross-coupling reactions molecule **27(*S*)** can be coupled side selectively with either the D-S subunit **10** or with the A1-S unit **17** as shown in Figure 63. Molecules **32(*S*)** could be synthesized in 30 % yield while Molecule **33(*S*)** was achieved in 67 % yield. In both reactions two equivalents of **27(*S*)** were necessary in order to prevent the coupling reaction from taking place twice on one BINOL molecule. Due to difficult separation problems neither the excess of **27(*S*)** can be easily recovered nor the desired products, **32(*S*)** and **33(*S*)**, can be completely purified. Compound **32(*S*)**, which showed less impurities than **33(*S*)**, was used in a cross-coupling reaction with **17** to form the D-S-B-A1-S part of series II dyes (**34(*S*)**). **34(*S*)** provides the aldehyde moiety as a synthetic handle to add the second acceptor or the SFR and was achieved in a yield of 75 %. Due to the problems in purification of **32(*S*)** and the excess of **27(*S*)**, that is necessary to prevent the cross-coupling reaction on both acetylene moieties, this synthetic strategy was not pursued any further.

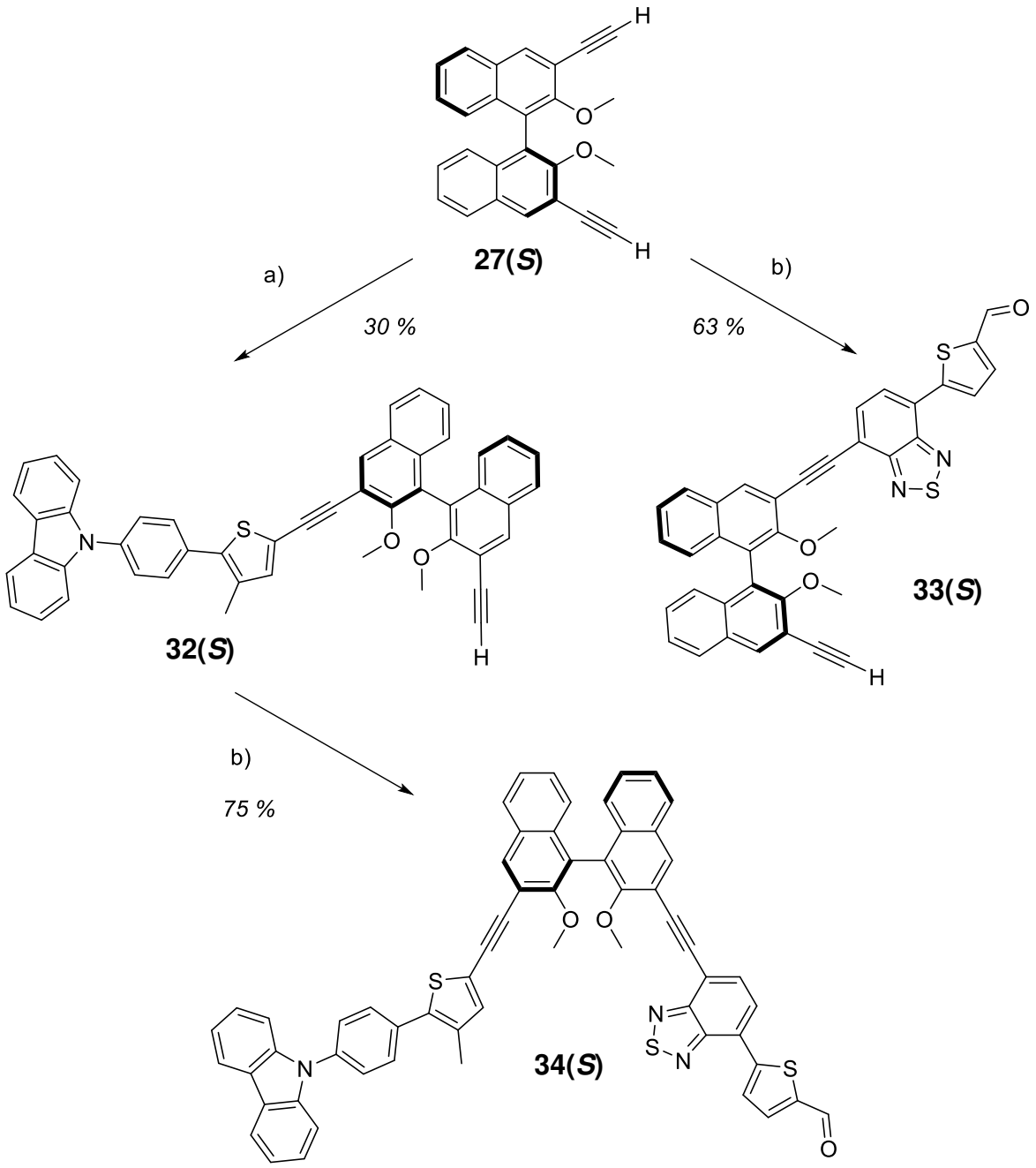


**Figure 63:** Synthetic strategy towards **34(*S*)**.
a) **10**, $Pd(PPh_3)_4$, CuI, $NEt_3$, THF, 60 °C. b) **17**, $Pd(PPh_3)_4$, CuI, $NEt_3$, THF, 60 °C.

Instead of providing B with the free acetylene units, necessary for the Sonogashira cross-coupling, the other building blocks, namely the D-S and the A1-S subunit were equipped with the acetylene linkers as previously shown in this chapter. This attempt allows the use of the quickly accessible **26(*S*)** as the chiral bridge building block. This easy access gives the possibility to synthesize the

series II dyes with the other enantiomer or even with another chiral bridge. The only requirements towards new bridge subunits are the two iodine atoms.

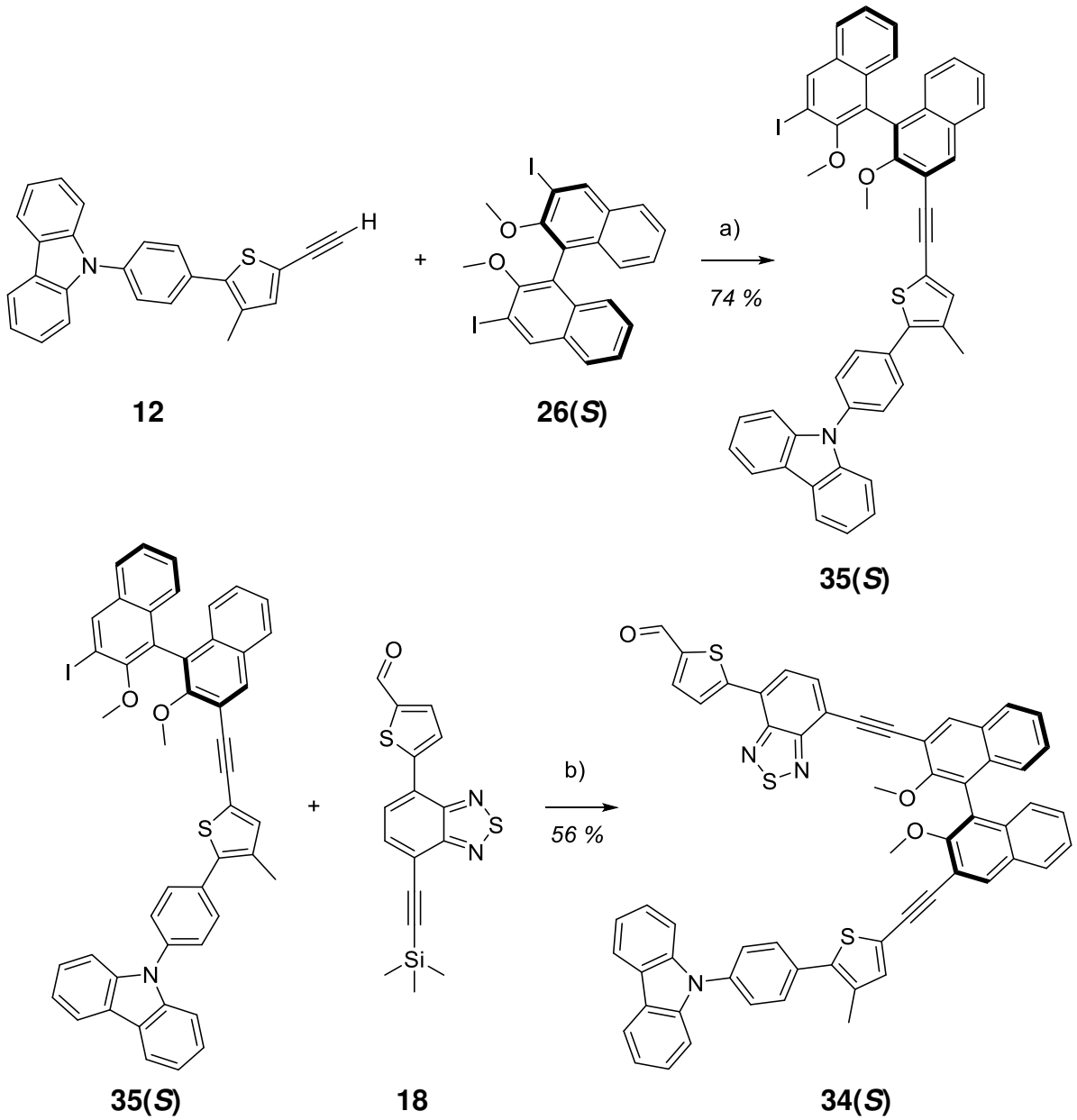


**12** **26(*S*)** **35(*S*)**

**35(*S*)** **18** **34(*S*)**

**Figure 64:** Combination of subunits for series II dye aldehyde **34(*S*)**.
a) $Pd(PPh_3)_4$, CuI, $NEt_3$, THF, rt, 16 h. b) $Pd(PPh_3)_4$, CuI, TBAF, $NEt_3$, THF, 60 °C, 2 h.

As shown in Figure 64 the D-S subunit **12** and the B subunit **26(*S*)** were combined by a Sonogashira cross-coupling forming molecule **35(*S*)**. Two equivalents of diiodo compound **26(*S*)** are used to reduce the chance of a second Sonogashira reaction at molecule **35(*S*)**. The excess of **26(*S*)** can be partially recovered during the column chromatographic purification. D-S-B building block

**35(*S*)** was cross-coupled with A1-S subunit **18** leading to the D-S-B-A1-S compound **34(*S*)**. Thereby, the TMS protected acetylene moiety of **18** was in situ deprotected with TBAF. A deprotection directly prior to use is not possible due to side reaction of the unprotected compound while removing the solvent. Molecule **34(*S*)** has an aldehyde moiety and can be coupled to A2 or R similar to series I dyes (Figure 65).

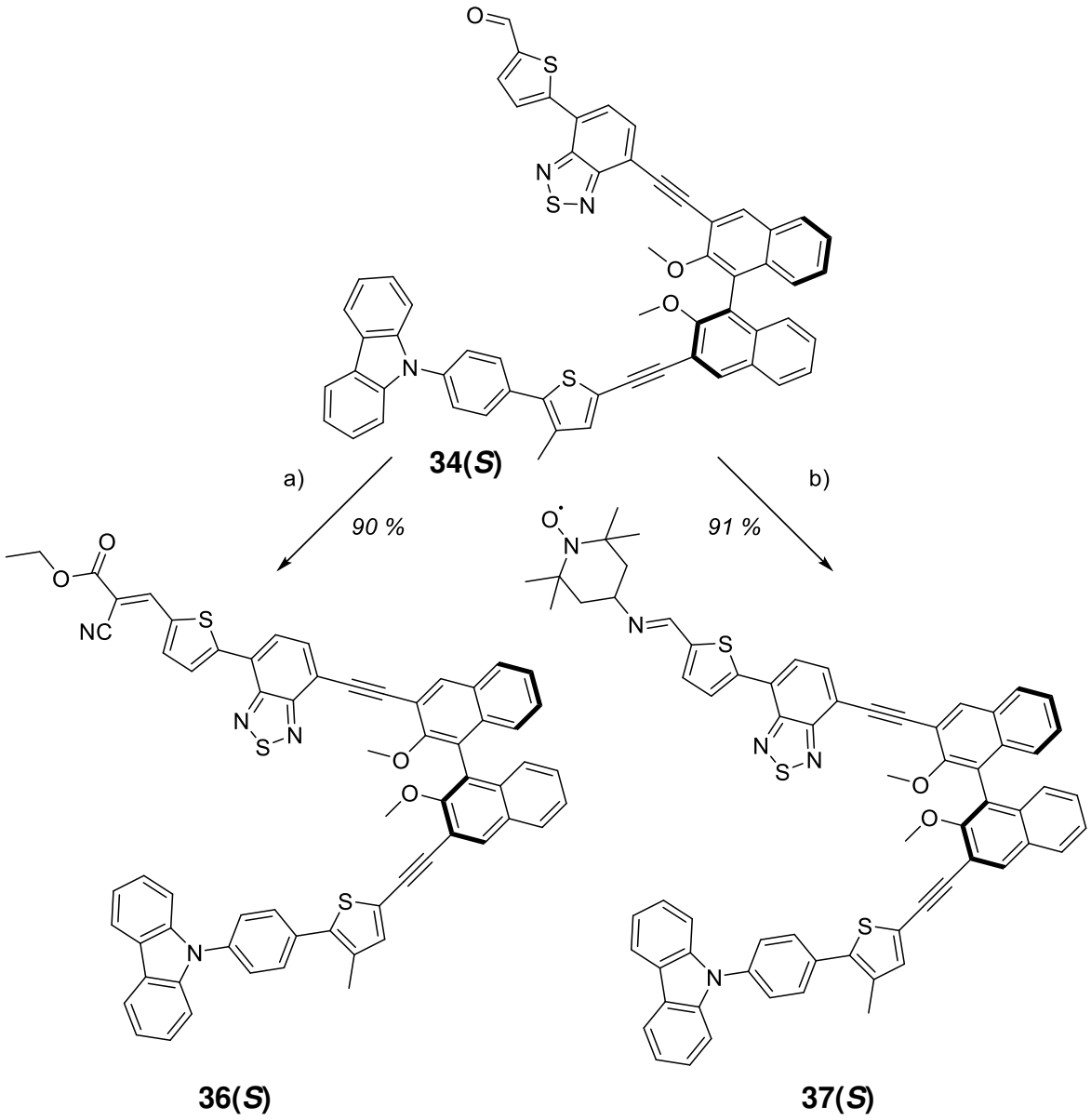


**Figure 65:** Substituting **34(*S*)** with either A2 or SFR.
a) Ethyl cyanoacetate, piperidine, DCM, rt, 20 h. b) TEMPO-amine, $Al_2O_3$, DCM, sonication, 2 h.

Molecules **36(*S*)** and **37(*S*)**, carrying A2 or SFR, respectively, were synthesized in yields comparable to the reaction for series I dyes. The purification of **37(*S*)** can be done like series I dyes by SXCC. The purity of **37(*S*)** was determined to 97 % by a SQUID measurement. The hydrolysis of the ester moiety of **36(*S*)** was not tested because a similar behavior as for **30(*S*)a** was expected.

## 2.3. Results of UV-Vis and Fluorescence Spectroscopy

Steady state UV-Vis absorption spectra of all new compounds were recorded at rt in HPLC grade DCM. Extinction coefficients were determined by taking the average of 3 measurements with different concentrations. Before taking the average the 3 measurements were compared to make sure that no concentration dependent effects were observed. The following discussion gives a possible explanation of the observed shifts but need to be verified by further experiments. The UV-Vis spectra of **4a** is shown in Figure 66.

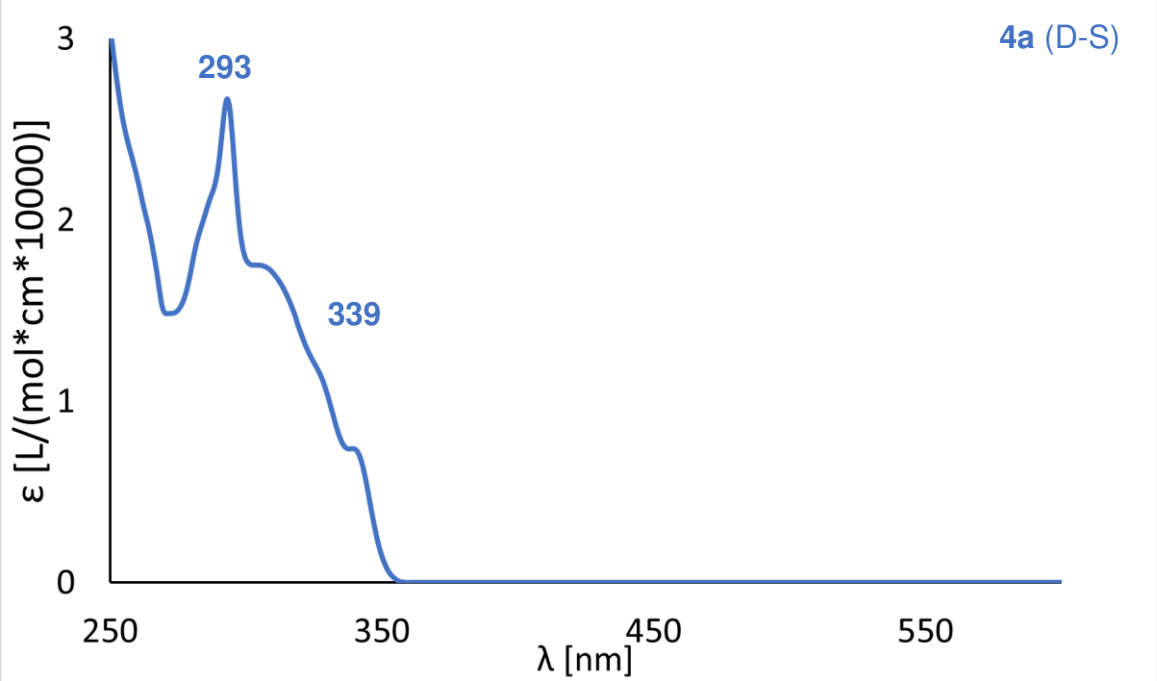


**Figure 66:** UV-Vis spectrum of **4a** in DCM at rt.

The strong absorption feature at 293 nm is based on the phenyl carbazole moiety and can be found in the spectra of pure 9-phenyl-9*H*-carbazole (9-PCz), too (Figure 67, blue line).[110] All compounds comprising the phenyl carbazole moiety, unsubstituted in the 3 and 6 position of the carbazole, show this band at 293 nm within a shift of 2 nm (0.03 eV). The group of Suryawanshi et al. assigns this band to the $\pi$-$\pi^*$ transition within the 9-PCz.[110] Further comparison between the absorption spectra of 9-PCz and **4a** shows low intensity absorptions between 300 and 350 nm for both compounds, which were assigned to the $n$-$\pi^*$ transition of 9-PCz.[110] The major difference between the spectra is the broad shoulder of the

band at 293 nm of **4a**. The shoulder is not visible in the spectra of 9-PCz and therefore could be related to the 3-methylthiophene moiety of **4a**.

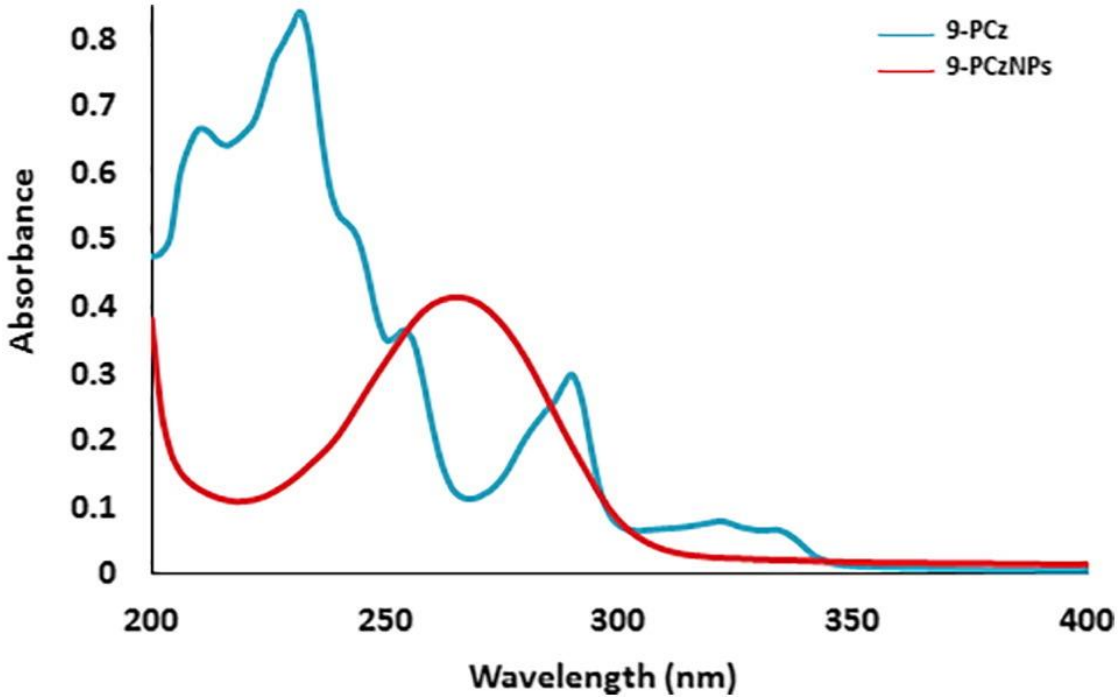


**Figure 67:** UV-Vis absorption spectra of 9-PCz (blue line) and 9-PCz nanoparticles (red line) in DCM.[110]
Reprinted from Suryawanshi, S. B.; Mahajan, P. G.; Bodake, A. J.; Kolekar, G. B.; Patil, S. R., Carbazole based nanoprobe for selective recognition of $Fe^{3+}$ ion in aqueous medium: Spectroscopic insight. *Spectrochim. Acta A Mol. Biomol. Spectrosc. 183*, 232-238, Copyright 2017, with permission from Elsevier.

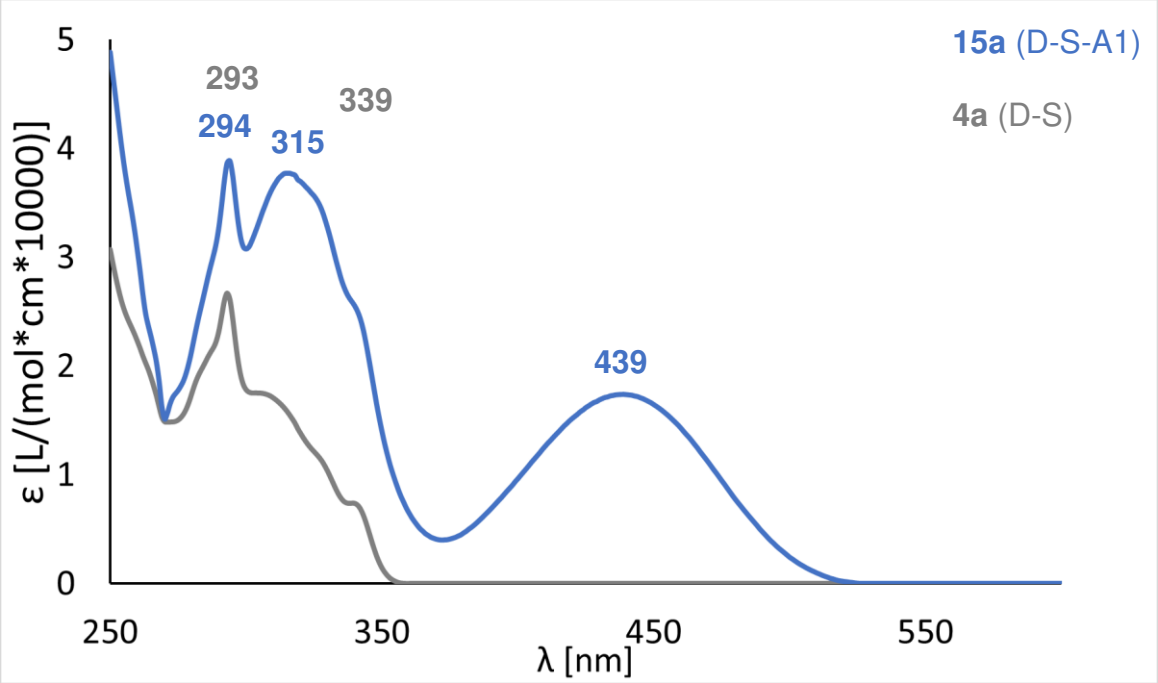


**Figure 68:** UV-Vis spectra of **15a** (blue) and **4a** (grey) in DCM at rt.

Comparing the UV-Vis spectrum of the D-S subunit, **4a**, with the spectrum of D-S-A1 molecule **15a** (Figure 68) shows changes in the visible and the UV part of the spectra. As already mentioned, the absorption at 294 nm should be based on the D and has only shifted by 1 nm (0.02 eV). The band at 315 nm is new in compound **15a** and could be based on the substituted BTDA moiety.[45i] At 439 nm a new absorption has raised which can be described as a CT band between D and A1.[15c, 20d, 24, 82c, 111]

Figure 69 shows the UV-Vis spectra of methoxy protected BINOL derivatives **22(*S*)** (red line) and **24(*S*)** (blue line). Changing the substitution of BINOL derivatives has led to a bathochromic shift of absorption bands. This shift could be based on the electron withdrawing nature of the attached aldehyde moiety. The absorption feature at 259 nm is only visible in TIPS-acetylene substituted BINOLs.

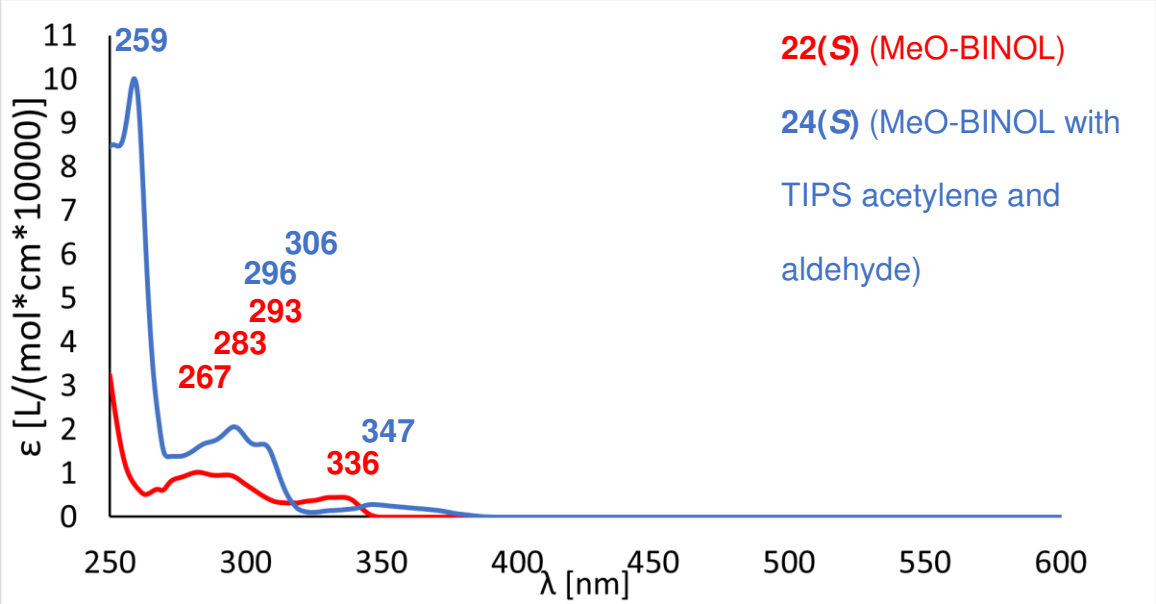


**Figure 69:** UV-Vis spectra of **22(*S*)** (red) and **24(*S*)** (blue) in DCM at rt.

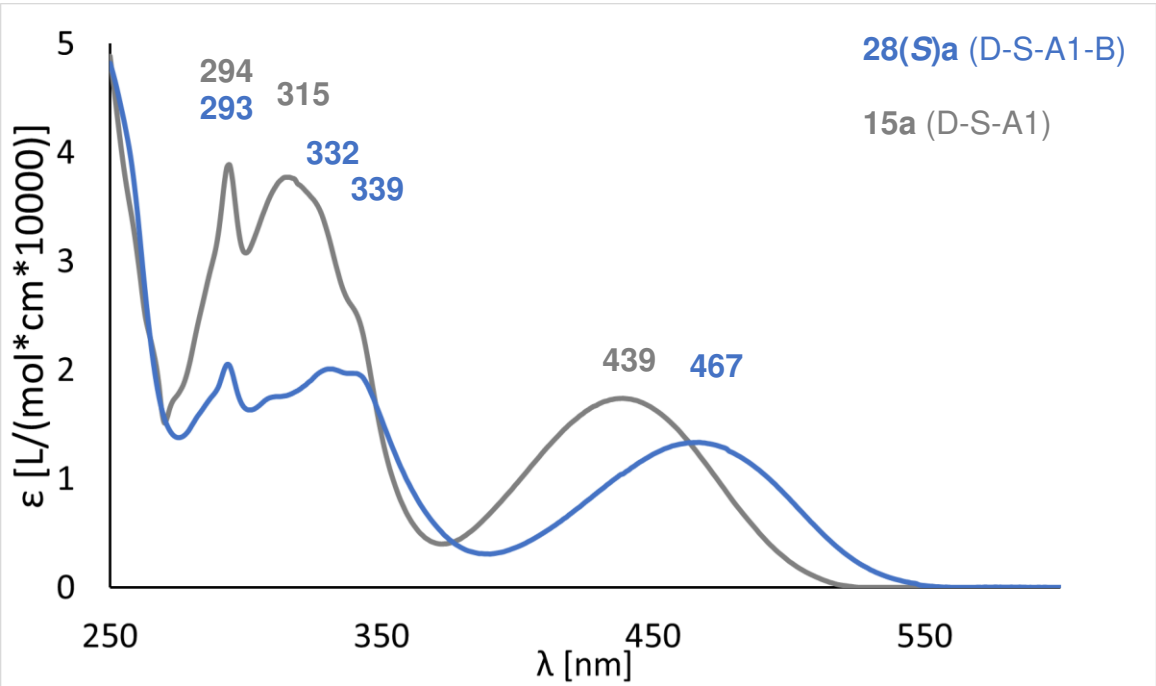


**Figure 70:** UV-Vis spectra of **28(*S*)a** (blue) and **15a** (grey) in DCM at rt.

The combination of D-S-A1 (**15a**) and the B (**24(*S*)**) subunit led to the formation of the D-S-A1-B molecule **28(*S*)a**. The absorption spectrum of **28(*S*)a** is shown in Figure 70. In comparison to the spectrum of **15a** the bands at 315 nm and 439 nm were bathochromically shifted by 17 and 28 nm (0.21 and 0.16 eV) to 332 and 467 nm, respectively. This shift could be explained by an expanded *π*-system, due to the combination of the two subunits. The donor is spatially

separated from A1 and B. Therefore, the $\pi$-$\pi^*$ transition of D at 293 nm is not affected by the expanded $\pi$-system.

Transforming the aldehyde moiety in **28(*S*)a** into a cyanoacrylic ester (**30(*S*)a**) or a TEMPO SFR (**31(*S*)a**) does not lead to a shift of the absorption bands of the compounds (Figure 71). The spatial distance between D or A1 and the aldehyde moiety is big. So, a modification of the aldehyde is not expected to result in a change of D (292 – 293 nm) or A1 (330 – 333 nm) absorption feature. Adding the cyanoacrylic ester as A2 was expected to influence the CT process during photoexcitation. In **28(*S*)a**, the CT can only take place from D to A1. Having a second acceptor in the molecule, A2 could impart in the CT process resulting in a CT from D to A2. Charge transfer from donor to secondary acceptor should show an absorption band different from the D to A1 CT. No significant change in the CT band between **28(*S*)a** (467 nm) and **30(*S*)a** (466 nm) can be observed. Therefore, there is no indication that a CT from D to A2 is taking place.

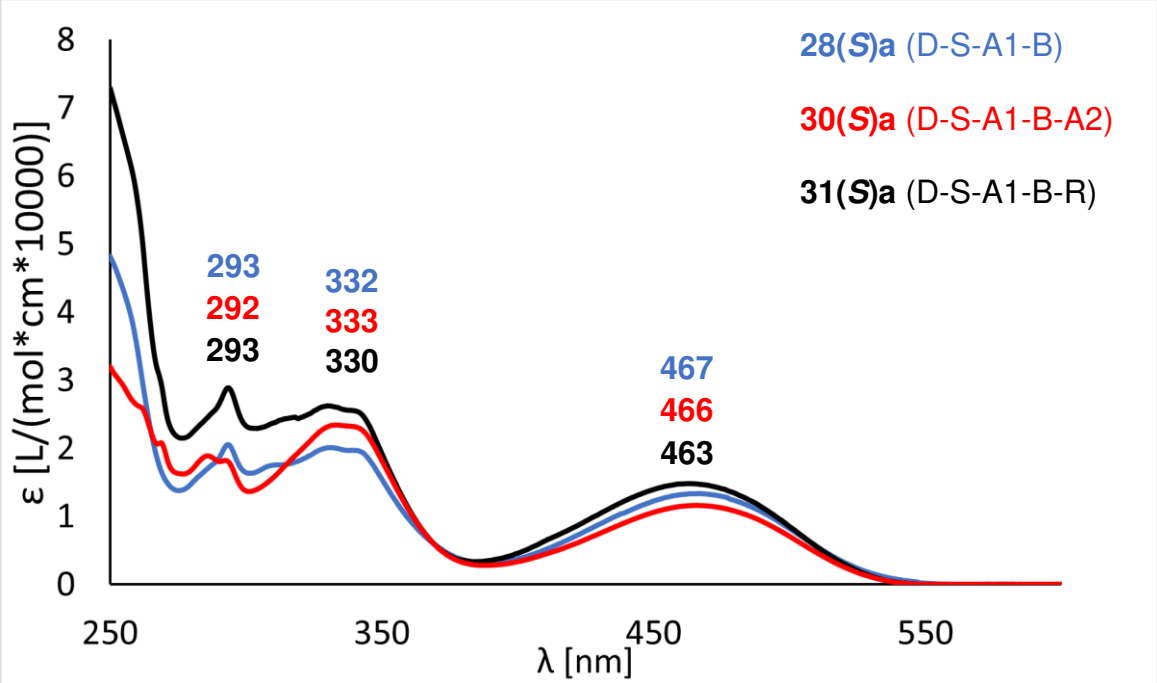


**Figure 71:** UV-Vis spectra of **28(*S*)a** (blue), **30(*S*)a** (red), and **31(*S*)a** (black) in DCM at rt.

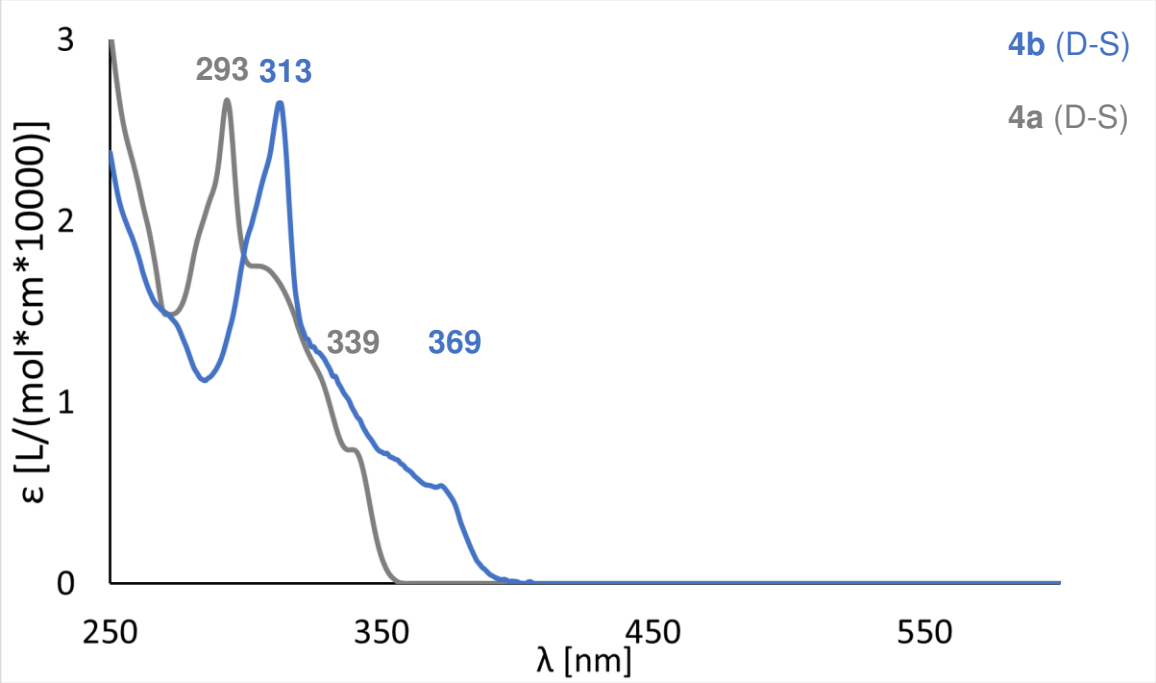


**Figure 72:** UV-Vis spectra of **4b** (blue) and **4a** (grey) in DCM at rt.

The *n*-butoxy substitution in 3 and 6 position of the carbazole increases the electron density and electron donating ability of the donor. The increased electron density leads to a bathochromic shift in the UV-Vis absorptions of *n*-butoxy substituted series I dyes. Shown in Figure 72 and Figure 73 are the UV-Vis spectra of the substituted D-S (**4b**) and the D-S-A1 (**15b**) subunits together with their unsubstituted counterparts. The *n*-butoxy substituted derivatives, **4b** and **15b**, show a redshift of the $\pi$-$\pi^*$ transition of D from 293 – 294 nm to 312 – 313 nm (0.27 eV) in comparison with the unsubstituted molecules, **4a** and **15a**. A similar redshift applies to the $n$-$\pi^*$ transition from 339 nm in **4a** to 369 nm (0.30 eV) in **4b**. With a shift of 5 nm (0.03 eV) the bathochromic shift is less pronounced for the CT band in **15b**. The absorption feature of A1 should be at about 315 nm and is probably overlayed in molecule **15b**.

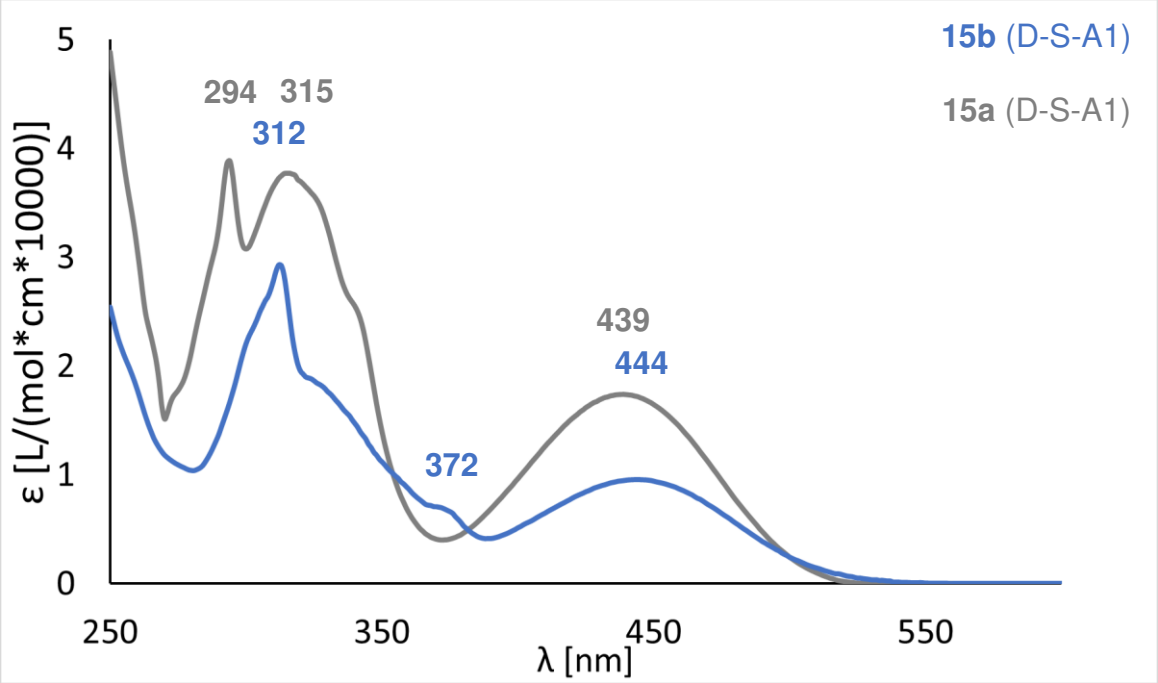


**Figure 73:** UV-Vis spectra of **15a** (blue) and **15b** (grey) in DCM at rt.

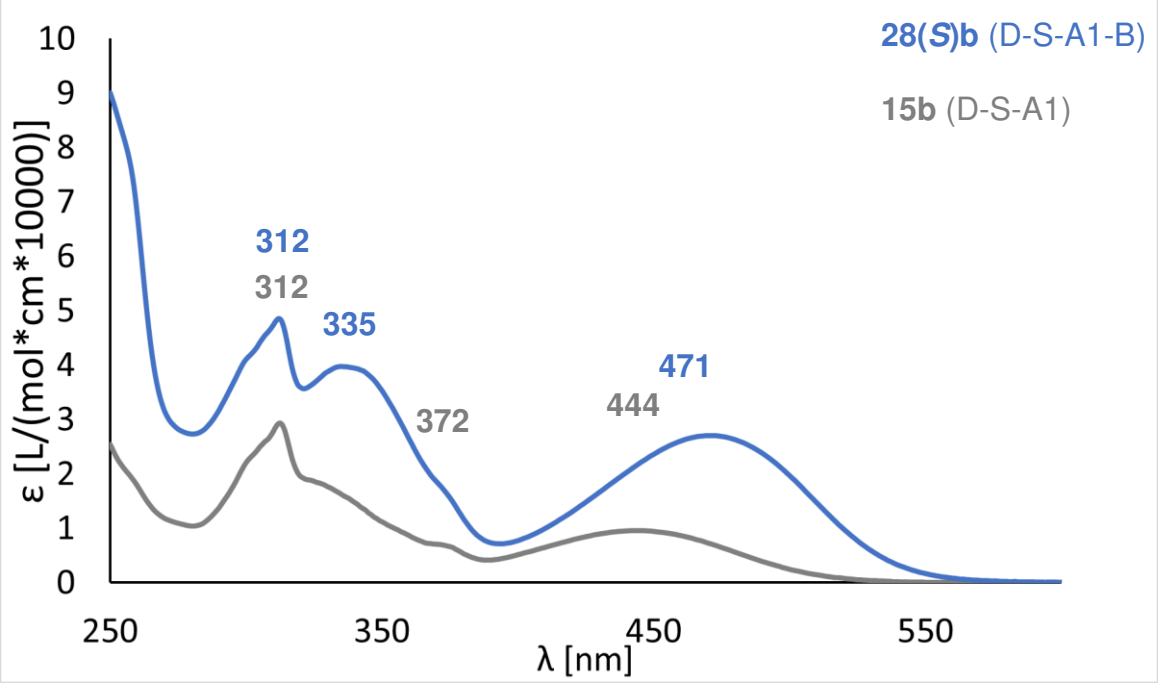


**Figure 74:** UV-Vis spectra of **28(*S*)b** (blue) and **15b** (grey) in DCM at rt.

Adding B to **15b** and forming **28(*S*)b** causes a bathochromic shift of absorption bands as shown in Figure 74. The CT band from D to A1 is shifted from 444 nm to 471 nm by 27 nm (0.16 eV). The redshift could be based on the chiral

bridge, which extends the *π*-system of A1. A similar effect was observed in series I dyes without the *n*-butoxy groups when adding B to **15a** and forming **28(*S*)a**.

Replacing the aldehyde moiety of **28(*S*)b** by a cyanoacrylic ester (**30(*S*)b**) or a SFR (**31(*S*)b**) leads to results comparable to the unsubstituted series I dyes (**30(*S*)a**, **31(*S*)a**) (Figure 75). In the *n*-butoxy substituted series I dyes the increased electron density was applied to improve the CT character of the dyes and allow a charge transfer from D to A2. However, no change of the CT band can be observed between **28(*S*)b** and **30(*S*)b**. Therefore, no indication for a D to A2 CT was confirmed. Nevertheless, *n*-butoxy substituted series I dyes show a significantly increased molar absorption coefficient in comparison to unsubstituted series I dyes. The increase ranges from 170 % for the SFR (**31(*S*)a**, **31(*S*)b**), 200 % for the aldehyde (**28(*S*)a**, **28(*S*)b**), to 370 % for the cyanoacrylic ester derivatives (**30(*S*)a**, **30(*S*)b**). An increase in molar absorption coefficients could be explained by improved spatial arrangement of the molecules, with an increased overlap of the ground and excited state wavefunctions.[78d, 112]

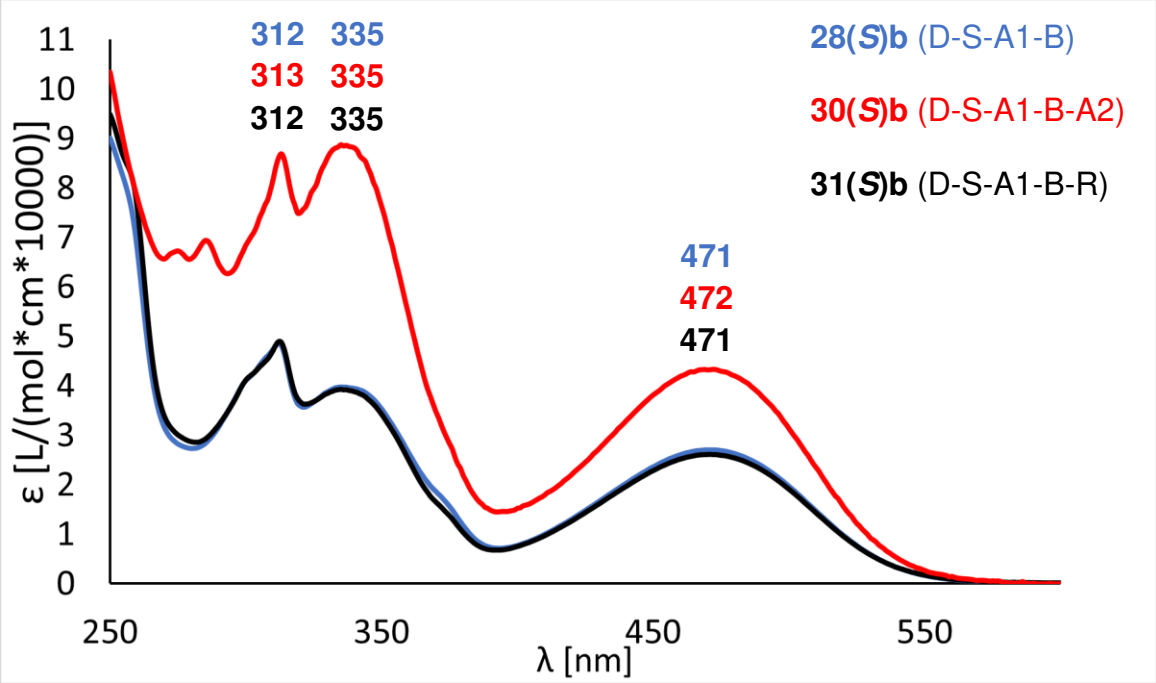


**Figure 75:** UV-Vis spectra of **28(*S*)b** (blue), **30(*S*)b** (red), and **31(*S*)b** (black) in DCM at rt.

In series II dyes D-S subunit is linked to the chiral bridge by an acetylene linker instead of A1. In molecule **12** an unprotected acetylene is attached to the D-S moiety **4a**. Comparing the UV-Vis spectra of **12** and **4a** (Figure 76) shows a shift of the absorption from a shoulder at 309 nm to a band at 324 nm. The absorption features based on the *n*-*π** transition (339 nm) and *π*-*π** transition (293 nm) of 9-PCz are not shifted. The bathochromic shifted of the absorption at 324 nm could be explained by the extended *π*-system, due to the linked acetylene unit. The increased *π*-system does not affect absorption bands of 9-PCz, indicating that thiophene and 9-PCz are electronically decoupled.

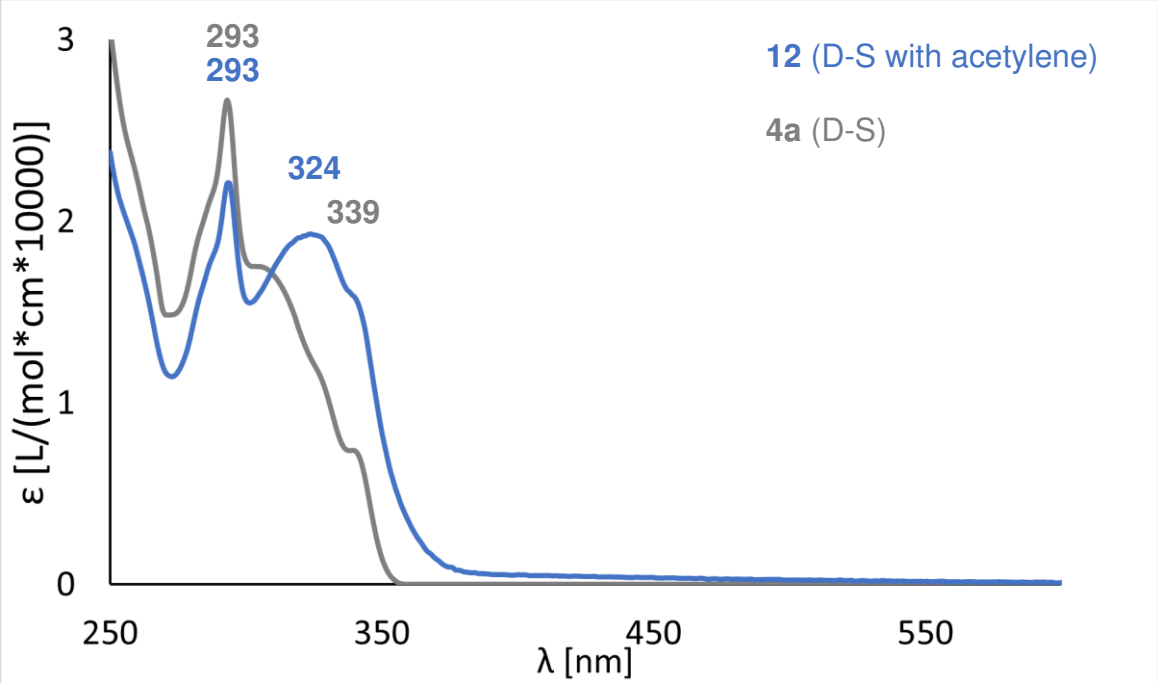


**Figure 76:** UV-Vis spectra of **12** (blue) and **4a** (grey) in DCM at rt.

In series II dyes A1 and D are on opposite sites of B. In molecule **17** one side of A1 is connected to a thiophene carbaldehyde, providing a synthetic handle to attach A2 or SFR. The other side of A1 is substituted by a bromine. Exchanging the bromine of **17** by a TMS-acetylene group forms **18**. The UV-Vis spectra of **17** and **18** are shown in Figure 77. The absorptions at 310 nm and 318 nm should be related to the substituted BTDA moiety and can be found at similar wavelengths for example in **15a** (315 nm), too. Both molecules show an absorption band between 398 nm and 414 nm. This feature can neither be assigned to BTDA nor to thiophene carbaldehyde and could be an CT between thiophene and BTDA.[113]

This hypothesis is also supported by the big Stokes shifts of 104 nm (0.645 eV) and 90 nm (0.535 eV) shown by **17** and **18**, respectively. In **18** this band is slightly red shifted in comparison to **17** (318 vs 310 nm), due to an extended *π*-system by the acetylene subunit.

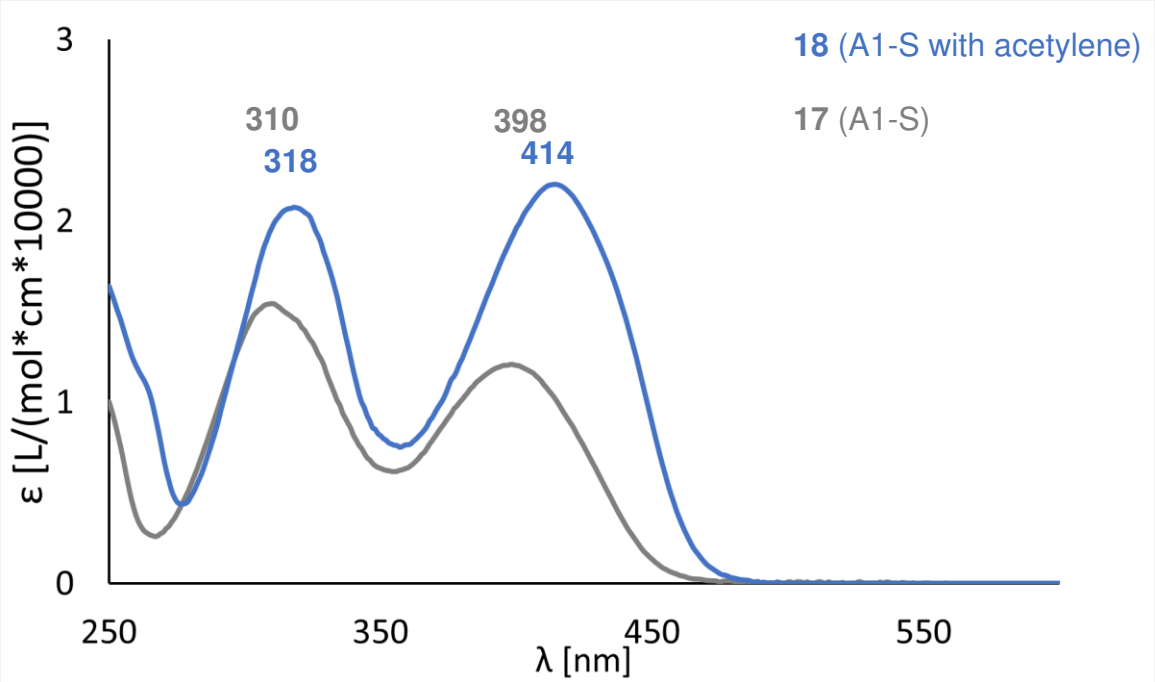


**Figure 77:** UV-Vis spectra of **18** (blue) and **17** (grey) in DCM at rt.

Combining D-S and B subunits of series II dyes leads to **35(*S*)**. The UV-Vis spectrum of **35(*S*)** compared to the spectrum of **12** is shown in Figure 78. While the absorption band of 9-PCz is not shifted by extending the $\pi$-system of the D-S part, the absorption at 324 nm is redshifted to 324 nm to 348 nm (24 nm, 0.27 eV).

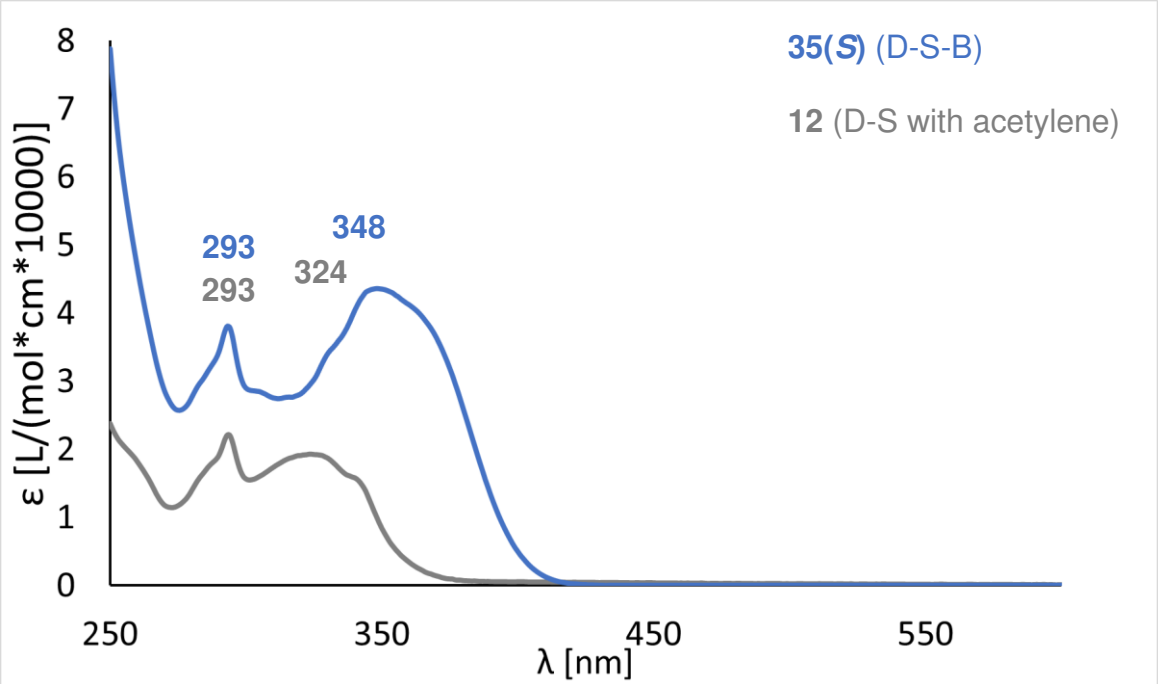


**Figure 78:** UV-Vis spectra of **35(*S*)** (blue) and **12** (grey) in DCM at rt.

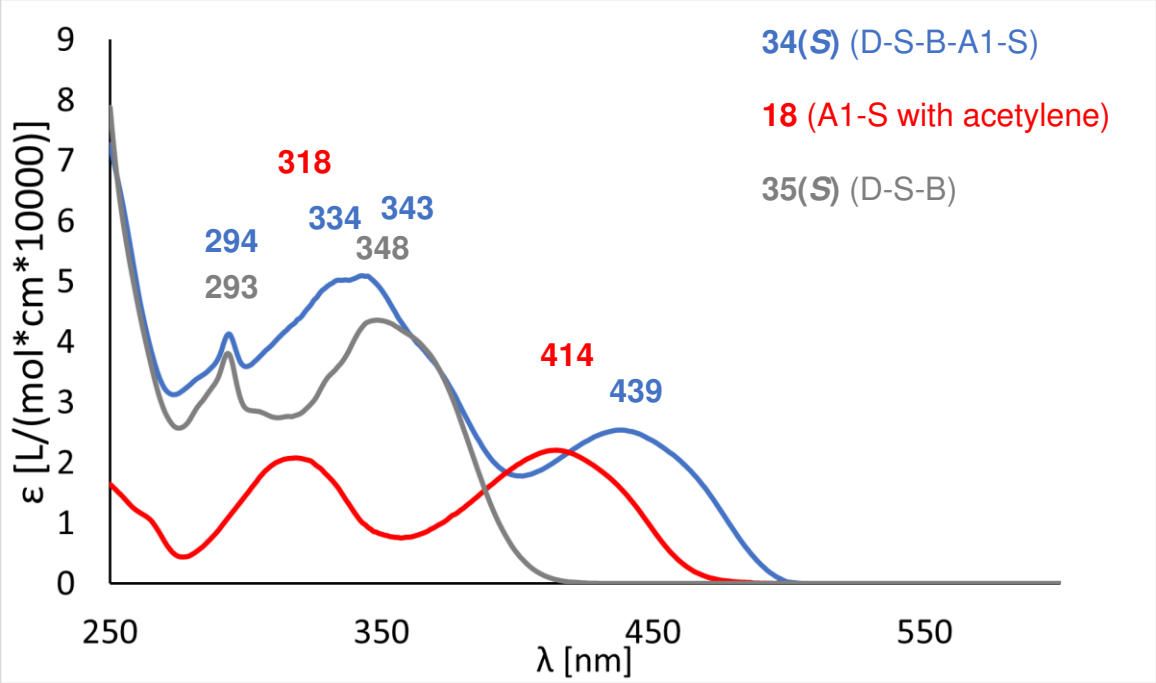


**Figure 79:** UV-Vis spectra of **34(*S*)** (blue), **18** (red), and **35(*S*)** (grey) in DCM at rt.

The UV-Vis spectra of **35(*S*)** (D-S-B, grey), **18** (A1-S, red), and **34(*S*)** (D-S-B-A1-S, blue) are shown in Figure 79. Adding the D-S-B part to A1-S leads to a 25 nm (0.18 eV) shift of the CT band from 414 nm to 439 nm. There are two possibilities to explain this shift. First one is, the CT in **34(*S*)** is taking place between D and A1, while CT took place from thiophene to A1 in **18**. A second explanation could be a bathochromic shift of the CT band by extending the $\pi$ system of the A1-S part. Redshifts for adding BINOL to A1 have shown to affect the CT band by similar values (0,16 eV for both molecules). The $n$-$\pi^*$ transition of the D moiety at 294 nm is almost not affected by the combination of D-S-B and A1-S and has shifted only by 1 nm.

In series II dyes exchanging the aldehyde group in **34(*S*)** does affect the CT band. The absorption feature is shifted from 439 nm by 9 nm (0.05 eV) to 448 nm in **37(*S*)** (SFR) and by 28 nm (0.17 eV) to 467 nm in **36(*S*)** (A2). This redshift could be based on the influence of A2 on the LUMO and the CT system. Other absorption bands within the molecules are not shifted by significant amounts.

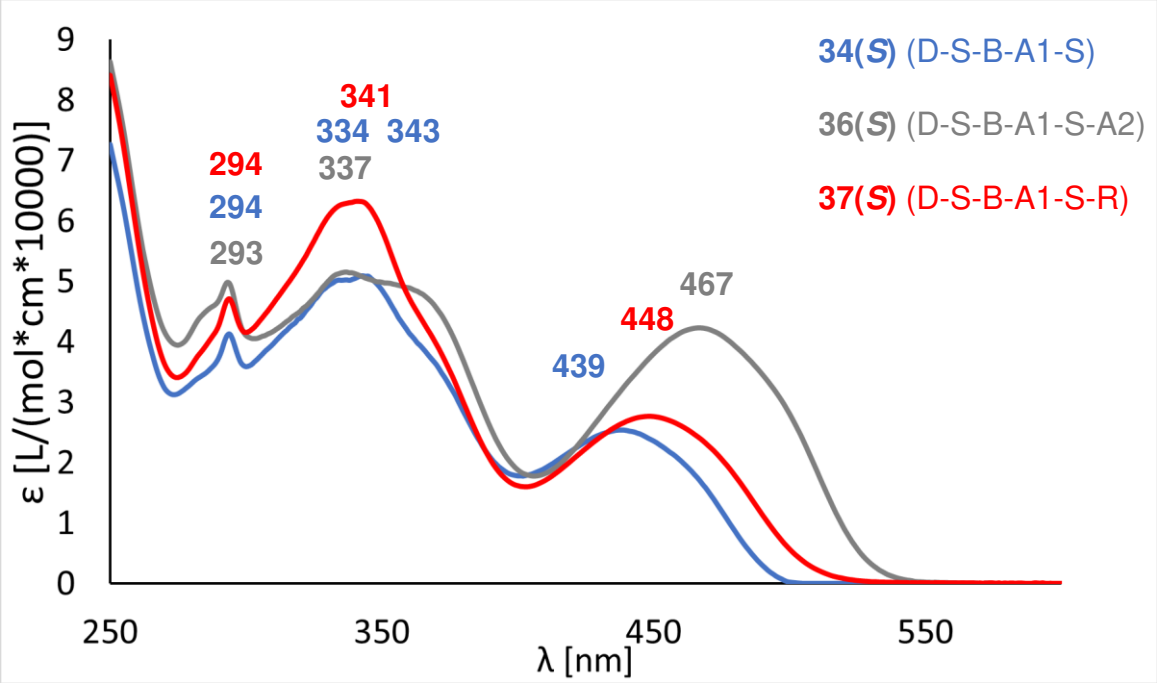


**Figure 80:** UV-Vis spectra of **34(*S*)** (blue), **36(*S*)** (grey), and **37(*S*)** (red) in DCM at rt.

Fluorescence measurements, including excitation and emission spectra as well as fluorescence quantum yields, were done on previously unknown compounds in DCM at rt. Molecules **10** and **15b** show changes of the emission spectra over time. Therefore, no fluorescence measurements of these compounds were done. Emission maxima, Stokes shifts and quantum yields of the aldehydes, SFRs and cyanoacrylic esters of series I and II dyes are shown in Table 3.

**Table 3:** Emission maxima, Stokes shifts and fluorescence quantum yields of aldehydes, SFRs and cyanoacrylic esters of series I and II dyes. Marked in yellow are series I dyes without *n*-butoxy groups; Marked in blue are series I dyes with *n*-butoxy groups; Marked in green are series II dyes.

| *Molecule* | *UV-Vis Maximum [nm]* | *Emission Maximum [nm]* | *Stokes Shift* | | *Φ [%]* |
|---|---|---|---|---|---|
| | | | ***[nm*** | ***eV]*** | |
| ***28(S)a*** | 467 | 615 | 148 | ***0.64*** | 54 |
| ***30(S)a*** | 466 | 620 | 154 | ***0.66*** | 50 |
| ***31(S)a*** | 463 | 620 | 157 | ***0.68*** | 47 |
| ***28(S)b*** | 471 | 665 | 194 | ***0.77*** | 1 |
| ***30(S)b*** | 472 | 672 | 200 | ***0.78*** | 2 |
| ***31(S)b*** | 471 | 633 | 162 | ***0.67*** | 1 |
| ***34(S)*** | 439 | 533 | 94 | ***0.50*** | 6 |
| ***36(S)*** | 467 | 548 | 81 | ***0.39*** | 5 |
| ***37(S)*** | 448 | 546 | 98 | ***0.50*** | 5 |

Comparing the Stokes shift of *n*-butoxy and non substituted series I dyes shows a shift towards lower energy fluorescence for the substituted dyes. The Stokes shift increased by 0.13 eV for the aldehydes and 0.12 eV for the A2 derivatives. This increased Stokes shift can be explained by the electron donating *n*-butoxy groups, which lead to a stronger CT character and a better stabilized charge separated state.[78d, 114] Comparing the SFR derivatives of series I dyes, **31(*S*)a** and **31(*S*)b**, shows a red shifted emission maximum but a decreased Stokes shift (by 0.01 eV) for the *n*-butoxy substituted compound **31(*S*)b**. Within the unsubstituted series I dyes the SFR shows the biggest Stokes shift, being 0.02 eV

and 0.04 eV greater than for the A2 and aldehyde derivative, respectively. In substituted series I dyes the SFR derivative shows the smallest Stokes shift, being 0.10 eV and 0.11 eV smaller than for the aldehyde and A2 derivative, respectively. In the unsubstituted SFR derivative **31(*S*)a** the TEMPO moiety is stabilizing the charge separated state compared to the aldehyde and A2. However, in the *n*-butoxy substituted derivative **31(*S*)b** the TEMPO moiety is destabilizing the charge separated state compared to the aldehyde and A2. Therefore, increasing the CT character of the molecule is influencing the interaction between the CT system and the SFR.

Comparing the Stokes shifts of unsubstituted series I and series II dyes show smaller Stokes shifts and higher energy emission maxima for series II dyes. A smaller Stokes shift indicates a less stabilized exited state for systems where D and A1 are separated by the chiral bride. In case a CT from D to A1 is taking place, a zwitterionic charge separated state with a $D^+$ and an $A1^-$ subunit is formed. In series I and series II dyes the spatial distance between the $D^+$ and $A1^-$ in the charge separated state is bigger than in series II dyes, where B is separating D and A1 (9.5 Å in series I dyes and 20.4 Å in series II dyes). The stabilizing Coulombic interactions between $D^+$ and $A1^-$ decrease with increasing distance between charges. Therefore, the excited charge separated state is less stabilized in series II dyes. This picture is very simplified but gives an idea on where the decreased stability of the exited state in series II dyes could be based on. The A2 derivate of series II dyes show with a shift of 81 nm or 0.39 eV the smallest Stokes shift within all the synthesized dyes. This shift is 0.11 eV smaller than the shifts for the SFR and the aldehyde derivates of series II dyes. Hence, the strong electron withdrawing substituent A2 seams to destabilizing the charge separated state of series II dyes in comparison to an aldehyde or SFR moiety.

Unsubstituted series I dyes show the most similar influence of the aldehyde, A2, SFR on the exited charge separated state. The Stokes shifts within unsubstituted series I dyes vary by 6 % while the variations are as large as 12 % and 21 % for *n*-butoxy substituted series I and series II dyes, respectively. With the given data no general rule of stabilizing or destabilizing interactions between the charge separated state and the aldehyde, A2 and SFR moiety can be given.

While for example the A2 derivative in substituted series I dyes show the greatest Stokes shift, the A2 derivative of series II dyes show the smallest.

The fluorescence quantum yields ($\Phi$) of unsubstituted series I dyes is ranging from 47 % for the SFR derivative to 54 % for the aldehyde and is one order of magnitude higher than the quantum yields of the other synthesized dyes. *N*-butoxy substituted series I dyes show the lowest $\Phi$ with yields between 1 % and 2 %. Series II dyes show $\Phi$ of 5 % and 6 %. Within the different categories of dyes $\Phi$ are barley varying. Hence, quantum yields of these molecules are mainly influenced by conformational arrangement of the exited state and the CT interaction between donor and acceptor. However, the substitution in form of aldehyde A2 or SFR does not significantly affect the $\Phi$.

## 2.4. Computational Analysis of Chiral Charge Transfer Dyes

The structure of cyanoacyrlic ester derivates of series I and series II dyes were optimized by density functional theory (DFT) calculations based on the B3LYP functional and the 6-31G* basis set without consideration of a solvent.[115] No conformational analysis was done. Therefore, optimized structures do not necessarily have to represent the global minimum of the potential energy surface of the molecule. The optimized structures were checked for imaginary frequencies to exclude that the results show transition states. Energies of orbitals were determined and the HOMO – LUMO gap was calculated. Molecular orbitals are given at contour values of 0.03. Discussions about charge transfer processes assume that the first exited state is highly HOMO-LUMO dominated. Therefore, it has to be taken into account that the following discussions are based on a very simplified model and the processes of excitation can be much more complicated. In further work the results can be improved by doing a confirmational analysis before optimizing the structures and by using time dependent DFT calculations to analyze the excitation processes.

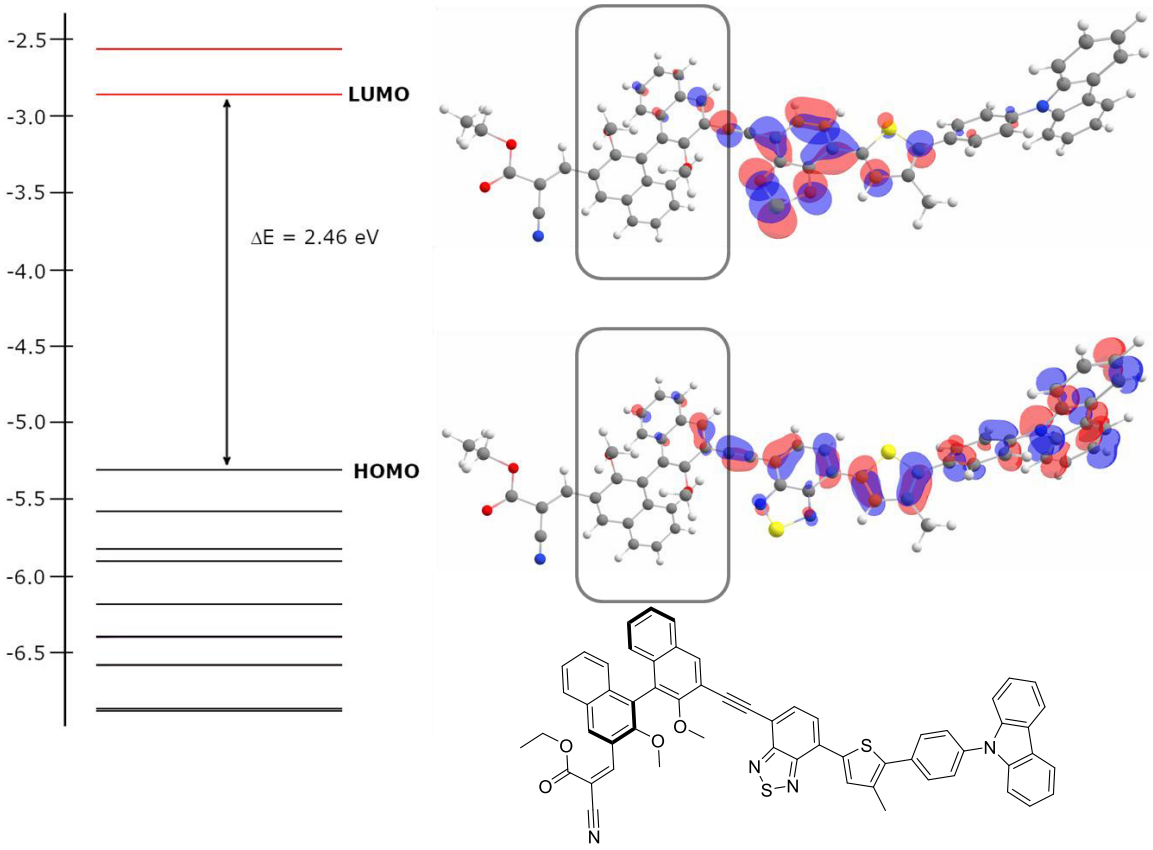


**Figure 81:** Computational results for **30(*S*)a** based on B3LYP/6-31G* level of theory. Energies in eV; counter values of orbitals 0.03; grey box frames B.

Shown in Figure 81 are the computational results for the A2 derivative of unsubstituted series I dyes, **30(*S*)a**. The energy of the HOMO and LUMO were calculated to – 5.30 eV and – 2.84 eV, respectively. The energy gap between HOMO and LUMO is 2.46 eV. The HOMO is spread over D, S and the phenyl ring of the BTDA moiety. The LUMO is located at the BTDA subunit. Therefore, CT during HOMO – LUMO excitation does not pass the chiral bridge and takes place between D-S and A1 subunits.

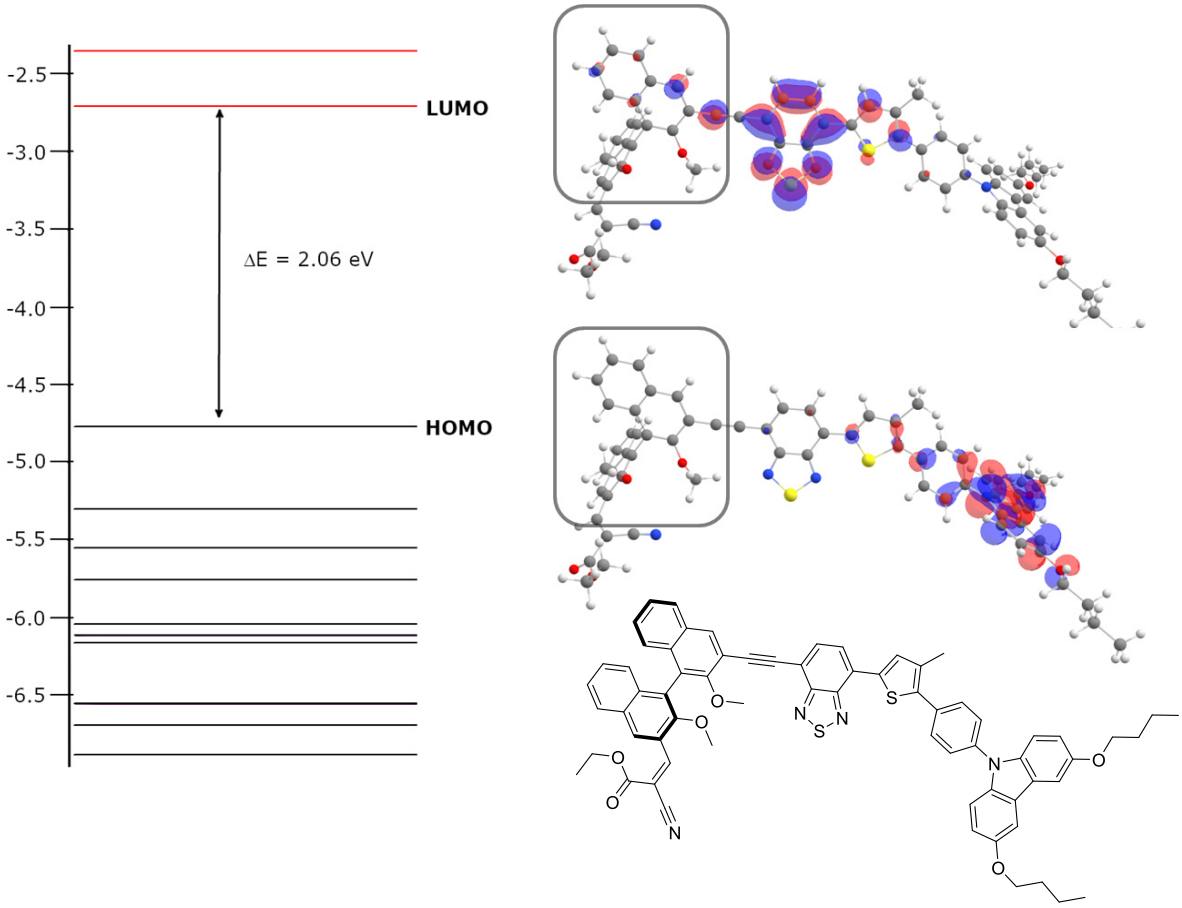


**Figure 82:** Computational results for **30(*S*)b** based on B3LYP/6-31G* level of theory. Energies in eV; counter values of orbitals 0.03; grey box frames B.

Comparing unsubstituted and *n*-butoxy substituted series I dyes (Figure 82) shows that the HOMO (– 4.76 eV) and LUMO (– 2.71 eV) are higher in energy by 0.54 eV and 0.13 eV, respectively, in the substituted derivative **30(*S*)b**. The HOMO – LUMO gap is reduced to 2.06 eV in **30(*S*)b**. The higher energy of the HOMO and the resulting smaller HOMO – LUMO gap is based on the increased electron density, due to the *n*-butoxy groups. The HOMO and LUMO orbitals of series I dyes are comparable to the orbitals of unsubstituted series I dyes, but with a HOMO limited to the D moiety. The orbitals in substituted and unsubstituted series I dyes are in good agreement with the results of UV-Vis experiments. CT does take place between D and A1 and is not influenced by the aldehyde, A2 or SFR moiety. This can be seen in the distribution of the orbitals and in the absence of a CT band shift in the UV-Vis spectra when comparing between aldehyde, A2 and SFR

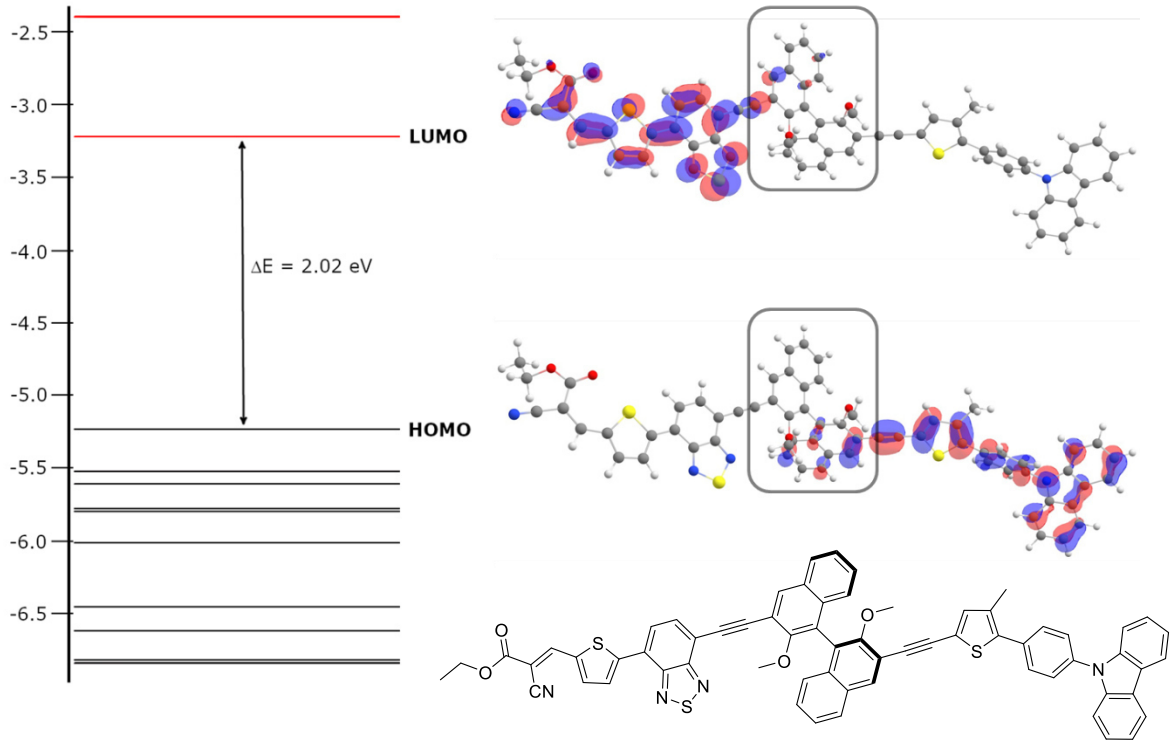


**Figure 83:** Computational results for **36(*S*)** based on B3LYP/6-31G* level of theory. Energies in eV; counter values of orbitals 0.03; grey box frames B.

The computational results of **36(*S*)** are shown in Figure 83. The HOMO of the molecule has an energy of – 5.24 eV and is located at the D-S subunit of the molecule. The LUMO of **36(*S*)** has an energy of – 3.22 eV, resulting in a HOMO – LUMO gap of 2.02 eV. The electron density distribution of the LUMO is located at the A1-S-A2 part of the molecule. **36(*S*)** is a series II dye, where D-S and A1-S-A2 subunits are separated by B. Therefore, an electron excited from the HOMO into the LUMO by light should pass the chiral bridge of the molecule. Distribution of the LUMO on A2 is in agreement with the results of UV-Vis measurements. Exchanging between aldehyde, A2 and SFR has influence on the CT band of the compounds. So A2 takes part on the LUMO.

In further research computations can be done on an improved level. Apart from confirmational optimization, the B3LYP method can be replaced by methods, which are able to describe CT interactions better.[116] In addition time dependent computations have to be done and solvent interactions can be considered in the calculation. [117]

# 3. Conclusion and Outlook

Presented in this work is the synthesis of two series of chiral CT dyes. Both series comprise a carbazole donor (D), a thiophene *π*-conjugated spacer (S), a BTDA primary acceptor (A1), and *S*-BINOL as a chiral bridge (B). The molecules were synthesized bearing an aldehyde moiety which can be used to append either a cyanoacrylic ester as a second acceptor (A2) or a TEMPO stable free radical (SFR) to the dyes. The molecules equipped with A2 can be used to study the chiral induced spin selectivity effect. The separation of spins within the system would grant applications in spin-valves and other spintronic devices. The molecules substituted with the SFR allow the study of radical-radical interactions between the unpaired spin of the SFR and the diradical charge transfer state. Studying these interactions could lead to potential applications in Quantum Information Science.

The two series vary in the arrangement of the different subunits within the dyes. In series I dyes a D-S-A1 subunit is separated from A2/SFR by B leading to a D-S-A1-B-A2/SFR arrangement. In series II dyes D and A1 are separated by the chiral bridge B. Therefore, the arrangement of series II dyes is D-S-B-A1-S-A2/SFR as shown in Figure 84. Series I dyes were synthesized either with an unsubstituted or with a 3,6-di-*n*-butoxy substituted carbazole donor. The butoxy substitution increases the electron density of the donor-subunit. Hence, the CT character between D and A should be increased by substitution.

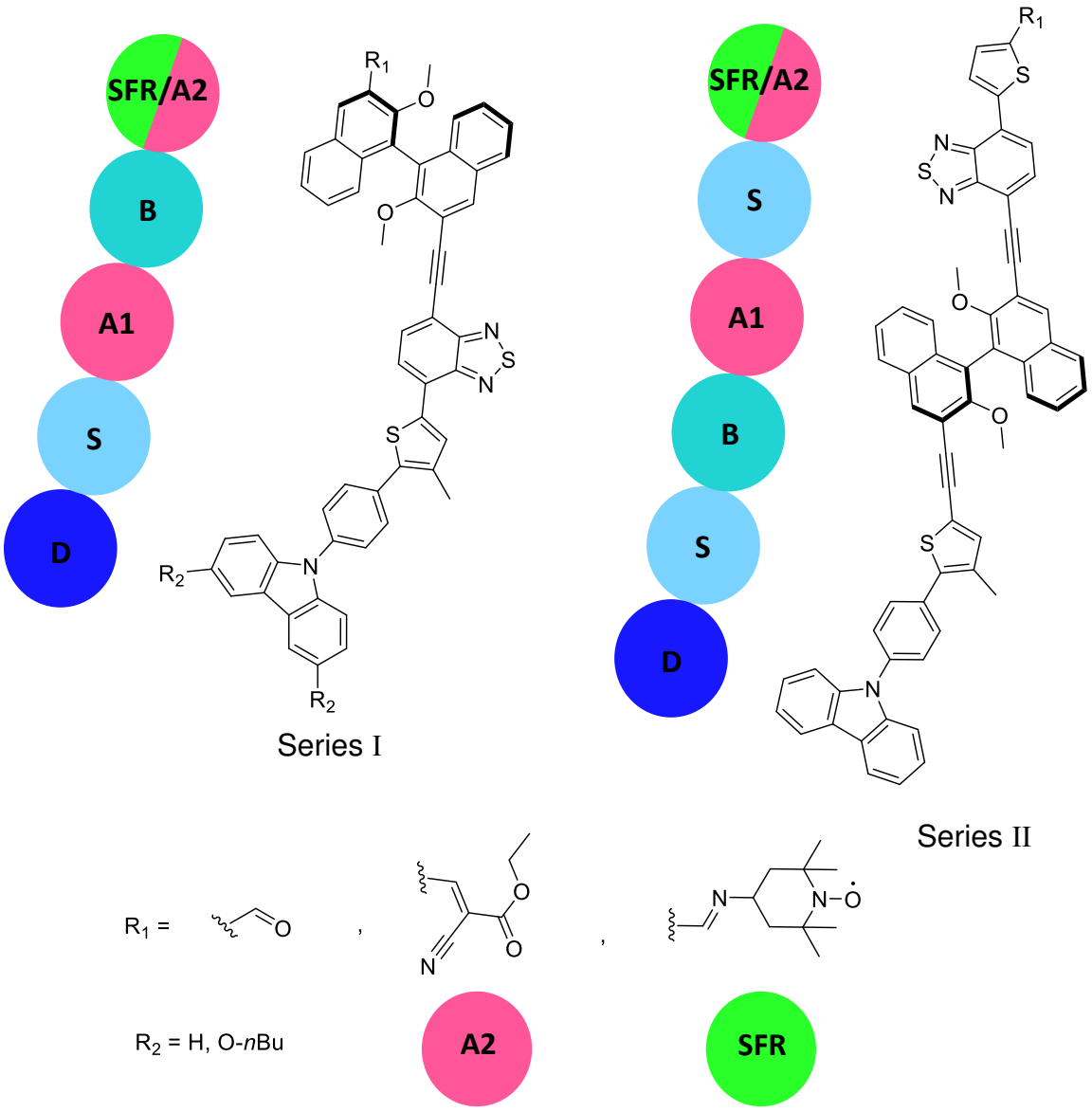


**Figure 84:** Arrangement of the subunits in series I (left) and series II dyes (right).

The dyes were synthesized by a modular procedure using multiple Palladium catalyzed cross-coupling reaction steps to combine different subunits. Modification of the aldehyde moiety into a SFR was accomplished by a protocol of Chernick et al., which was developed to connect a benzaldehyde substituted pentacene with TEMPO-amine.[96] Unlike Chernick et al., SFR substituted dyes could not be recrystallized for purification. Silica- and alumina-based column chromatography cannot be used, due to hydrolyzation sensitivity of the imine bond connecting TEMPO to the rest of the dye. Size exclusion chromatography on BIOBeads® SX3 with toluene as a liquid phase allowed the separation of TEMPO-amine and SFR substituted dyes, based on size difference of the

compounds. The purity of SFR substituted compounds was determined by SQUID measurements. The project originally aimed for a cyanoacetic acid group as A2. During the synthesis substitution of the chiral dyes with a cyanoacrylic acid turned out to be challenging. Neither direct substitution of the aldehyde nor deprotection of ethyl cyanoacrylic ester derivatives allowed isolation of the aimed acids. Hence, the ethyl cyanoacrylic ester substituted dyes are presented in this work. Further synthetic effort can be done in the future to accomplish molecules with cyanoacrylic acid as A2. Different solvent systems and catalysts could allow the direct insertion of cyanoacetic acid by a Knoevenagel reaction. In case there is no success, various cyanoacetic esters, for example *t*-butyl or thioesters, can be coupled to the dyes, allowing cleavage of the ester functionality under very mild conditions.

UV-Vis and fluorescence measurements were done on new compounds. The results of the UV-Vis experiments of series I dyes showed a charge transfer absorption band when D and A1 are combined within one molecule. Variation of the aldehyde moiety to SFR or A2 does not shift the CT band. These results indicate that CT in series I dyes does take place between D and A1. A2 is not participating the CT process and no electron density is distributed on A2 in the exited charge separated state. The increased electron density in *n*-butoxy substituted series I dyes decreased the HOMO – LUMO gap of the molecule and improved the CT interaction. However, the improved CT interaction of substituted series I does still not allow CT interaction between D and A2. Series II dyes show CT bands as soon as BTDA and thiophene carbaldehyde are connected (A1-S subunit). The CT band shifts to lower wavelength by combining D-S-B and A1-S subunits. This shift can either be based on a CT from D to A1 or on an increased $\pi$- system shifting the CT visible in the A1-S subunit to lower energy. To proof or refuse the hypothesis of an increased $\pi$-system a B-A1-S molecule could be investigated by UV-Vis spectroscopy. Further transient absorption spectroscopy experiments will be done by collaborators to find spectroscopic signatures of either $D^+$ or $S^+$ in the excited state of the molecules. Derivatization from aldehyde to SFR and A2 does influence the CT in series II dyes. Hence, in contrast to series I, A2 does influence the CT either by having electron withdrawing effects on A1 or by CT from D to A2.

Fluorescence data of series I and series II dyes have shown Stokes shifts typical for CT dyes. Stokes shifts of series II dyes are generally smaller than for series I dyes. Fluorescence quantum yields are highest for unsubstituted series I dyes and lowest for substituted series I dyes. Therefore, $\Phi$ are strongly influenced by conformational arrangements and interactions within the CT system. Within derivatization from aldehyde to SFR or A2 $\Phi$ does not change significantly.

DFT calculations based on B3LYP/6-31G* were done for ethyl cyanoacrylic ester substituted series I and series II dyes. The energy levels and spatial distributions of orbitals were determined and evaluated. Based on very simplifying assumptions of for example a HOMO-LUMO dominated $S_1$ state, HOMO and LUMO orbitals are in good agreement with the results found by UV-Vis experiments. Time dependent DFT calculations, solvent models and other DFT functionals could be used in further work to improve the meaningfulness of computational results.

The synthesized dyes will be investigated in cooperation with other national and international working groups to investigate further into their photophysical properties, their charge transfer behavior, and intramolecular CISS effects. The formation and nature of the excited charge separated state will be studied by transient absorption spectroscopy and time dependent EPR spectroscopy. Time dependent EPR studies would additionally allow insight in the interaction between the charge separated state and the SFR. Comparing these interactions in series I and series II dyes can help to understand the influence of the chiral bridge on radical – radical interactions. Deposition of the molecules on an inorganic surface like Ag or MgO allows the study of intramolecular CISS effects with devices similar to the spin valve shown in Figure 5 in the Spintronic and Quantum Information Science chapter. Having access to a cyanoacrylic acid as A2 would allow sufficient binding of the dyes on MgO surfaces. Binding on Ag surfaces can be achieved alternatively by derivatization of the aldehyde moiety to for example thiol bearing groups. Development of Spintronic application, including the use of CISS, opens possibilities to the efficient use of renewable and cheap organic materials to store and process digital data.

When CISS effects or potential uses in spintronics are discernable the basic synthetic plan presented within this work can be modified to synthesize a variety of new chiral dyes. Modifications can be made at several places in the molecule. Changes on the chiral bridge should directly influence CISS effects. For example, BINOL can be substituted in the 6 and 6’ position with electron donating or accepting groups. Also the connection between the B and the rest of the system can be changed from the 3 and 3’ position to the 6 and 6’ position. Additionally, BINOL as a chiral bridge can be completely replaced by for example helicacenes or DNA strands to increase the length of the actual chiral moiety and therefore the CISS effect. The modular approach of the synthesis allows the exchange of donor or acceptor groups to affect the formation and lifetime of the charge separated state. Smaller modifications of the donor system can also be done by replacing the *n*-butoxy substituents on the carbazole moiety by different other groups. Cross-coupling reactions on the brominated carbazole **9** can be used to connect a variety of groups to the D moiety. Different other linking groups could replace A2 to allow sufficient deposition on surfaces.

The synthesis presented in this work is a first step to explore the field of chiral organic charge transfer dyes. Further work needs to be done to study their properties and their potential use in quantum information science. The synthetic plan can be modified to optimize the molecules for a variety of applications.

# 4. Experimental

## 4.1. General Information

Solvents for chromatography and workup including technical grade diethylether, ethyl acetate (EtOAc), hexane and dichloromethane (DCM) were distilled prior to use with a rotary evaporator or purchased as HPLC grade. DCM, hexane, tetrahydrofuran (THF) and toluene used for the synthetic reactions were purified by a SPS system (MBraun MB-SPS-800). DMF, *n*-BuLi (2.5 M in hexane) and TMEDA used in the synthetic reactions were bought anhydrous and under inert atmosphere from Sigma-Aldrich. Triethylamine was distilled over CaH under $N_2$-atmosphere prior to use. Methanol for the recrystallization and synthetic reactions was purchased as HPLC grade. Concentrated $HCl_{(aq)}$ was used as technical grade and diluted to 1 M concentration. 4-Amino-2,2,6,6-tetramethylpiperidinyloxyl free radical (TEMPO-Amine), $Al_2O_3$, 9-(4-bromophenyl)-9H-carbazole (**2a**), CuI, CsF, $CSCO_3$, ethylcyanacetate, 1-Fluoro-4-iodobenzene, piperidine, $I_2$, $K_2CO_3$, $PdCl_2$, tetra-*n*-butylammoniumfluoride (TBAF), tributyltinchloride, tri-*iso*propylsilylacetylene, trimethylsilylacetylene and tri-*t*-butylphosphine were used without further purification. DCM-$d_2$ and $CDCl_3$ was purified directly before use by passing through a basic alumina column. Solvent impurities and water were not fully removed by this technique, leading to impurities. $^1$H-NMR gave signals at 1.52 (water), 1.26 (grease) and 0.08 (grease) ppm. $^{13}$C-NMR gave signals at 1.2 (grease) ppm.[118] Tetrakis (triphenylphosphine)palladium(0)[119], 3,6-di-*n*-butoxy-9*H*-carbazole (**1**)[99], tributyl(3-methylthiophene-2-yl)stannane (**3**)[120], 3,6-dibromo-9-(4-iodophenyl)-9H-carbazole (**9**)[98], 4,7-dibromobenzo[c][1,2,5]thiadiazole (**14**)[121], 5-(7-bromobenzo[c][1,2,5]thiadiazol-4-yl)thiophene-2-carbaldehyde (**17**)[101], 2,2'-dimethoxy-1,1'-binaphthalene (**20(*S*)**)[102], and 3,3'-diiodo-2,2'-dimethoxy-1,1'-binaphthalene (**26(*S*)**)[87a] were synthesized according to reported literature. 3-Iodo-2,2'-dimethoxy-1,1'-binaphthalene (**22(*S*)**) was synthesized in a modified synthetic procedure of reported literature in improved yields.[103]

Thin Layer Chromatography (TLC) was performed on silica TLC plates (Macherey-Nagel, Polygram Sil G/UV) and visualized by illumination with an UV lamp (254 nm and 365 nm wavelength). Silica gel (Macherey-Nagel,

0.04–0.063 mm) was used as received. Size exclusion chromatography was performed on Bio-Beads™ S-X3 Resin with toluene as an eluent.

All NMR spectra were recorded at 298 K on 400 MHz and 700 MHz Bruker Avance III spectrometers. $^{1}$H and $^{13}$C shifts were referenced to the residual solvent signal ($CD_2Cl_2$, $^{1}$H-NMR: $\delta$ = 5.32 ppm, $^{13}$C-NMR: $\delta$ = 53.84 ppm and $CDCl_3$, $^{1}$H-NMR: $\delta$ = 7.26 ppm, $^{13}$C-NMR: $\delta$ = 77.16 ppm).[118] All assignments were deduced with a combination of 2D experiments (COSY, NOESY, HSQC and HMBC). Mass spectrometry measurements were recorded on a maXis 4G-UHR-TOF Bruker Daltonics spectrometer using the ESI or the APCI technique. UV/Vis spectra were recorded at room temperature in a 1 cm quarz cuvette using a Perkin-Elmer Lambda 1050 spectrophotometer. Fluorescence spectra were recorded on a PTI Quantamaster QM4, equipped with a 75 W steady-state xenon short arc lamp for excitation. The emission was recorded with a PTI P1.7R detector module covering UV-Vis-NIR wavelength (200 – 1000 nm). When necessary, long pass filter glass plates (Schott, 3 mm thickness) were used in the emission path. Spectral selection was achieved by single grating monochromators (excitation: 1200 grooves/mm, 300 nm blaze and UV-Vis emission: 1200 grooves/mm, 500 nm blaze). Samples were dissolved in HPLC grade solvents without further purification. An absorbance of 0.1 at the excitation wavelength was used without degassing. Fluorescence quantum yields were determined by the method introduced by Parker and Rees using the following equation:[122]

$$\Phi_x = \Phi_R * \frac{Grad_x}{Grad_R} * \frac{n_x^2}{n_R^2}$$

Where $n$ is the refractive index (ACN: $n$ = 1.344, DCM: $n$ = 1.424, $H_2O$: $n$ = 1.330, 0.1 M $H_2SO_4$: $n$ = 1.334) and $Grad$ is the linearly fitted slope from the plot of the integrated luminescence intensity versus the absorbance at the excitation wavelength. The subscripts '$x$' and '$R$' refer to the sample and the reference, respectively. Quinine sulfate in 0.1 M $H_2SO_4$ was used as a reference material, with a fluorescence quantum yield of 54.6 %, for **2b**, **4a**, **4b**, **11**, **12**, **23(*S*)**, **24(*S*)** and **32(*S*)**.[123] Coumarin 153 in ACN was used as a reference material, with a fluorescence quantum yield of 43 %, for **15a**, **18**, **28(*S*)a**, **30(*S*)a** and **31(*S*)a**.[124] Tris(2,2'-bipyridyl)dichloro ruthenium(II) * 6 $H_2O$ in water was used as a reference

material, with a fluorescence quantum yield of 2.8 %, for **28(*S*)b**, **30(*S*)b**, **31(*S*)b**, **34(*S*)**, **36(*S*)** and **37(*S*)**.[125] EPR measurements were performed on a Bruker ESP300E X-Band instrument, operating at a microwave frequency of 9.84 GHz. IR-spectra were recorded at rt using a Jasco FT/IR4100 spectrometer with an ATR application. Optical rotations were measured at a Jasco P-1020 at 295 K and a concentration of 0.1 and 0.01 in DCM. Melting Points were measured with a Büchi Melting Point B540.

Calculations were performed using the Gaussian16 package.[126] Geometries were optimized in the gas phase using the B3LYP[115a, 127] functional and the 6-31G*[115b, 115c] basis set for all atoms. Frequency analyses were performed at the same level of theory to conform that the obtained geometries correspond to minima.

SQUID measurements were performed on a Quantum Design spectrometer, equipped with a 1822-MPMS Controller, a 1802 R/G Bridge, a Model 2000 VHF SQUID Amplifier, and a Model 2010 SQUID Controller. The magnetic susceptibility was measured between 5 and 300 K. The molar magnetic susceptibility $\chi_{mol}$ was calculated by the Curie-Weiss-law, where $C$ is the Curie constant, $T$ is the temperature in K and $\theta$ is the Weiss constant. The equation was expanded with a temperature independent correction factor $\chi_0$, for the diamagnetic correction and the diamagnetic probe container.[108]

$$\chi_{mol} = \frac{C}{T - \theta} + \chi_0$$

The experimental Bohr magneton $\mu_{exp}$ was calculated by $\mu_{exp} = 2.83 * \sqrt{C}$. The amount of unpaired spin was calculated by the spin only formula, where $g = 2.00023$ is the gyromagnetic ratio for a free electron and $S$ is the number of unpaired electrons.[108]

$$\mu_{exp} = g\sqrt{S(S+1)}$$

Reactions under $N_2$-atmosphere were carried out in oven dried glassware, that were evacuated and refilled with $N_2$ 3 times.

## 4.2. Synthetic Procedures

***3,6-Dibutoxy-9-(4-iodophenyl)-9H-carbazole*** (**2b**)

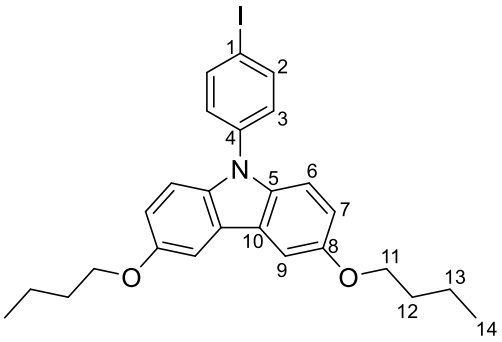


**1** (1.3 g, 4.2 mmol)[99], 1-Fluoro-4-iodobenzene (5.4 g, 24 mmol) and $CsCO_3$ (5.3 mg, 16.3 mmol), were dissolved in 13 mL DMF and heated to 150°C for 36 h. After cooling to rt, water was added, and the mixture was extracted with EtOAc. The organic layer was separated, washed with brine and dried over $MgSO_4$.The solvent was removed under reduced pressure and the crude product was purified by column chromatography (silica, hex/DCM 3:1). **2b** (1.31 g, 61 %) was isolated as a colorless solid. **Mp** = 125 °C. $\mathbf{R_f}$ = 0.41 (hexane/DCM 3:2). **UV-Vis** (DCM) $\lambda_{max}$ ($\varepsilon$) = 312 (29200), 357 (3980), 370 (4110) nm. **Fluorescence** (DCM) $\lambda_{max}$ = 387 nm, $\Phi$ = 3 %. **IR** (ATR) = 1456 (s), 1203 (s), 1162 (s), 801 (s). **$^1$H-NMR** (400 MHz, $CD_2Cl_2$, 298 K): $\delta$ = 7.92 – 7.90 (m, 2 arom. H, 2), 7.54 (d, $^4J_{7,9}$ = 2.5 Hz, 2 arom. H, 9), 7.34 – 7.30 (m, 4 arom. H, 3, 6), 7.02 (dd, $^3J_{6,7}$ = 8.9 Hz, $^4J_{7,9}$ = 2.5 Hz, 2 arom. H, 7), 4.08 (t, $J$ = 6.6 Hz, 4 H, 11), 1.86 – 1.79 (m, 4 H, 12), 1.59 – 1.50 (m, 4 H, 13), 1.01 (t, $J$ = 7.4 Hz, 6 H, 14) ppm. **$^{13}$C{$^1$H}-NMR** (100.6 MHz, $CD_2Cl_2$, 298 K): $\delta$ = 154.2 (8), 139.3 (2). 138.5 (4), 136.1 (5), 128.7 (3), 124.3 (10), 116.0 (7), 110.8 (6), 104.2 (9), 91.3 (1), 69.0 (11), 32.0 (12), 19.8 (13), 14.1 (14) ppm. **APCI-HRMS** calcd. for $C_{26}H_{28}INO_2$ + $Na^+$ (M + $Na^+$) 536.10570, found 536.10638.

***9-(4-(3-Methylthiophen-2-yl)phenyl)-9H-carbazole*** (**4a**)

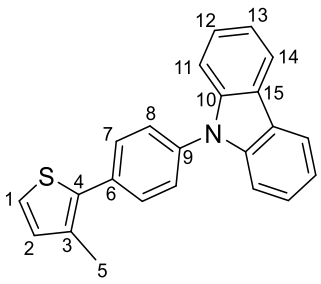


Under $N_2$-atmosphere **2a** (0.64 g, 2.0 mmol) and **3** (0.88 g, 2.4 mmol)[120] were dissolved in 10 mL DMF. $PdCl_2$ (7 mg, 0.039mmol), CuI (15 mg, 0.079 mmol) P*t*-$Bu_3$ (16 mg, 0.079 mmol) and CsF (0.61 g, 4.0 mmol) were added. The reaction was heated to 100 °C for 16 h. After cooling to rt, water was added, and the mixture was extracted with hexane. The organic layer was separated, washed with brine and dried over $MgSO_4$. The solvent was removed under reduced pressure and the crude product was purified by column chromatography (silica, hex/DCM 9:1). **4a** (397 mg, 58 %) was isolated as a colorless solid. **Mp** = 127 °C. $R_f$ = 0.2 (hexane/DCM 9:1). **UV-Vis** (DCM) $\lambda_{max}$ ($\varepsilon$) = 293 (26700), 303 (17500, shoulder), 339 (7380) nm. **Fluorescence** (DCM) $\lambda_{max}$ = 367 nm, $\Phi$ = 23 %. **IR** (ATR) = 1509 (m), 1450 (s), 1316 (m), 1233 (m). **$^1$H-NMR** (400 MHz, $CD_2Cl_2$, 298 K): $\delta$ = 8.17 (d, $^3J_{13,14}$ = 7.8 Hz, 2 arom. H, 14), 7.74 – 7.72 (m, 2 arom. H, 7), 7.65 – 7.62 (m, 2 arom. H, 8), 7.50 (d, $^3J_{11,12}$ = 8.1 Hz, 2 arom. H, 11), 7.46 – 7.42 (m, 2 arom. H, 12), 7.33 – 7.29 (m, 3 arom. H, 1; 13), 7.01 (d, $^3J_{1,2}$ = 5.1 Hz, 1 arom. H, 2), 2.44 (s, 3 H, 5) ppm. **$^{13}$C{$^1$H}-NMR** (100.6 MHz, $CD_2Cl_2$, 298 K): $\delta$ = 141.2 (10), 137.2 (3), 136.9 (9), 134.4 (5), 134.3 (6), 131,8 (2), 130.7 (7), 127.4 (8), 126.4 (12), 124.2 (1), 123.8 (15), 120.6 (14), 120.4 (13), 110.2 (11), 15.2 (4) ppm. **ESI-HRMS** calcd for $C_{23}H_{17}NS^{\bullet+}$ ($M^{\bullet+}$) 339.10762, found 339.1079.

***3,6-Dibutoxy-9-(4-(3-methylthiophen-2-yl)phenyl)-9H-carbazole*** (**4b**)

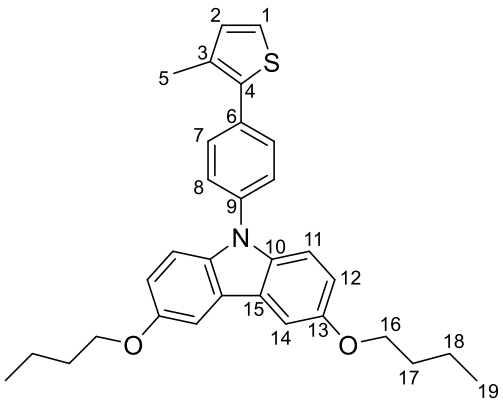


Under $N_2$-atmosphere **2b** (1.2 g, 2.3 mmol) and **3** (1.0 g, 2.6 mmol)[120] were dissolved in 40 mL DMF. $Pd(PPh_3)_4$ (250 mg, 0.22 mmol), CuI (84 mg, 0.44 mmol) and CsF (670 mg, 4.4 mmol) were added and the reaction was stirred at rt overnight. Water was added to the mixture and the mixture was extracted with hexane. The organic layer was separated, washed with brine and dried over $MgSO_4$. The solvent was removed under reduced pressure and the crude product was purified by column chromatography (silica, hex/DCM 1:1). **4b** (866 mg, 78 %) was isolated as a colorless solid. **Mp** = 95 °C. $\mathbf{R_f}$ = 0.21 (hexane/DCM 1:1). **UV-Vis** (DCM) $\lambda_{max}$ ($\varepsilon$) = 313 (26500), 324 (13100, shoulder), 369 (5410) nm. **Fluorescence** (DCM) $\lambda_{max}$ = 390 nm, $\Phi$ = 20 %. **IR** (ATR) = 1457 (sh s), 1200 (s), 1162 (s), 806 (s). **$^1$H-NMR** (400 MHz, $CD_2Cl_2$, 298 K): $\delta$ = 7.70 – 7.67 (m, 2 arom. H, 7), 7.61 – 7.59 (m, 2 arom. H, 8), 7.57 (d, $^4J_{12,14}$ = 2.5 Hz, 2 arom. H, 14), 7.40 (d, $^3J_{11,12}$ = 8.9 Hz, 2 arom. H, 11), 7.28 (d, $^3J_{1,2}$ = 5.1 Hz, 1 arom. H, 1), 7.04 (dd, $^3J_{11,12}$ = 8.9 Hz, $^4J_{12,14}$ = 2.5 Hz, 2 arom. H, 12), 7.00 (d, $^3J_{1,2}$ = 5.1 Hz, 1 arom. H, 2), 4.10 (t, $J$ = 6.6 Hz, 4 H, 16), 2.42 (s, 3 H, 5), 1.87 – 1.80 (m, 4 H, 17), 1.61 – 1.51 (m, 4 H, 18), 1.02 (t, $J$ = 7.4 Hz, 6 H, 19) ppm. **$^{13}$C{$^1$H}-NMR** (100.6 MHz, $CD_2Cl_2$, 298K): $\delta$ = 154.1 (13), 137.5 (9), 137.3 (3), 136.4 (10), 134.1 (4), 133.7 (6), 131.8 (2), 130.6 (7), 126.8 (8), 124.1 (15), 124.0 (1), 116.0 (12), 111.0 (11), 104.1 (14), 69.0 (16), 32.0 (17), 19.8 (18), 15.2 (5), 14.1 (19) ppm. **APCI-HRMS** calcd for $C_{31}H_{32}NO_2S + H^+$ ($M+H^+$) 484.23048, found 484.23068.

***9-(4-(5-Iodo-3-methylthiophen-2-yl)phenyl)-9H-carbazole*** (**10**)

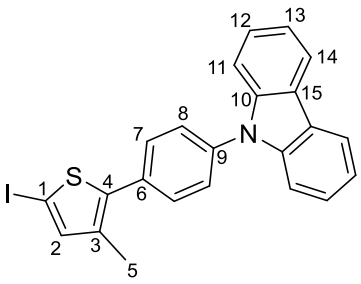


Under $N_2$-atmosphere **4a** (200 mg, 0.59 mmol) was dissolved in 15 mL THF and cooled to – 78 °C. *n*-BuLi (2.5 $_M$ in hexane) (403 $\mu$L, 1.0 mmol) was added dropwise over 5 min and the reaction was stirred for 30 min. $I_2$ (381 mg, 1.5 mmol) dissolved in 5 mL THF was added and the reaction was allowed to warm to rt overnight. Sat. $NaSO_{3(aq)}$ was added and the mixture was extracted with EtOAc. The separated organic layer was washed with brine and dried over $MgSO_4$. The solvent was removed under reduced pressure. **10** (266 mg, 97 %) was isolated as a colorless solid. **Mp** = 176.5 °C. $R_f$ = 0.23 (hexane/DCM 9:1). **UV-Vis** (DCM) $\lambda_{max}$ ($\varepsilon$) = 293 (24900), 316 (19200), 337 (12600, shoulder) nm.[128] **IR** (ATR) = 1449 (s), 1230 (m), 830 (s), 751 (s). **$^1$H-NMR** (400 MHz, $CD_2Cl_2$, 298 K): $\delta$ = 8.16 (d, $^3J_{13,14}$ = 8.0 Hz, 2 arom. H, 14), 7.66 – 7.63 (m, 4 arom. H, 7, 8), 7.49 (d, $^3J_{11,12}$ = 8.2 Hz, 2 arom. H, 11), 7.45 – 7.43 (m, 2 arom. H, 12), 7.32 – 7.30 (m, 2 arom. H, 13), 7.16 (s, 1 arom. H, 2), 2.39 (s, 3 H, 5) ppm. **$^{13}$C{$^1$H}-NMR** (100.6 MHz, $CD_2Cl_2$, 298 K): $\delta$ = 143.5 (4), 141.5 (2), 141.1 (10), 137.4 (9), 136.2 (3), 133.1 (6), 130.6 (7), 127.4 (8), 126.4 (12), 123.8 (15), 120.6 (14), 120.5 (13), 110.2 (11), 71.7 (1), 14.8 (5) ppm. **APCI-HRMS** calcd for $C_{23}H_{16}INS + H^+$ ($M+H^+$) 466.01209, found 466.01292.

***9-(4-(3-Methyl-5-((trimethylsilyl)ethynyl)thiophen-2-yl)phenyl)-9H-carbazole*** (**11**)

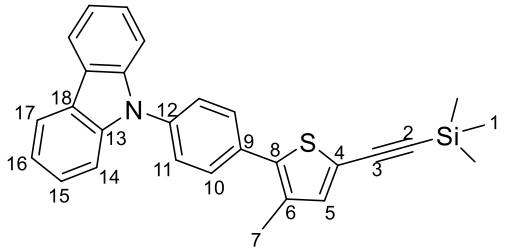


Under $N_2$-atmosphere **10** (470 mg, 1.0 mmol), TMS-Acetylene (280 $\mu$L, 2 mmol), $Pd(PPh_3)_4$ (23 mg, 0.02 mmol), CuI (19 mg, 0.1 mmol) and $NEt_3$ (3.5 mL, 25 mmol) were dissolved in 40 mL THF. After stirring for 5 h at rt, water was added, and the mixture was extracted with DCM. The separated organic layer was washed with brine and dried over $MgSO_4$. The solvent was removed under reduced pressure and the crude product was purified by column chromatography (silica, hex/DCM 4:1). **11** (400 mg, 92 %) was isolated as a colorless solid. **Mp** = 88 °C. **$R_f$** = 0.34 (hex/DCM 4:1). **UV-Vis** (DCM) $\lambda_{max}$ ($\varepsilon$) = 294 (58000), 327 (62900), 336 (58900, shoulder) nm. **Fluorescence** (DCM) $\lambda_{max}$ = 414 nm, $\Phi$ = 37 %. **IR** (ATR) = 2144 (m), 1450 (s), 1223 (s), 838 (s,sh). **$^1$H-NMR** (400 MHz, $CD_2Cl_2$, 298 K): $\delta$ = 8.16 (d, $^3J_{16,17}$ = 7.9 Hz, 2 arom. H, 17), 7.71 – 7.69 (m, 2 arom. H, 10), 7.65 – 7.63 (m, 2 arom. H, 11), 7.50 (d, $^3J_{14,15}$ = 8.1 Hz, 2 arom. H, 14), 7.46 – 7.42 (m, 2 arom. H, 15), 7.33 – 7.29 (m, 2 arom. H, 16), 7.13 (s, 1 arom. H, 5), 2.38 (s, 3 H, 7), 0.27 (s, 9 H, 1) ppm. **$^{13}$C{$^1$H}-NMR** (100.6 MHz, $CD_2Cl_2$, 298K): $\delta$ = 141.1 (13), 139.2 (8), 137.4 (12), 137.2 (5), 134.3 (6), 133.3 (9), 130.7 (10), 127.4 (11), 126.4 (15), 123.8 (18), 121.4 (4), 120.6 (17), 120.5 (16), 110.2 (14), 99.8 (2), 97.7 (3), 15.2 (7), – 0.1 (1) ppm. **APCI-HRMS** calcd for $C_{25}H_{25}NSSI + H^+$ ($M+H^+$) 436.15497, found 436.15543.

***9-(4-(5-Ethynyl-3-methylthiophen-2-yl)phenyl)-9H-carbazole*** (**12**)

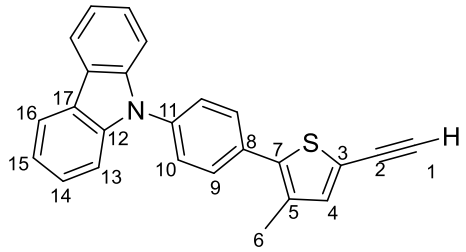


**11** (650 mg, 1.5 mmol) was dissolved in 32 mL THF and 32 mL MeOH . $K_2CO_3$ (230 mg, 1.7 mmol) was added and the reaction was stirred for 1 h at rt. Sat. $NH_4Cl_{(aq)}$ was added and the mixture was extracted with EtOAc. The separated organic layer was washed with sat. $NaHCO_{3(aq)}$, water, brine, and dried over $MgSO_4$. The solvent was removed under reduced pressure and the crude product was recrystallized out of MeOH. **12** (490 mg, 90 %) was isolated as a colorless solid. **Mp** = 151 °C. $\mathbf{R_f}$ = 0.28 (hex/DCM 4:1). **UV-Vis** (DCM) $\lambda_{max}$ ($\varepsilon$) = 293 (22100), 324 (19300), 337 (16300, shoulder) nm. **Fluorescence** (DCM) $\lambda_{max}$ = 410 nm, $\Phi$ = 31 %. **IR** (ATR) = 1511 (m), 1449 (s), 1230 (s), 833 (s). **$^1$H-NMR** (400 MHz, $CD_2Cl_2$, 298 K): $\delta$ = 8.16 (d, $^3J_{15,16}$ = 7.9 Hz, 2 arom. H, 16), 7.72 – 7.70 (m, 2 arom. H, 9), 7.66 – 7.64 (m, 2 arom. H, 10), 7.49 (d, $^3J_{13,14}$ = 8.1 Hz, 2 arom. H, 13), 7.46 – 7.42 (m, 2 arom. H, 14), 7.33 – 7.29 (m, 2 arom. H, 15), 7.18 (s, 1 arom. H, 4), 3.47 (s, 1 H, 1), 2.39 (s, 3 H, 6) ppm. **$^{13}$C{$^1$H}-NMR** (100.6 MHz, $CD_2Cl_2$, 298K): $\delta$ = 141.1 (12), 139.5 (7), 137.6 (4), 137.5 (11), 134.3 (5), 133.2 (8), 130.7 (9), 127.4 (10), 126.4 (14), 123.8 (17), 120.7 (16), 120.5 (15), 120.2 (3), 110.2 (13), 82.1 (1), 77.2 (2), 15.1 (6) ppm. **APCI-HRMS** calcd for $C_{25}H_{17}NS + H^+$ ($M + H^+$) 364.11545, found 364.11602.

***3,6-dibromo-9-(4-(3-methylthiophen-2-yl)phenyl)-9H-carbazole*** (**13**)

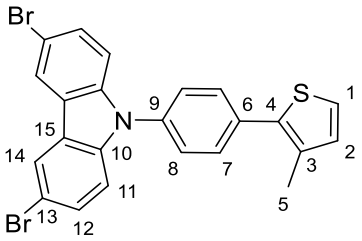


Under $N_2$-atmosphere **3** (161 mg, 0.42 mmol) and **9** (220 mg, 0.42 mmol)[98], $Pd(PPh_3)_4$ (48 mg, 0.04 mmol), CuI (16 mg, 0.08 mmol) and CsF (161 mg, 0.83 mmol) were dissolved in 8 mL DMF. The reaction was stirred for 3 h at rt. Water was added, and the mixture was extracted with DCM. Solvent was removed. A short chromatography on silica with hex:DCM 3:1 was made to remove yellow impurities. The separated organic layer was washed with brine and dried over $MgSO_4$. The solvent was removed under reduced pressure and crude product was purified by column chromatography (silica, hex/DCM 3:1). **13** (186 mg, 89 %) was isolated as a colorless solid. $\mathbf{R_f}$ = 0.54 (hex/DCM 3:1). **$^1$H-NMR** (400 MHz, $CD_2Cl_2$, 298 K): $\delta$ = 8.24 (d, $^4J_{12,14}$ = 1.9 Hz, 2 arom. H, 14), 7.73 – 7.71 (m, 2 arom. H, 7), 7.58 – 7.54 (m, 4 arom. H, 8, 12), 7.37 (d, $^3J_{11,12}$ = 8.8 Hz, 2 arom. H, 11), 7.30 (d, $^3J_{1,2}$ = 5.2 Hz, 1 arom. H, 1), 7.01 (d, $^3J_{1,2}$ = 5.2 Hz, 1 arom. H, 2), 2.43 (s, 3 H, 5) ppm. **$^{13}$C{$^1$H}-NMR** (100.6 MHz, $CD_2Cl_2$, 298K): $\delta$ = 140.3 (10), 136.9 (4), 135.9 (9), 135.1 (6), 134.5 (3), 131.8 (2), 130.8 (7), 129.8 (12), 127.3 (8), 124.4 (1, 13), 123.6 (14), 113.4 (15), 112.1 (11), 15.2 (5) ppm.

***4-(5-(4-(9H-Carbazol-9-yl)phenyl)-4-methylthiophen-2-yl)-7-bromobenzo[c][1,2,5]thiadiazole*** (**15a**)

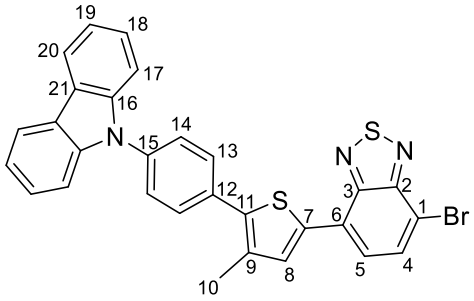


Under $N_2$-atmosphere **4a** (397 mg, 1.2 mmol) was dissolved in 30 mL THF and cooled to – 78 °C. *n*-BuLi (2.5 M in hexane) (468 µL, 1.2 mmol) was added over 5 min and the reaction was stirred for 30 min. Tributyltin chloride (380 µl, 1.4 mmol) was added, and reaction was allowed to warm up to rt. After 1 h, 10 mL sat. $KF_{(aq)}$ was added and the mixture was stirred for 16 h. The organic layer was separated, and the aqueous layer was extracted with ether. The combined organic layers were dried over $MgSO_4$ and solvent was removed under reduced pressure to isolated crude **5a** as a slightly yellowish oil. No further purification was made.

Under $N_2$-atmosphere **14** (382 mg, 1.3 mmol)[121], $Pd(PPh_3)_4$ (75 mg, 0.065 mmol), **5a** (803 mg, 1.2 mmol), CsF (395 mg, 2.6 mmol) and CuI (23 mg, 0.13 mmol) were suspended in 40 mL toluene. The reaction was heated to 80 °C for 16 h. The reaction was quenched with water and the mixture was extracted with $Et_2O$. The organic phase was washed with water, brine, and dried over $MgSO_4$. The solvent was removed and the crude product was purified by column chromatography (silica, hex/DCM 1:1) and recrystallized out of MeOH. **15a** (330 mg, 50 %) was isolated as an orange solid. **Mp** = 237 °C. $R_f$ = 0.22 (hexane/DCM 1:1). **UV-Vis** (DCM) $\lambda_{max}$ ($\varepsilon$) = 294 (38900), 316 (37700), 338 (25900, shoulder), 439 (17400) nm. **Fluorescence** (DCM) $\lambda_{max}$ = 619 nm, $\Phi$ = 39 %. **IR** (ATR) = 2955 (w), 2936 (w), 2868 (w), 1490 (m), 1456 (s), 1198 (s). **$^1$H-NMR** (700 MHz, $CD_2Cl_2$, 298 K): $\delta$ = 8.17 (d, $^3J_{19,20}$ = 7.7 Hz, 2 arom. H, 20), 8.03 (s, 1 arom. H, 8), 7.89 (d, $^3J_{4,5}$ = 7.7 Hz, 1 arom. H, 4), 7.82 – 7.81 (m, 2 arom. H, 13), 7.77 (d, $^3J_{4,5}$ = 7.7 Hz, 1 arom. H, 5), 7.69 – 7.68 (m, 2 arom. H, 14), 7.52 (d, $^3J_{17,18}$ = 8.0 Hz, 2 arom. H, 17), 7.46 – 7.44 (m, 2 arom. H, 18), 7.32 – 7.30 (m, 2 arom. H, 19), 2.53 (s, 3 H, 10) ppm. **$^{13}$C{$^1$H}-NMR**

(176.1 MHz, $CD_2Cl_2$, 298K): $\delta$ = 154.3 (2), 152.2 (3). 141.1 (16), 139.5 (11), 137.3 (15), 136.8 (7), 135.4 (9), 133.8 (12), 132.8 (8), 132.7 (4), 130.6 (13), 127.5 (14), 127.2 (6), 126.4 (18), 125.8 (5), 123.8 (21), 120.7 (20), 120.5 (19), 112.5 (1), 110.2 (17), 15.6 (10) ppm. **ESI-HRMS** calcd for $C_{29}H_{18}BrN_3S_2^{\bullet+}$ ($M^{\bullet+}$) 551.01200, found 551.01228.

***4-Bromo-7-(5-(4-(3,6-dibutoxy-9H-carbazol-9-yl)phenyl)-4-methylthiophen-2-yl)benzo[c][1,2,5]thiadiazole*** (**15b**)

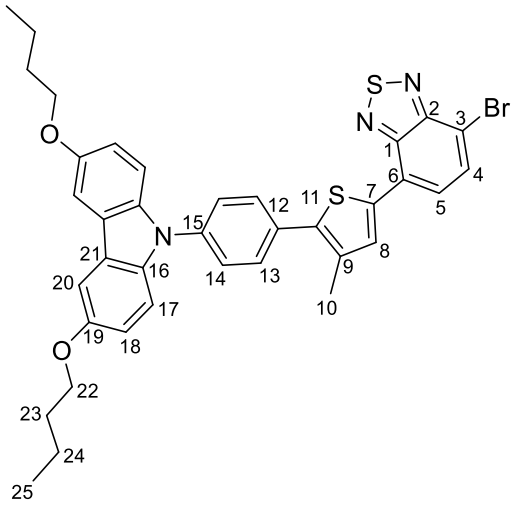


Under $N_2$-atmosphere **4b** (48 mg, 0.10 mmol) was dissolved in 3 mL THF and cooled to – 78 °C. *n*-BuLi (2.5 M in hexane) (41 $\mu$L, 0.10 mmol) was added over 5 min and the reaction was stirred for 30 min. Tributyltin chloride (33 $\mu$l, 0.12 mmol) was added and reaction was allowed to warm up to rt. After 1 h 1 mL sat. $KF_{(aq)}$ was added and the mixture was stirred for 16 h. The organic layer was separated, and the aqueous layer was extracted with ether. The combined organic layers were dried over $MgSO_4$ and solvent was removed under reduced pressure to isolated crude **5b** as a slightly yellowish oil. No further purification was made.

Under $N_2$-atmosphere **14** (34 mg, 0.11 mmol)[121], $Pd(PPh_3)_4$ (7 mg, 0.01 mmol), **5b** (80 mg, 0.10 mmol), CuI (2 mg, 0.01 mmol) and CsF (35 mg, 0.23 mmol) were suspended in 3 mL toluene. The reaction was heated to 80°C for 4 h. The reaction was cooled to rt and water was added. The mixture was extracted with DCM. The organic layer was separated, washed with brine and dried over $MgSO_4$. The solvent was removed under reduced pressure and the crude product was purified by column chromatography (silica, hex/DCM

1:1). **15b** (20 mg, 29 %) was isolated as an orange solid. **Mp** = 150 °C. **$R_f$** = 0.10 (hexane/DCM 1:1). **UV-Vis** (DCM) $\lambda_{max}$ ($\varepsilon$) = 312 (29200), 320 (19500, shoulder), 372 (4130), 444 (9550) nm.[128] **IR** (ATR) = 1458 (s), 1326 (m), 1166 (s), 812 (s). **$^1$H-NMR** (400 MHz, $CD_2Cl_2$, 298 K): $\delta$ = 8.03 (s, 1 arom. H, 8), 7.88 (d, $^3J_{4,5}$ = 7.8 Hz, 1 arom. H, 4), 7.79 – 7.76 (m, 3 arom. H, 5, 13), 7.66 – 7.64 (m, 2 arom. H, 14), 7.56 (d, $^4J_{18,20}$ = 2.5 Hz, 2 arom. H, 20), 7.43 (d, $^3J_{17,18}$ = 8.9 Hz, 2 arom. H, 17), 7.05 (dd, $^3J_{17,18}$ = 8.9 Hz, $^4J_{18,20}$ = 2.5 Hz, 2 arom. H, 18), 4.10 (t, $^3J_{22,23}$ = 6.6 Hz, 4 H, 22), 2.51 (s, 3 H, 10), 1.87 – 1.80 (m, 4 H, 23), 1.61 – 1.51 (m, 4 H, 24), 1.02 (t, $^3J_{24,25}$ = 7.4 Hz, 6 H, 25) ppm. **$^{13}$C{$^1$H}-NMR** (100.6 MHz, $CD_2Cl_2$, 298 K): $\delta$ = 154.2 (2), 154.1 (19), 152.2 (1), 139.6 (11), 137.9 (15), 136.6 (7), 136.3 (16), 135.3 (9), 133.1 (12), 132.8 (8), 132.7 (4), 130.5 (13), 127.2 (6), 126.8 (14), 125.7 (5), 124.2 (21), 116.0 (18), 112.4 (3), 111.0 (17), 104.1 (20), 69.0 (22), 32.0 (23), 19.8 (24), 15.6 (10), 14.1 (25) ppm. **APCI-HRMS** calcd for $C_{37}H_{34}BrN_3O_2S_2$ + $H^+$ ($M + H^+$) 696.13486, found 696.13608.

***5-(7-((Trimethylsilyl)ethynyl)benzo[c][1,2,5]thiadiazol-4-yl)thiophene-2-carbaldehyde*** (**18**)

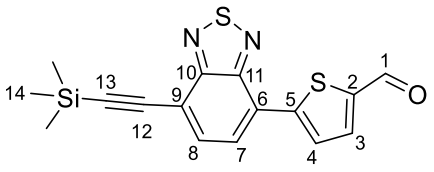


Under $N_2$-atmosphere **17** (110 mg, 0.34 mmol)[101], TMS-Acetylene (95 $\mu$L, 0.68 mmol), $Pd(PPh_3)_4$ (8 mg, 0.007 mmol), CuI (6 mg, 0.03 mmol) and $NEt_3$ (1.2 mL, 8.5 mmol) were dissolved in 15 mL THF. The reaction was stirred for 5 h at 60°C. After cooling to rt, water was added, and the mixture was extracted with DCM. The separated organic layer was washed with brine and dried over $MgSO_4$. The solvent was removed under reduced pressure and crude product was purified by column chromatography (silica, hex/DCM 1:4). **18** (97 mg, 83 %) was isolated as a yellow solid. **Mp** = 143 °C. **$R_f$** = 0.23 (hex/DCM 1:4). **UV-Vis** (DCM) $\lambda_{max}$ ($\varepsilon$) = 318 (20800), 414 (22000) nm. **Fluorescence** (DCM) $\lambda_{max}$ = 504 nm, $\Phi$ = 27 %. **IR** (ATR) = 2148 (w), 1662 (m), 1446 (m), 835 (s). **$^1$H-NMR** (400 MHz, $CD_2Cl_2$, 298 K): $\delta$ = 9.96 (s, 1 H, 1), 8.20 (d, $^3J_{3,4}$ = 4.0 Hz, 1 arom. H, 4), 7.96 (d, $^3J_{7,8}$ = 7.4 Hz, 1 arom. H, 7), 7.85 (d,

$^3J_{3,4}$ = 4.0 Hz, 1 arom. H, 3), 7.81 (d, $^3J_{7,8}$ = 7.4 Hz, 1 arom. H, 8), 0.34 (s, 9 H, 14) ppm. **$^{13}$C{$^1$H}-NMR** (100.6 MHz, $CD_2Cl_2$, 298K): $\delta$ = 183.4 (1), 155.5 (10), 152.0 (11), 148.0 (5), 144.6 (2), 137.0 (3), 133.8 (8), 129.0 (4), 127.0 (7), 126.9 (6) 117.5 (9), 103.7 (12), 100.5 (13), – 0.1 (14)ppm. **ESI-HRMS** calcd for $C_{16}H_{14}N_2OS_2Si$ + $Na^+$ ($M+Na^+$) 365.02090, found 365.02140.

***3-Iodo-2,2'-dimethoxy-1,1'-binaphthalene*** (**22(*S*)**)

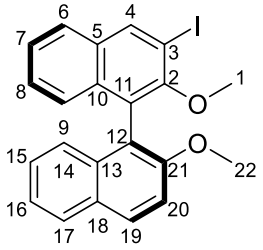


Under $N_2$-atmosphere **20(*S*)** (200 mg, 0.64 mmol)[102] was dissolved in 11 mL THF. The solution was cooled to 0 °C and *n*-BuLi (2.5 M in hexane, 0.31 mL, 0.76 mmol) was added over 5 min. The solution was stirred for 5 h at 0 °C and then cooled to –78 °C. A solution of $I_2$ (194 mg, 0.76 mmol) in 1 mL THF was added dropwise over 1 min and the solution was allowed to warm to rt. The reaction was stirred for 16 h, then quenched with sat. $NaS_2O_{3(aq)}$. The mixture was extracted with EtOAc. The organic layer was washed with brine and dried over $MgSO_4$. The solvent was removed, and the crude product was purified by column chromatography (silica, hex/DCM 1:1). **22(*S*)** (140 mg, 50 %) was isolated as a colorless solid. **$^1$H-NMR** (400 MHz, $CD_2Cl_2$, 298 K): $\delta$ = 8.52 (s, 1 arom. H, 4), 8.06 (d, $^3J_{19,20}$ = 9.2 Hz, 1 arom. H, 20), 7.90 (d, $^3J_{14,15}$ = 8.1 Hz, 1 arom. H, 14), 7.80 (d, $^3J_{8,9}$ = 8.1 Hz, 1 arom. H, 9), 7.50 (d. $^3J_{19,20}$ = 9.2 Hz, 1 arom. H, 19), 7.42 – 7.38 (m, 1 arom. H, 8), 7.36 – 7.32 (m, 1 arom. H, 15), 7.27 – 7.22 (m, 2 arom. H, 7, 16), 7.08 – 7.02 (m, 2 arom. H, 6, 17), 3.81 (s, 3 H, 22), 3.40 (s, 3 H, 1) ppm. **$^{13}$C{$^1$H}-NMR** (100.6 MHz, $CD_2Cl_2$, 298K): $\delta$ = 155.2 (21), 154.8 (2), 139.5 (4). 134.5 (13), 134.1 (11), 132.8 (10), 130.6 (20), 129.4 (18), 128.4 (14), 127.3 (9), 127.1 (7, 16), 126.4 (5), 126.0 (8), 125.9 (6/17), 125.2 (6/17). 124.1 (15), 118.8 (12), 113.6 (19), 92.9 (3), 61.1 (1), 56.6 (22) ppm. **ESI-HRMS** calcd for $C_{22}H_{17}IO_2$ + $Na^+$ ($M$ + $Na^+$) 463.01655, found 463.01642. Full characterization corresponds with reported literature.[103]

***((2,2'-Dimethoxy-[1,1'-binaphthalen]-3-yl)ethynyl)triisopropylsilane*** (**23(*S*)**)

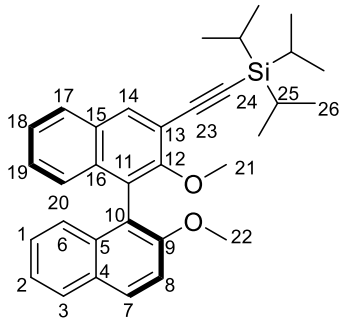


Under $N_2$-atmosphere **22(*S*)** (150 mg, 0.33 mmol), tri-*iso*propylsilylacetylene (73 mg, 0.40 mmol), CuI (3 mg, 0.015 mmol), and $Pd(PPh_3)_4$ (63 mg, 0.055 mmol) was dissolved in $NEt_3$ (3.0 mL, 22 mmol) and 3 mL DMF. The reaction was heated to 50 °C for 8 h. After cooling to rt the reaction was quenched with water and the mixture was extracted with EtOAc. The organic layer was washed with brine and dried over $MgSO_4$. The solvent was removed under reduced pressure and the crude product was purified by column chromatography (silica, hex/DCM 3:2). **23(*S*)** (133 mg, 81 %) was isolated as a colorless solid. **Mp** = 125 °C. $R_f$ = 0.22 (hexane/DCM 3:2). **UV-Vis** (DCM) $\lambda_{max}$ ($\varepsilon$) = 259 (59700), 284 (14800), 294 (16100), 302 (11100, shoulder), 337 (4120) nm. **Fluorescence** (DCM) $\lambda_{max}$ = 382 nm, $\Phi$ = 24 %. **[α]$^{22}$** = –58.0 (c = 0.1, DCM). **IR** (ATR) = 2941 (m, sh), 2890 (w), 2862 (m), 1265 (s), 1247 (s), 668 (s). **$^1$H-NMR** (400 MHz, $CD_2Cl_2$, 298 K): $\delta$ = $^1$H-NMR (400 MHz, $CD_2Cl_2$, 300 K): $\delta$ = 8.16 (s, 1 arom. H, 14), 8.04 (d, $^3J_{7,8}$ = 9.1 Hz, 1 arom. H, 7), 7.90 (d, $^3J_{2,3}$ = 8.4 Hz, 1 arom. H, 3), 7.85 (d, $^3J_{17,18}$ = 8.4 Hz, 1 arom. H, 17), 7.50 (d, $^3J_{7,8}$ = 9.1 Hz, 1 arom. H, 8), 7.42 – 7.38 (m, 1 arom. H, 18), 7.35 – 7.31 (m, 1 arom. H, 2), 7.25 – 7.21 (m, 2 arom. H, 1, 19), 7.06 – 7.03 (m, 2 arom. H, 6, 20), 3.81 (s, 3 H, 22), 3.63 (s, 3 H, 21), 1.18 (s, 21 H, 25, 26) ppm. **$^{13}$C{$^1$H}-NMR** (100.6 MHz, $CD_2Cl_2$, 298K): $\delta$ = 156.2 (12), 155.2 (9), 135.0 (14), 134.4 (5), 130.7 (16), 130.2 (7), 129.4 (4), 128.4 (3), 128.1 (17), 127.5 (19), 126.9 (1), 126.1 (15), 125.9 (20), 125.7 (18), 125.3 (6), 124.0 (2), 118.8 (10), 118.0 (11, 13), 113.7 (8), 104.1 (23), 95.8 (24), 61.2 (21), 56.6 (22), 18.9 (25/26), 11.9 (25/26) ppm. **ESI-HRMS** calcd for $C_{33}H_{38}O_2Si + Na^+$ (M + $Na^+$) 517.25333, found 517.25338.

***2,2'-Dimethoxy-3'-((triisopropylsilyl)ethynyl)-[1,1'-binaphthalene]-3-carbaldehyde*** (**24(*S*)**)

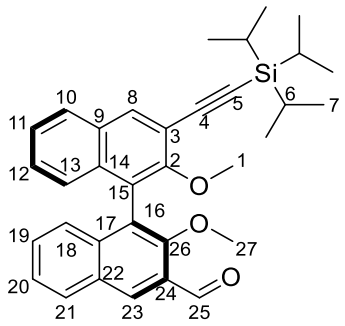


Under $N_2$-atmosphere **23(*S*)** (71 mg, 0.14 mmol) was dissolved in 0.5 mL TMEDA. *n*-BuLi (2.5 M in hexane, 75 µL, 0.19 mmol) was added dropwise over 2 min and the reaction was stirred for 2 h at rt. DMF (0.5 mL, 6.5 mmol) was added. The solution was stirred for 16 h before 2 mL 1 M $HCl_{(aq)}$ was added. The mixture was extracted with EtOAc and the organic layer was washed with sat. $NaHCO_{3(aq)}$ and brine and dried over $MgSO_4$. The solvent was removed under reduced pressure, and the crude product was purified by column chromatography (silica, hex/$Et_2O$ 6:1). **24(*S*)** (71 mg, 97 %) was isolated as a colorless solid. **Mp** 68 °C. $R_f$ = 0.32 (hexane/$Et_2O$ 3:2). **UV-Vis** (DCM) $\lambda_{max}$ ($\varepsilon$) = 259 (100000), 286 (17000, shoulder), 296 (20600), 306 (16700), 347 (2910) nm. **Fluorescence** (DCM) $\lambda_{max}$ = 446 nm, $\Phi$ = 1 %. **[α]$^{22}$** = –22.6 (c = 0.1, DCM). **IR** (ATR) = 2942 (w, br), 2863 (w), 1690 (m), 1102 (s), 750 (s). **$^1$H-NMR** (400 MHz, $CD_2Cl_2$, 298 K): $\delta$ = 10.53 (s, 1 H, 25), 8.57 (s, 1 arom. H, 23), 8.23 (s, 1 arom. H, 8), 8.08 (d, $^3J_{18,19}$ = 8.2 Hz, 1 arom. H, 18), 7.89 (d, $^3J_{12,13}$ = 8.2 Hz, 1 arom. H, 13), 7.50 – 7.46 (m, 1 arom. H, 19), 7.45 – 7.41 (m, 1 arom. H, 12), 7.40 – 7.36 (m, 1 arom. H, 20), 7.31 – 7.26 (m, 1 arom. H, 11), 7.15 – 7.08 (m, 2 arom. H, 10; 21), 3.68 (s, 3 H, 1), 3.50 (s, 3 H, 27), 1.18 (s, 21 H, 6, 7) ppm. **$^{13}$C{$^1$H}-NMR** (100.6 MHz, $CD_2Cl_2$, 298K): $\delta$ = 190.7 (25), 156.9 (26), 156.4 (2), 137.5 (16), 135.9 (8), 134.2 (15), 132.1 (23), 130.6 (21, 14), 130.4 (22, 17), 129.5 (20), 129.1 (24), 128.3 (10), 127.9 (11), 126.2 (19), 126.0 (18) 125.9 (12, 13), 124.6 (9), 117.9 (3), 103.8 (4), 96.5 (5), 63.2 (27), 61.4 (1), 18.9 (6/7), 11.8 (6/7) ppm. **ESI-HRMS** calcd for $C_{34}H_{38}O_3Si + Na^+$ (M + $Na^+$) 545.24824, found 545.24847.

***((2,2'-dimethoxy-[1,1'-binaphthalene]-3,3'-diyl)bis(ethyne-2,1-diyl))bis(trimethylsilane)*** (**27(*S*)**)

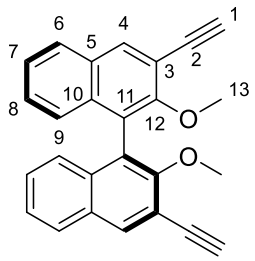


Under $N_2$-atmosphere **26(*S*)** (200 mg, 0.35 mmol), $Pd(PPh_3)_4$ (8 mg, 0.007 mmol), CuI (8 mg, 0.04 mmol), $NEt_3$ (1 mL, 7.7 mmol) and TMS-acetylene (145 $\mu$L, 1.05 mmol) were dissolved in 10 mL THF. The reaction was stirred for 20 h at 60 °C. After cooling to rt water was added, and the mixture was extracted with EtOAc. The separated organic layer was washed with brine and dried over $MgSO_4$. The solvent was removed under reduced pressure.

The crude product and TBAF (183 mg, 0.7 mmol) was dissolved in 10 mL THF. The solution was stirred for 10 min at rt. Water was added, and the mixture was extracted with EtOAc. The organic layer was washed with brine and dried over $MgSO_4$. The solvent was removed under reduced pressure and the crude product was purified by column chromatography (silica, hex/EtOAc 19:1). **27(*S*)** (106 mg, 91 %) was isolated as a colorless solid. $R_f$ = 0.20 (hex/EtOAc 19:1). **$^1$H-NMR** (400 MHz, $CDCl_3$, 298 K): $\delta$ = 8.19 (s, 2 arom. H, 4), 7.83 (d, $^3J_{8,9}$ = 8.4 Hz, 2 arom. H, 9), 7.40 – 7.35 (m, 2 arom. H, 8), 7.26 – 7.22 (m, 2 arom. H, 7 and $CDCl_3$), 7.09 (d, $^3J_{6,7}$ = 8.5 Hz, 2 arom. H, 6), 3.66 (s, 6 H, 13), 3.35 (s, 1 H, 1) ppm. **$^{13}$C{$^1$H}-NMR** (100.6 MHz, $CDCl_3$, 298K): $\delta$ = 156.0 (12), 135.4 (4), 134.1 (11), 130.1 (10), 127.9 (9), 127.6 (7), 125.8 (6), 125.5 (8), 125.0 (5), 116.3 (3), 81.7 (1), 80.6 (2), 61.3 (13) ppm.

***3'-((7-(5-(4-(9H-Carbazol-9-yl)phenyl)-4-methylthiophen-2-yl)benzo[c][1,2,5]thiadiazol-4-yl)ethynyl)-2,2'-dimethoxy-[1,1'-binaphthalene]-3-carbaldehyde*** (**28(*S*)a**)

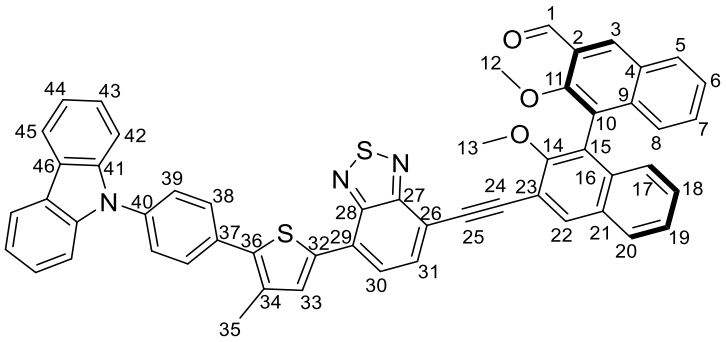

**24(*S*)** (117 mg, 0.22 mmol) was dissolved under $N_2$-atmosphere in 50 mL THF. The solution was cooled to 0 °C and TBAF (77 mg, 0.25 mmol) was added. After stirring for 15 min at 0 °C, the reaction was quenched with water. The mixture was extracted with EtOAc. The organic layer was washed with brine and dried over $MgSO_4$. The solvent was removed, and the crude product was filtered through a silica plug while dissolved in $Et_2O$. After removing the solvent under reduced pressure, crude **25(*S*)** was isolated as a colorless solid and then carried on to the next reaction without further purification.

Under $N_2$-atmosphere **15a** (106 mg, 0.19 mmol), **25(*S*)** (70 mg, 0.14mmol), $Pd(PPh_3)_4$ (22 mg, 0.019 mmol), CuI (2 mg, 0.011 mmol) and $NEt_3$ (0.5 mL, 3.6 mmol) were dissolved in 5 mL THF. The reaction was heated to 60 °C for 16 h. Water was added, and the mixture was extracted with DCM. The organic layer was washed with brine and dried over $MgSO_4$. The solvent was removed under reduced pressure and the crude product was purified by column chromatography (silica, Hex/DCM 1:3) and recrystallized out of MeOH. **28(*S*)a** (88 mg, 75 %) was isolated as an orange solid. **Mp** = 175 °C, decomposition. $R_f$ = 0.21 (hexane/DCM 1:3). **UV-Vis** (DCM) $\lambda_{max}$ ($\varepsilon$) = 293 (20500), 332 (20100), 339 (19700), 344 (19000, shoulder), 467 (13400) nm. **Fluorescence** (DCM) $\lambda_{max}$ = 615 nm, $\Phi$ = 54 %. $[\alpha]^{22}$ = –30.6 (c = 0.1, DCM). **IR** (ATR) = 3051 (w, br), 2940 (w, br), 2862 (w, br), 2839 (w, br), 1687 (m), 1449 (m), 747 (s). **$^1$H-NMR** (700 MHz, $CD_2Cl_2$, 298 K): $\delta$ = 10.56 (s, 1 H, 1), 8.60 (s, 1 arom. H, 3), 8.41 (s, 1 arom. H, 22), 8.17 (d, $^3J_{44,45}$ = 7.7 Hz, 2 arom. H, 45), 8.10 (d, $^3J_{7,8}$ = 8.5 Hz, 1 arom. H, 8), 8.08 (s, 1 arom. H, 33), 7.96 (d,

$^3J_{17,18}$ = 8.5 Hz, 1 arom. H, 17), 7.89 – 7.86 (m, 2 arom. H, 30, 31), 7.82 – 7.80 (m, 2 arom. H, 39), 7.67 – 7.66 (m, 2 arom. H, 38), 7.52 – 7.49 (m, 3 arom. H, 7; 42), 7.48 – 7.46 (m, 1 arom. H, 18), 7.45 – 7.43 (m, 2 arom. H, 43), 7.42 – 7.40 (m, 1 arom. H, 19), 7.34 – 7.30 (m, 3 arom. H, 6; 44), 7.25 – 7.23 (m, 1 arom. H, 5), 7.17 – 7.15 (m, 1 arom. H, 20), 3.90 (s, 3 H, 13), 3.57 (s, 3 H, 12), 2.52 (s, 3 H, 35) ppm. **$^{13}C\{^1H\}$-NMR** (176.1 MHz, $CD_2Cl_2$, 298K): $\delta$ = 190.7 (1), 156.9 (11), 156.2 (14), 155.7 (27), 152.1 (28), 141.1 (41), 139.9 (35), 137.4 (10), 137.3 (37), 137.2 (32), 135.5 (22), 135.4 (34), 134.4 (15), 133.7 (40), 133.3 (31), 133.1 (33), 132.1 (3), 130.7 (8/17), 130.6 (16), 130.5 (39), 130.3 (9), 129.6 (6), 129.1 (2), 128.5 (8/17), 128.1 (19), 127.9 (29), 127.4 (38), 126.4 (43), 126.3 (7), 126.1 (4), 126.0 (18; 5), 125.9 (20), 125.0 (30), 124.7 (21), 123.8 (46), 120.6 (45), 120.5 (44), 117.2 (23), 115.2 (26), 110.2 (42), 93.3 (24), 90.9 (25), 63.2 (12), 61.9 (13), 15.6 (36) ppm. **APCI-HRMS** calcd for $C_{54}H_{35}N_3O_3S_2$ + $H^+$ (M + $H^+$) 838.21926, found 838.22087.

***3'-((7-(5-(4-(3,6-Dibutoxy-9H-carbazol-9-yl)phenyl)-4-methylthiophen-2-yl)benzo[c][1,2,5]thiadiazol-4-yl)ethynyl)-2,2'-dimethoxy-[1,1'-binaphthalene]-3-carbaldehyde*** (**28(*S*)b**)

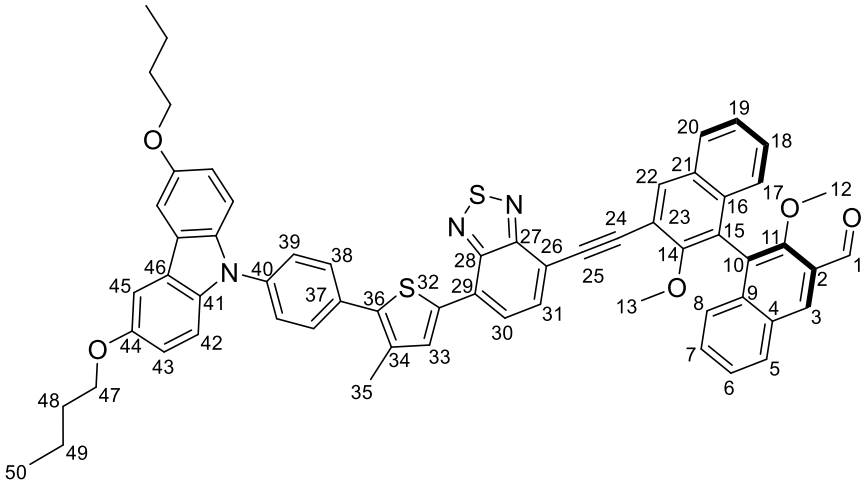


**24(*S*)** (117 mg, 0.22 mmol) was dissolved under $N_2$-atmosphere in 50 mL THF. The solution was cooled to 0 °C and TBAF (77 mg, 0.25 mmol) was added. After stirring for 15 min at 0 °C, the reaction was quenched with water. The mixture was extracted with EtOAc. The organic layer was washed with brine and dried over $MgSO_4$. The solvent was removed, and the crude product was filtered through a silica plug while dissolved in $Et_2O$. After removing the solvent under reduced

pressure, crude **25(*S*)** was isolated as a colorless solid and then carried on to the next reaction without further purification.

Under $N_2$-atmosphere **15b** (85 mg, 0.12 mmol), $Pd(PPh_3)_4$ (14 mg, 0.012 mmol), **25(*S*)** (67 mg, 0.18 mmol), CuI (2 mg, 0.011 mmol) and $NEt_3$ (0.4 mL, 2.9 mmol) were suspended in 5 mL THF. The reaction was heated to 60°C overnight. The reaction was cooled to rt and water was added. The mixture was extracted with DCM. The organic layer was separated, washed with brine, and dried over $MgSO_4$. The solvent was removed under reduced pressure and the crude product was purified by column chromatography (silica, hex/DCM 1:2). **28(*S*)b** (106 mg, 90 %) was isolated as a red solid. **Mp** = 135 °C, decomposition. **$R_f$** = 0.30 (hexane/DCM 1:3). **UV-Vis** (DCM) $\lambda_{max}$ ($\varepsilon$) = 300 (41600, shoulder), 312 (48500), 335 (39700), 370 (18600, shoulder), 471 (27000) nm. **Fluorescence** (DCM) $\lambda_{max}$ = 665 nm, $\Phi$ = 1 %. **$[\alpha]^{22}$** = –28.2 (c = 0.1, DCM). **IR** (ATR) = 1689 (m), 1454 (s), 1196 (m), 749 (m). **$^1$H-NMR** (700 MHz, $CD_2Cl_2$, 298 K): $\delta$ = 10.56 (s, 1 H, 1), 8.60 (s, 1 arom. H, 3), 8.40 (s, 1 arom. H, 22), 8.09 (d, $^3J_{7,8}$ = 8.2 Hz, 1 arom. H, 8), 8.05 (s, 1 arom. H, 33), 7.96 (d, $^3J_{17,18}$ = 8.1 Hz, 1 arom. H, 17), 7.84 (s, 2 arom. H, 30, 31), 7.76 – 7.75 (m, 2 arom. H, 38), 7.63 – 7.62 (m, 2 arom. H, 39), 7.56 (d, $^4J_{43,45}$ = 2.5 Hz, 2 arom. H, 45), 7.51 – 7.48 (m, 1 arom. H, 7), 7.47 – 7.45 (m, 1 arom. H, 18), 7.42 – 7.39 (m, 3 arom. H, 6, 42), 7.34 – 7.32 (m, 1 arom. H, 19), 7.24 (d, $^3J_{5,6}$ = 8.8 Hz, 1 arom. H, 5), 7.16 (d, $^3J_{19,20}$ = 8.6 Hz, 1 arom. H, 20), 7.04 (dd, $^3J_{42,43}$ = 8.8 Hz, $^4J_{43,45}$ = 2.5 Hz, 2 arom. H, 43), 4.10 (t, $^3J_{47,48}$ = 6.6 Hz, 4 H, 47), 3.90 (s, 3 H, 13), 3.57 (s, 3 H, 12), 2.49 (s, 3 H, 35), 1.86 – 1.82 (m, 4 H, 48), 1.59 – 1.54 (m, 4 H, 49), 1.03 (t, $^3J_{49,50}$ = 7.5 Hz, 6 H, 50) ppm. **$^{13}$C{$^1$H}-NMR** (176.1 MHz, $CD_2Cl_2$, 298K): $\delta$ = 190.7 (1), 156.9 (11), 156.2 (14), 155.7 (27), 154.1 (44), 152.1 (28), 140.0 (36), 137.9 (40), 137.4 (10), 137.1 (32), 136.2 (41), 135.4 (22), 135.3 (34), 134.4 (15), 133.3 (31), 133.1 (33), 133.0 (37), 132.1 (3), 130.7 (8), 130.6 (16), 130.40 (38), 130.35 (9), 129.6 (6), 129.1 (2), 128.5 (17), 128.1 (19), 127.9 (29), 126.8 (39), 126.3 (7), 126.1 (4), 126.0 (20, 5), 125.9 (18), 124.9 (30), 124.7 (21), 124.2 (46), 117.2 (23), 116.0 (43), 115.1 (26), 111.0 (42), 104.2 (45), 93.3 (24), 91.0 (25), 69.0 (47), 63.2 (12), 61.9 (13), 32.0 (48), 19.8 (49), 15.6 (35), 14.1 (50) ppm. **ESI-HRMS** calcd for $C_{62}H_{51}N_3O_5S_2Na^+$ ($M + Na^+$) 1004.31623, found 1004.31570.

***3'-((7-(5-(4-(3,6-Dibutoxy-9H-carbazol-9-yl)phenyl)-4-methylthiophen-2-yl)benzo[c][1,2,5]thiadiazol-4-yl)ethynyl)-2,2'-dimethoxy-[1,1'-binaphthalene]-3-carbaldehyde*** (**30(*S*)a**)

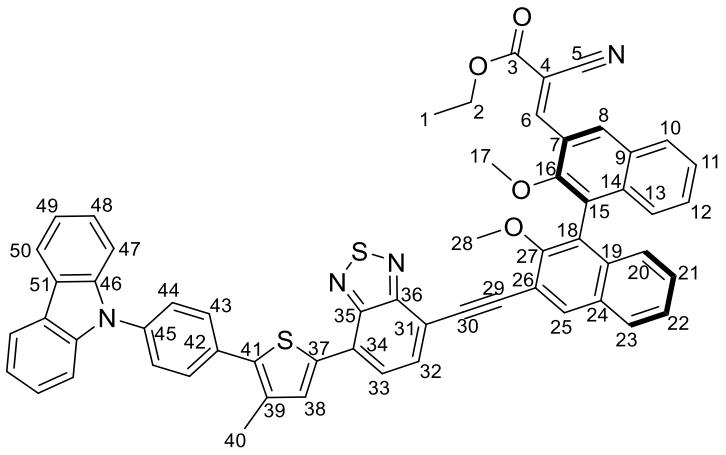

**28(*S*)a** (25 mg, 0.030 mmol) was dissolved in 10 mL DCM. EtOAc (65 $\mu$L, 0.61 mmol) and piperidine (12 $\mu$L, 0.12 mmol) were added and the reaction was stirred for 64 h at rt. The reaction was quenched with water and the mixture was extracted with DCM. The organic layer was washed with brine and dried over $MgSO_4$. The solvent was removed under reduced pressure and the crude product was purified by column chromatography (silica, hexane/DCM 1:3) and recrystallized out of MeOH. **30(*S*)a** (24 mg, 86 %) was isolated as an orange solid. **Mp** 168 °C. $R_f$ = 0.29 (hexane/DCM 1:3). **UV-Vis** (DCM) $\lambda_{max}$ ($\varepsilon$) = 260 (26200, shoulder), 269 (20700), 286 (18900), 292 (18200) 333 (23400), 339 (23200, shoulder), 466 (11600) nm. **Fluorescence** (DCM) $\lambda_{max}$ = 620 nm, $\Phi$ = 47 %. **[α]$^{22}$** = 122.2 (c = 0.1, DCM). **IR** (ATR) = 3059 (vw, br), 2980 (vw, br), 2941 (vw, br), 2224 (w, sh), 1722 (m), 1449 (s), 1229 (s), 747 (s). **$^1$H-NMR** (700 MHz, $CD_2Cl_2$, 298 K): $\delta$ = 9.01 (s, 1 arom. H, 8), 8.81 (s, 1 arom. H, 6), 8.42 (s, 1 arom. H, 25), 8.17 (d, $^3J_{49,50}$ = 7.8 Hz, 2 arom. H, 50), 8.13 (s, 1 arom. H, 38), 8.09 (d, $^3J_{12,13}$ = 8.2 Hz, 1 arom. H, 13), 7.98 (d, $^3J_{20,21}$ = 8.2 Hz, 1 arom. H, 20), 7.95 – 7.92 (m, 2 arom. H, 32, 33), 7.84 – 7.83 (m, 2 arom. H, 44), 7.70 – 7.69 (m, 2 arom. H, 43), 7.53 – 7.51 (m, 3 arom. H, 12, 47), 7.49 – 7.47 (m, 1 arom. H, 21), 7.46 – 7.44 (m, 2 arom. H, 48), 7.42 – 7.40 (m, 1 arom. H, 11), 7.35 – 7.31 (m, 3 arom. H, 22; 49), 7.22 – 7.20 (m, 1 arom. H, 10), 7.15 – 7.14 (m, 1 arom. H, 23), 4.41 (q, $^3J_{1,2}$ = 7.4 Hz, 2 H, 2), 3.89 (s, 3 H, 28), 3.46 (s, 3 H, 17), 2.55 (s, 3 H, 40), 1.42 (t, $^3J_{1,2}$ = 7.4 Hz, 3 H, 1) ppm. **$^{13}$C{$^1$H}-NMR** (176.1 MHz, $CD_2Cl_2$, 298K):

$\delta$ = 162.8 (3), 156.2 (27), 155.8 (36), 155.2 (16), 152.3 (35), 150.6 (6), 141.1 (46), 139.9 (41), 137.4 (42), 137.3 (37), 136.7 (15), 135.6 (39), 135.5 (25), 134.3 (18), 133.8 (45), 133.4 (32), 133.2 (38), 131.7 (8), 130.7 (19), 130.6 (44), 130.5 (14), 130.0 (13), 129.5 (11), 128.5 (20), 128.2 (22), 128.0 (34), 127.5 (43), 126.4 (12, 48), 126.1 (21), 126.06 (10), 125.96 (23), 125.7 (7), 125.6 (9), 125.1 (33), 124.7 (24), 123.8 (51), 120.7 (50), 120.5 (49), 117.2 (26), 116.1 (5), 115.3 (31), 110.2 (47), 105.1 (4) 93.3 (29), 90.9 (30), 63.2 (2), 62.8 (17), 61.9 (28), 15.6 (40), 14.4 (1) ppm. **ESI-HRMS** calcd for $C_{59}H_{40}N_4O_4S_2$ + $Na^+$ (M + $Na^+$) 955.23832, found 955.23804.

***Ethyl (E)-2-cyano-3-(3'-((7-(5-(4-(3,6-dibutoxy-9H-carbazol-9-yl)phenyl)-4-methylthiophen-2-yl)benzo[c][1,2,5]thiadiazol-4-yl)ethynyl)-2,2'-dimethoxy-[1,1'-binaphthalen]-3-yl)acrylate*** (**30(*S*)b**)

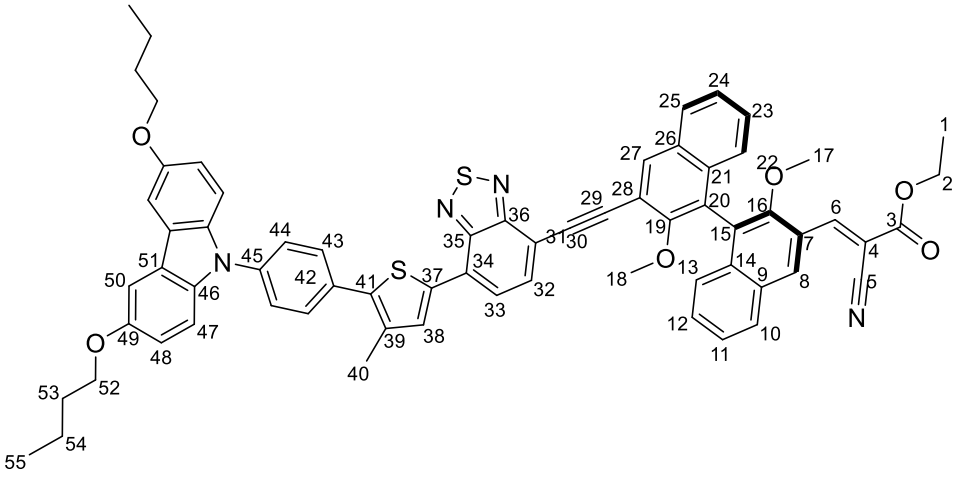

**28(*S*)b** (30 mg, 0.031 mmol), cyanoacetic acid (64 $\mu$L, 0.60 mmol) and piperidine (12 $\mu$L, 0.12 mmol) were dissolved in 5 mL DCM and stirred at rt for 20 h. 20 mL MeOH was added and the DCM was removed under reduced pressure. A red solid precipitated and was filtered off. **30(*S*)b** (31 mg, 93 %) was isolated as a red solid. **Mp** = 141 °C. **$R_f$** = 0.40 (DCM). **UV-Vis** (DCM) $\lambda_{max}$ ($\varepsilon$) = 275 (67300), 285 (69400), 313 (86900), 335 (88800), 472 (43400) nm. **Fluorescence** (DCM) $\lambda_{max}$ = 672 nm, $\Phi$ = 2 %. **$[\alpha]^{22}$** = 136° (c = 0.1, DCM). **IR** (ATR) = 1724 (m), 1457 (s), 1196 (s), 1162 (s). **$^1$H-NMR** (700 MHz, $CD_2Cl_2$, 298 K): $\delta$ = 9.01 (s, 1 arom. H, 8), 8.81 (s, 1 H, 6), 8.40 (s, 1 arom. H, 27), 8.09 – 8.08 (m, 2 arom. H, 13, 38) 7.96 (d, $^3J_{22,23}$ = 8.2 Hz, 1 arom. H, 22), 7.90 – 7.87 (m, 2 arom. H, 32, 33), 7.78 – 7.77 (m, 2 arom. H, 43), 7.65 – 7.64 (m,

2 arom. H, 44), 7.57 (d, $^4J_{48,50}$ = 2.5 Hz, 2 arom. H, 50), 7.53 – 7.50 (m, 1 arom. H, 12), 7.48 – 7.46 (m, 1 arom. H, 23), 7.43 – 7.39 (m, 3 arom. H, 11 ,47), 7.34 – 7.32 (m, 1 arom. H, 24), 7.21 (d, $^3J_{10,11}$ = 8.5 Hz, 1 arom. H, 10), 7.15 (d, $^3J_{24,25}$ = 8.5 Hz, 1 arom. H, 25), 7.04 (dd, $^3J_{47,48}$ = 8.9 Hz, $^4J_{48,50}$ = 2.5 Hz, 2 arom. H, 48), 4.41 (q, $^3J_{1,2}$ = 7.1 Hz, 2 H, 2), 4.10 (t, $^3J_{52,53}$ = 6.6 Hz, 4 H, 52), 3.90 (s, 3 H, 18), 3.47 (s, 3 H, 17), 2.51 (s, 3 H, 40), 1.86 – 1.82 (m, 4 H, 53), 1.59 – 1.54 (m, 4 H, 54), 1.42 (t, $^3J_{1,2}$ = 7.1 Hz, 3 H, 1), 1.02 (t, $^3J_{54,55}$ = 7.5 Hz, 6 H, 55) ppm. **$^{13}$C{$^1$H}-NMR** (176.1 MHz, $CD_2Cl_2$, 298K): $\delta$ = 162.7 (3), 156.2 (19), 155.7 (35), 155.2 (16), 154.1 (49), 152.2 (36), 150.6 (6), 140.0 (41), 137.9 (45), 137.1 (37), 136.7 (15), 136.3 (46), 135.5 (27), 135.4 (39), 134.3 (20), 133.3 (32), 133.15 (38), 133.05 (42), 131.7 (8), 130.7 (21), 130.5 (14), 130.4 (43), 130.0 (13), 129.5 (11), 128.5 (22), 128.2 (24), 128.0 (34), 126.8 (44), 126.4 (12), 126.04 (23), 125.96 (10), 125.94 (25), 125.7 (9), 125.6 (7), 125.0 (33), 124.7 (26), 124.2 (51), 117.2 (28), 116.1 (5), 116.0 (48), 115.2 (31), 111.0 (47), 105.0 (4), 104.2 (50), 93.3 (29), 91.0 (30), 69.0 (52), 63.2 (2), 62.8 (17), 61.9 (18), 32.0 (53), 19.8 (54), 15.6 (40), 14.4 (1), 14.1 (55) ppm. **APCI-HRMS** calcd for $C_{67}H_{56}N_4O_6S_2 + H^+$ ($M+H^+$) 1077.37140, found 1077.37245.

***4-(((3'-((7-(5-(4-(9H-Carbazol-9-yl)phenyl)-4-methylthiophen-2-yl)benzo[c][1,2,5]thiadiazol-4-yl)ethynyl)-2,2'-dimethoxy-[1,1'-binaphthalen]-3-yl)methylene)amino)-2,2,6,6-tetramethylpiperidin-1-oxyl*** (**31(*S*)a**)

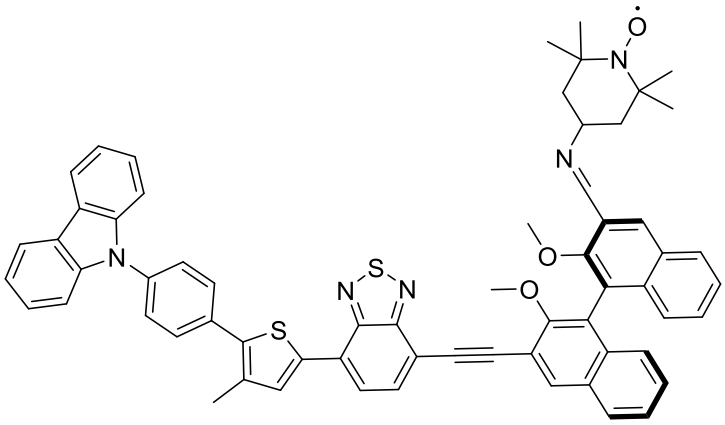

**28(*S*)a** (20 mg, 0.024 mmol) was dissolved in 2 mL DCM. TEMPO-Amine (47.2 mg, 0.28 mmol) and 190 mg of $Al_2O_3$ was added and the mixture was sonicated for 2 h. The $Al_2O_3$ was removed by filtration and the solvent was removed under reduced pressure. The crude product was purified by size exclusion chromatography (BioBeads SX 3 in Tol). **31(*S*)a** (23 mg, 97 %) was achieved as an orange solid. **Mp** = 126 °C, decomposition. **UV-Vis** (DCM) $\lambda_{max}$ ($\varepsilon$) = 293 (28800), 318 (24500), 330 (26200), 342 (25100, shoulder), 463 (14800) nm. **Fluorescence** (DCM) $\lambda_{max}$ = 620 nm, $\Phi$ = 47 %. **[α]$^{22}$** = 91° (c = 0.1, DCM). **IR** (ATR) = 2924 (w, br), 2853 (w, br), 1452 (m), 1264 (m), 735 (s, sh). **CW-EPR** (9.84 GHz, DCM, 300K): center field = 3500.00 G, $a_N$ = 16 G (resonances = 3486 G, 3502 G, 3518 G), $g$ = 2.0000. **ESI-HRMS** calcd for $C_{63}H_{52}N_5O_3S_2 + H^+$ ($M + H^+$) 991.35843, found 991.35855. **SQUID** C = 0.39739 gives: $\mu_{exp}$ = 1.784 $\mu_B$, corresponds to 1.045 electrons per molecule and therefor a purity of 104.5% which lies within the error range of the experimental equipment and technique.[108-109]

***(E)-4-(((3'-((7-(5-(4-(3,6-dibutoxy-9H-carbazol-9-yl)phenyl)-4-methylthiophen-2-yl)benzo[c][1,2,5]thiadiazol-4-yl)ethynyl)-2,2'-dimethoxy-[1,1'-binaphthalen]-3-yl)methylene)amino)-2,2,6,6-tetramethylpiperidin-1-oxyl*** (**31(*S*)b**)

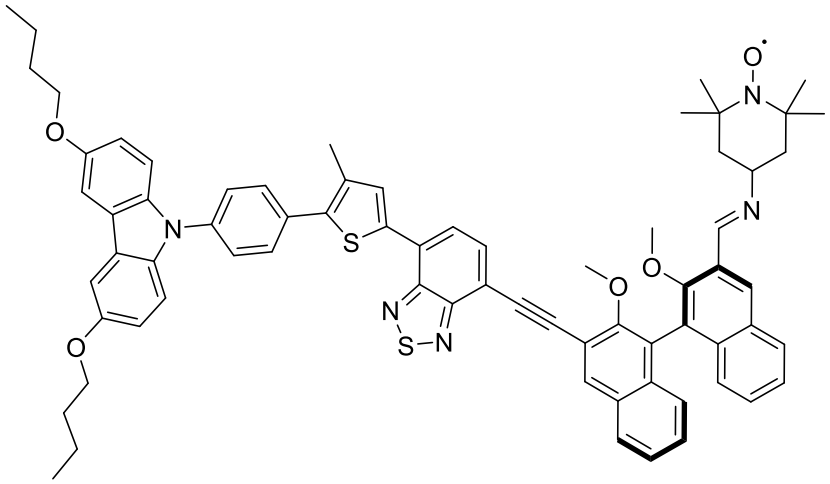

**28(*S*)b** (20 mg, 0.020 mmol) was dissolved in 5 mL DCM. TEMPO-Amine (86 mg, 0.50 mmol) and 200 mg of $Al_2O_3$ was added and the mixture was sonicated for 2 h at rt. The $Al_2O_3$ was removed by filtration and the solvent was removed under reduced pressure. The crude product was purified by size exclusion chromatography (BioBeads SX 3 in Tol). **31(*S*)b** (21 mg, 92 %) was achieved as a red solid. **Mp** = 164 °C. **UV-Vis** (DCM) $\lambda_{max}$ ($\varepsilon$) = 254 (87700, shoulder), 300 (41200, shoulder), 312 (48900), 335 (39300), 369 (17000, shoulder), 471 (26100) nm. **Fluorescence** (DCM) $\lambda_{max}$ = 633 nm, $\Phi$ = 1 %. **[α]$^{22}$** = 52° (c = 0.1, DCM). **IR** (ATR) = 1490 (s), 1456 (s), 1196 (s), 833 (s). **CW-EPR** (9.84 GHz, DCM, 300K): center field = 3500.00 G, $a_N$ = 16 G (resonances = 3486 G, 3502 G, 3518 G), $g$ = 2.0000. **APCI-HRMS** calcd for $C_{71}H_{68}N_5O_5S_2 + H^+$ (M + H$^+$) 1135.47346, found 1135.47461.[129]

***9-(4-(5-((3'-ethynyl-2,2'-dimethoxy-[1,1'-binaphthalen]-3-yl)ethynyl)-3-methylthiophen-2-yl)phenyl)-9H-carbazole*** (**32(*S*)**)

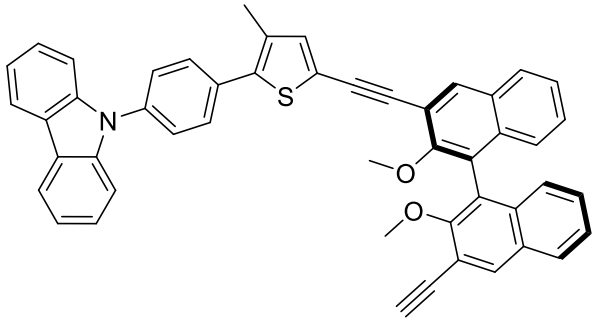

Under $N_2$-atmosphere **27(*S*)** (88 mg, 0.24 mmol), **10** (56 mg, 0.12 mmol), $Pd(PPh_3)_4$ (6 mg, 0.005 mmol), CuI (4 mg, 0.02 mmol) and $NEt_3$ (831 $\mu$L, 6 mmol) were dissolved in 10 mL THF. The reaction was stirred for 16 h at rt. Water was added and the mixture was extracted with DCM. The separated organic layer was washed with brine and dried over $MgSO_4$. The solvent was removed under reduced pressure and the crude product was purified by column chromatography (silica, hex/EtOAc 7:3). **32(*S*)** (25 mg, 30 %) was isolated as a colorless solid. $R_f$ = 0.6 (hex/EtOAc 7:3). **$^1$H-NMR** (400 MHz, $CD_2Cl_2$, 298 K): $\delta$ = 8.25 (s, 1 arom. H), 8.24 (s, 1 arom. H), 8.17 (d, 7.5 Hz, 2 arom. H), 7.93 – 7.89 (m, 2 arom. H), 7.76 – 7.74 (m, 2 arom. H), 7.67 – 7.65 (m, 2 arom. H), 7.51 (d, 7.8 Hz, 2 arom. H), 7.47 – 7.43 (m, 4 arom. H), 7.33 – 7.27 (m, 5 arom. H), 7.14 – 7.09 (m, 2 arom. H), 3.75 (s, 3 H), 3.68 (s, 3 H), 3.46 (s, 1 H), 2.44 (s, 3 H) ppm.

***5-(7-((3'-ethynyl-2,2'-dimethoxy-[1,1'-binaphthalen]-3-yl)ethynyl)benzo[c][1,2,5]thiadiazol-4-yl)thiophene-2-carbaldehyde*** (**33(*S*)**)

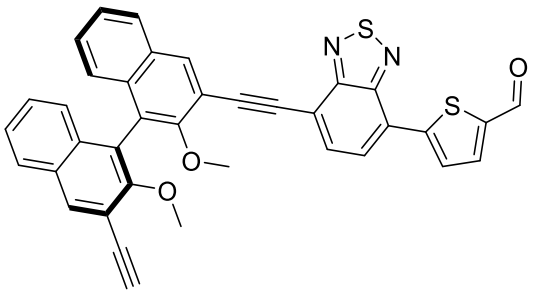

Under $N_2$-atmosphere **27(*S*)** (109 mg, 0.3 mmol), **17** (50 mg, 0.15 mmol), $Pd(PPh_3)_4$ (3 mg, 0.003 mmol), CuI (3 mg, 0.02 mmol) and $NEt_3$ (520 $\mu$L, 3.75 mmol) were dissolved in 10 mL THF. The reaction stirred for 16 h at 60 °C. Water was added, and the mixture was extracted with EtOAc. The

separated organic layer was washed with brine and dried over $MgSO_4$. The solvent was removed under reduced pressure and the crude product was purified by column chromatography (silica, hex/$Et_2O$/DCM (8:1:1) and recrystallization out of hexane. **33(*S*)** (97 mg, 63 %) was isolated as an orange solid. $R_f$ = 0.33 (hex/$Et_2O$/DCM 3:1:1). **$^1$H-NMR** (700 MHz, $CD_2Cl_2$, 298 K): $\delta$ = 9.97 (s, 1 H), 8.39 (s, 1 arom. H), 8.24 (s, 1 arom. H), 8.23 (d, 4.0 Hz, 1 arom. H), 8.04 (d, 7.4 Hz, 1 arom. H), 7.96 (d, 8.4 Hz, 1 arom. H), 7.93 (d, 7.4 Hz, 1 arom. H), 7.90 (d, 8.4 Hz, 1 arom. H), 7.86 (d, 4.0 Hz, 1 arom. H), 7.48 – 7.44 (m, 2 arom. H + impurity), 7.33 – 7.30 (m, 2 arom. H + impurity), 7.15 (d, 8.3 Hz, 1 arom. H), 7.12 (d, 8.6 Hz, 1 arom. H), 3.86 (s, 3 H), 3.68 (s, 3 H), 3.46 (s, 1 H) ppm.

***5-(7-((3'-((5-(4-(9H-Carbazol-9-yl)phenyl)-4-methylthiophen-2-yl)ethynyl)-2,2'-dimethoxy-[1,1'-binaphthalen]-3-yl)ethynyl)benzo[c][1,2,5]thiadiazol-4-yl)thiophene-2-carbaldehyde*** (**34(*S*)**)

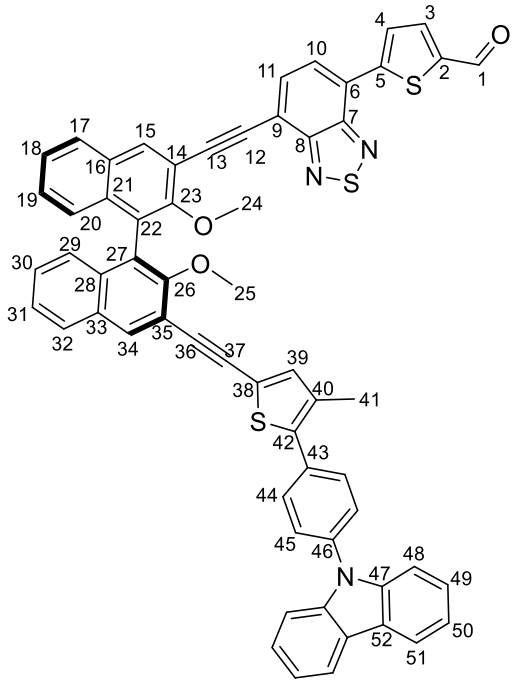

Method A:

Under $N_2$-atmosphere **17** (10 mg, 0.03 mmol), **32(*S*)** (17 mg, 0.028 mmol), $Pd(PPh_3)_4$ (1 mg, 0.001 mmol), CuI (1 mg, 0.005 mmol) and $NEt_3$ (100 $\mu$l, 0.7 mmol) were dissolved in 2 ml THF. The reaction was stirred at rt for 72 h. Water was added to the reaction and the mixture was extracted with EtOAc. The separated organic layer was washed with brine, dried over $MgSO_4$ and

the solvent was removed under reduced pressure. The crude product was purified by column chromatography (silica, DCM). **34(*S*)** (20 mg, 75 %) was isolated as an orange solid

Method B:

Under $N_2$-atmosphere **18** (10 mg, 0.03 mmol), **35(*S*)** (24 mg, 0.03 mmol), $Pd(PPh_3)_4$ (1 mg, 0.001 mmol), CuI (1 mg, 0.005 mmol) CsF (5 mg, 0.03 mmol) and $NEt_3$ (100 µl, 0.72 mmol) were dissolved in 10 mL THF. TBAF (1 M in THF, 30 µl, 0.03 mmol) was added and the reaction was heated to 60°C for 2 h. After cooling to rt, water was added, and the mixture was extracted with DCM. The separated organic layer was washed with brine, dried over $MgSO_4$, and the solvent was removed under reduced pressure. The crude product was purified by column chromatography (silica, DCM). **34(*S*)** (16 mg, 56 %) was isolated as an orange solid. **Mp** = 163 °C. **$R_f$** = 0.39 (DCM). **UV-Vis** (DCM) $\lambda_{max}$ ($\varepsilon$) = 294 (41300), 332 (49800, shoulder) 343 (50900), 370 (36200, shoulder), 439 (25400) nm. **Fluorescence** (DCM) $\lambda_{max}$ = 533 nm, $\Phi$ = 6 %. **$[\alpha]^{22}$** =527° (c = 0.1, DCM). **IR** (ATR): = 2195 (wb), 1662 (s), 1514 (s), 1447 (s). **$^1$H-NMR** (700 MHz, $CD_2Cl_2$, 298 K): $\delta$ = 9.97 (s, 1 H, 1), 8.40 (s, 1 arom H, 15), 8.27 (s, 1 aroms. H, 34), 8.24 (d, $^3J_{3,4}$ = 4.0 Hz, 1 arom. H, 4), 8.16 (d, $^3J_{50,51}$ = 7.8 Hz, 2 arom H, 51), 8.05 (d, $^3J_{10,11}$ = 7.6 Hz, 1 arom H, 10), 7.97 (d, $^3J_{19,20}$ = 8.3 Hz, 1 arom H, 20), 7.95 – 7.93 (m, 2 arom. H, 11, 29), 7.87 (d, $^3J_{3,4}$ = 4.0 Hz, 1 arom H, 3), 7.75 – 7.74 (m, 2 arom. H, 44), 7.67 – 7.65 (m, 2 arom. H, 45), 7.51 – 7.43 (m, 6 arom. H, 19, 30, 48, 49), 7.36 – 7.29 (m, 4 arom. H, 18, ,31, 50), 7.27 (s, 1 arom. H, 39), 7.18 – 7.16 (m, 2 arom. H, 17, 32), 3.88 (s, 3 H, 24), 3.77 (s, 3 H, 25), 2.44 (s, 3 H, 41) ppm. **$^{13}$C{$^1$H}-NMR** (176.1 MHz, $CD_2Cl_2$, 298K): $\delta$ = 183.4 (1), 156.1 (23), 155.8 (26), 155.6 (8), 152.1 (7), 148.2 (5), 144.6 (2), 141.1 (47), 139.7 (42), 137.5 (46), 137.1 (3), 136.7 (39), 135.3 (15), 134.69 (16), 134.65 (40), 134.4 (34), 134.2 (33), 133.3 (43), 132.9 (11), 130.73 (21), 130.68 (28), 130.65 (44) 129.0 (4), 128.5 (20), 128.4 (29), 128.1 (18), 127.8 (31), 127.5 (45), 127.3 (10), 126.7 (6), 126.4 (49), 126.1 (17), 126.02 (19), 126.00 (32), 125.9 (30), 125.5 (22), 125.3 (27), 123.8 (52), 121.5 (38), 120.7 (51), 120.5 (50), 117.8 (9), 117.3 (35), 116.9 (14), 110.2 (48), 94.8 (13), 91.2 (36), 90.3 (12), 87.5 (37),

61.9 (24), 61.6 (25), 15.3 (41) ppm. **APCI-HRMS** calcd for $C_{60}H_{37}N_3O_3S_3$ + $H^+$ (M + $H^+$) 944.20698, found 944.20781.

***9-(4-(5-((3'-Iodo-2,2'-dimethoxy-[1,1'-binaphthalen]-3-yl)ethynyl)-3-methylthiophen-2-yl)phenyl)-9H-carbazole*** (**35(*S*)**)

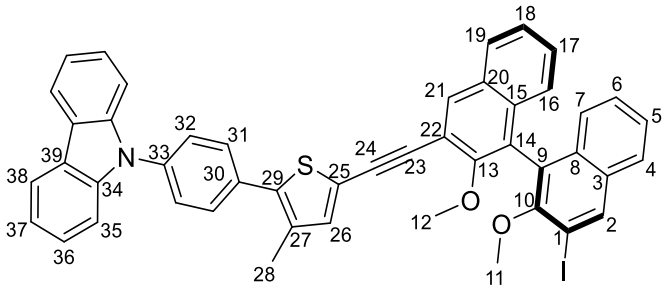


Under $N_2$-atmosphere **12** (270 mg, 0.74 mmol), **26(*S*)** (840 mg, 1.5 mmol), $Pd(PPh_3)_4$ (17 mg, 0.015 mmol), CuI (13 mg, 0.068 mmol) and $NEt_3$ (2.6 mL, 18.8 mmol) were dissolved in 30 mL THF. The reaction was stirred at rt overnight. Water was added and the mixture was extracted with DCM. The separated organic layer was washed with brine and dried over $MgSO_4$. The solvent was removed under reduced pressure and crude product was purified by column chromatography (silica, hex/DCM 3:2). The product was recrystallized out of hexane. **35(*S*)** (440 mg, 74 %) and isolated as a colorless solid. **Mp** 130 °C. **$R_f$** = 0.26 (hex/DCM 3:2). **UV-Vis** (DCM) $\lambda_{max}$ ($\varepsilon$) = 293 (38000), 301 (28700, shoulder), 316 (27600), 332 (34900, shoulder), 348 (43600) nm. **Fluorescence** (DCM) $\lambda_{max}$ = 438 nm, $\Phi$ = 38 %. **$[\alpha]^{22}$** = 30° (c = 0.1, DCM). **IR** (ATR) = 2934 (w, br), 1514 (s), 1450 (s), 1229 (s). **$^1$H-NMR** (700 MHz, $CD_2Cl_2$, 298 K): $\delta$ = 8.57 (s, 1 arom H, 2), 8.26 (s, 1 aroms. H, 21), 8.17 (d, $^3J_{37,38}$ = 7.7 Hz, 2 arom. H, 38), 7.92 (d, $^3J_{16,17}$ = 8.1 Hz, 1 arom. H, 16), 7.84 (d, $^3J_{6,7}$ = 8.2 Hz, 1 arom. H, 7), 7.75 – 7.74 (m, 2 arom. H, 31), 7.67 – 7.66 (m, 2 arom. H, 32), 7.50 (d, $^3J_{35,36}$ = 8.2 Hz, 2 arom. H, 35), 7.46 – 7.43 (m, 4 arom. H, 6, 17, 36), 7.32 – 7.29 (m, 4 arom. H, 5, 18, 37), 7.26 (s, 1 arom. H, 26), 7.13 (d, $^3J_{4,5}$ = 8.6 Hz, 1 arom. H, 4), 7.07 (d, $^3J_{18,19}$ = 8.5 Hz, 1 arom. H, 19), 3.75 (s, 3 H, 12), 3.45 (s, 3 H, 11), 2.44 (s, 3 H, 28) ppm. **$^{13}$C{$^1$H}-NMR** (176.1 MHz, $CD_2Cl_2$, 298K): $\delta$ = 155.8 (10), 154.8 (13), 141.1 (34), 140.0 (2), 139.7 (29), 137.5 (33), 136.7 (26), 134.7 (27), 134.6 (21), 134.3 (3), 134.1 (20), 133.3 (30), 132.7 (8), 130.7 (31), 130.6 (15), 128.3 (16), 127.9 (18), 127.5 (32), 127.4 (7), 127.3 (5), 126.4 (36), 126.1 (4),

126.04 (19), 125.98 (17), 125.93 (6), 125.8 (9), 125.3 (14), 123.8 (39), 121.4 (25), 120.7 (38), 120.5 (37), 117.2 (22), 110.2 (35), 92.7 (1), 91.0 (23), 87.7 (24), 61.5 (12), 61.4 (11), 15.3 (28) ppm. **APCI-HRMS** calcd for $C_{47}H_{32}INO_2S$ + $H^+$ (M + $H^+$) 802.12712, found 802.12839.

***Ethyl 3-(5-(7-((3'-((5-(4-(9H-carbazol-9-yl)phenyl)-4-methylthiophen-2-yl)ethynyl)-2,2'-dimethoxy-[1,1'-binaphthalen]-3-yl)ethynyl)benzo[c][1,2,5]thiadiazol-4-yl)thiophen-2-yl)-2-cyanoacrylate*** (**36(*S*)**)

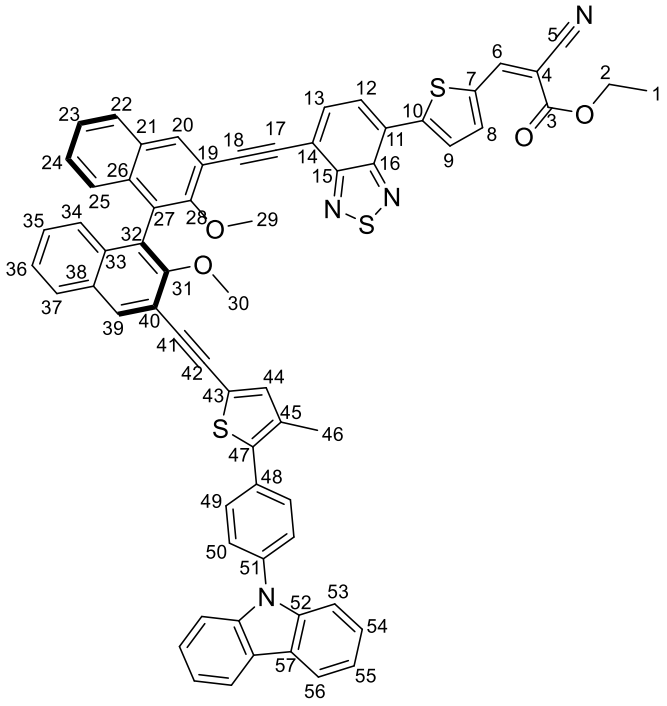

**34(*S*)** (30 mg, 0.032 mmol), cyanoacetic acid (68 $\mu$L, 0.64 mmol) and piperidine (13 $\mu$L, 0.13 mmol) were dissolved in 5 mL DCM and stirred at rt for 20 h. 20 mL MeOH was added to the reaction, and DCM was removed under reduced pressure. A red solid precipitated and was filtered off. **36(*S*)** (30 mg, 90 %) was isolated as an orange solid. **Mp** = 169 °C. $\mathbf{R_f}$ = 0.52 (DCM). **UV-Vis** (DCM) $\lambda_{max}$ ($\varepsilon$) = 283 (43400, shoulder), 293 (49800), 337 (51500), 371 (45000, shoulder) 467 (42300) nm. **Fluorescence** (DCM) $\lambda_{max}$ = 548 nm, $\Phi$ = 5 %. $\mathbf{[\alpha]^{22}}$ =752° (c = 0.1, DCM). **IR** (ATR) = 1715 (m), 1581 (s), 1450 (s), 1202 (s). **$^1$H-NMR** (700 MHz, $CD_2Cl_2$, 298 K): $\delta$ = 8.40 (s, 1 arom H, 20), 8.37 (s, 1 H, 6), 8.27 – 8.26 (m, 2 aroms. H, 4, 39), 8.16 (d, $^3J_{55,56}$ = 7.6 Hz, 2 arom. H, 56), 8.08 (d, $^3J_{12,13}$ = 7.6 Hz, 1 arom. H, 12), 7.97 (d, $^3J_{24,25}$ = 8.1 Hz, 1 arom. H, 25),

7.95 – 7.94 (m, 2 arom. H, 13, 34), 7.91 (d, $^{3}J_{8,9}$ = 4.2 Hz, 1 arom. H, 8), 7.75 – 7.74 (m, 2 arom. H, 49), 7.67 – 7.65 (m, 2 arom. H, 50), 7.51 – 7.43 (m, 6 arom. H, 24, 35, 52, 53), 7.36 – 7.29 (m, 4 arom. H, 23, 36, 55), 7.27 (s, 1 arom. H, 44), 7.18 – 7.16 (m, 2 arom. H, 22, 37), 4.36 (q, $^{3}J_{1,2}$ = 7.2 Hz, 2 H, 2), 3.88 (s, 3 H, 29), 3.77 (s, 3 H, 30), 2.44 (s, 3 H, 46), 1.39 (t, $^{3}J_{1,2}$ = 7.2 Hz, 3 H, 1) ppm. **$^{13}$C{$^{1}$H}-NMR** (176.1 MHz, $CD_2Cl_2$, 298K): $\delta$ = 163.0 (3), 156.1 (28), 155.8 (31), 155.6 (16), 152.1 (15), 148.5 (10), 146.4 (6), 141.1 (52), 139.7 (47), 138.7 (8), 137.53 (7), 137.48 (51), 136.7 (44), 135.3 (20), 134.71 (45), 134.66 (21), 134.4 (39), 134.3 (38), 133.3 (48), 133.0 (13), 130.74 (33), 130.68 (26), 130.66 (49) 129.2 (9), 128.5 (25), 128.4 (34), 128.1 (23), 127.8 (36), 127.5 (50), 127.4 (12), 126.43 (54), 126.40 (11), 126.1 (22), 126.03 (37), 126.01 (24), 125.9 (35), 125.5 (27), 125.3 (32), 123.8 (57), 121.5 (43), 120.7 (56), 120.5 (55), 117.9 (14), 117.3 (40), 116.9 (19), 116.4 (5), 110.2 (53), 99.7 (4), 95,1 (41), 91.2 (18), 90.4 (17), 87.5 (42), 63.0 (2), 62.0 (29), 61.6 (30), 15.3 (46), 14.4 (1) ppm. **APCI-HRMS** calcd for $C_{65}H_{42}N_4O_4S_3$ + $H^+$ ($M+H^+$) 1039.24410, found 1039.24612.

***(E)-4-(((5-(7-((3'-((5-(4-(9H-Carbazol-9-yl)phenyl)-4-methylthiophen-2-yl)ethynyl)-2,2'-dimethoxy-[1,1'-binaphthalen]-3-yl)ethynyl)benzo[c][1,2,5]thiadiazol-4-yl)thiophen-2-yl)methylene)amino)-2,2,6,6-tetramethylpiperidin-1-oxyl*** (**37(*S*)**)

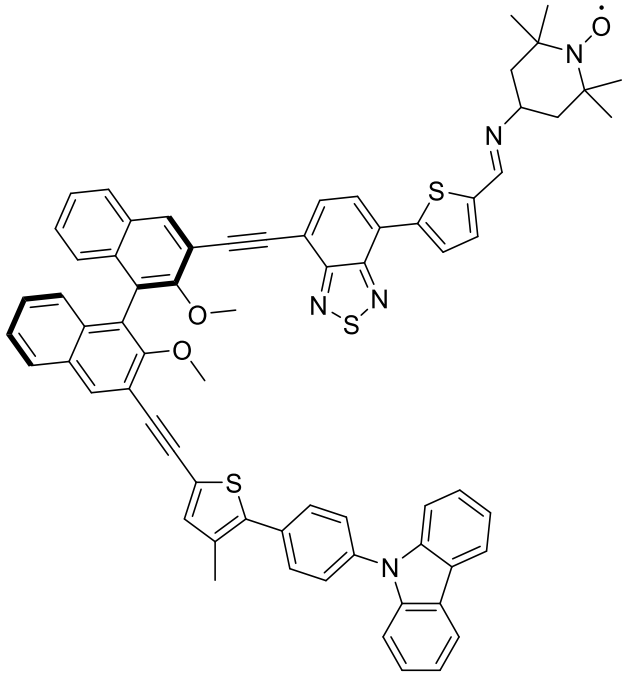

**34(*S*)** (110 mg, 0.12 mmol) was dissolved in 20 mL DCM. TEMPO-Amine (470 mg, 2.7 mmol) and 1.1 g of $Al_2O_3$ was added and the mixture was sonicated for 2 h at rt. The $Al_2O_3$ was removed by filtration, and the solvent was removed under reduced pressure. The crude product was purified by size exclusion chromatography (BioBeads SX 3 in Tol). **37(*S*)** (120 mg, 91 %) was achieved as a red solid. **Mp** = 166 °C. **UV-Vis** (DCM) $\lambda_{max}$ ($\varepsilon$) = 286 (39800, shoulder), 294 (47000), 333 (62100, shoulder), 341 (63200), 368 (41100, shoulder), 448 (27600) nm. **Fluorescence** (DCM) $\lambda_{max}$ = 546 nm, $\Phi$ = 5 %. **[α]$^{22}$** =501° (c = 0.1, DCM). **IR** (ATR) 1624 (m), 1449 (s), 1227 (s, sh), 835 (s). **CW-EPR** (9.84 GHz, DCM, 300K): center field = 3500.00 G, $a_N$ = 16 G (resonances = 3486 G, 3502 G, 3518 G), $g$ = 2.0000. **APCI-HRMS** calcd for $C_{69}H_{54}N_5O_3S_3$ + $H^+$ (M + $H^+$) 1097.34616, found 1097.34826. **SQUID** C = 0.35843 gives: $\mu_{exp}$ = 1.694 $\mu_B$, corresponds to 0.967 electrons per molecule and a purity of 97%.[108-109]

# 5. Appendix

## 5.1. NMR-Spectra

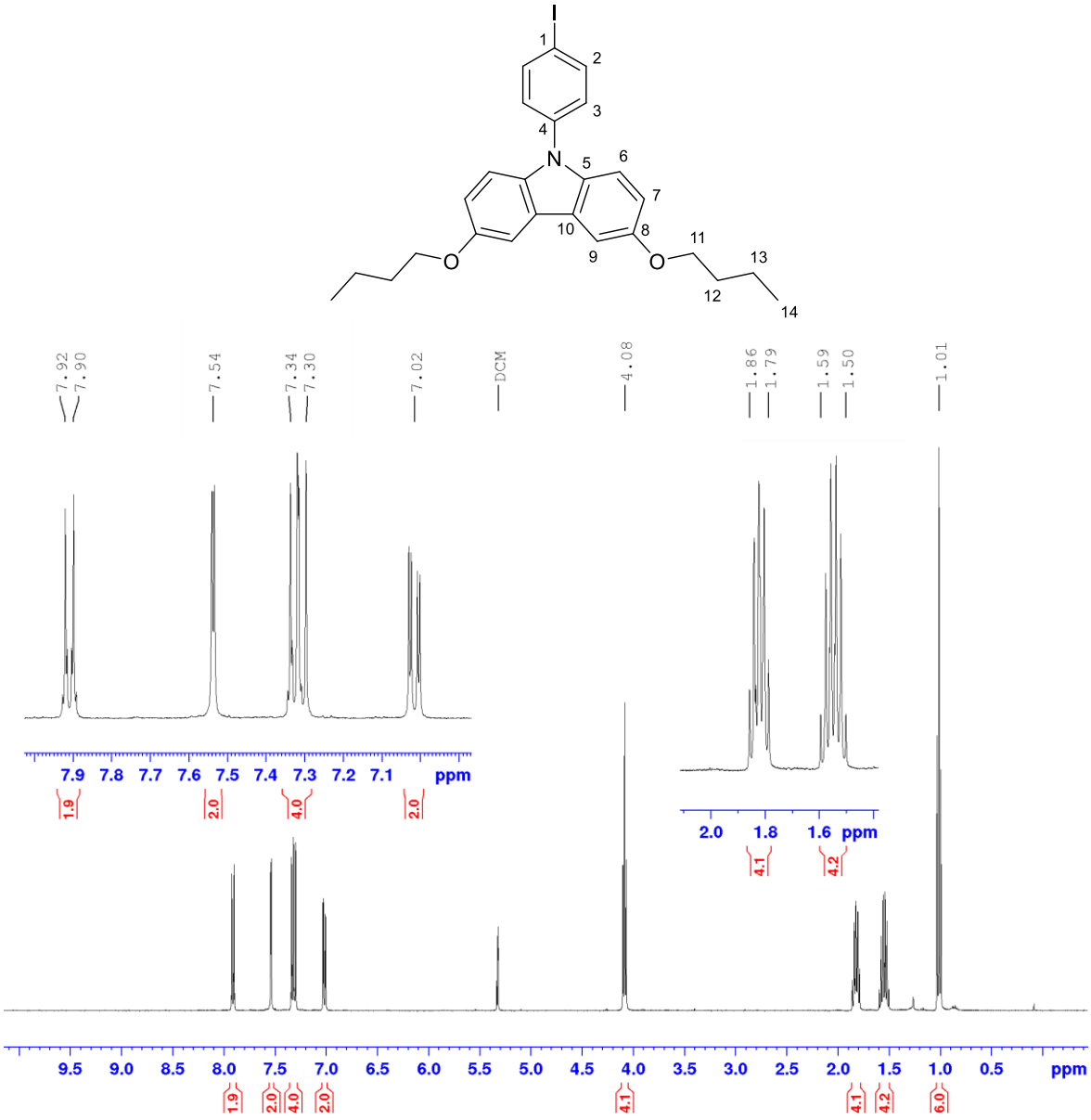


**Figure A1:** $^{1}$H NMR of **2b** in $CD_2Cl_2$ at a 400 MHz spectrometer at 298 K.

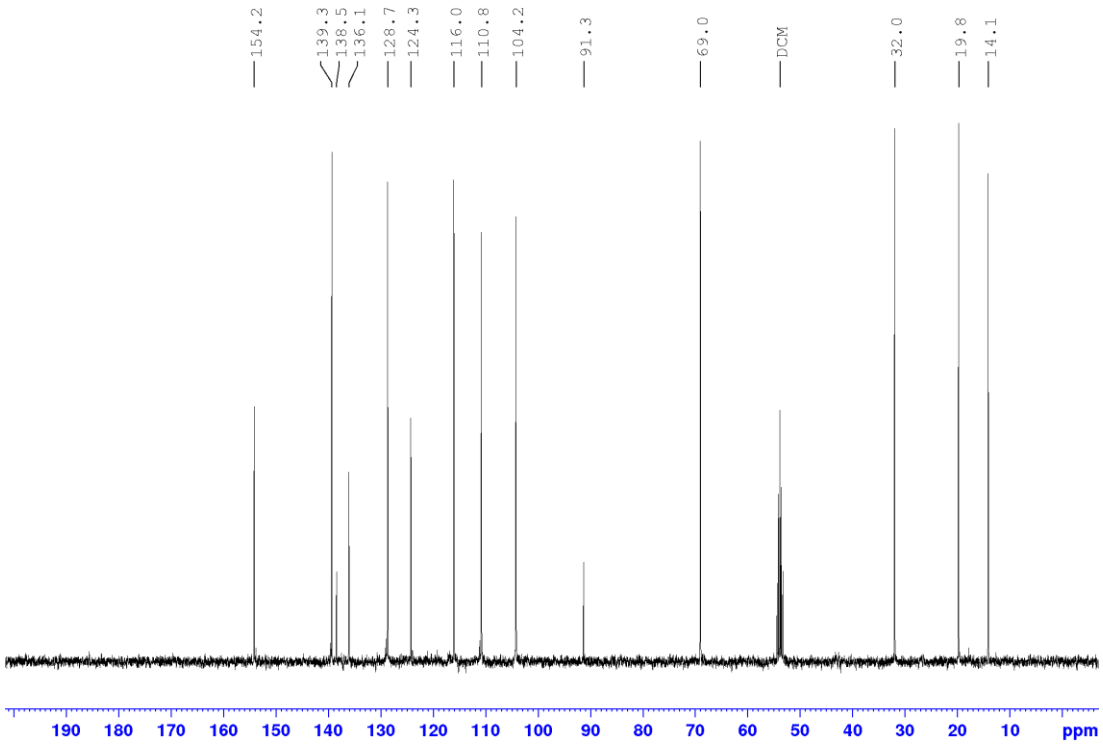


**Figure A2:** $^{13}C\{^{1}H\}$ NMR of **2b** in $CD_2Cl_2$ at a 100.6 MHz spectrometer at 298 K.

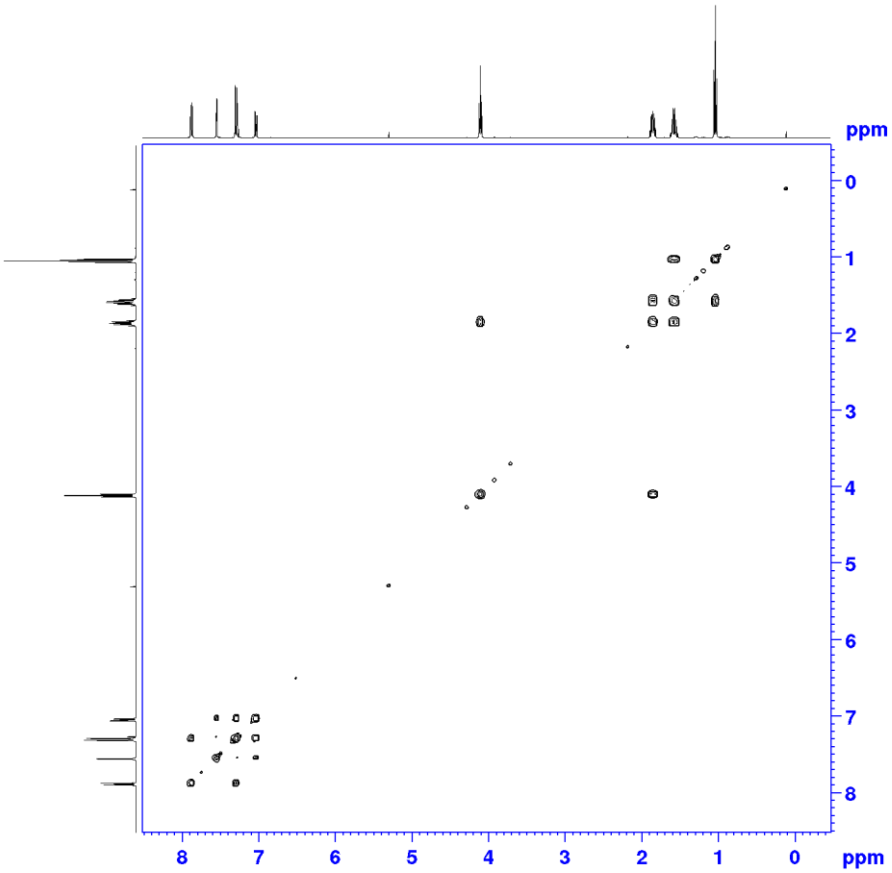


**Figure A3:** $^{1}H,^{1}H$ COSY NMR spectrum of **2b** in $CDCl_3$ at a 400 MHz spectrometer at 298 K.

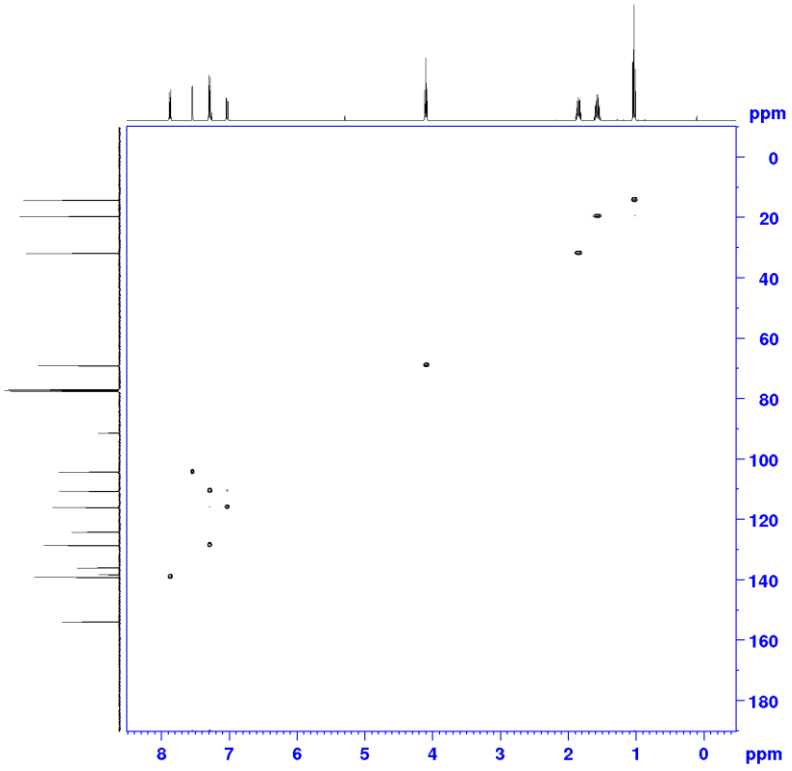


**Figure A4:** $^{1}H,^{13}C$ HSQC NMR spectrum of **2b** in $CDCl_3$ at a 400 MHz spectrometer at 298 K.

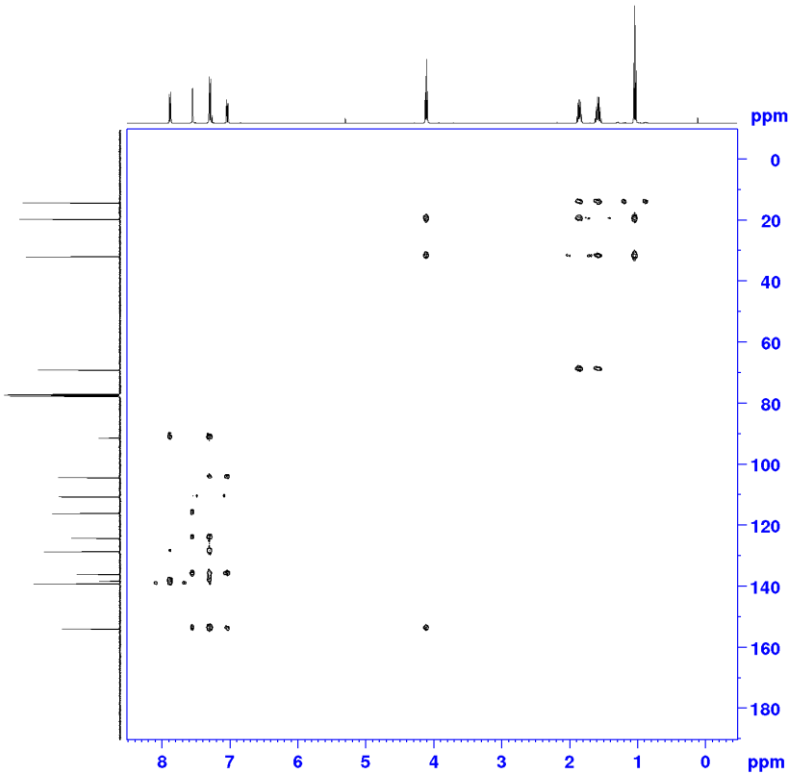


**Figure A5:** $^{1}H,^{13}C$ HMBC NMR spectrum of **2b** in $CDCl_3$ at a 400 MHz spectrometer at 298 K.

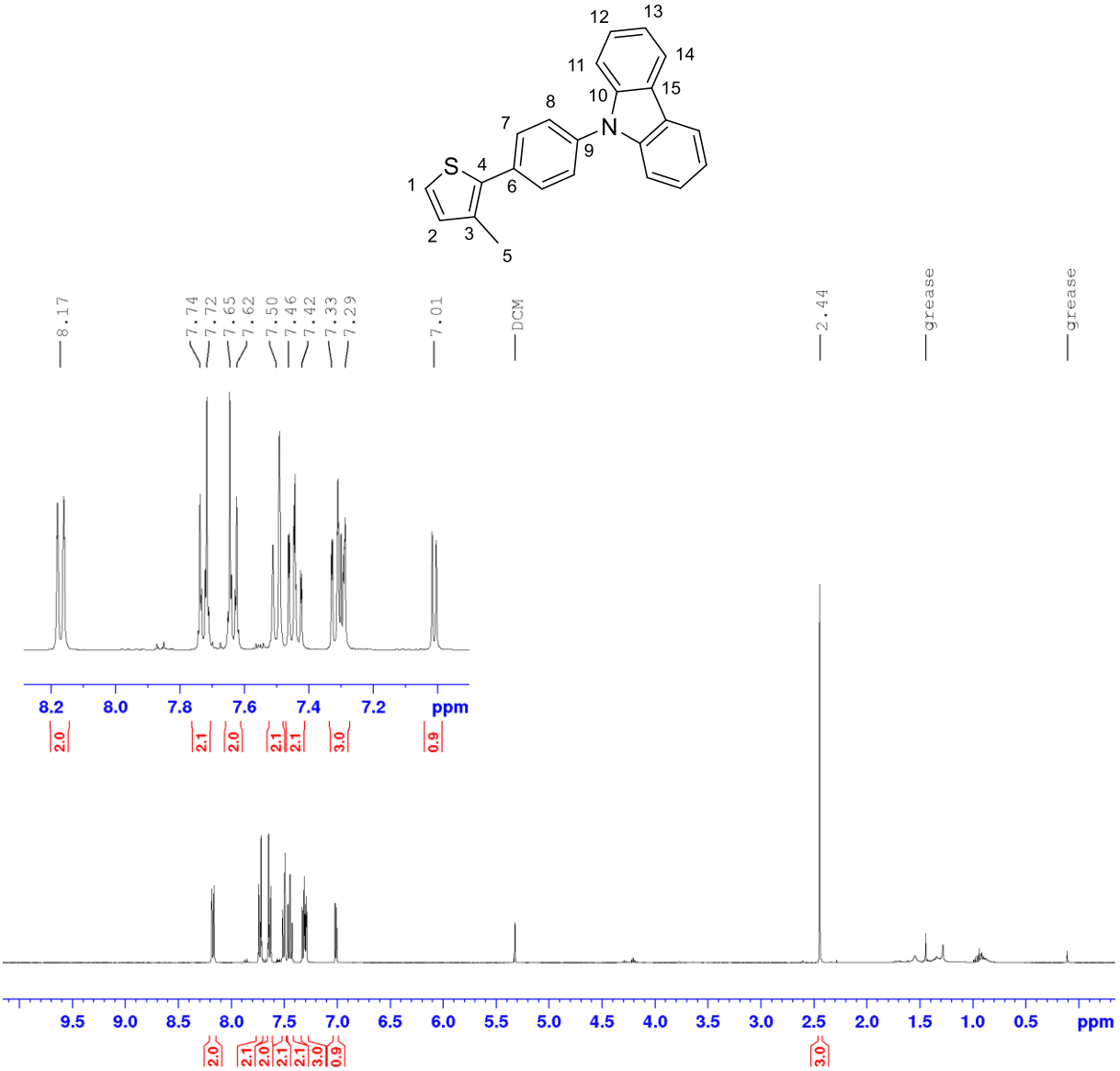


**Figure A6:** $^{1}$H NMR of zt**4a** in $CD_2Cl_2$ at a 400 MHz spectrometer a 298 K.

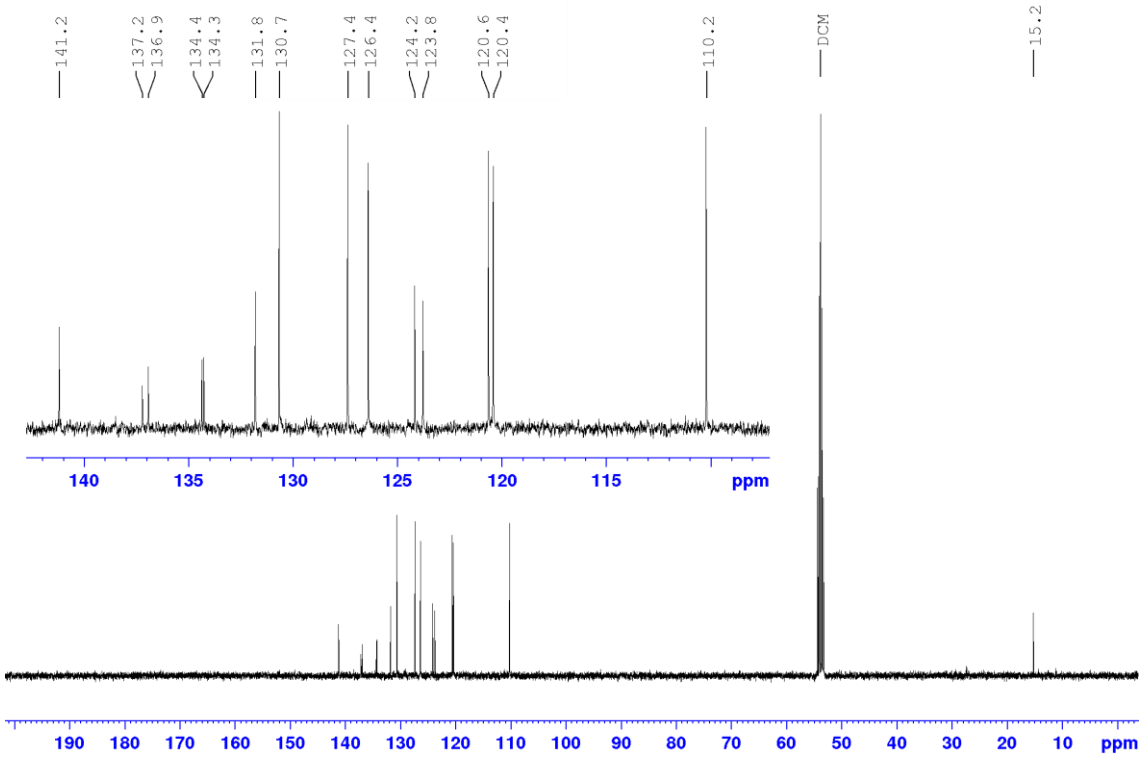


**Figure A7:** $^{13}C\{^{1}H\}$ NMR of **4a** in $CD_2Cl_2$ at a 100.6 MHz spectrometer at 298 K.

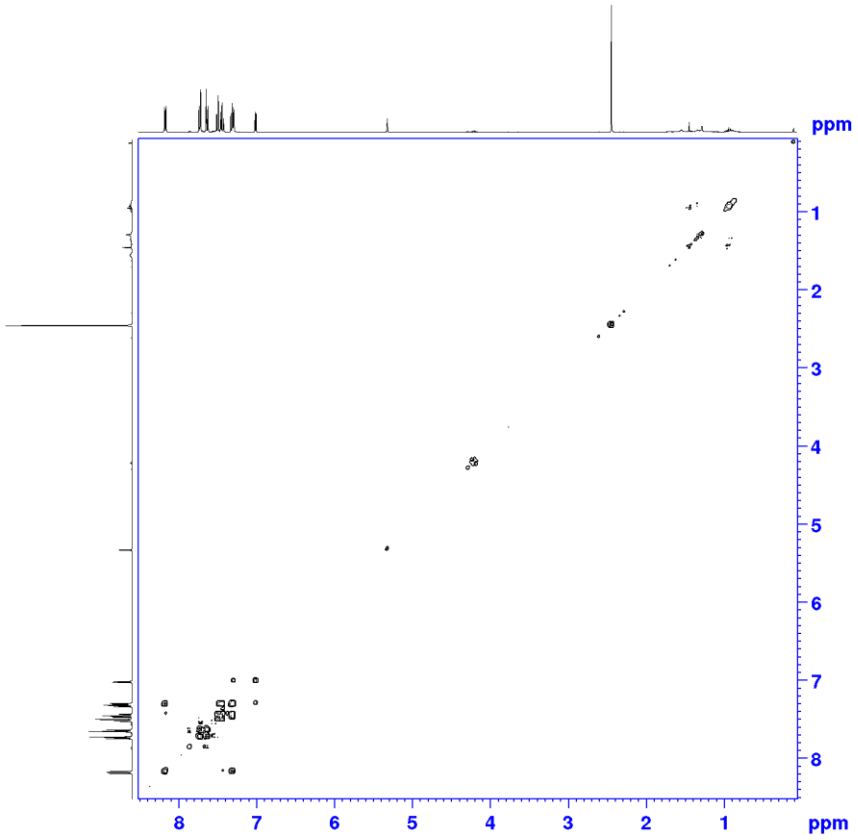


**Figure A8:** $^{1}H,^{1}H$ COSY NMR spectrum of **4a** in $CD_2Cl_2$ at a 400 MHz spectrometer at 298 K.

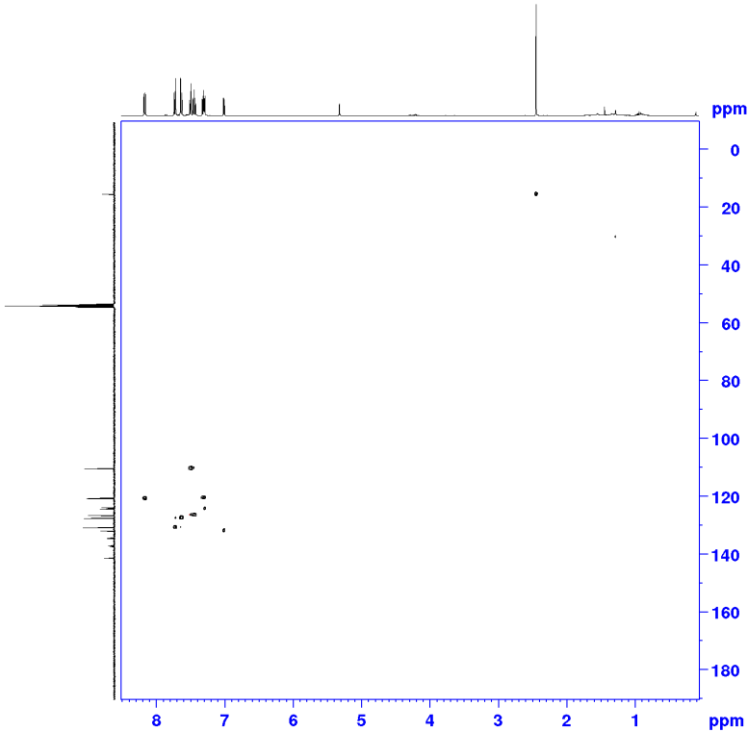


**Figure A9:** $^{1}H,^{13}C$ HSQC NMR spectrum of **4a** in $CD_2Cl_2$ at a 400 MHz spectrometer at 298 K.

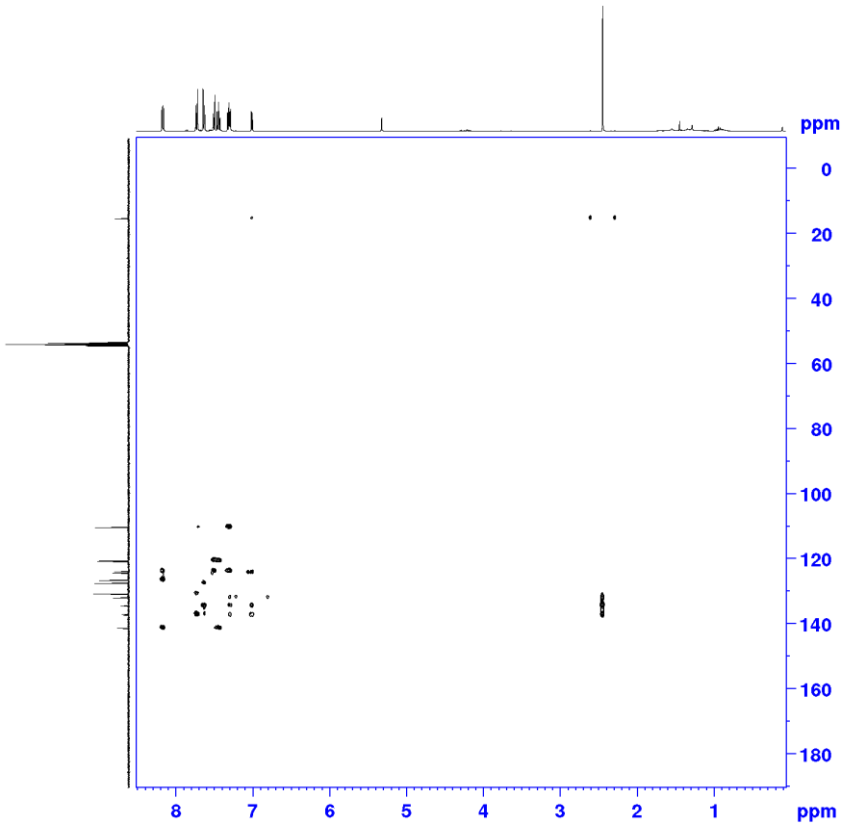


**Figure A10:** $^{1}H,^{13}C$ HMBC NMR spectrum of **4a** in $CD_2Cl_2$ at a 400 MHz spectrometer at 298 K.

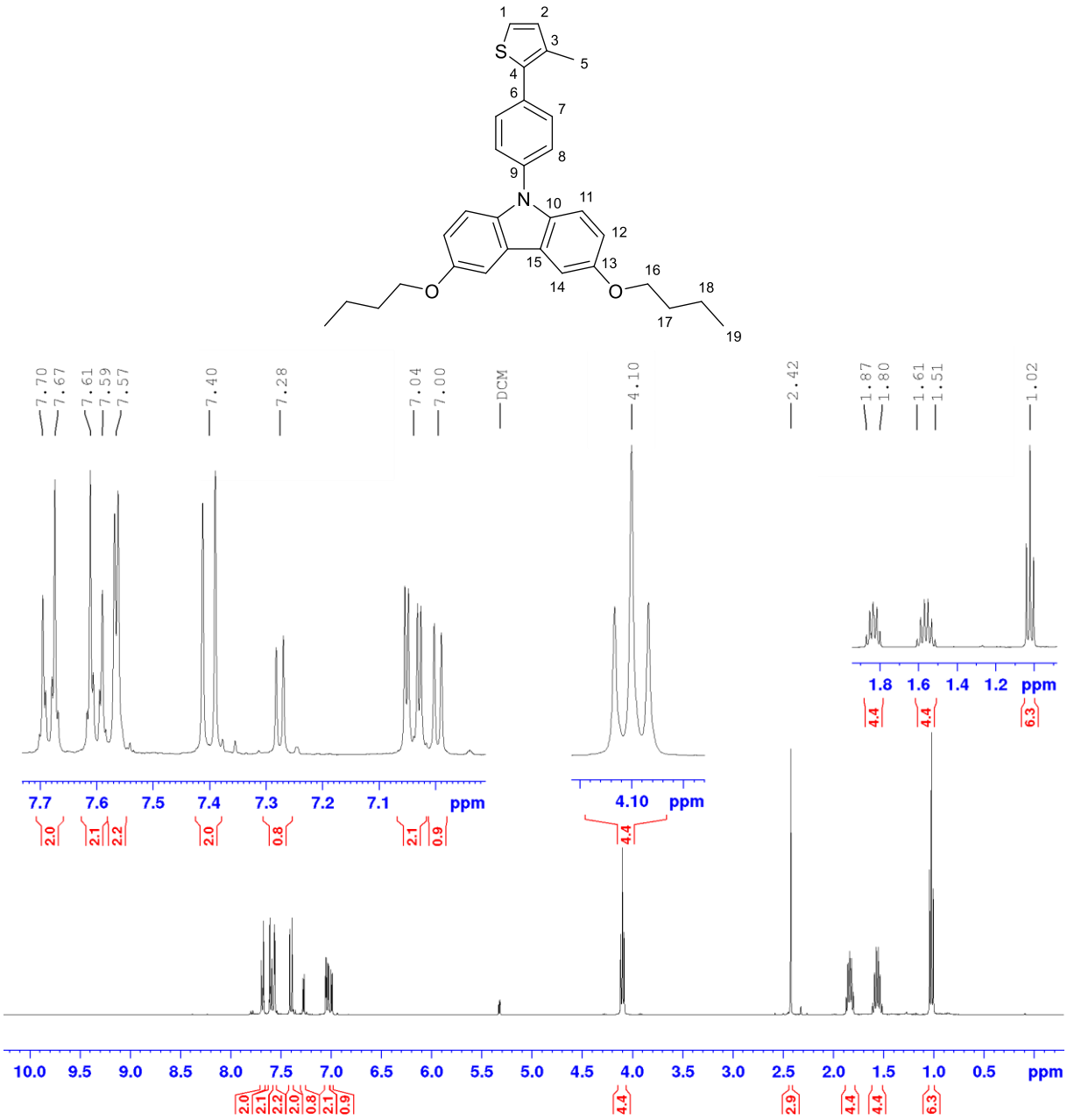


**Figure A11:** $^{1}$H NMR of **4b** in $CD_2Cl_2$ at a 400 MHz spectrometer at 298 K.

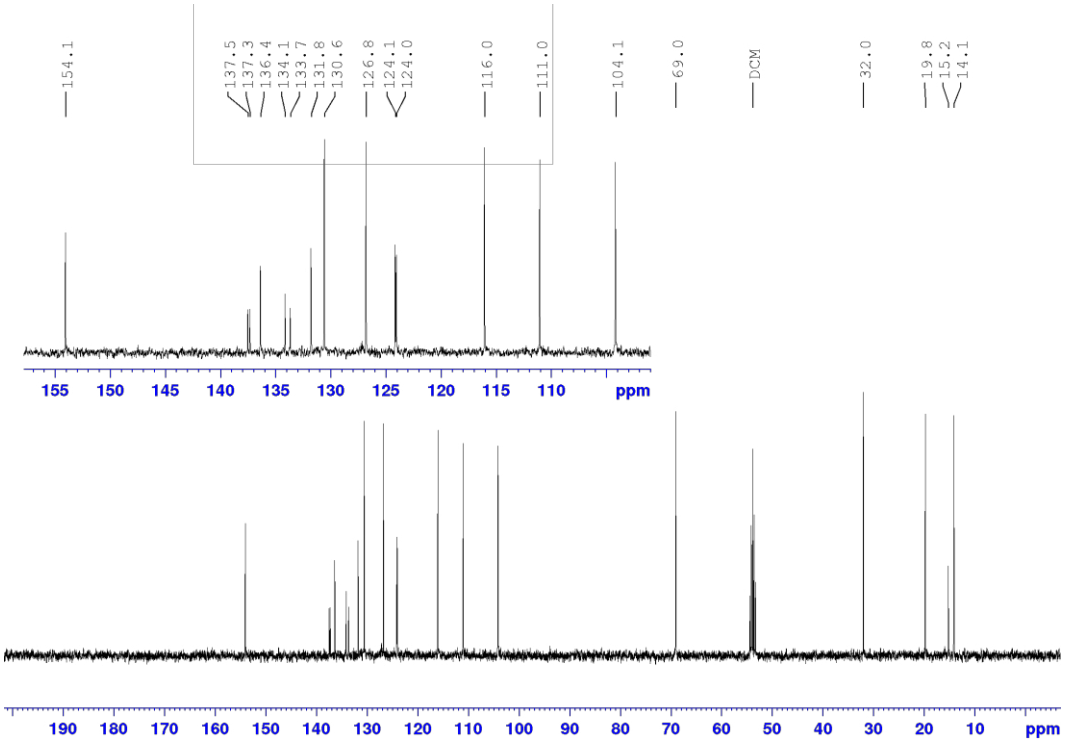


**Figure A12:** $^{13}C\{^{1}H\}$ NMR of **4b** in $CD_2Cl_2$ at a 100.6 MHz spectrometer at 298 K.

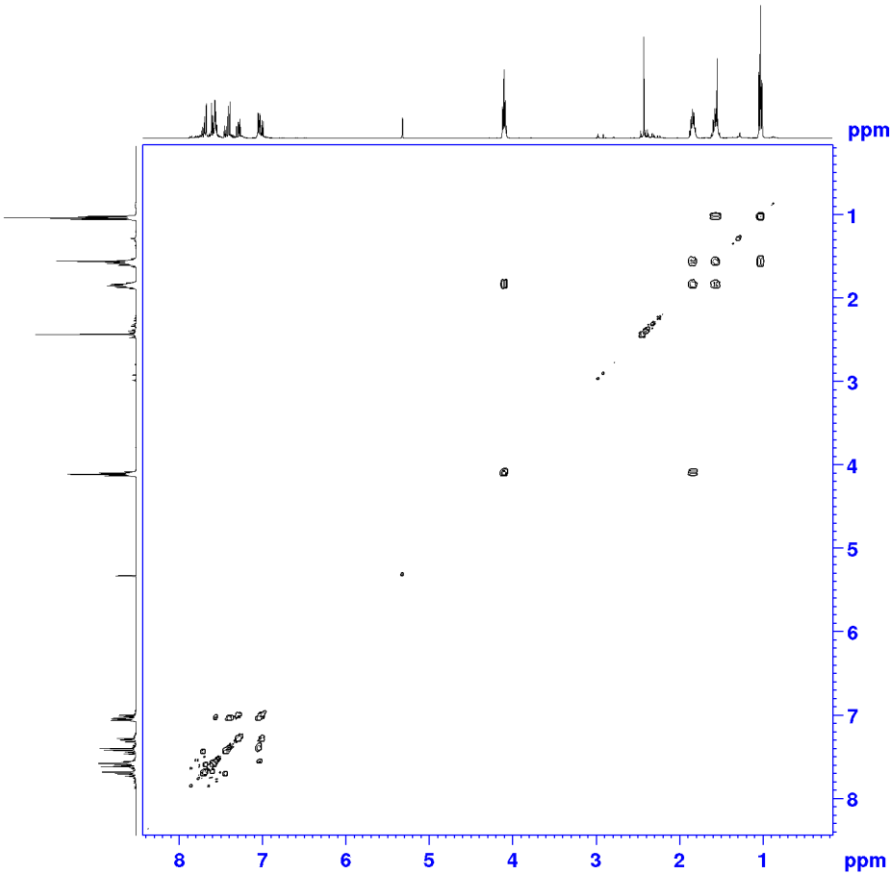


**Figure A13:** $^{1}H,^{1}H$ COSY NMR spectrum of **4b** in $CD_2Cl_2$ at a 400 MHz spectrometer at 298 K.

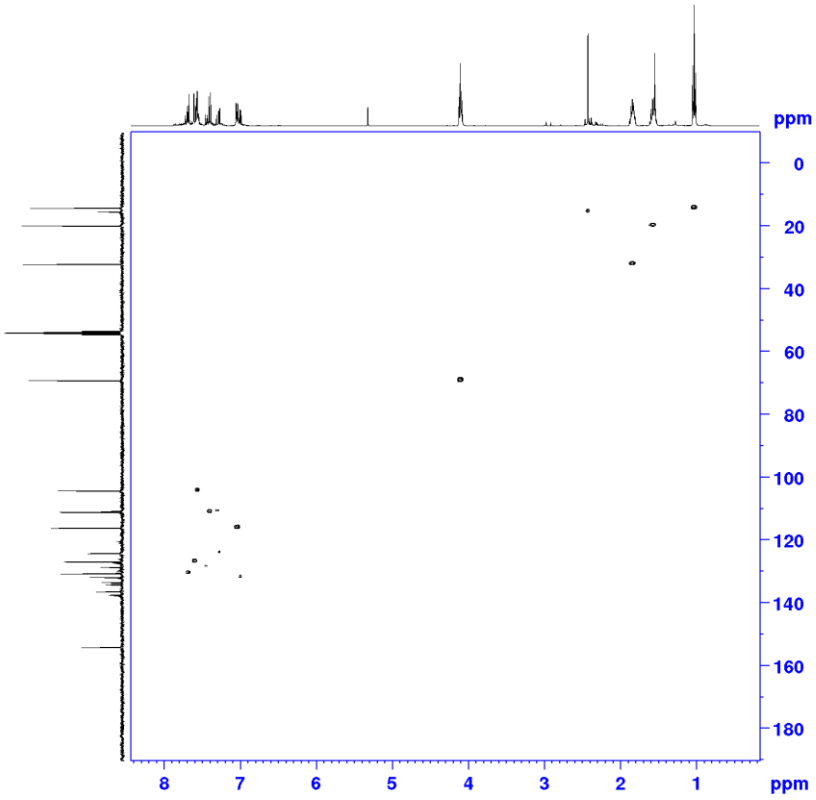


**Figure A14:** $^{1}H,^{13}C$ HSQC NMR spectrum of **4b** in $CD_2Cl_2$ at a 400 MHz spectrometer at 298 K.

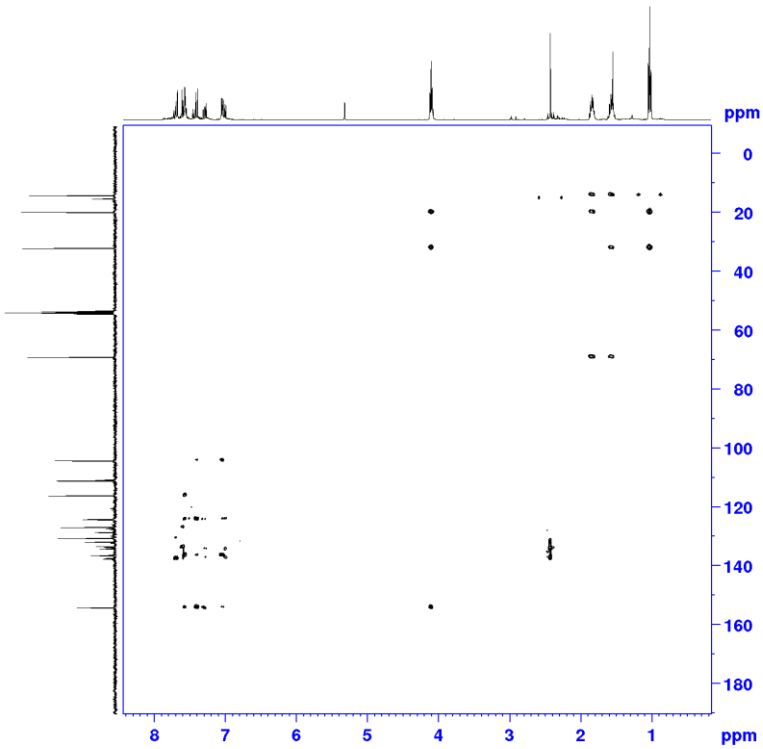


**Figure A15:** $^{1}H,^{13}C$ HMBC NMR spectrum of **4b** in $CD_2Cl_2$ at a 400 MHz spectrometer at 298 K.

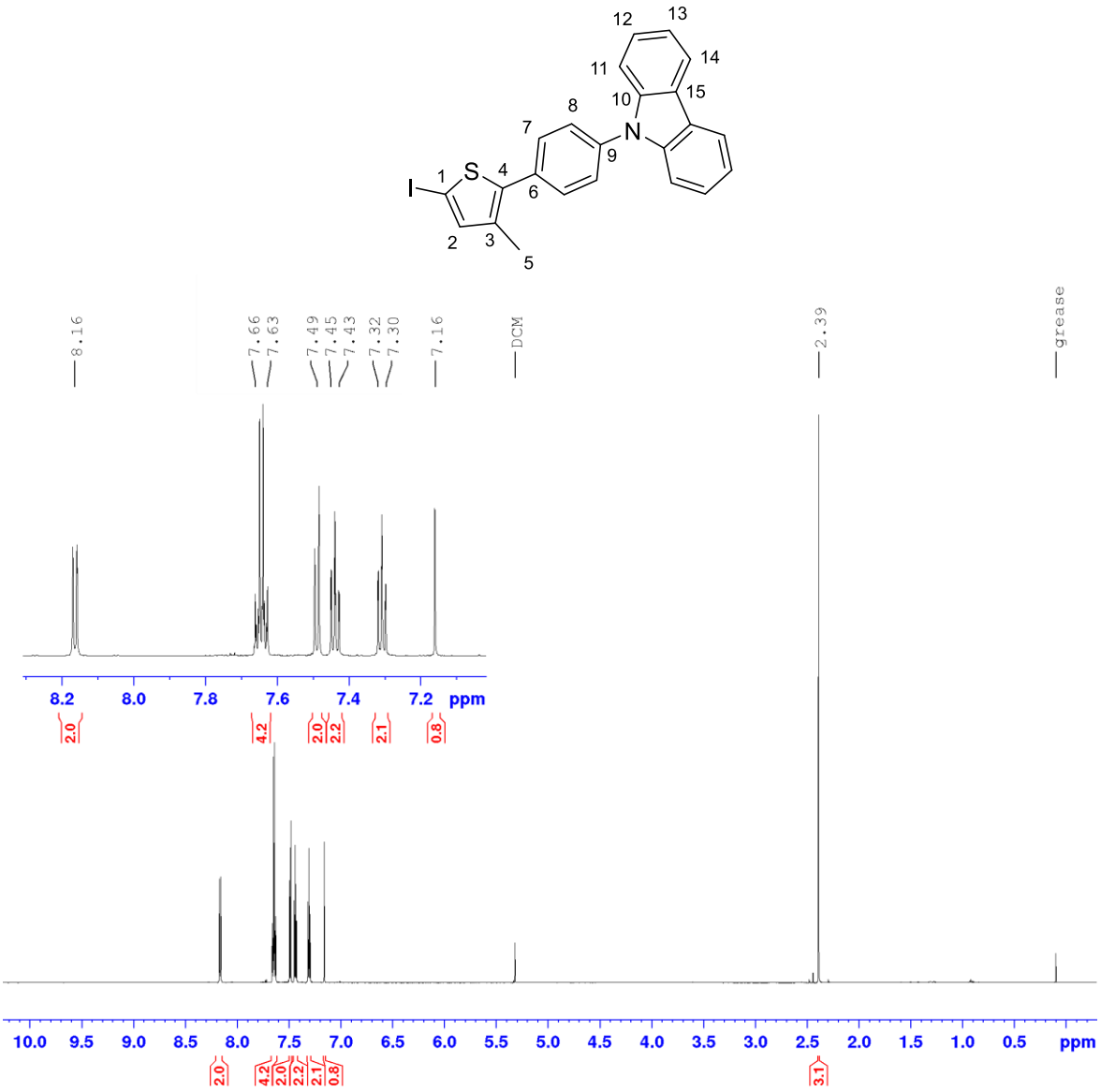


**Figure A16:** $^{1}H$ NMR of **5a** in $CD_2Cl_2$ at a 400 MHz spectrometer at 298 K.

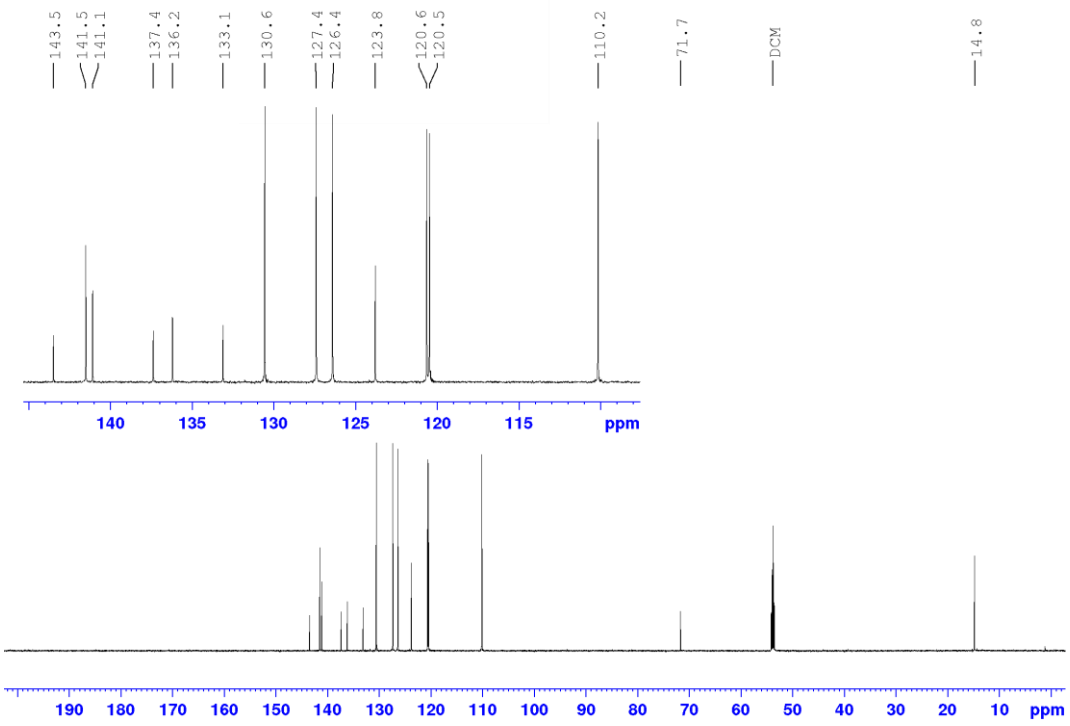


**Figure A17:** $^{13}C\{^{1}H\}$ NMR of **5a** in $CD_2Cl_2$ at a 100.6 MHz spectrometer at 298 K.

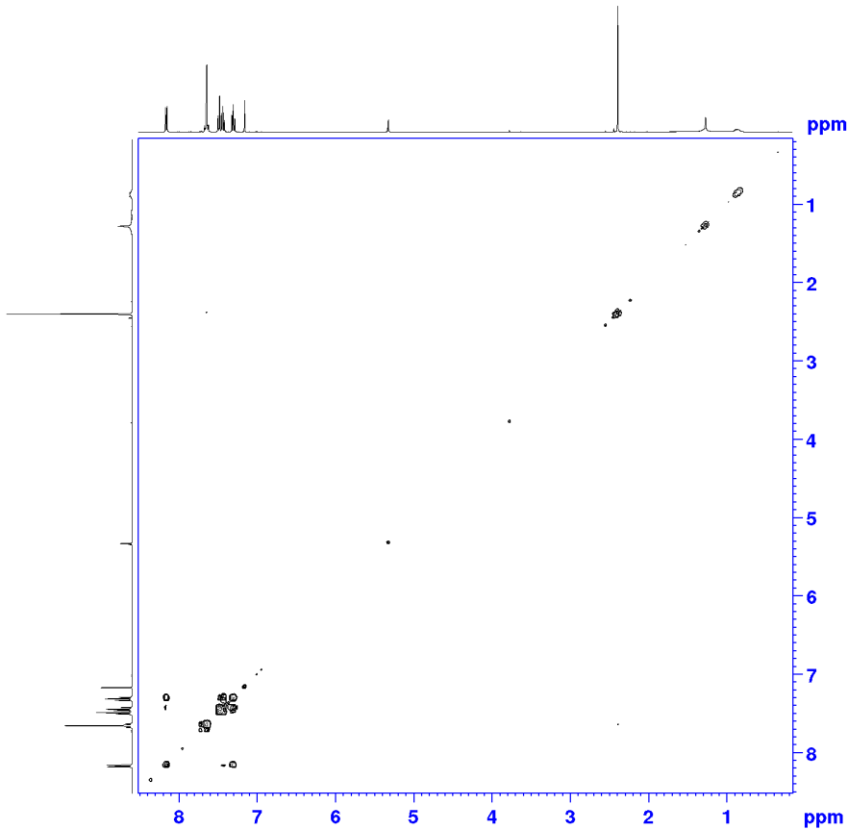


**Figure A18:** $^{1}H,^{1}H$ COSY NMR spectrum of **5a** in $CD_2Cl_2$ at a 400 MHz spectrometer at 298 K.

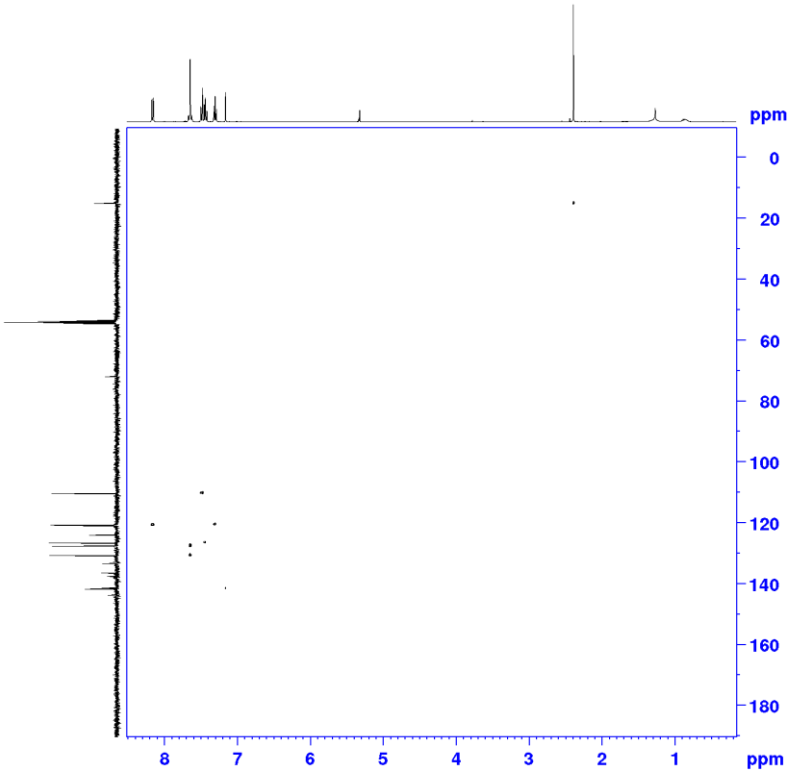


**Figure A19:** $^{1}H,^{13}C$ HSQC NMR spectrum of **5a** in $CD_2Cl_2$ at a 400 MHz spectrometer at 298 K.

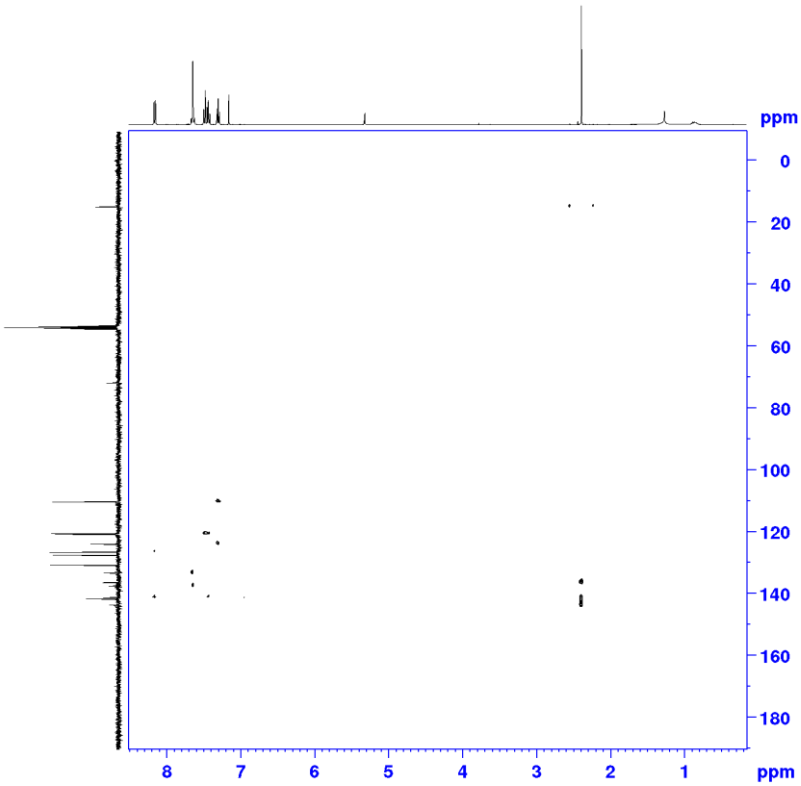


**Figure A20:** $^{1}H,^{13}C$ HMBC NMR spectrum of **5a** in $CD_2Cl_2$ at a 400 MHz spectrometer at 298 K.

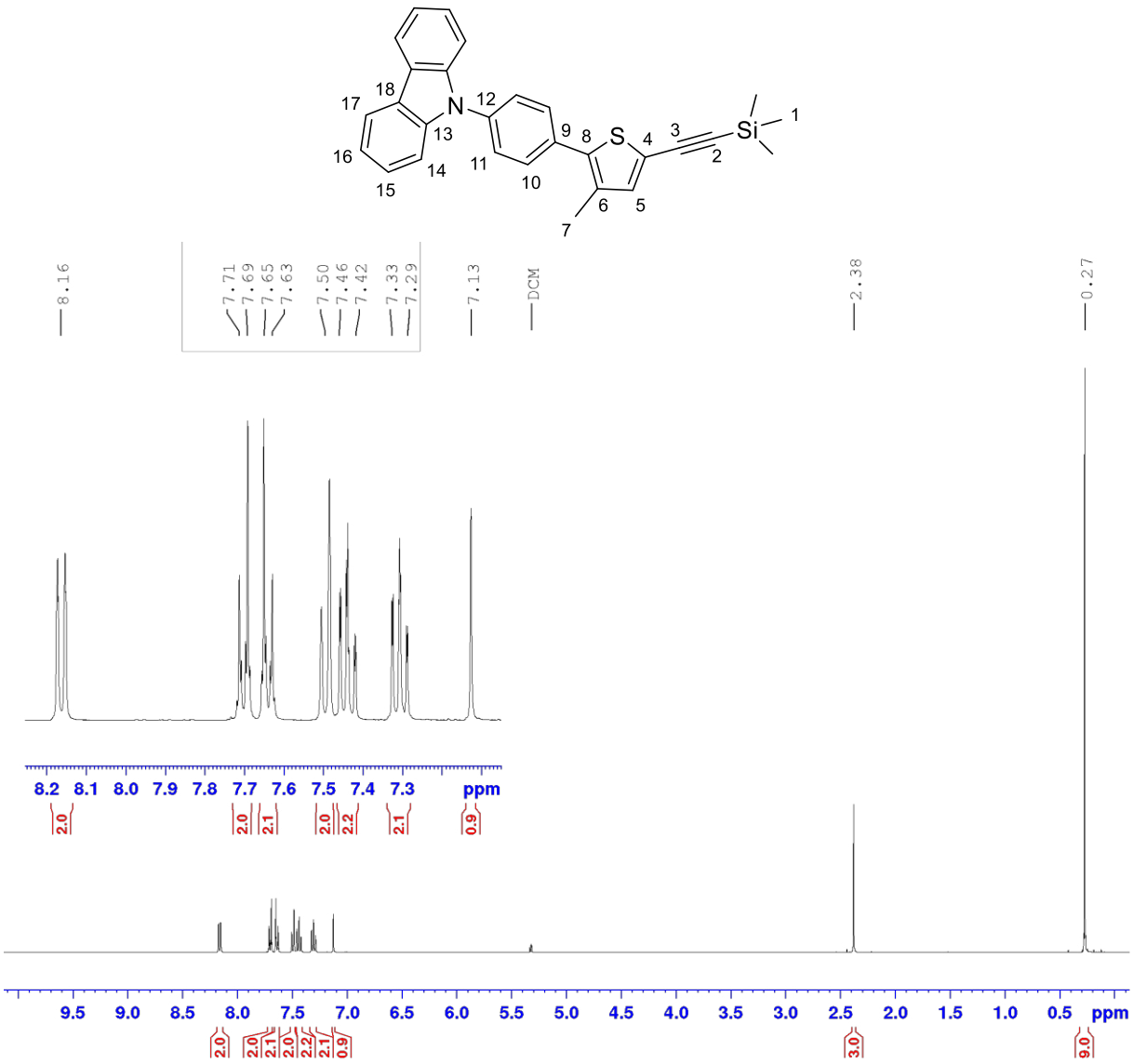


**Figure A21:** $^{1}$H NMR of **11** in $CD_2Cl_2$ at a 400 MHz spectrometer at 298 K.

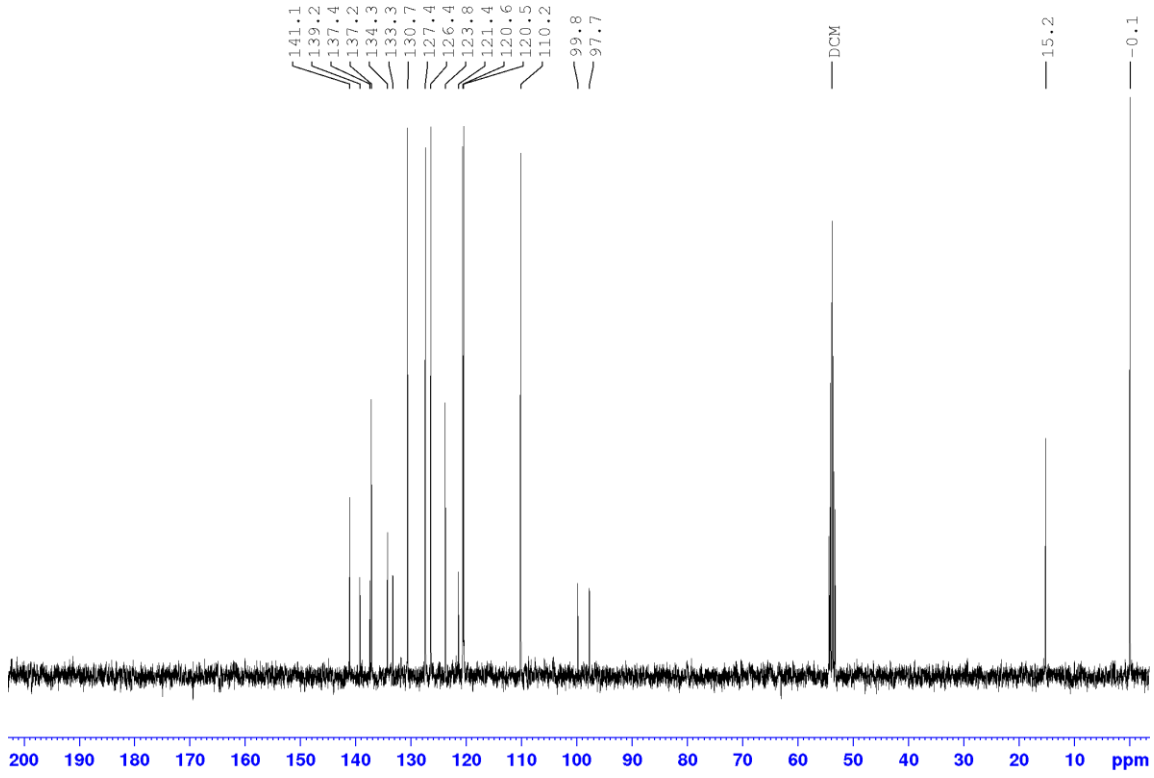


**Figure A22:** $^{13}C\{^{1}H\}$ NMR of **11** in $CD_2Cl_2$ at a 100.6 MHz spectrometer at 298 K.

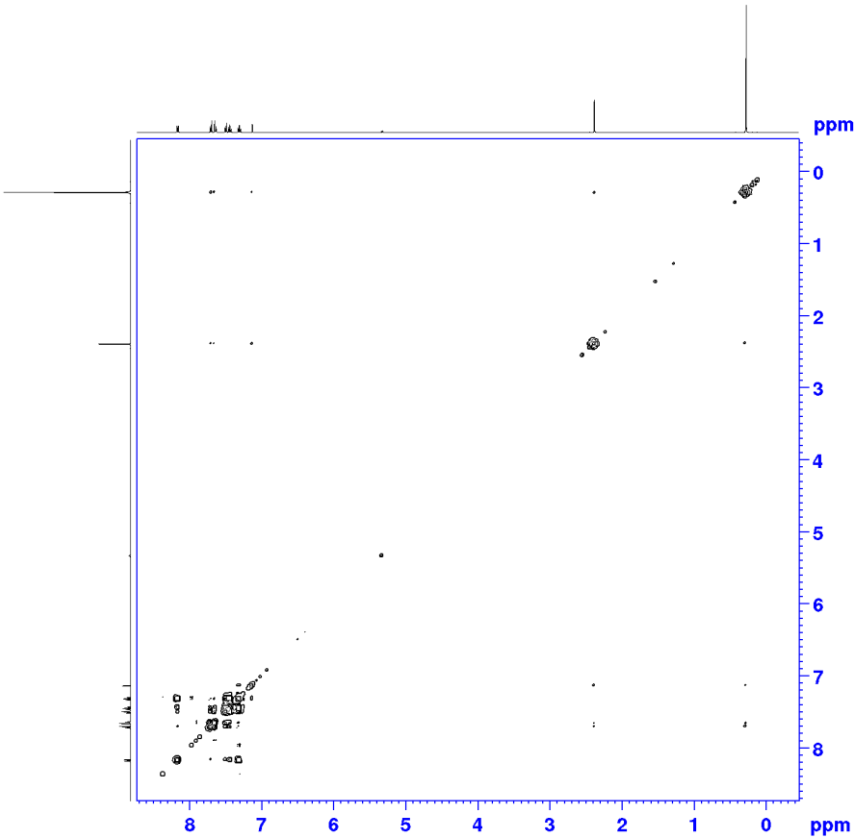


**Figure A23:** $^{1}H,^{1}H$ COSY NMR spectrum of **11** in $CD_2Cl_2$ at a 400 MHz spectrometer at 298 K.

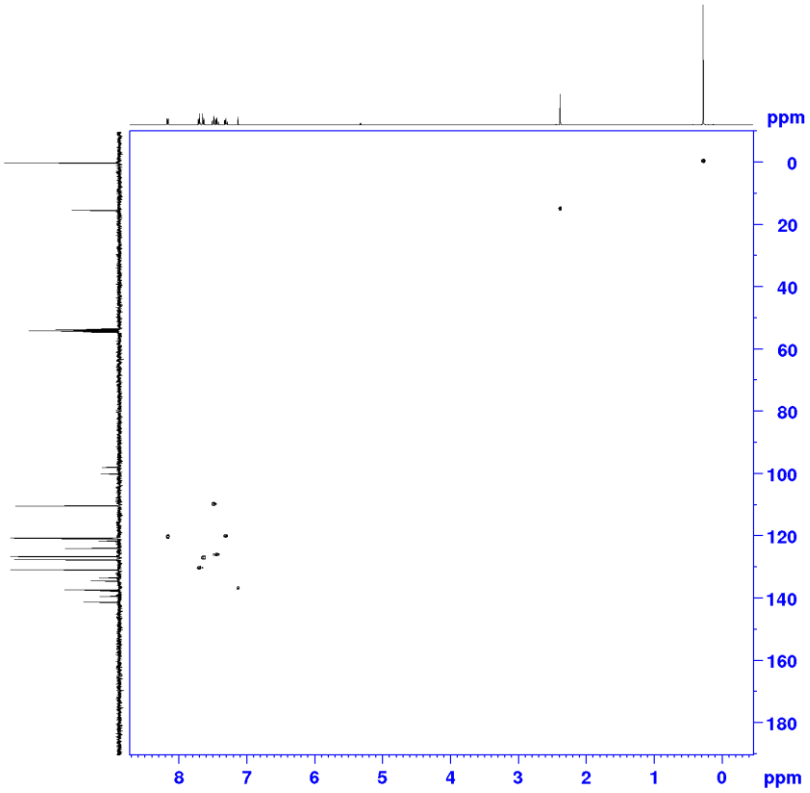


**Figure A24:** $^{1}H,^{13}C$ HSQC NMR spectrum of **11** in $CD_2Cl_2$ at a 400 MHz spectrometer at 298 K.

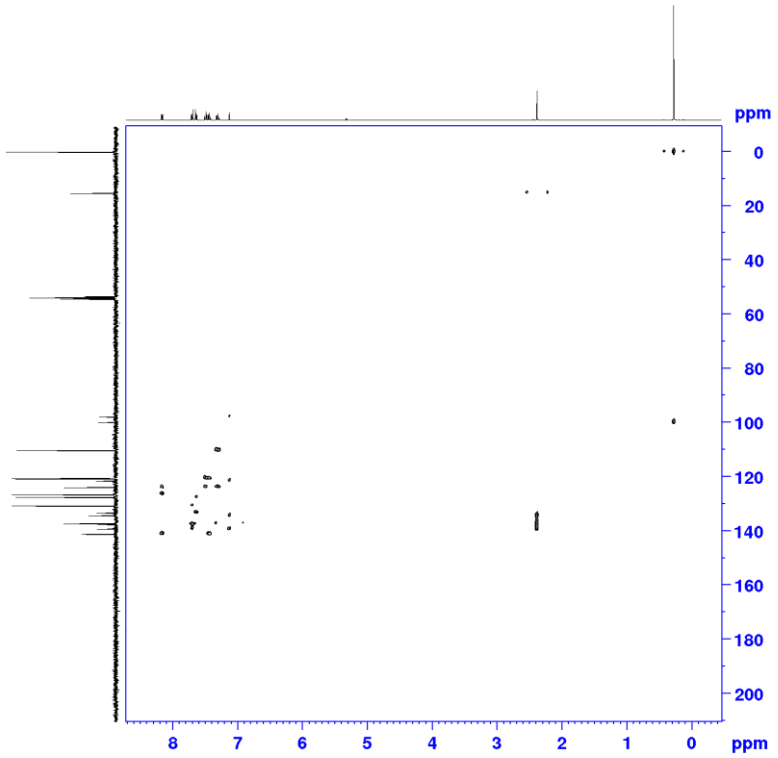


**Figure A25:** $^{1}H,^{13}C$ HMBC NMR spectrum of **11** in $CD_2Cl_2$ at a 400 MHz spectrometer at 298 K.

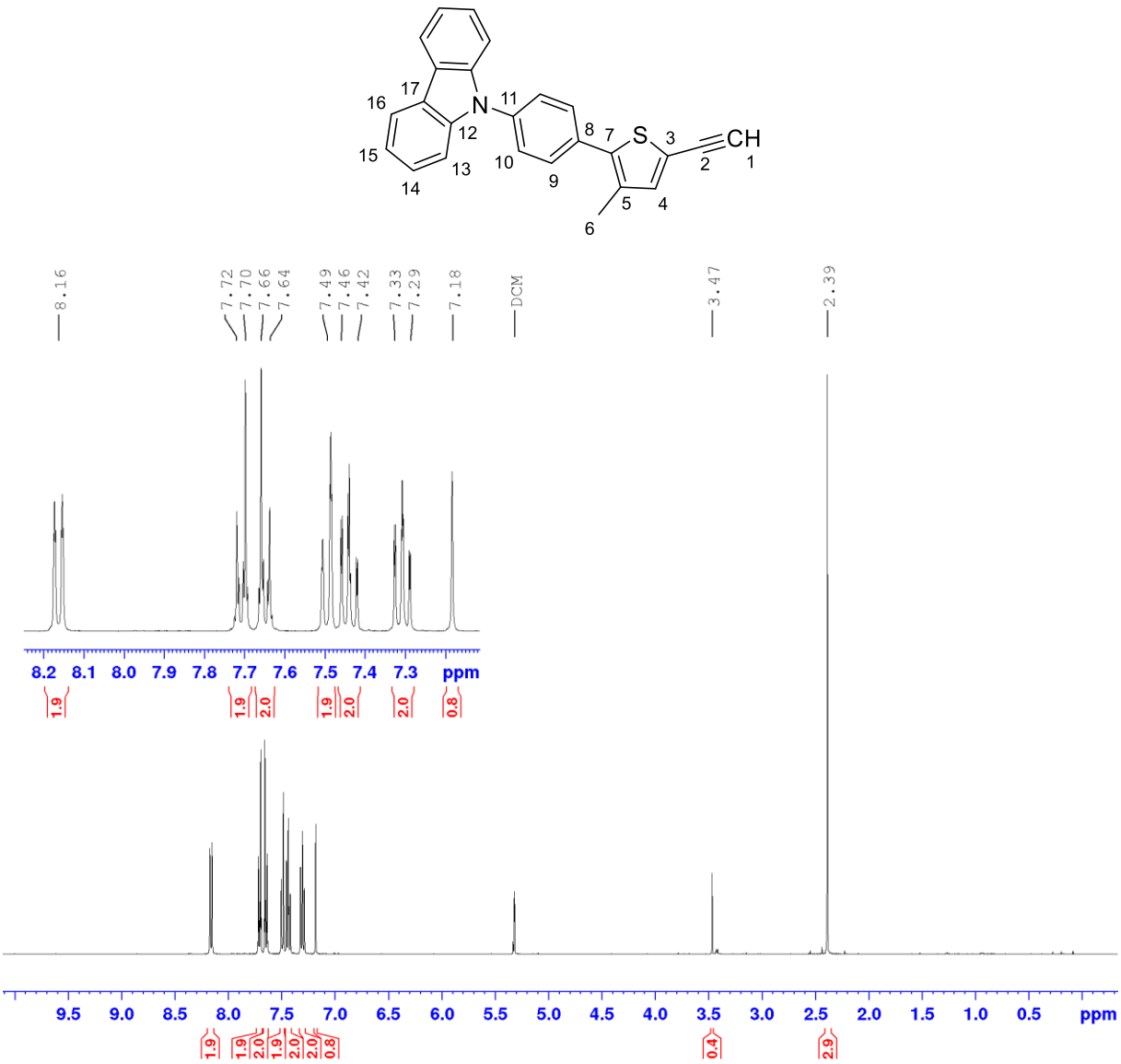


**Figure A26:** $^{1}H$ NMR of **12** in $CD_2Cl_2$ at a 400 MHz spectrometer at 298 K.

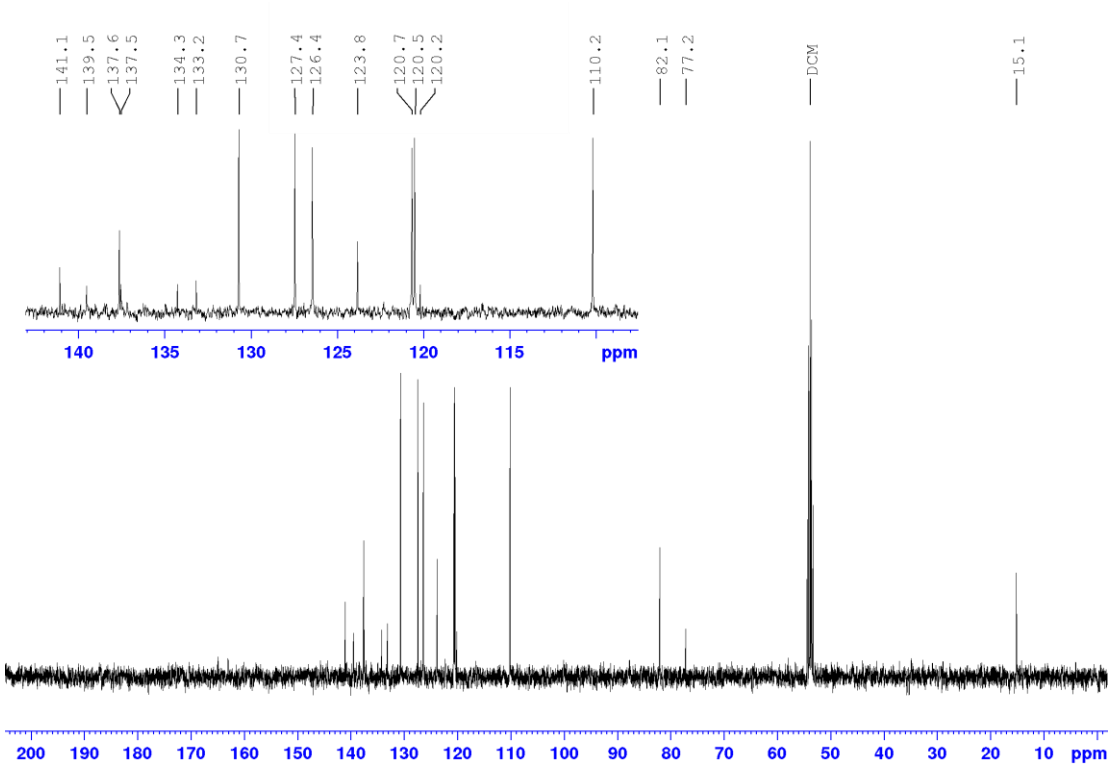


**Figure A27:** $^{13}C\{^{1}H\}$ NMR of **12** in $CD_2Cl_2$ at a 100.6 MHz spectrometer at 298 K.

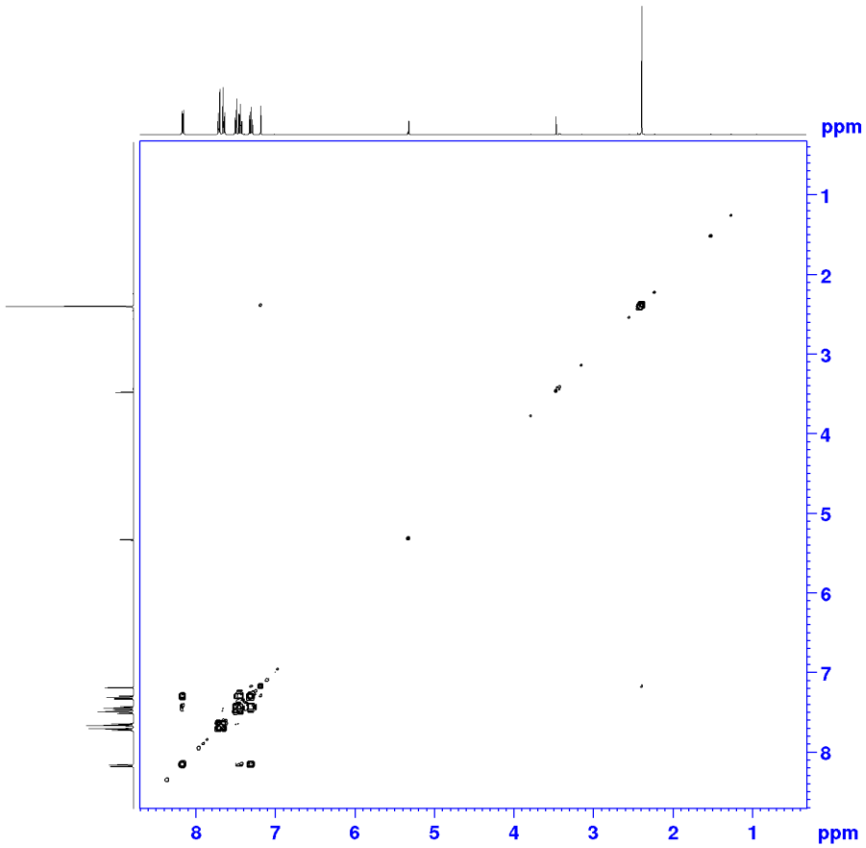


**Figure A28:** $^{1}H,^{1}H$ COSY NMR spectrum of **12** in $CD_2Cl_2$ at a 400 MHz spectrometer at 298 K.

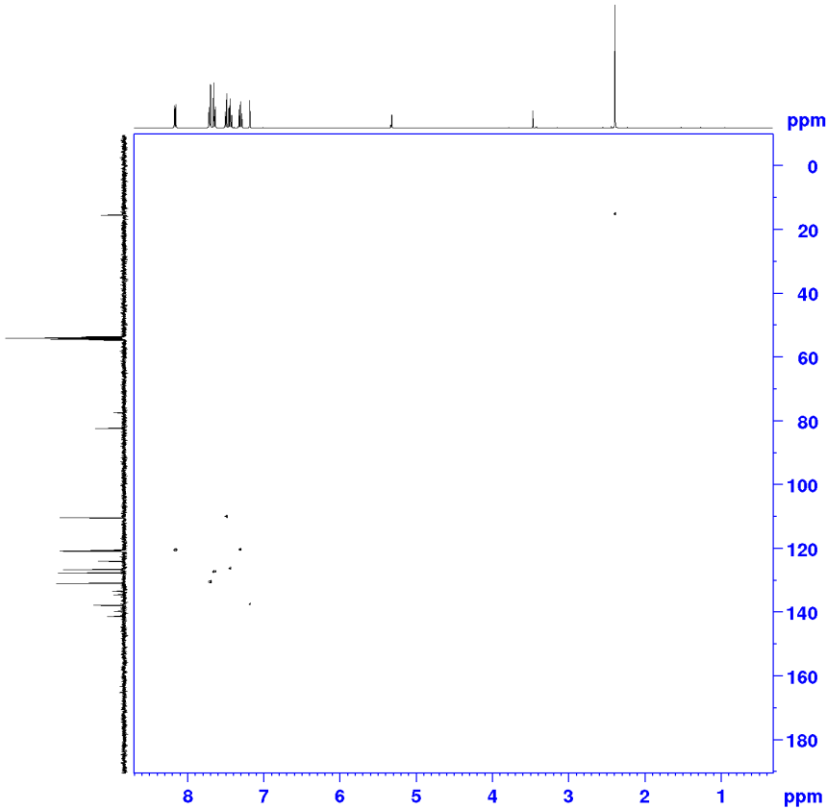


**Figure A29:** $^{1}H,^{13}C$ HSQC NMR spectrum of **12** in $CD_2Cl_2$ at a 400 MHz spectrometer at 298 K.

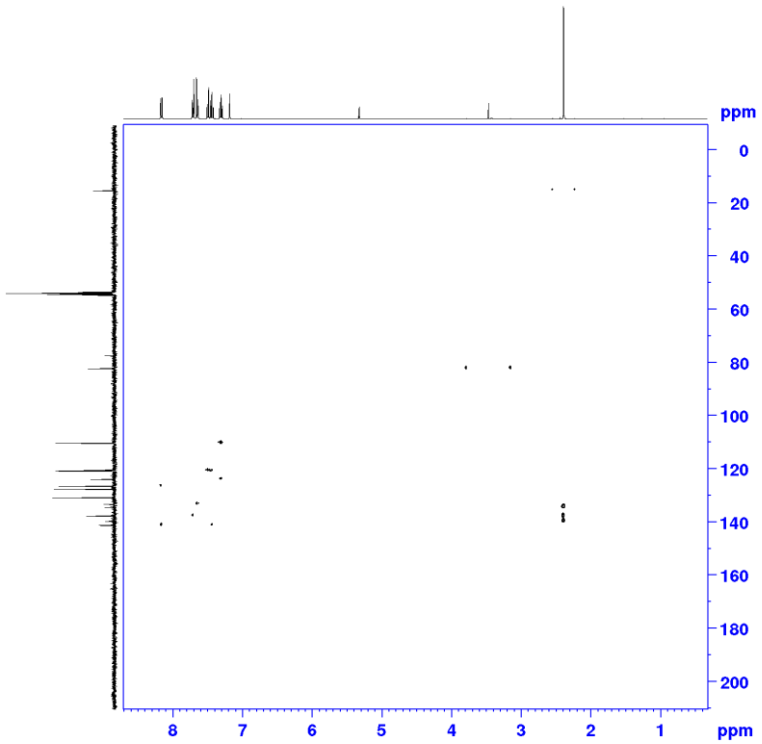


**Figure A30:** $^{1}H,^{13}C$ HMBC NMR spectrum of **12** in $CD_2Cl_2$ at a 400 MHz spectrometer at 298 K.

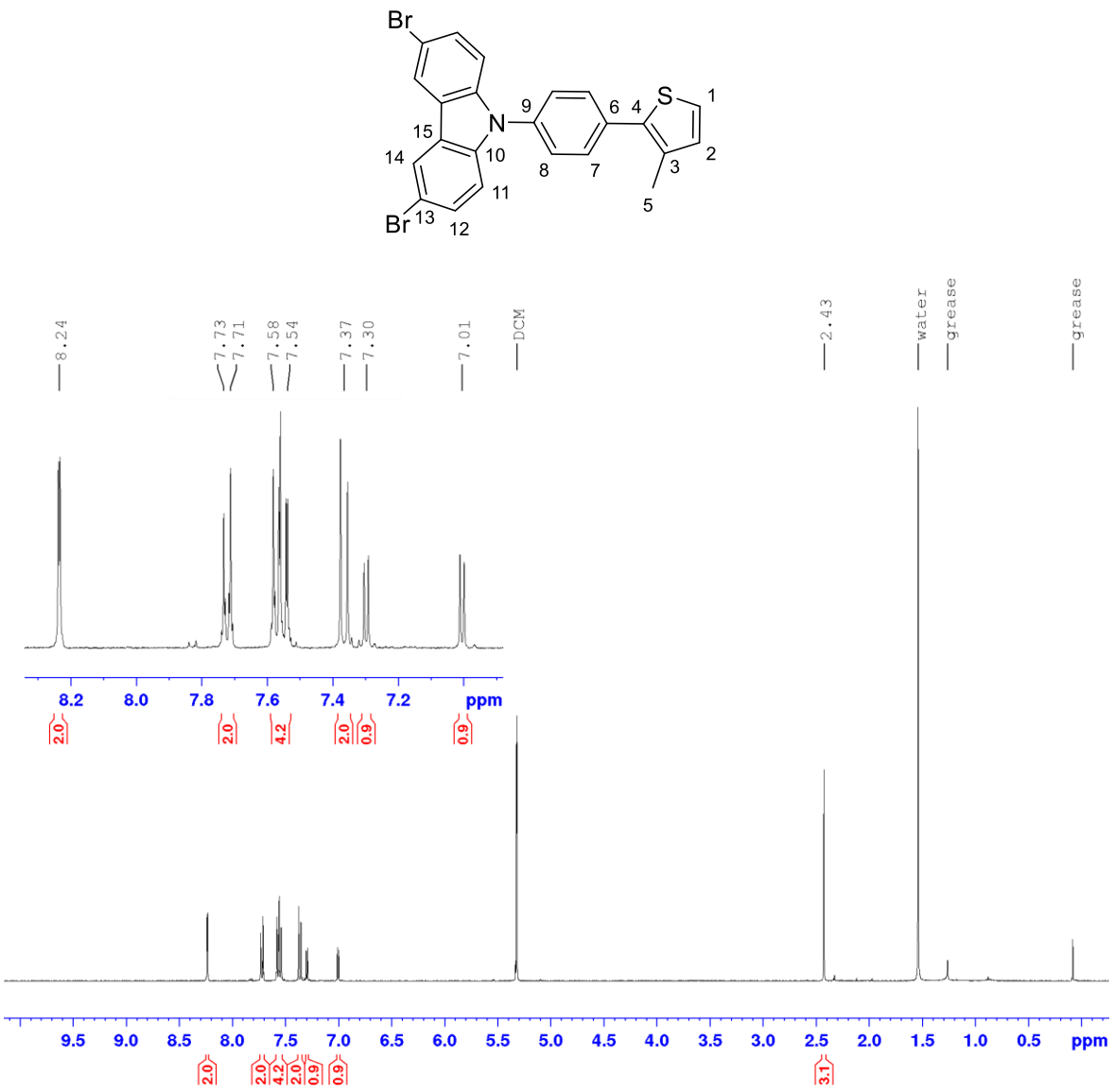


**Figure A31:** $^{1}H$ NMR of **13** in $CD_2Cl_2$ at a 400 MHz spectrometer at 298 K.

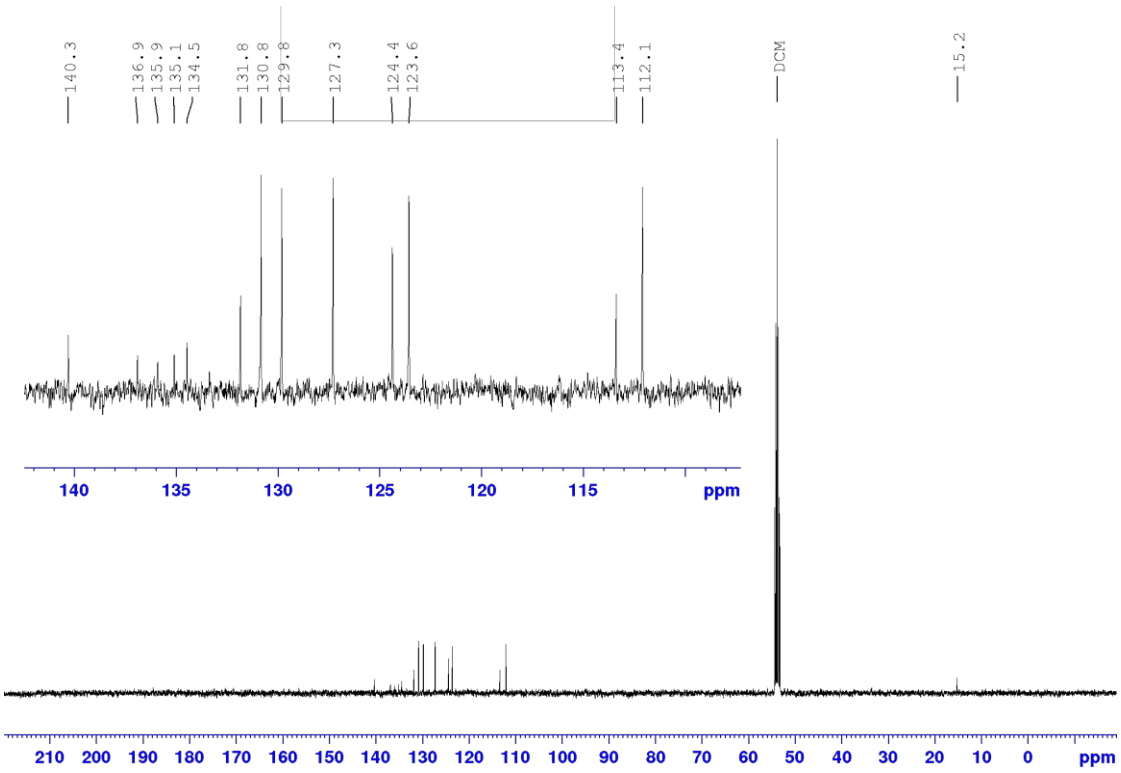


**Figure A32:** $^{13}C\{^{1}H\}$ NMR of **13** in $CD_2Cl_2$ at a 100.6 MHz spectrometer at 298 K.

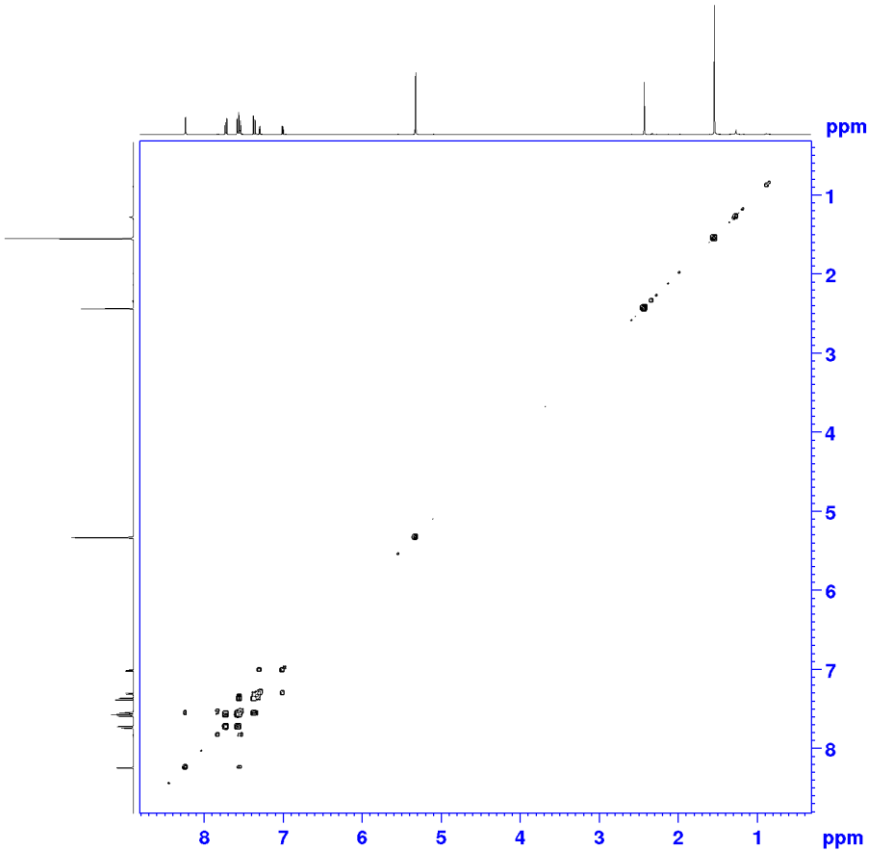


**Figure A33:** $^{1}H,^{1}H$ COSY NMR spectrum of **13** in $CD_2Cl_2$ at a 400 MHz spectrometer at 298 K.

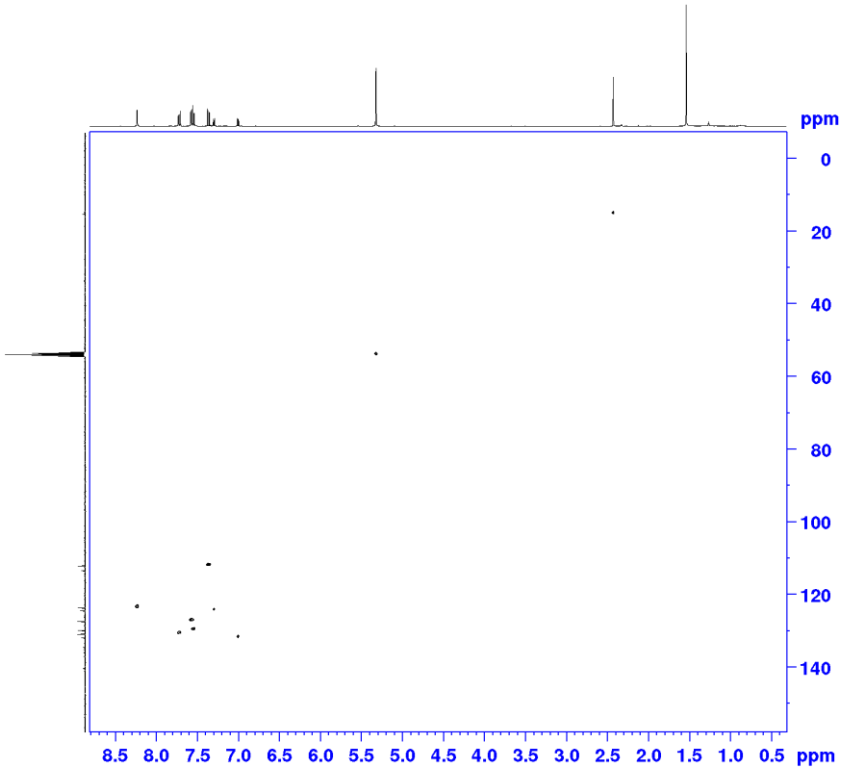


**Figure A34:** $^{1}H,^{13}C$ HSQC NMR spectrum of **13** in $CD_2Cl_2$ at a 400 MHz spectrometer at 298 K.

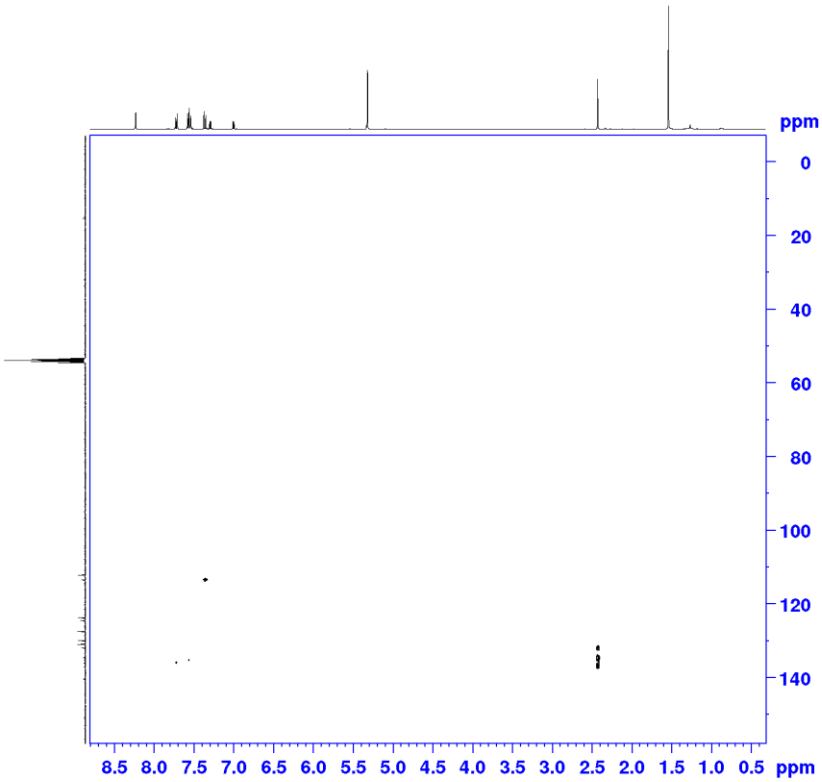


**Figure A35:** $^{1}H,^{13}C$ HMBC NMR spectrum of **13** in $CD_2Cl_2$ at a 400 MHz spectrometer at 298 K.

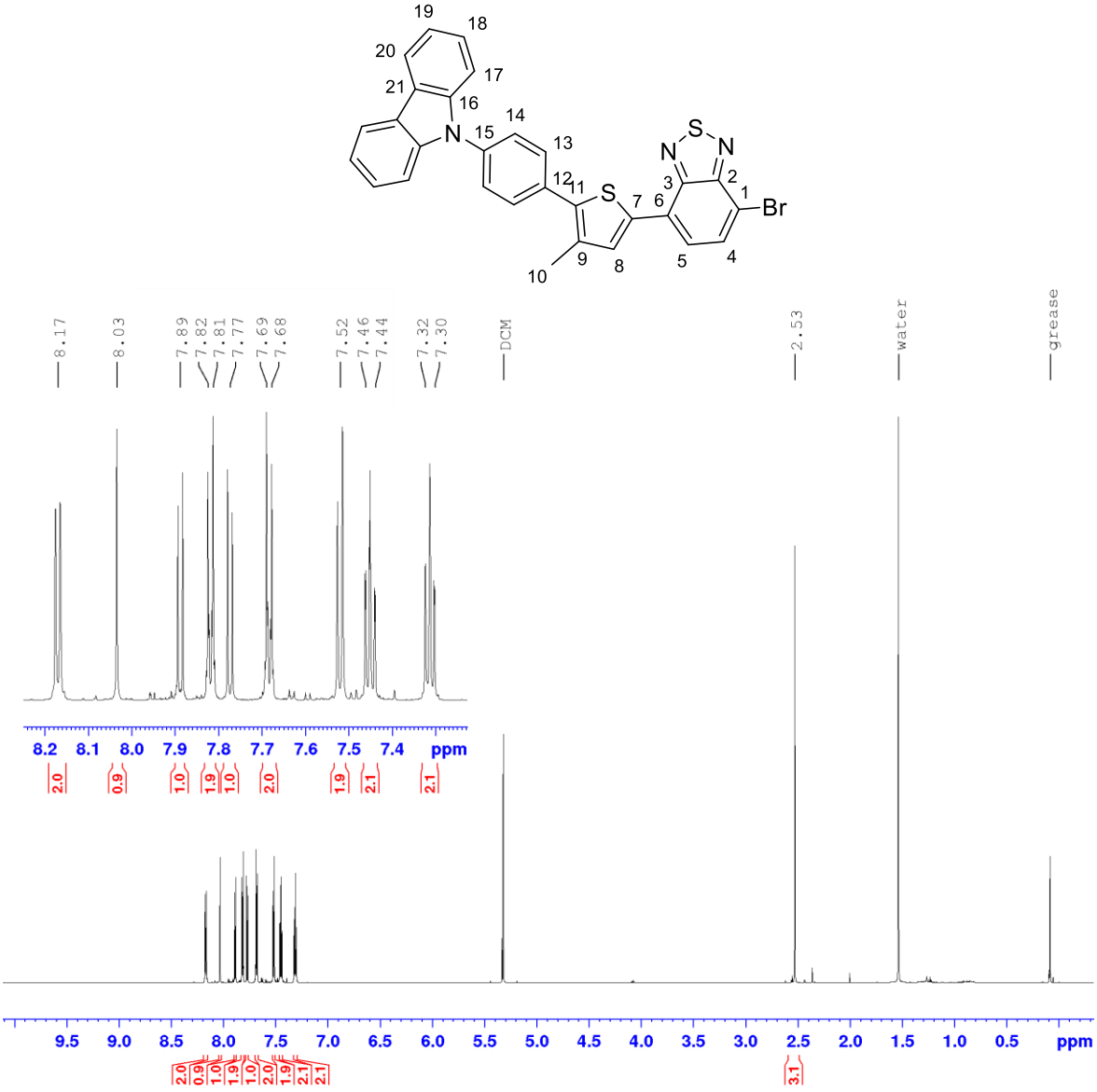


**Figure A36:** $^{1}$H NMR of **15a** in $CD_2Cl_2$ at a 700 MHz spectrometer at 298 K.

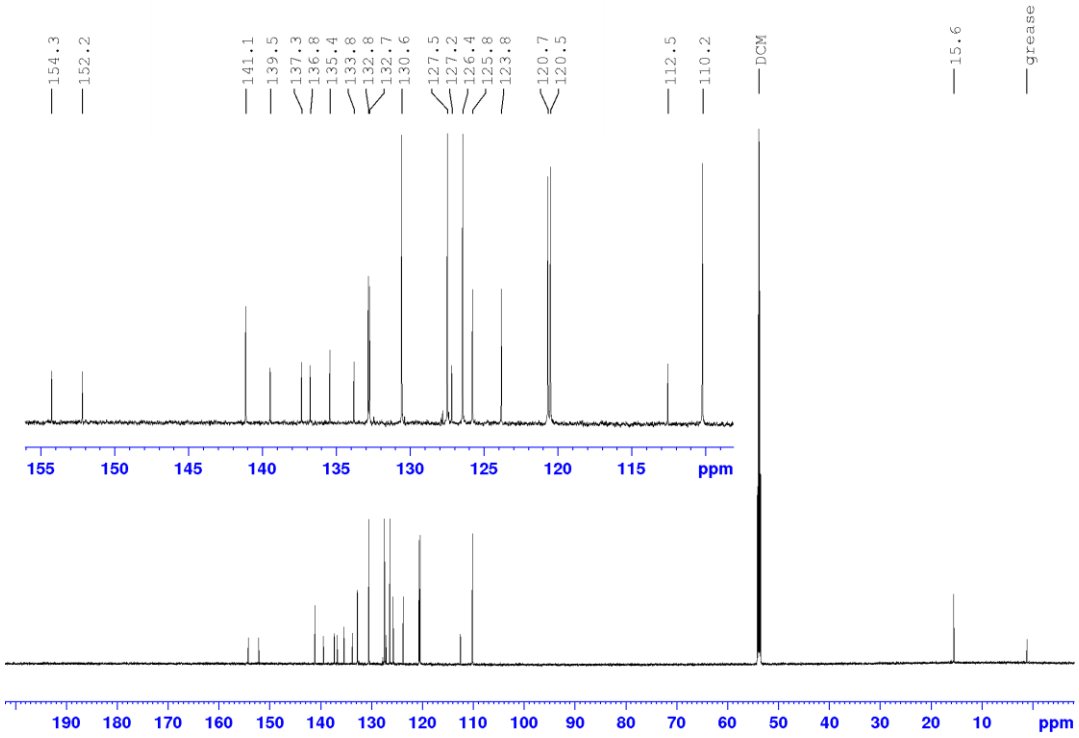


**Figure A37:** $^{13}C\{^{1}H\}$ NMR of **15a** in $CD_2Cl_2$ at a 176.1 MHz spectrometer at 298 K.

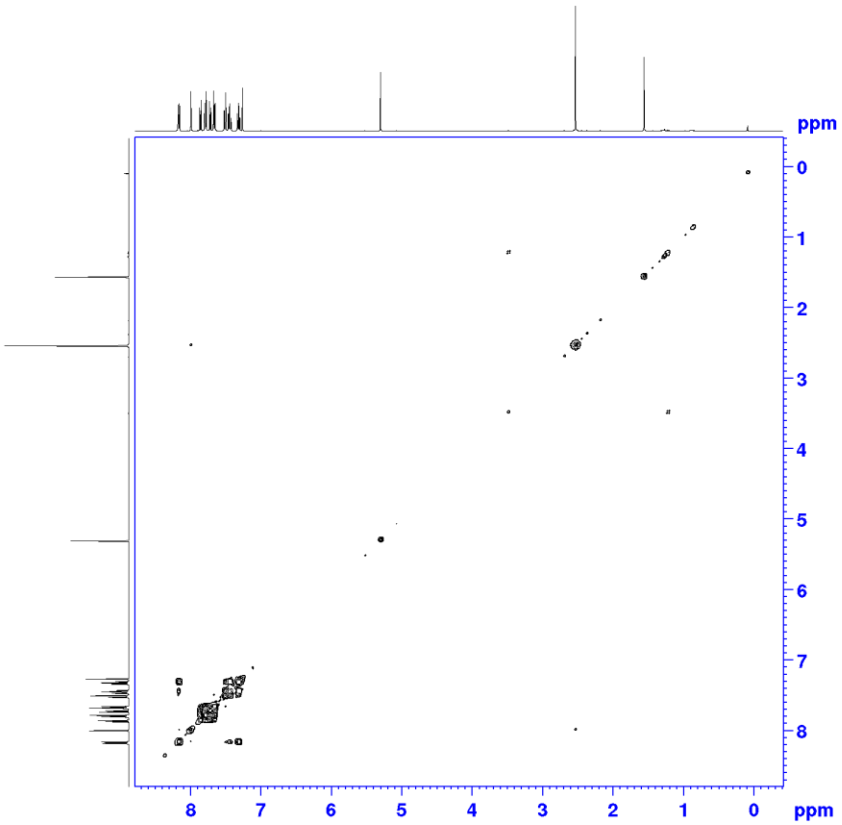


**Figure A38:** $^{1}H,^{1}H$ COSY NMR spectrum of **15a** in $CDCl_3$ at a 700 MHz spectrometer at 298 K.

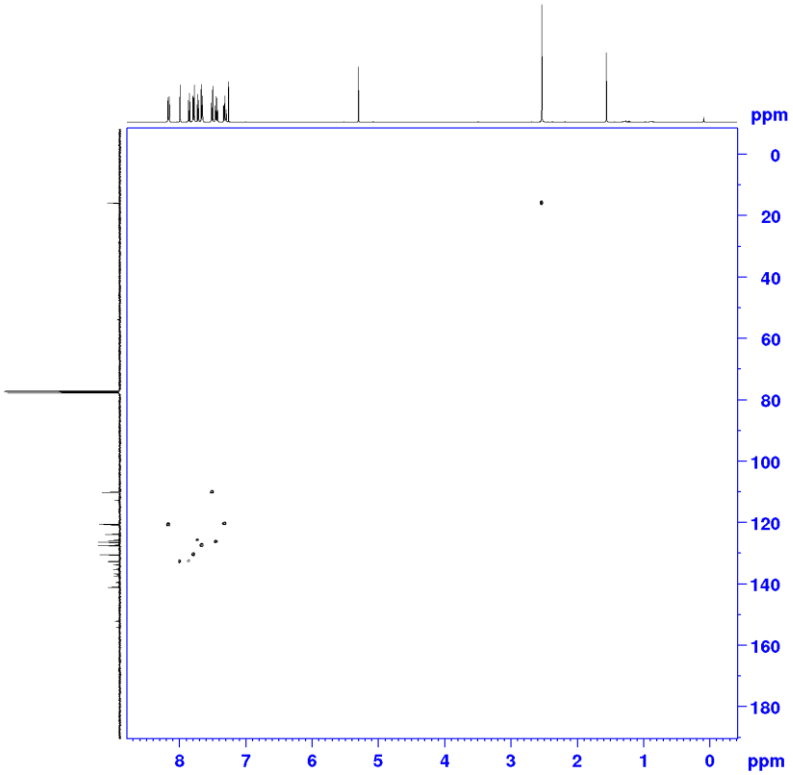


**Figure A39:** $^{1}H,^{13}C$ HSQC NMR spectrum of **15a** in $CDCl_3$ at a 700 MHz spectrometer at 298 K.

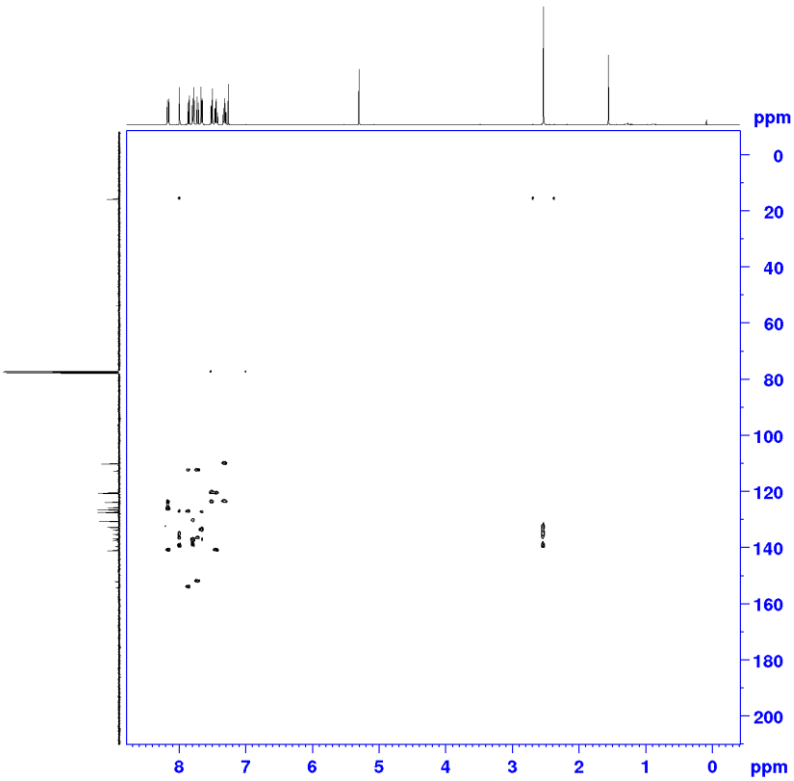


**Figure A40:** $^{1}H,^{13}C$ HMBC NMR spectrum of **15a** in $CDCl_3$ at a 700 MHz spectrometer at 298 K.

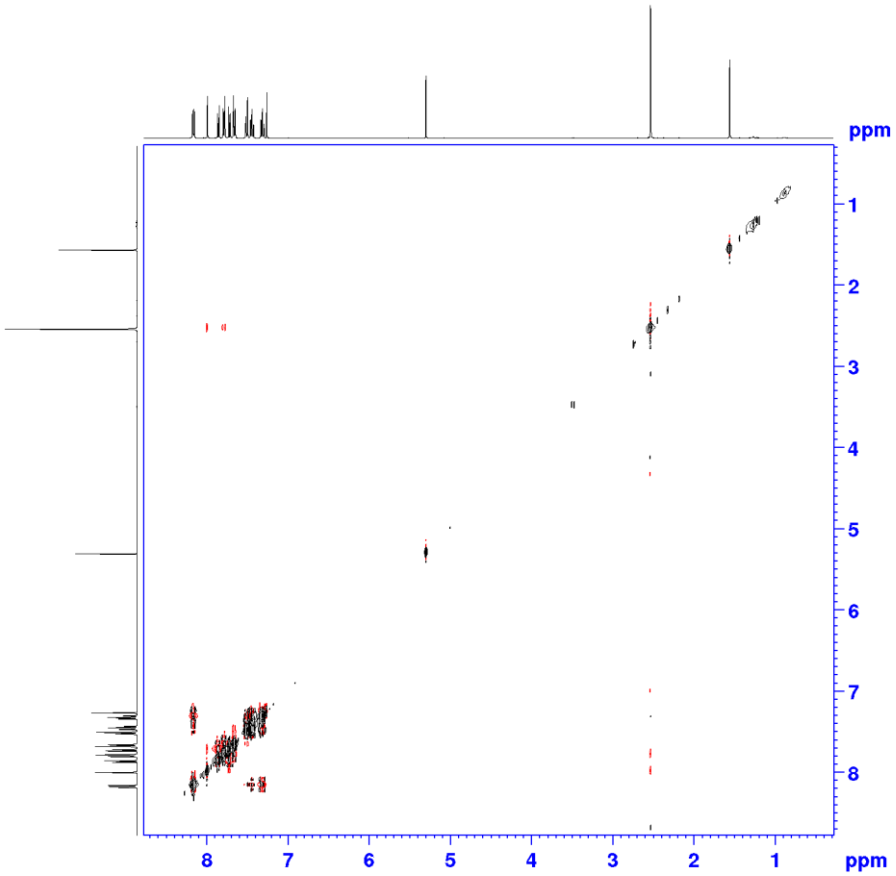


**Figure A41:** $^{1}H,^{1}H$ NOESY NMR spectrum of **15a** in $CDCl_3$ at a 700 MHz spectrometer at 298 K.

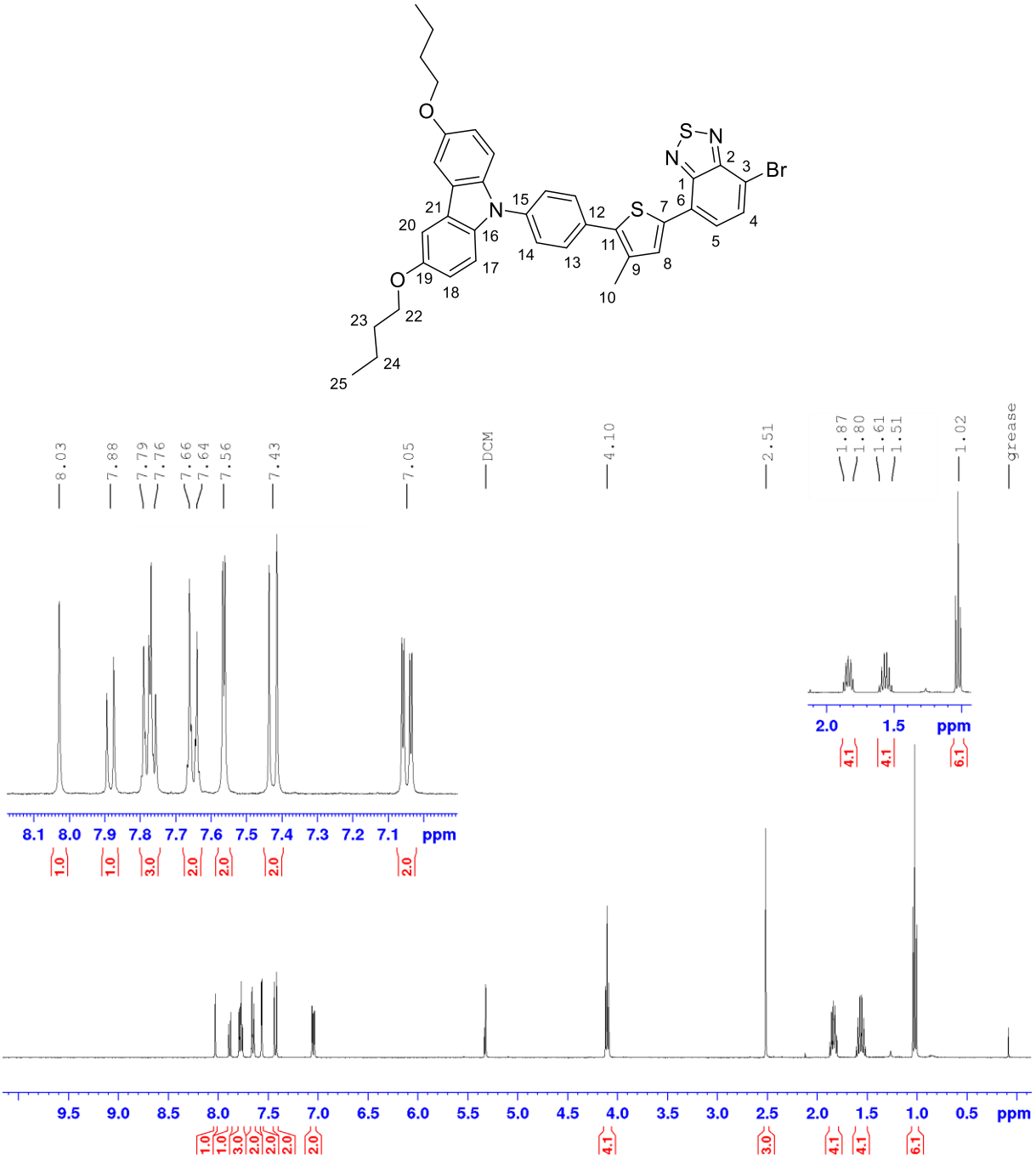


**Figure A42:** $^{1}H$ NMR of **15b** in $CD_2Cl_2$ at a 400 MHz spectrometer at 298 K.

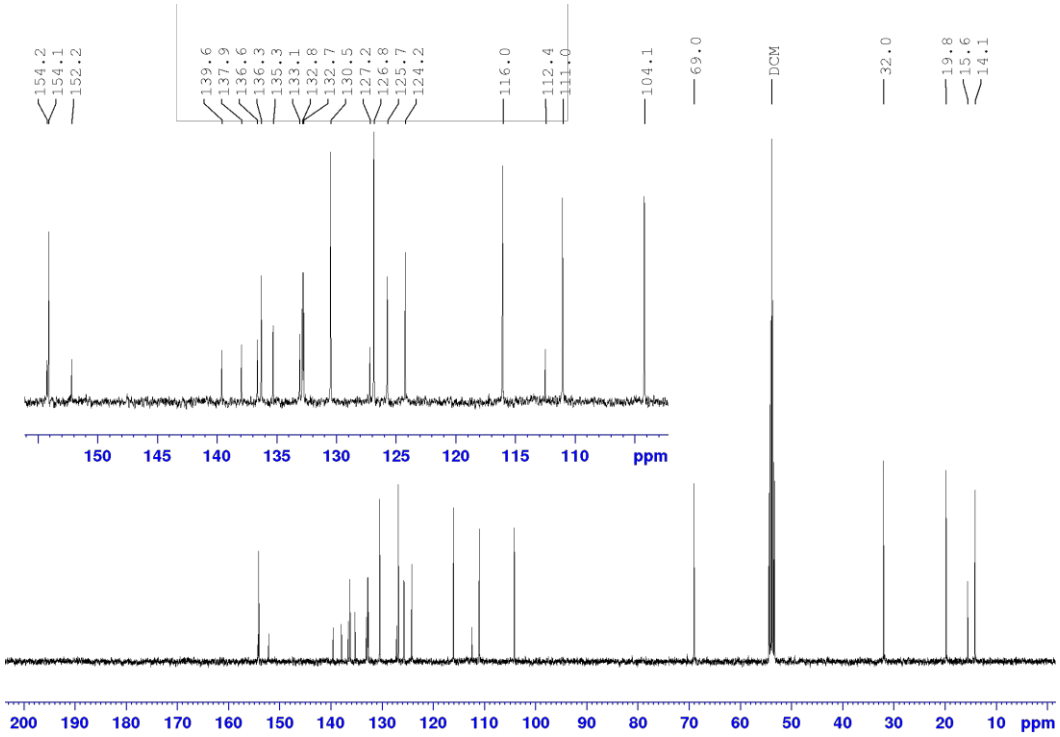


**Figure A43:** $^{13}C\{^{1}H\}$ NMR of **15b** in $CD_2Cl_2$ at a 100.6 MHz spectrometer at 298 K.

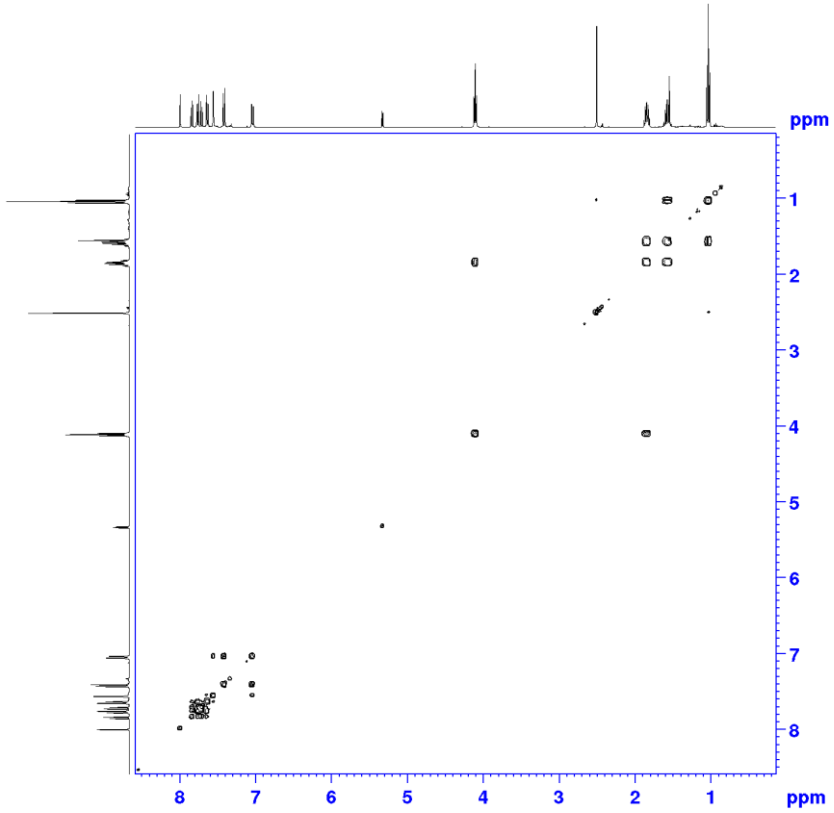


**Figure A44:** $^{1}H,^{1}H$ COSY NMR spectrum of **15b** in $CD_2Cl_2$ at a 400 MHz spectrometer at 298 K.

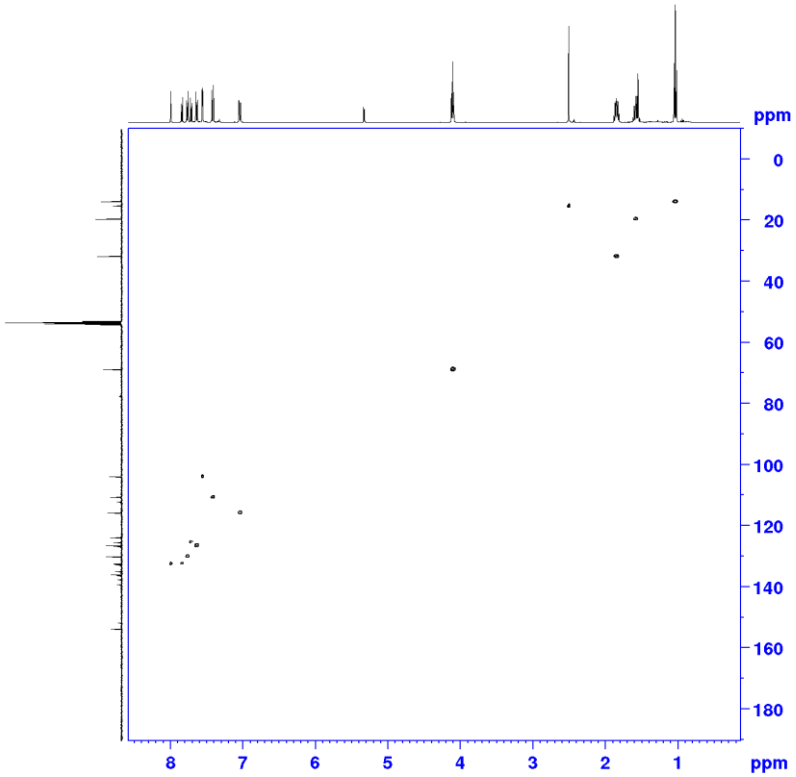


**Figure A45:** $^{1}H,^{13}C$ HSQC NMR spectrum of **15b** in $CD_2Cl_2$ at a 400 MHz spectrometer at 298 K.

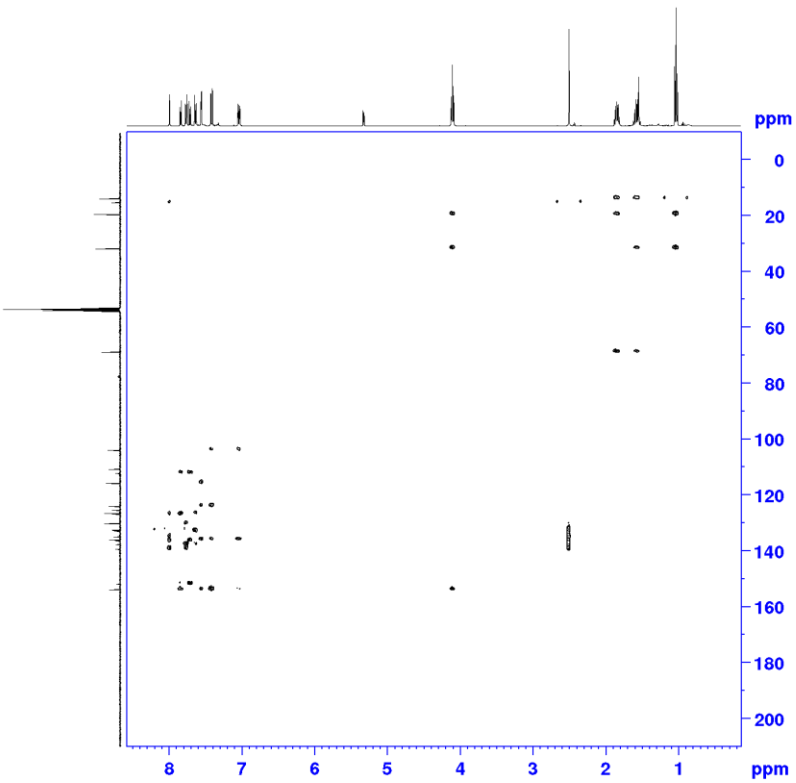


**Figure A46:** $^{1}H,^{13}C$ HMBC NMR spectrum of **15b** in $CD_2Cl_2$ at a 400 MHz spectrometer at 298 K.

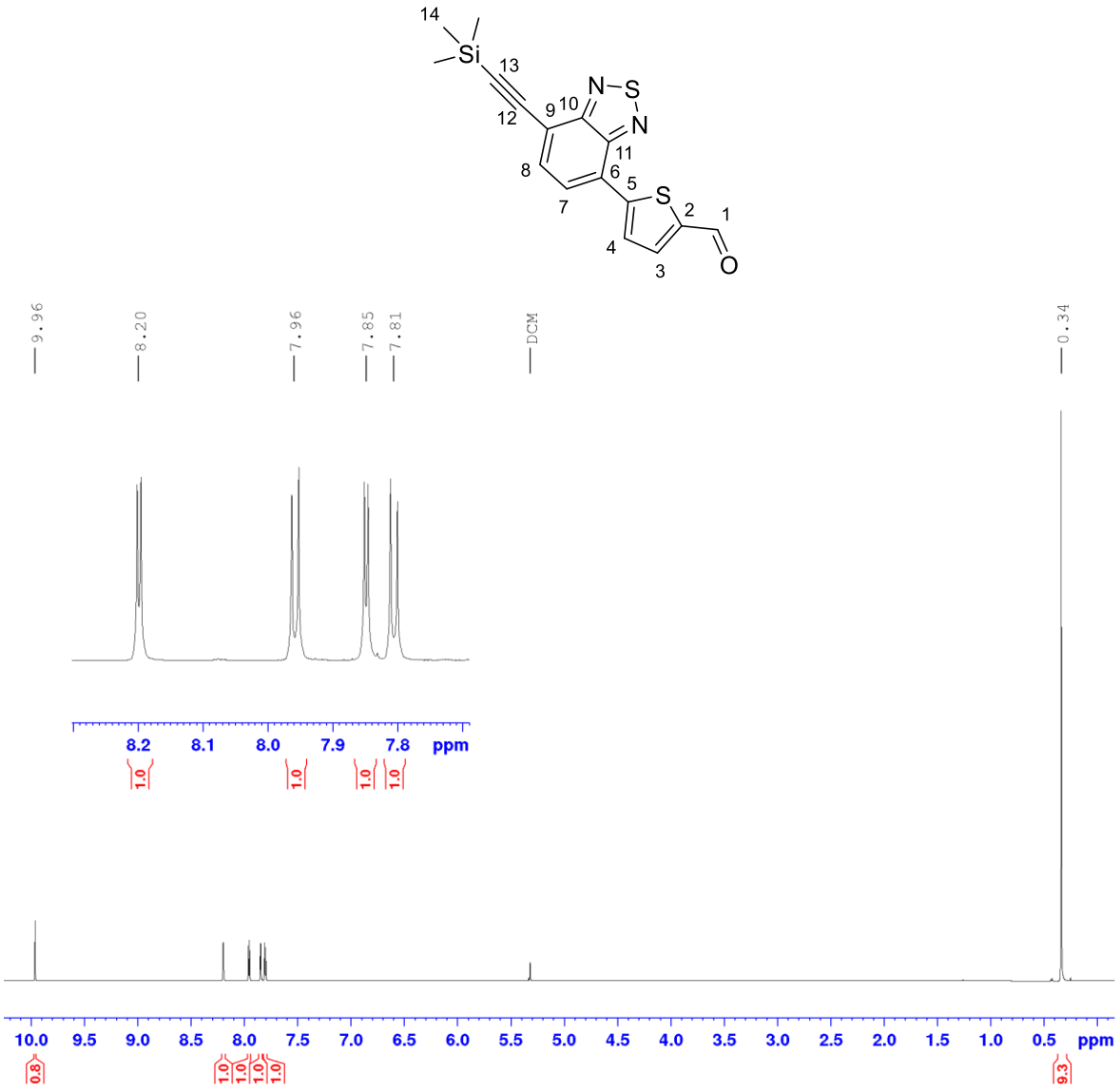


**Figure A47:** $^{1}H$ NMR of **18** in $CD_2Cl_2$ at a 400 MHz spectrometer at 298 K.

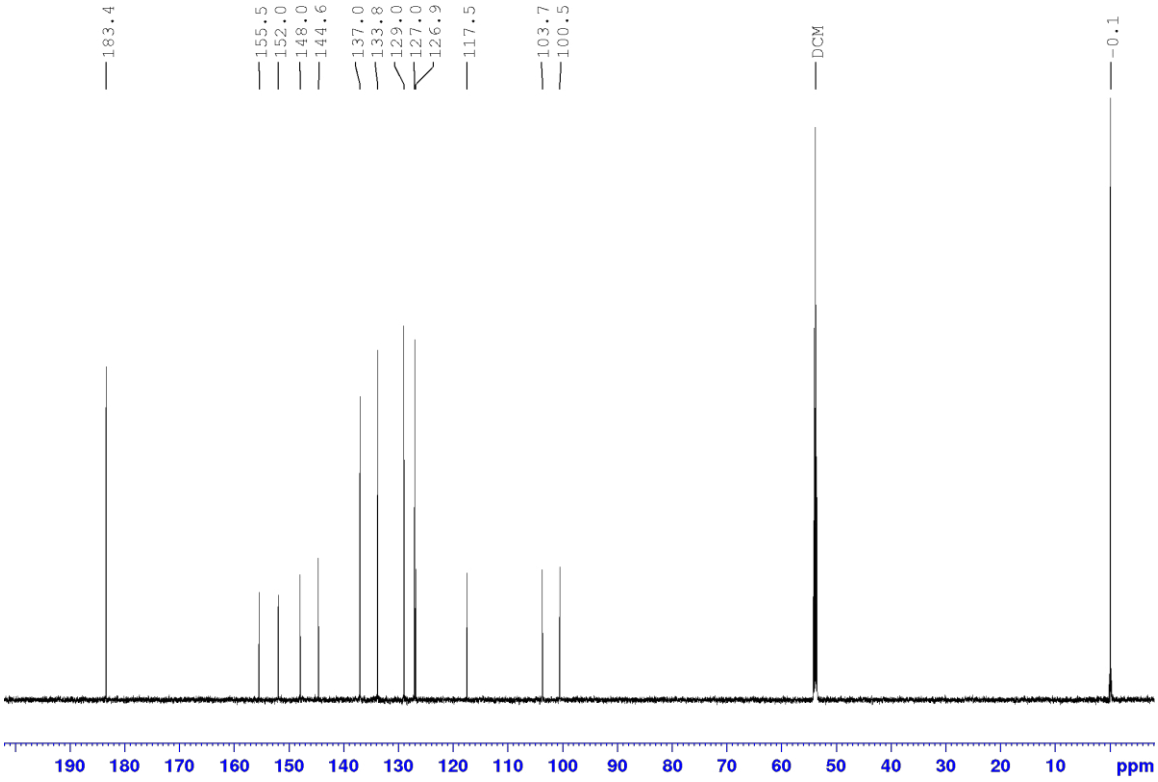


**Figure A48:** $^{13}C\{^{1}H\}$ NMR of **18** in $CD_2Cl_2$ at a 100.6 MHz spectrometer at 298 K.

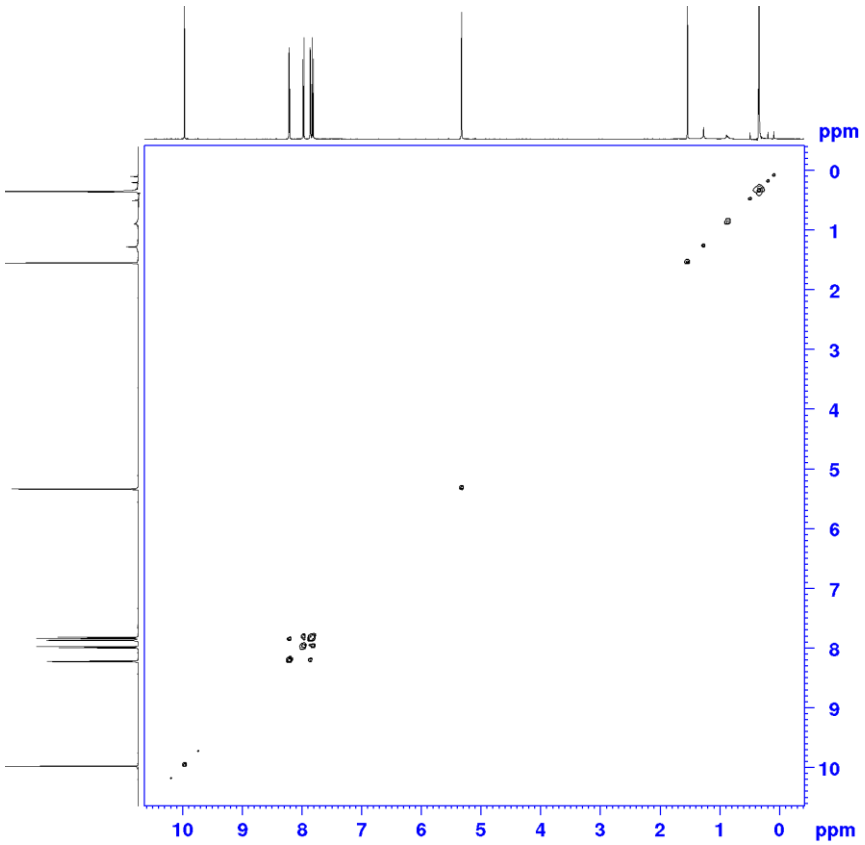


**Figure A49:** $^{1}H,^{1}H$ COSY NMR spectrum of **18** in $CD_2Cl_2$ at a 400 MHz spectrometer at 298 K.

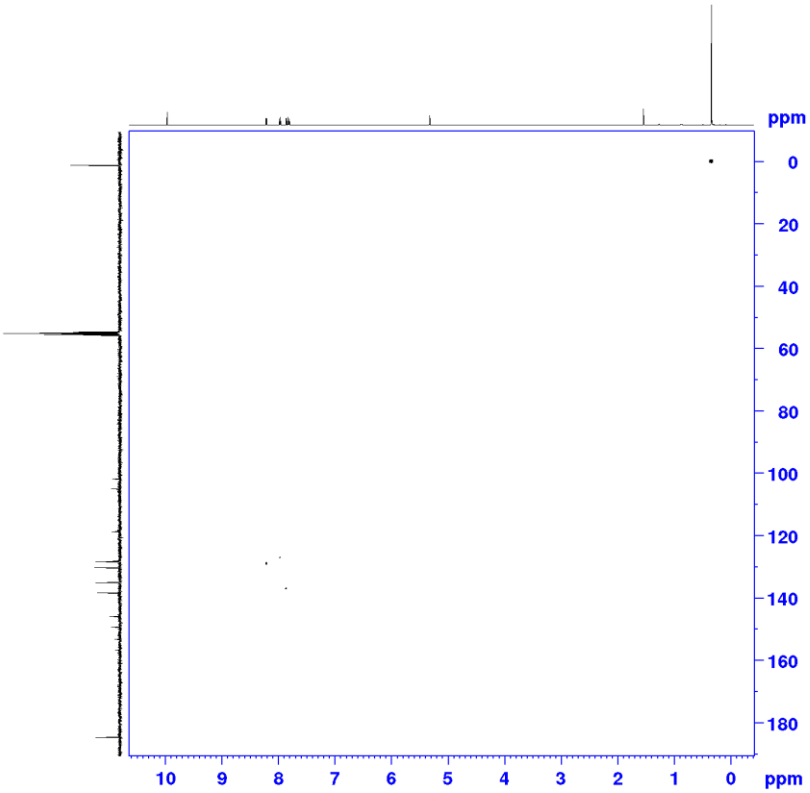


**Figure A50:** $^{1}H,^{13}C$ HSQC NMR spectrum of **18** in $CD_2Cl_2$ at a 400 MHz spectrometer at 298 K.

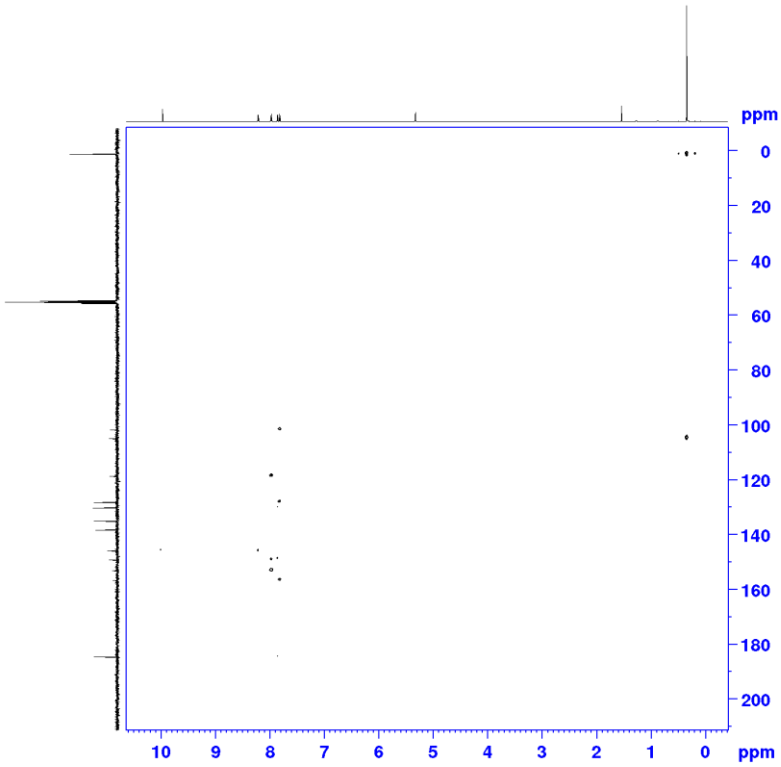


**Figure A51:** $^{1}H,^{13}C$ HMBC NMR spectrum of **18** in $CD_2Cl_2$ at a 400 MHz spectrometer at 298 K.

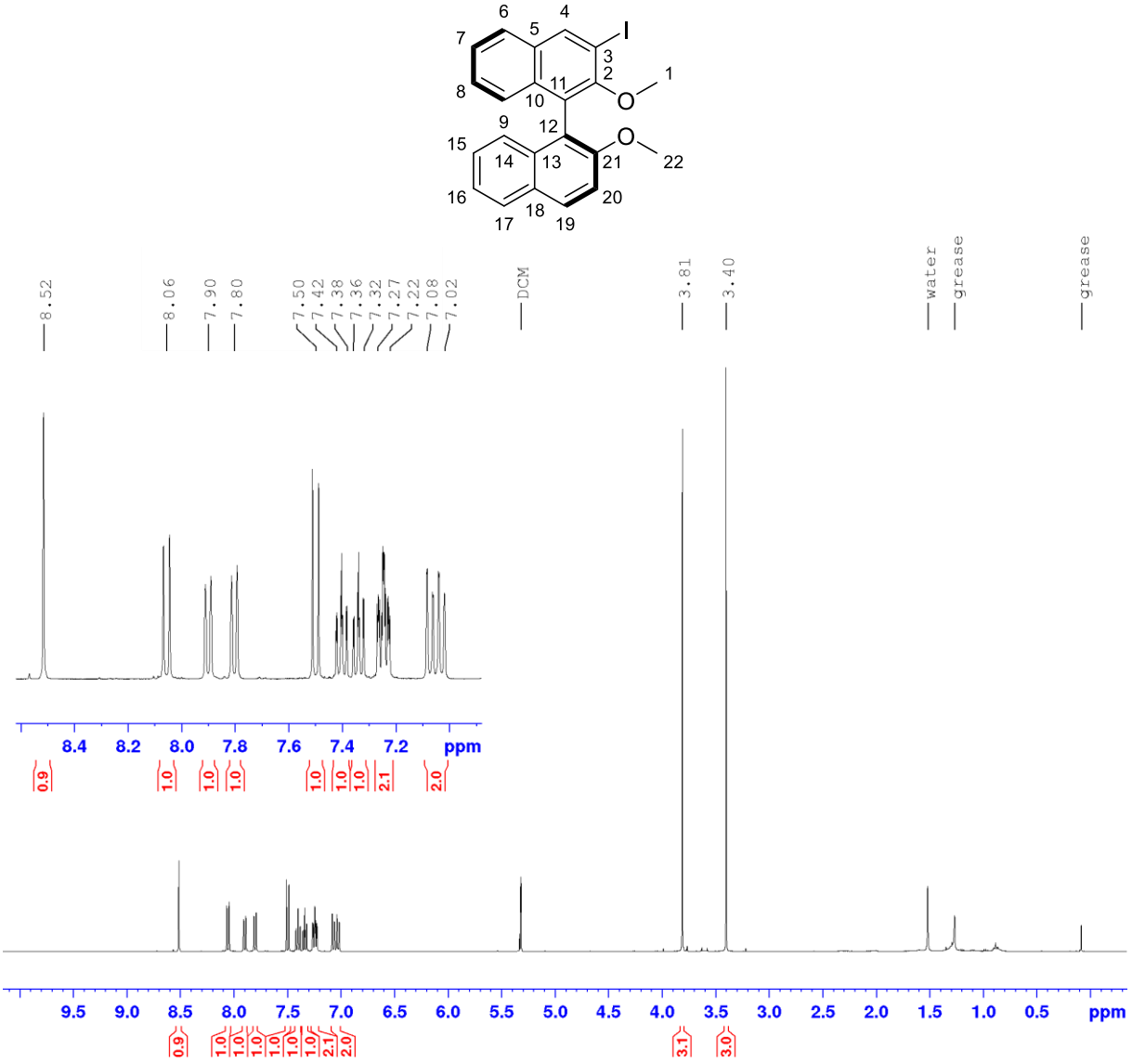


**Figure A52:** $^{1}H$ NMR of **22(*S*)** in $CD_2Cl_2$ at a 400 MHz spectrometer at 298 K.

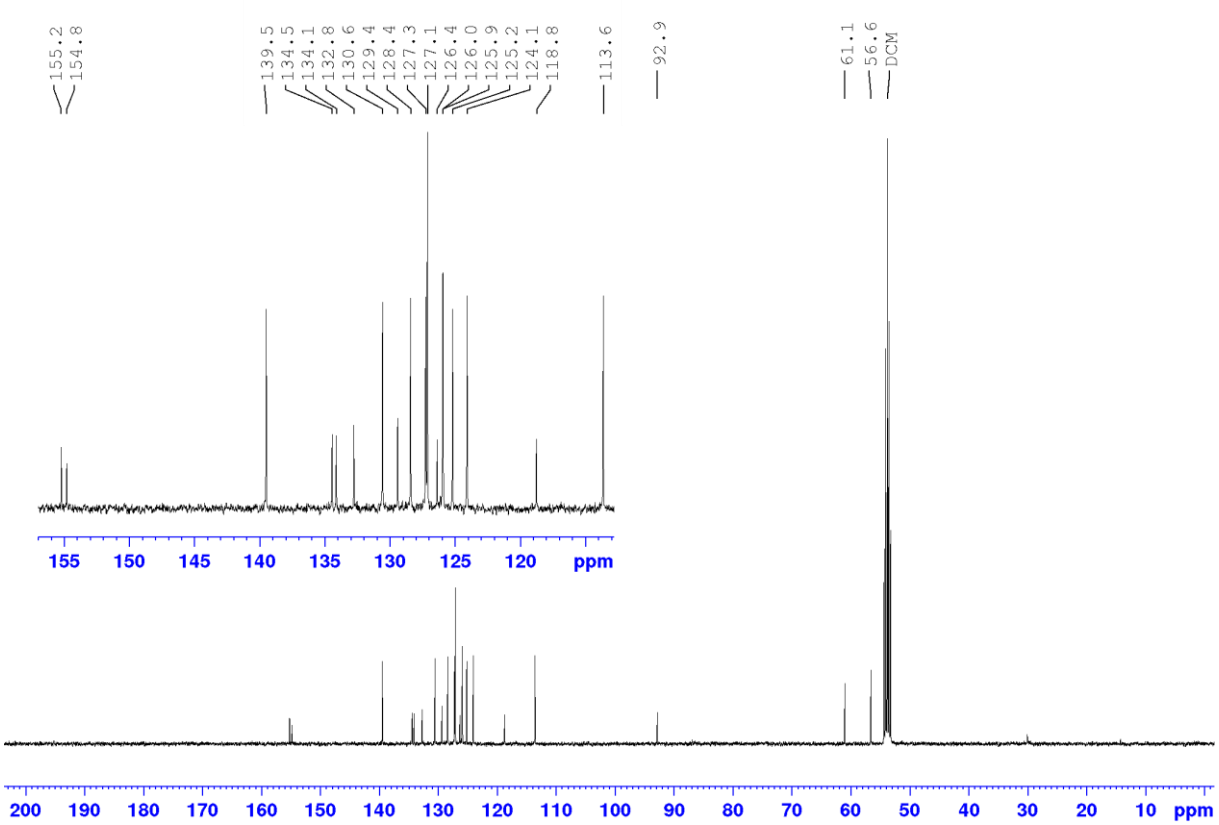


**Figure A53:** $^{13}C\{^{1}H\}$ NMR of **22(*S*)** in $CD_2Cl_2$ at a 100.6 MHz spectrometer at 298 K.

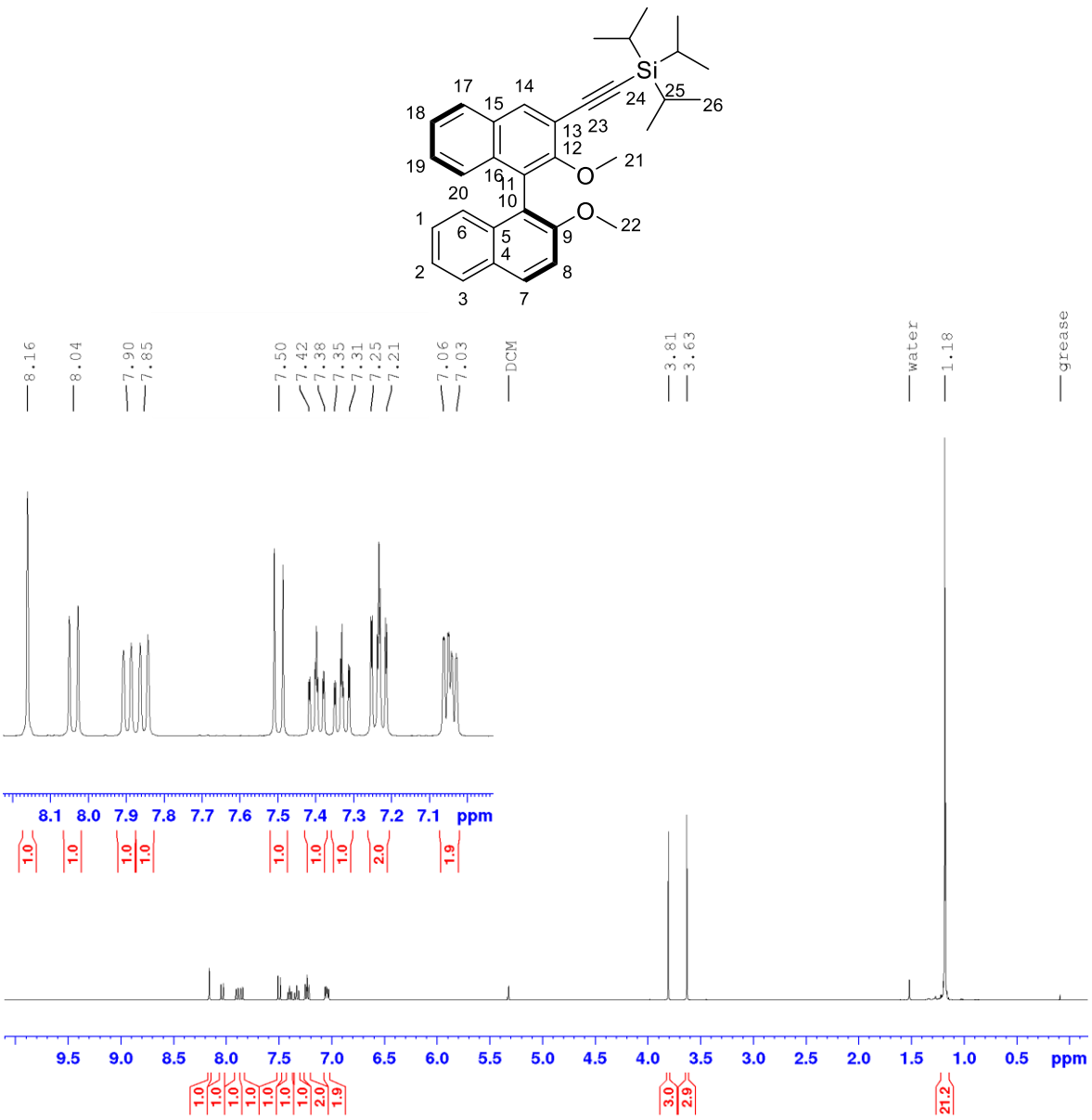


**Figure A54:** $^{1}$H NMR of **23(*S*)** in $CD_2Cl_2$ at a 400 MHz spectrometer at 298 K.

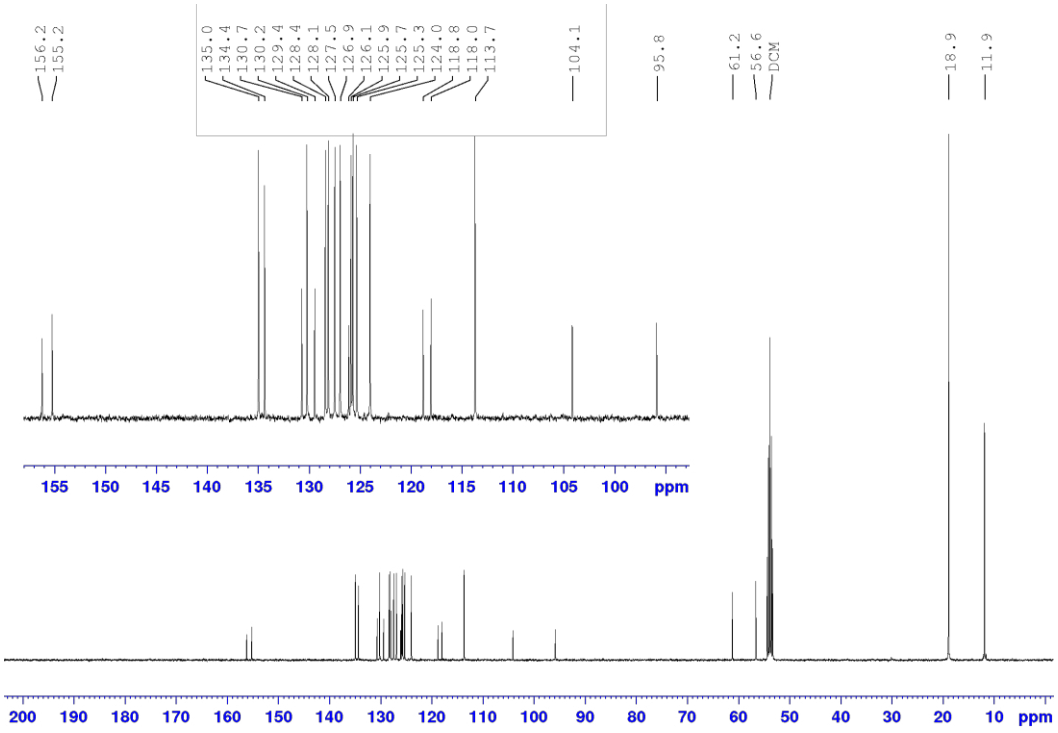


**Figure A55:** $^{13}C\{^{1}H\}$ NMR of **23(*S*)** in $CD_2Cl_2$ at a 100.6 MHz spectrometer at 298 K.

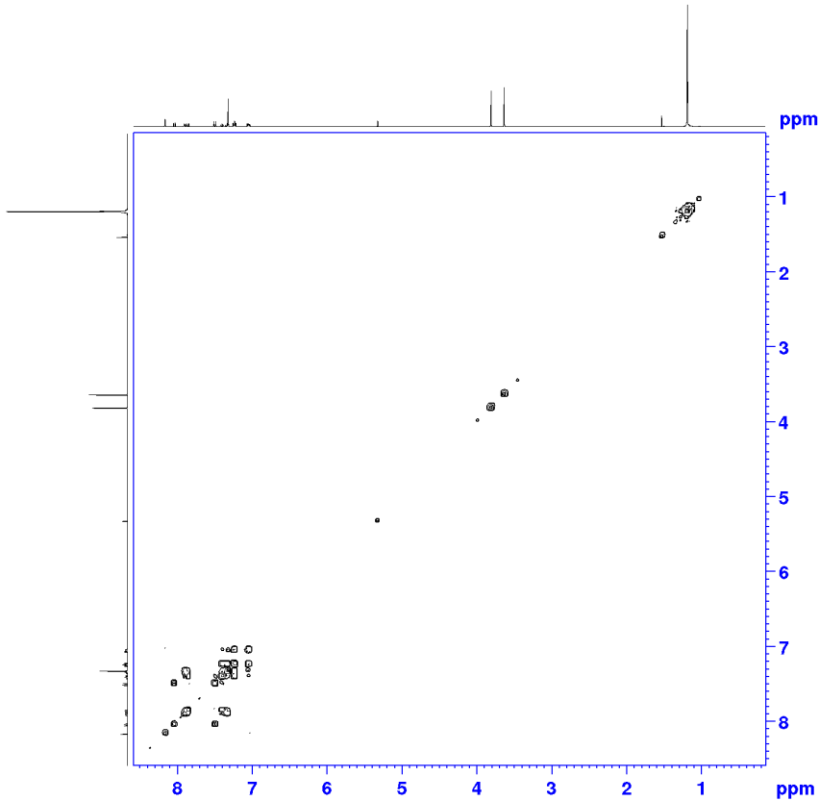


**Figure A56:** $^{1}H,^{1}H$ COSY NMR spectrum of **23(*S*)** in $CD_2Cl_2$ at a 400 MHz spectrometer at 298 K.

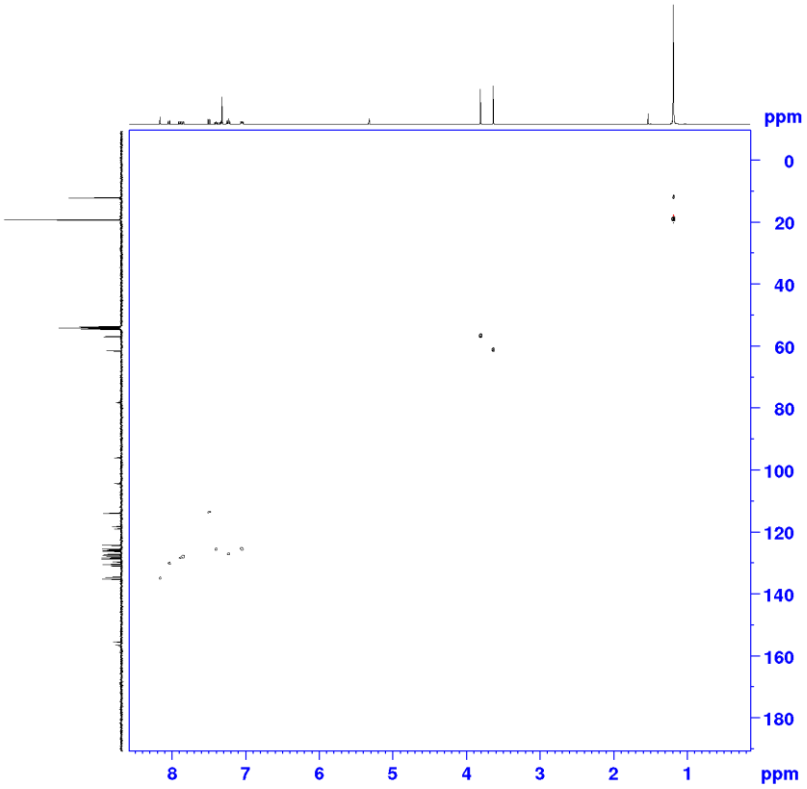


**Figure A57:** $^{1}H,^{13}C$ HSQC NMR spectrum of **23(*S*)** in $CD_2Cl_2$ at a 400 MHz spectrometer at 298 K.

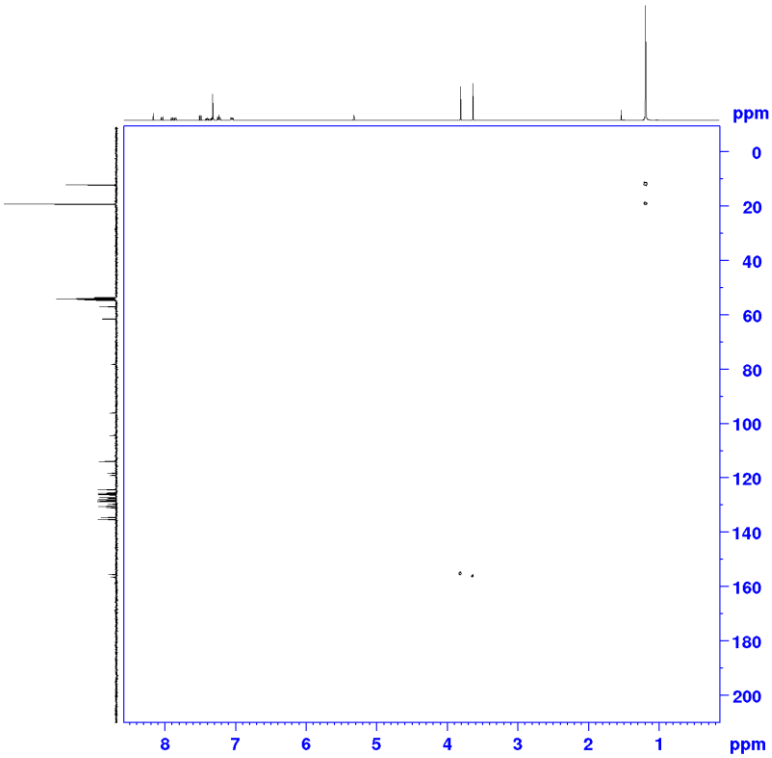


**Figure A58:** $^{1}H,^{13}C$ HMBC NMR spectrum of **23(*S*)** in $CD_2Cl_2$ at a 400 MHz spectrometer at 298 K.

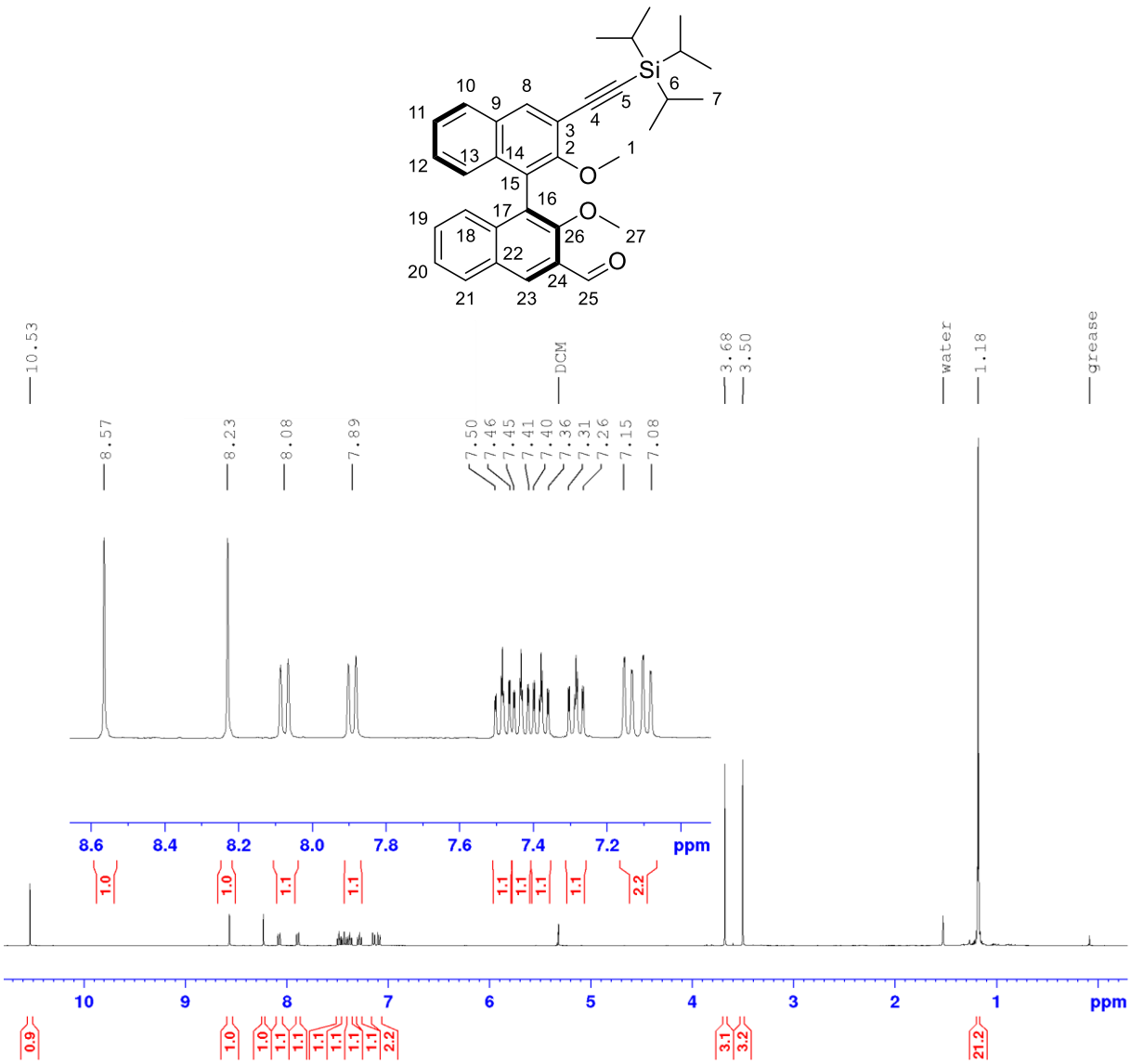


**Figure A59:** $^{1}$H NMR of **24(*S*)** in $CD_2Cl_2$ at a 400 MHz spectrometer at 298 K.

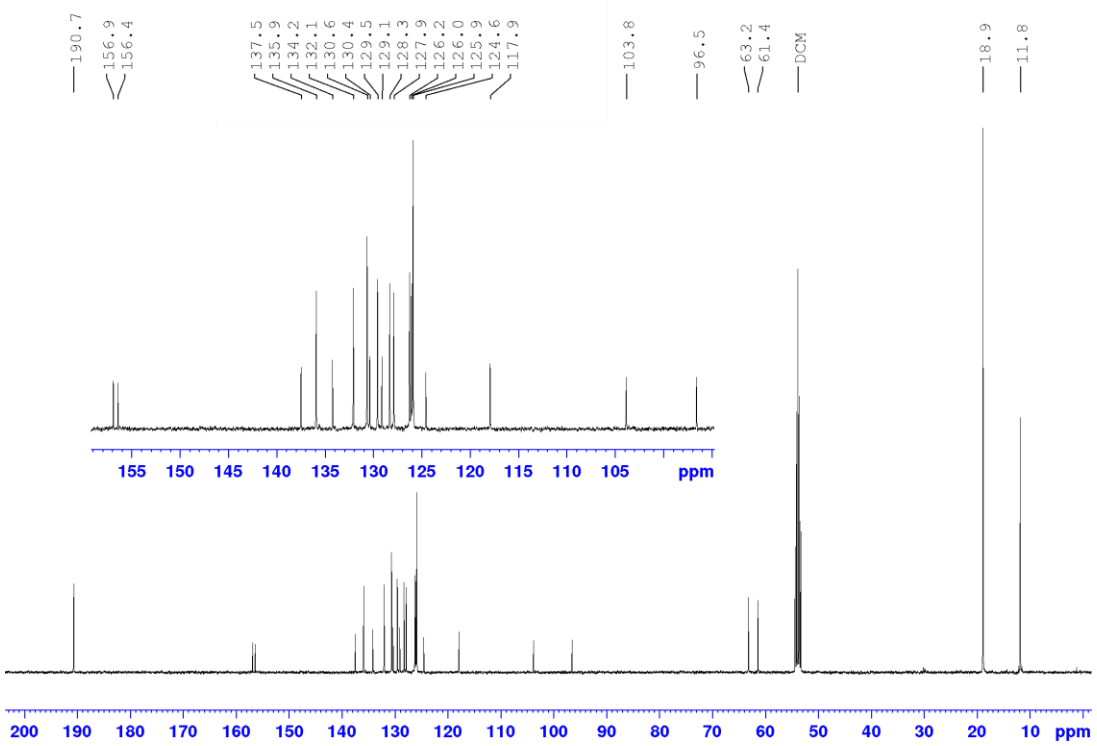


**Figure A60:** $^{13}C\{^{1}H\}$ NMR of **24(*S*)** in $CD_2Cl_2$ at a 100.6 MHz spectrometer at 298 K.

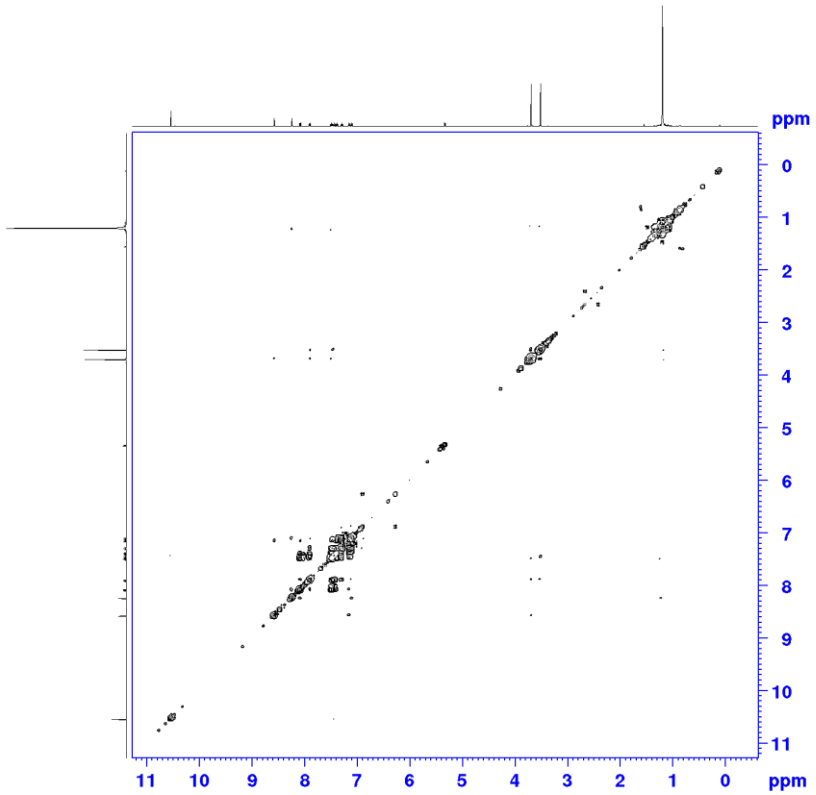


**Figure A61:** $^{1}H,^{1}H$ COSY NMR spectrum of **24(*S*)** in $CDCl_3$ at a 400 MHz spectrometer at 298 K.

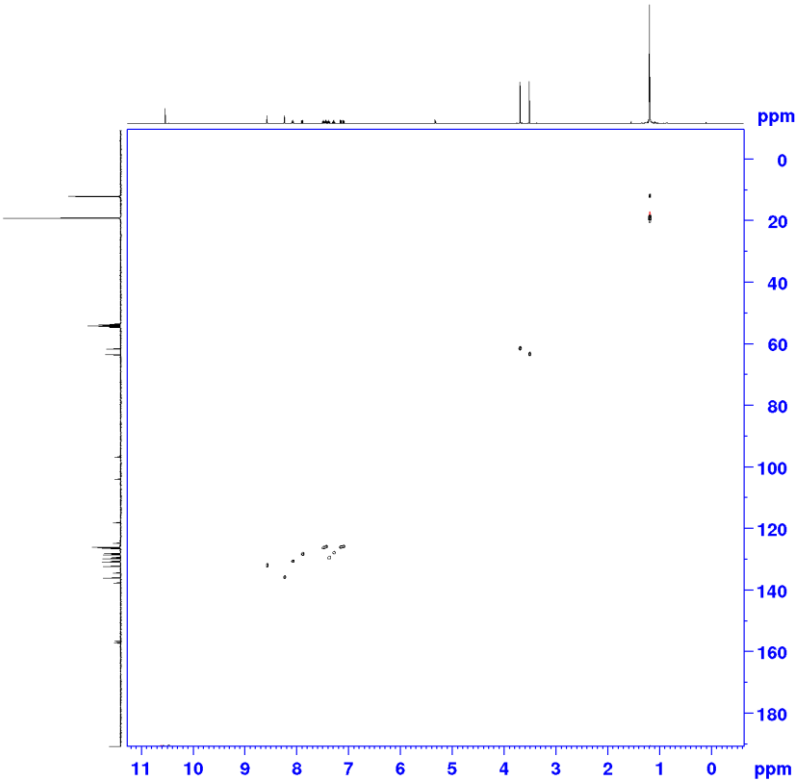


**Figure A62:** $^{1}H,^{13}C$ HSQC NMR spectrum of **24(*S*)** in $CDCl_3$ at a 400 MHz spectrometer at 298 K.

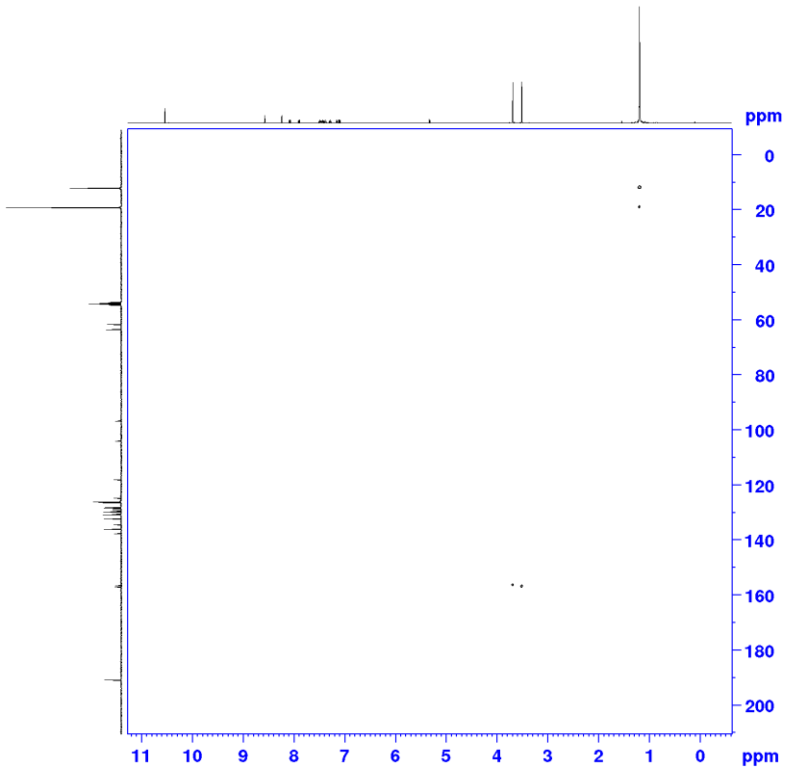


**Figure A63:** $^{1}H,^{13}C$ HMBC NMR spectrum of **24(*S*)** in $CDCl_3$ at a 400 MHz spectrometer at 298 K.

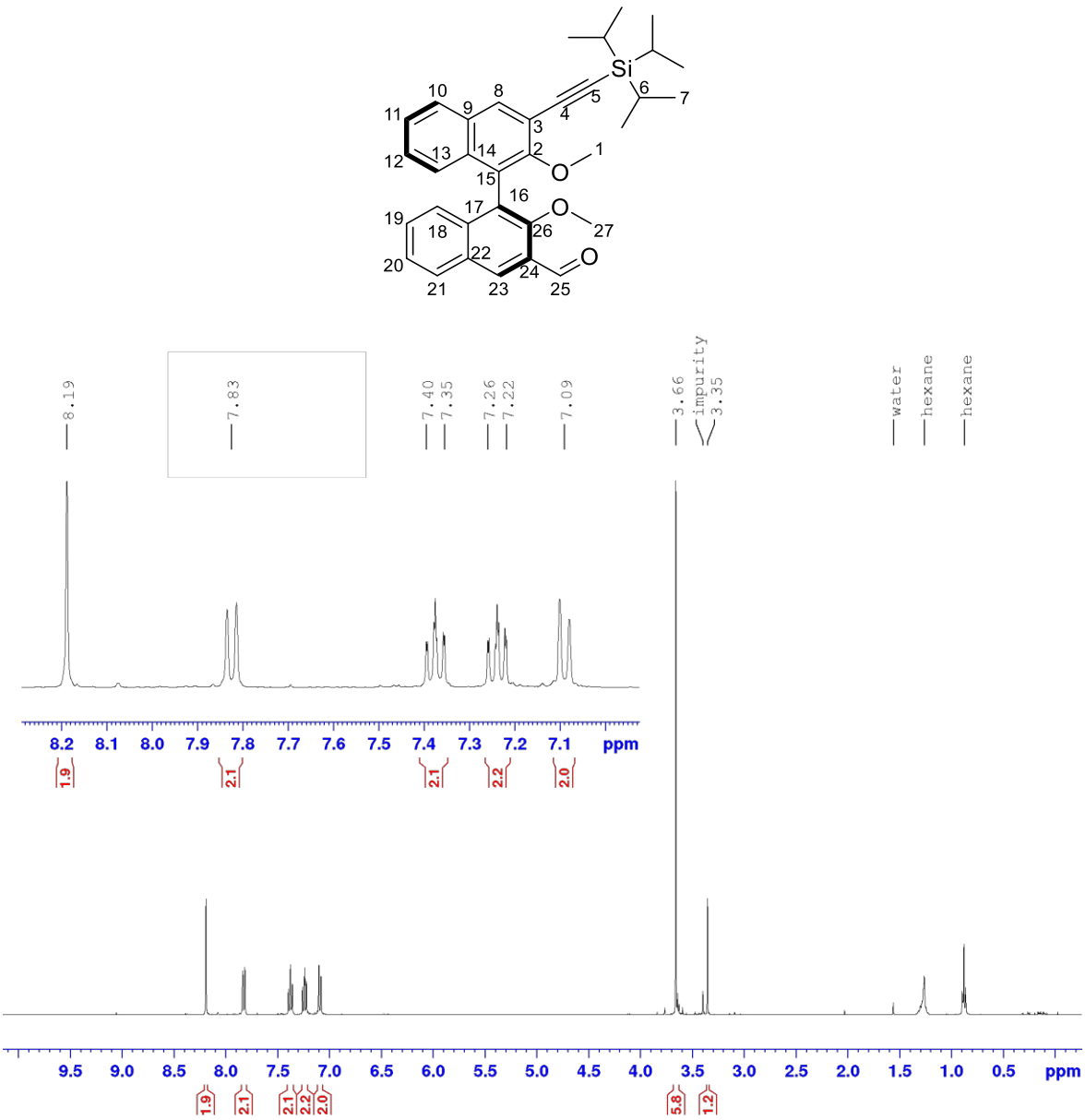


**Figure A64:** $^{1}$H NMR of **27(*S*)** in $CD_2Cl_2$ at a 400 MHz spectrometer at 298 K.

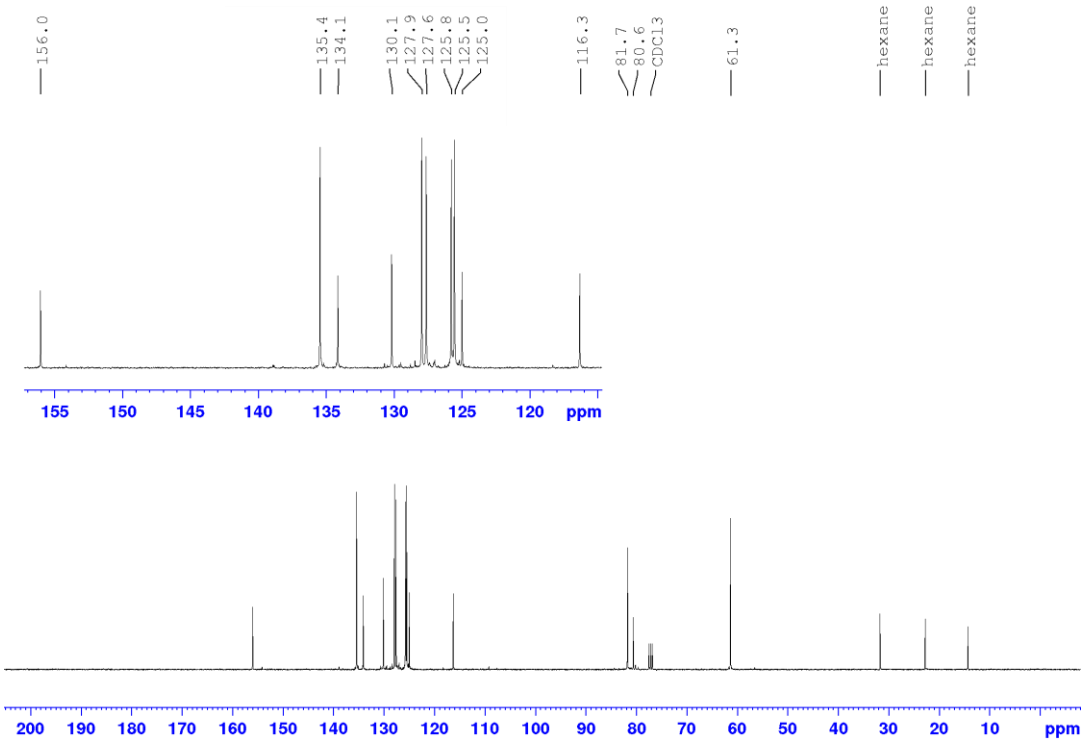


**Figure A65:** $^{13}C\{^{1}H\}$ NMR of **27(*S*)** in $CD_2Cl_2$ at a 100.6 MHz spectrometer at 298 K.

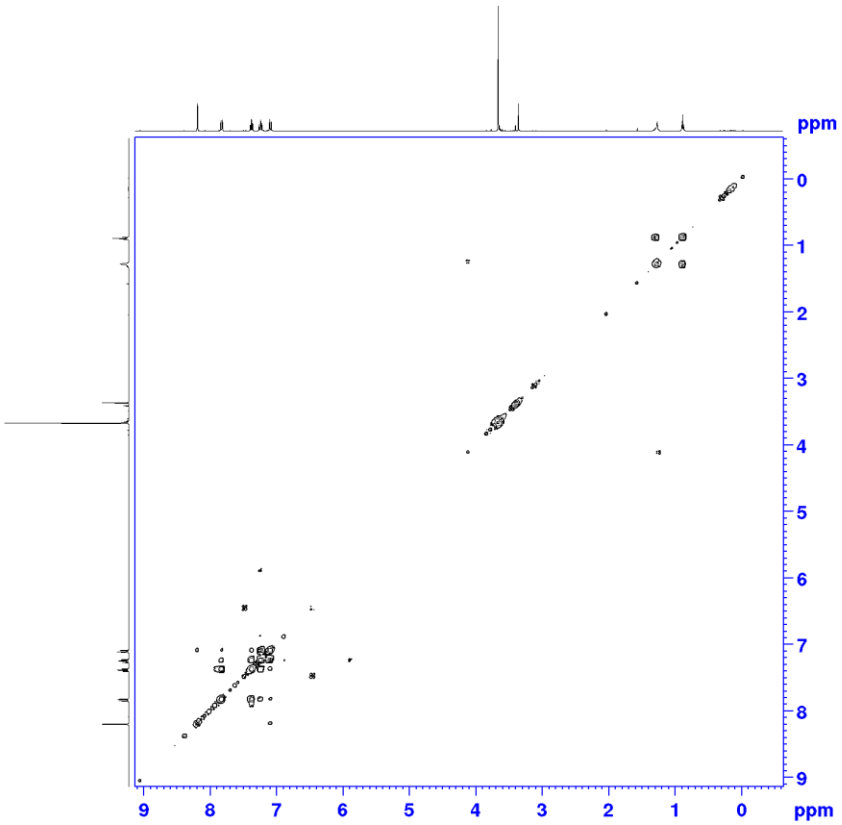


**Figure A66:** $^{1}H,^{1}H$ COSY NMR spectrum of **27(*S*)** in $CDCl_3$ at a 400 MHz spectrometer at 298 K.

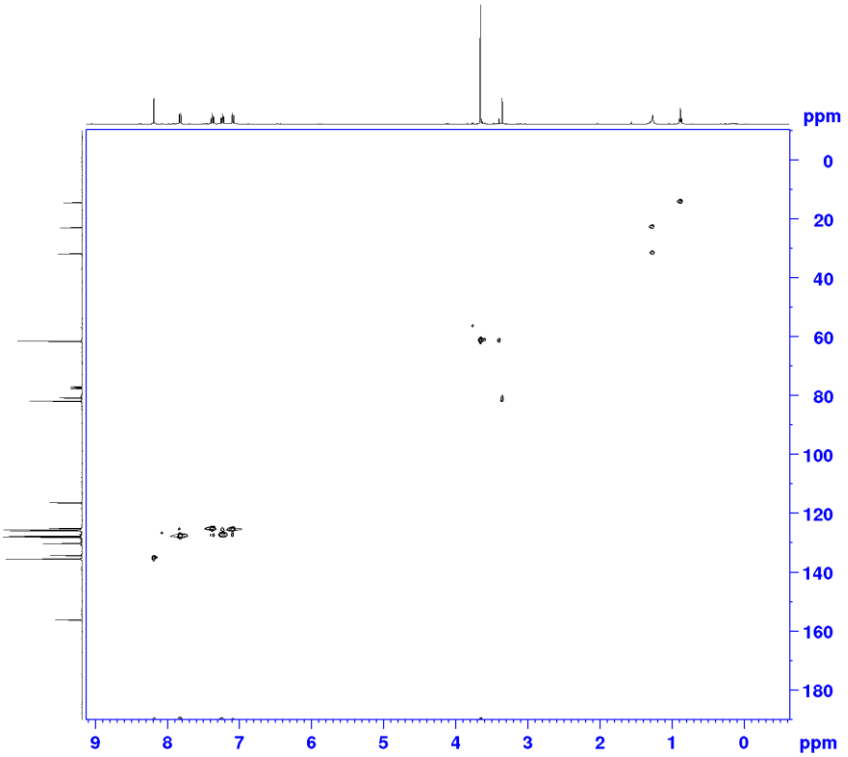


**Figure A67:** $^{1}H,^{13}C$ HSQC NMR spectrum of **27(*S*)** in $CDCl_3$ at a 400 MHz spectrometer at 298 K.

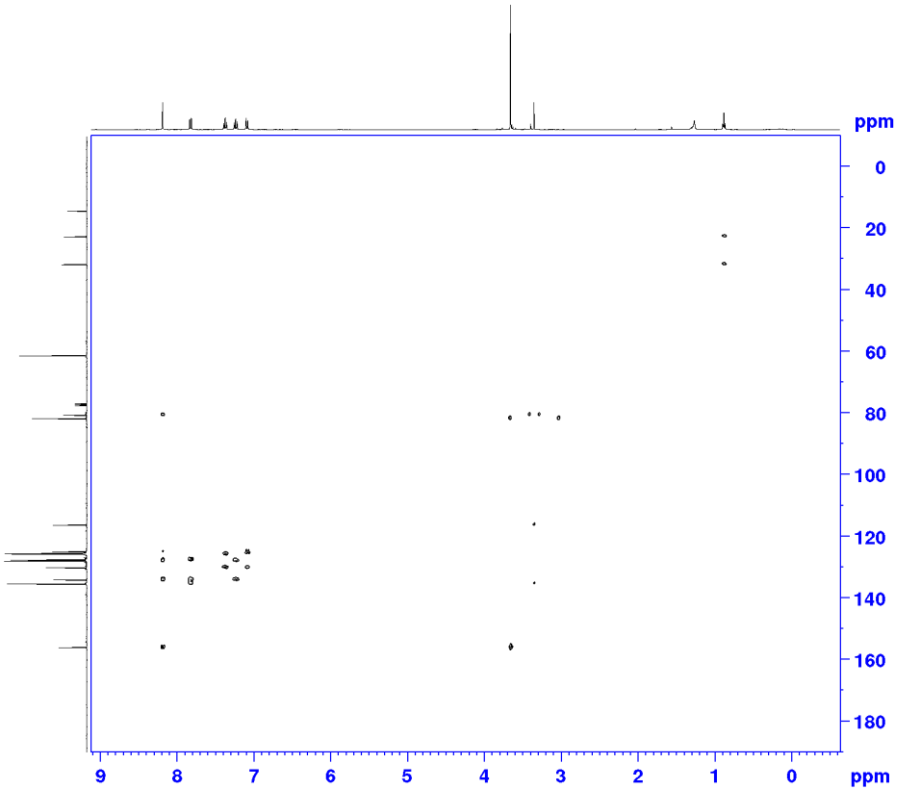


**Figure A68:** $^{1}H,^{13}C$ HMBC NMR spectrum of **27(*S*)** in $CDCl_3$ at a 400 MHz spectrometer at 298 K.

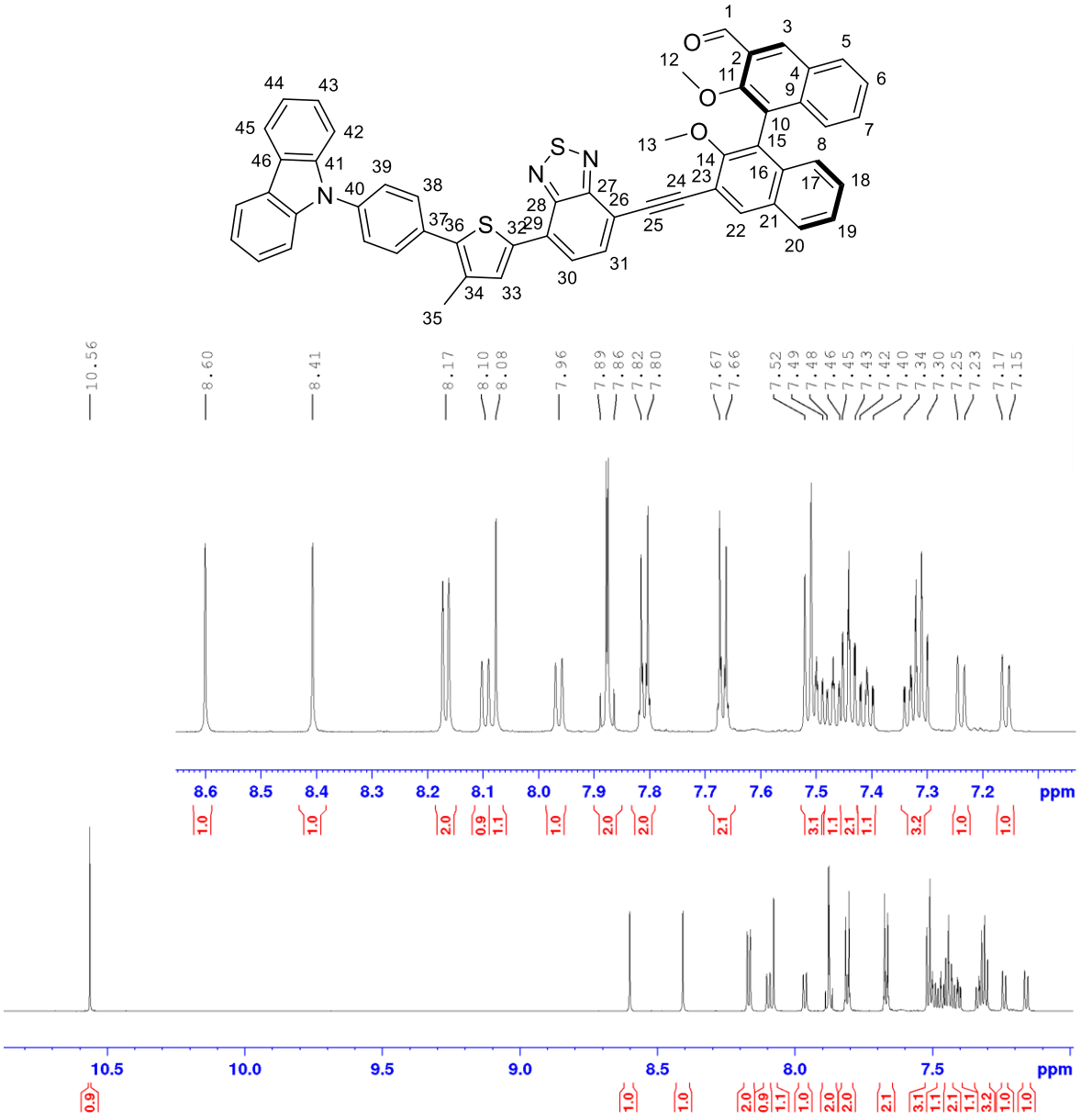


**Figure A69:** $^{1}$H NMR of **28(*S*)a** in $CD_2Cl_2$ at a 700 MHz spectrometer at 298 K, Part 1 (10.7 ppm – 7.0 ppm).

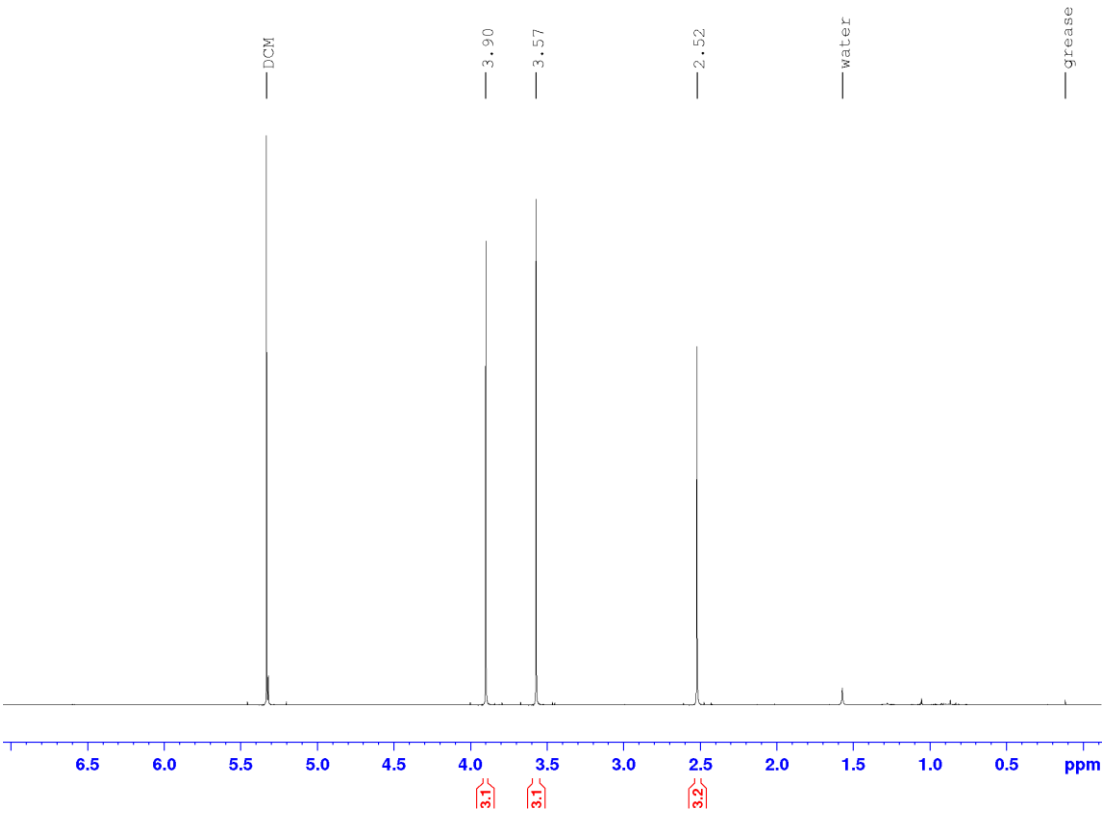


**Figure A70:** $^{1}$H NMR of **28(*S*)a** in $CD_2Cl_2$ at a 700 MHz spectrometer at 298 K, Part 2 (7.0 ppm – 0.0 ppm).

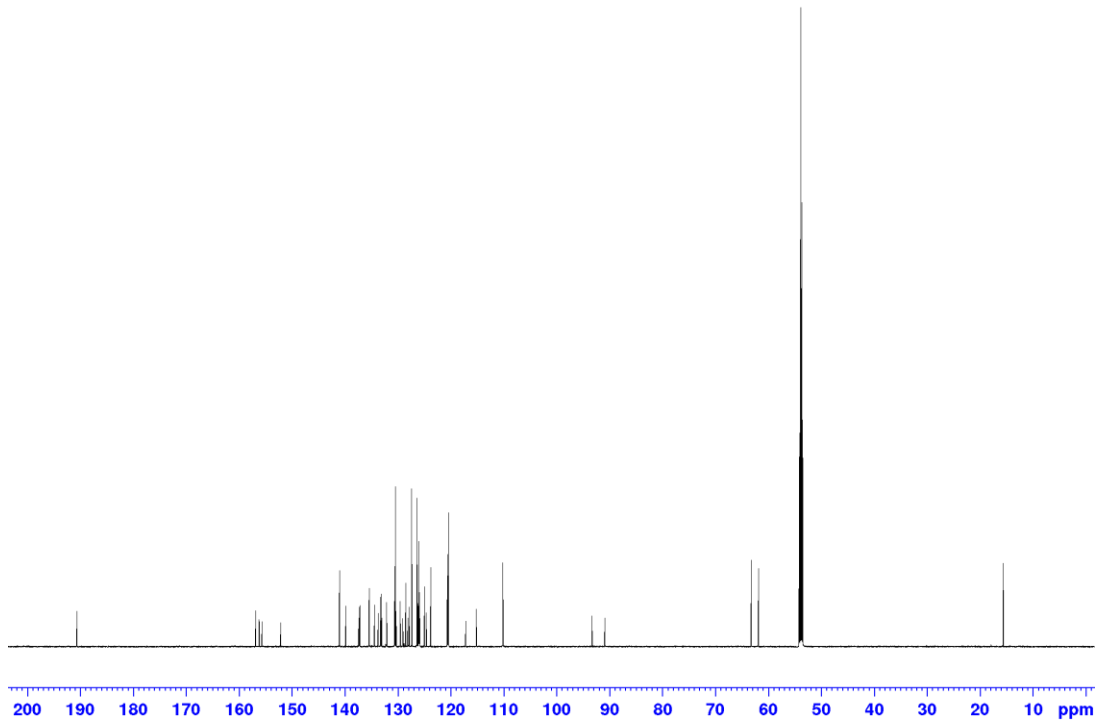


**Figure A71:** $^{13}C\{^{1}H\}$ NMR of **28(*S*)a** in $CD_2Cl_2$ at a 176.1 MHz spectrometer at 298 K, Overview.

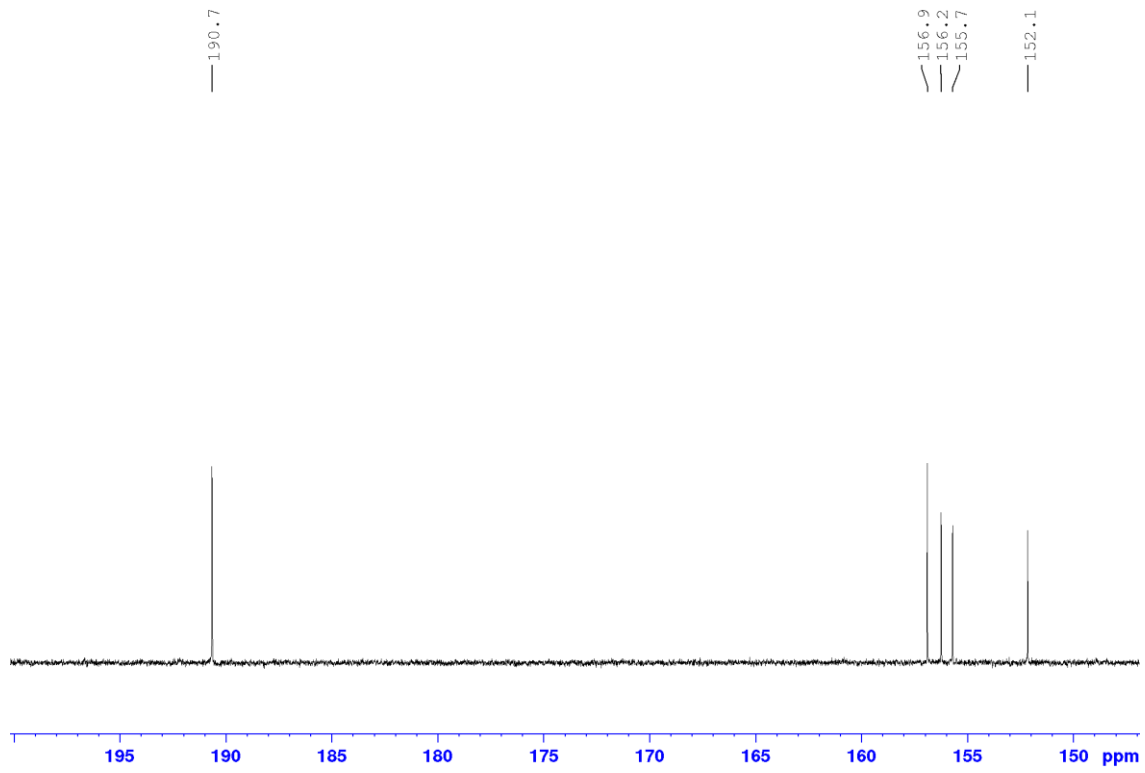


**Figure A72:** $^{13}C\{^{1}H\}$ NMR of **28(*S*)a** in $CD_2Cl_2$ at a 176.1 MHz spectrometer at 298 K, Part 1 (200 ppm – 147 ppm).

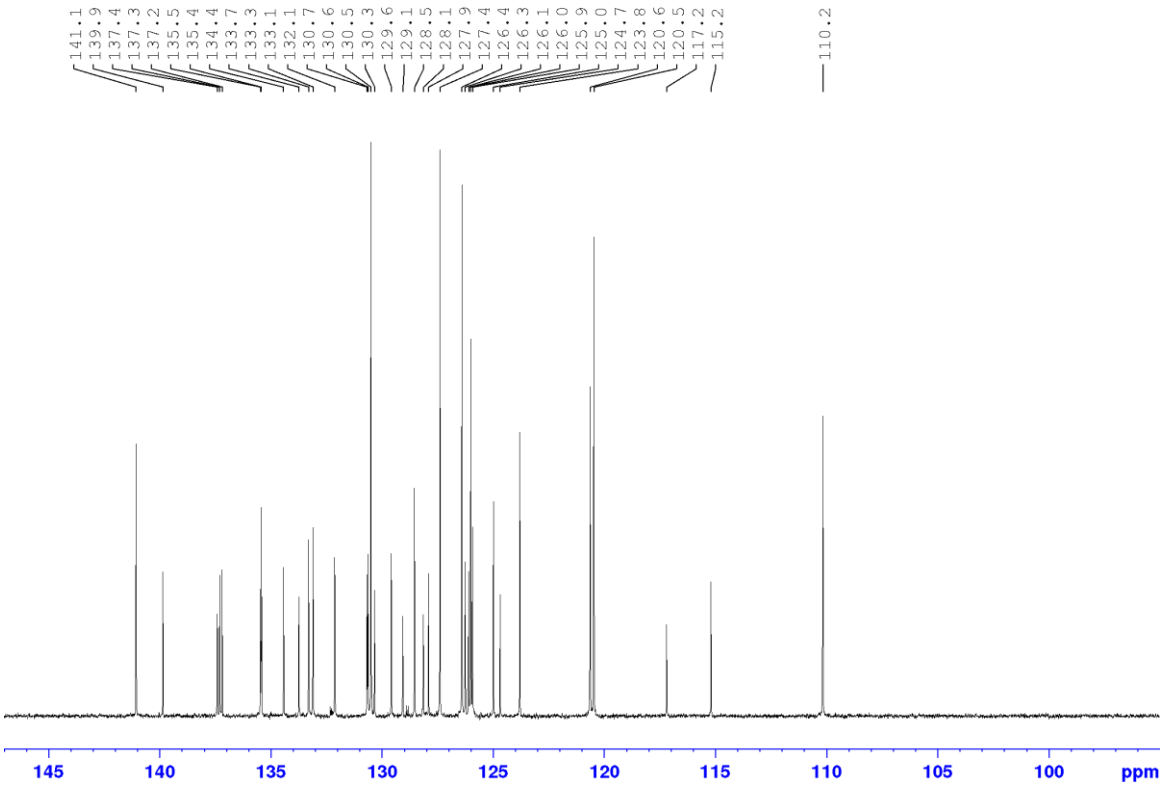


**Figure A73:** $^{13}C\{^{1}H\}$ NMR of **28(*S*)a** in $CD_2Cl_2$ at a 176.1 MHz spectrometer at 298 K, Part 2 (147 ppm – 95 ppm).

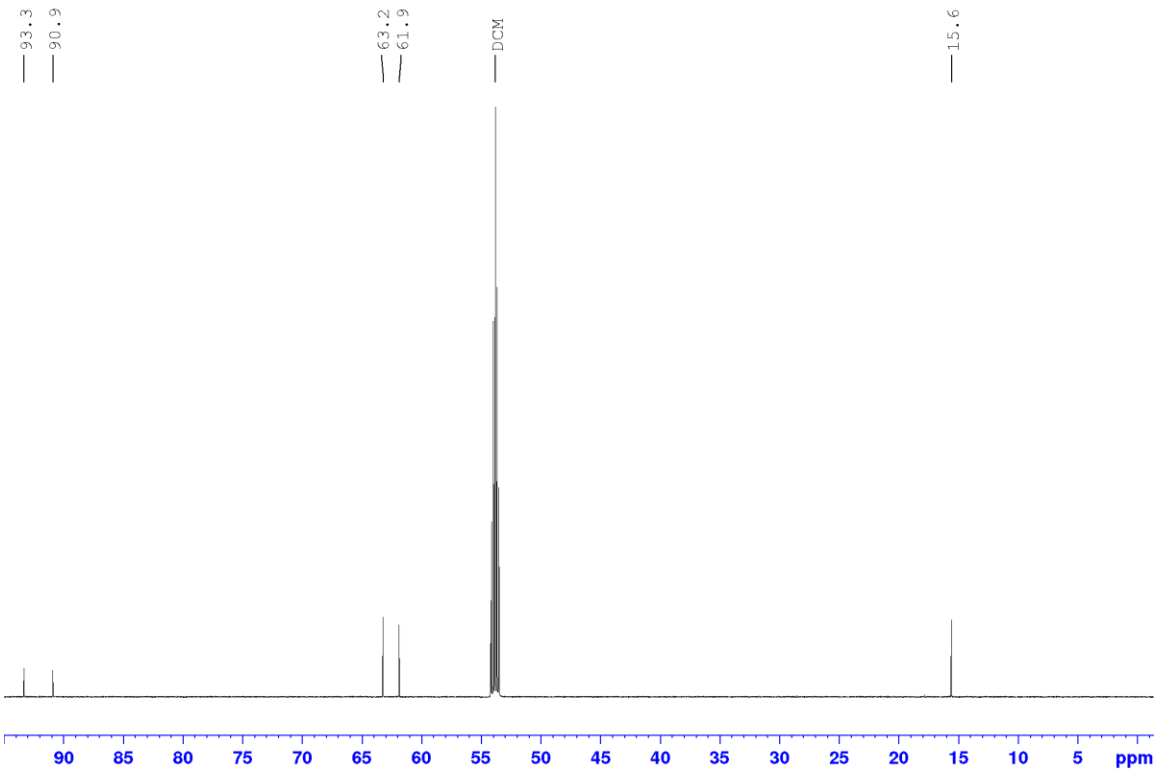


**Figure A74:** $^{13}C\{^{1}H\}$ NMR of **28(*S*)a** in $CD_2Cl_2$ at a 176.1 MHz spectrometer at 298 K, Part 3 (95 ppm – 0 ppm).

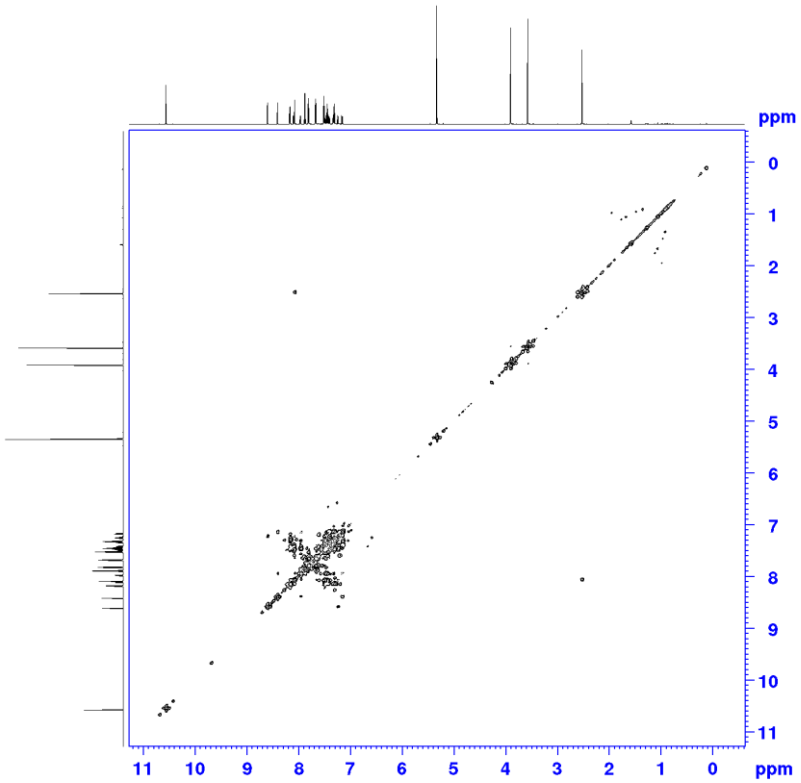


**Figure A75:** $^{1}H,^{1}H$ COSY NMR spectrum of **28(*S*)a** in $CD_2Cl_2$ at a 700 MHz spectrometer at 298 K.

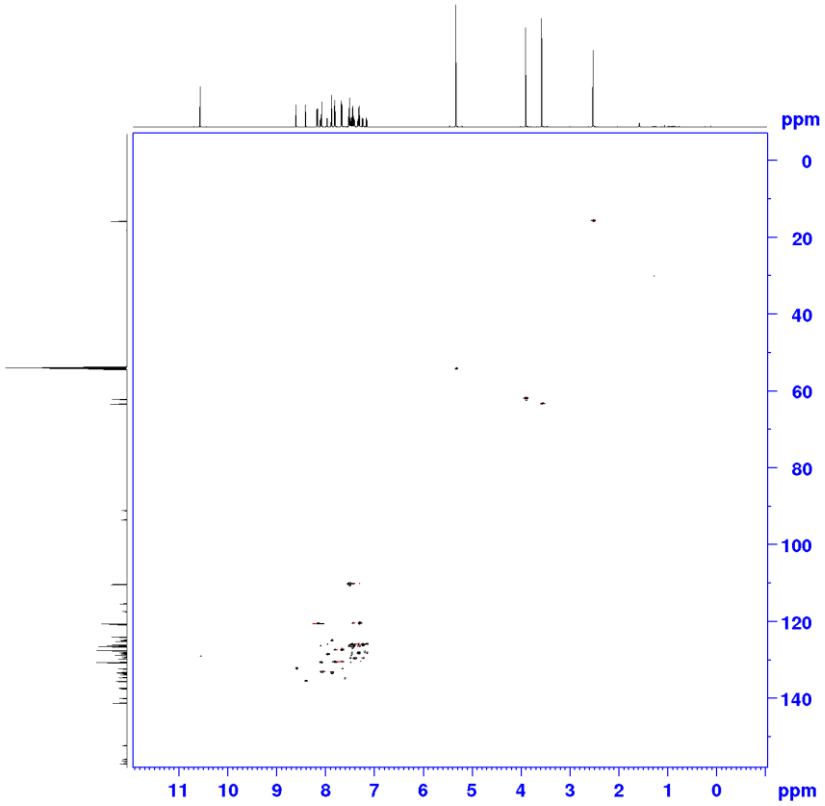


**Figure A76:** $^{1}H,^{13}C$ HSQC NMR spectrum of **28(*S*)a** in $CD_2Cl_2$ at a 700 MHz spectrometer at 298 K.

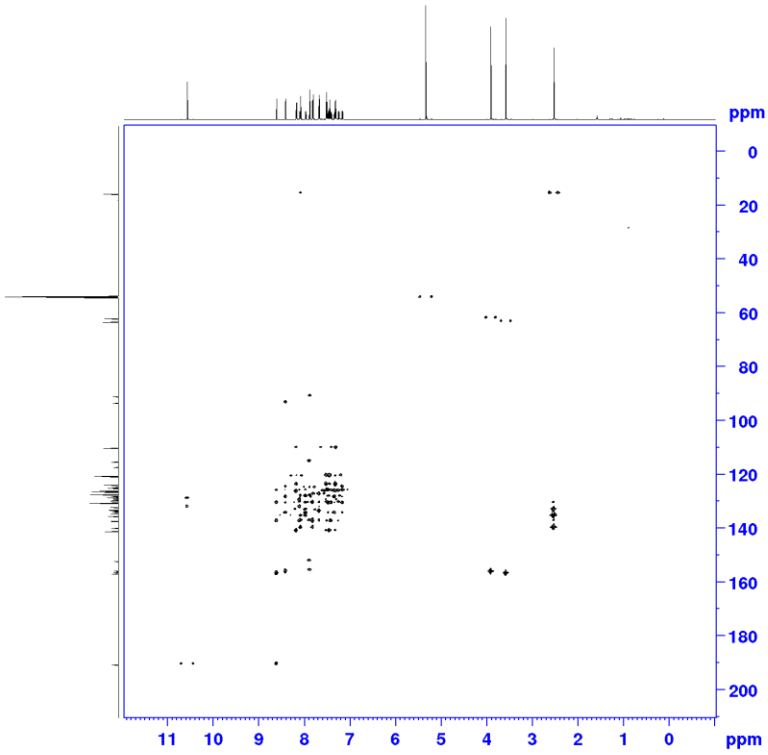


**Figure A77:** $^{1}H,^{13}C$ HMBC NMR spectrum of **28(*S*)a** in $CD_2Cl_2$ at a 700 MHz spectrometer at 298 K.

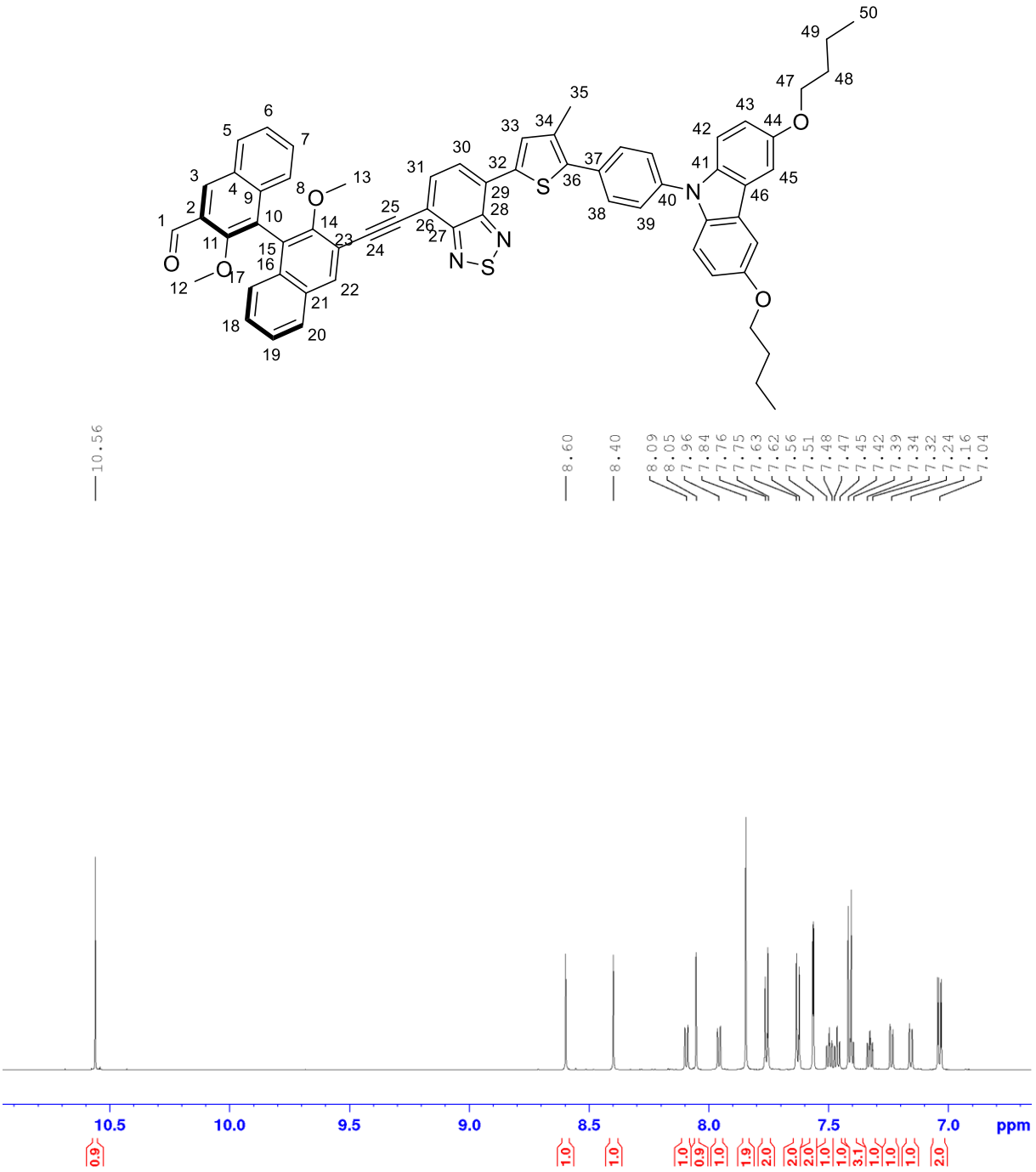


**Figure A78:** $^{1}$H NMR of **28(*S*)b** in $CD_2Cl_2$ at a 700 MHz spectrometer at 298 K, Part 1 (10.9 ppm – 6.7 ppm).

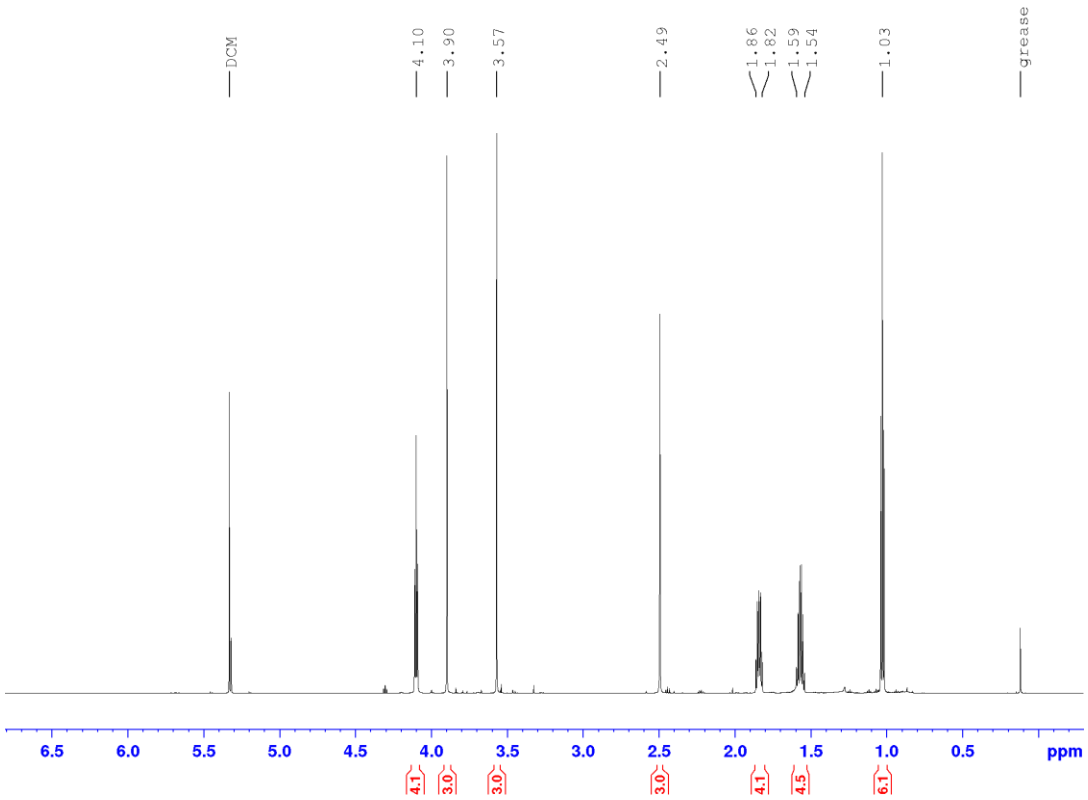


**Figure A79:** $^{1}$H NMR of **28(*S*)b** in $CD_2Cl_2$ at a 700 MHz spectrometer at 298 K, Part 2 (6.8 ppm – 0.0 ppm).

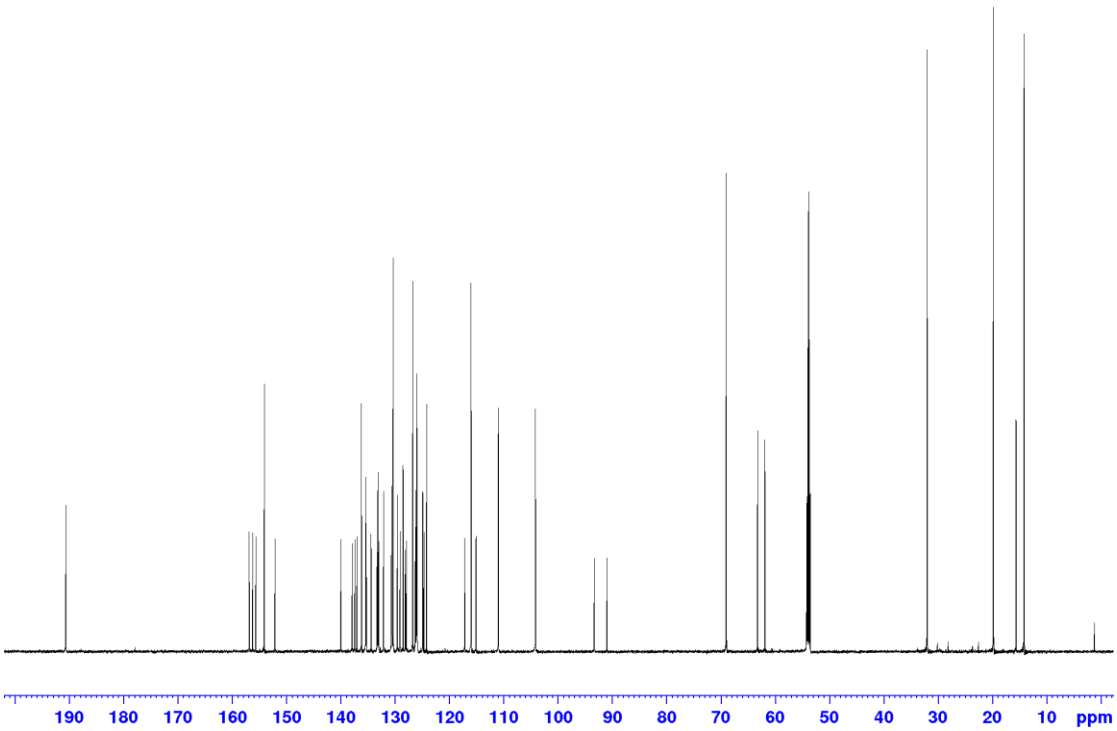


**Figure A80:** $^{13}C\{^{1}H\}$ NMR of **28(*S*)b** in $CD_2Cl_2$ at a 176.1 MHz spectrometer at 298 K, Overview.

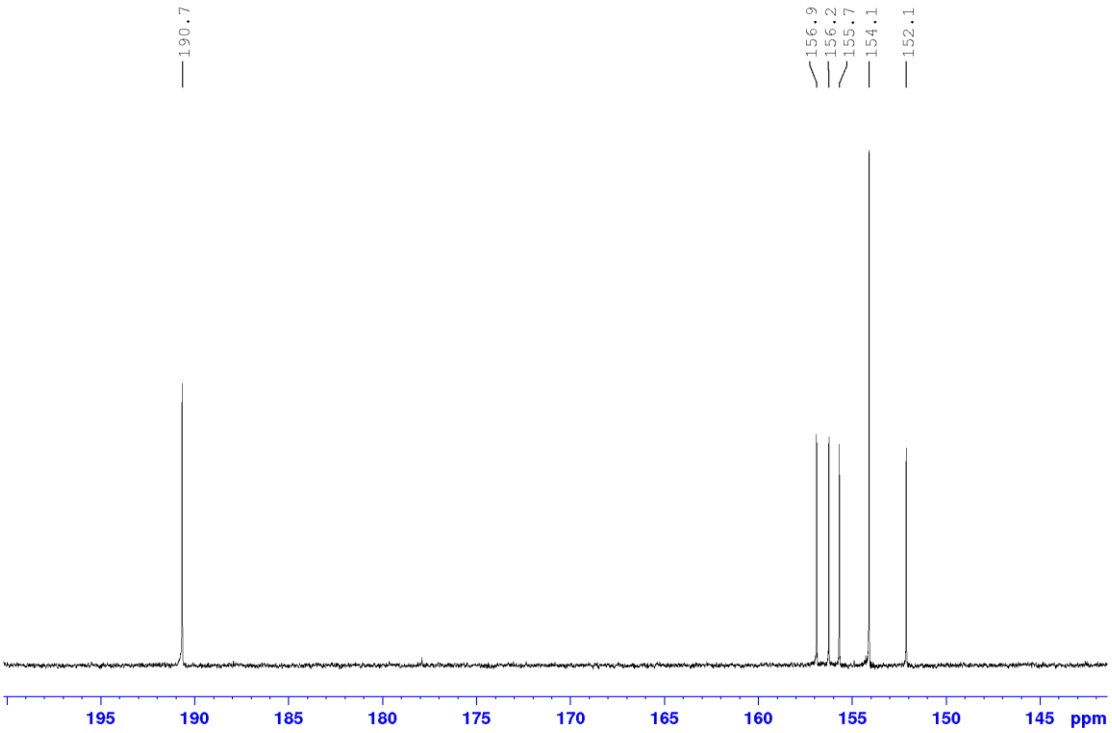


**Figure A81:** $^{13}C\{^{1}H\}$ NMR of **28(*S*)b** in $CD_2Cl_2$ at a 176.1 MHz spectrometer at 298 K, Part 1 (200 ppm – 143 ppm).

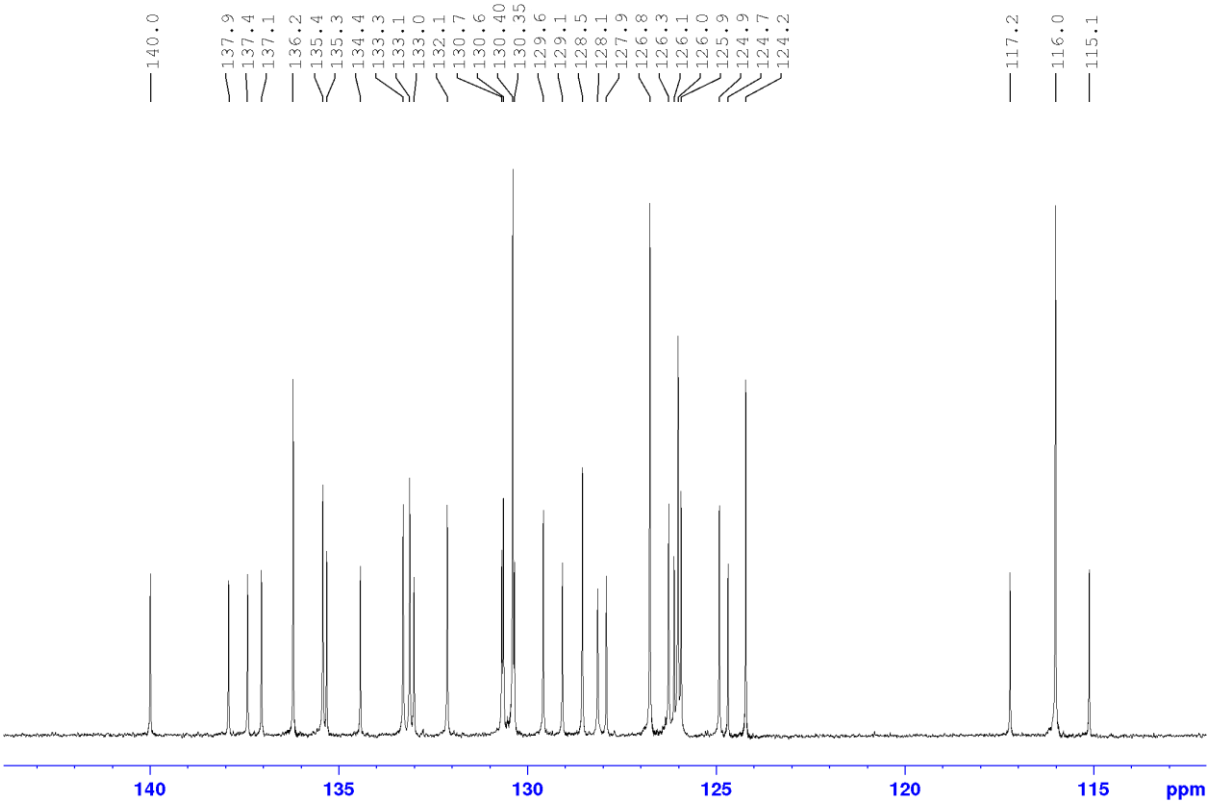


**Figure A82:** $^{13}C\{^{1}H\}$ NMR of **28(*S*)b** in $CD_2Cl_2$ at a 176.1 MHz spectrometer at 298 K, Part 2 (143 ppm – 113 ppm).

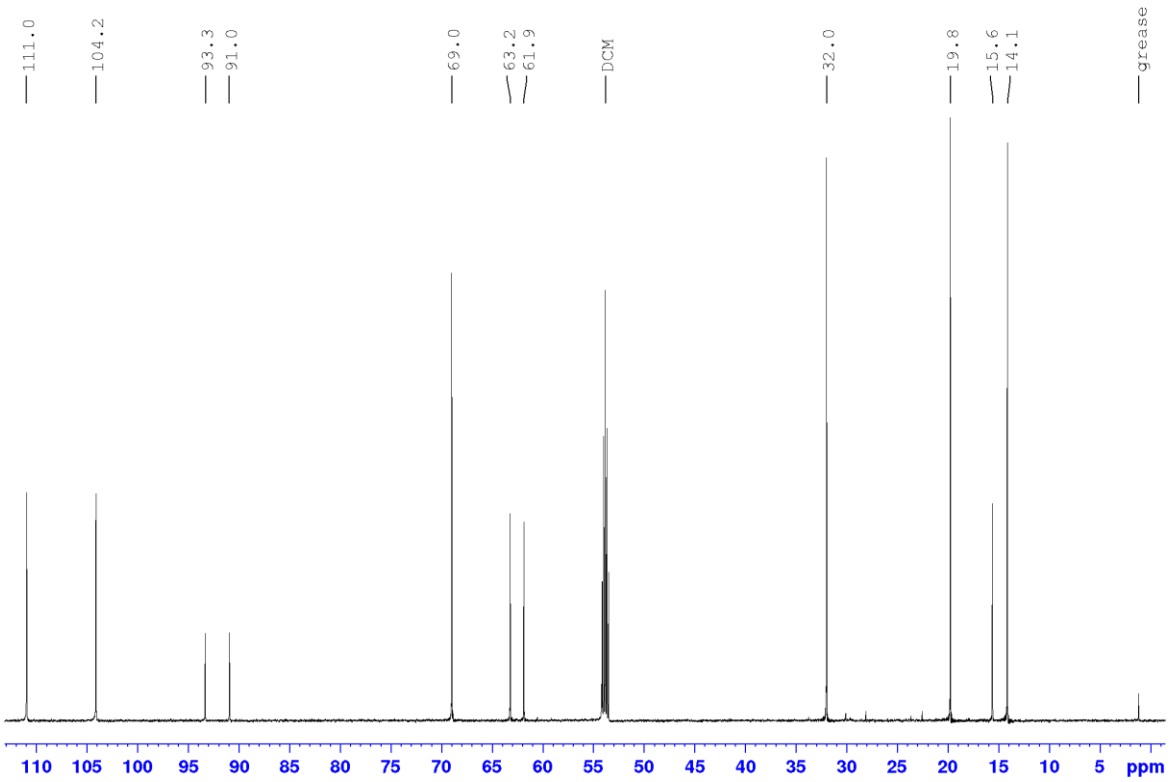


**Figure A83:** $^{13}C\{^{1}H\}$ NMR of **28(*S*)b** in $CD_2Cl_2$ at a 176.1 MHz spectrometer at 298 K, Part 3 (113 ppm – 0 ppm).

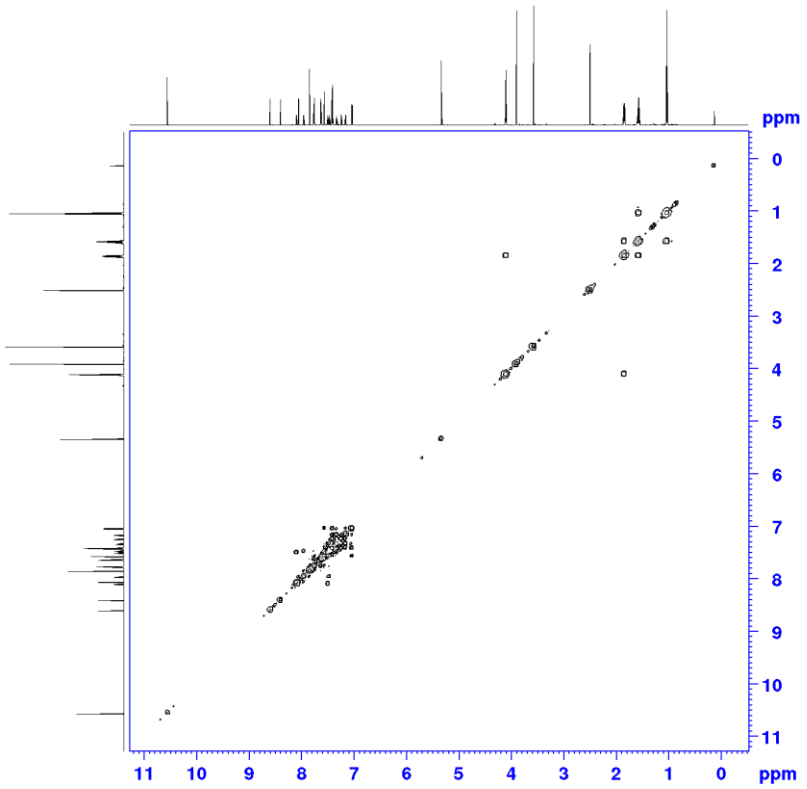


**Figure A84:** $^{1}H,^{1}H$ COSY NMR spectrum of **28(*S*)b** in $CD_2Cl_2$ at a 700 MHz spectrometer at 298 K.

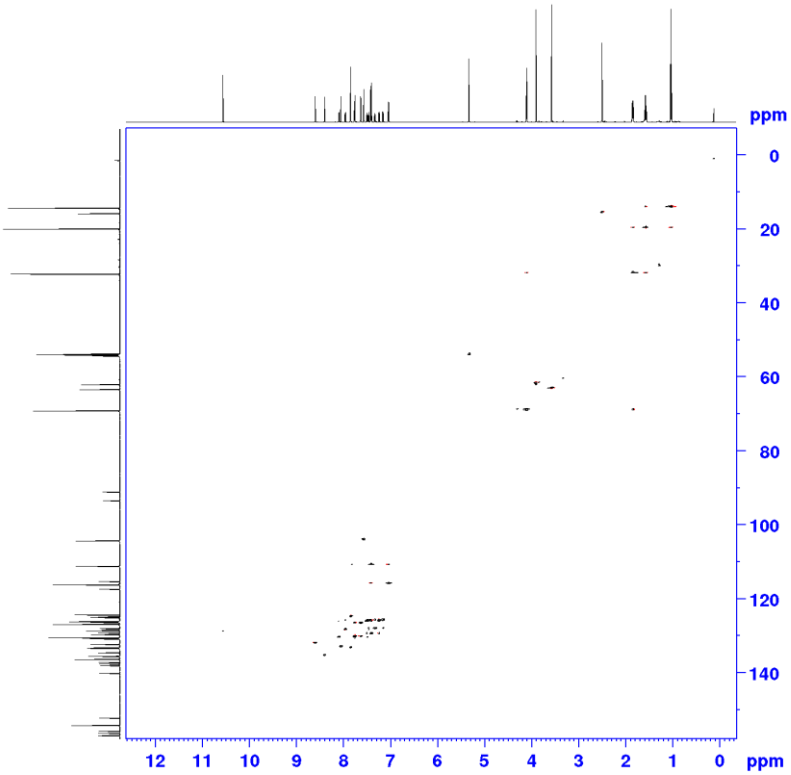


**Figure A85:** $^{1}H,^{13}C$ HSQC NMR spectrum of **28(*S*)b** in $CD_2Cl_2$ at a 700 MHz spectrometer at 298 K.

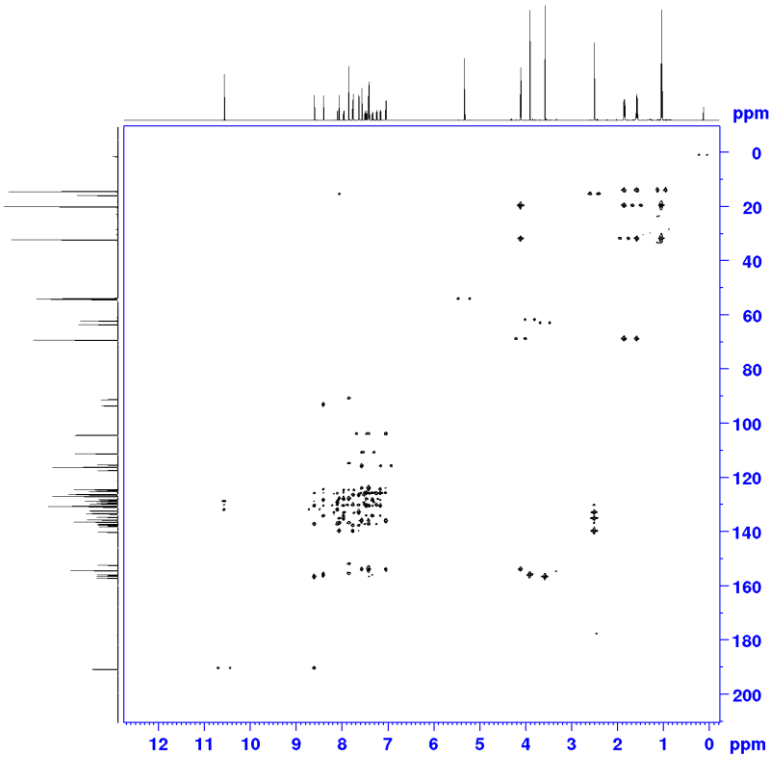


**Figure A86:** $^{1}H,^{13}C$ HMBC NMR spectrum of **28(*S*)b** in $CD_2Cl_2$ at a 700 MHz spectrometer at 298 K.

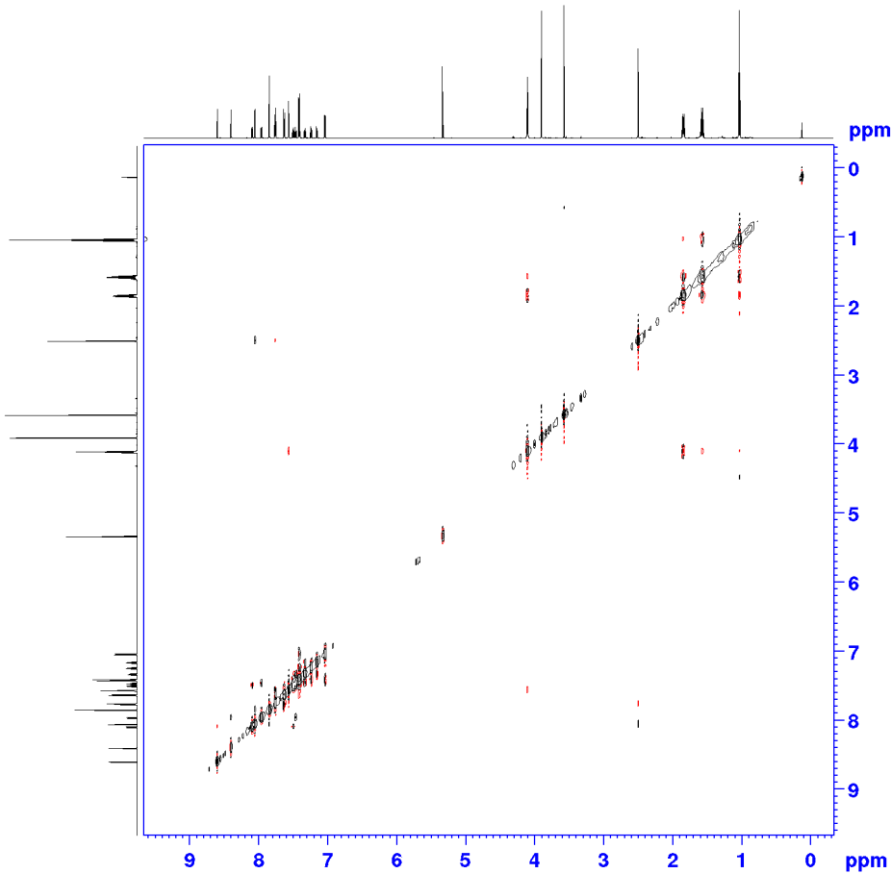


**Figure A87:** $^{1}H,^{1}H$ NOESY NMR spectrum of **28(*S*)b** in $CD_2Cl_2$ at a 700 MHz spectrometer at 298 K.

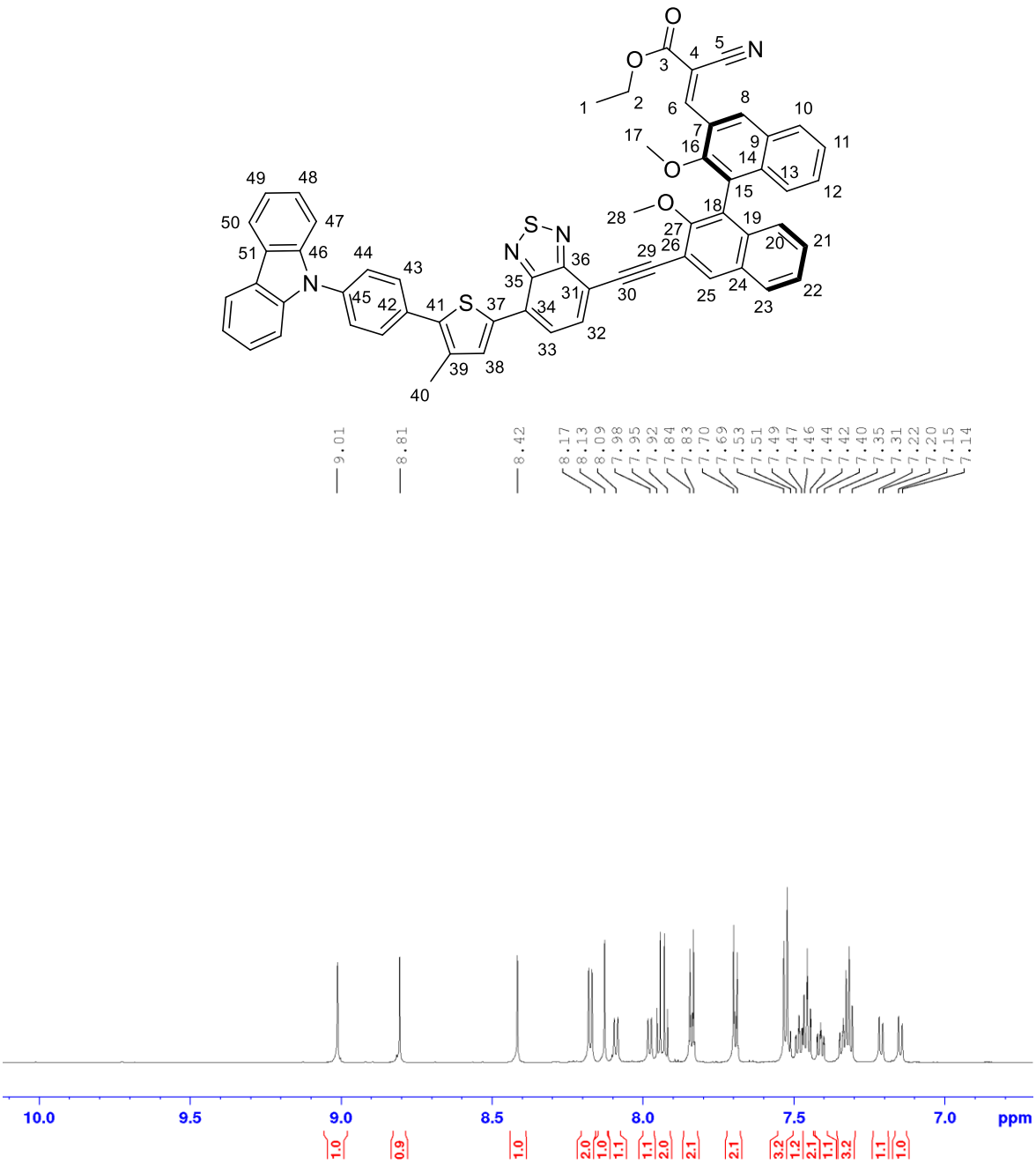


**Figure A88:** $^{1}$H NMR of **30(*S*)a** in $CD_2Cl_2$ at a 700 MHz spectrometer at 298 K, Part 1 (10.1 ppm – 6.8 ppm).

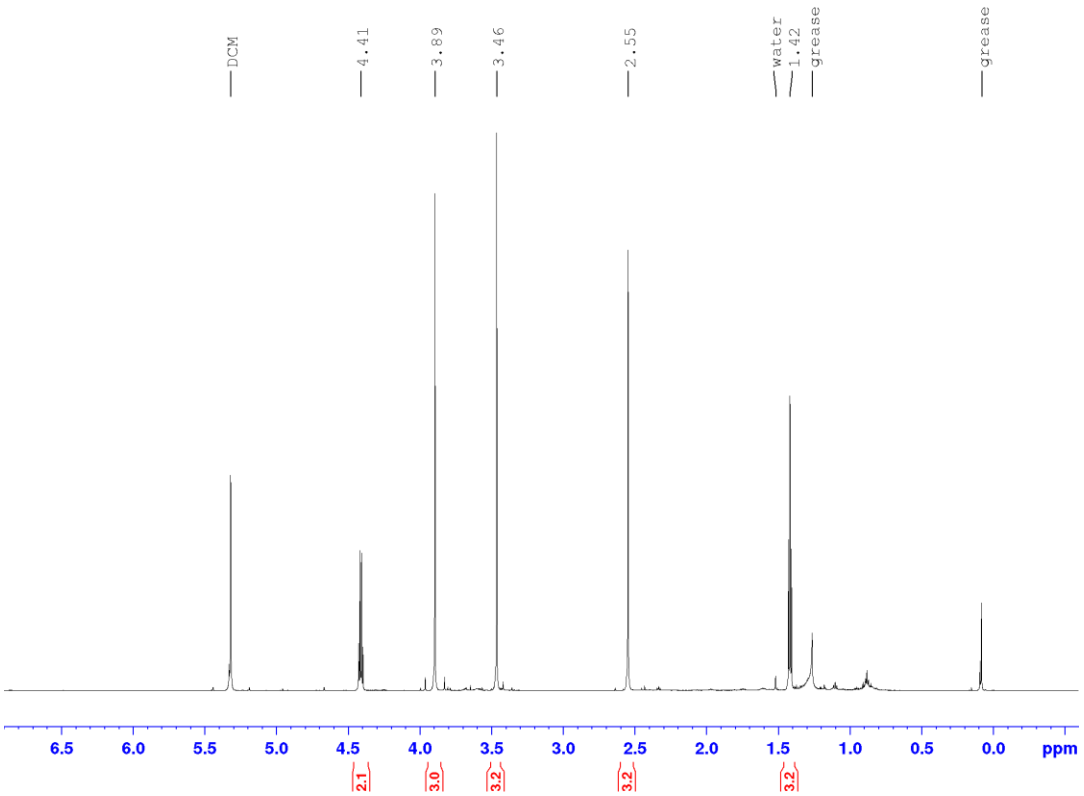


**Figure A89:** $^{1}$H NMR of **30(*S*)a** in $CD_2Cl_2$ at a 700 MHz spectrometer at 298 K, Part 2 (6.8 ppm – –1.0 ppm).

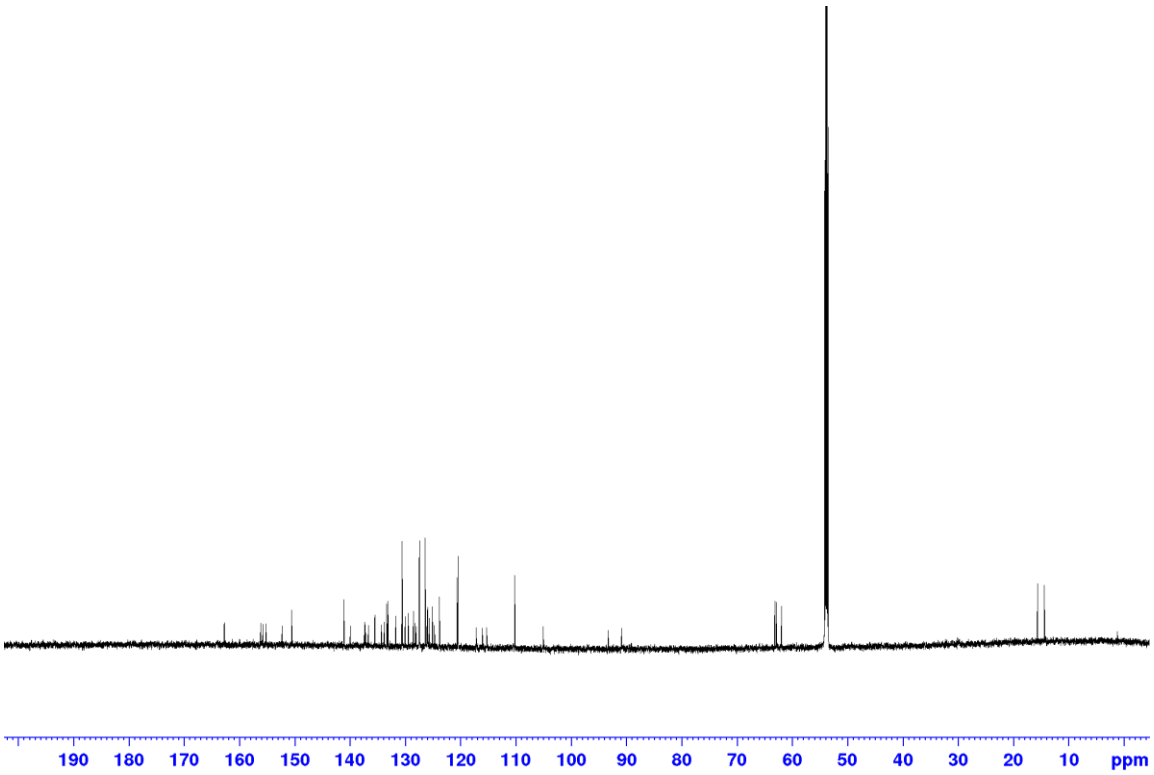


**Figure A90:** $^{13}C\{^{1}H\}$ NMR of **30(*S*)a** in $CD_2Cl_2$ at a 176.1 MHz spectrometer at 298 K, Overview.

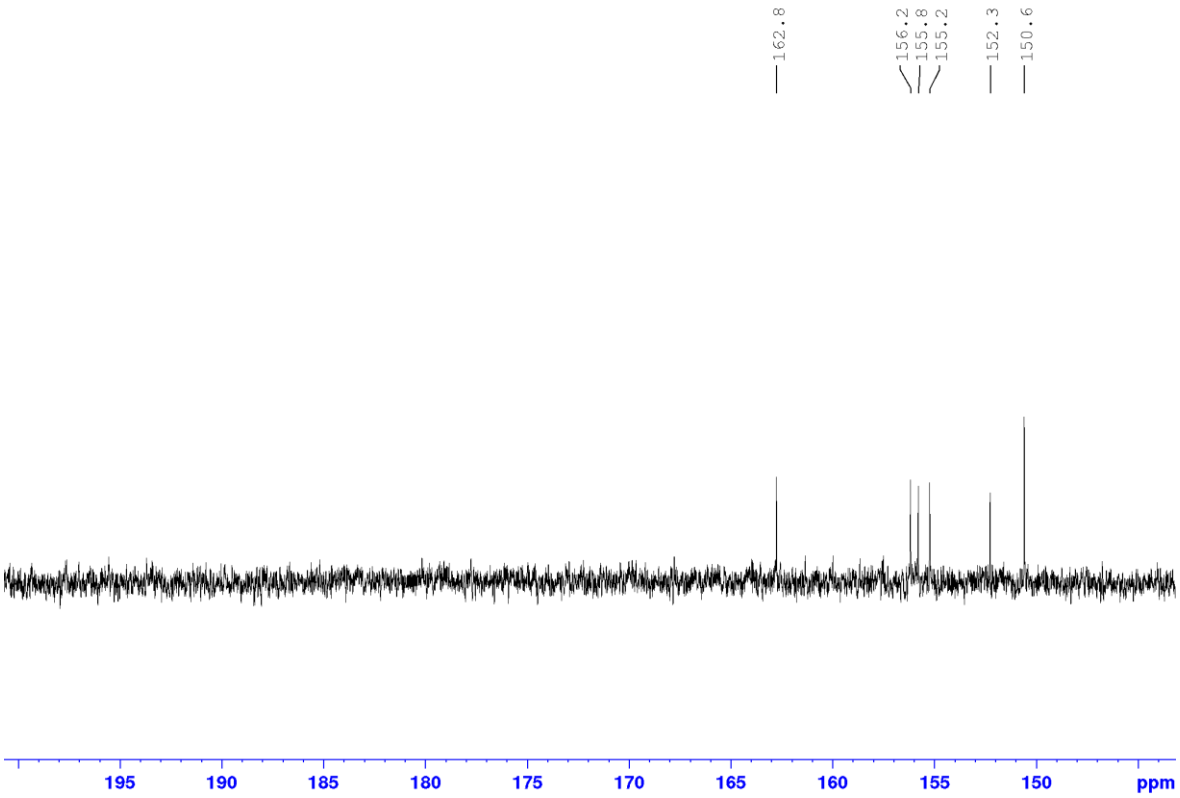


**Figure A91:** $^{13}C\{^{1}H\}$ NMR of **30(*S*)a** in $CD_2Cl_2$ at a 176.1 MHz spectrometer at 298 K, Part 1 (200 ppm – 144 ppm).

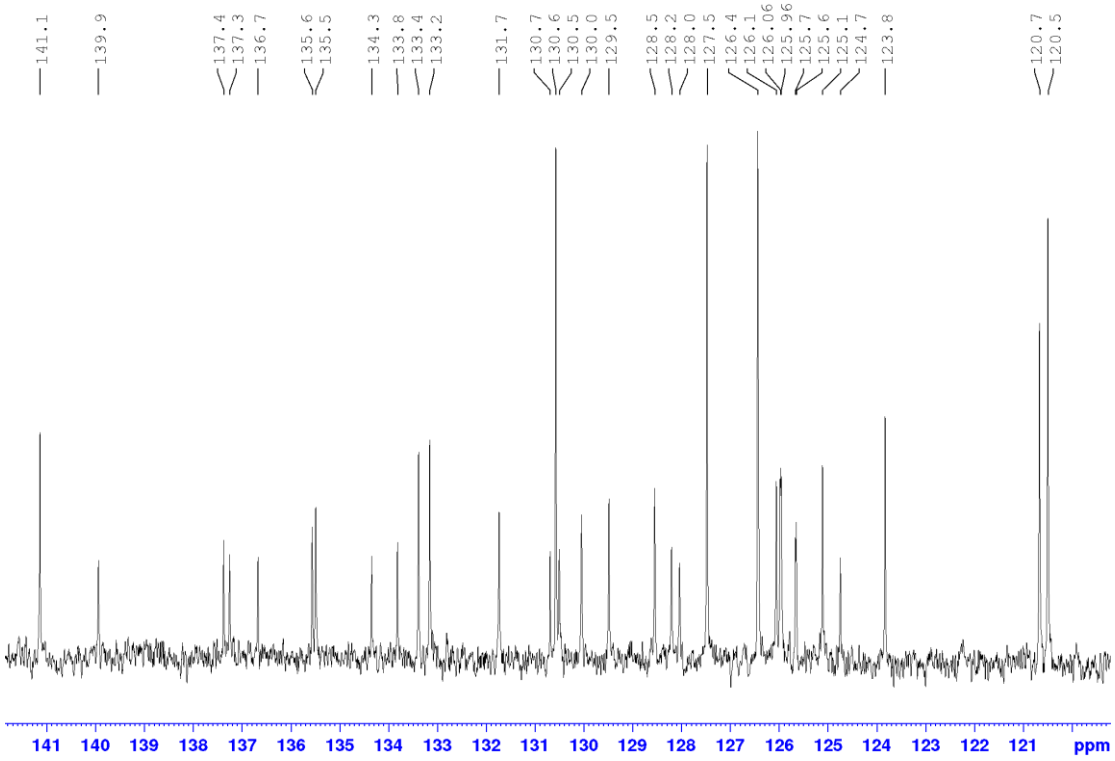


**Figure A92:** $^{13}C\{^{1}H\}$ NMR of **30(*S*)a** in $CD_2Cl_2$ at a 176.1 MHz spectrometer at 298 K, Part 2 (144 ppm – 119 ppm).

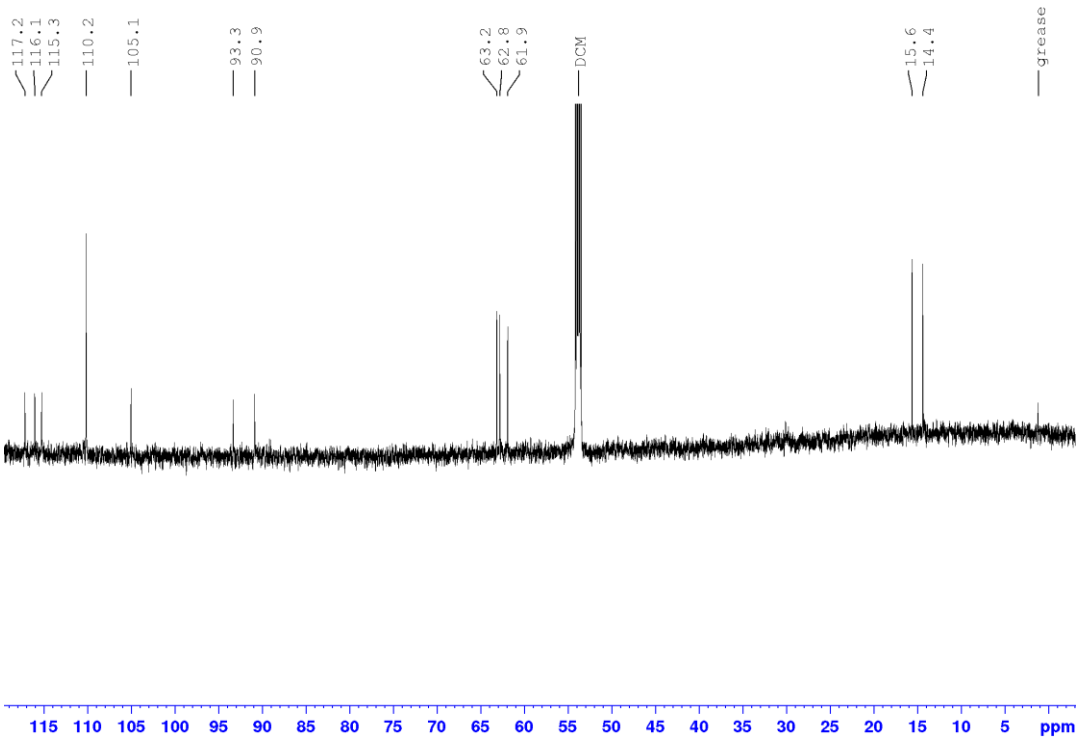


**Figure A93:** $^{13}C\{^{1}H\}$ NMR of **30(*S*)a** in $CD_2Cl_2$ at a 176.1 MHz spectrometer at 298 K, Part 3 (119 ppm – 0 ppm).

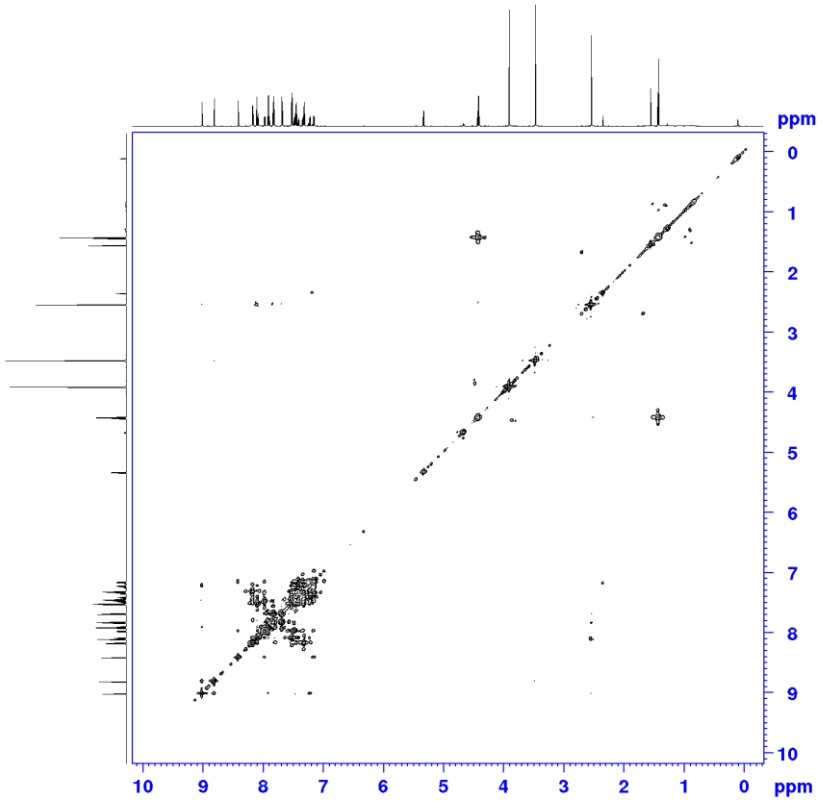


**Figure A94:** $^{1}H,^{1}H$ COSY NMR spectrum of **30(*S*)a** in $CD_2Cl_2$ at a 700 MHz Spectrometer at 298 K.

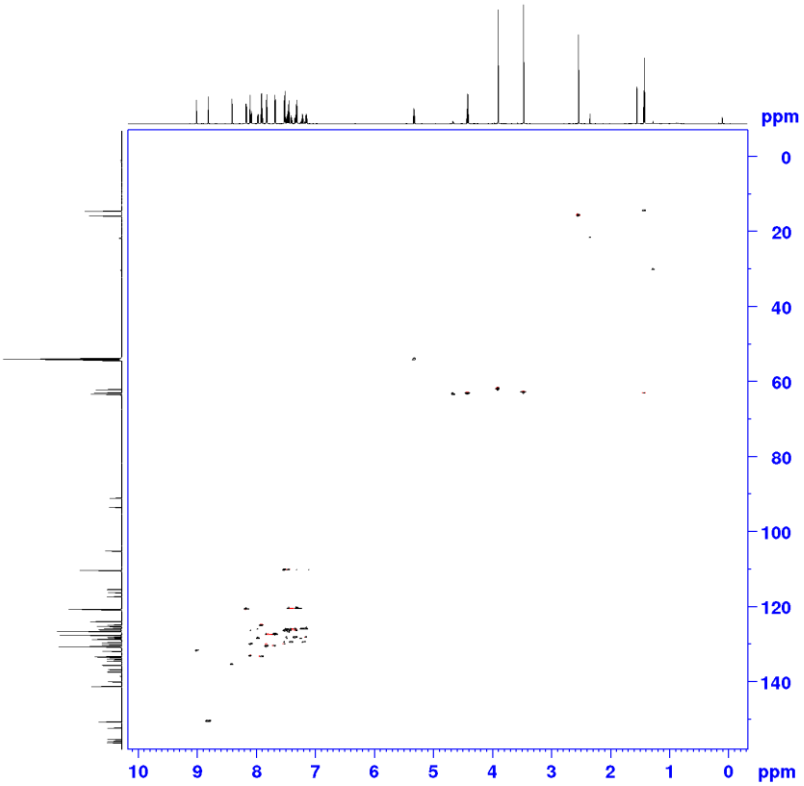


**Figure A95:** $^{1}H,^{13}C$ HSQC NMR spectrum of **30(*S*)a** in $CD_2Cl_2$ at a 700 MHz Spectrometer at 298 K.

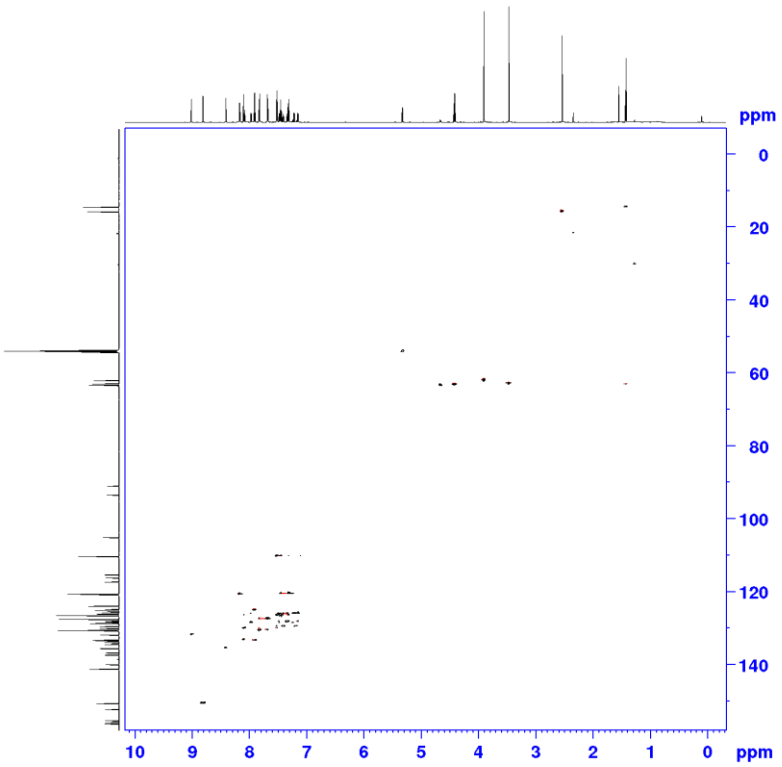


**Figure A96:** $^{1}H,^{13}C$ HMBC NMR spectrum of **30(*S*)a** in $CD_2Cl_2$ at a 700 MHz Spectrometer at 298 K.

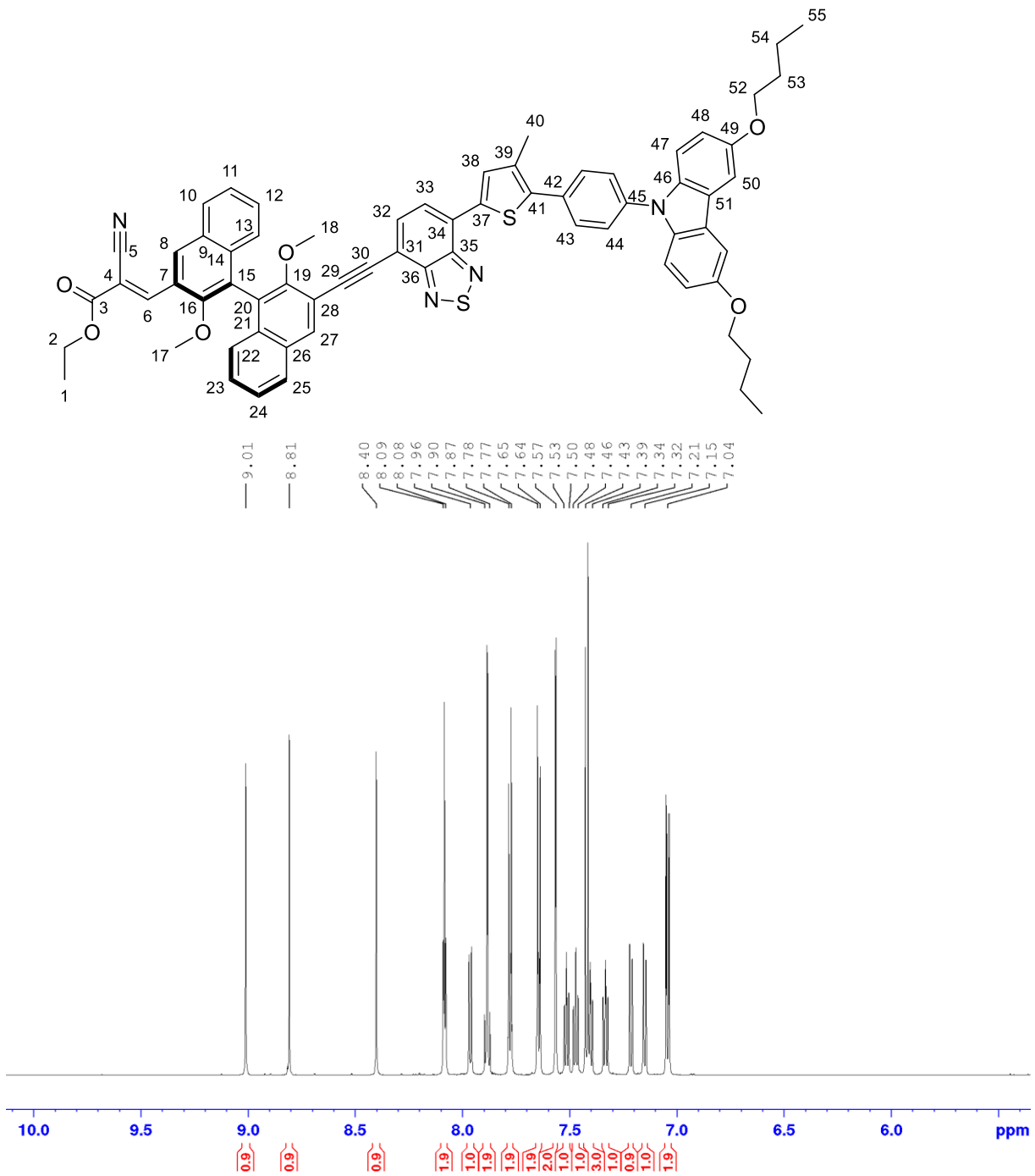


**Figure A97:** $^{1}$H NMR of **30(*S*)b** in $CD_2Cl_2$ at a 700MHz spectrometer at 298 K, Part 1 (10.4 ppm – 5.4 ppm).

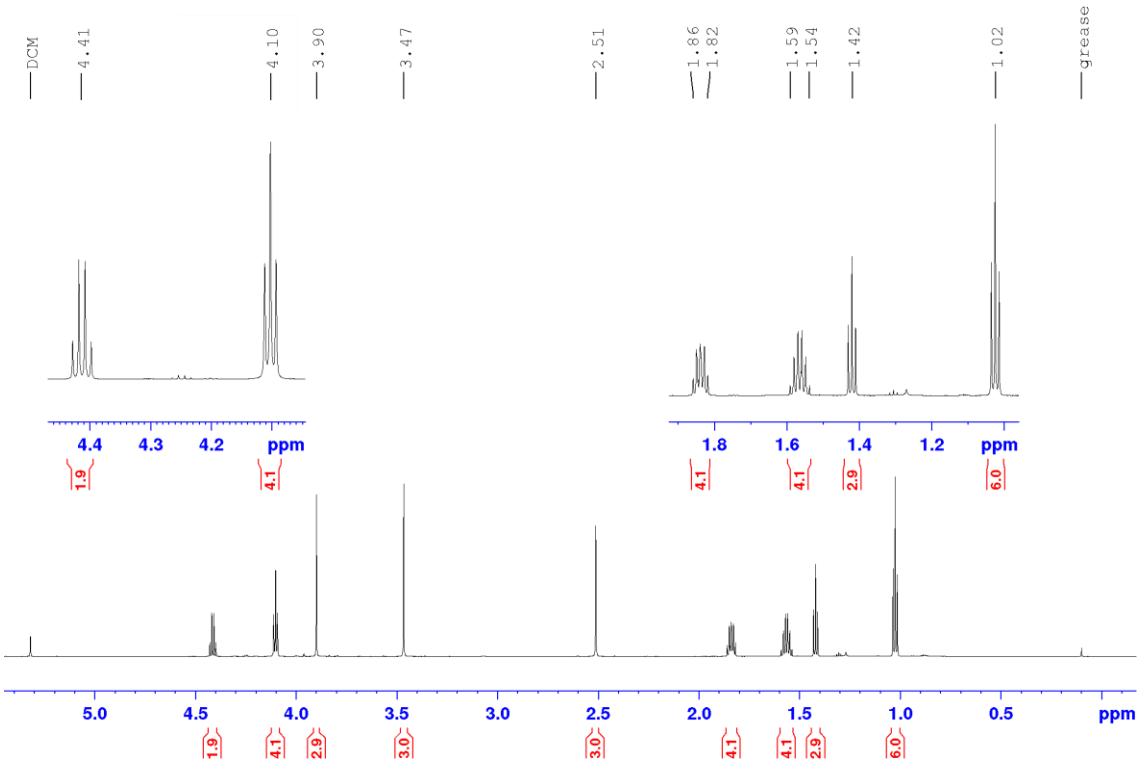


**Figure A98:** $^{1}H$ NMR of **30(*S*)b** in $CD_2Cl_2$ at a 700 MHz spectrometer at 298 K, Part 2 (5.4 ppm – 0.0 ppm).

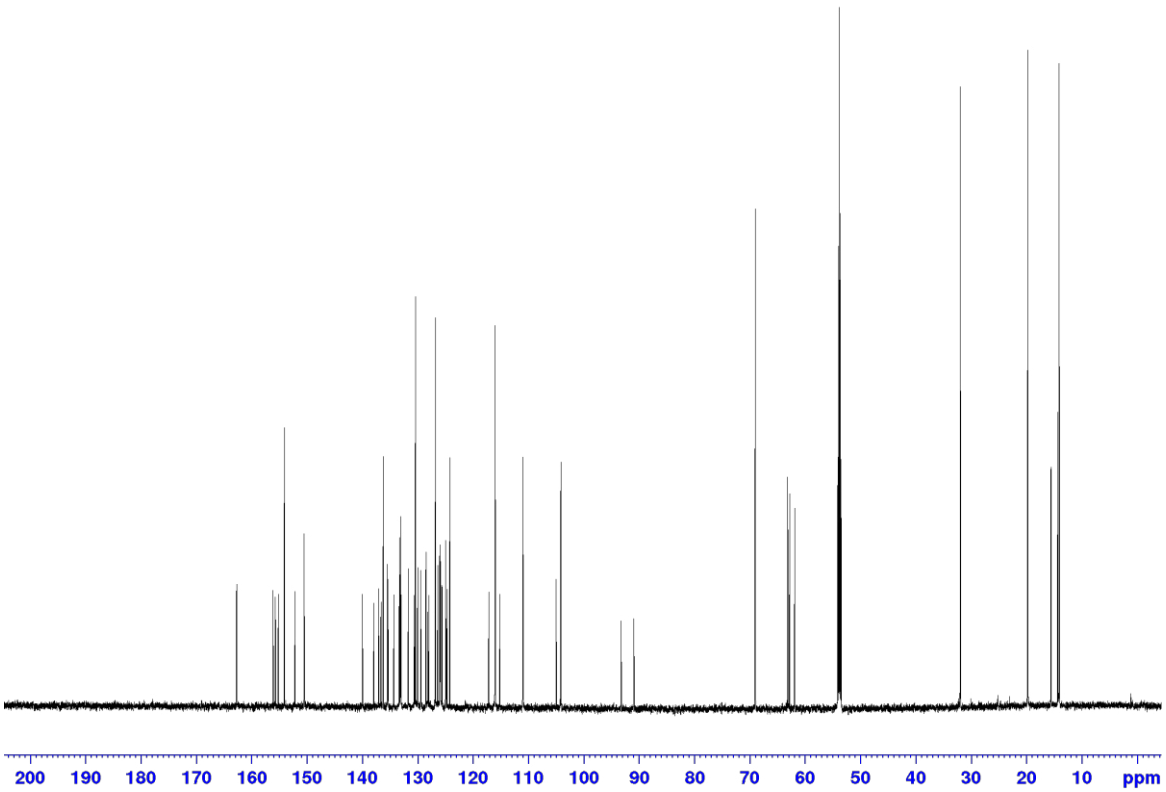


**Figure A99:** $^{13}C\{^{1}H\}$ NMR of **30(*S*)b** in $CD_2Cl_2$ at a 176.1 MHz spectrometer at 298 K, Overview.

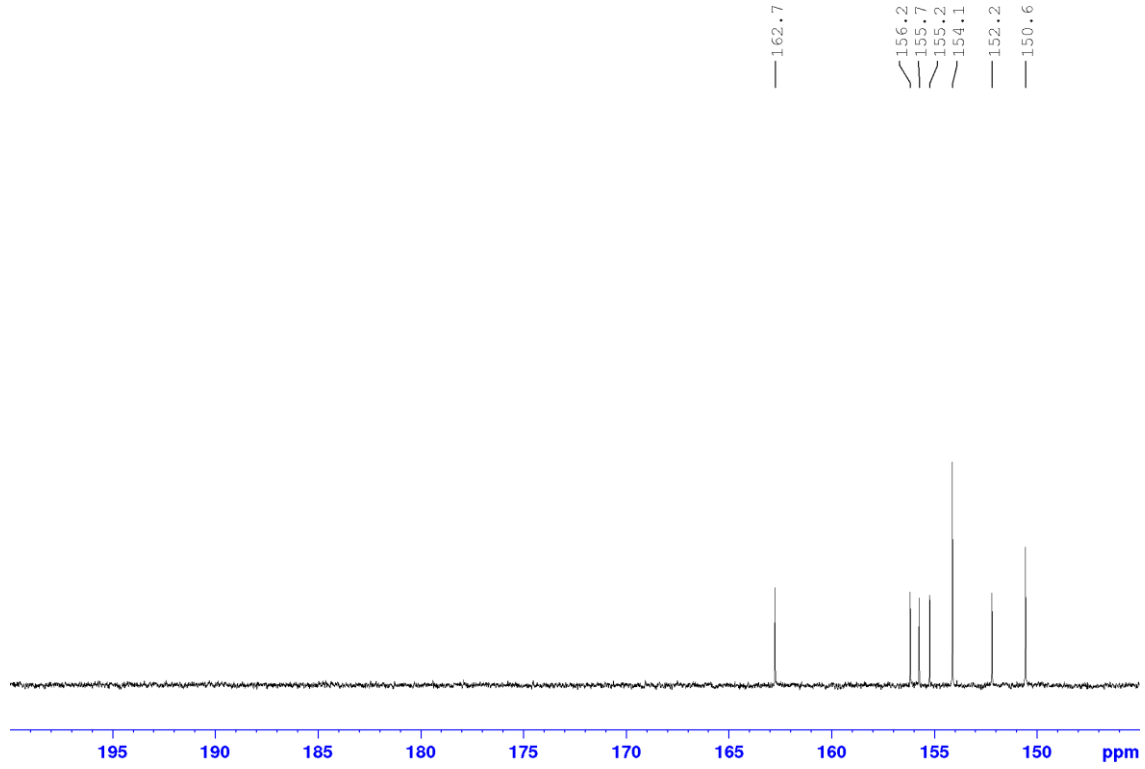


**Figure A100:** $^{13}C\{^{1}H\}$ NMR of **30(*S*)b** in $CD_2Cl_2$ at a 176.1 MHz spectrometer at 298 K, Part 1 (200 ppm – 145 ppm).

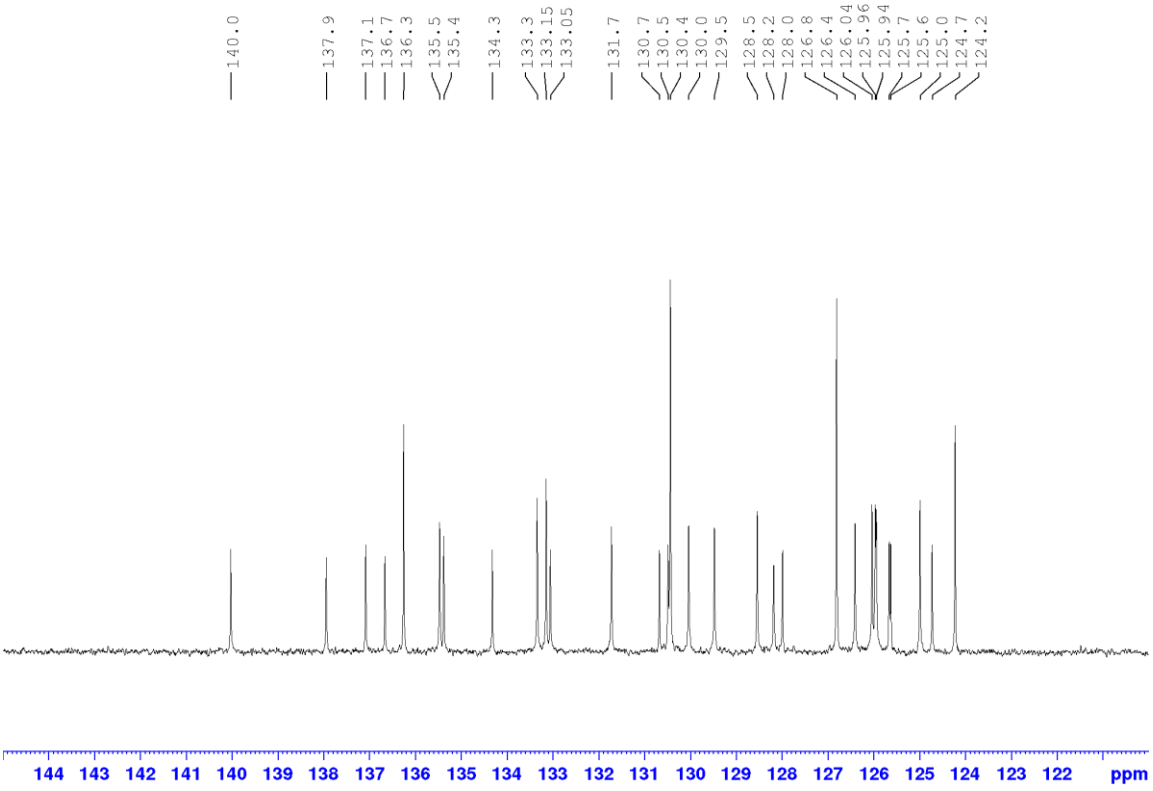


**Figure A101:** $^{13}C\{^{1}H\}$ NMR of **30(*S*)b** in $CD_2Cl_2$ at a 176.1 MHz spectrometer at 298 K, Part 2 (145 ppm – 120 ppm).

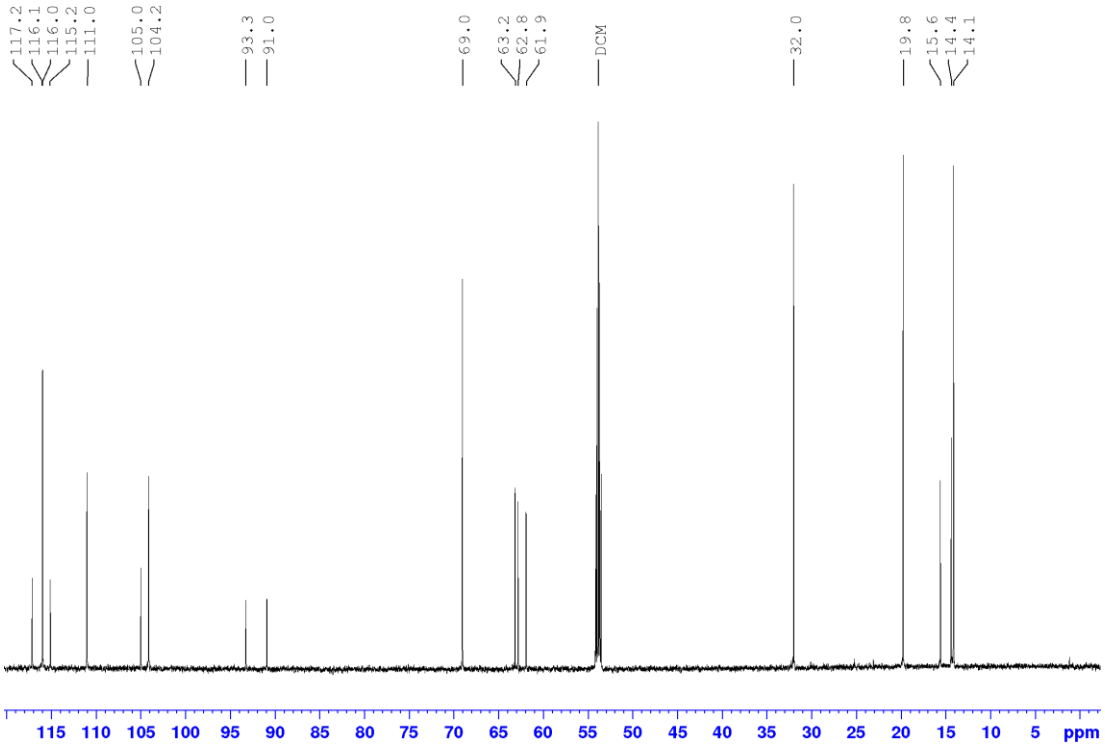


**Figure A102:** $^{13}C\{^{1}H\}$ NMR of **30(*S*)b** in $CD_2Cl_2$ at a 176.1 MHz spectrometer at 298 K, Part 3 (120 ppm – 0 ppm).

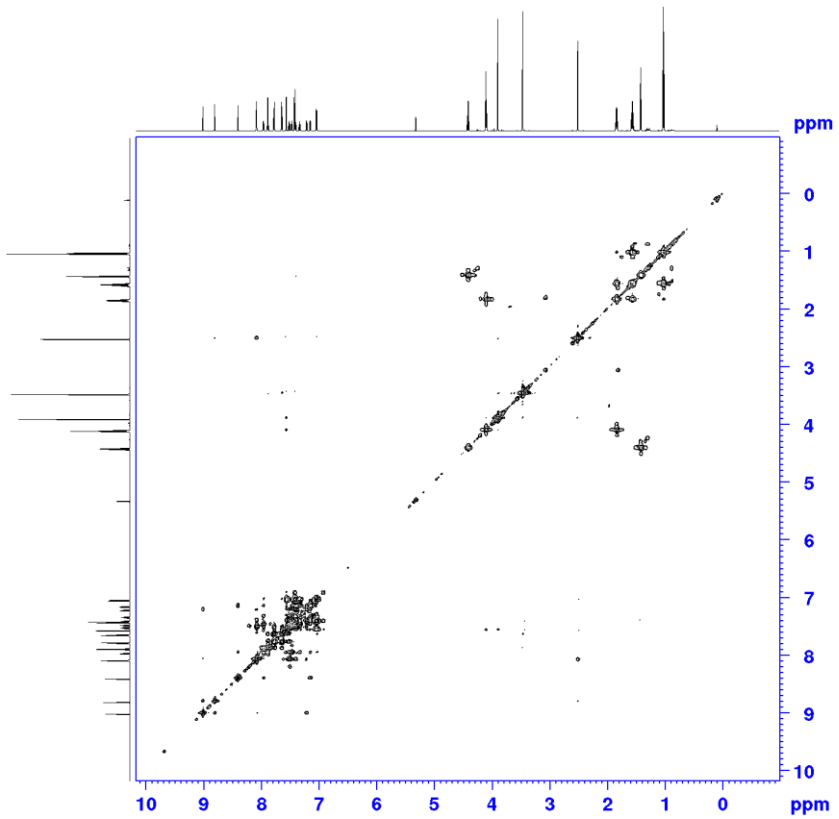


**Figure A103:** $^{1}H,^{1}H$ COSY NMR spectrum of **30(*S*)b** in $CD_2Cl_2$ at a 700 MHz spectrometer at 298 K.

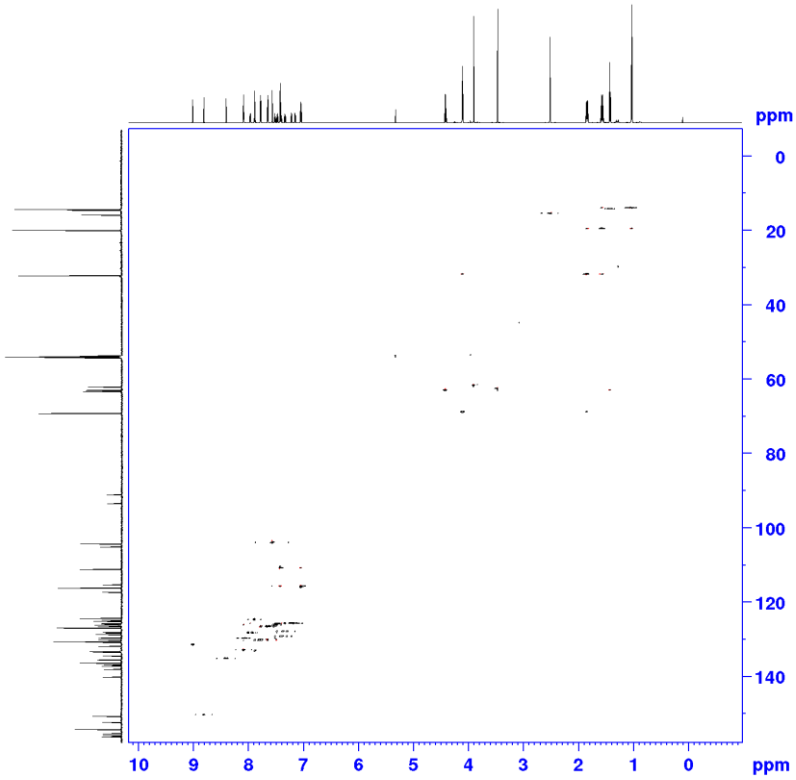


**Figure A104:** $^{1}H,^{13}C$ HSQC NMR spectrum of **30(*S*)b** in $CD_2Cl_2$ at a 700 MHz spectrometer at 298 K.

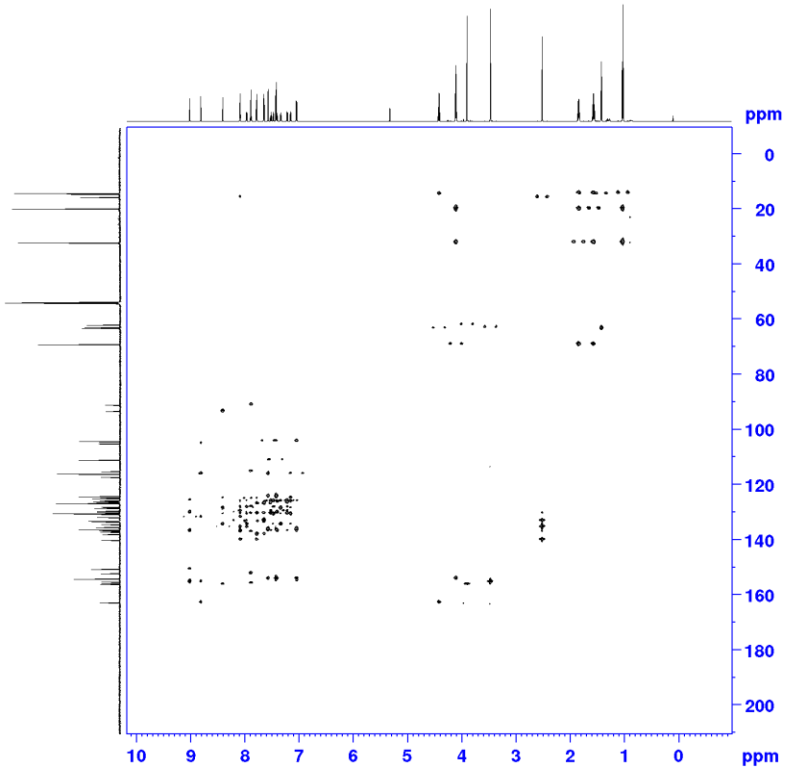


**Figure A105:** $^{1}H,^{13}C$ HMBC NMR spectrum of **30(*S*)b** in $CD_2Cl_2$ at a 700 MHz spectrometer at 298 K.

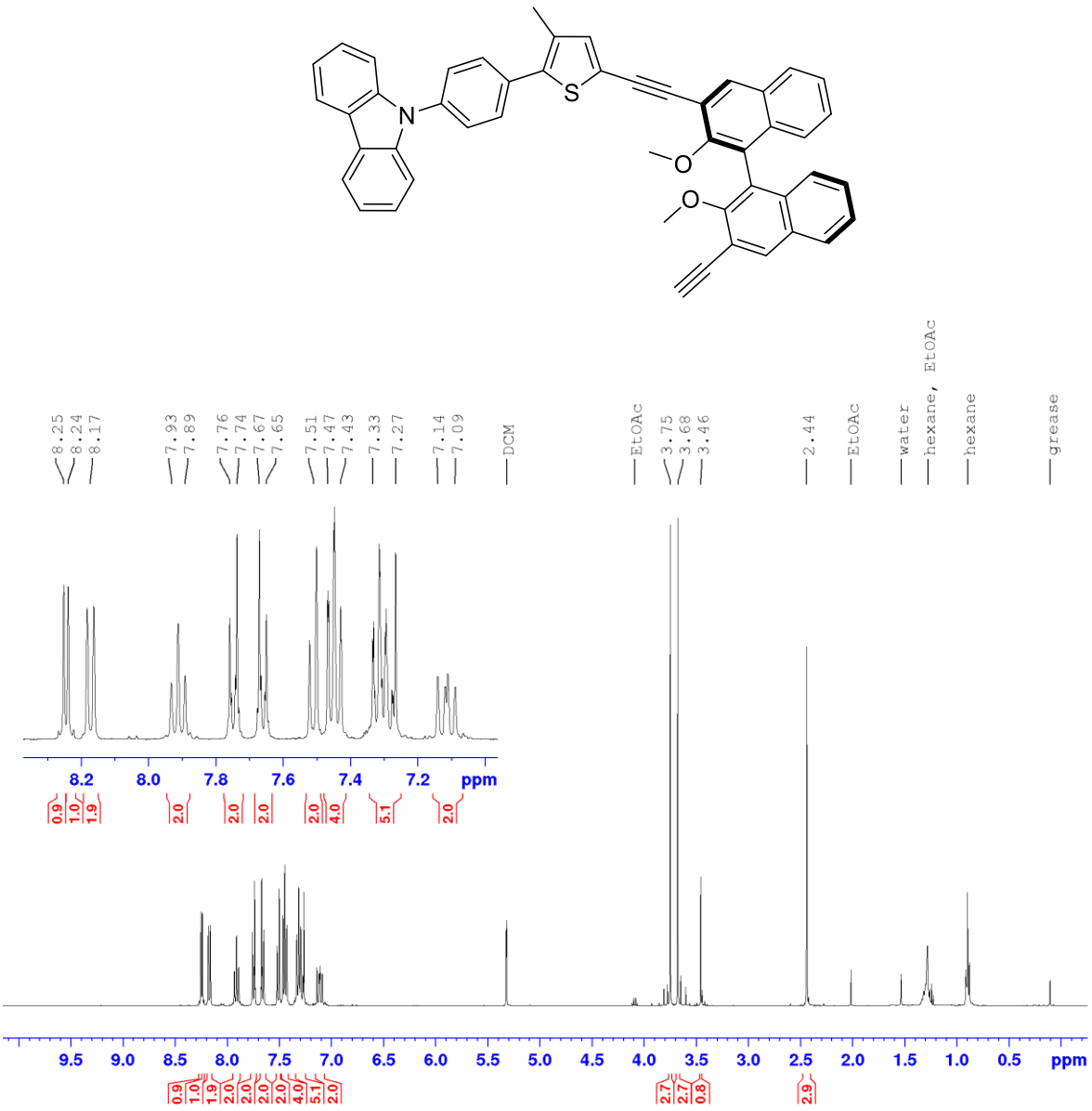


**Figure A106:** $^{1}$H NMR of **32(*S*)** in $CD_2Cl_2$ at a 400 MHz spectrometer at 298 K.

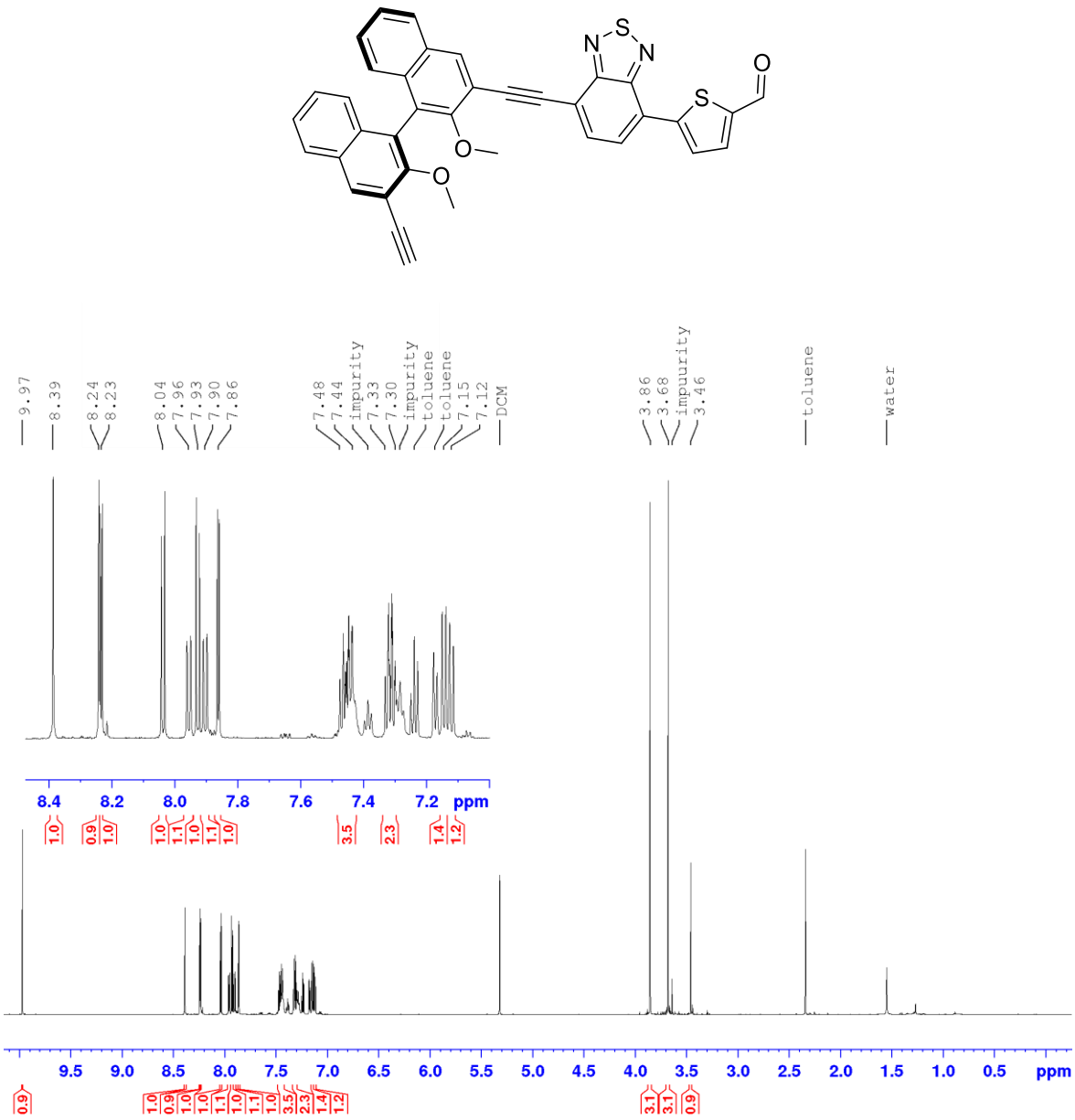


**Figure A107:** $^{1}H$ NMR of **33(*S*)** in $CD_2Cl_2$ at a 400 MHz spectrometer at 298 K.

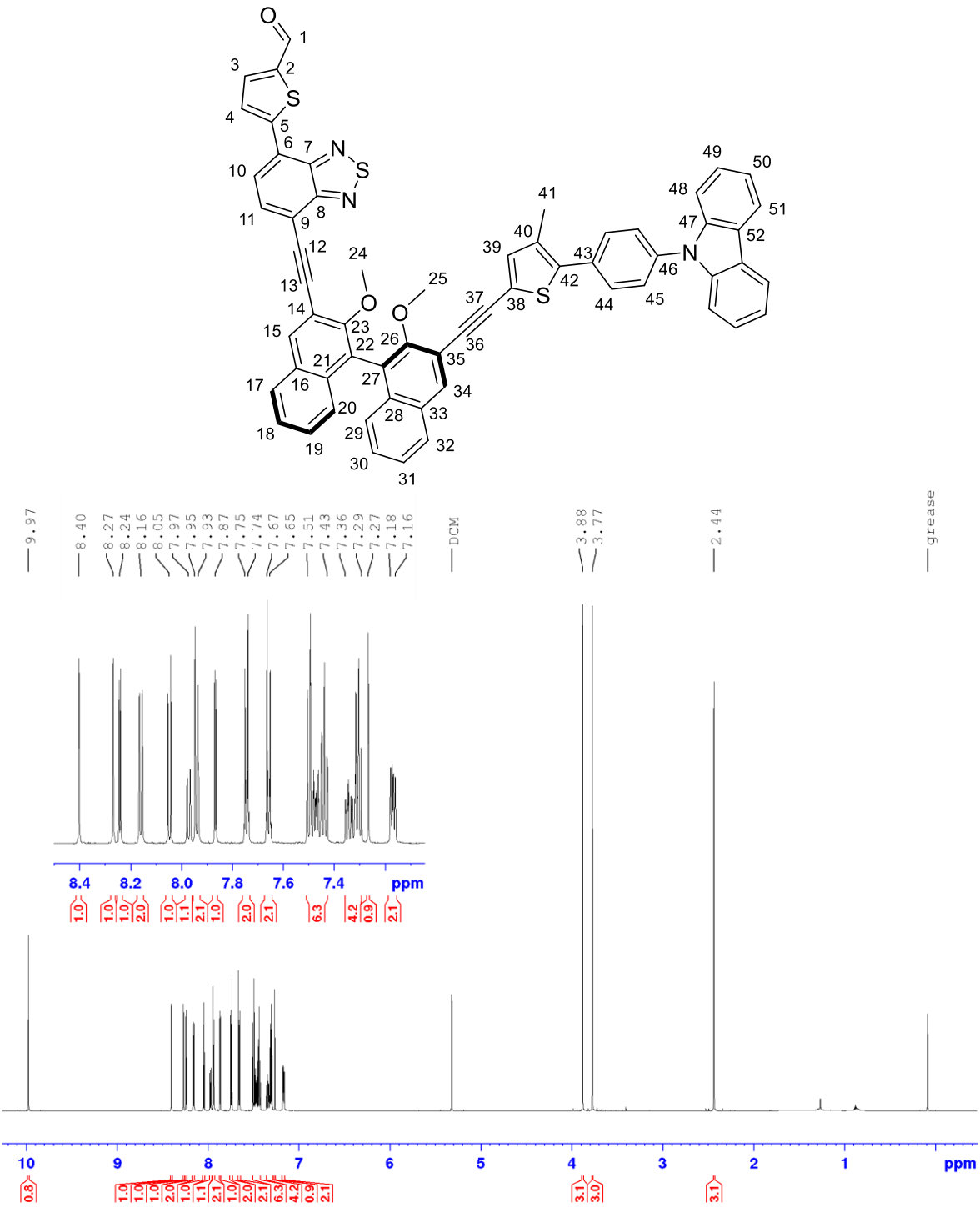


**Figure A108:** $^{1}$H NMR of **34(*S*)** in $CD_2Cl_2$ at a 700 MHz spectrometer at 298 K.

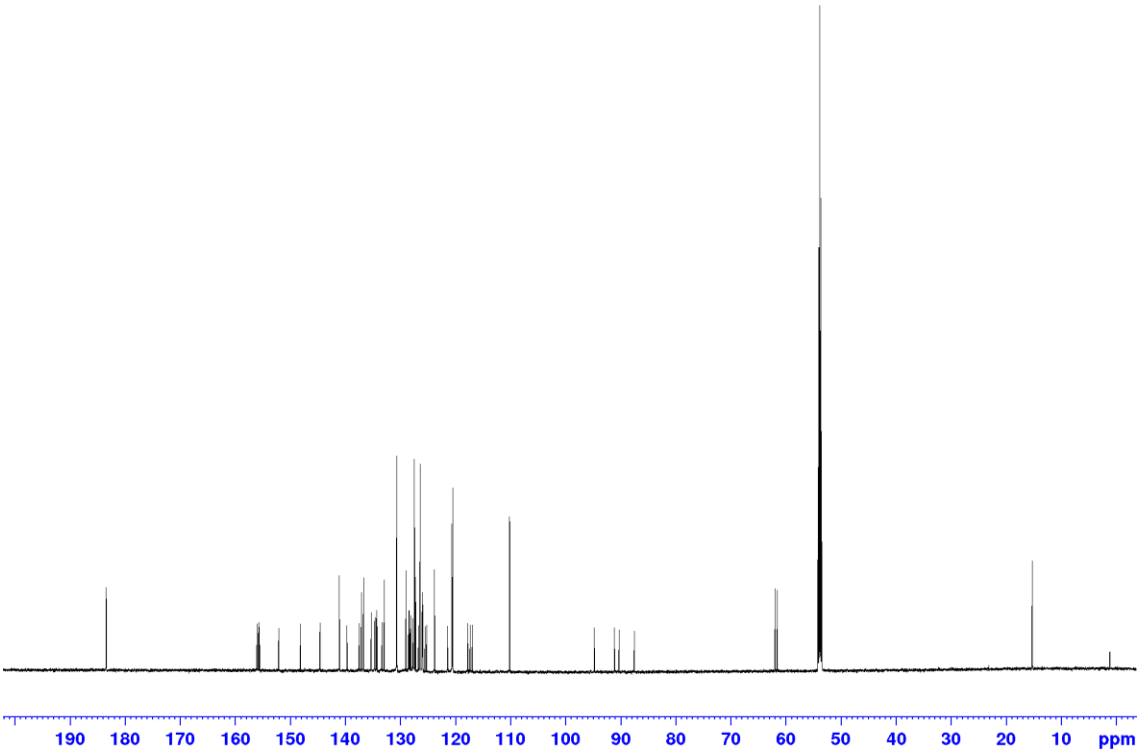


**Figure A109:** $^{13}C\{^{1}H\}$ NMR of **34(*S*)** in $CD_2Cl_2$ at a 176.1 MHz spectrometer at 298 K, Overview.

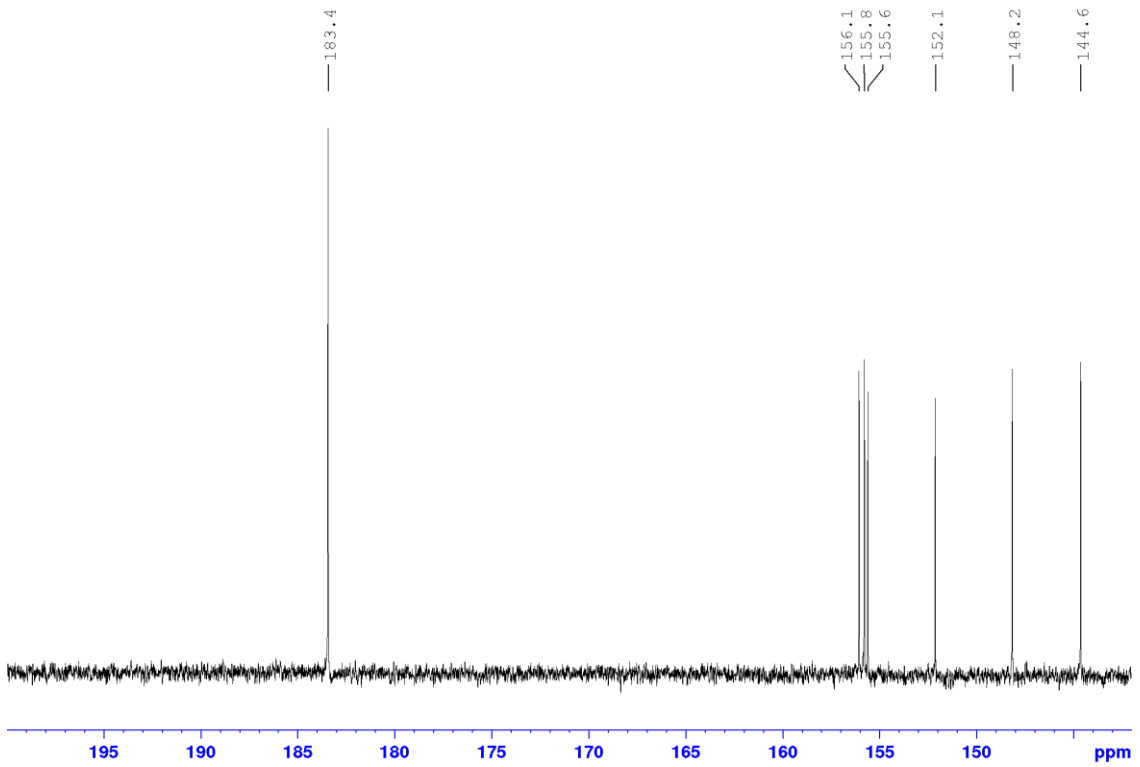


**Figure A110:** $^{13}C\{^{1}H\}$ NMR of **34(*S*)** in $CD_2Cl_2$ at a 176.1 MHz spectrometer at 298 K, Part 1 (200 ppm – 142 ppm).

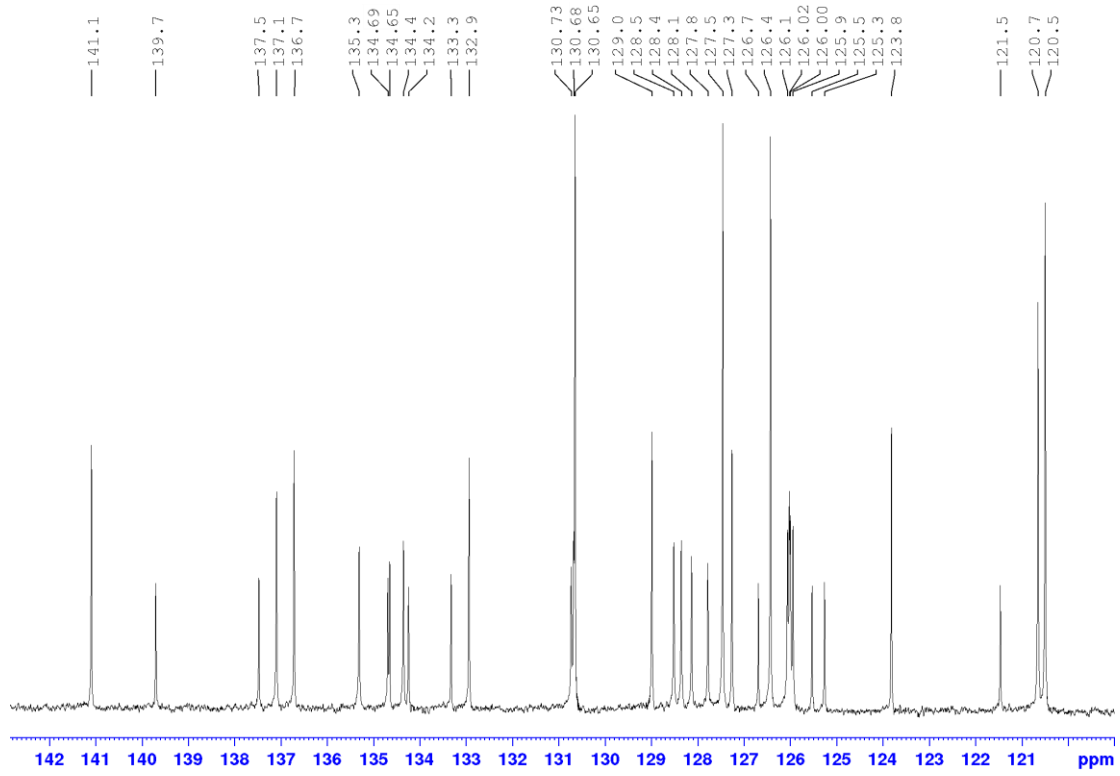


**Figure A111:** $^{13}C\{^{1}H\}$ NMR of **34(*S*)** in $CD_2Cl_2$ at a 176.1 MHz spectrometer at 298 K, Part 2 (142.5 ppm – 119 ppm).

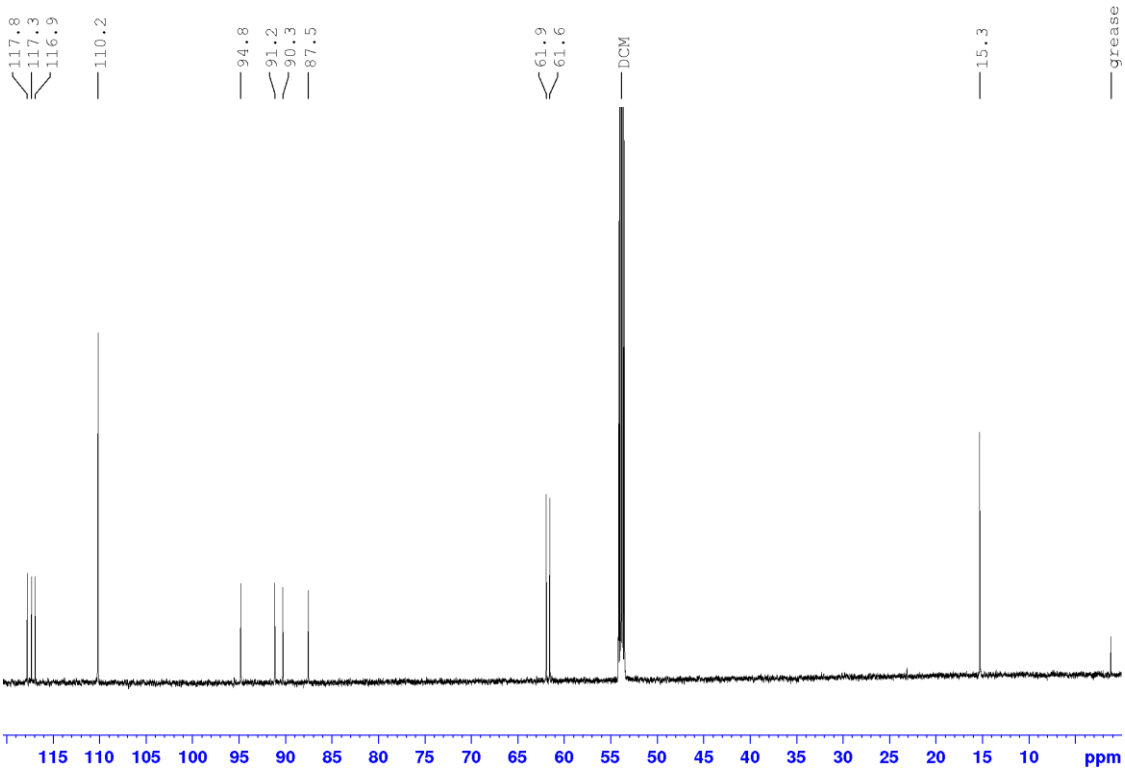


**Figure A112:** $^{13}C\{^{1}H\}$ NMR of **34(*S*)** in $CD_2Cl_2$ at a 176.1 MHz spectrometer at 298 K, Part 3 (120 ppm – 0 ppm).

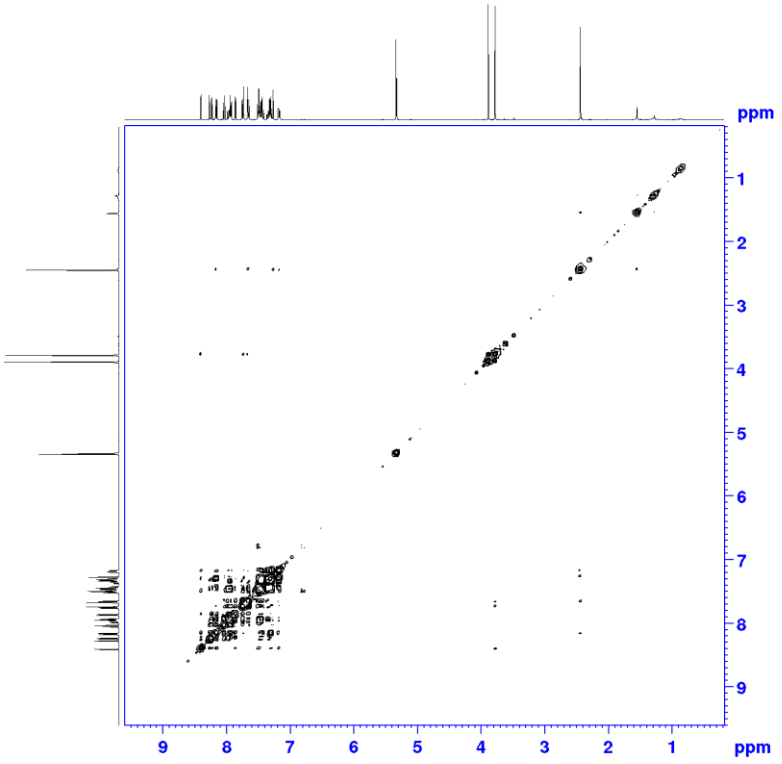


**Figure A113:** $^{1}H,^{1}H$ COSY NMR spectrum of **34(*S*)** in $CD_2Cl_2$ at a 700 MHz spectrometer at 298 K.

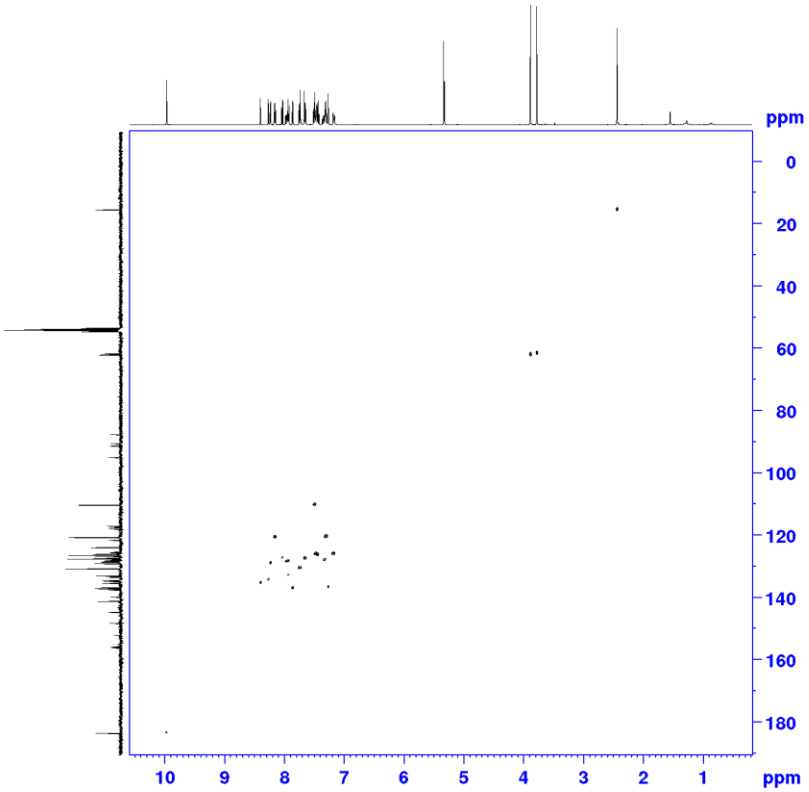


**Figure A114:** $^{1}H,^{13}C$ HSQC NMR spectrum of **34(*S*)** in $CD_2Cl_2$ at a 700 MHz spectrometer at 298 K.

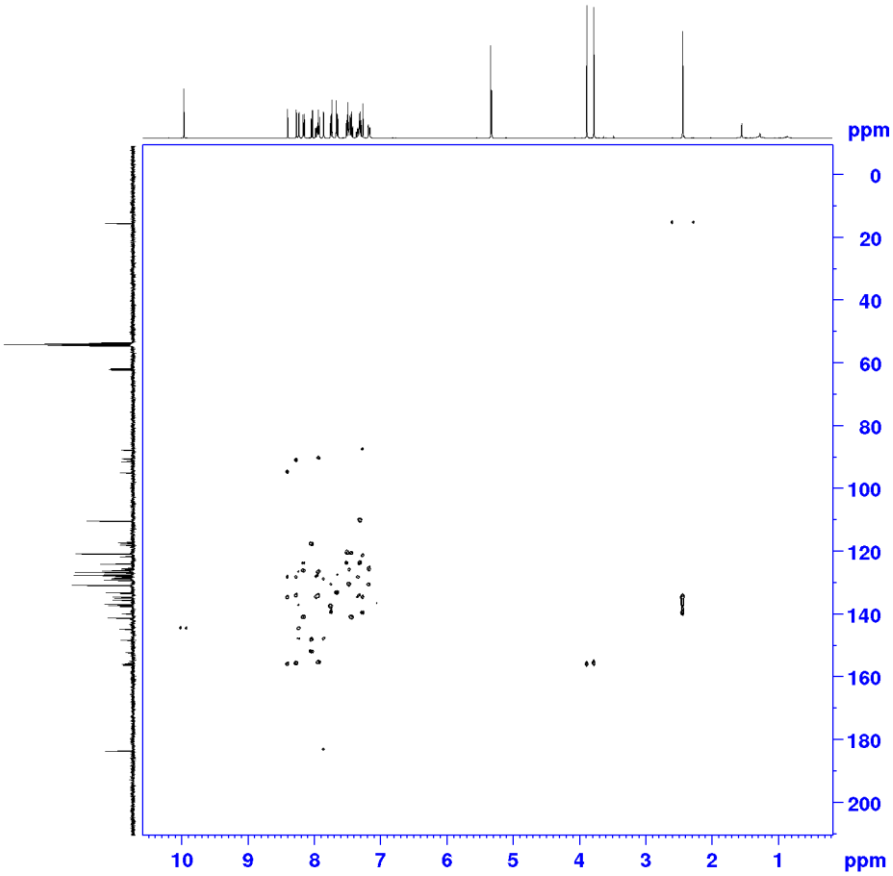


**Figure A115:** $^{1}H,^{13}C$ HMBC NMR spectrum of **34(*S*)** in $CD_2Cl_2$ at a 700 MHz spectrometer at 298 K.

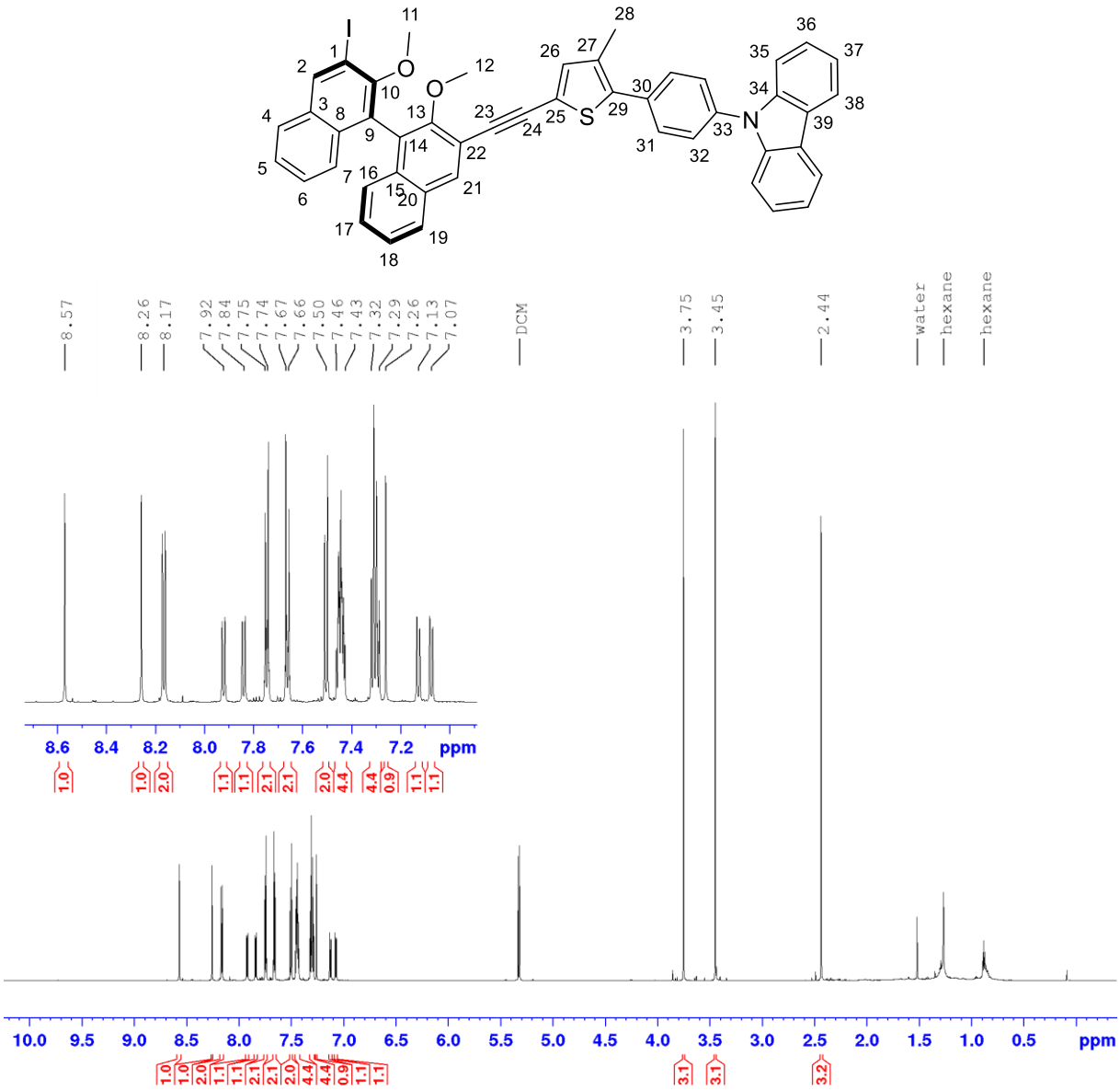


**Figure A116:** $^{1}$H NMR of **35(*S*)** in $CD_2Cl_2$ at a 700 MHz spectrometer at 298 K.

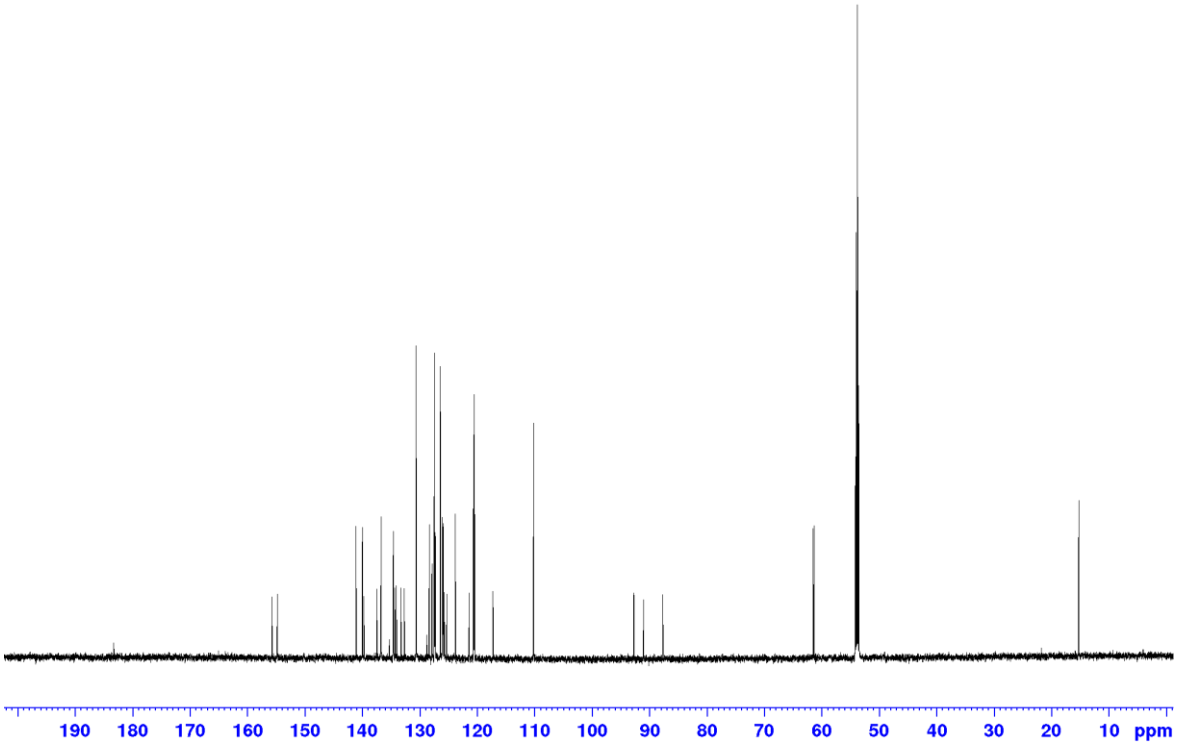


**Figure A117:** $^{13}C\{^{1}H\}$ NMR of **35(*S*)** in $CD_2Cl_2$ at a 176.1 MHz spectrometer at 298 K, Overview.

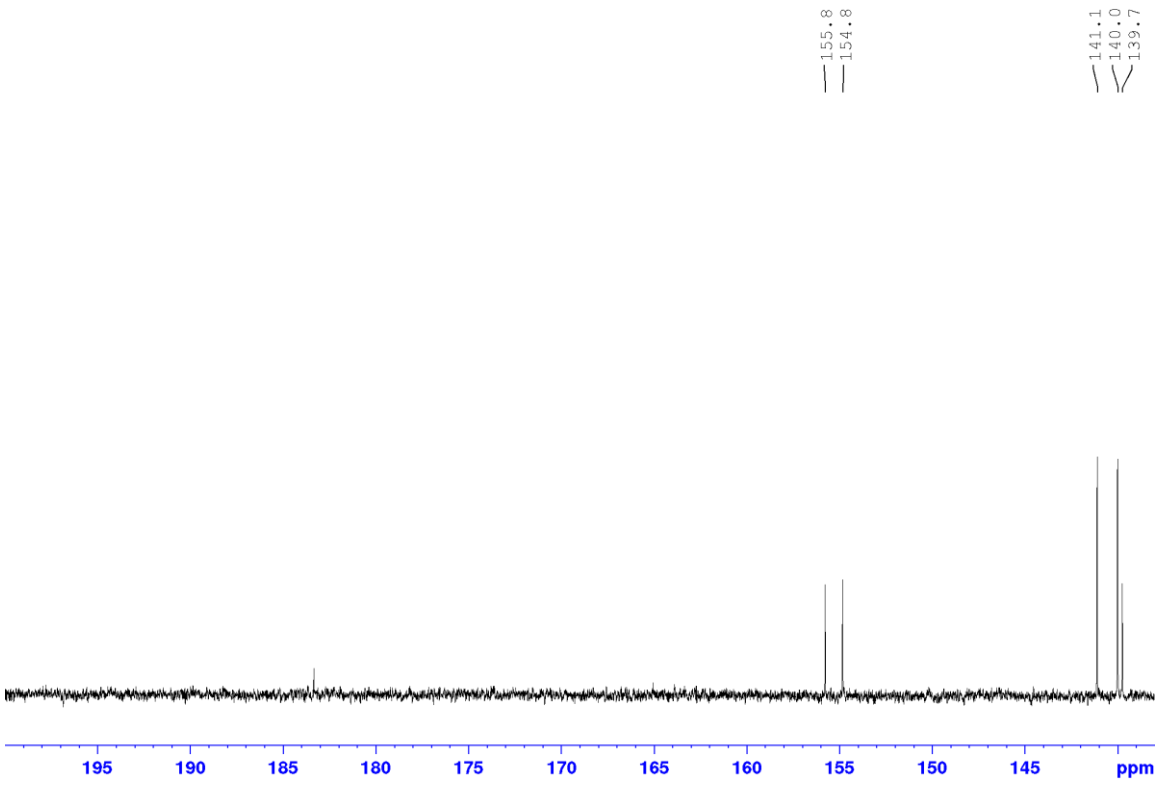


**Figure A118:** $^{13}C\{^{1}H\}$ NMR of **35(*S*)** in $CD_2Cl_2$ at a 176.1 MHz spectrometer at 298 K, Part 1 (200 ppm – 138 ppm).

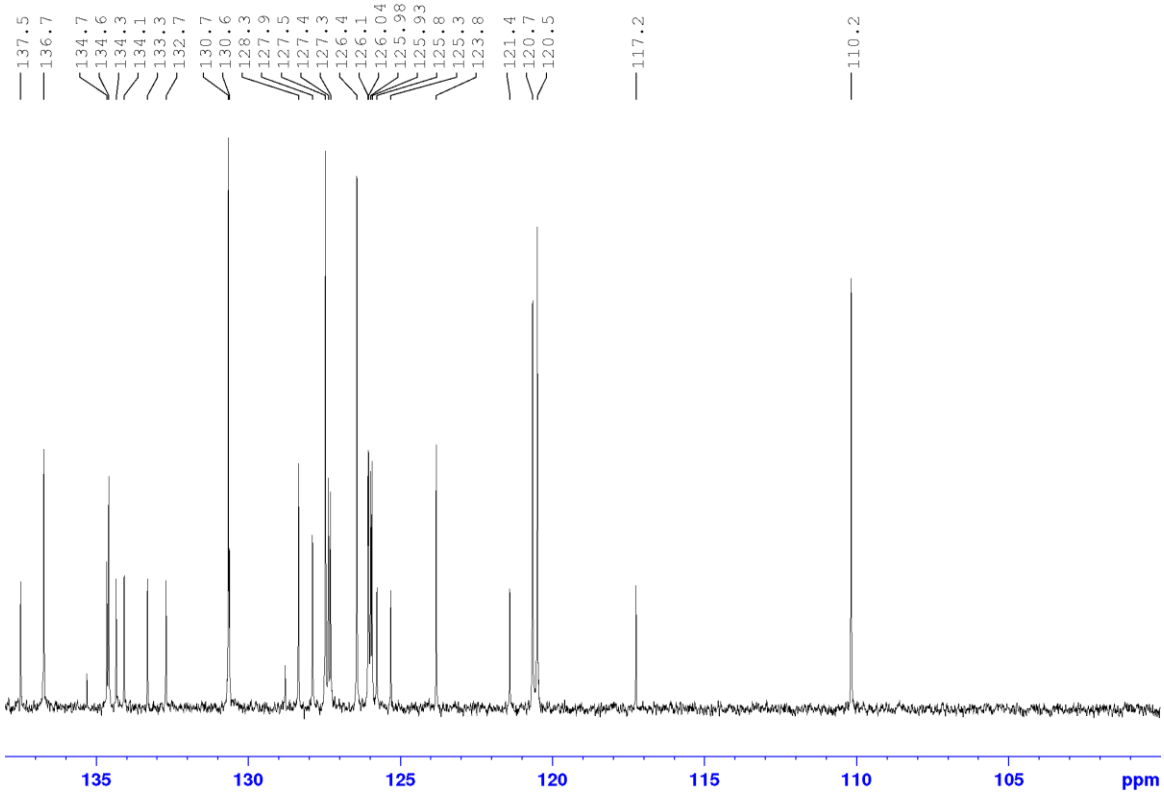


**Figure A119:** $^{13}C\{^{1}H\}$ NMR of **35(*S*)** in $CD_2Cl_2$ at a 176.1 MHz spectrometer at 298 K, Part 2 (138 ppm – 100 ppm).

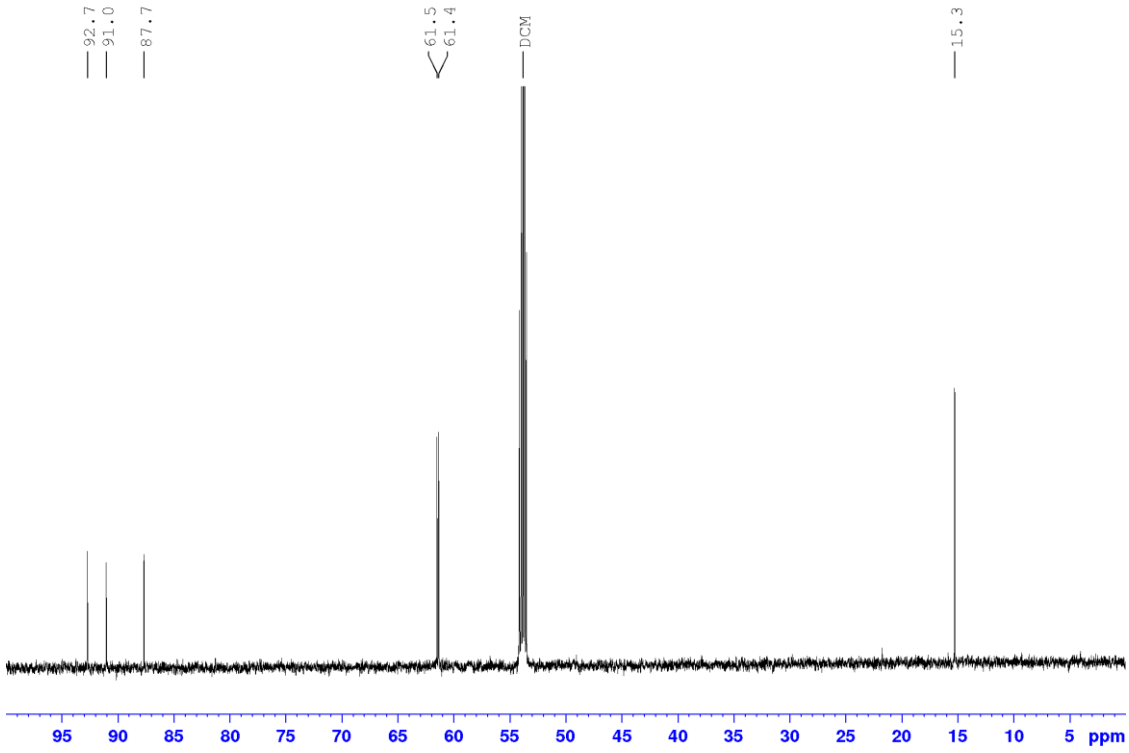


**Figure A120:** $^{13}C\{^{1}H\}$ NMR of **35(*S*)** in $CD_2Cl_2$ at a 176.1 MHz spectrometer at 298 K, Part 3 (100 ppm – 0 ppm).

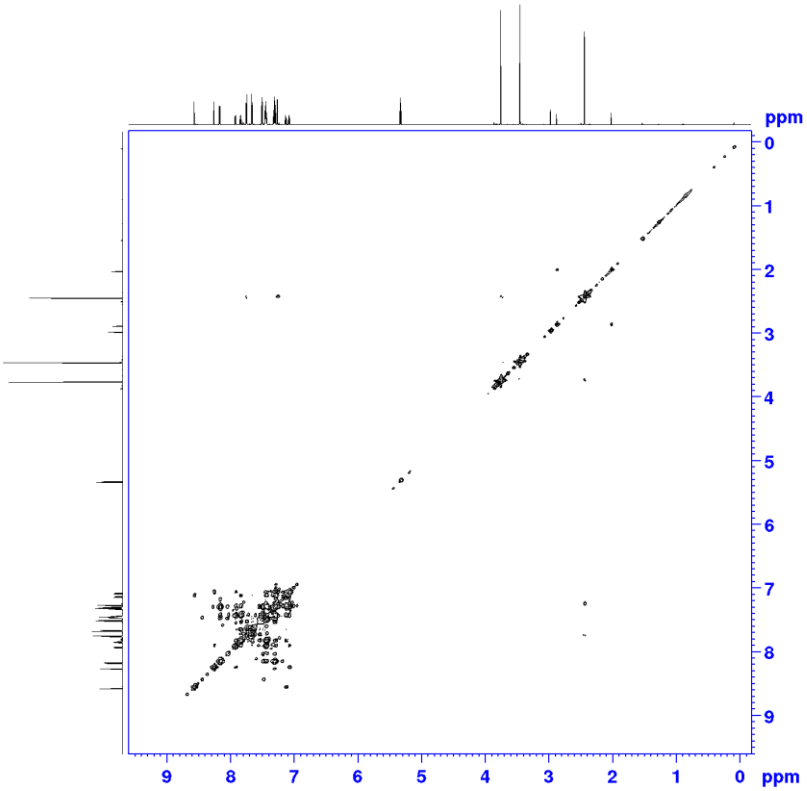


**Figure A121:** $^{1}H,^{1}H$ COSY NMR spectrum of **35(*S*)** in $CD_2Cl_2$ at a 700 MHz spectrometer at 298 K.

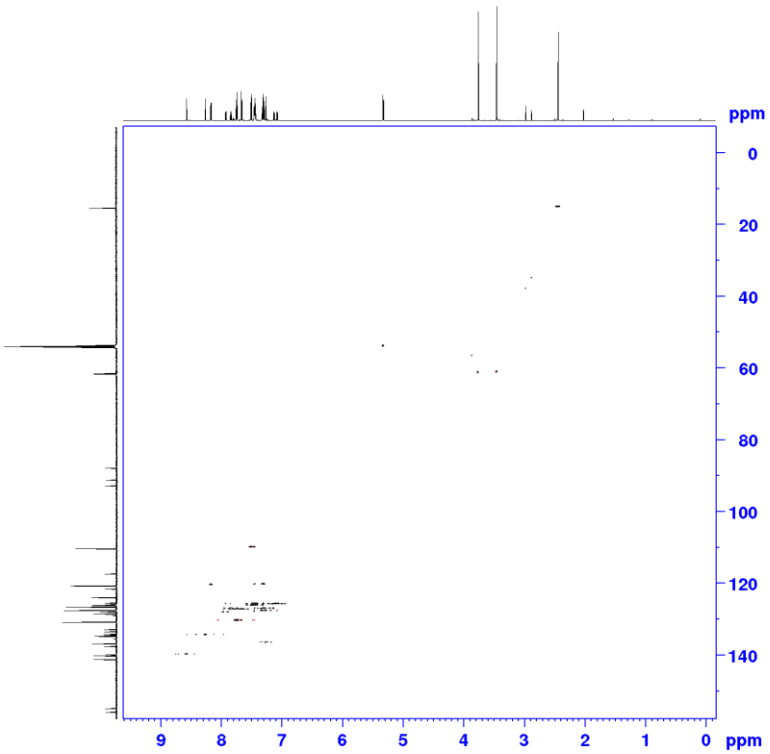


**Figure A122:** $^{1}H,^{13}C$ HSQC NMR spectrum of **35(*S*)** in $CD_2Cl_2$ at a 700 MHz spectrometer at 298 K.

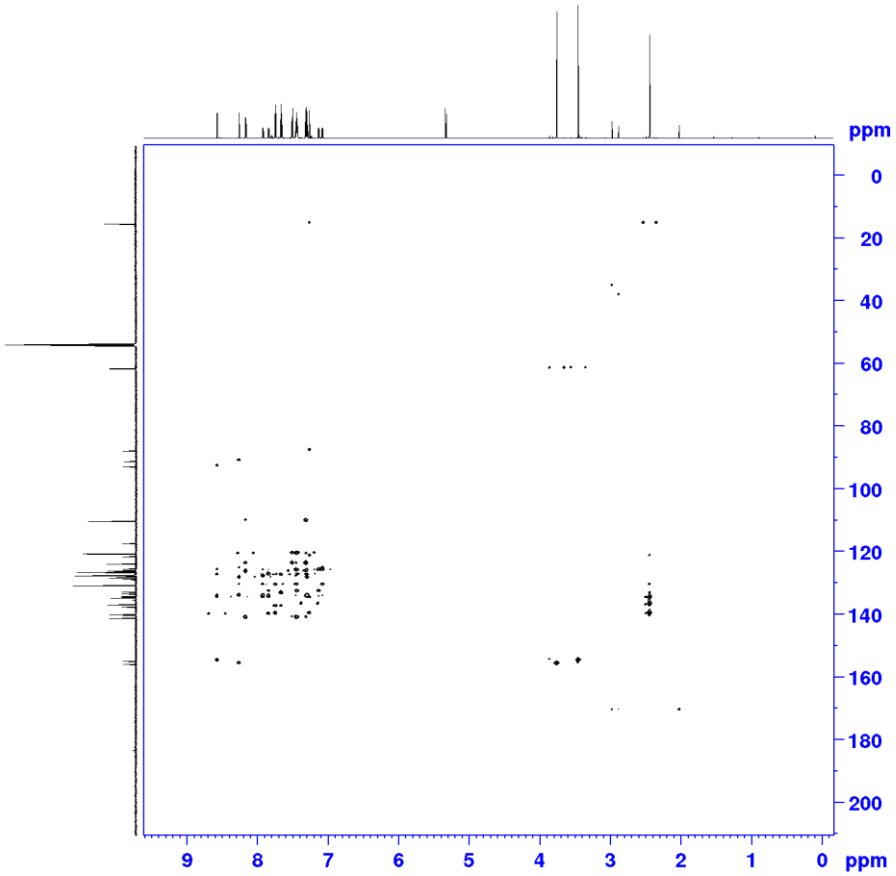


**Figure A123:** $^{1}H,^{13}C$ HMBC NMR spectrum of **35(*S*)** in $CD_2Cl_2$ at a 700 MHz spectrometer at 298 K.

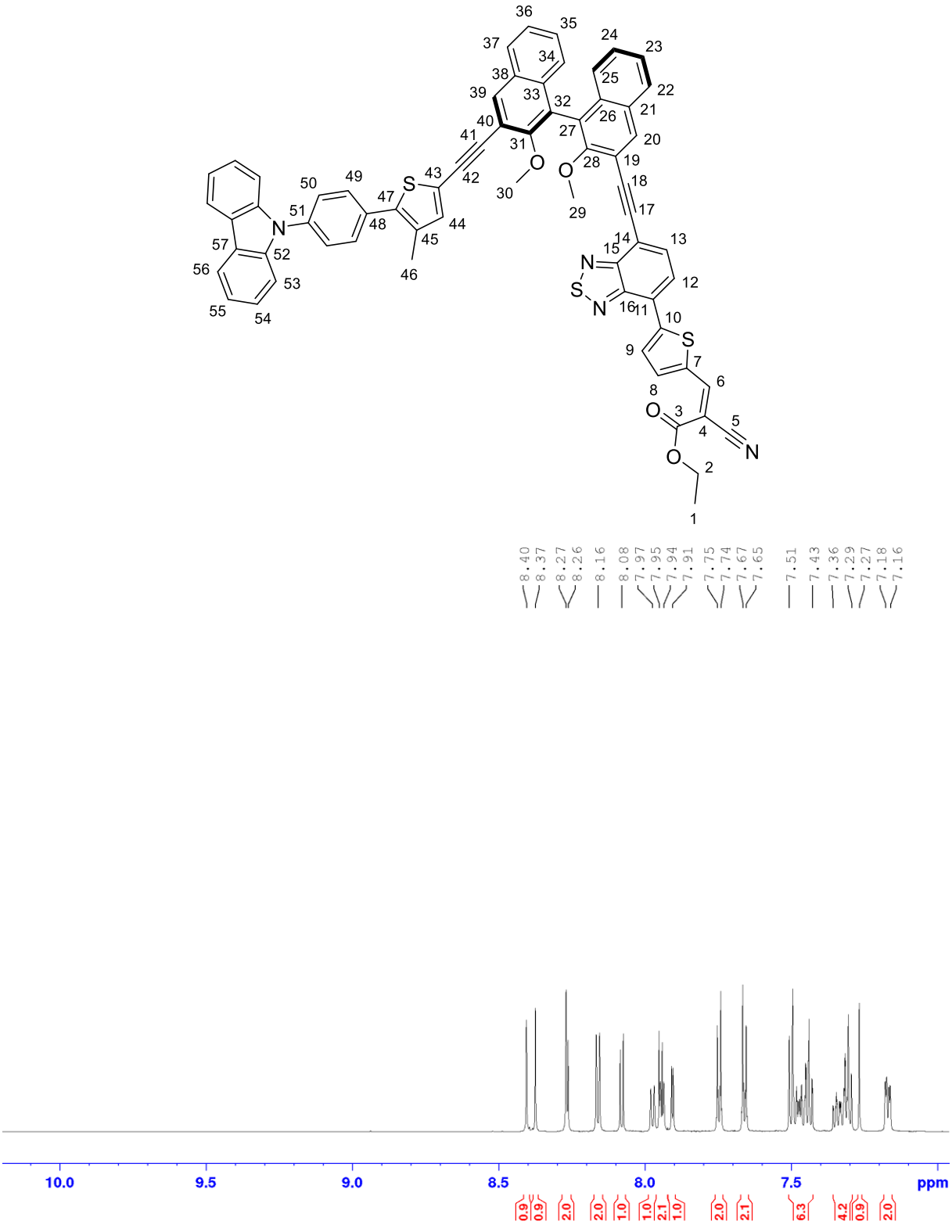


**Figure A124:** $^{1}$H NMR of **36(*S*)** in $CD_2Cl_2$ at a 700 MHz spectrometer at 298 K, Part 1 (10.1 ppm – 7.0 ppm).

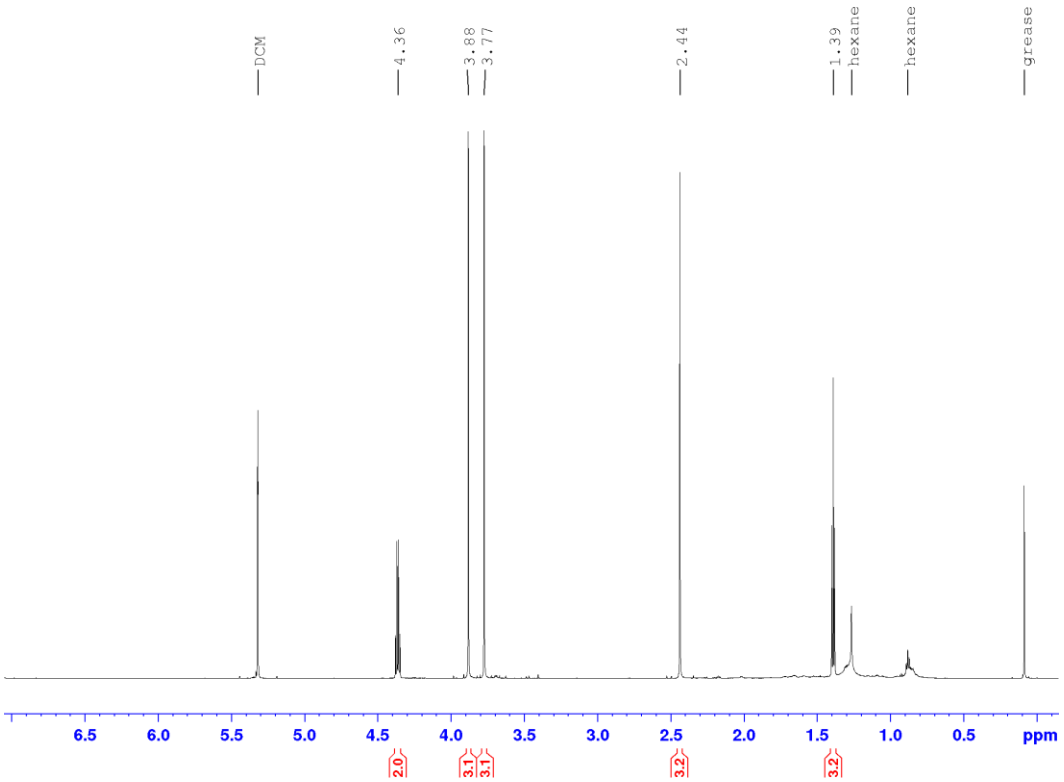


**Figure A125:** $^{1}$H NMR of **36(*S*)** in $CD_2Cl_2$ at a 700 MHz spectrometer at 298 K, Part 2 (7.0 ppm – 0.0 ppm).

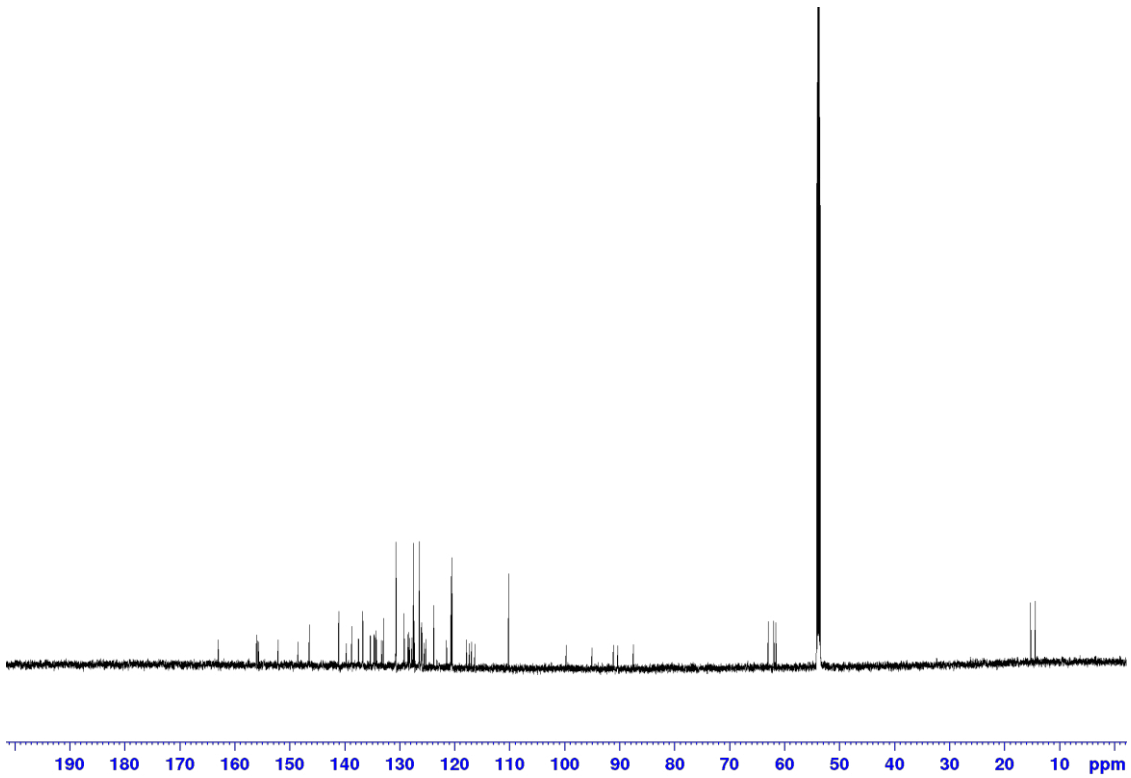


**Figure A126:** $^{13}C\{^{1}H\}$ NMR of **36(*S*)** in $CD_2Cl_2$ at a 176.1 MHz spectrometer at 298 K, Overview.

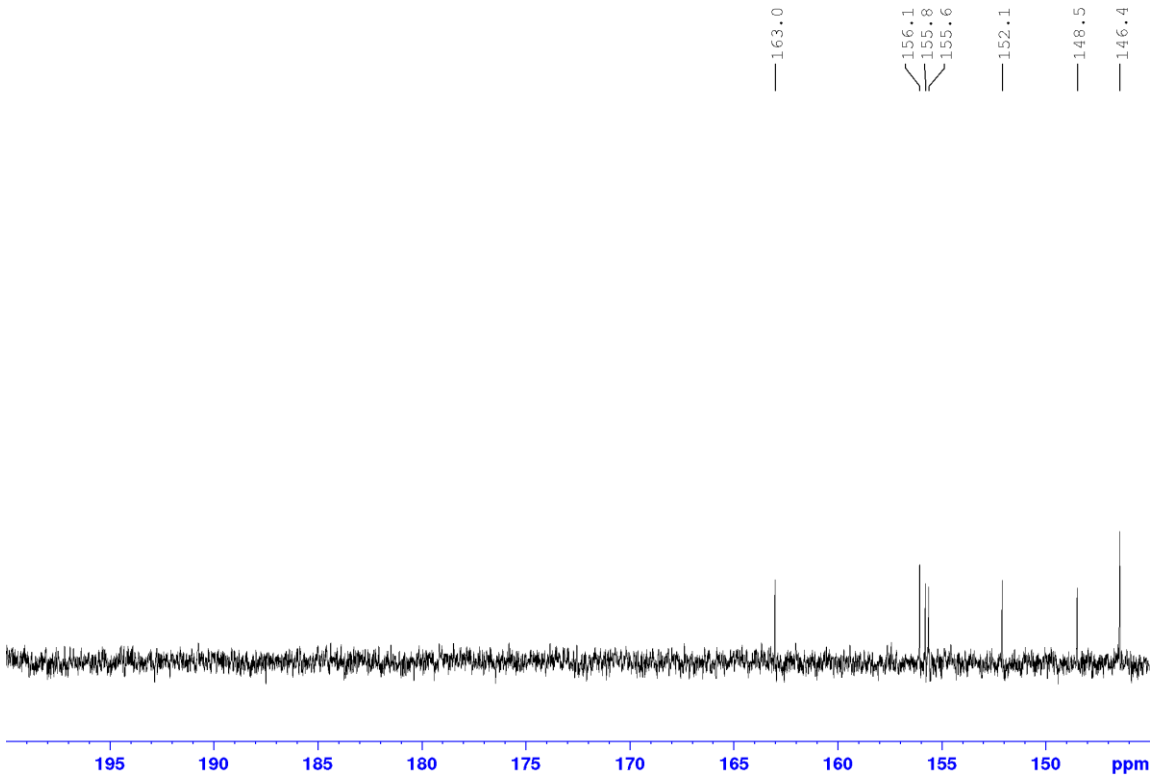


**Figure A127:** $^{13}C\{^{1}H\}$ NMR of **36(*S*)** in $CD_2Cl_2$ at a 176.1 MHz spectrometer at 298 K, Part 1 (190 ppm – 145 ppm).

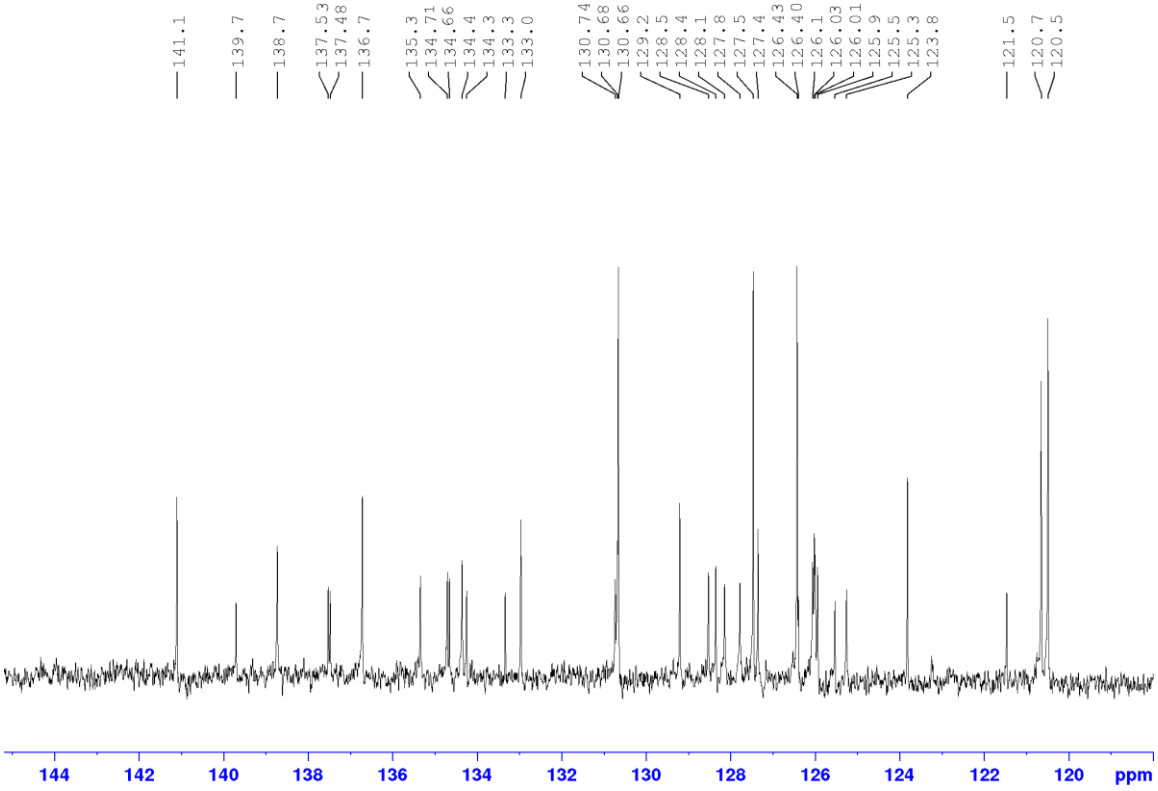


**Figure A128:** $^{13}C$ NMR of **36(*S*)** in $CD_2Cl_2$ at a 176.1 MHz spectrometer at 298 K, Part 2 (145 ppm – 118 ppm).

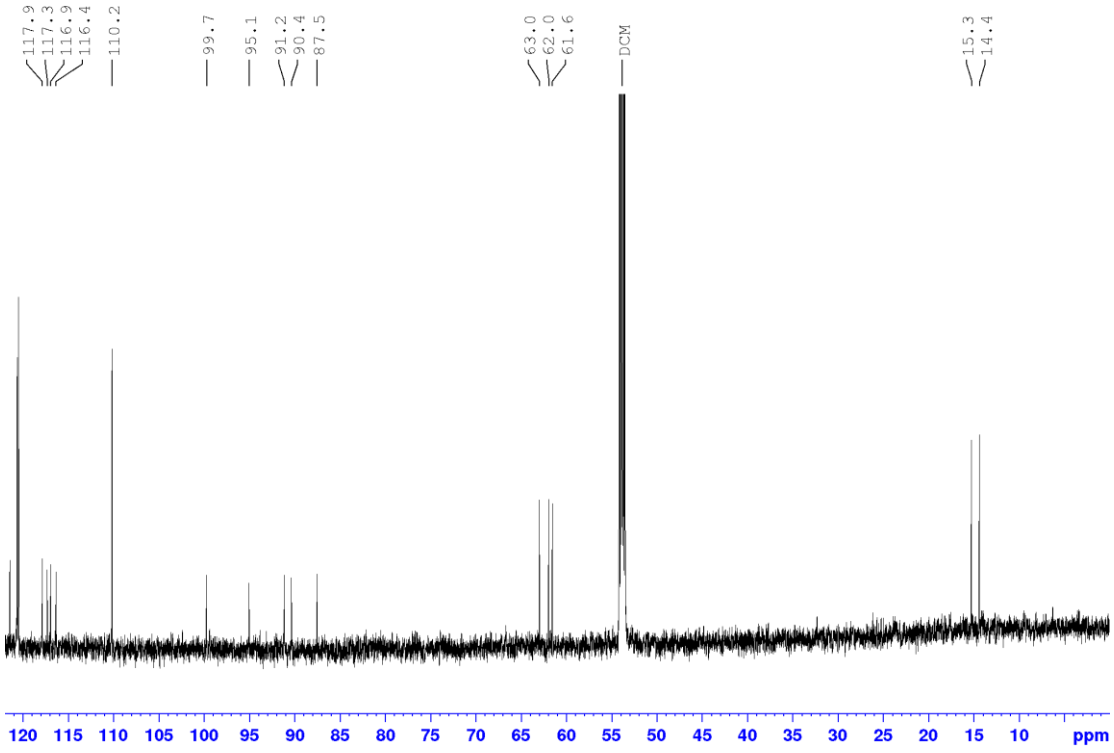


**Figure A129:** $^{13}C$ NMR of **36(*S*)** in $CD_2Cl_2$ at a 176.1 MHz spectrometer at 298 K, Part 3 (122 ppm – 0 ppm).

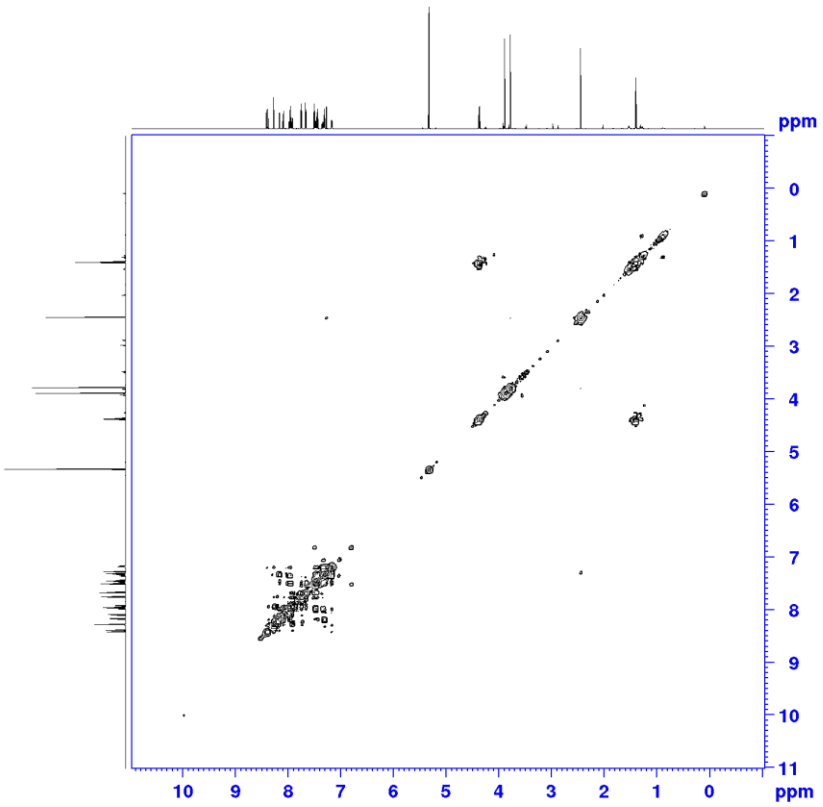


**Figure A130:** $^{1}H,^{1}H$ COSY NMR spectrum of **36(*S*)** in $CD_2Cl_2$ at a 700 MHz spectrometer at 298 K.

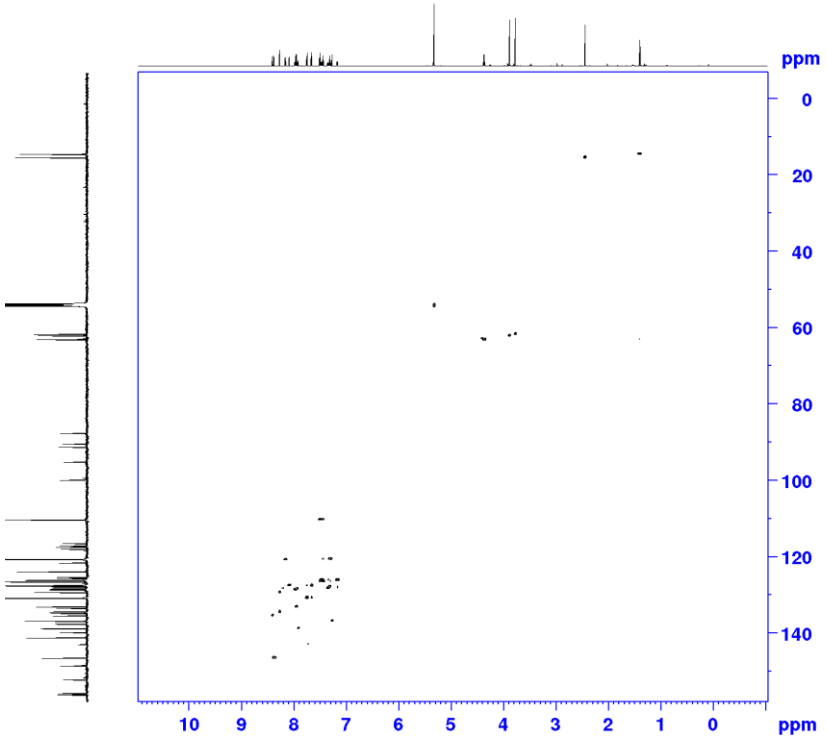


**Figure A131:** $^{1}H,^{13}C$ HSQC NMR spectrum of **36(*S*)** in $CD_2Cl_2$ at a 700 MHz spectrometer at 298 K.

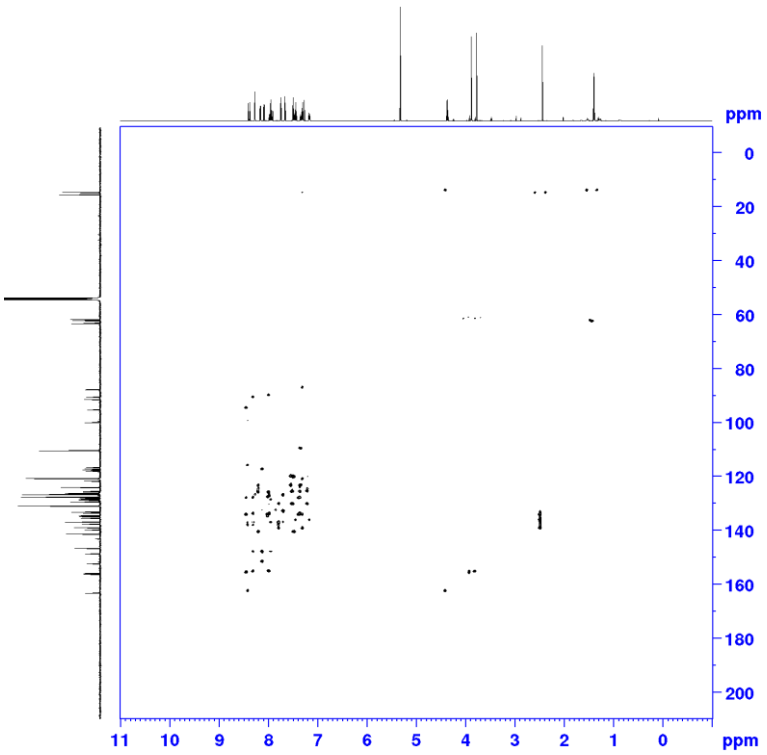


**Figure A132:** $^{1}H,^{13}C$ HMBC NMR spectrum of **36(*S*)** in $CD_2Cl_2$ at a 700 MHz spectrometer at 298 K.

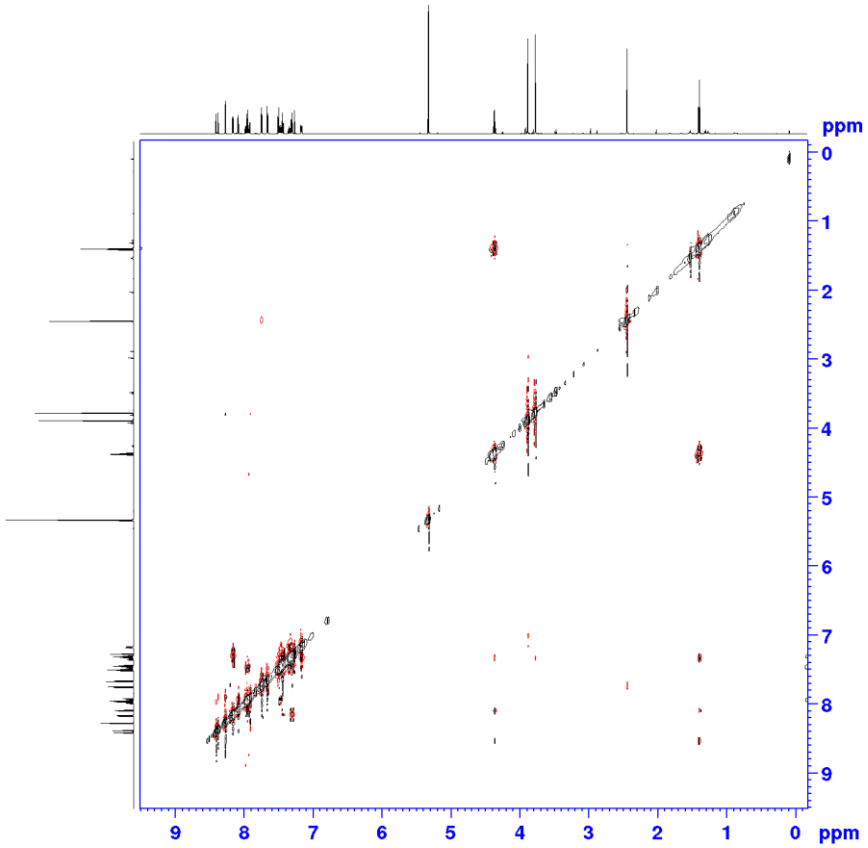


**Figure A133:** $^{1}H,^{1}H$ NOESY NMR spectrum of **36(*S*)** in $CD_2Cl_2$ at a 700 MHz spectrometer at 298 K.

## 5.2. UV-Vis- and Fluorescence Spectra

The fluorescence spectra were scaled to the UV-Vis spectra (absorption coefficients and quantum yields are assigned in Table S1).

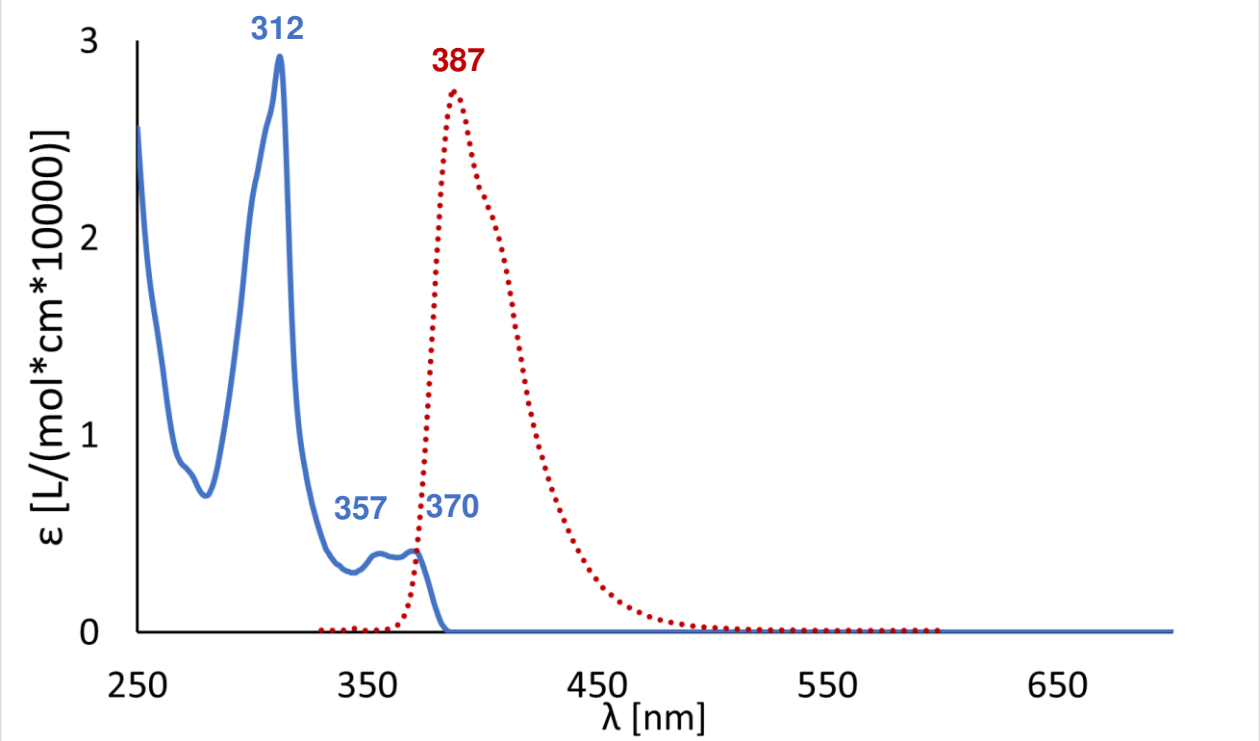


**Figure A134:** UV-Vis (blue line)- and Fluorescence (red dotted line) spectra of **2b** in DCM.

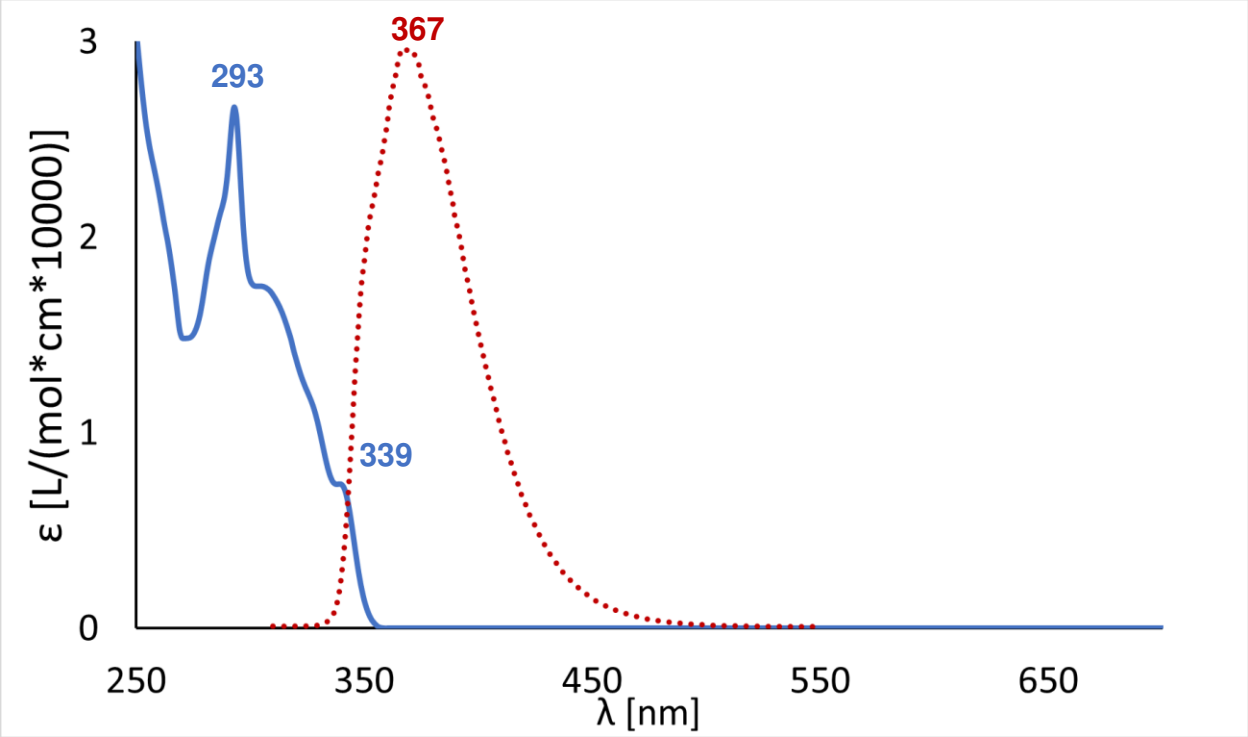


**Figure A135:** UV-Vis (blue line)- and Fluorescence (red dotted line) spectra of **4a** in DCM.

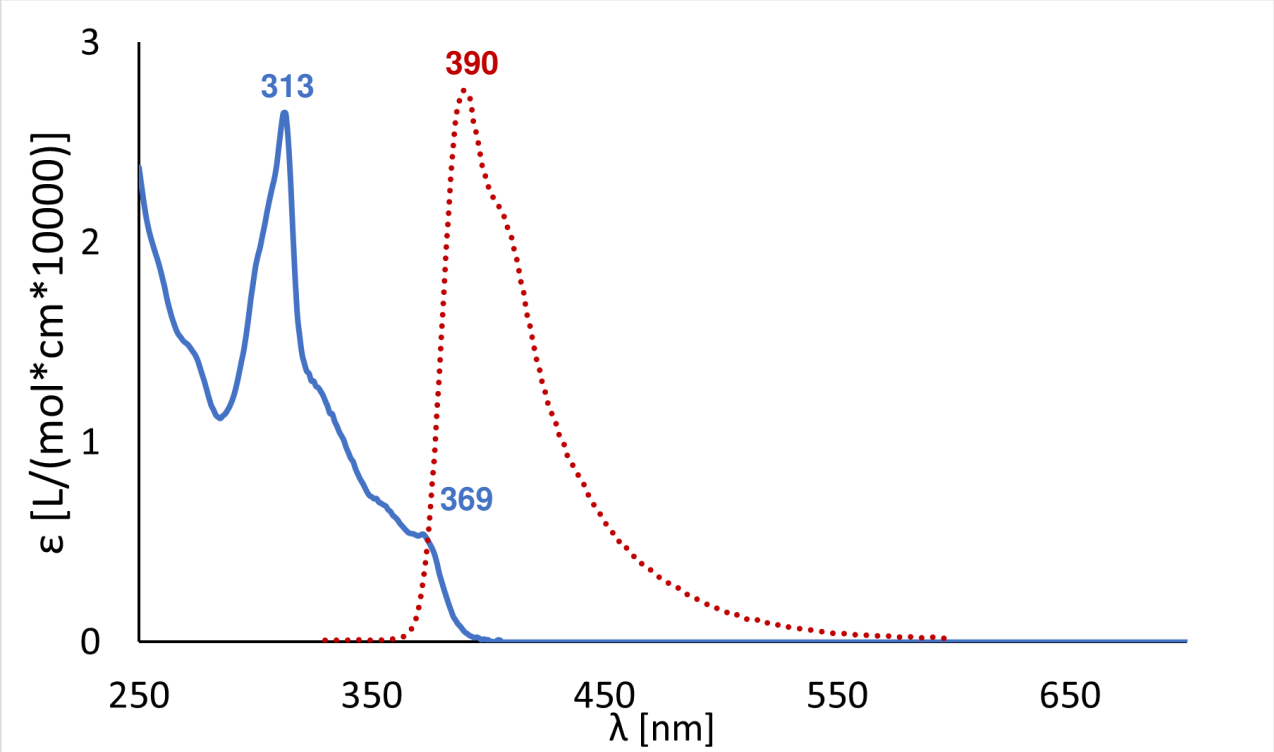


**Figure A136:** UV-Vis (blue line)- and Fluorescence (red dotted line) spectra of **4b** in DCM.

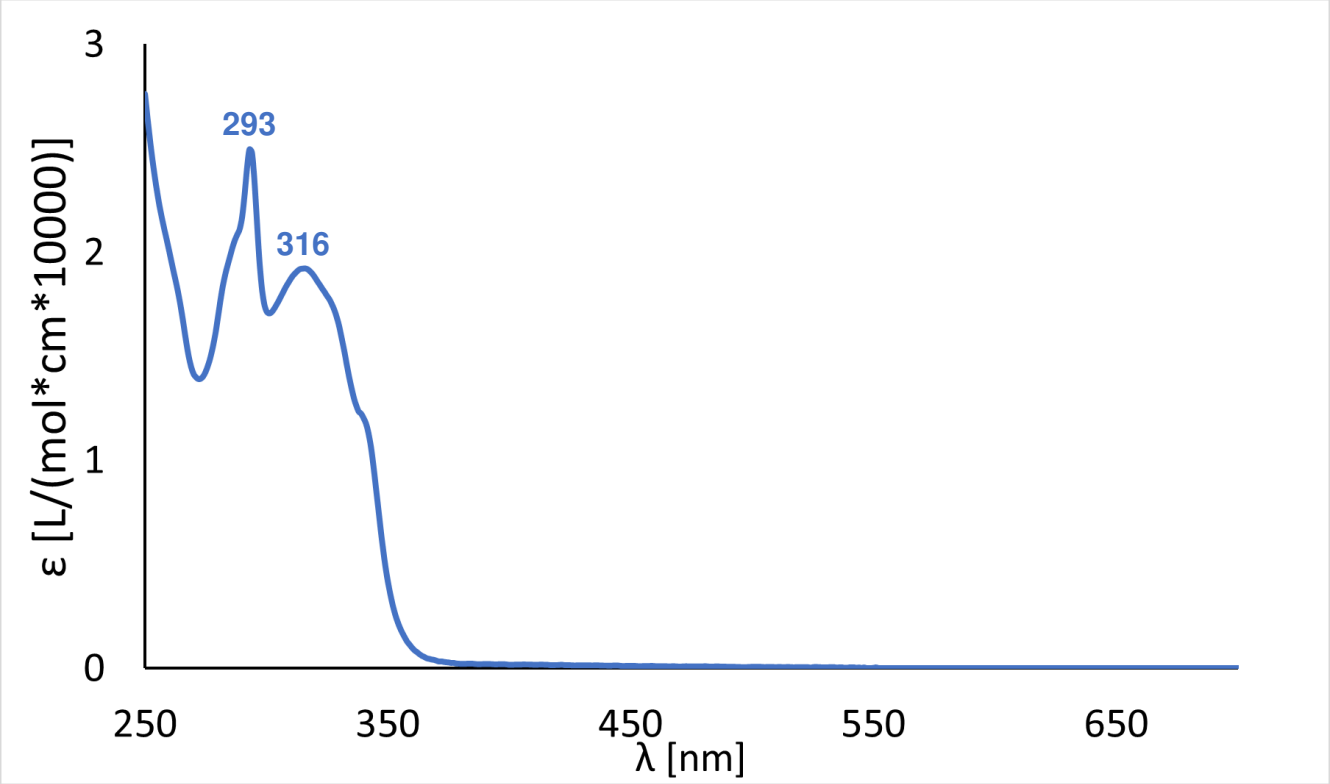


**Figure A137:** UV-Vis spectra of **10** in DCM.

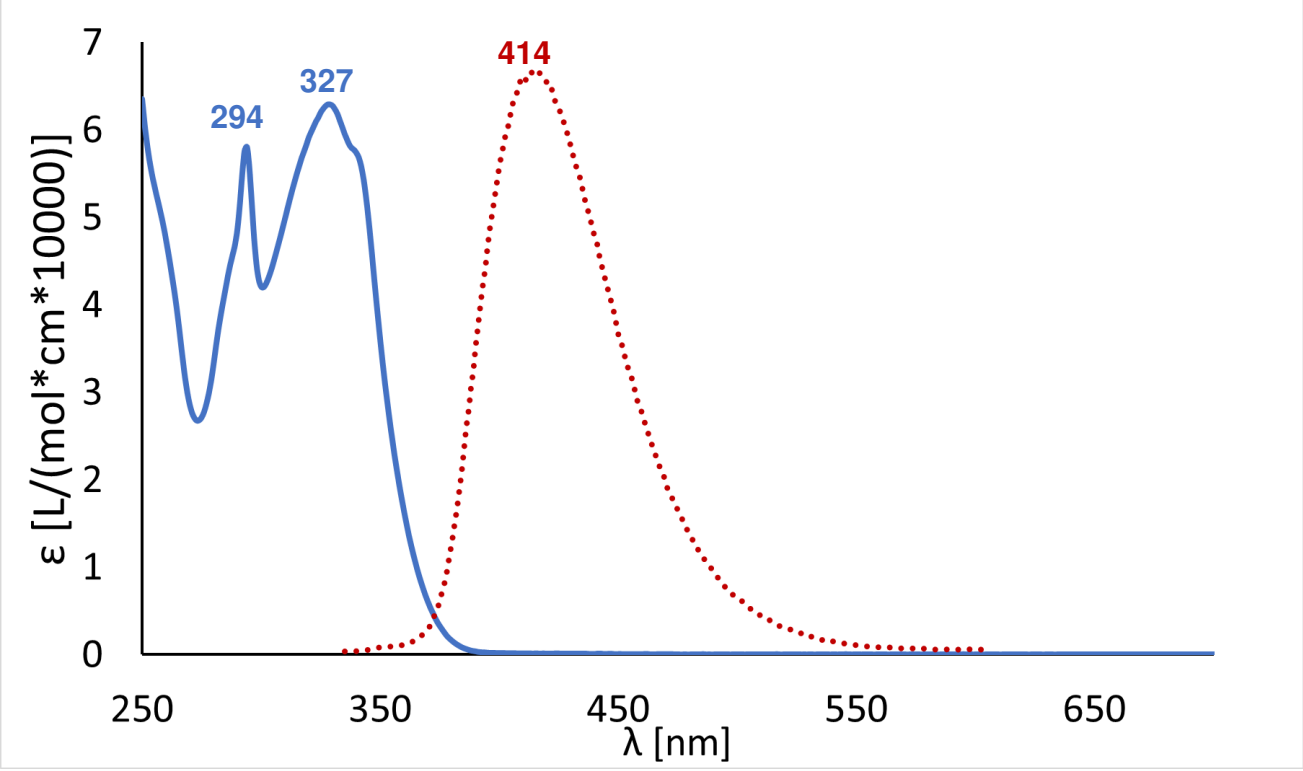


**Figure A138:** UV-Vis (blue line)- and Fluorescence (red dotted line) spectra of **11** in DCM.

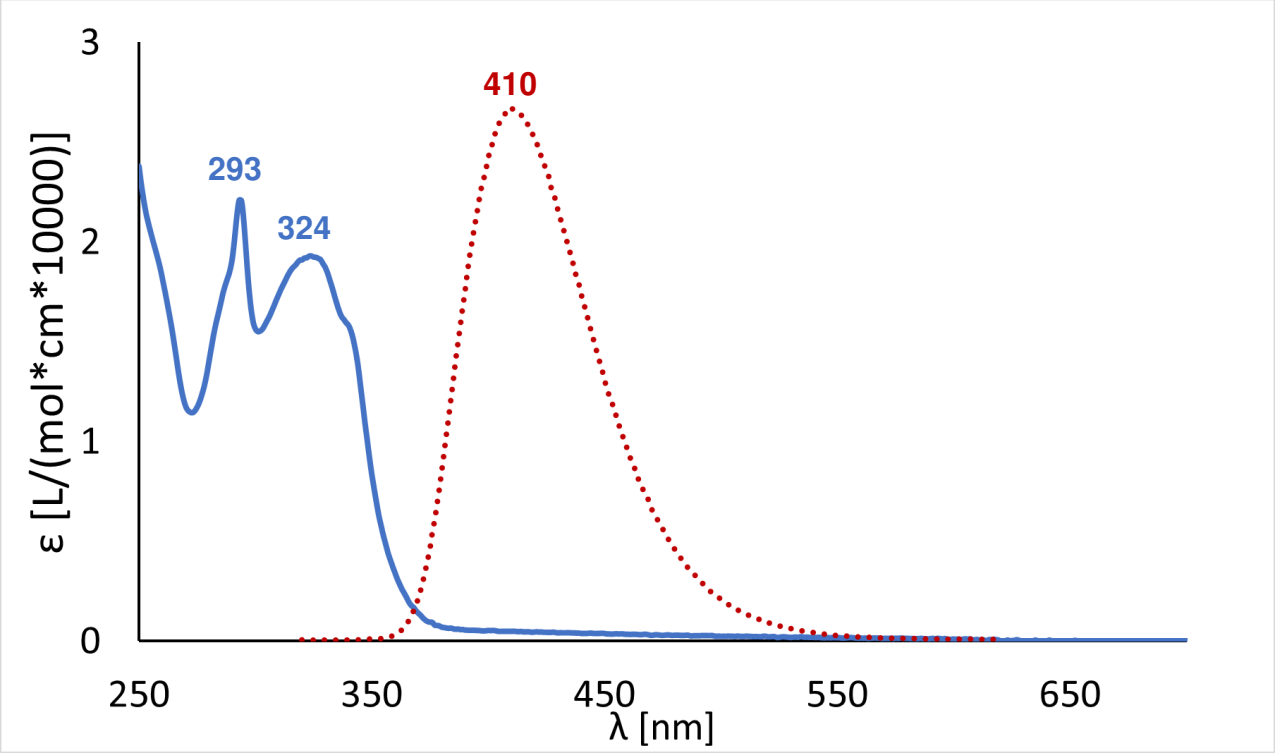


**Figure A139:** UV-Vis (blue line)- and Fluorescence (red dotted line) spectra of **12** in DCM.

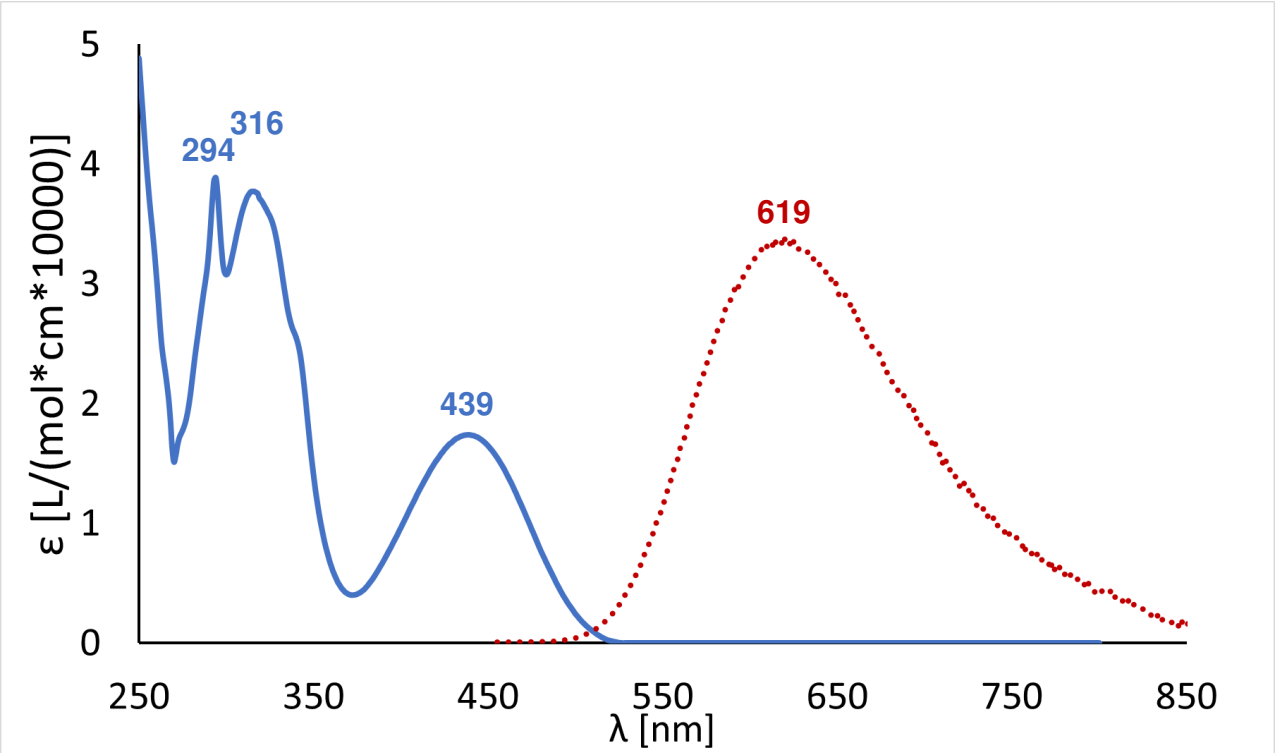


**Figure A140:** UV-Vis (blue line)- and Fluorescence (red dotted line) spectra of **15a** in DCM.

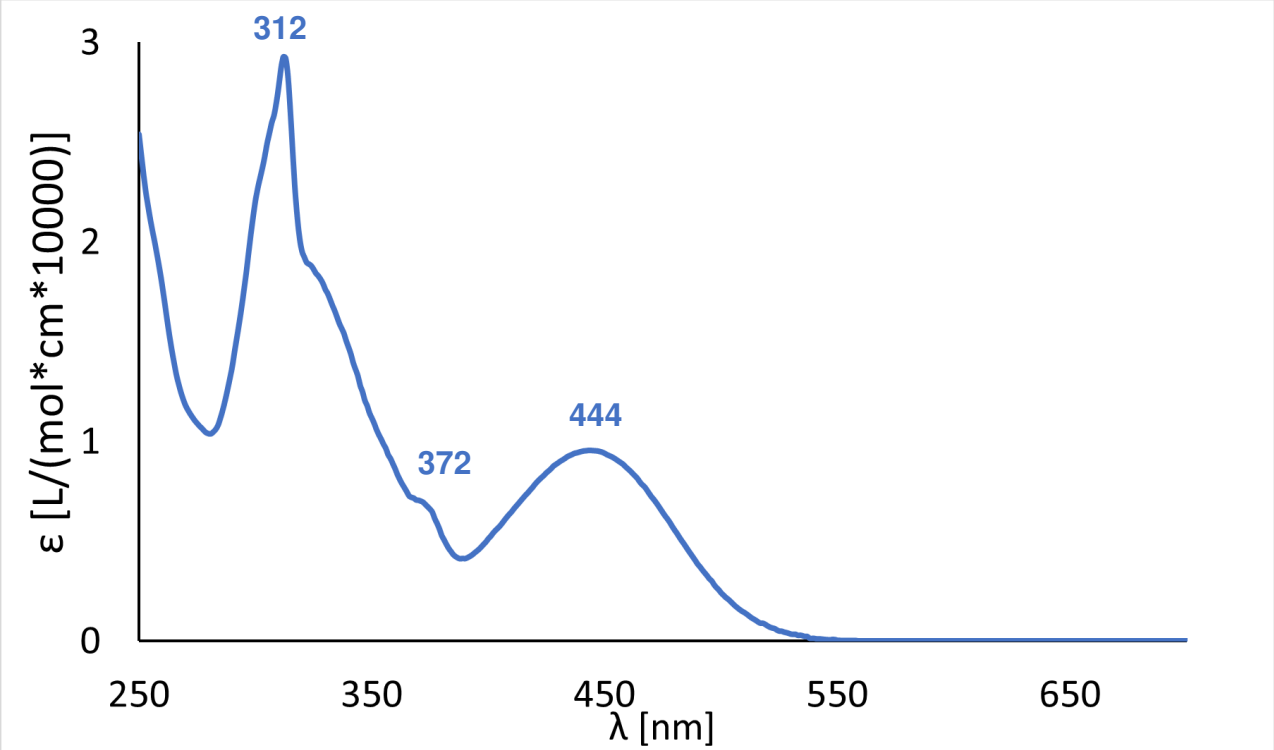


**Figure A141:** UV-Vis spectra of **15b** in DCM.

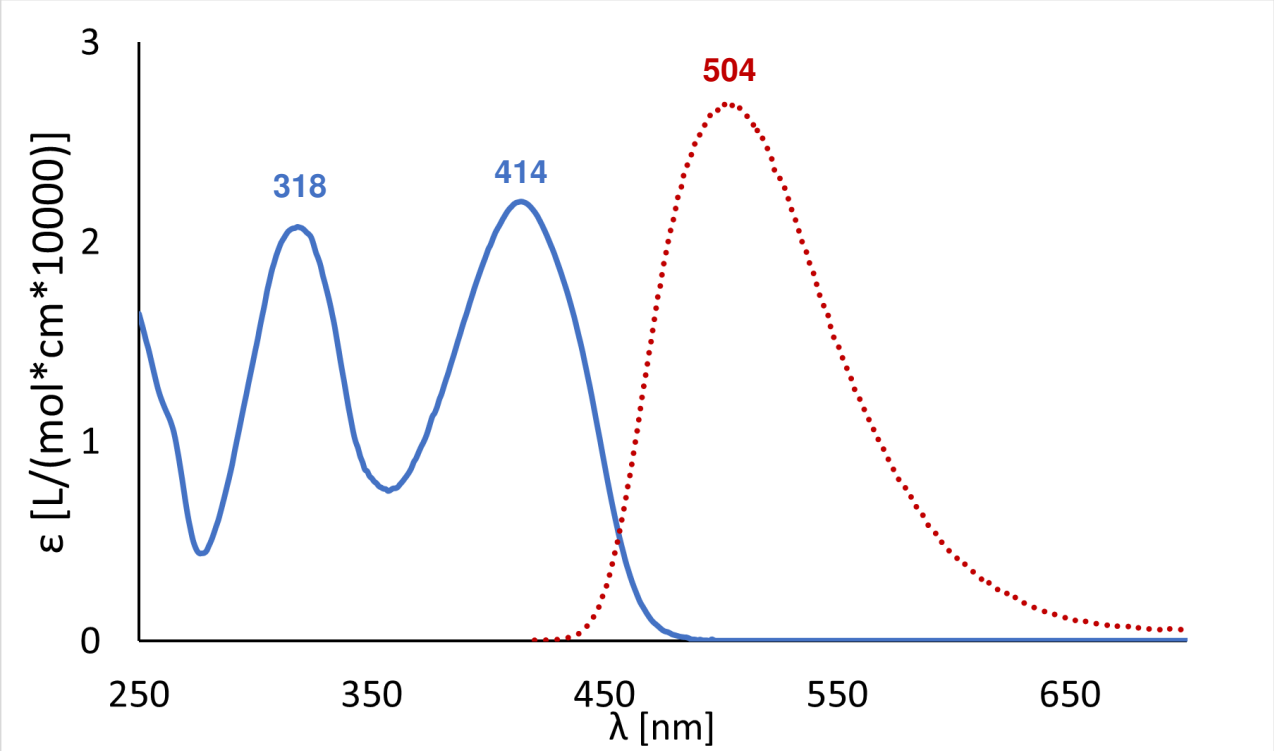


**Figure A142:** UV-Vis (blue line)- and Fluorescence (red dotted line) spectra of **18** in DCM.

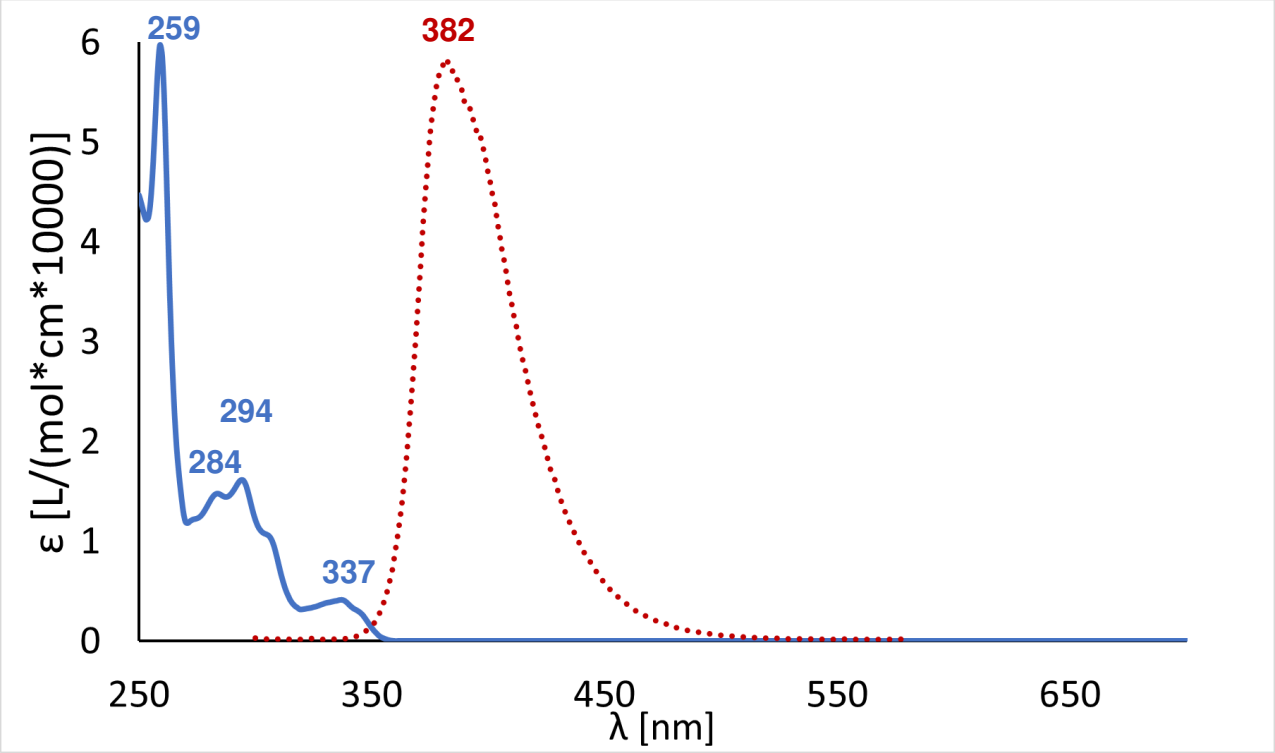


**Figure A143:** UV-Vis (blue line)- and Fluorescence (red dotted line) spectra of **23(*S*)** in DCM.

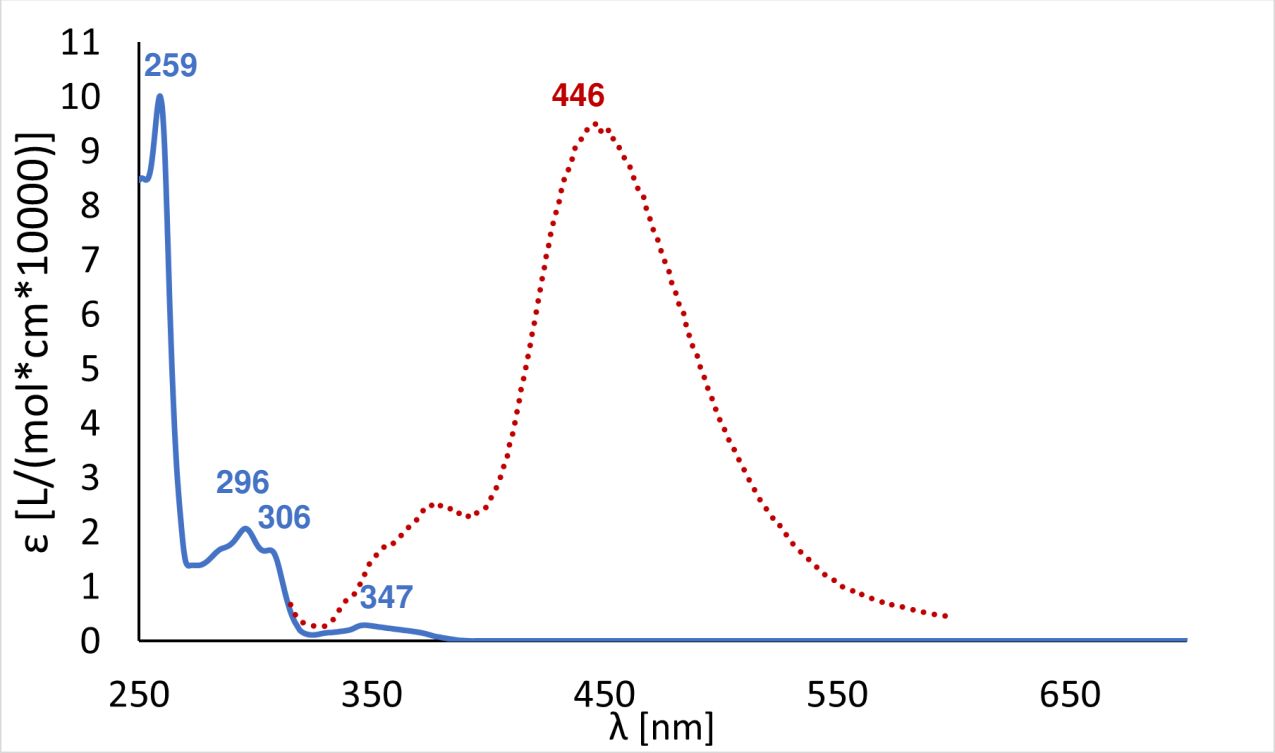


**Figure A144:** UV-Vis (blue line)- and Fluorescence (red dotted line) spectra of **24(*S*)** in DCM.

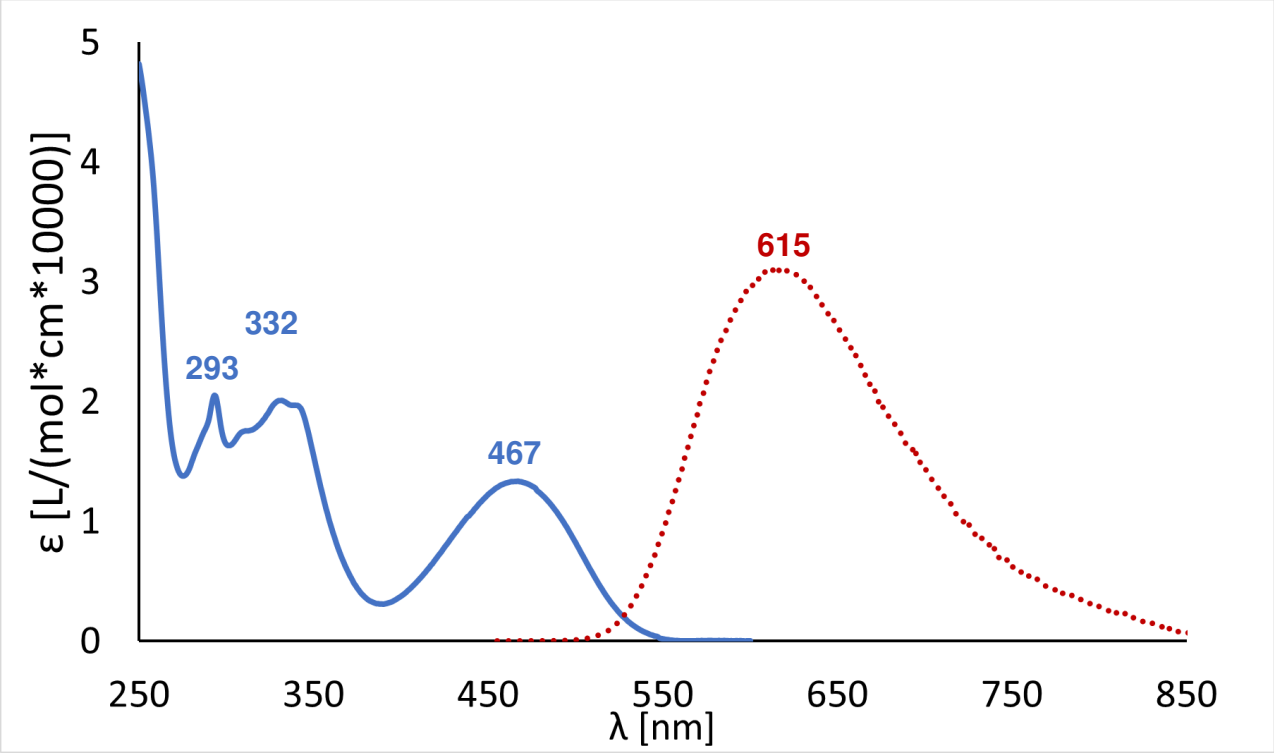


**Figure A145:** UV-Vis (blue line)- and Fluorescence (red dotted line) spectra of **28(*S*)a** in DCM.

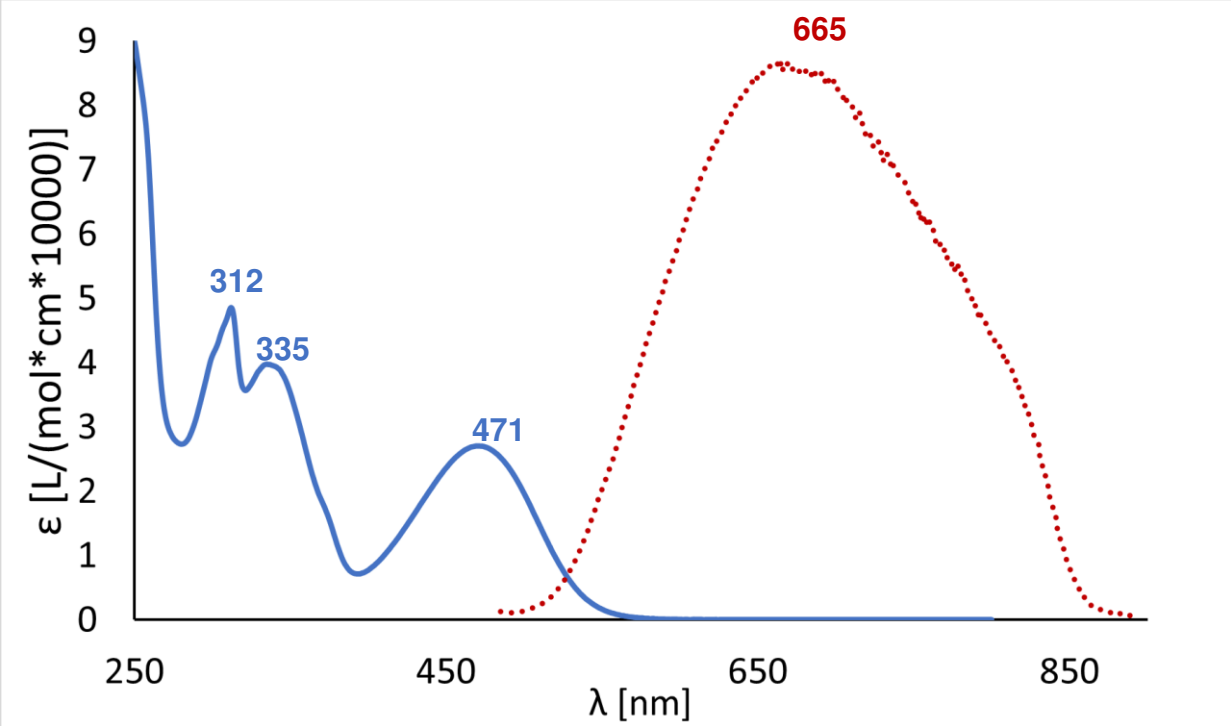


**Figure A146:** UV-Vis (blue line)- and Fluorescence (red dotted line) spectra of **28(*S*)b** in DCM.

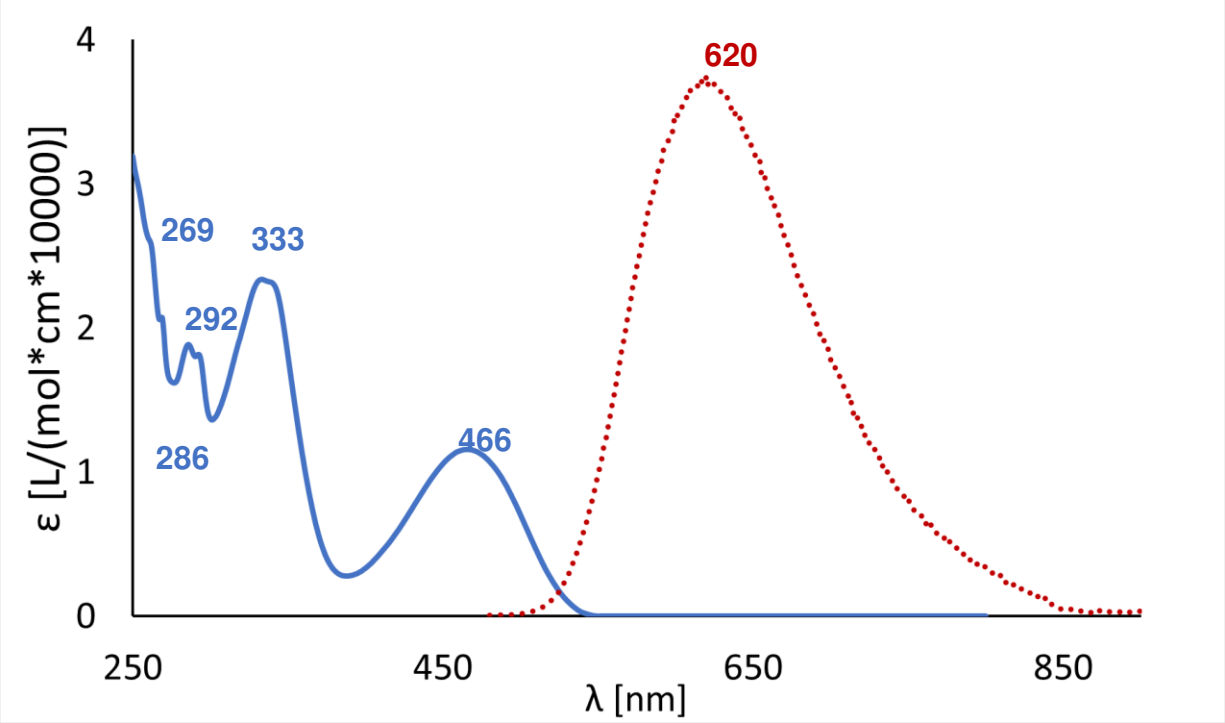


**Figure A147:** UV-Vis (blue line)- and Fluorescence (red dotted line) spectra of **30(*S*)a** in DCM.

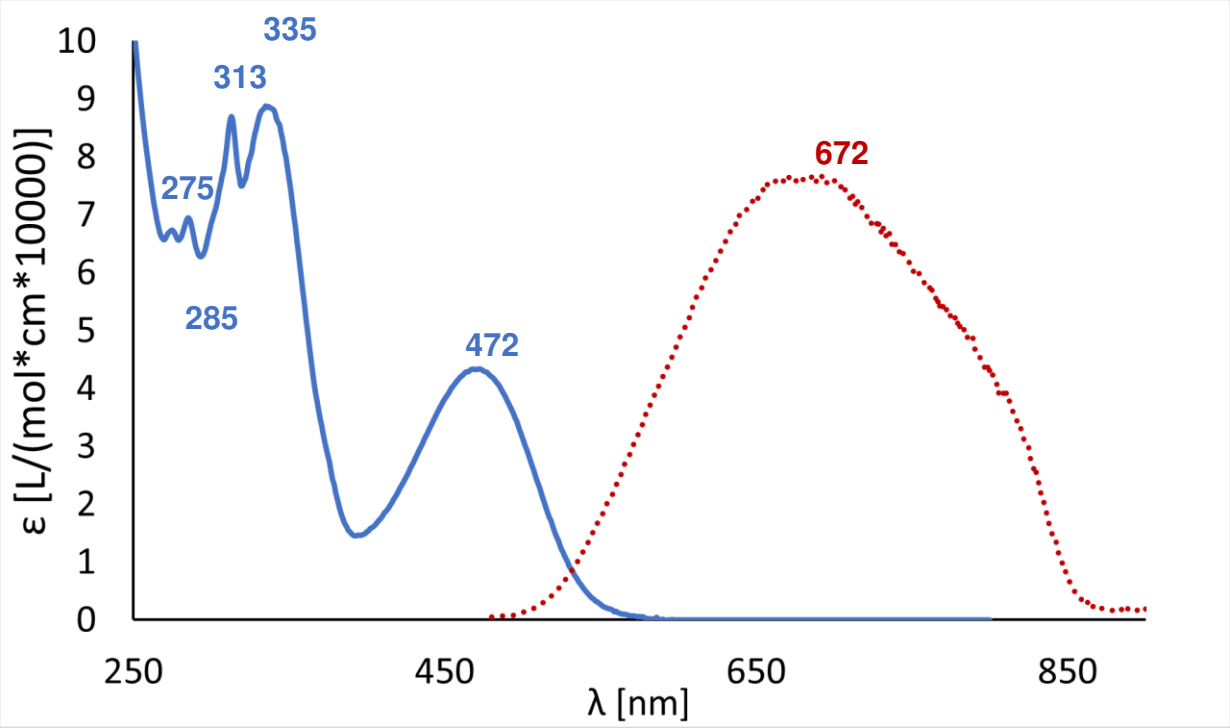


**Figure A148:** UV-Vis (blue line)- and Fluorescence (red dotted line) spectra of **30(*S*)b** in DCM.

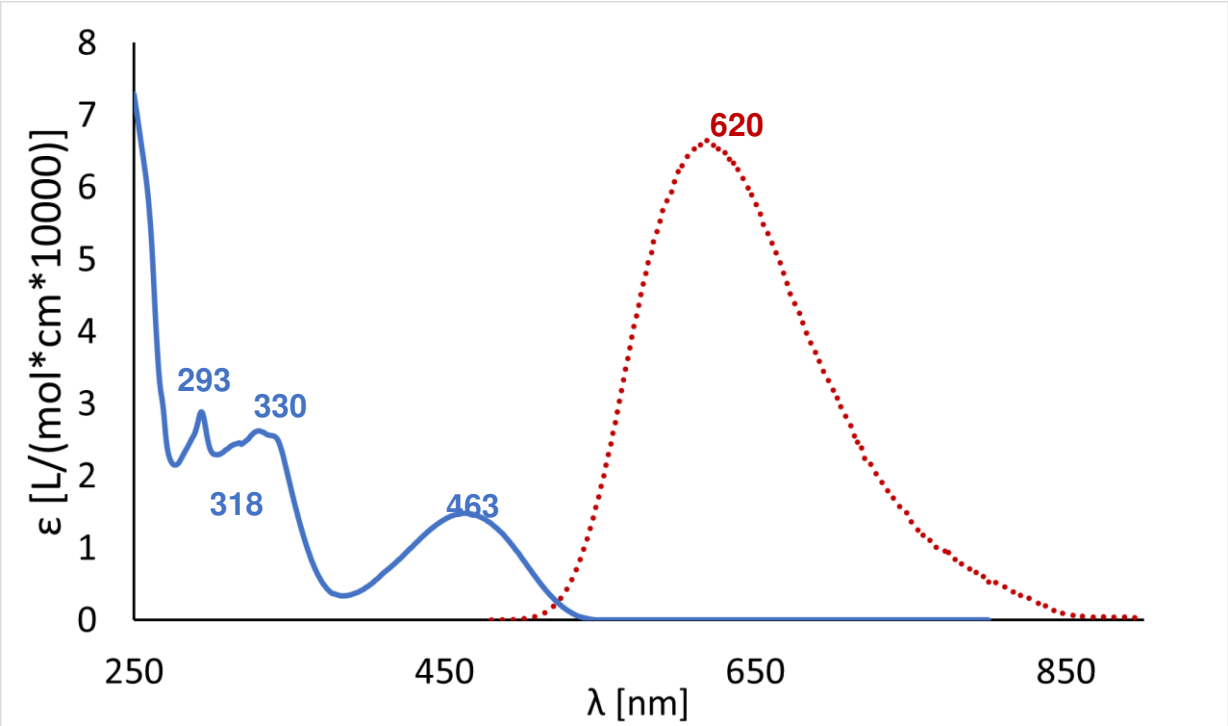


**Figure A149:** UV-Vis (blue line)- and Fluorescence (red dotted line) spectra of **31(*S*)a** in DCM.

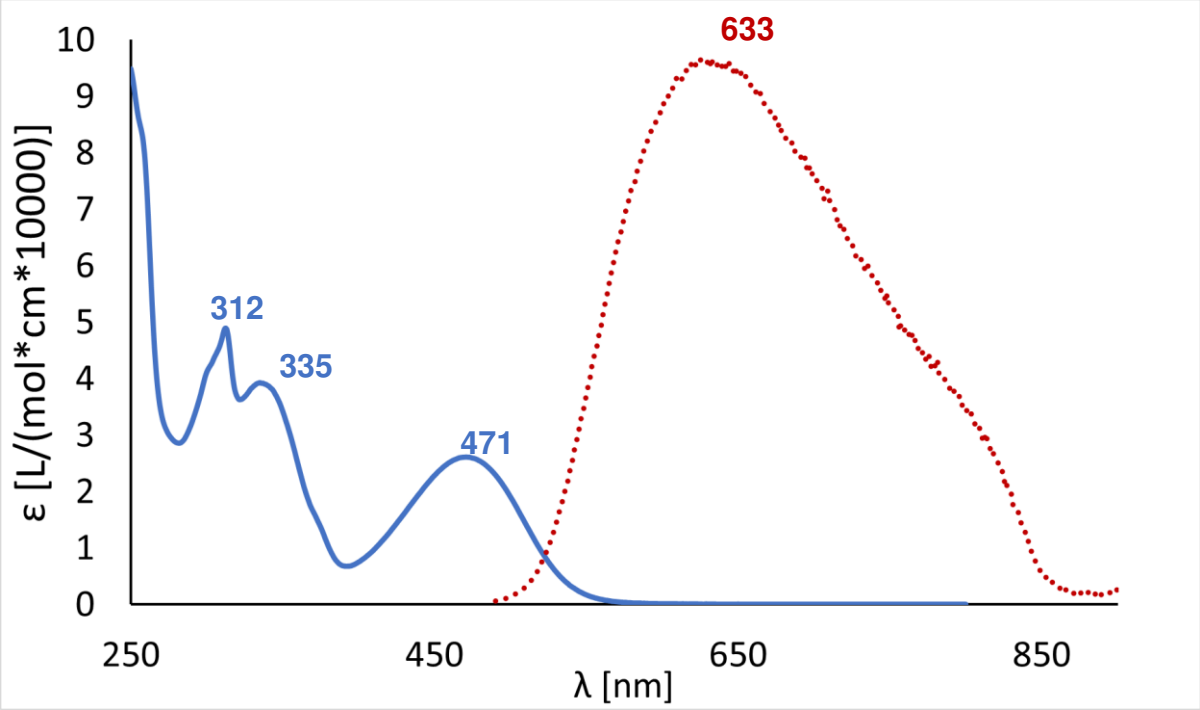


**Figure A150:** UV-Vis (blue line)- and Fluorescence (red dotted line) spectra of **31(*S*)b** in DCM.

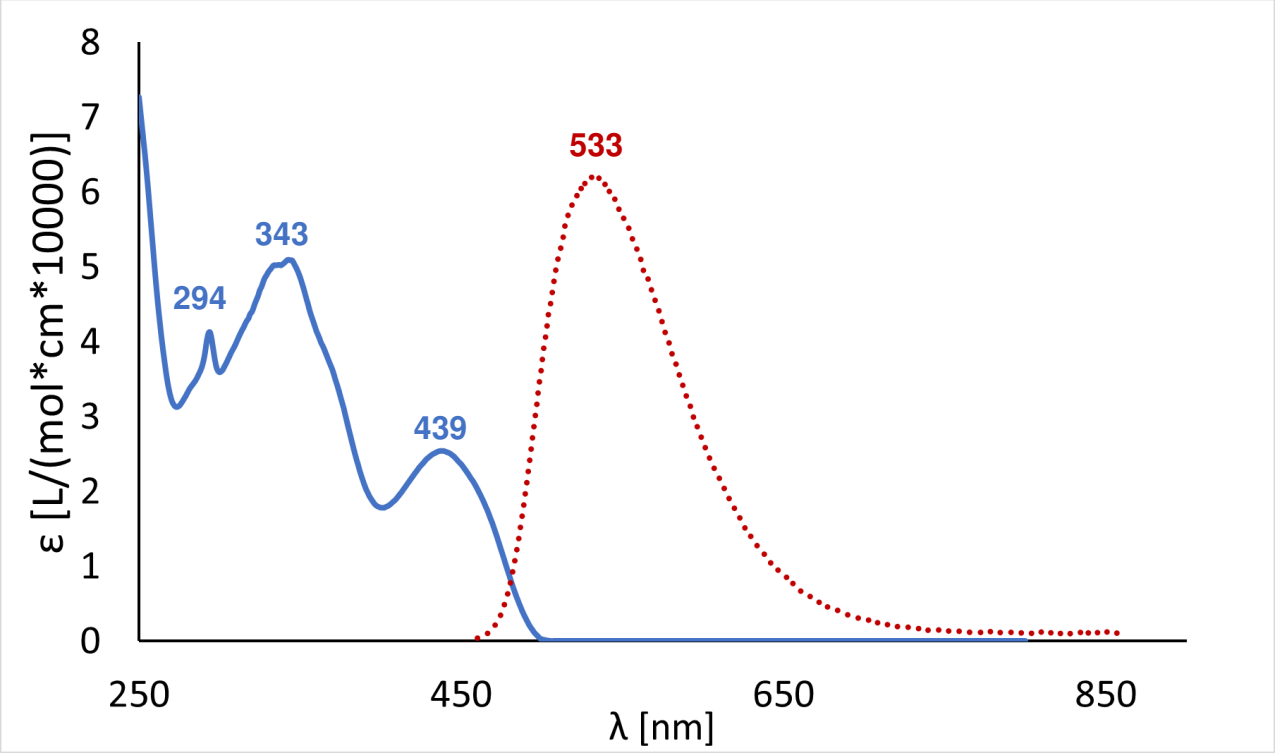


**Figure A151:** UV-Vis (blue line)- and Fluorescence (red dotted line) spectra of **34(*S*)** in DCM.

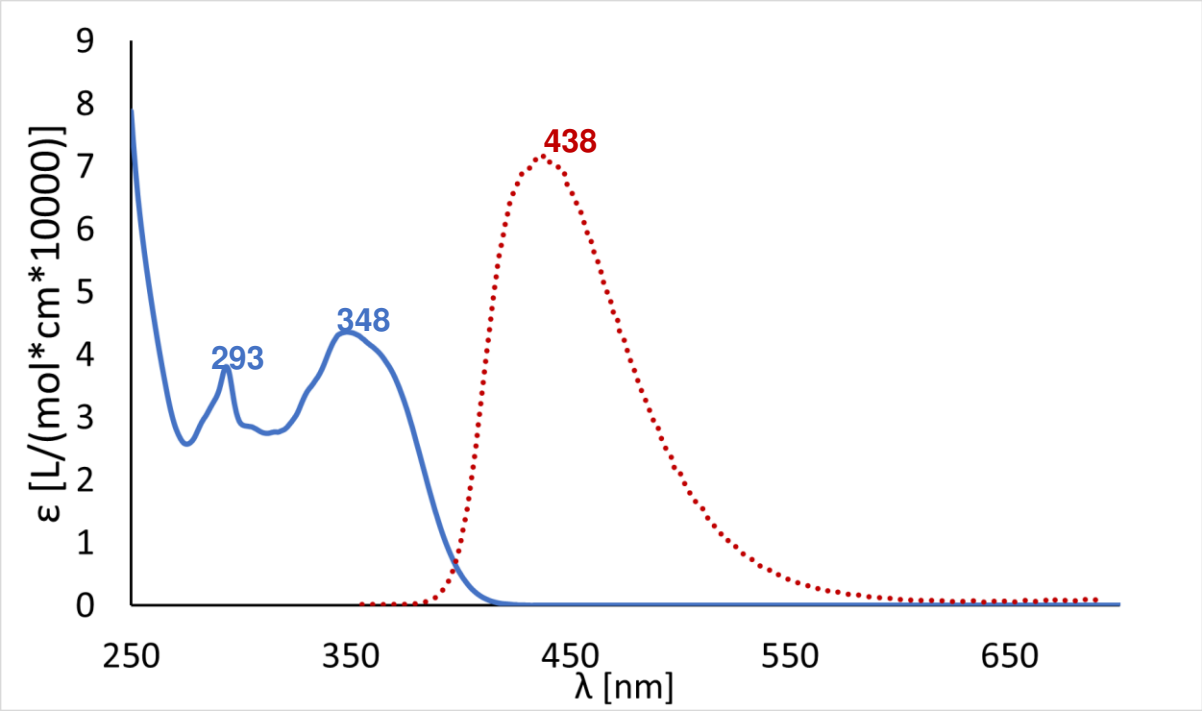


**Figure A152:** UV-Vis (blue line)- and Fluorescence (red dotted line) spectra of **35(*S*)** in DCM.

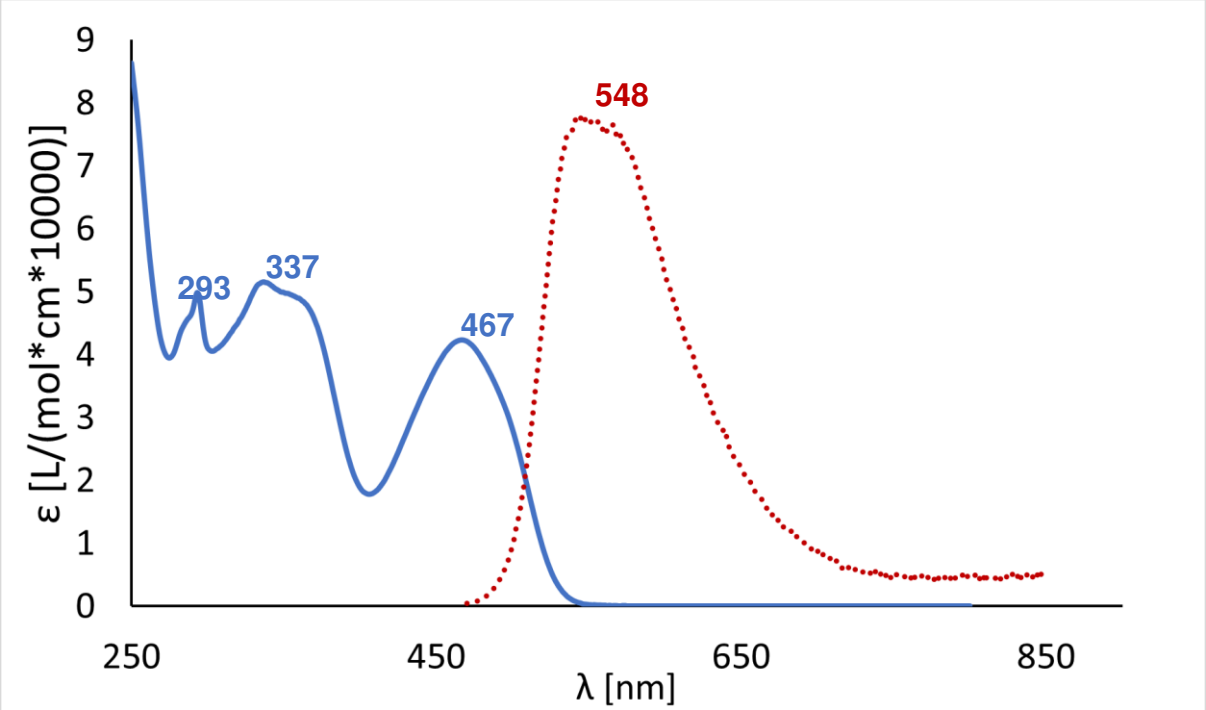


**Figure A153:** UV-Vis (blue line)- and Fluorescence (red dotted line) spectra of **36(*S*)** in DCM.

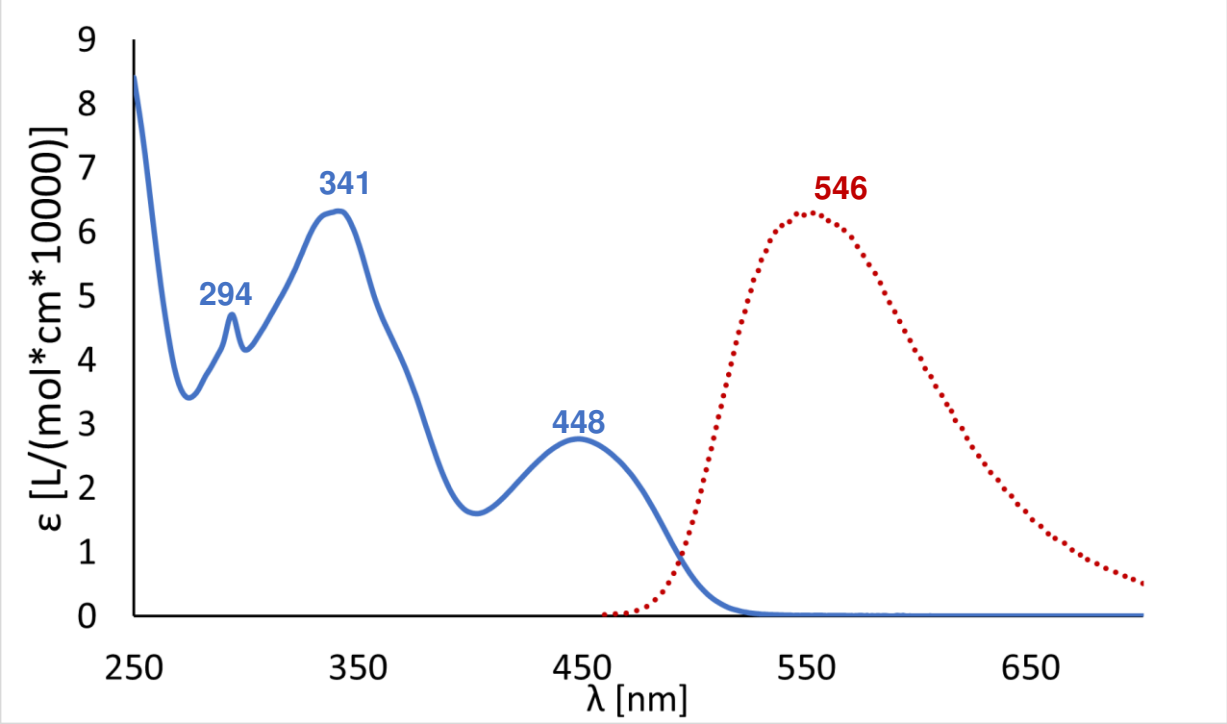


**Figure A154:** UV-Vis (blue line)- and Fluorescence (red dotted line) spectra of **37(*S*)** in DCM.

**Table S1:** The UV-Vis absorption maxima with the highest wavelength [nm], fluorescence maxima [nm], stokes shifts [nm] and fluorescence quantum yields ($\Phi$), and $R^2$ value of the linear fitting slope. All measurements were carried out in DCM.

| Molecule | UV-Vis maximum [nm] | Emission maximum [nm] | Stokes shift [nm] | $\Phi$ [%] | $R^2$ for $\Phi$ |
|---|---|---|---|---|---|
| **2b** | 370 | 387 | 17 | 3 | 0.997 |
| **4a** | 340 | 367 | 27 | 23 | 0.999 |
| **4b** | 369 | 390 | 21 | 20 | 0.999 |
| **11** | 327 | 414 | 87 | 37 | 0.999 |
| **12** | 324 | 410 | 86 | 31 | 0.999 |
| **15a** | 441 | 619 | 178 | 39 | 0.999 |
| **18** | 414 | 504 | 90 | 27 | 0.997 |
| **23(*S*)** | 337 | 382 | 45 | 24 | 0.999 |
| **24(*S*)** | 347 | 446 | 99 | 1 | 0.999 |
| **28(*S*)a** | 465 | 615 | 150 | 54 | 0.999 |
| **28(*S*)b** | 471 | 665 | 194 | 1 | 0.997 |
| **30(*S*)a** | 466 | 620 | 154 | 50 | 0.996 |
| **30(*S*)b** | 472 | 672 | 200 | 2 | 0.990 |
| **31(*S*)a** | 464 | 620 | 156 | 47 | 0.995 |
| **31(*S*)b** | 471 | 633 | 162 | 1 | 0.999 |
| **34(*S*)** | 439 | 533 | 94 | 6 | 0.999 |
| **35(*S*)** | 348 | 438 | 90 | 38 | 0.997 |
| **36(*S*)** | 467 | 548 | 81 | 5 | 0.998 |
| **37(*S*)** | 448 | 546 | 98 | 5 | 0.997 |

## 5.3. CW-EPR spectra

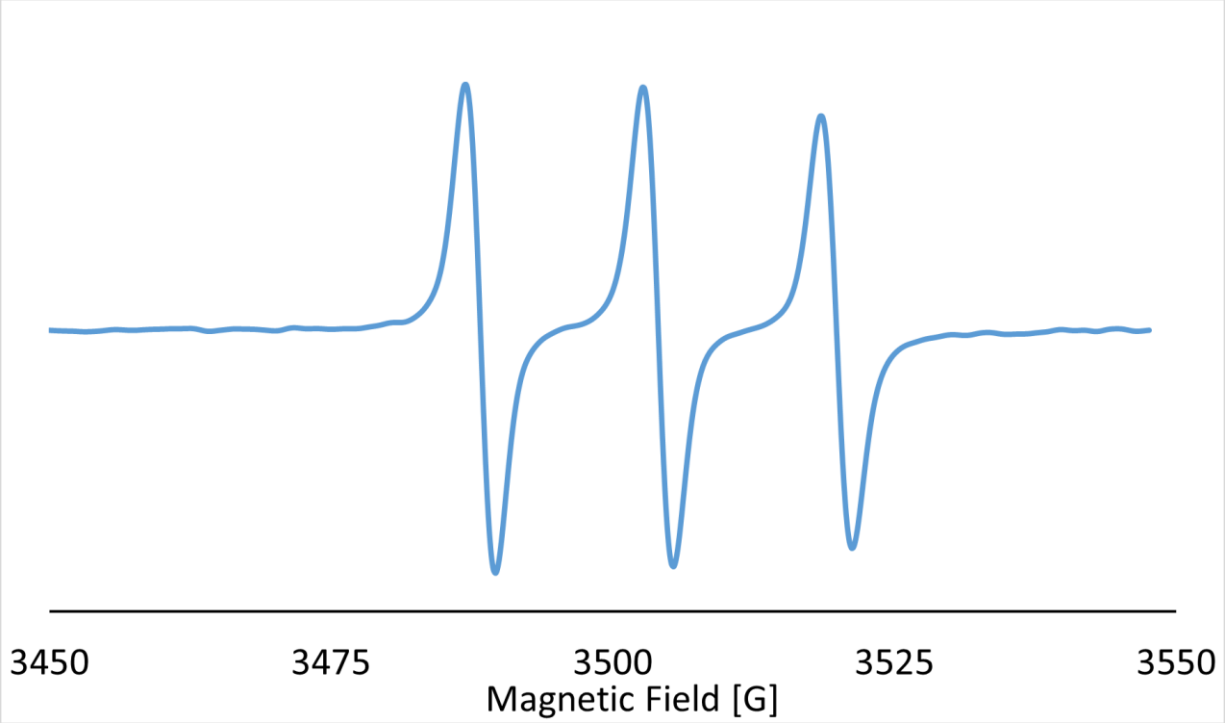


**Figure A155:** CW-EPR spectra of compound **31(*S*)a** at X-band (9.8 GHz) in DCM obtained at room temperature with a 2.0 G modulation amplitude.

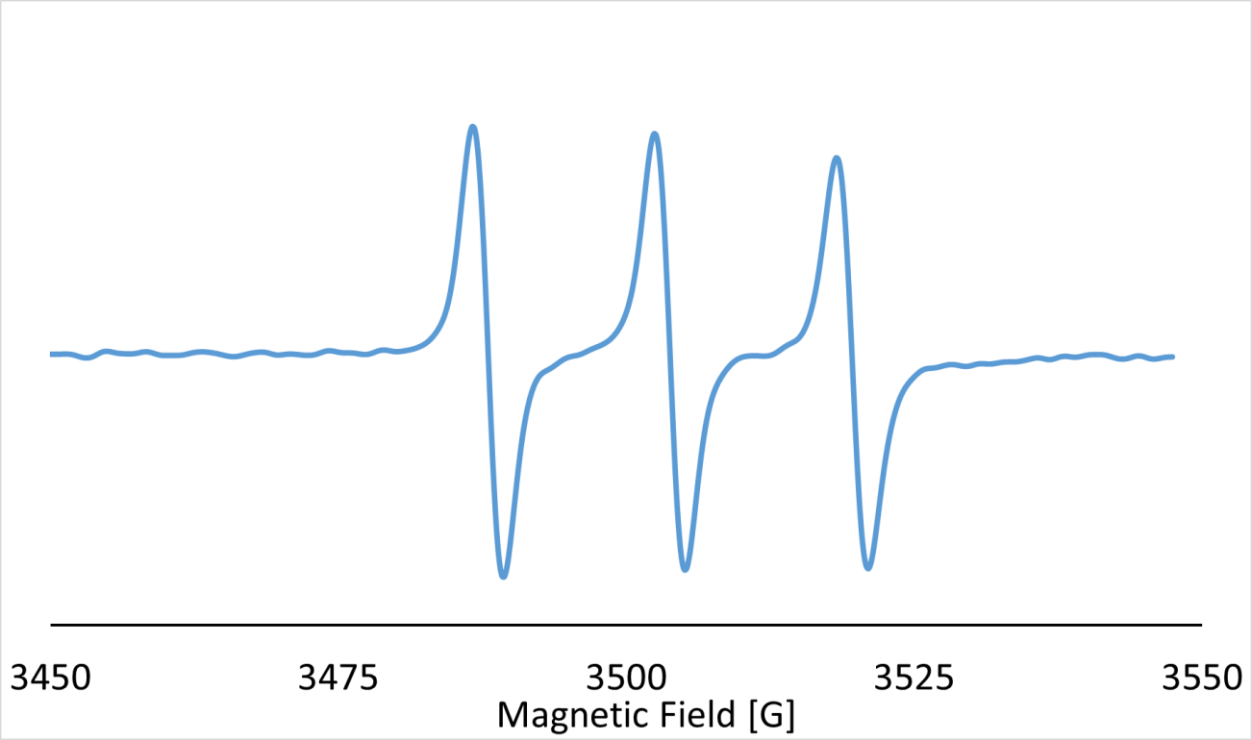


**Figure A156:** CW-EPR spectra of compound **31(*S*)b** at X-band (9.8 GHz) in DCM obtained at room temperature with a 2.0 G modulation amplitude.

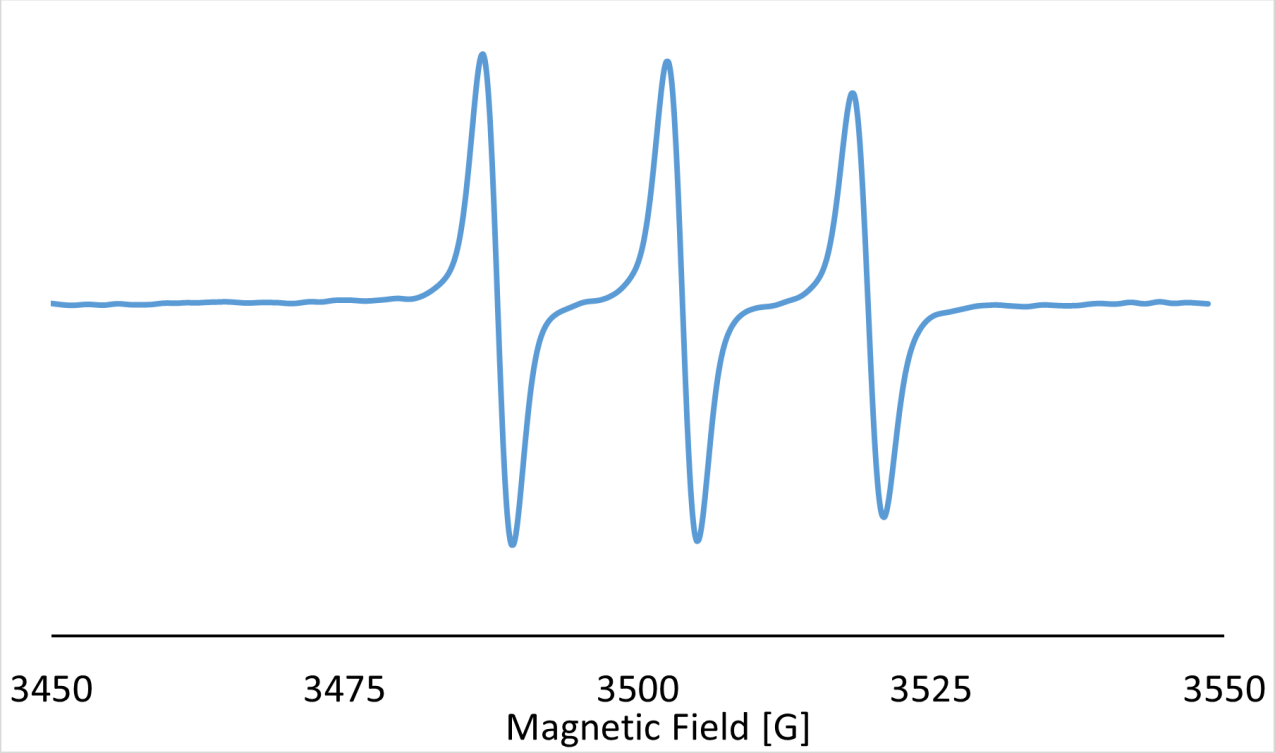


**Figure A157:** CW-EPR spectra of compound **37(*S*)** at X-band (9.8 GHz) in DCM obtained at room temperature with a 2.0 G modulation amplitude.

## 5.4. SQUID Measurements

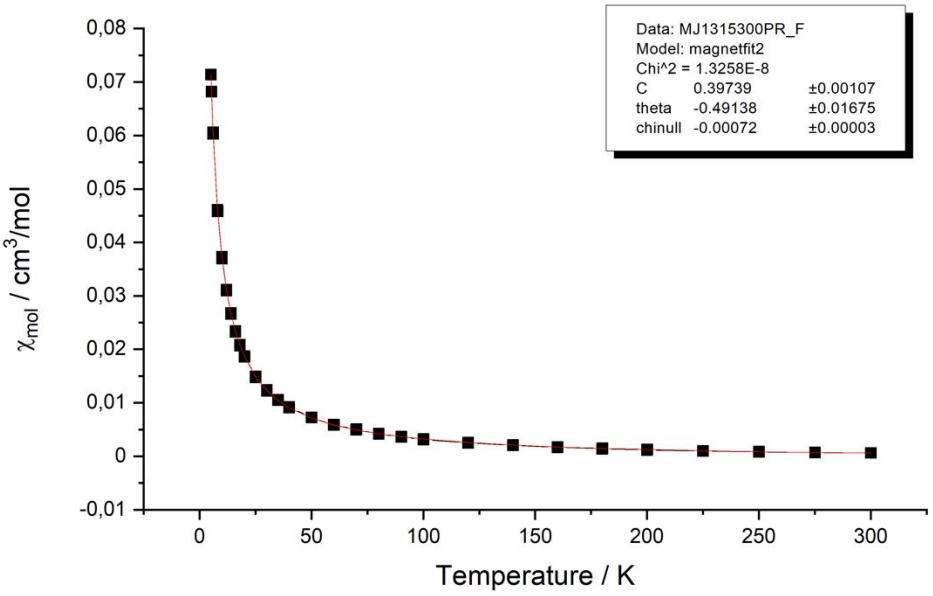


**Figure A158:** SQUID measurement of **31(*S*)a**.

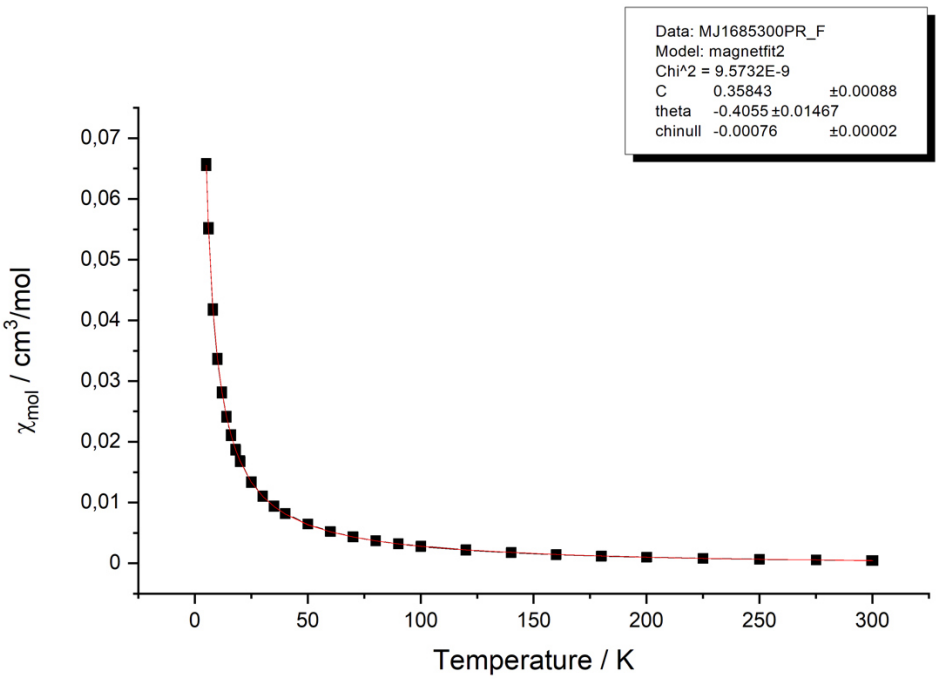


**Figure A159:** SQUID measurement of **37(*S*)**.

## 5.5. ESI/APCI-High Resolution Mass Spectrum

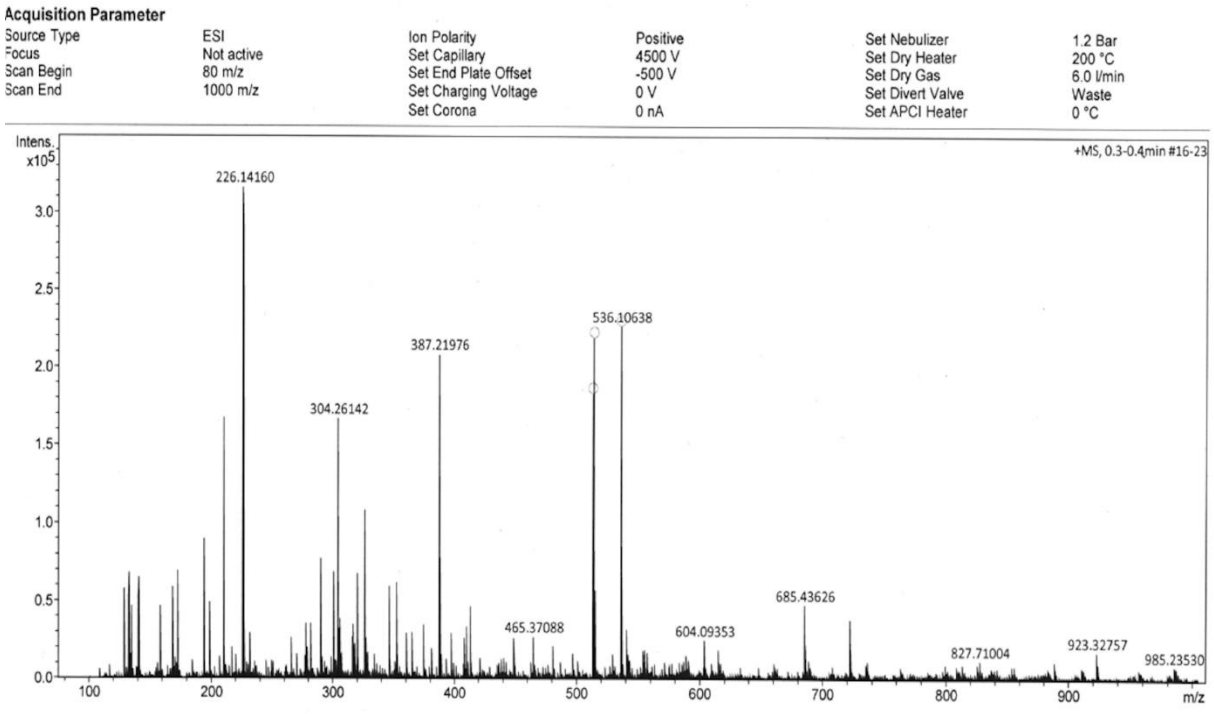


**Figure A160:** APCI-HRMS of **2b**.

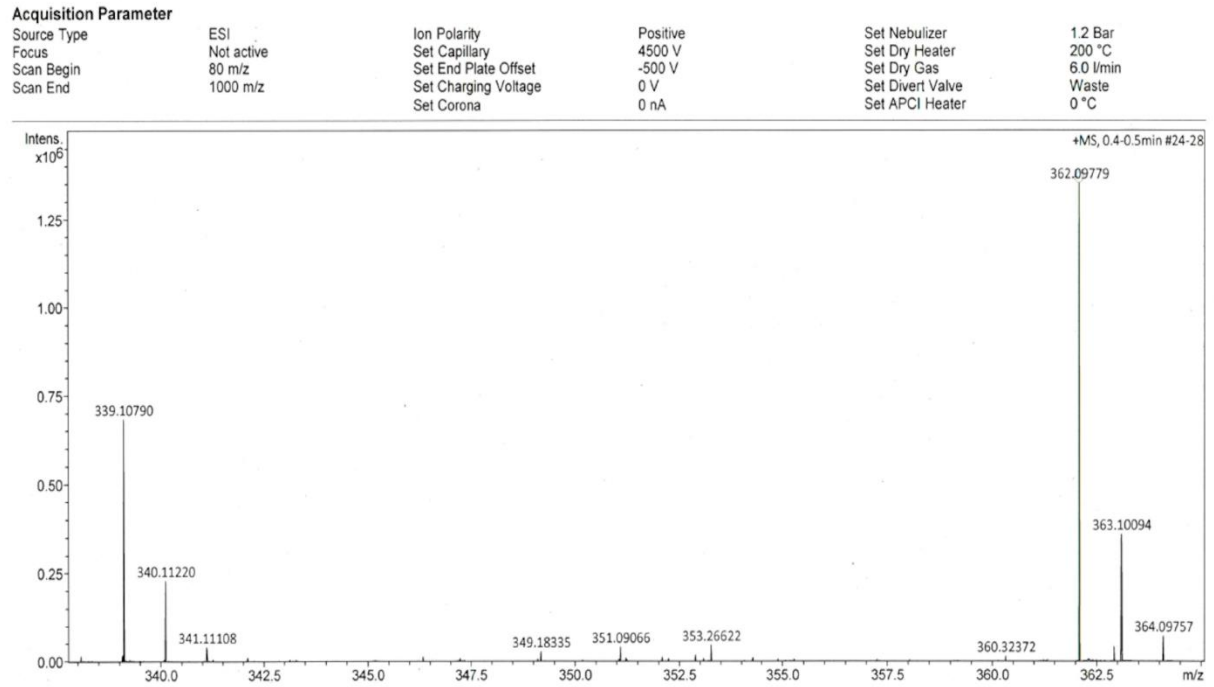


**Figure A161:** ESI-HRMS of **4a**.

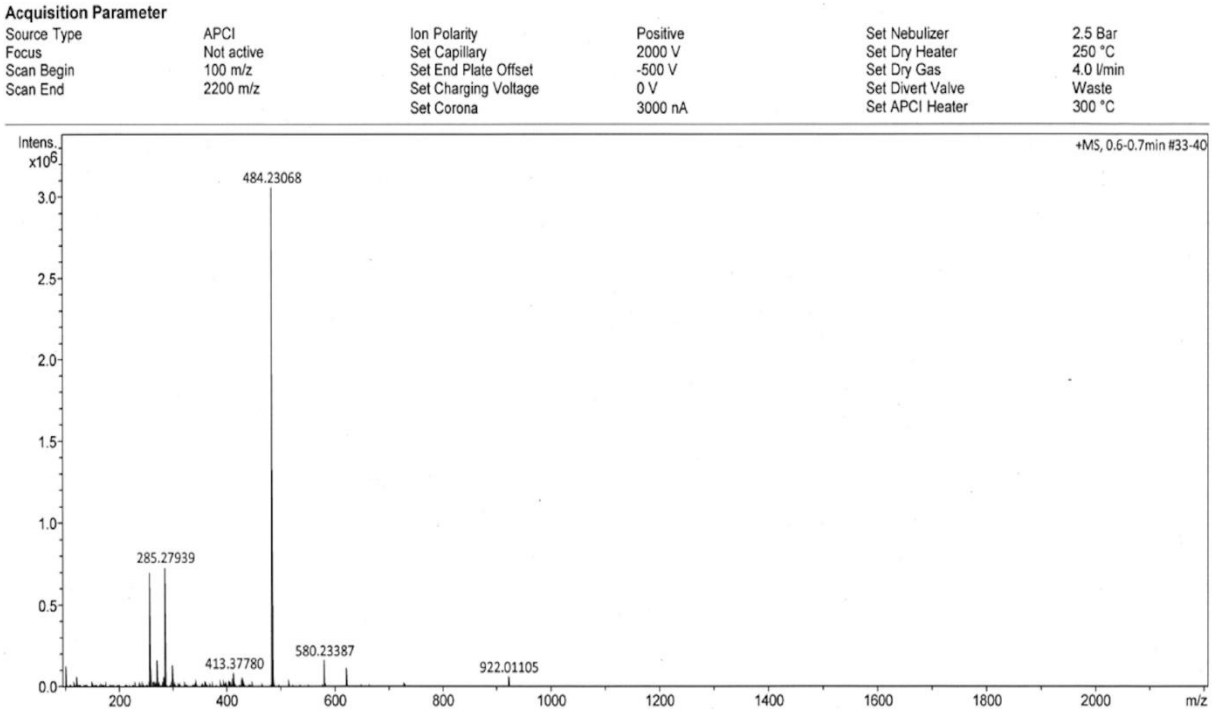


**Figure A162:** APCI-HRMS of **4b**.

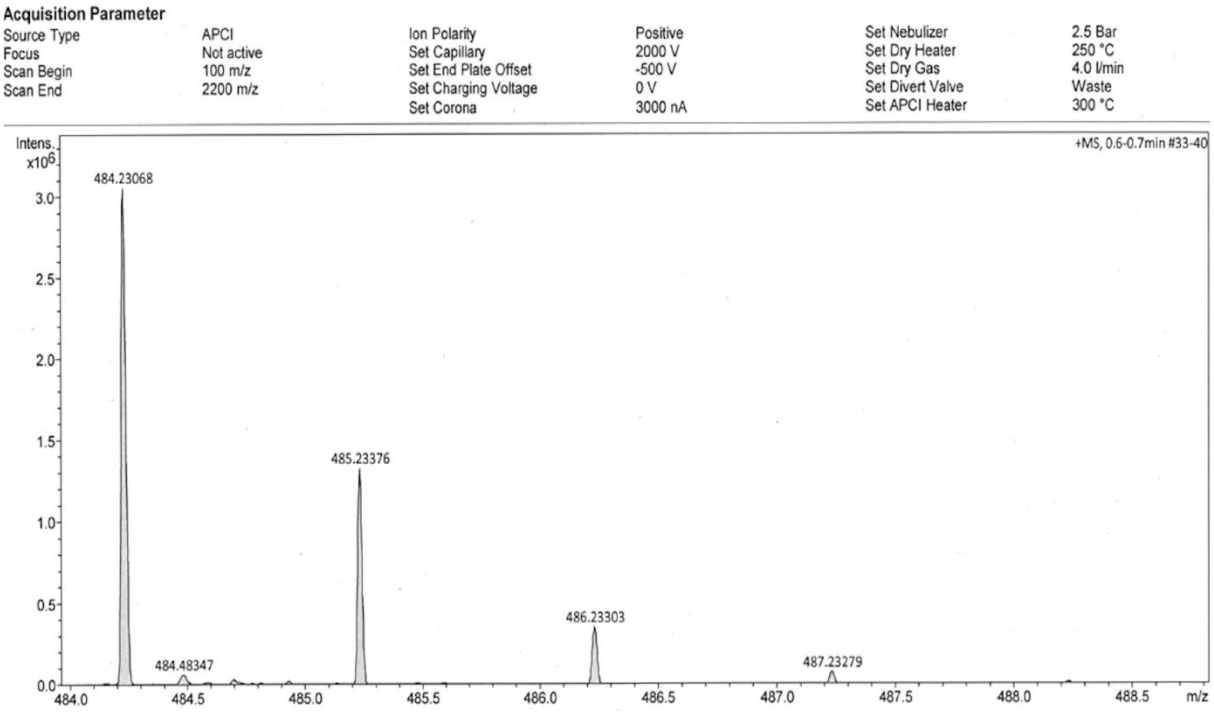


**Figure A163:** APCI-HRMS of **4b**.

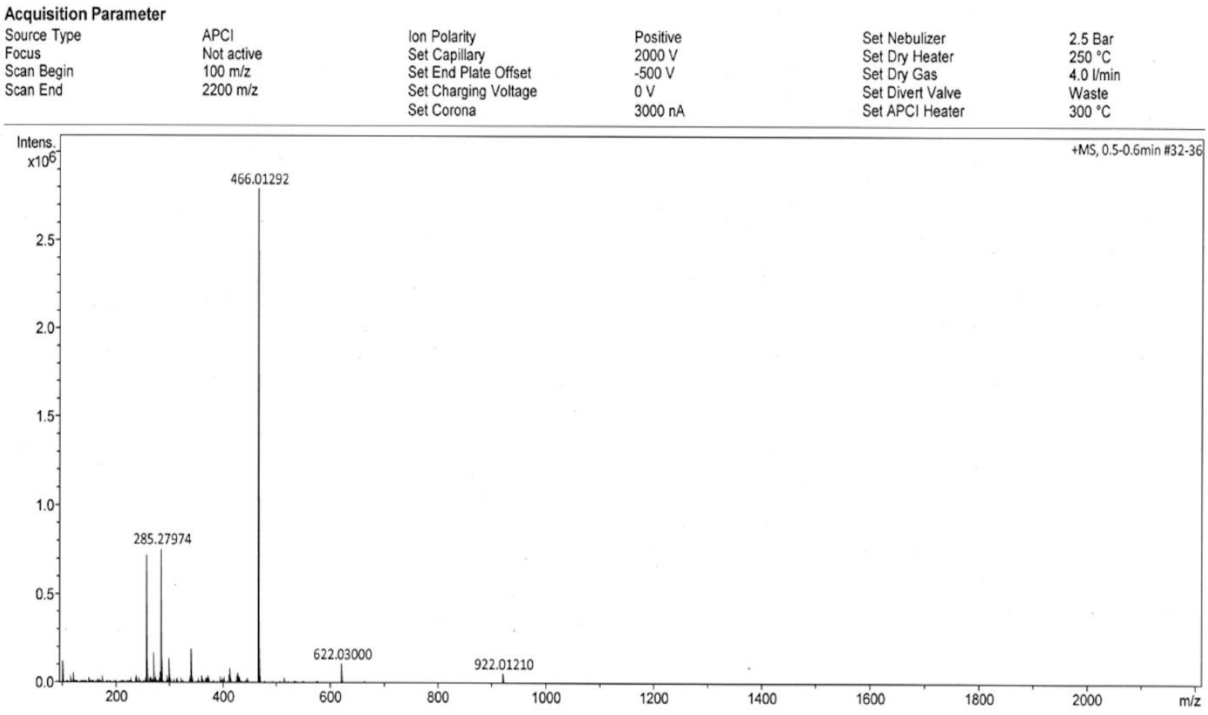


**Figure A164:** APCI-HRMS of **10**.

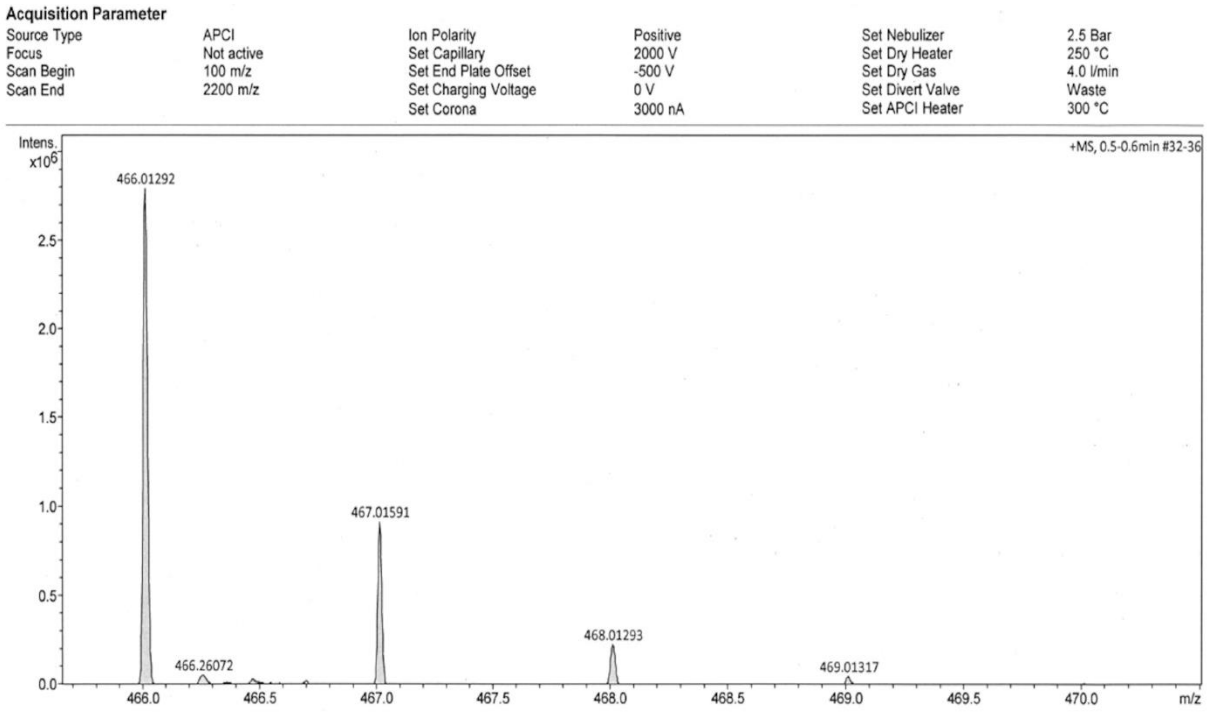


**Figure A165:** APCI-HRMS of **10**.

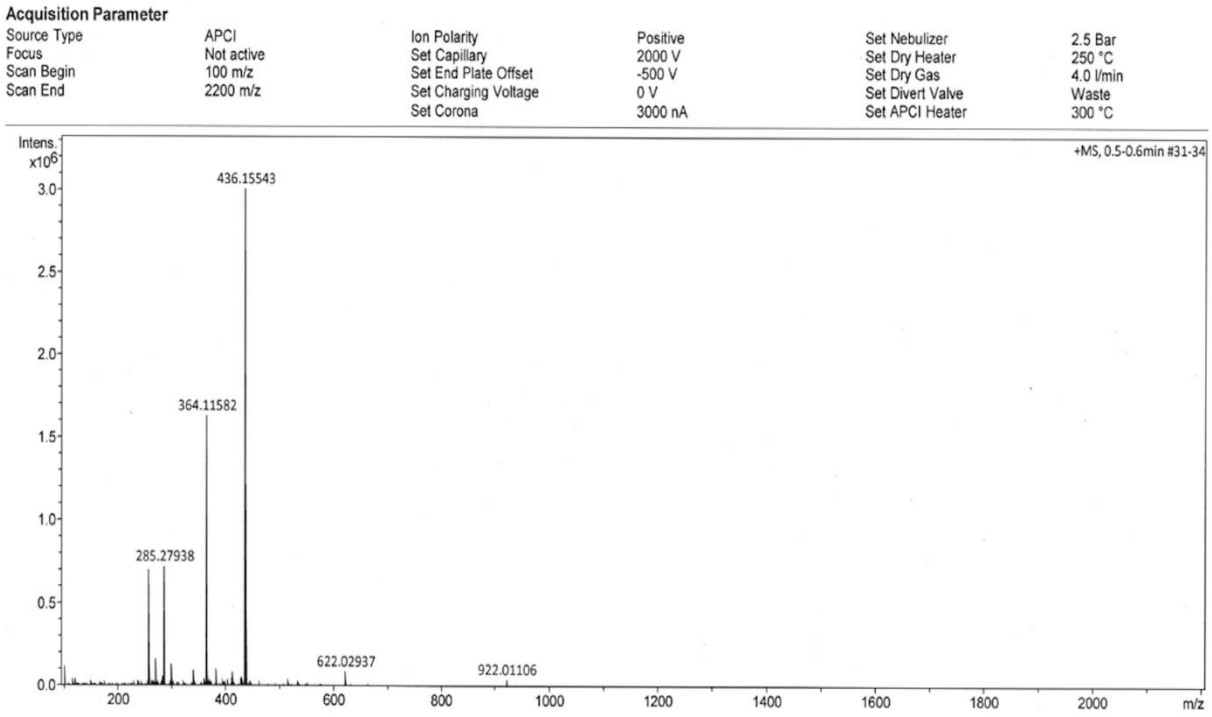


**Figure A166:** APCI-HRMS of **11**.

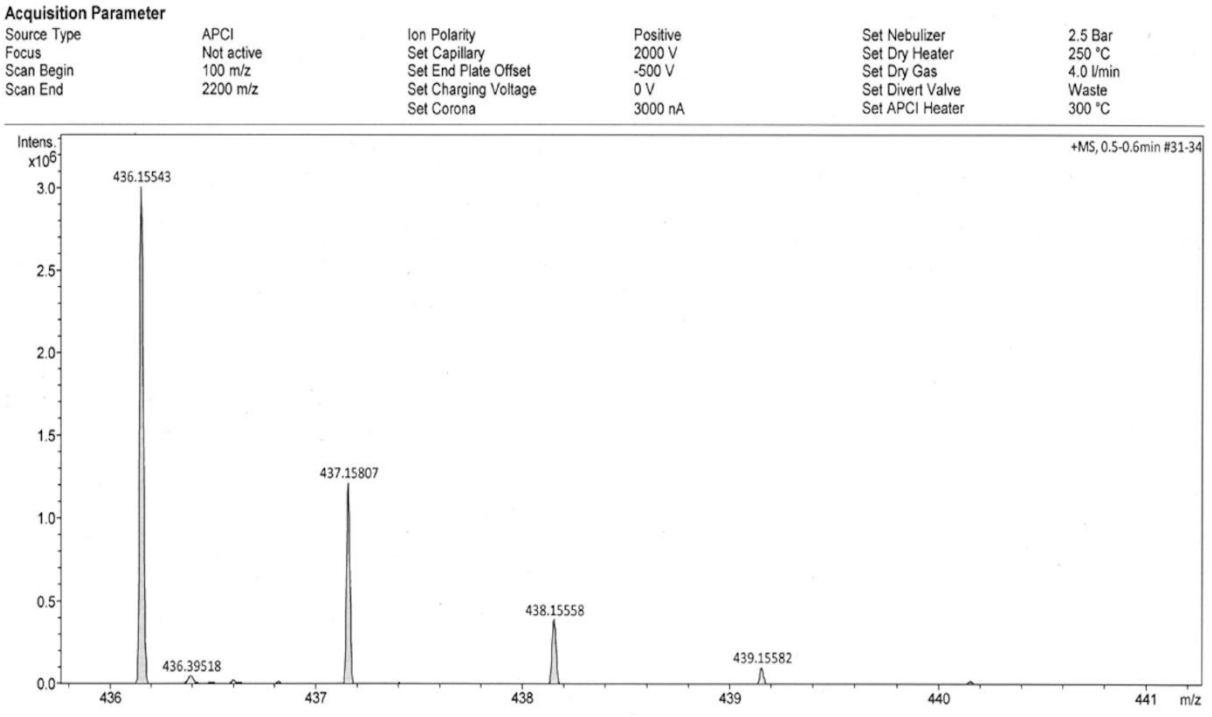


**Figure A167:** APCI-HRMS of **11**.

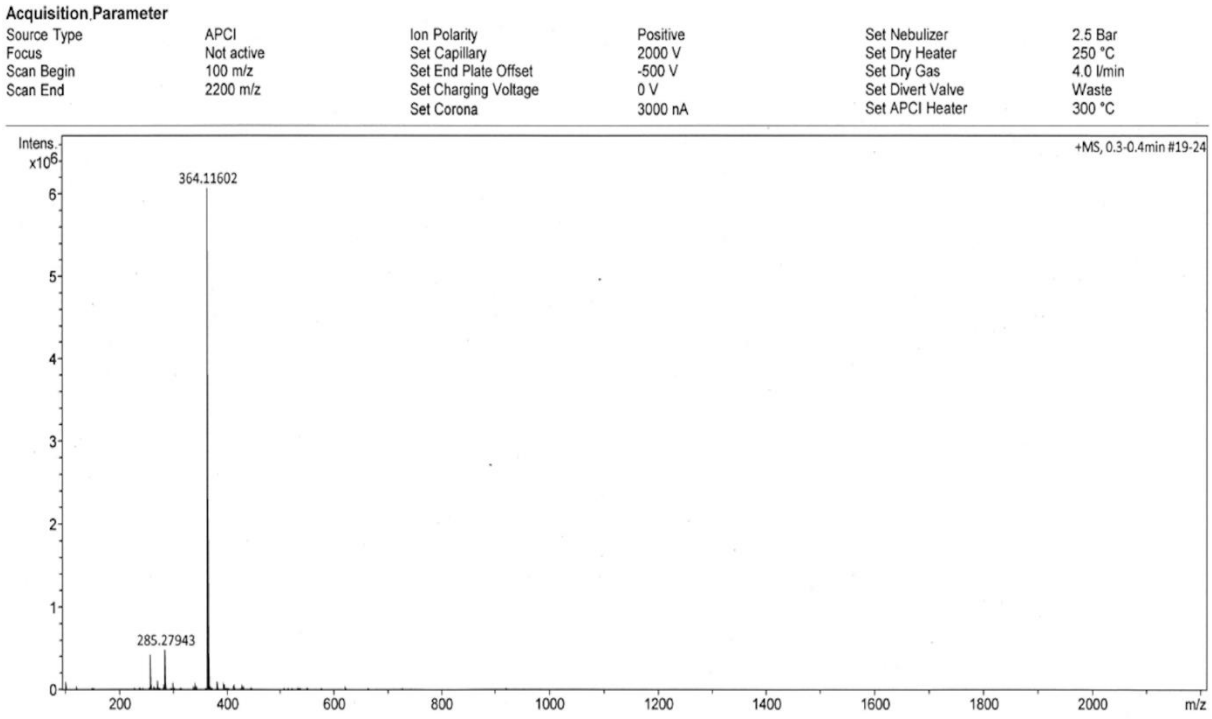


**Figure A168:** APCI-HRMS of **12**.

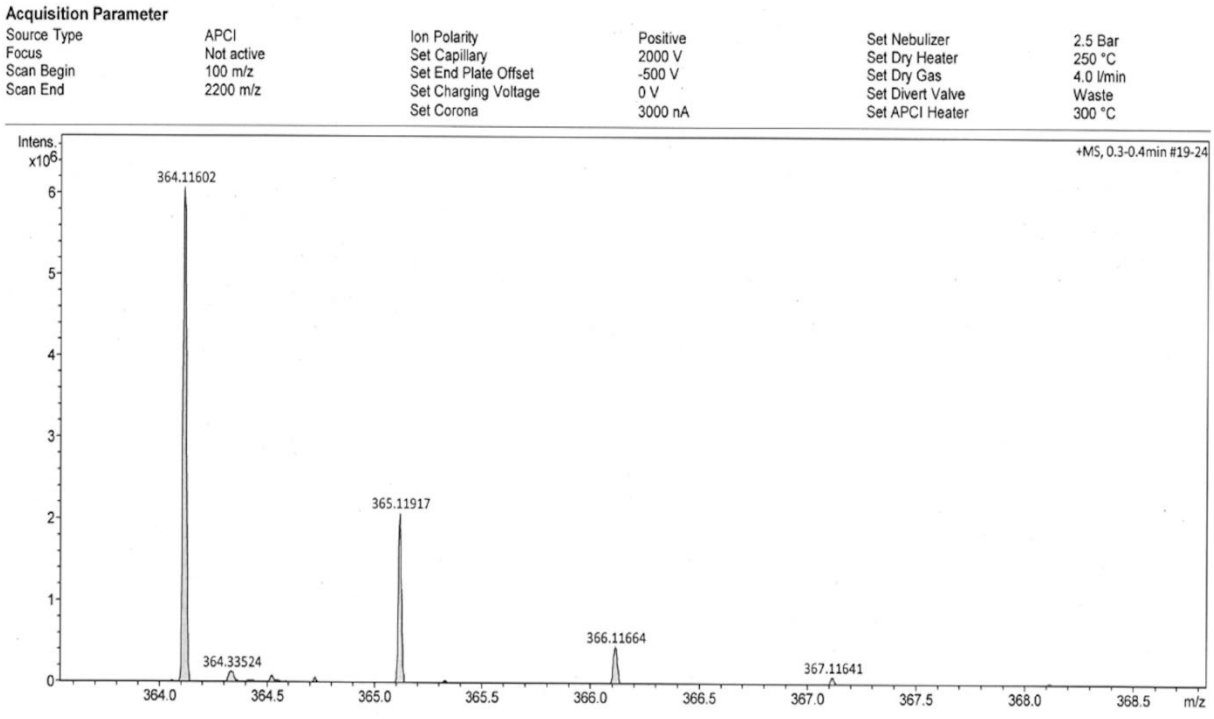


**Figure A169:** APCI-HRMS of **12**.

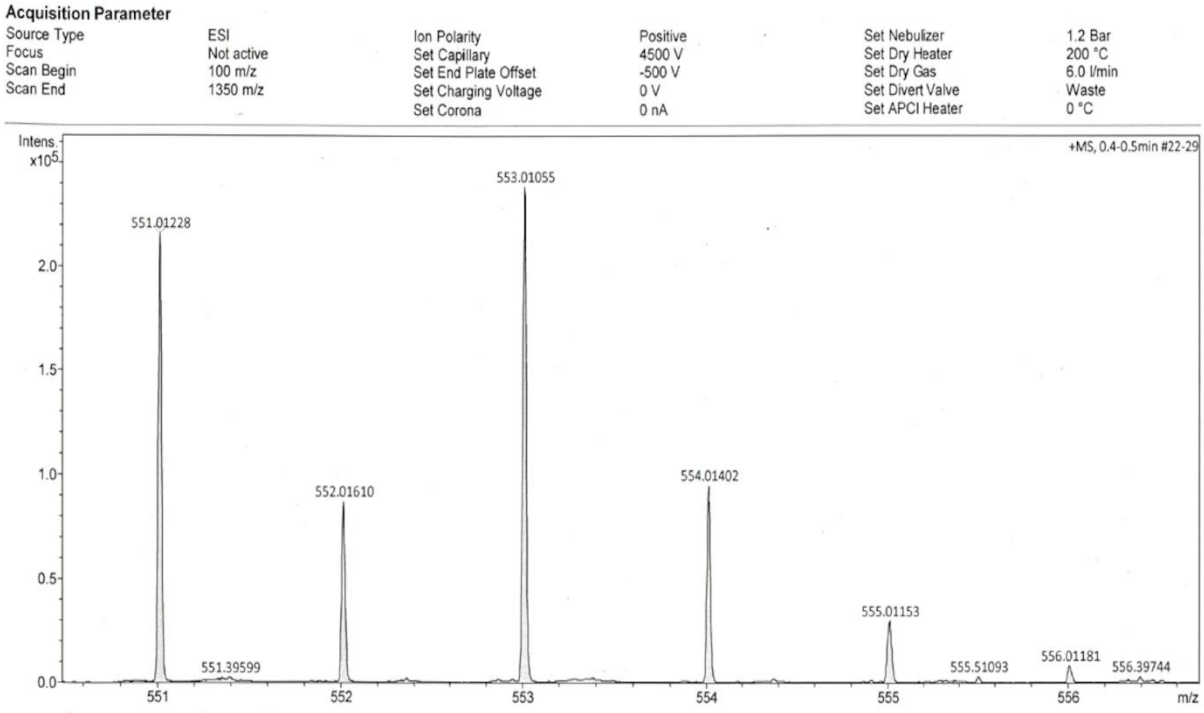


**Figure A170:** ESI-HRMS of **15a**.

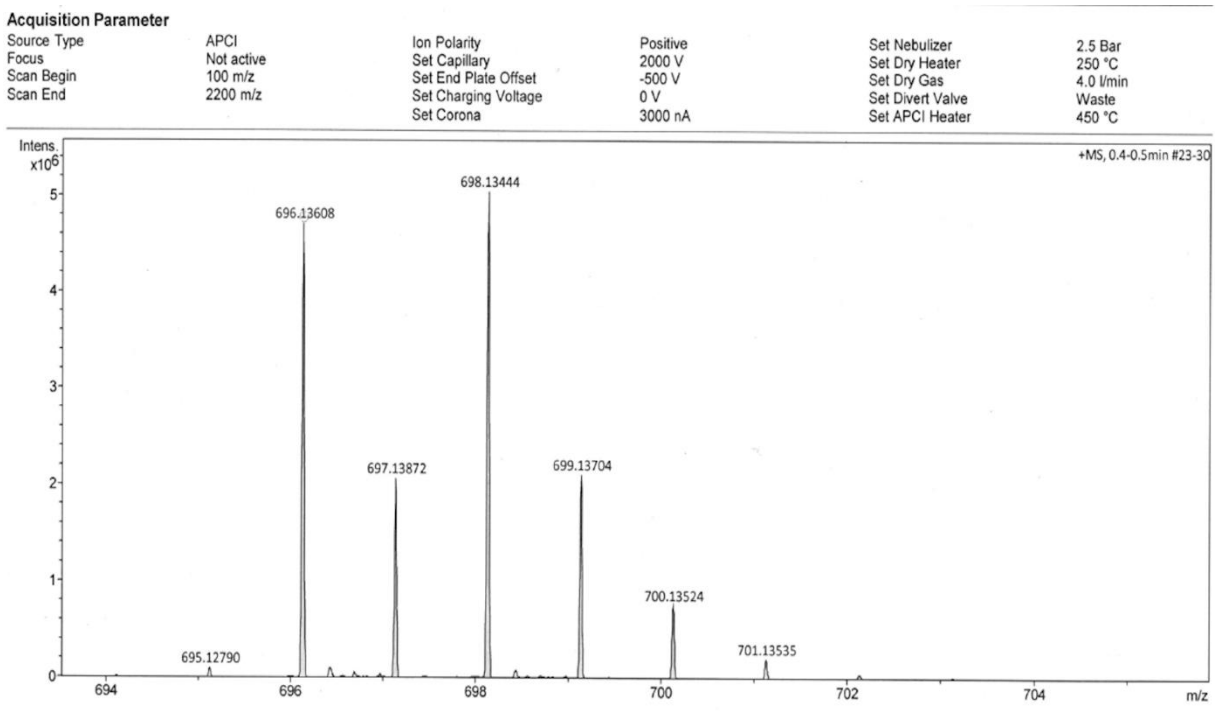


**Figure A171:** APCI-HRMS of **15b**.

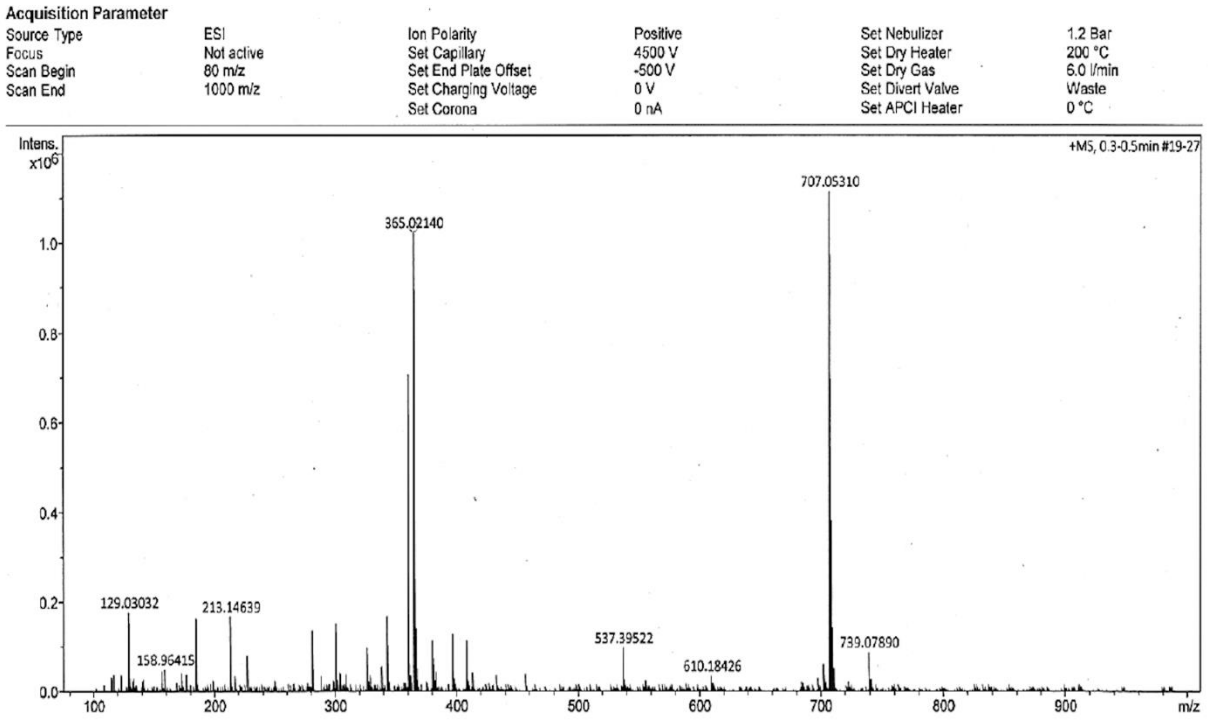


**Figure A172:** ESI-HRMS of **18**.

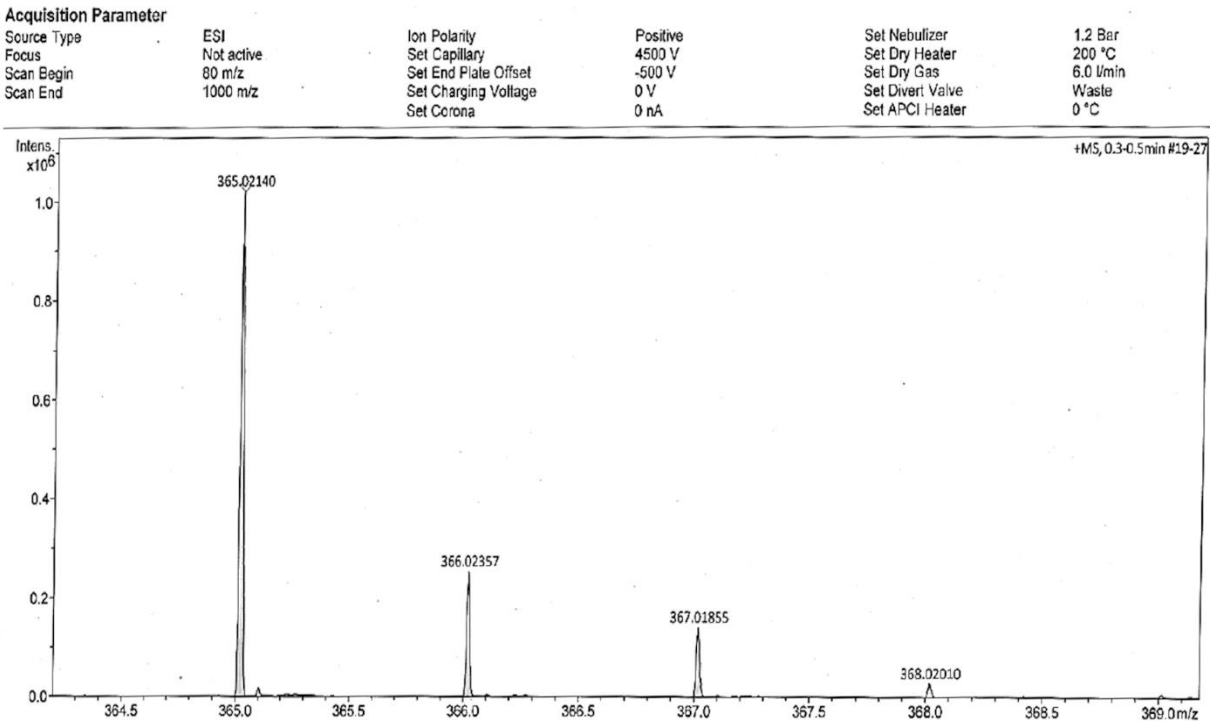


**Figure A173:** ESI-HRMS of **18**.

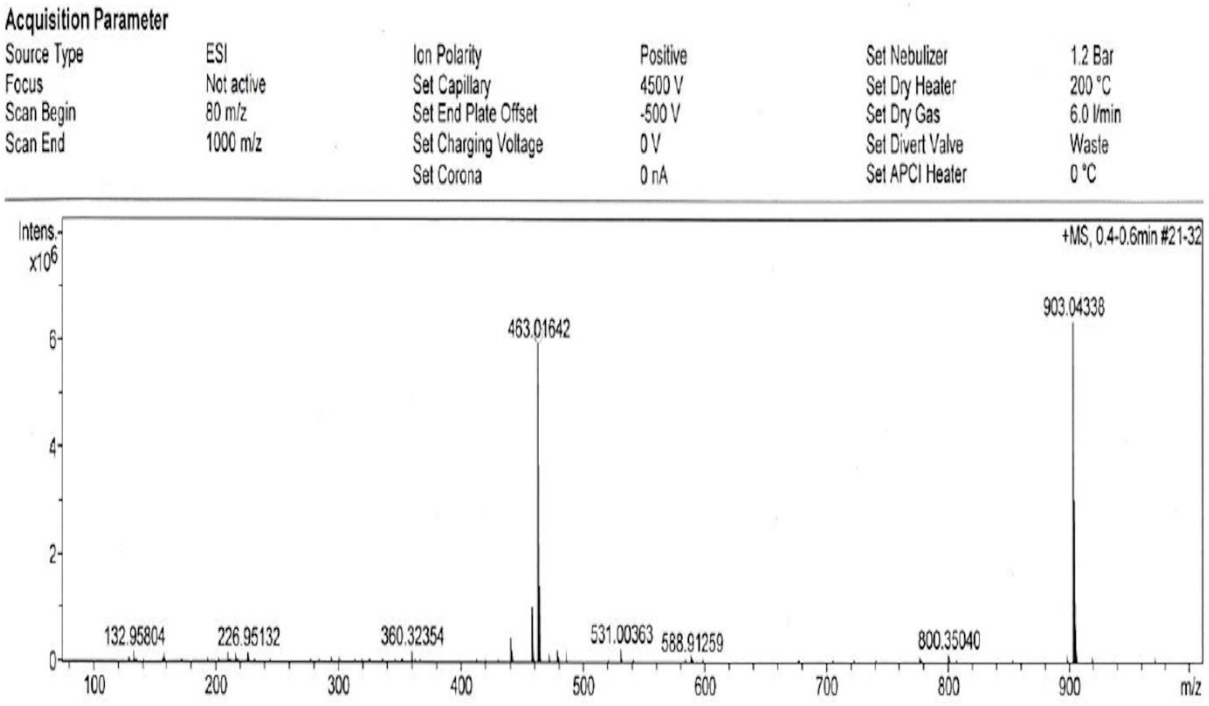


**Figure A174:** ESI-HRMS of **22(*S*)**.

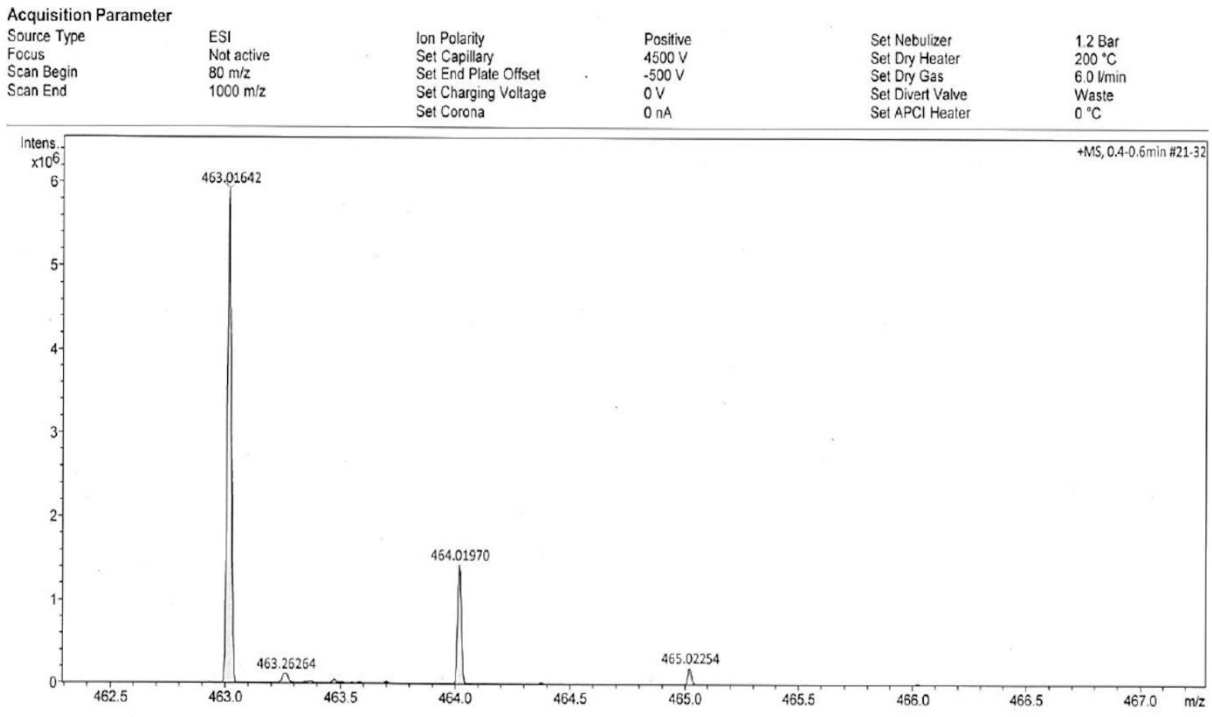


**Figure A175:** ESI-HRMS of **22(*S*)**.

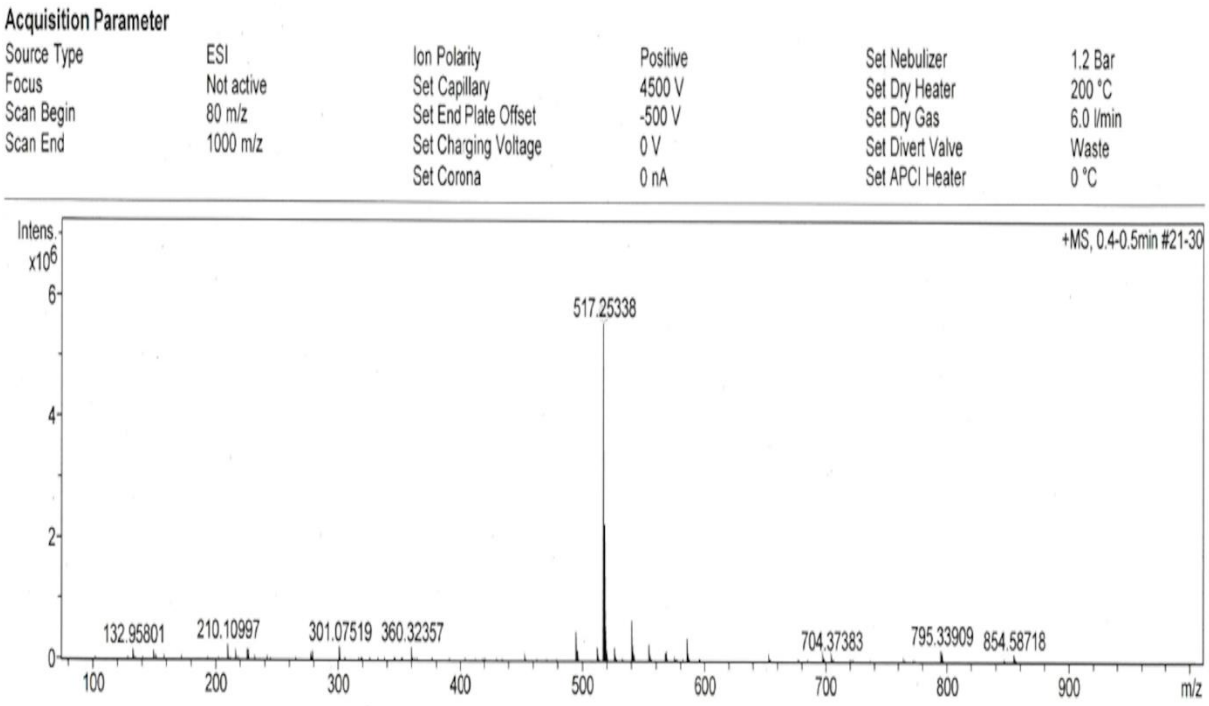


**Figure A176:** ESI-HRMS of **23(*S*)**.

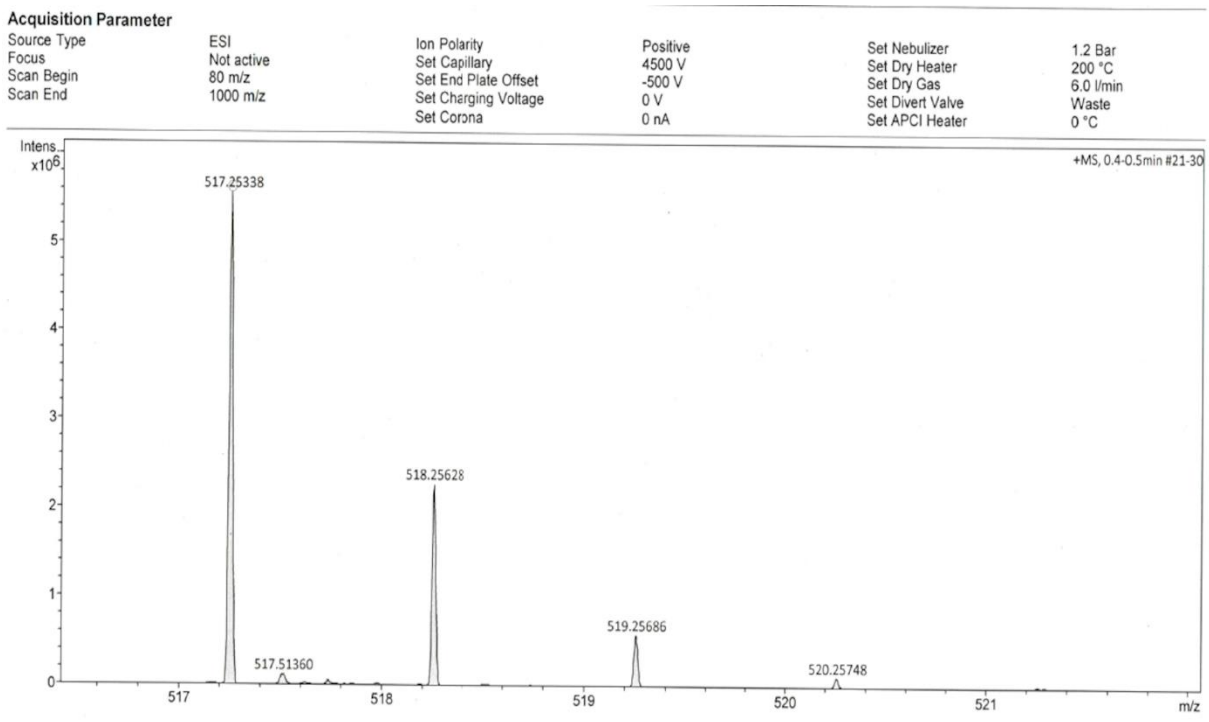


**Figure A177:** ESI-HRMS of **23(*S*)**.

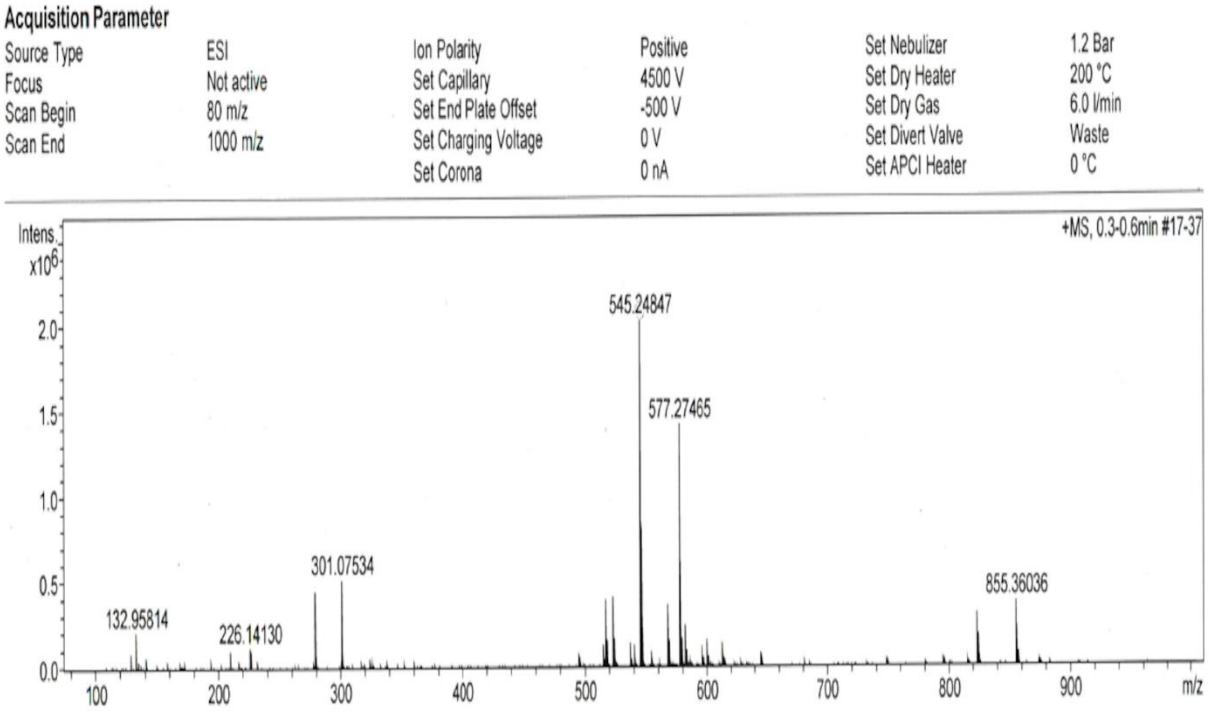


**Figure A178:** ESI-HRMS of **24(*S*)**.

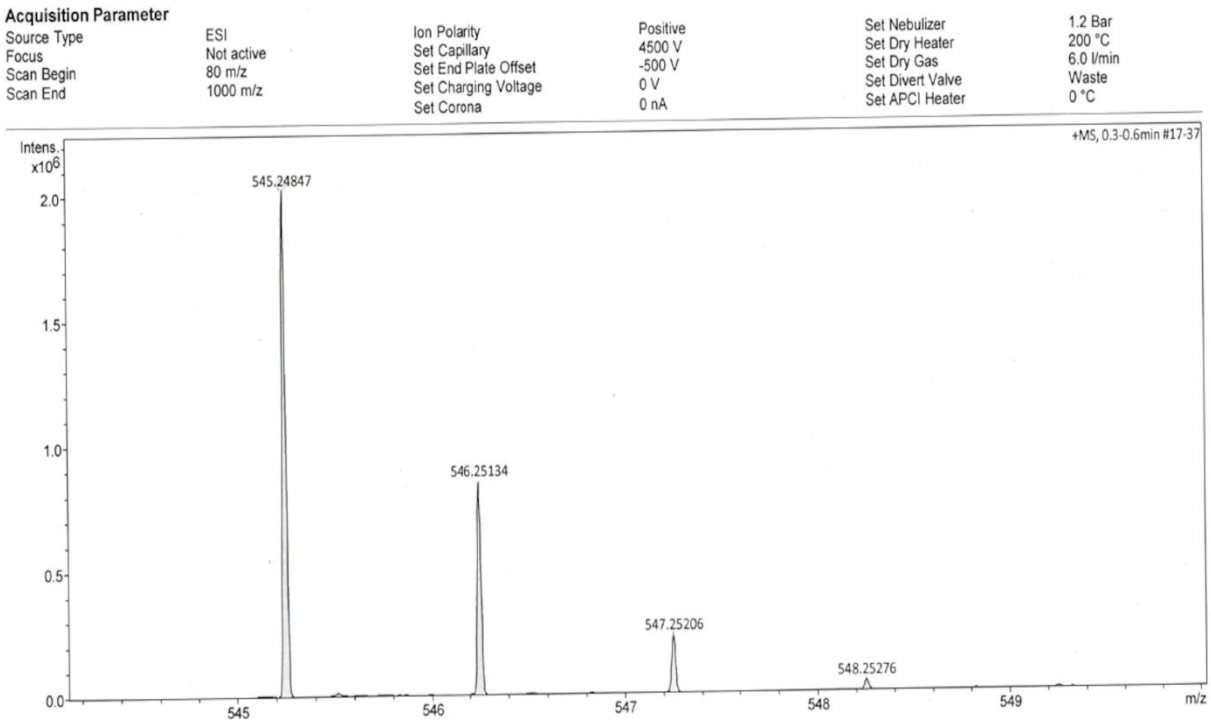


**Figure A179:** ESI-HRMS of **24(*S*)**.

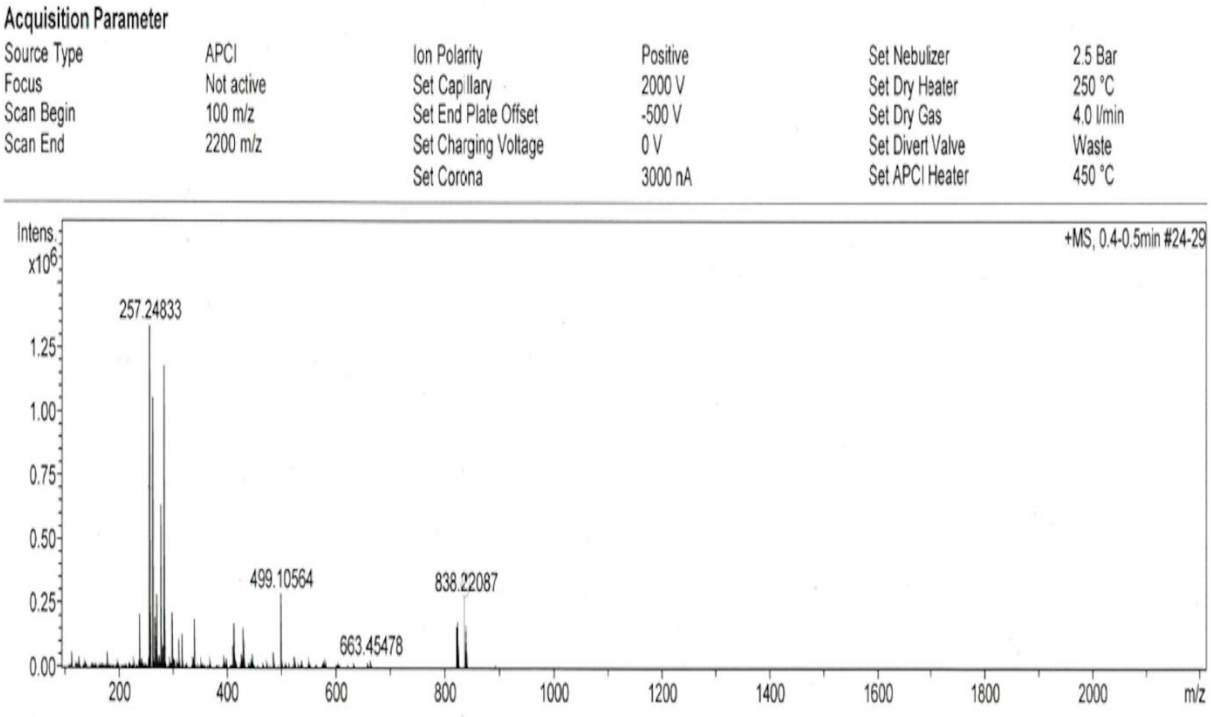


**Figure A180:** APCI-HRMS of **28(*S*)a**.

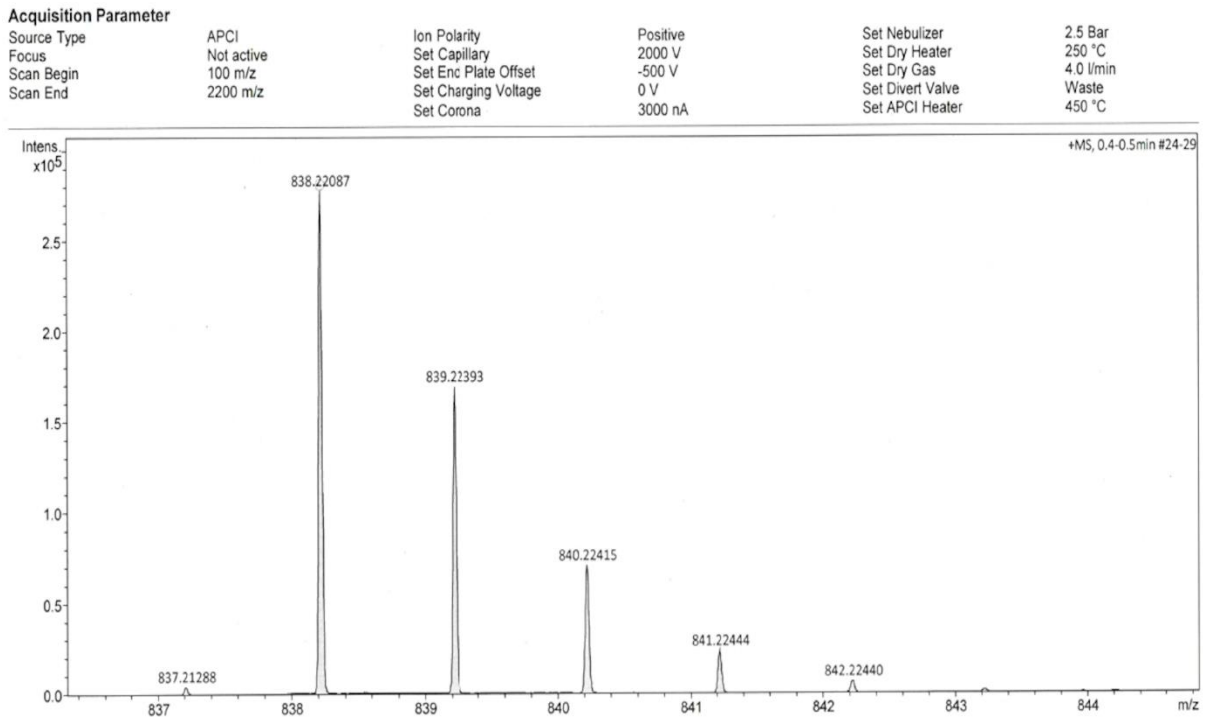


**Figure A181:** APCI-HRMS of **28(*S*)a**.

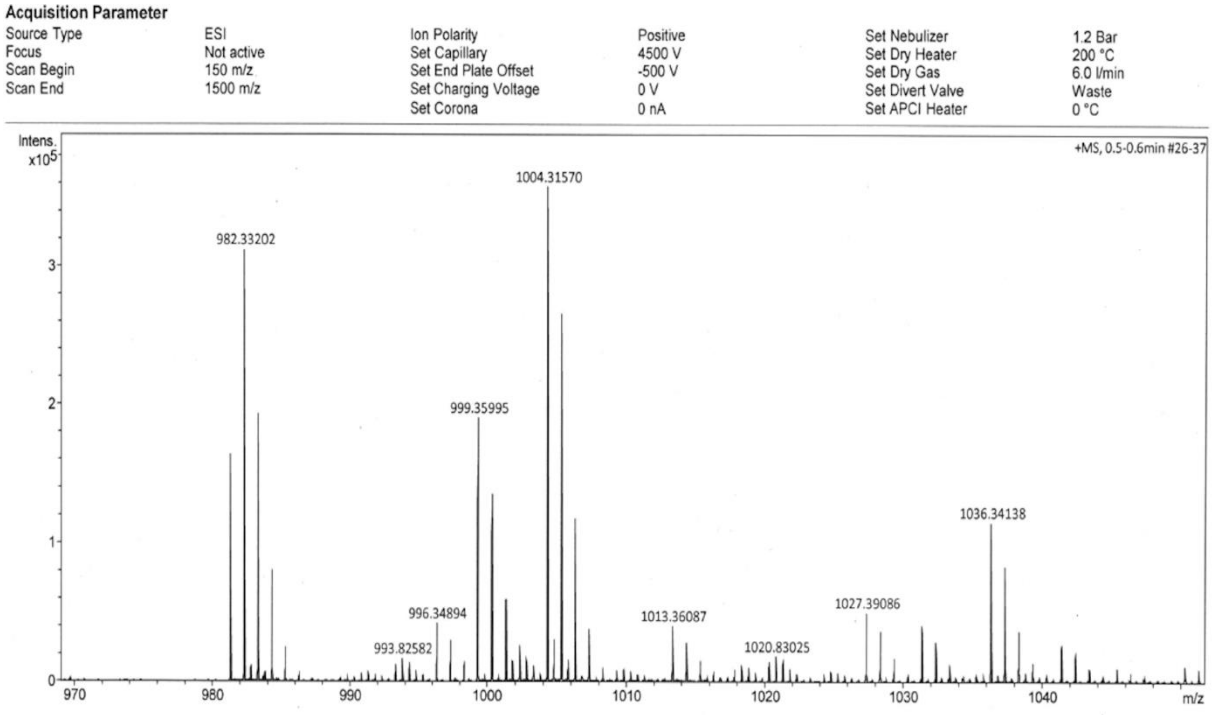


**Figure A182:** ESI-HRMS of **28(*S*)b**.

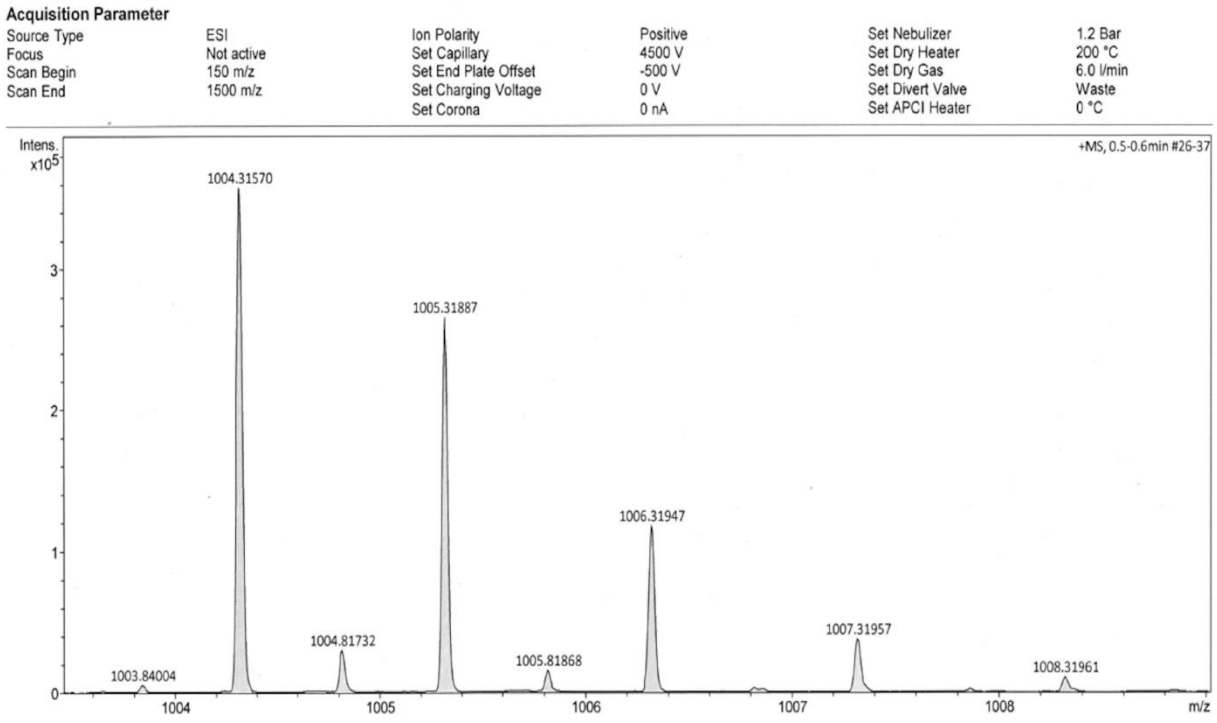


**Figure A183:** ESI-HRMS of **28(*S*)b**.

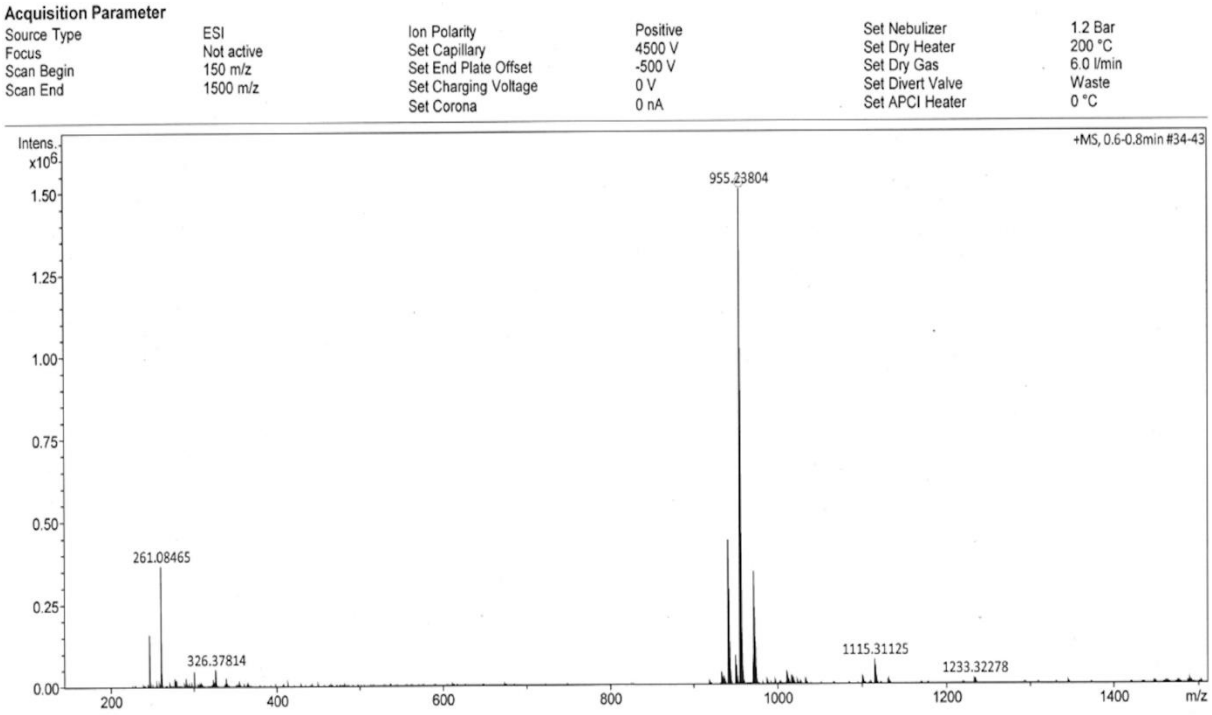


**Figure A184:** ESI-HRMS of **30(*S*)a**.

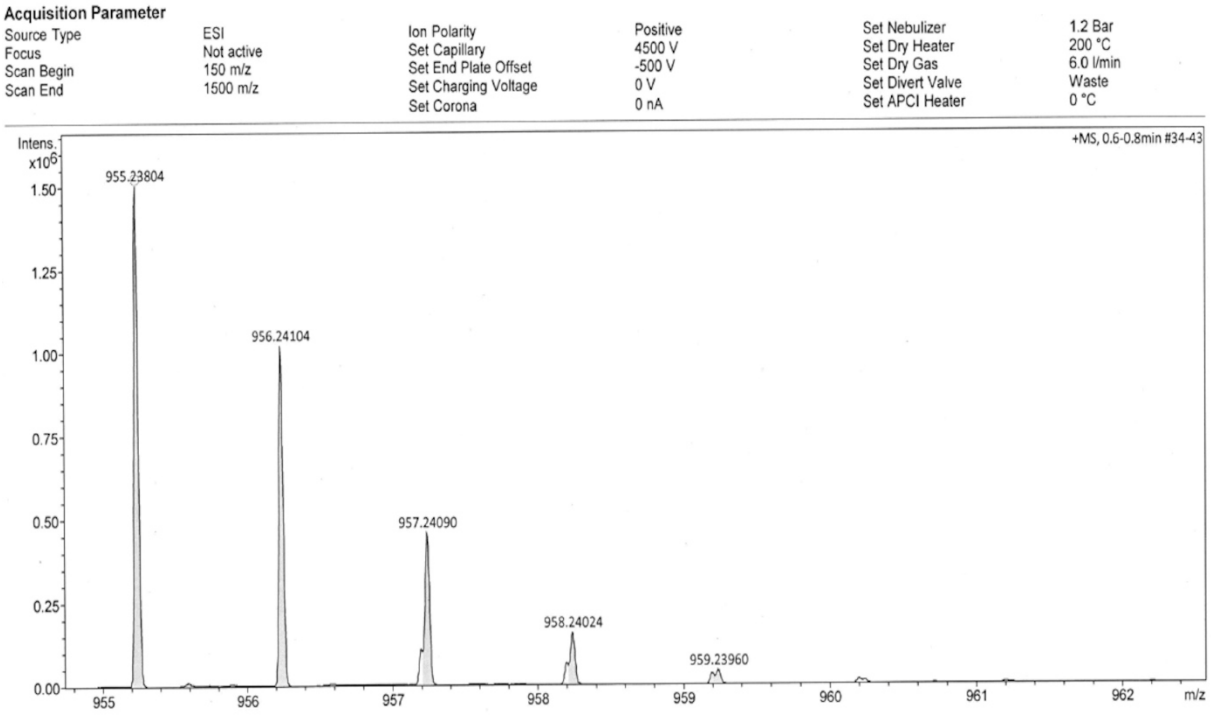


**Figure A185:** ESI-HRMS of **30(*S*)a**.

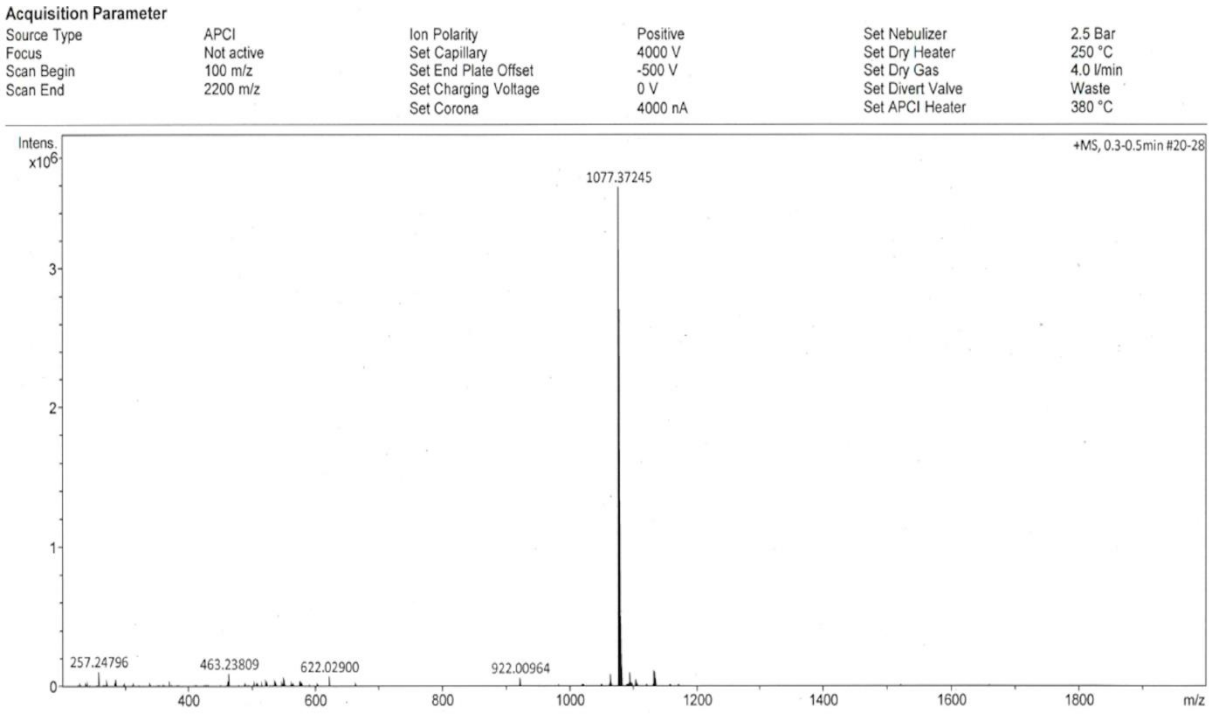


**Figure A186:** APCI-HRMS of **30(*S*)b**.

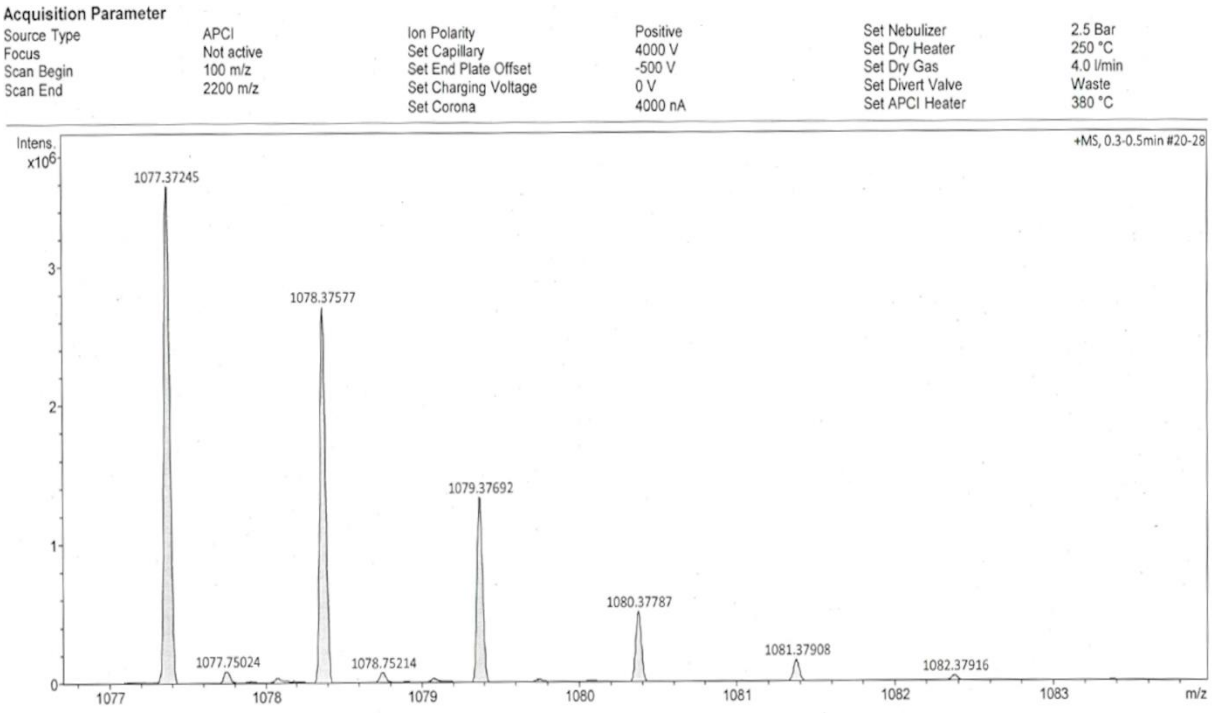


**Figure A187:** APCI-HRMS of **30(*S*)b**.

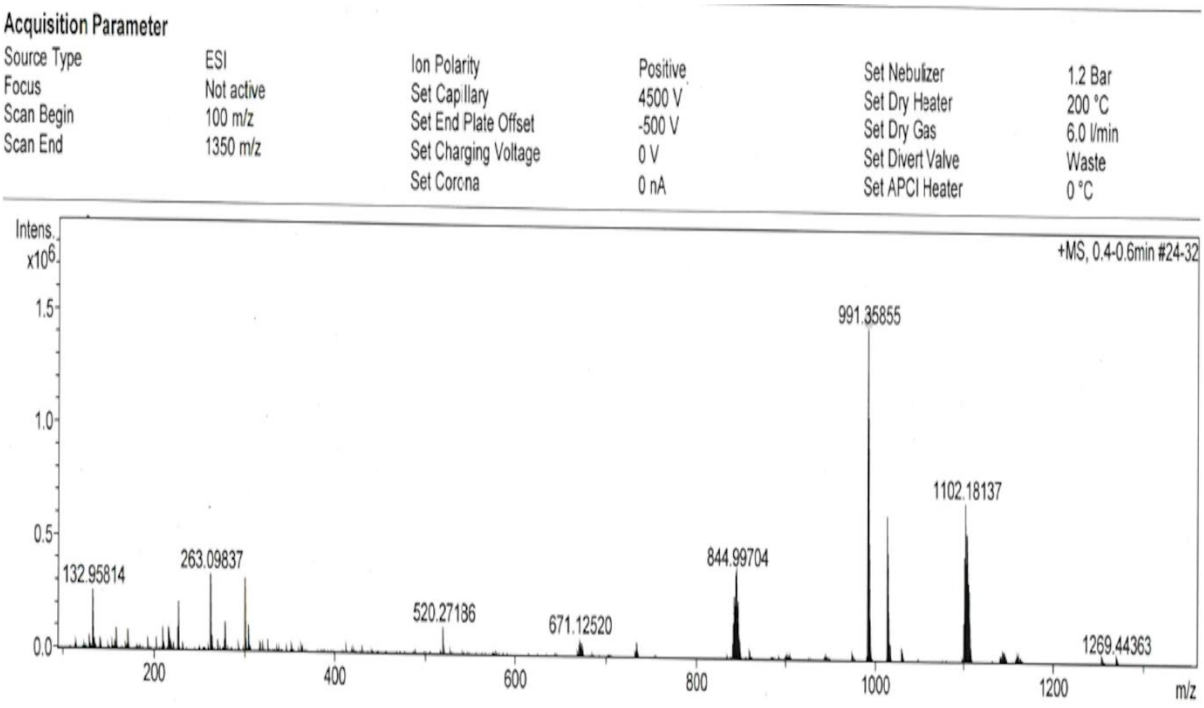


**Figure A188:** ESI-HRMS of **31(*S*)a**.

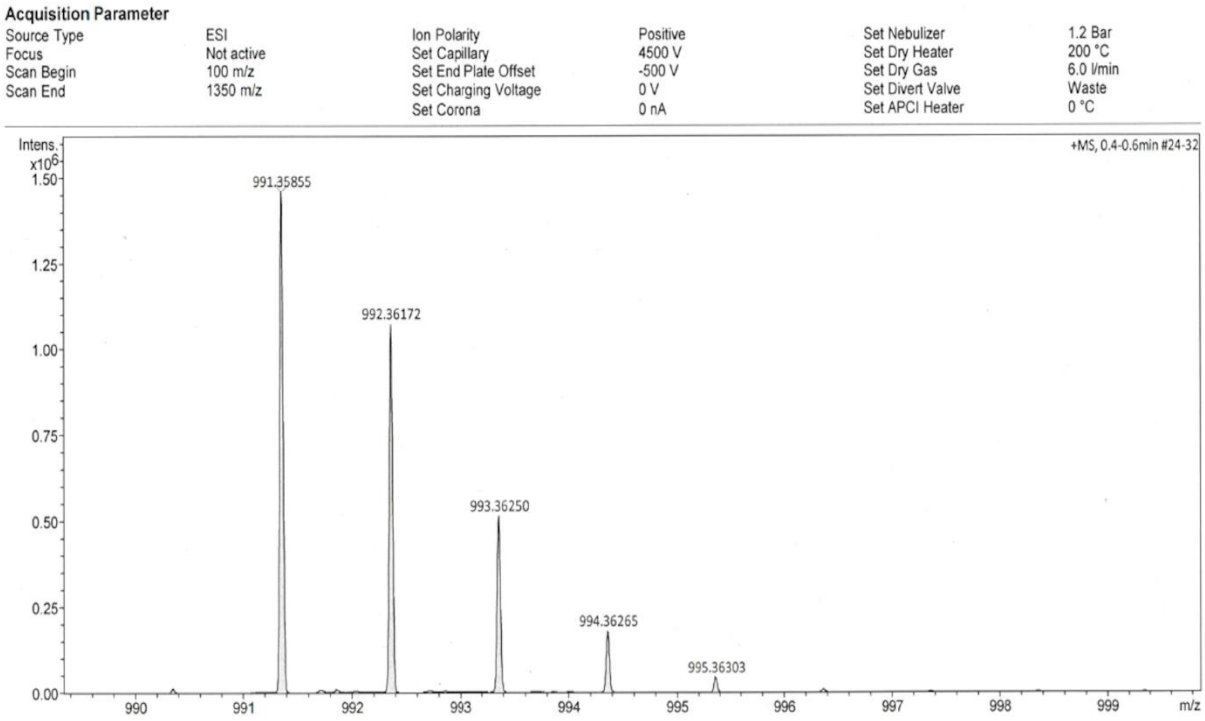


**Figure A189:** ESI-HRMS of **31(*S*)a**.

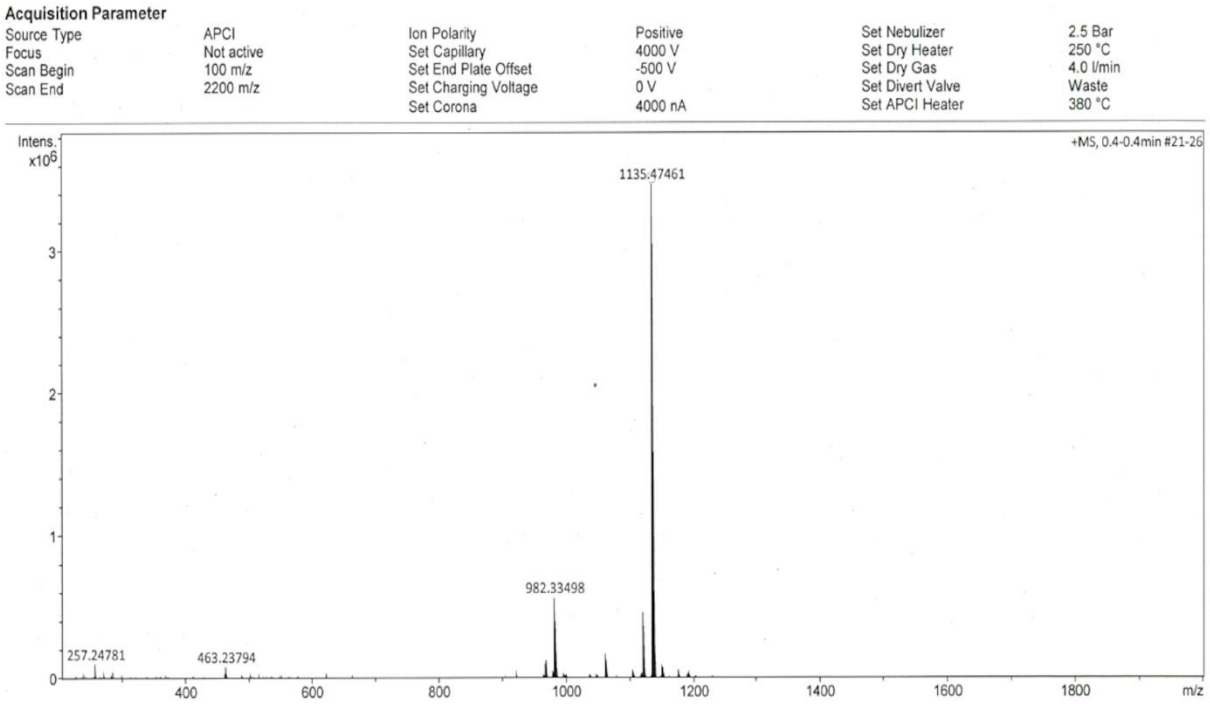


**Figure A190:** APCI-HRMS of **31(*S*)b**.

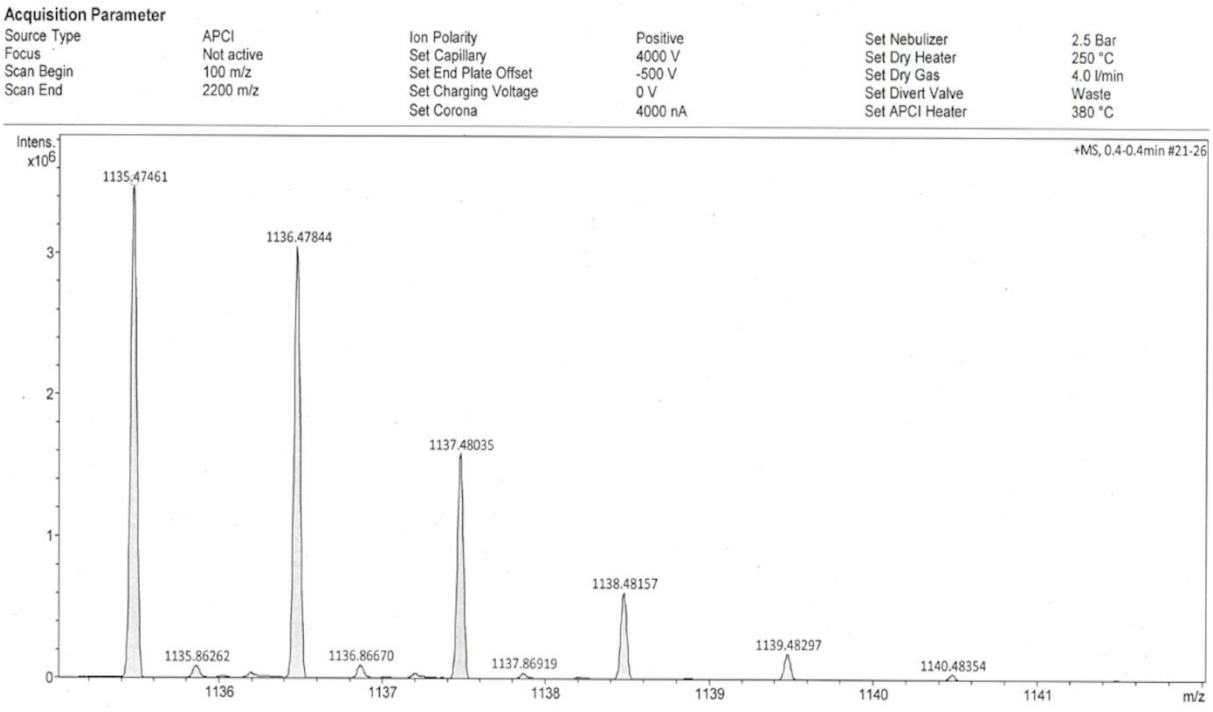


**Figure A191:** APCI-HRMS of **31(*S*)b**.

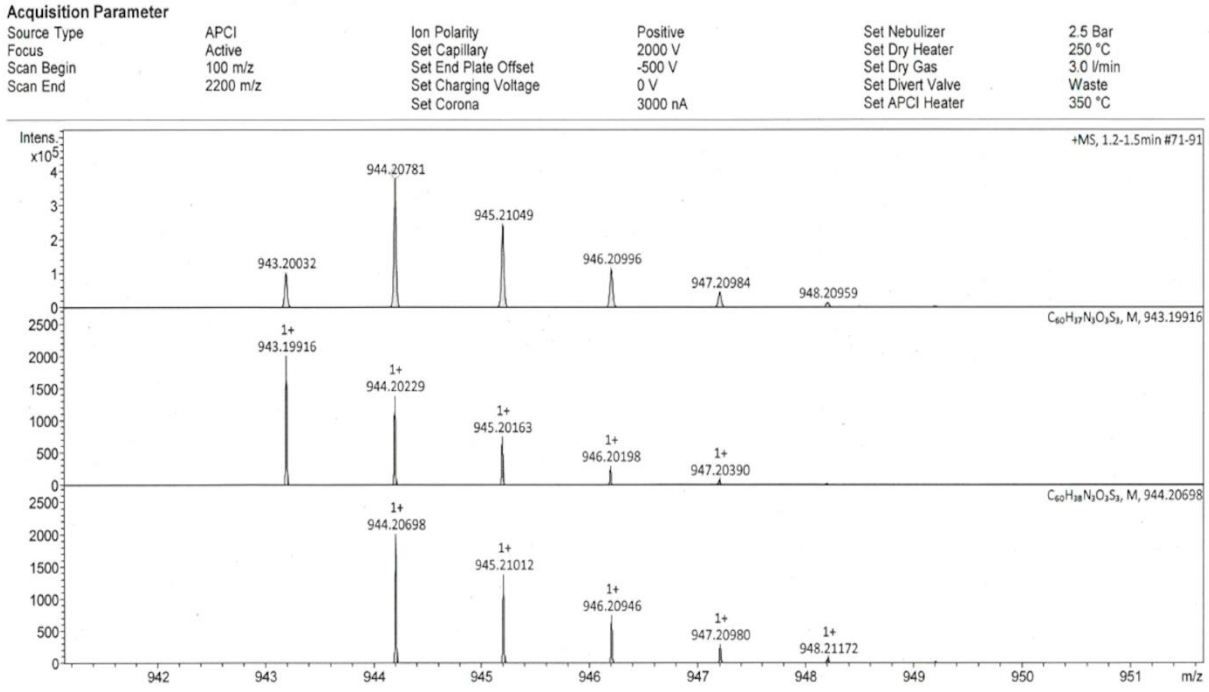


**Figure A192:** APCI-HRMS of **34(*S*)**.

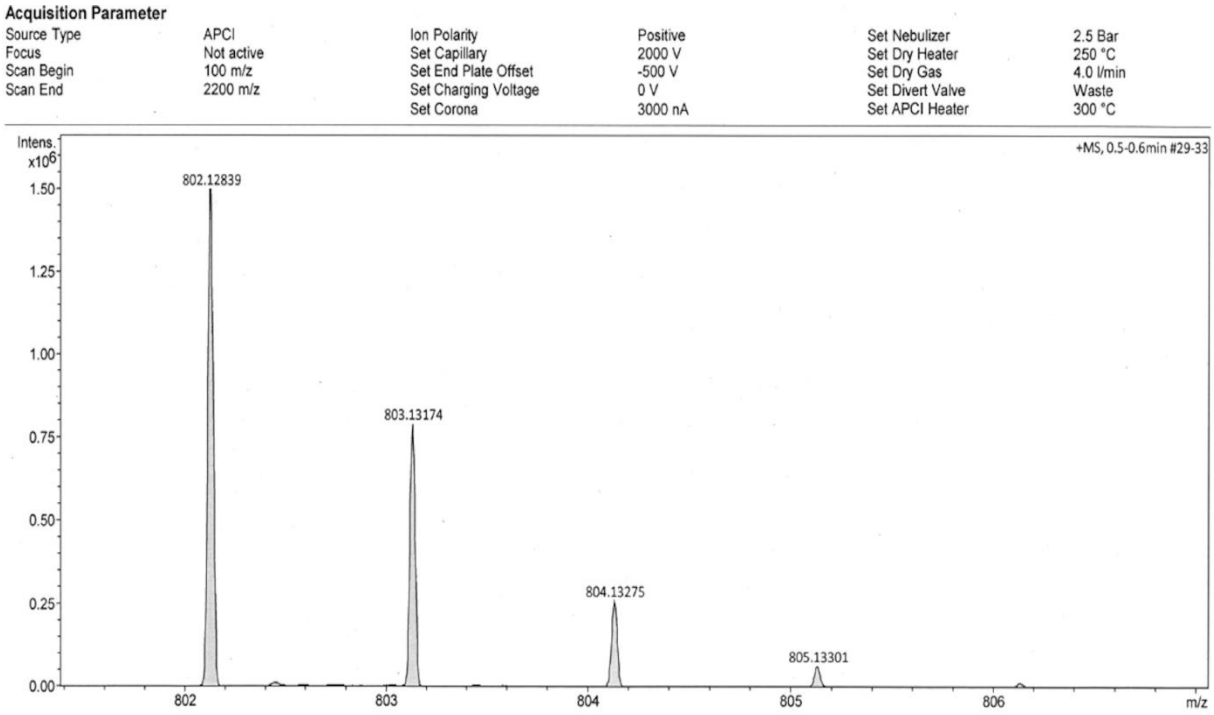


**Figure A193:** APCI-HRMS of **35(*S*)**.

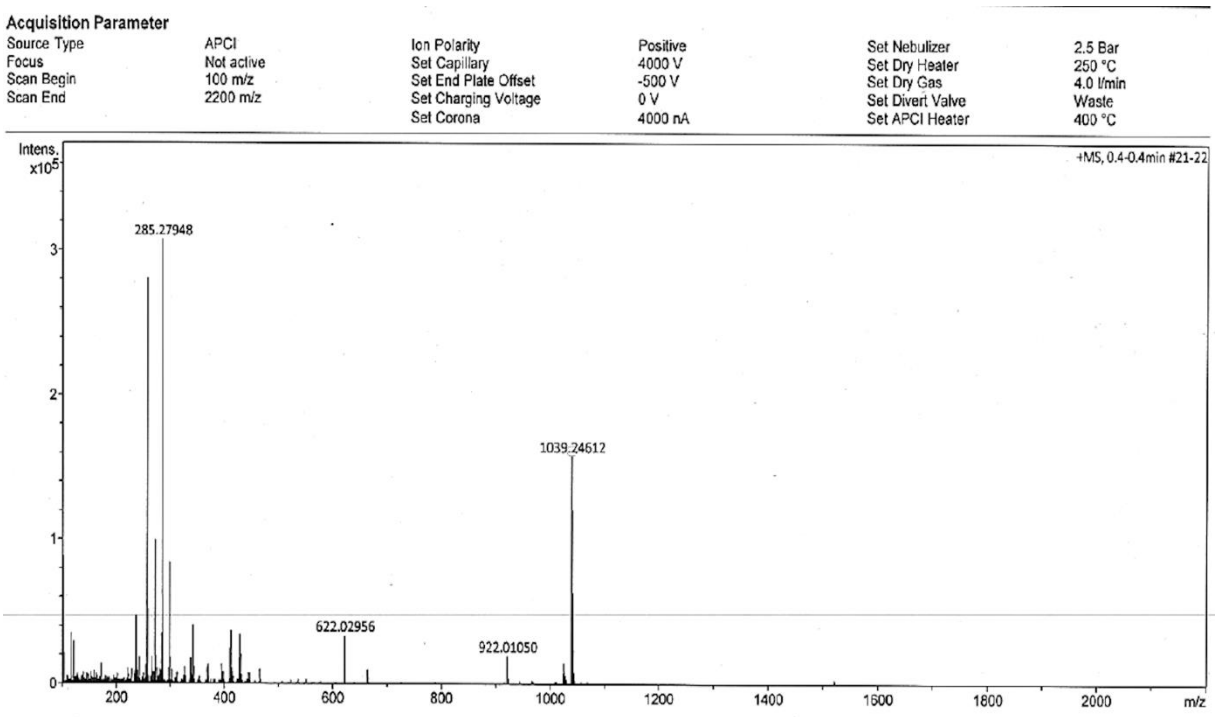


**Figure A194:** APCI-HRMS of **36(*S*)**.

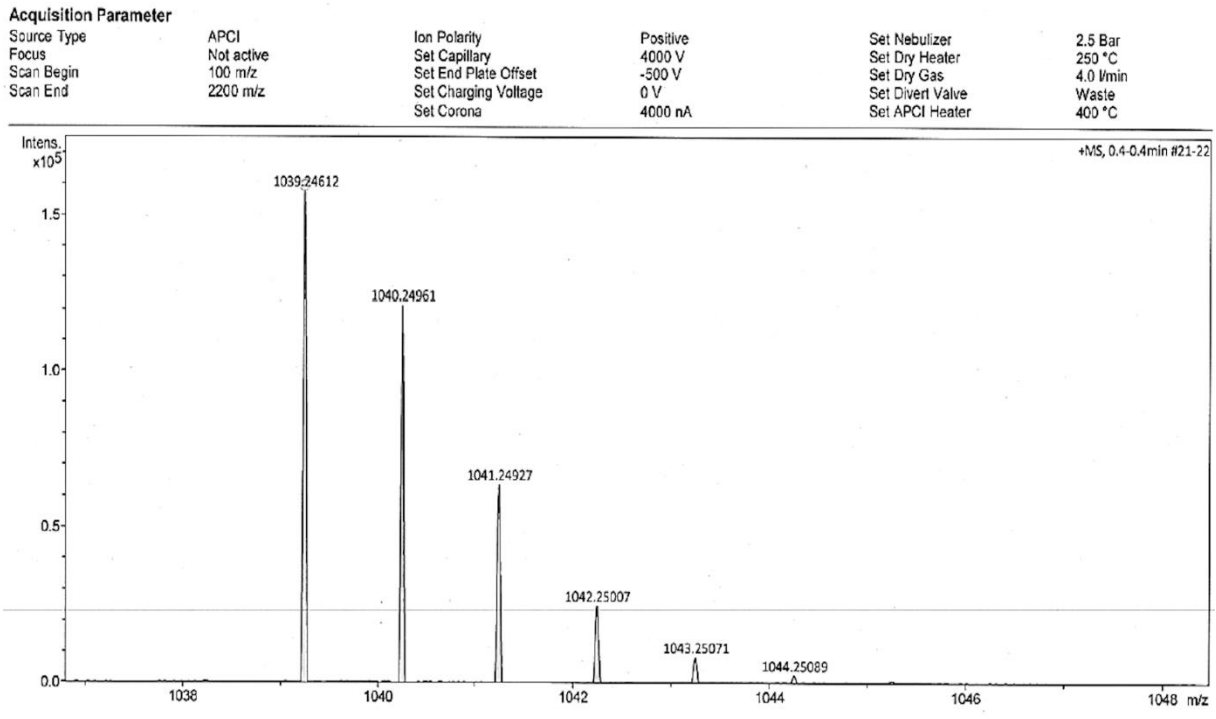


**Figure A195:** APCI-HRMS of **36(*S*)**.

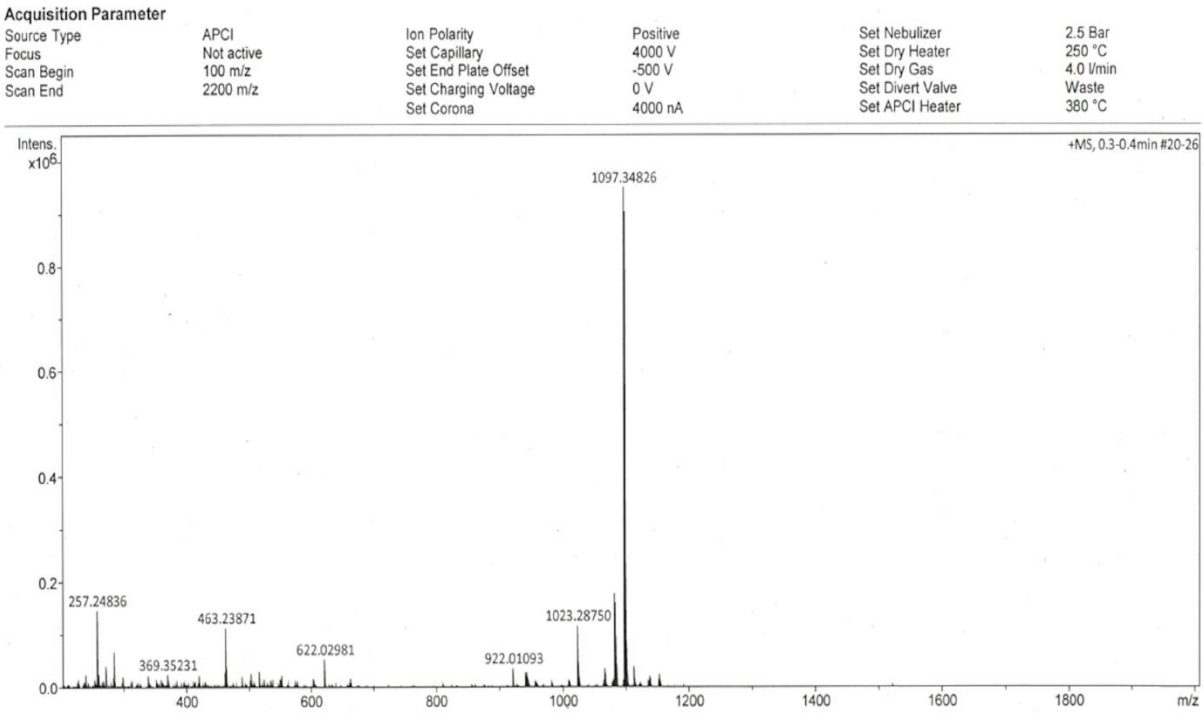


**Figure A196:** APCI-HRMS of **37(*S*)**.

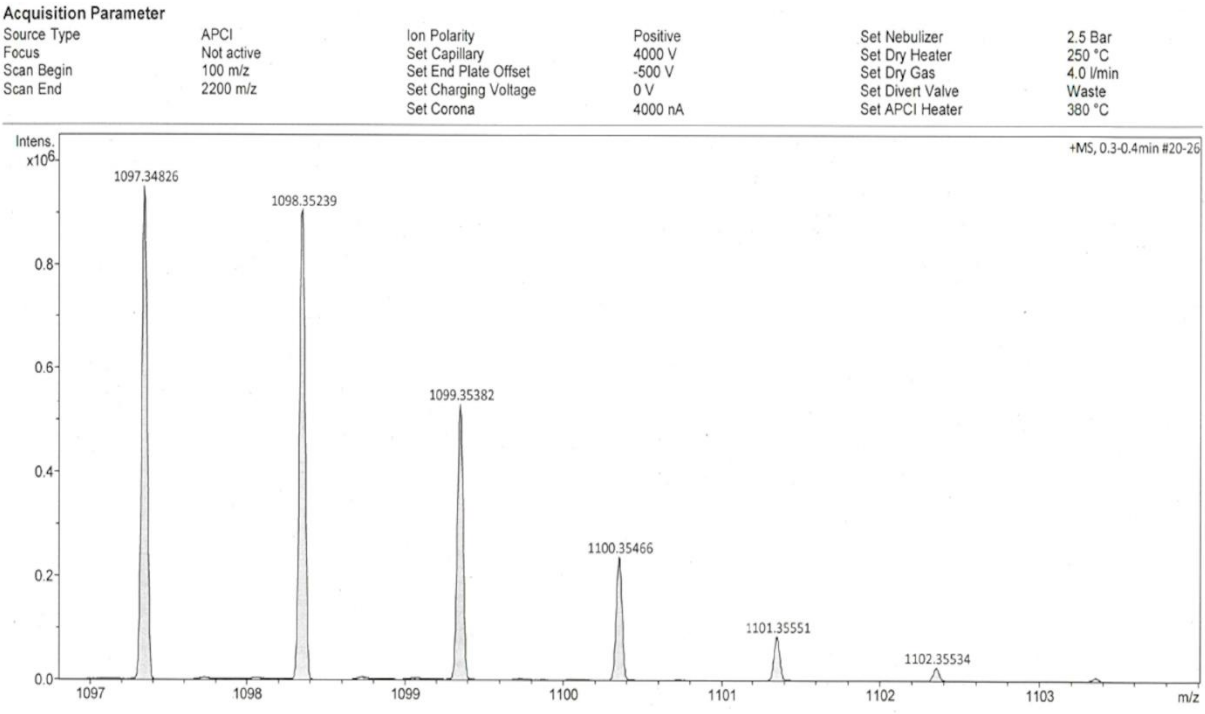


**Figure A197:** APCI-HRMS of **37(*S*)**.

## 5.6. Computational Chemistry

**Table A2:** HOMO-1, HOMO, LUMO and LUMO+1 energy levels of the optimized structures.

| Molecule | HOMO -1 [eV] | HOMO [eV] | LUMO [eV] | LUMO +1 [eV] |
|---|---|---|---|---|
| **30(*S*)a** | – 5.57 | – 5.30 | – 2.84 | – 2.44 |
| **30(*S*)b** | – 5.30 | – 4.76 | – 2.71 | – 2.35 |
| **36(*S*)** | – 5.53 | – 5.24 | – 3.22 | – 2.39 |

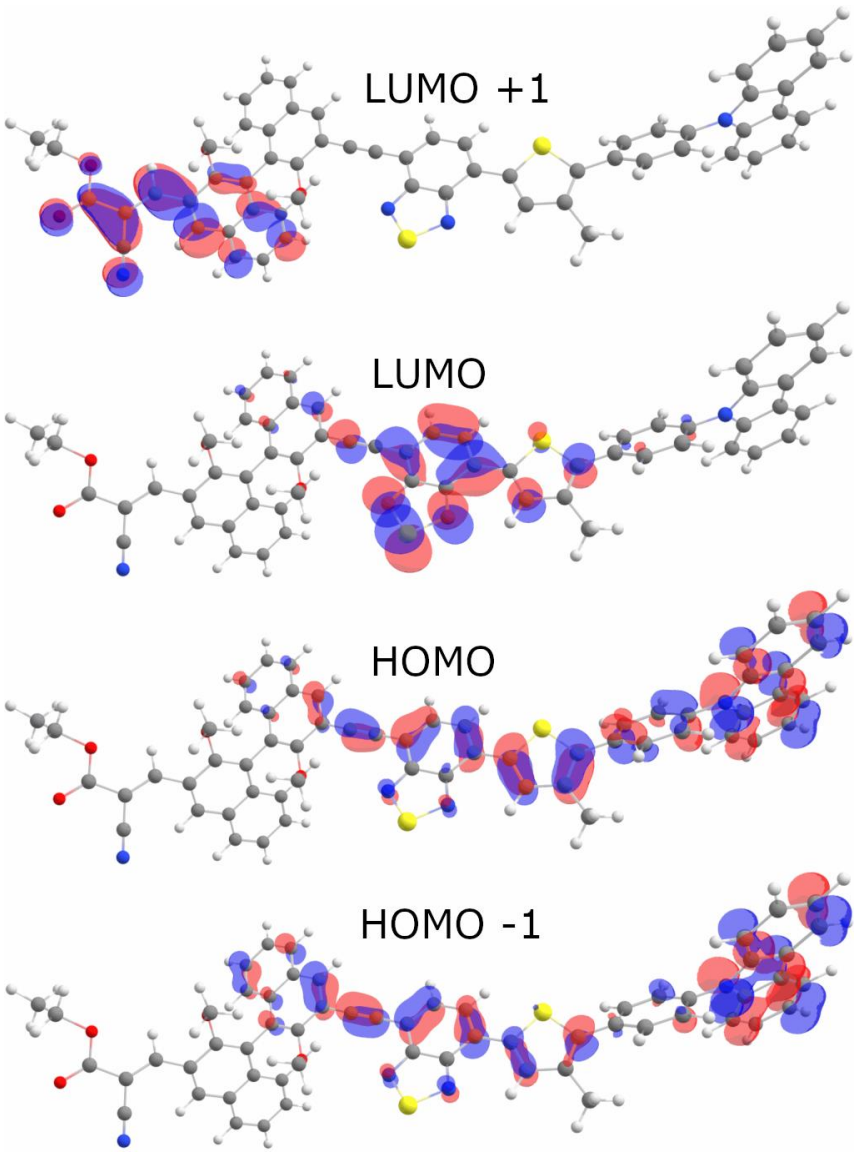


**Figure A198:** Frontier orbitals of **30(*S*)a** at B3LYP, 6-31G* level of theory and 0.03 contour value.

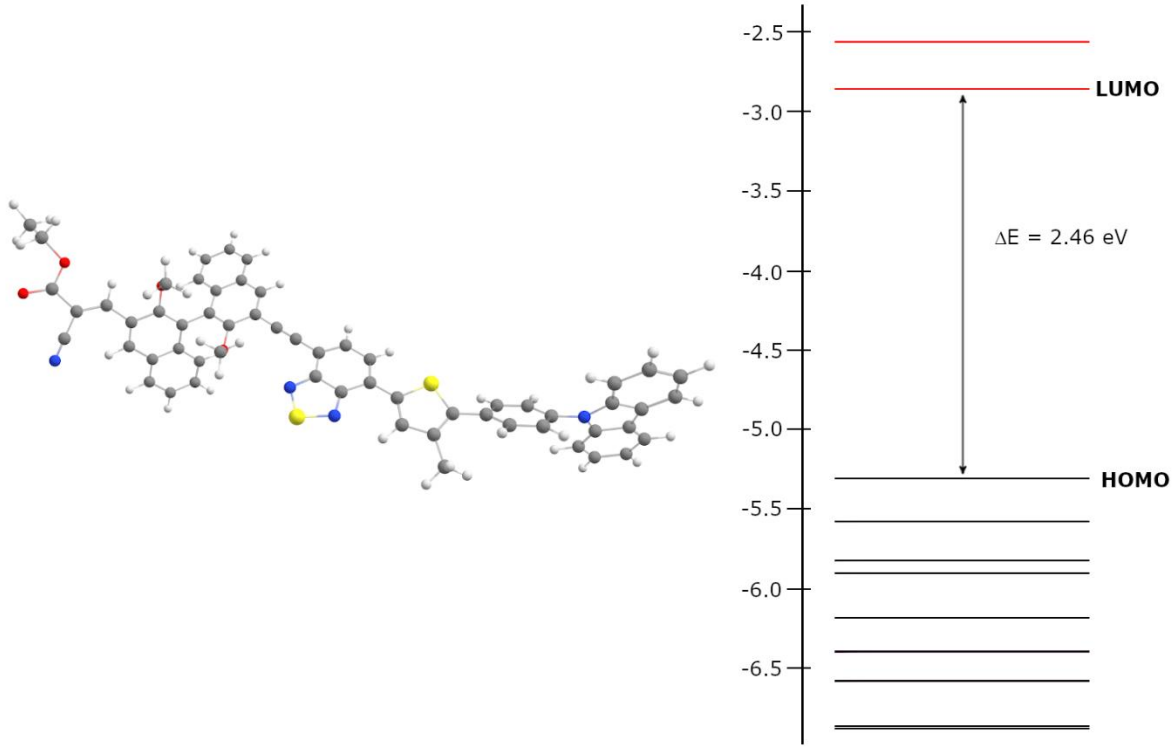


**Figure A199:** Optimized geometry and energy diagram, in eV, of **30(*S*)a** at B3LYP, 6-31G* level of theory.

**Table A3:** Cartesian coordinates of **30(*S*)a** optimized at B3LYP, 6-31G*, distances in angstrom.

| | | | |
|---|---|---|---|
| **C** | -13.076399 | 0.439691 | 0.774803 |
| **C** | -12.813648 | 0.333325 | 2.143381 |
| **H** | -11.828119 | 0.065857 | 2.509802 |
| **C** | -13.864506 | 0.574102 | 3.0262 |
| **H** | -13.683812 | 0.498881 | 4.095071 |
| **C** | -15.149002 | 0.907032 | 2.56337 |
| **H** | -15.946123 | 1.090621 | 3.278077 |
| **C** | -15.40795 | 0.996865 | 1.198815 |
| **H** | -16.404431 | 1.24351 | 0.841639 |
| **C** | -14.37008 | 0.759366 | 0.290227 |
| **C** | -14.292774 | 0.746993 | -1.155808 |
| **C** | -15.220993 | 0.99516 | -2.173618 |
| **H** | -16.249269 | 1.248444 | -1.928924 |
| **C** | -14.808966 | 0.919691 | -3.500895 |

| | | | |
|---|---|---|---|
| **H** | -15.520659 | 1.108867 | -4.299408 |
| **C** | -13.476182 | 0.6068 | -3.818317 |
| **H** | -13.170537 | 0.562705 | -4.860158 |
| **C** | -12.532333 | 0.354787 | -2.824701 |
| **H** | -11.502847 | 0.125762 | -3.079179 |
| **C** | -12.955854 | 0.417207 | -1.49424 |
| **C** | -10.846881 | -0.10906 | -0.238739 |
| **C** | -10.35572 | -1.233947 | -0.913674 |
| **H** | -11.037225 | -1.850413 | -1.491252 |
| **C** | -9.004388 | -1.559499 | -0.846919 |
| **H** | -8.637842 | -2.413068 | -1.407092 |
| **C** | -8.106198 | -0.792759 | -0.080952 |
| **C** | -8.616889 | 0.331791 | 0.595365 |
| **H** | -7.949809 | 0.940081 | 1.199256 |
| **C** | -9.961266 | 0.676889 | 0.510722 |
| **H** | -10.331895 | 1.559333 | 1.022512 |
| **C** | -6.680916 | -1.141968 | -0.004934 |
| **C** | -6.075519 | -2.38297 | 0.099186 |
| **C** | -4.656054 | -2.290148 | 0.151349 |
| **H** | -4.011518 | -3.154226 | 0.244874 |
| **C** | -4.153818 | -1.006089 | 0.09207 |
| **C** | -6.791457 | -3.706275 | 0.199889 |
| **H** | -7.799066 | -3.594252 | 0.609916 |
| **H** | -6.235138 | -4.391702 | 0.848045 |
| **H** | -6.884654 | -4.194993 | -0.779125 |
| **C** | -2.773515 | -0.54626 | 0.129591 |
| **C** | -2.43973 | 0.80227 | 0.172874 |
| **C** | -1.113292 | 1.288919 | 0.203209 |
| **C** | -0.005235 | 0.453523 | 0.196758 |
| **C** | -0.282696 | -0.958123 | 0.14977 |
| **C** | -1.650041 | -1.456089 | 0.1183 |
| **C** | 1.320553 | 0.943006 | 0.233294 |

| | | | |
|---|---|---|---|
| **C** | 2.462454 | 1.364585 | 0.268699 |
| **C** | 3.783289 | 1.887167 | 0.297627 |
| **C** | 4.003632 | 3.238633 | 0.074003 |
| **H** | 3.157541 | 3.881086 | -0.152869 |
| **C** | 5.295711 | 3.80257 | 0.160114 |
| **C** | 5.505541 | 5.194227 | -0.044799 |
| **H** | 4.648957 | 5.817521 | -0.290065 |
| **C** | 6.760985 | 5.742638 | 0.071148 |
| **H** | 6.911047 | 6.80729 | -0.084681 |
| **C** | 7.86087 | 4.915764 | 0.401741 |
| **H** | 8.85062 | 5.353061 | 0.501043 |
| **C** | 7.690706 | 3.562949 | 0.599641 |
| **H** | 8.543171 | 2.943347 | 0.853599 |
| **C** | 6.410548 | 2.959544 | 0.480511 |
| **C** | 6.192984 | 1.55314 | 0.67805 |
| **C** | 4.906492 | 1.040407 | 0.598744 |
| **C** | 4.327899 | -1.169821 | -0.137425 |
| **H** | 3.468616 | -0.802664 | -0.704551 |
| **H** | 4.053714 | -2.107817 | 0.347573 |
| **H** | 5.180375 | -1.339912 | -0.806956 |
| **C** | 7.33435 | 0.633489 | 0.989559 |
| **C** | 7.476528 | 0.044597 | 2.291875 |
| **C** | 6.582449 | 0.318149 | 3.359805 |
| **H** | 5.752291 | 0.994673 | 3.193193 |
| **C** | 6.757572 | -0.263208 | 4.596624 |
| **H** | 6.059873 | -0.037538 | 5.398525 |
| **C** | 7.833133 | -1.152056 | 4.836778 |
| **H** | 7.953192 | -1.604518 | 5.816972 |
| **C** | 8.72268 | -1.433885 | 3.828032 |
| **H** | 9.55774 | -2.109488 | 3.994693 |
| **C** | 8.573229 | -0.84502 | 2.54066 |
| **C** | 9.504651 | -1.112658 | 1.515216 |

| | | | |
|---|---|---|---|
| **H** | 10.333708 | -1.773433 | 1.738689 |
| **C** | 9.395797 | -0.526732 | 0.260138 |
| **C** | 8.282616 | 0.356126 | 0.020153 |
| **C** | 7.473036 | 0.313629 | -2.222715 |
| **H** | 6.408443 | 0.273143 | -1.967957 |
| **H** | 7.850086 | -0.70451 | -2.385409 |
| **H** | 7.604815 | 0.900043 | -3.134532 |
| **C** | 10.361399 | -0.694869 | -0.81366 |
| **H** | 10.253756 | 0.021099 | -1.620602 |
| **N** | -12.220916 | 0.231988 | -0.315519 |
| **O** | 4.69194 | -0.274612 | 0.919217 |
| **O** | 8.21805 | 0.987133 | -1.205511 |
| **C** | 11.373536 | -1.593286 | -0.979061 |
| **S** | -5.482307 | 0.13647 | -0.045664 |
| **N** | -1.715013 | -2.790869 | 0.073043 |
| **S** | -0.168926 | -3.347707 | 0.070035 |
| **N** | 0.642162 | -1.920122 | 0.124428 |
| **H** | -0.955697 | 2.362132 | 0.239524 |
| **H** | -3.236171 | 1.54046 | 0.191717 |
| **C** | 11.67989 | -2.647112 | -0.060688 |
| **C** | 12.265478 | -1.55986 | -2.178142 |
| **N** | 11.916535 | -3.498244 | 0.697222 |
| **O** | 13.174853 | -2.344877 | -2.353924 |
| **O** | 11.939394 | -0.568755 | -3.037254 |
| **C** | 12.760696 | -0.453205 | -4.225807 |
| **H** | 13.013462 | -1.457032 | -4.574786 |
| **H** | 12.107068 | 0.032437 | -4.9545 |
| **C** | 14.010662 | 0.37078 | -3.958227 |
| **H** | 14.65923 | -0.135808 | -3.238258 |
| **H** | 14.571307 | 0.504927 | -4.890497 |
| **H** | 13.74989 | 1.36002 | -3.568134 |

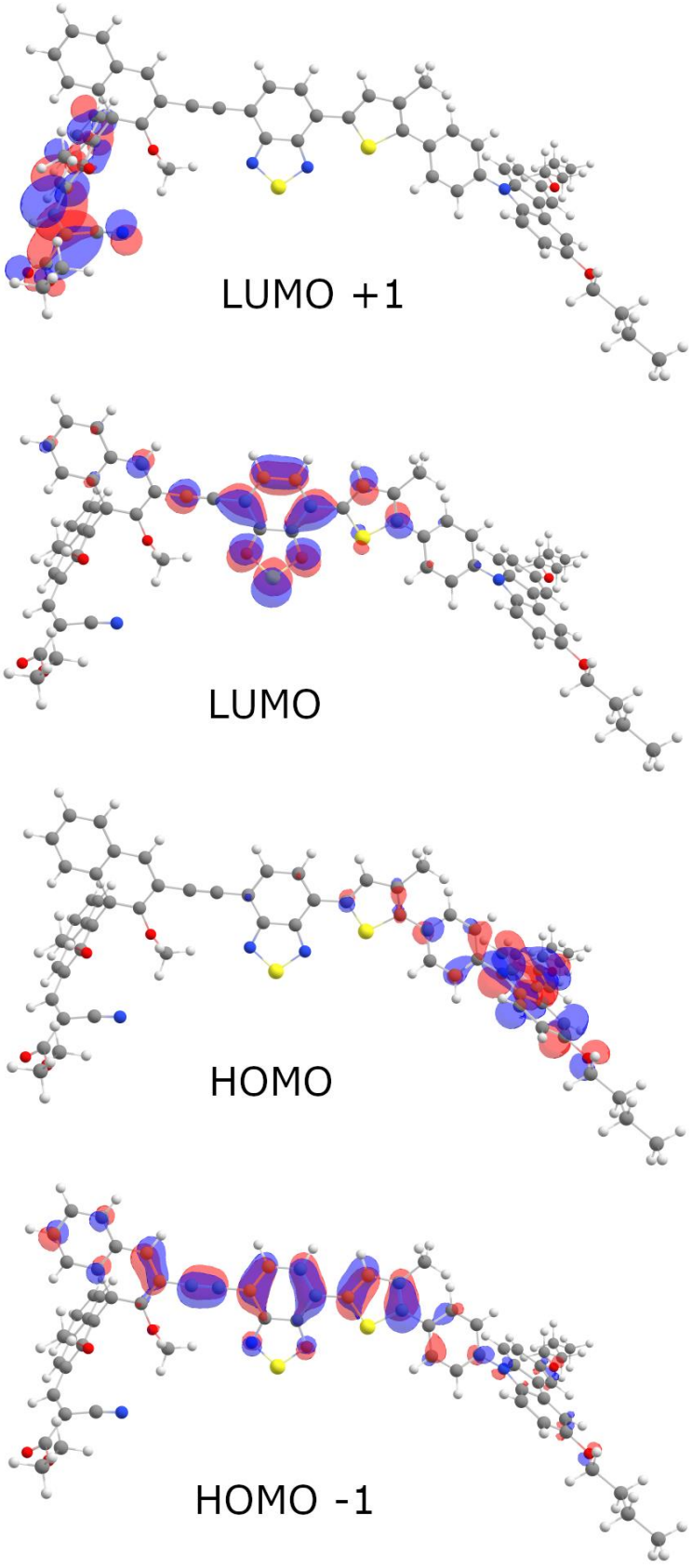


**Figure A200:** Frontier orbitals of **30(*S*)b** at B3LYP, 6-31G* level of theory and 0.03 contour value.

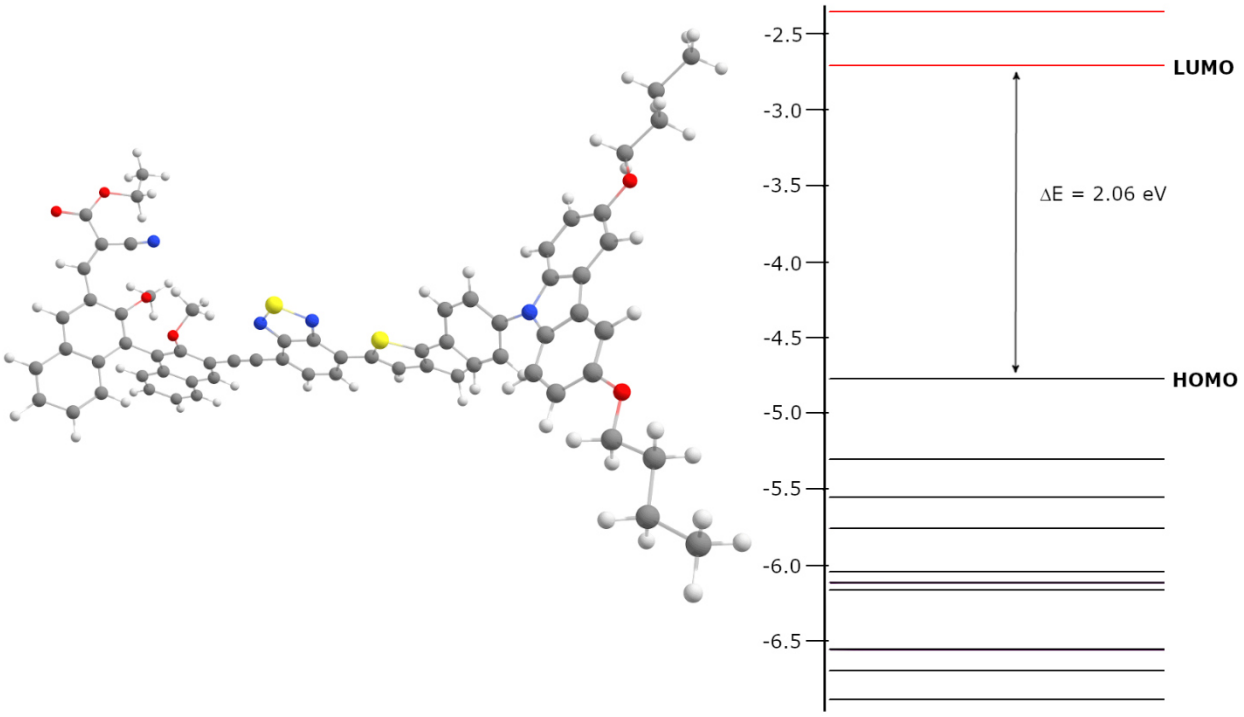


**Figure A201:**. Optimized geometry and energy diagram, in eV, of **30(*S*)b** at B3LYP, 6-31G* level of theory.

**Table A4:** Cartesian coordinates of **30(*S*)b** optimized at B3LYP, 6-31G*, distances in angstrom.

| | | | |
|---|---|---|---|
| **C** | -11.650983 | -3.287704 | -0.141183 |
| **C** | -12.017073 | -2.053502 | 0.402406 |
| **C** | -11.122266 | -0.986244 | 0.332487 |
| **C** | -9.853845 | -1.158726 | -0.278506 |
| **C** | -9.493556 | -2.382771 | -0.837884 |
| **C** | -10.397158 | -3.445197 | -0.762051 |
| **C** | -11.196694 | 0.395514 | 0.764259 |
| **C** | -9.972222 | 1.008703 | 0.394637 |
| **N** | -9.154886 | 0.059151 | -0.240618 |
| **C** | -12.17449 | 1.130938 | 1.433364 |
| **C** | -11.929477 | 2.472238 | 1.739373 |
| **C** | -10.704002 | 3.068007 | 1.38492 |
| **C** | -9.717747 | 2.340539 | 0.714815 |
| **C** | -7.857504 | 0.288826 | -0.752945 |

| | | | |
|---|---|---|---|
| **C** | -6.794973 | -0.56044 | -0.41089 |
| **C** | -5.523485 | -0.340338 | -0.928213 |
| **C** | -5.258367 | 0.745451 | -1.785215 |
| **C** | -6.329862 | 1.601545 | -2.10256 |
| **C** | -7.610216 | 1.371084 | -1.60927 |
| **C** | -3.907204 | 0.98648 | -2.310252 |
| **C** | -3.512992 | 1.39666 | -3.57554 |
| **C** | -2.10151 | 1.493483 | -3.682157 |
| **C** | -1.399223 | 1.173081 | -2.534272 |
| **S** | -2.525799 | 0.722007 | -1.269074 |
| **C** | -4.428525 | 1.662667 | -4.743866 |
| **O** | -12.583347 | -4.286149 | -0.026152 |
| **O** | -12.942271 | 3.125957 | 2.392346 |
| **C** | -12.758692 | 4.488882 | 2.758757 |
| **C** | -14.023035 | 4.953819 | 3.469445 |
| **C** | -13.945554 | 6.419524 | 3.915052 |
| **C** | -15.215727 | 6.890192 | 4.630914 |
| **C** | -12.286843 | -5.570654 | -0.562549 |
| **C** | -13.482648 | -6.474686 | -0.293112 |
| **C** | -13.280169 | -7.897626 | -0.828931 |
| **C** | -14.481095 | -8.809978 | -0.559277 |
| **C** | 2.156205 | 0.707122 | -1.063652 |
| **C** | 0.710405 | 0.661931 | -1.199718 |
| **C** | 0.045311 | 1.21423 | -2.352588 |
| **C** | 0.887462 | 1.795449 | -3.294745 |
| **C** | 2.294465 | 1.837356 | -3.171156 |
| **C** | 2.975418 | 1.310739 | -2.080441 |
| **N** | 2.60584 | 0.148824 | 0.06248 |
| **S** | 1.285773 | -0.3863 | 0.882167 |
| **N** | 0.105539 | 0.069931 | -0.166134 |
| **C** | 11.863493 | 2.690712 | -2.765398 |
| **C** | 11.134733 | 3.025643 | -3.932113 |

| | | | |
|---|---|---|---|
| **C** | 9.775784 | 2.818675 | -3.970026 |
| **C** | 9.087534 | 2.271596 | -2.852102 |
| **C** | 9.820732 | 1.936999 | -1.665175 |
| **C** | 11.226082 | 2.162658 | -1.663541 |
| **C** | 7.69338 | 2.058042 | -2.878216 |
| **C** | 7.010434 | 1.520936 | -1.793444 |
| **C** | 7.753493 | 1.152312 | -0.615915 |
| **C** | 9.124383 | 1.36886 | -0.550474 |
| **C** | 9.855444 | 0.992021 | 0.700661 |
| **C** | 10.123068 | -0.340169 | 0.966351 |
| **C** | 10.836065 | -0.74461 | 2.142697 |
| **C** | 11.320583 | 0.242428 | 2.992008 |
| **C** | 11.04305 | 1.609946 | 2.782761 |
| **C** | 10.280244 | 1.996581 | 1.631772 |
| **C** | 11.493074 | 2.606077 | 3.692919 |
| **C** | 11.195994 | 3.932373 | 3.486415 |
| **C** | 10.430701 | 4.315553 | 2.358344 |
| **C** | 9.986034 | 3.375372 | 1.454729 |
| **O** | 7.147098 | 0.656685 | 0.490611 |
| **O** | 9.700998 | -1.308748 | 0.085736 |
| **C** | 10.658038 | -1.679469 | -0.910513 |
| **C** | 6.308828 | -0.512934 | 0.373842 |
| **C** | 11.115875 | -2.126329 | 2.5168 |
| **C** | 10.392333 | -3.269946 | 2.373602 |
| **C** | 5.594904 | 1.415362 | -1.853271 |
| **C** | 4.382844 | 1.365263 | -1.961729 |
| **C** | 9.039561 | -3.3143 | 1.919439 |
| **C** | 11.013298 | -4.526097 | 2.954672 |
| **N** | 7.913457 | -3.421238 | 1.642111 |
| **O** | 11.848426 | -4.465719 | 3.82972 |
| **O** | 10.617978 | -5.735304 | 2.507122 |
| **H** | -12.994599 | -1.951342 | 0.863393 |

| | | | |
|---|---|---|---|
| **H** | -8.537514 | -2.519899 | -1.331796 |
| **H** | -10.115172 | -4.397691 | -1.194947 |
| **H** | -13.120286 | 0.688355 | 1.73015 |
| **H** | -10.506025 | 4.104279 | 1.63217 |
| **H** | -8.773958 | 2.812689 | 0.463629 |
| **H** | -6.970689 | -1.389028 | 0.267568 |
| **H** | -4.71964 | -1.022414 | -0.666774 |
| **H** | -6.155653 | 2.466182 | -2.734429 |
| **H** | -8.427205 | 2.028884 | -1.888001 |
| **H** | -1.615416 | 1.768225 | -4.612614 |
| **H** | -5.359488 | 1.093843 | -4.66672 |
| **H** | -3.940042 | 1.386339 | -5.684683 |
| **H** | -4.697318 | 2.724733 | -4.821127 |
| **H** | -12.571504 | 5.100215 | 1.862488 |
| **H** | -11.883937 | 4.588791 | 3.419578 |
| **H** | -14.195803 | 4.304824 | 4.337781 |
| **H** | -14.877295 | 4.809794 | 2.795198 |
| **H** | -13.761488 | 7.059221 | 3.040235 |
| **H** | -13.080663 | 6.555111 | 4.579808 |
| **H** | -16.093546 | 6.799874 | 3.979735 |
| **H** | -15.134277 | 7.938784 | 4.938227 |
| **H** | -15.407763 | 6.29232 | 5.530016 |
| **H** | -11.379563 | -5.977923 | -0.090418 |
| **H** | -12.094945 | -5.494571 | -1.643927 |
| **H** | -14.373213 | -6.023459 | -0.749596 |
| **H** | -13.664485 | -6.502064 | 0.789133 |
| **H** | -12.380101 | -8.335565 | -0.374583 |
| **H** | -13.087763 | -7.857939 | -1.910493 |
| **H** | -14.677472 | -8.898135 | 0.516079 |
| **H** | -14.310697 | -9.818829 | -0.951456 |
| **H** | -15.390154 | -8.417237 | -1.030566 |

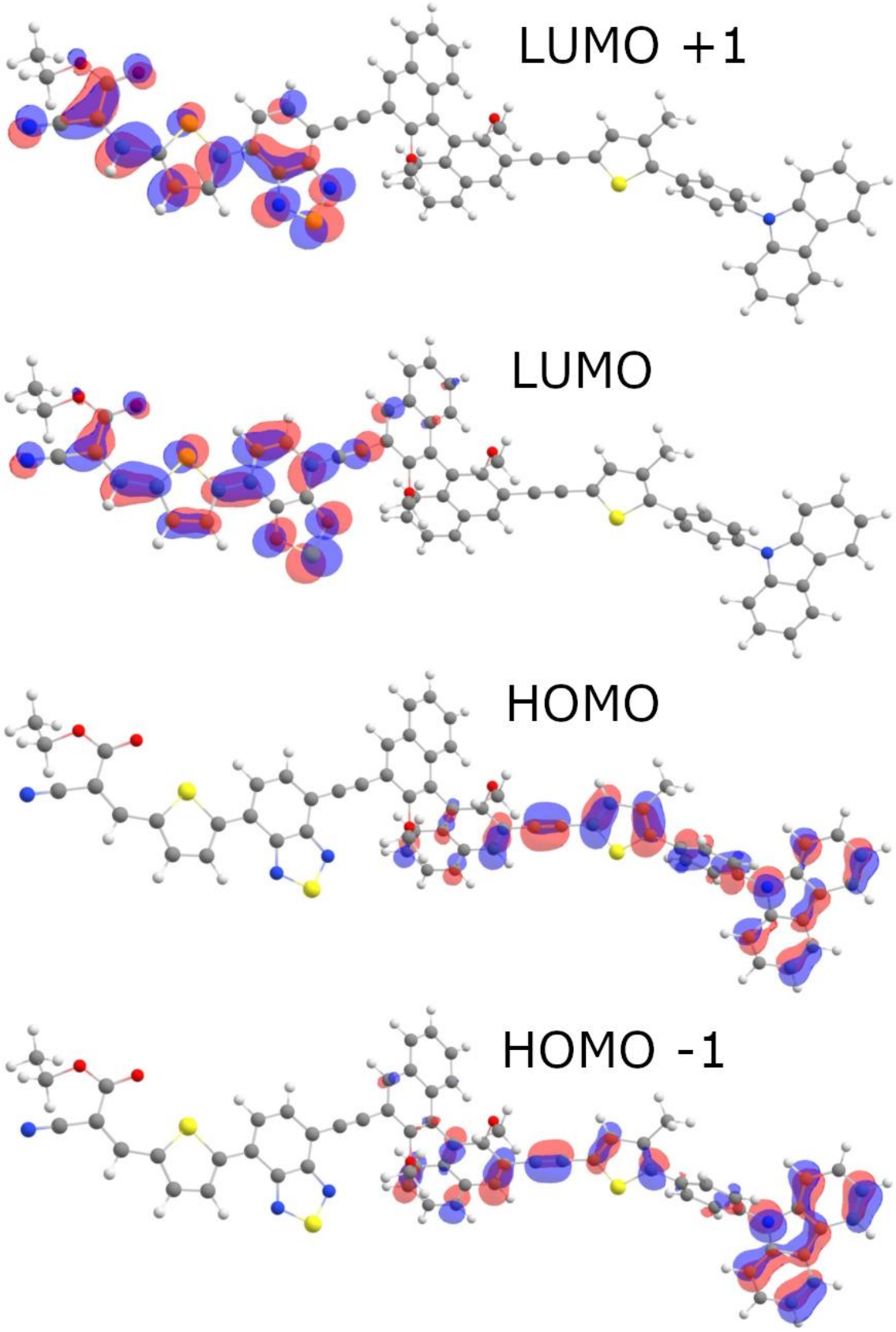


**Figure A202:** Frontier orbitals of **36(*S*)** at B3LYP, 6-31G* level of theory and 0.03 contour value.

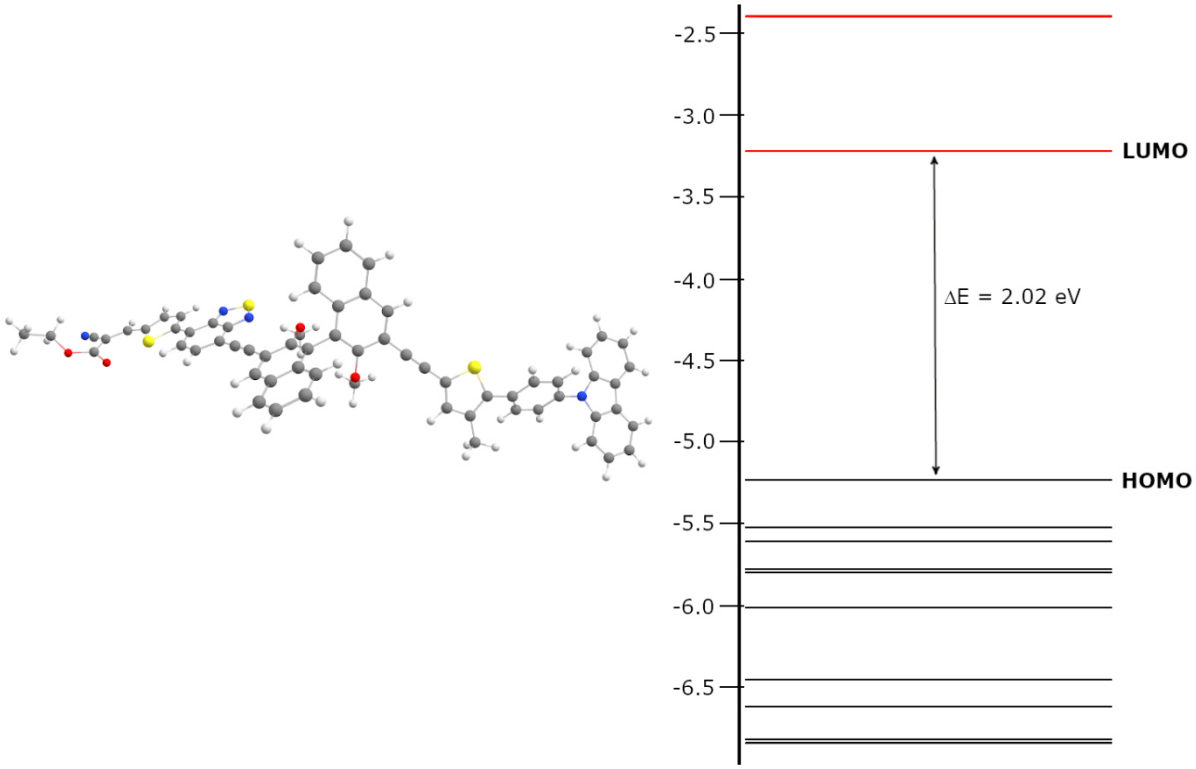


**Figure A203:** Optimized geometry and energy diagram, in eV, of **36(*S*)** at B3LYP, 6-31G* level of theory.

**Table A5:** Cartesian coordinates of **36(*S*)** optimized at B3LYP, 6-31G*, distances in angstrom.

| | | | |
|---|---|---|---|
| **C** | -16.776986 | -2.527563 | -2.81604 |
| **C** | -16.890109 | -2.696943 | -1.43921 |
| **C** | -15.778973 | -2.443058 | -0.626784 |
| **C** | -14.560113 | -2.026278 | -1.219684 |
| **C** | -14.444566 | -1.840234 | -2.600059 |
| **C** | -15.565819 | -2.099152 | -3.385758 |
| **C** | -15.555159 | -2.494866 | 0.802982 |
| **C** | -14.209876 | -2.104771 | 1.023793 |
| **N** | -13.609924 | -1.821641 | -0.210506 |
| **C** | -16.3602 | -2.844193 | 1.89343 |
| **C** | -15.819217 | -2.808037 | 3.175248 |
| **C** | -14.479292 | -2.433927 | 3.374705 |
| **C** | -13.656518 | -2.08094 | 2.307019 |

| | | | |
|---|---|---|---|
| **C** | -12.270992 | -1.397659 | -0.405 |
| **C** | -11.426813 | -2.092467 | -1.280539 |
| **C** | -10.114633 | -1.671518 | -1.474488 |
| **C** | -9.600584 | -0.548899 | -0.798542 |
| **C** | -10.458433 | 0.130479 | 0.087805 |
| **C** | -11.773171 | -0.280138 | 0.278488 |
| **C** | -8.21122 | -0.111123 | -0.993737 |
| **C** | -7.457547 | -0.04864 | -2.155912 |
| **C** | -6.144083 | 0.445796 | -1.922576 |
| **C** | -5.875426 | 0.763703 | -0.606152 |
| **S** | -7.283822 | 0.439319 | 0.389224 |
| **C** | -4.691159 | 1.273136 | -0.049878 |
| **C** | -3.669643 | 1.717597 | 0.444117 |
| **C** | 0.262466 | 5.995123 | -2.229017 |
| **C** | 1.425667 | 6.077088 | -3.032952 |
| **C** | 2.453057 | 5.185122 | -2.839013 |
| **C** | 2.362499 | 4.176505 | -1.839509 |
| **C** | 1.18345 | 4.086715 | -1.027998 |
| **C** | 0.143722 | 5.028552 | -1.255048 |
| **C** | 3.418952 | 3.271731 | -1.613146 |
| **C** | 3.348976 | 2.290507 | -0.629464 |
| **C** | 2.14736 | 2.177956 | 0.155575 |
| **C** | 1.09029 | 3.058809 | -0.035084 |
| **C** | -0.137667 | 2.925547 | 0.812844 |
| **C** | -1.285733 | 2.379681 | 0.268623 |
| **C** | -2.490836 | 2.242764 | 1.038407 |
| **C** | -2.490959 | 2.660021 | 2.361483 |
| **C** | -1.340545 | 3.226842 | 2.955423 |
| **C** | -0.146358 | 3.375931 | 2.175716 |
| **C** | -1.349816 | 3.667005 | 4.307596 |
| **C** | -0.232292 | 4.235916 | 4.872416 |
| **C** | 0.945108 | 4.390144 | 4.102707 |

| | | | |
|---|---|---|---|
| **C** | 0.986602 | 3.971185 | 2.790671 |
| **O** | 2.019833 | 1.266916 | 1.161676 |
| **O** | -1.304157 | 2.018811 | -1.058284 |
| **C** | -1.171931 | 0.619597 | -1.316388 |
| **C** | 2.311632 | -0.117045 | 0.920483 |
| **C** | 4.492616 | 1.482883 | -0.393435 |
| **C** | 5.515436 | 0.838945 | -0.237403 |
| **C** | 6.77087 | -0.985881 | 0.895129 |
| **C** | 7.9991 | -1.739946 | 1.092282 |
| **C** | 9.190967 | -1.423062 | 0.339356 |
| **C** | 9.062427 | -0.366212 | -0.556222 |
| **C** | 7.871956 | 0.367813 | -0.749505 |
| **C** | 6.702802 | 0.099536 | -0.048848 |
| **N** | 5.756384 | -1.399578 | 1.656702 |
| **S** | 6.323725 | -2.650234 | 2.556889 |
| **N** | 7.871123 | -2.706988 | 2.007086 |
| **C** | 10.440718 | -2.153361 | 0.499735 |
| **C** | 10.736066 | -3.180236 | 1.391225 |
| **C** | 12.047455 | -3.653906 | 1.257833 |
| **C** | 12.799518 | -3.010186 | 0.273818 |
| **S** | 11.817289 | -1.795416 | -0.525617 |
| **C** | 14.16722 | -3.355463 | 0.048655 |
| **C** | 15.189593 | -2.823031 | -0.70068 |
| **C** | 16.439261 | -3.515808 | -0.656546 |
| **C** | 15.036868 | -1.651246 | -1.614619 |
| **N** | 17.452471 | -4.091438 | -0.632189 |
| **O** | 13.972665 | -1.396104 | -2.143519 |
| **O** | 16.101321 | -0.8743 | -1.895597 |
| **H** | -17.632118 | -2.722837 | -3.456791 |
| **H** | -17.830488 | -3.017619 | -0.998461 |
| **H** | -13.516901 | -1.499134 | -3.047397 |
| **H** | -15.499511 | -1.962784 | -4.461798 |

| | | | |
|---|---|---|---|
| **H** | -17.39336 | -3.144473 | 1.739081 |
| **H** | -16.434598 | -3.07559 | 4.029453 |
| **H** | -14.07158 | -2.42143 | 4.381885 |
| **H** | -12.620121 | -1.804485 | 2.469611 |
| **H** | -11.795682 | -2.978757 | -1.787135 |
| **H** | -9.466522 | -2.247023 | -2.126911 |
| **H** | -10.097862 | 1.013198 | 0.608104 |
| **H** | -12.428156 | 0.276546 | 0.941162 |
| **C** | -7.943749 | -0.401778 | -3.539283 |
| **H** | -5.411115 | 0.585678 | -2.709986 |
| **H** | -0.546439 | 6.704137 | -2.383138 |
| **H** | 1.502534 | 6.845258 | -3.797289 |
| **H** | 3.354758 | 5.236957 | -3.444609 |
| **H** | -0.753674 | 4.977219 | -0.648859 |
| **H** | 4.325238 | 3.353232 | -2.206488 |
| **H** | -3.399437 | 2.561761 | 2.948868 |
| **H** | -2.262463 | 3.546568 | 4.88643 |
| **H** | -0.250748 | 4.569496 | 5.906299 |
| **H** | 1.825059 | 4.842919 | 4.55156 |
| **H** | 1.894994 | 4.094249 | 2.211152 |
| **H** | -1.222464 | 0.50574 | -2.401502 |
| **H** | -1.983344 | 0.047743 | -0.85197 |
| **H** | -0.205927 | 0.245066 | -0.955252 |
| **H** | 1.603016 | -0.681598 | 1.53317 |
| **H** | 3.333051 | -0.365141 | 1.215879 |
| **H** | 2.162063 | -0.375274 | -0.134067 |
| **H** | 9.922872 | -0.070335 | -1.149021 |
| **H** | 7.872916 | 1.177527 | -1.471735 |
| **H** | 10.016638 | -3.562639 | 2.101166 |
| **H** | 12.465635 | -4.446139 | 1.870875 |
| **H** | 14.458416 | -4.22096 | 0.642325 |
| **C** | 17.264289 | -0.747955 | -1.038855 |

| | | | |
|---|---|---|---|
| **H** | -9.029617 | -0.305183 | -3.624927 |
| **H** | -7.680363 | -1.431658 | -3.814755 |
| **H** | -7.485221 | 0.256932 | -4.284705 |
| **C** | 17.777713 | 0.673096 | -1.192035 |
| **H** | 18.013607 | -1.480194 | -1.349637 |
| **H** | 16.983969 | -0.957962 | -0.001489 |
| **H** | 18.031277 | 0.880329 | -2.236108 |
| **H** | 18.678767 | 0.807516 | -0.583341 |
| **H** | 17.024714 | 1.398181 | -0.868351 |

# 6. References


1. a) Sanvito, S., Molecular Spintronics. *Chem. Soc. Rev.* **2011**, *40* (6), 3336-3355; b) Troiani, F.; Affronte, M., Molecular Spins for Quantum Information Technologies. *Chem. Soc. Rev.* **2011**, *40* (6), 3119-3129; c) Liu, X.; Hersam, M. C., 2D Materials for Quantum Information Science. *Nat. Rev. Mater.* **2019**, *4* (10), 669-684; d) Wasielewski, M. R.; Forbes, M. D. E.; Frank, N. L.; Kowalski, K.; Scholes, G. D.; Yuen-Zhou, J.; Baldo, M. A.; Freedman, D. E.; Goldsmith, R. H.; Goodson, T.; Kirk, M. L.; McCusker, J. K.; Ogilvie, J. P.; Shultz, D. A.; Stoll, S.; Whaley, K. B., Exploiting Chemistry and Molecular Systems for Quantum Information Science. *Nat. Rev. Chem.* **2020**, *4* (9), 490-504.

2. a) Barla, P.; Joshi, V. K.; Bhat, S., Spintronic Devices: A Promising Alternative to CMOS Devices. *J. Comput. Electron.* **2021**; b) Ivanov, K. L.; Wagenpfahl, A.; Deibel, C.; Matysik, J., Spin-Chemistry Concepts for Spintronics Scientists. *Beilstein J. Nanotechnol.* **2017**, *8*, 1427-1445; c) Joshi, V. K., Spintronics: A Contemporary Review of Emerging Electronics Devices. *Eng. Sci. Technol. an Int. J.* **2016**, *19* (3), 1503-1513; d) Lin, X.; Yang, W.; Wang, K. L.; Zhao, W., Two-Dimensional Spintronics for Low-Power Electronics. *Nat. Electron.* **2019**, *2* (7), 274-283.

3. a) Binasch, G.; Grünberg, P.; Saurenbach, F.; Zinn, W., Enhanced Magnetoresistance in Layered Magnetic Structures with Antiferromagnetic Interlayer Exchange. *Phys. Rev. B* **1989**, *39* (7), 4828-4830; b) Chappert, C.; Fert, A.; Van Dau, F. N., The Emergence of Spin Electronics in Data Storage. *Nat. Mater.* **2007**, *6* (11), 813-823; c) Ennen, I.; Kappe, D.; Rempel, T.; Glenske, C.; Huetten, A., Giant Magnetoresistance: Basic Concepts, Microstructure, Magnetic Interactions and Applications. *Sensors* **2016**, *16* (6), 904/901-904/924; d) Levy, P. M.; Zhang, S.; Fert, A., Electrical Conductivity of Magnetic Multilayered Structures. *Phys. Rev. Lett.* **1990**, *65* (13), 1643-1646; e) Sun, D.; Yin, L.; Sun, C.; Guo, H.; Gai, Z.; Zhang, X. G.; Ward, T. Z.; Cheng, Z.; Shen, J., Giant Magnetoresistance in Organic Spin Valves. *Phys. Rev. Lett.* **2010**, *104* (23), 236602/236601-236602/236604; f) Valet, T.; Fert, A., Theory of the Perpendicular Magnetoresistance in Magnetic Multilayers. *Phys. Rev. B* **1993**, *48* (10), 7099-7113.

4. Waldrop, M. M., The Chips are Down for Moore's Law. *Nature* **2016**, *530* (7589), 144-147.

5. Göhler, B.; Hamelbeck, V.; Markus, T. Z.; Kettner, M.; Hanne, G. F.; Vager, Z.; Naaman, R.; Zacharias, H., Spin Selectivity in Electron Transmission Through Self-Assembled Monolayers of Double-Stranded DNA. *Science* **2011**, *331* (6019), 894-897.

6. a) Michaeli, K.; Kantor-Uriel, N.; Naaman, R.; Waldeck, D. H., The Electron's Spin and Molecular Chirality - How are They Related and How do They Affect Life Processes? *Chem. Soc. Rev.* **2016**, *45* (23), 6478-6487; b) Naaman, R.; Paltiel, Y.; Waldeck, D. H., Chiral Molecules and the Electron Spin. *Nat. Rev. Chem.* **2019**, *3* (4), 250-260; c) Naaman, R.; Waldeck, D. H., Chiral-Induced Spin Selectivity Effect. *J. Phys. Chem. Lett.* **2012**, *3* (16), 2178-2187.

7. Ray, K.; Ananthavel, S. P.; Waldeck, D. H.; Naaman, R., Asymmetric Scattering of Polarized Electrons by Organized Organic Films of Chiral Molecules. *Science* **1999**, *283* (5403), 814-816.

8. Naaman, R.; Waldeck, D. H., Spintronics and Chirality: Spin Selectivity in Electron Transport Through Chiral Molecules. *Annu. Rev. Phys. Chem.* **2015**, *66* (1), 263-281.

9. Mishra, S.; Mondal, A. K.; Pal, S.; Das, T. K.; Smolinsky, E. Z. B.; Siligardi, G.; Naaman, R., Length-Dependent Electron Spin Polarization in Oligopeptides and DNA. *J. Phys. Chem. C* **2020**, *124* (19), 10776-10782.

10. Kulkarni, C.; Mondal, A. K.; Das, T. K.; Grinbom, G.; Tassinari, F.; Mabesoone, M. F. J.; Meijer, E. W.; Naaman, R., Highly Efficient and Tunable Filtering of Electrons' Spin by Supramolecular Chirality of Nanofiber-Based Materials. *Adv. Mater.* **2020**, *32* (7), 1904965/1904961-1904965/1904967.

11. Senthil Kumar, K.; Kantor-Uriel, N.; Mathew, S. P.; Guliamov, R.; Naaman, R., A Device for Measuring Spin Selectivity in Electron Transfer. *Phys. Chem. Chem. Phys.* **2013**, *15* (42), 18357-18362.

12. Mathew, S. P.; Mondal, P. C.; Moshe, H.; Mastai, Y.; Naaman, R., Non-Magnetic Organic/Inorganic Spin Injector at Room Temperature. *Appl. Phys. Lett.* **2014**, *105* (24), 242408/242401-242408/242404.

13. a) Moshe, H.; Levi, G.; Sharon, D.; Mastai, Y., Atomic Layer Deposition of Enantioselective Thin Film of Alumina on Chiral Self-Assembled-Monolayer. *Surf. Sci.* **2014**, *629*, 88-93; b) Moshe, H.; Vanbel, M.; Valev, V. K.; Verbiest, T.; Dressler, D.; Mastai, Y., Chiral Thin Films of Metal Oxide. *Chem. Eur. J.* **2013**, *19* (31), 10295-10301.

14. Rugg, B. K.; Phelan, B. T.; Horwitz, N. E.; Young, R. M.; Krzyaniak, M. D.; Ratner, M. A.; Wasielewski, M. R., Spin-Selective Photoreduction of a Stable Radical Within a Covalent Donor–Acceptor–Radical Triad. *J. Am. Chem. Soc.* **2017**, *139* (44), 15660-15663.

15. a) Mulliken, R. S., Forces Intermoléculaires de Transfert de Charge. *J. Chim. Phys.* **1954**, *51*, 341-344; b) Ouyang, X.; Li, X.-L.; Zhang, X.; Islam, A.; Ge, Z.; Su, S.-J., Effective Management of Intramolecular Charge Transfer to Obtain from Blue to Violet-Blue OLEDs Based on a Couple of Phenanthrene Isomers. *Dyes Pigm.* **2015**, *122*, 264-271; c) Misra, R.; Bhattacharyya, S. P., *Intramolecular Charge Transfer: Theory and Application*. Wiley-VCH: **2018**; d) Tamura, H.; Burghardt, I., Potential Barrier and Excess Energy for Electron–Hole Separation from the Charge-Transfer Exciton at Donor–Acceptor Heterojunctions of Organic Solar Cells. *J. Phys. Chem. C* **2013**, *117* (29), 15020-15025.

16. a) Chernick, E. T.; Mi, Q.; Kelley, R. F.; Weiss, E. A.; Jones, B. A.; Marks, T. J.; Ratner, M. A.; Wasielewski, M. R., Electron Donor−Bridge−Acceptor Molecules with Bridging Nitronyl Nitroxide Radicals: Influence of a Third Spin on Charge- and Spin-Transfer Dynamics. *J. Am. Chem. Soc.* **2006**, *128* (13), 4356-4364; b) Weiss, E. A.; Chernick, E. T.; Wasielewski, M. R., Modulation of Radical

Ion Pair Lifetimes by the Presence of a Third Spin in Rodlike Donor−Acceptor Triads. *J. Am. Chem. Soc.* **2004**, *126* (8), 2326-2327.

17. Voet, D.; Voet, J. G., *Biochemistry*. 4. ed.; Wiley: Hoboken, **2011**.

18. a) Vlček, A., Mechanistic Roles of Metal-to-Ligand Charge-Transfer Excited States in Organometallic Photochemistry. *Coord. Chem. Rev.* **1998**, *177* (1), 219-256; b) Vogler, A.; Kunkely, H., Photochemistry Induced by Metal-to-Ligand Charge Transfer Excitation. *Coord. Chem. Rev.* **2000**, *208* (1), 321-329; c) Zhao, R.; Shi, L., A Renaissance of Ligand-to-Metal Charge Transfer by Cerium Photocatalysis. *Org. Chem. Front.* **2018**, *5* (20), 3018-3021; d) Mulliken, R. S.; Person, W. B., *Molecular Complexes A Lecture and Reprint Volume*. Wiley-Interscience: New York, **1969**.

19. a) Mulliken, R. S., Report on Notation for the Spectra of Polyatomic Molecules. *J. Chem. Phys.* **1955**, *23* (11), 1997-2011; b) Mulliken, R. S., Lewis Acids and Bases and Molecular Complexes. *J. Chem. Phys.* **1951**, *19* (4), 514-515; c) Mulliken, R. S., Molecular Compounds and Their Spectra. II. *J. Am. Chem. Soc.* **1952**, *74* (3), 811-824; d) Mulliken, R. S., Overlap Integrals and Chemical Binding. *J. Am. Chem. Soc.* **1950**, *72* (10), 4493-4503; e) Mulliken, R. S., Molecular Compounds and Their Spectra. III. The Interaction of Electron Donors and Acceptors. *J. Phys. Chem.* **1952**, *56* (7), 801-822.

20. a) Grabowski, Z. R.; Rotkiewicz, K.; Rettig, W., Structural Changes Accompanying Intramolecular Electron Transfer: Focus on Twisted Intramolecular Charge-Transfer States and Structures. *Chem. Rev.* **2003**, *103* (10), 3899-4032; b) Cetin, M. M.; Beldjoudi, Y.; Roy, I.; Anamimoghadam, O.; Bae, Y. J.; Young, R. M.; Krzyaniak, M. D.; Stern, C. L.; Philp, D.; Alsubaie, F. M.; Wasielewski, M. R.; Stoddart, J. F., Combining Intra- and Intermolecular Charge Transfer with Polycationic Cyclophanes To Design 2D Tessellations. *J. Am. Chem. Soc.* **2019**, *141* (47), 18727-18739; c) Verhoeven, J. W.; Dirkx, I. P.; De Boer, T. J., Studies of Inter- and Intra-Molecular Donor-Acceptor Interactions—IV: Intramolecular Charge Transfer Phenomena in Substituted N-Aralkyl-Pyridinium Ions. *Tetrahedron* **1969**, *25* (17), 4037-4055; d) Goetz, K. P.; Vermeulen, D.; Payne, M. E.; Kloc, C.; McNeil, L. E.; Jurchescu, O. D., Charge-Transfer Complexes: New Perspectives on an Old Class of Compounds. *J. Mater. Chem. C* **2014**, *2* (17), 3065-3076.

21. Ferraris, J.; Cowan, D. O.; Walatka, V.; Perlstein, J. H., Electron Transfer in a New Highly Conducting Donor-Acceptor Complex. *J. Am. Chem. Soc.* **1973**, *95* (3), 948-949.

22. a) Jones, G.; Lu, L. N.; Fu, H.; Farahat, C. W.; Oh, C.; Greenfield, S. R.; Gosztola, D. J.; Wasielewski, M. R., Intramolecular Electron Transfer Across Amino Acid Spacers in the Picosecond Time Regime. Charge-Transfer Interaction through Peptide Bonds. *J. Phys. Chem. B* **1999**, *103* (3), 572-581; b) Jones, G.; Lu, L. N.; Vullev, V.; Gosztola, D. J.; Greenfield, S. R.; Wasielewski, M. R., Photoinduced Electron Transfer for Pyrenesulfonamide Conjugates of Tryptophan-Containing Peptides. Mitigation of Fluoroprobe Behavior in *N*-Terminal Labeling Experiments. *Bioorg. Med. Chem. Lett.* **1995**, *5* (20), 2385-2390; c) Li, Q.; Hu, J.; Lv, J.; Wang, X.; Shao, S.; Wang, L.; Jing, X.; Wang, F., Through-Space Charge-Transfer Polynorbornenes with Fixed and Controllable Spatial Alignment of Donor

and Acceptor for High-Efficiency Blue Thermally Activated Delayed Fluorescence. *Angew. Chem. Int. Ed.* **2020**, *59* (45), 20174-20182; d) Li, Q.; Hu, J.; Lv, J.; Wang, X.; Shao, S.; Wang, L.; Jing, X.; Wang, F., Through-Space Charge-Transfer Polynorbornenes with Fixed and Controllable Spatial Alignment of Donor and Acceptor for High-Efficiency Blue Thermally Activated Delayed Fluorescence. *Angew. Chem. Germ. Ed.* **2020**, *132* (45), 20349-20357.

23. a) Haberhauer, G., Planarized and Twisted Intramolecular Charge Transfer: A Concept for Fluorophores Showing Two Independent Rotations in Excited State. *Chem. Eur. J.* **2017**, *23* (39), 9288-9296; b) Il'ichev, Y. V.; Kühnle, W.; Zachariasse, K. A., Intramolecular Charge Transfer in Dual Fluorescent 4-(Dialkylamino)benzonitriles. Reaction Efficiency Enhancement by Increasing the Size of the Amino and Benzonitrile Subunits by Alkyl Substituents. *J. Phys. Chem. A* **1998**, *102* (28), 5670-5680; c) Misra, R.; Bhattacharyya, S. P., Introduction. In *Intramolecular Charge Transfer*, Wiley VCH: **2018**; pp 1-27.

24. Misra, R.; Bhattacharyya, S. P., Brief History of ICT Molecules. In *Intramolecular Charge Transfer*, Wiley VCH: **2018**; pp 29-69.

25. a) Franck, J.; Dymond, E. G., Elementary Processes of Photochemical Reactions. *Trans. Faraday Soc.* **1926**, *21* (February), 536–542; b) Condon, E., A Theory of Intensity Distribution in Band Systems. *Phys. Rev.* **1926**, *28* (6), 1182–1201; c) Condon, E. U., Nuclear Motions Associated with Electron Transitions in Diatomic Molecules. *Phys. Rev.* **1928**, *32* (6), 858–872.

26. Kasha, M., Characterization of Electronic Transitions in Complex Molecules. *Discuss. Faraday Soc.* **1950**, *9* (0), 14-19.

27. a) Berezin, M. Y.; Achilefu, S., Fluorescence Lifetime Measurements and Biological Imaging. *Chem. Rev.* **2010**, *110* (5), 2641-2684; b) Lichtman, J. W.; Conchello, J.-A., Fluorescence Microscopy. *Nat. Methods* **2005**, *2* (12), 910-919.

28. Gómez, I.; Castro, P. J.; Reguero, M., Insight into the Mechanisms of Luminescence of Aminobenzonitrile and Dimethylaminobenzonitrile in Polar Solvents. An ab Initio Study. *J. Phys. Chem. A* **2015**, *119* (10), 1983-1995.

29. a) Berera, R.; van Grondelle, R.; Kennis, J. T. M., Ultrafast Transient Absorption Spectroscopy: Principles and Application to Photosynthetic Systems. *Photosynth. Res.* **2009**, *101* (2-3), 105-118; b) Schenter, G. K.; Duke, C. B., Theory of Photoinduced Twisting Dynamics in Polar Solvents: Application to dimethylaminobenzonitrile in Propanol at Low Temperatures. *Chem. Phys. Lett.* **1991**, *176* (6), 563-570; c) Wang, Y.; McAuliffe, M.; Novak, F.; Eisenthal, K. B., Picosecond Dynamics of Twisted Internal Charge-Transfer Phenomena. *J. Phys. Chem.* **1981**, *85* (25), 3736-3739; d) Okamoto, H.; Inishi, H.; Nakamura, Y.; Kohtani, S.; Nakagaki, R., Picosecond Infrared Spectra of Isotope-Substituted 4-(Dimethylamino)benzonitriles and Molecular Structure of the Charge-Transfer Singlet Excited State. *J. Phys. Chem. A* **2001**, *105* (17), 4182-4188; e) Marcus, R. A., Chemical and Electrochemical Electron-Transfer Theory. *Annu. Rev. Phys. Chem.* **1964**, *15* (1), 155-196; f) Marcus, R. A., On the Theory of Electron-Transfer Reactions. VI. Unified Treatment for Homogeneous and Electrode Reactions. *J. Chem. Phys.* **1965**, *43* (2), 679-701; g) Marcus, R. A., On the Theory of

Chemiluminescent Electron-Transfer Reactions. *J. Chem. Phys.* **1965**, *43* (8), 2654-2657; h) Marcus, R. A., Electrostatic Free Energy and Other Properties of States Having Nonequilibrium Polarization. I. *J. Chem. Phys.* **1956**, *24* (5), 979-989; i) Marcus, R. A., On the Theory of Oxidation-Reduction Reactions Involving Electron Transfer. I. *J. Chem. Phys.* **1956**, *24* (5), 966-978.

30. a) Lippert, E., Dipolmoment und Elektronenstruktur von Angeregten Molekülen. *Z. Naturforsch.* **1955**, *10a*, 541-545; b) Lippert, E.; Lueder, W.; Moll, F.; Naegele, W.; Boos, H.; Prigge, H.; Seibold-Blankenstein, I., Umwandlung von Elektronenanregungsenergie. *Angew. Chem.* **1961**, *73*, 695-706.

31. Kalcic, C.; Harris, D.; Dantus, M., Controlling the Excited State Charge Transfer in DMABN Using Shaped Femtosecond Pulses. *Conference on Quantum Electronics and Laser Science (QELS) - Technical Digest Series* **2007**.

32. Foerster, T., Farbe und Konstitution Organischer Verbindungen vom Standpunkt der Modernen Physikalischen Theorie. *Z. Elektrochem. angew. phys. Chem.* **1939**, *45*, 548-573.

33. Arrhenius, S., Über die Reaktionsgeschwindigkeit bei der Inversion von Rohrzucker durch Säuren. *Z. Phys. Chem.* **1889**, *4U* (1), 226-248.

34. a) Misra, R.; Bhattacharyya, S. P., New Theoretical and Experimental Techniques for Studying the ICT Process. In *Intramolecular Charge Transfer*, Wiley VCH: **2018**; pp 71-113; b) Zachariasse, K. A., Comment on “Pseudo-Jahn–Teller and TICT-Models: a Photophysical Comparison of *Meta*-and *Para*-DMABN Derivatives” [Chem. Phys. Lett. 305 (1999) 8]: The PICT Model for Dual Fluorescence of Aminobenzonitriles. *Chem. Phys. Lett.* **2000**, *320* (1), 8-13.

35. a) Lewis, F. D.; Holman, B., Singlet States of Benzonitrile and *p*-Dimethylaminobenzonitrile. *J. Phys. Chem.* **1980**, *84* (18), 2326-2328; b) Sobolewski, A. L.; Domcke, W., Promotion of Intramolecular Charge Transfer in Dimethylamino Derivatives: Twisting Versus Acceptor-Group Rehybridization. *Chem. Phys. Lett.* **1996**, *259* (1), 119-127.

36. a) Rotkiewicz, K.; Grellmann, K. H.; Grabowski, Z. R., Reinterpretation of the Anomalous Fluorescense of *p*-*N*,*N*-Dimethylamino-Benzonitrile. *Chem. Phys. Lett.* **1973**, *19* (3), 315-318; b) Rettig, W., Charge Separation in Excited States of Decoupled Systems—TICT Compounds and Implications Regarding the Development of New Laser Dyes and the Primary Process of Vision and Photosynthesis. *Angew. Chem. Int. Ed.* **1986**, *25* (11), 971-988; c) Rettig, W., Ladungstrennung in Angeregten Zuständen Entkoppelter Systeme – TICT-Verbindungen und Implikationen für die Entwicklung Neuer Laserfarbstoffe sowie für den Primärprozeß von Sehvorgang und Photosynthese. *Angew. Chem. Germ. Ed.* **1986**, *98* (11), 969 - 986; d) Sasaki, S.; Drummen, G. P. C.; Konishi, G.-i., Recent Advances in Twisted Intramolecular Charge Transfer (TICT) Fluorescence and Related Phenomena in Materials Chemistry. *J. Mater. Chem. C* **2016**, *4* (14), 2731-2743.

37. Coto, P. B.; Serrano-Andrés, L.; Gustavsson, T.; Fujiwara, T.; Lim, E. C., Intramolecular Charge Transfer and Dual Fluorescence of 4-

(Dimethylamino)benzonitrile: Ultrafast Branching Followed by a Two-Fold Decay Mechanism. *Phys. Chem. Chem. Phys.* **2011**, *13* (33), 15182-15188.

38. Yoshihara, T.; Druzhinin, S. I.; Zachariasse, K. A., Fast Intramolecular Charge Transfer with a Planar Rigidized Electron Donor/Acceptor Molecule. *J. Am. Chem. Soc.* **2004**, *126* (27), 8535-8539.

39. a) Segado, M.; Gómez, I.; Reguero, M., Intramolecular Charge Transfer in Aminobenzonitriles and Tetrafluoro Counterparts: Fluorescence Explained by Competition Between Low-Lying Excited States and Radiationless Deactivation. Part I: A Mechanistic Overview of the Parent System ABN. *Phys. Chem. Chem. Phys.* **2016**, *18* (9), 6861-6874; b) Segado, M.; Mercier, Y.; Gómez, I.; Reguero, M., Intramolecular Charge Transfer in Aminobenzonitriles and Tetrafluoro Counterparts: Fluorescence Explained by Competition Between Low Lying Excited States and Radiationless Deactivation. Part II: Influence of Substitution on Luminescence Patterns. *Phys. Chem. Chem. Phys.* **2016**, *18* (9), 6875-6884.

40. Zhong, C., The Driving Forces for Twisted or Planar Intramolecular Charge Transfer. *Phys. Chem. Chem. Phys.* **2015**, *17* (14), 9248-9257.

41. a) Myers, A. B., Resonance Raman Intensities and Charge-Transfer Reorganization Energies. *Chem. Rev.* **1996**, *96* (3), 911-926; b) Okamoto, H.; Kinoshita, M.; Kohtani, S.; Nakagaki, R.; Zachariasse, K. A., Picosecond Infrared Spectra and Structure of Locally Excited and Charge Transfer Excited States of Isotope-Labeled 4-(Dimethylamino)benzonitriles. *Bull. Chem. Soc. Jpn.* **2002**, *75* (5), 957-963.

42. a) Farr, E. P.; Quintana, J. C.; Reynoso, V.; Ruberry, J. D.; Shin, W. R.; Swartz, K. R., Introduction to Time-Resolved Spectroscopy: Nanosecond Transient Absorption and Time-Resolved Fluorescence of Eosin B. *J. Chem. Educ.* **2018**, *95* (5), 864-871; b) Samuel, A. P. S.; Co, D. T.; Stern, C. L.; Wasielewski, M. R., Ultrafast Photodriven Intramolecular Electron Transfer from a Zinc Porphyrin to a Readily Reduced Diiron Hydrogenase Model Complex. *J. Am. Chem. Soc.* **2010**, *132* (26), 8813-8815; c) Vagnini, M. T.; Smeigh, A. L.; Blakemore, J. D.; Eaton, S. W.; Schley, N. D.; D'Souza, F.; Crabtree, R. H.; Brudvig, G. W.; Co, D. T.; Wasielewski, M. R., Ultrafast Photodriven Intramolecular Electron Transfer From an Iridium-Based Water-Oxidation Catalyst to Perylene Diimide Derivatives. *Proc. Natl. Acad. Sci. U.S.A.* **2012**, *109* (39), 15651-15656.

43. a) Smidt, J.; Hafner, W., Eine Reaktion von Palladiumchlorid mit Allylalkohol. *Angew. Chem. Germ. Ed.* **1959**, *71* (8), 284-284; b) Lindlar, H., Ein neuer Katalysator für selektive Hydrierungen. *Helv. Chim. Acta* **1952**, *35* (2), 446-450; c) Liu, X.; Astruc, D., Development of the Applications of Palladium on Charcoal in Organic Synthesis. *Adv. Synth. Catal.* **2018**, *360* (18), 3426-3459.

44. a) Mahdavi, A. F.; Reynolds, J. L., The Wurtz Cross-Coupling Reaction Revisited. *Main Group Met. Chem.* **1994**, *17* (6), 399-402; b) Wurtz, A., Ueber eine Neue Klasse Organischer Radicale. *Justus Liebigs Ann. Chem.* **1855**, *96* (3), 364–375; c) Fittig, R., Ueber das Monobrombenzol. *Justus Liebigs Ann. Chem.* **1862**, *121* (3), 361–365; d) Tollens, B.; Fittig, R., Ueber die Synthese der Kohlenwasserstoffe der Benzolreihe. *Justus Liebigs Ann. Chem.* **1864**, *131* (3),

303–323; e) Tollens, B.; Fittig, R., Vorläufige Notiz über Gemischte Alkoholradicale der Aethyl- und Phenylreihe. *Justus Liebigs Ann. Chem.* **1864**, *129* (3), 369–370; f) Grignard, V., Sur Quelques Nouvelles Combinaisons Organométalliques du Magnèsium et Leur Application à des Synthèses d'Alcools et d'Hydrocarbures. *C.R. Hebd. Séances Acad. Sci.* **1900**, *130*, 1322–1324.

45. a) Johansson Seechurn, C. C. C.; Kitching, M. O.; Colacot, T. J.; Snieckus, V., Palladium-Catalyzed Cross-Coupling: A Historical Contextual Perspective to the 2010 Nobel Prize. *Angew. Chem. Int. Ed.* **2012**, *51* (21), 5062-5085; b) Johansson Seechurn, C. C. C.; Kitching, M. O.; Colacot, T. J.; Snieckus, V., Palladiumkatalysierte Kreuzkupplungen: Eine Historische Perspektive im Kontext der Nobel-Preise 2010. *Angew. Chem. Germ. Ed.* **2012**, *124* (21), 5150-5174; c) Seyferth, D., Alkyl and Aryl Derivatives of the Alkali Metals: Useful Synthetic Reagents as Strong Bases and Potent Nucleophiles. 1. Conversion of Organic Halides to Organoalkali-Metal Compounds. *Organometallics* **2006**, *25* (1), 2-24; d) Glaser, C., Beiträge zur Kenntniss des Acetenylbenzols. *Ber. Dtsch. Chem. Ges.* **1869**, *2* (1), 422–424; e) Glaser, C., Untersuchungen über einige Derivate der Zimmtsäure. *Justus Liebigs Ann. Chem.* **1870**, *154* (2), 137–171; f) Siemsen, P.; Livingston, R. C.; Diederich, F., Acetylenic Coupling: A Powerful Tool in Molecular Construction. *Angew. Chem. Int. Ed.* **2000**, *39* (15), 2632-2657; g) Siemsen, P.; Livingston, R. C.; Diederich, F., Acetylenkupplungen: Eine Leistungsfähige Methode für den Aufbau von Molekülen. *Angew. Chem. Germ. Ed.* **2000**, *112* (15), 2740-2767; h) Hassan, J.; Sévignon, M.; Gozzi, C.; Schulz, E.; Lemaire, M., Aryl−Aryl Bond Formation One Century after the Discovery of the Ullmann Reaction. *Chem. Rev.* **2002**, *102* (5), 1359-1470; i) Tao, Y.-M.; Li, H.-Y.; Xu, Q.-L.; Zhu, Y.-C.; Kang, L.-C.; Zheng, Y.-X.; Zuo, J.-L.; You, X.-Z., Synthesis and Characterization of Efficient Luminescent Materials Based on 2,1,3-Benzothiadiazole with Carbazole Moieties. *Synth. Met.* **2011**, *161* (9), 718-723; j) Ullmann, F.; Bielecki, J., Ueber Synthesen in der Biphenylreihe. *Ber. Dtsch. Chem. Ges.* **1901**, *34* (2), 2174–2185.

46. a) Heck, R. F., Acylation, Methylation, and Carboxyalkylation of Olefins by Group VIII Metal Derivatives. *J. Am. Chem. Soc.* **1968**, *90* (20), 5518-5526; b) Heck, R. F., The Arylation of Allylic Alcohols with Organopalladium Compounds. A New Synthesis of 3-Aryl Aldehydes and Ketones. *J. Am. Chem. Soc.* **1968**, *90* (20), 5526-5531; c) Heck, R. F., The Palladium-Catalyzed Arylation of Enol Esters, Ethers, and Halides. A New Synthesis of 2-Aryl Aldehydes and Ketones. *J. Am. Chem. Soc.* **1968**, *90* (20), 5535-5538.

47. a) Heck, R. F.; Nolley, J. P., Palladium-Catalyzed Vinylic Hydrogen Substitution Reactions with Aryl, Benzyl, and Styryl Halides. *J. Org. Chem.* **1972**, *37* (14), 2320-2322; b) Tsutomu, M.; Kunio, M.; Atsumu, O., Arylation of Olefin With Aryl Iodide Catalyzed by Palladium. *Bull. Chem. Soc. Jpn.* **1971**, *44* (2), 581-581.

48. a) Cordovilla, C.; Bartolomé, C.; Martínez-Ilarduya, J. M.; Espinet, P., The Stille Reaction, 38 Years Later. *ACS Catal.* **2015**, *5* (5), 3040-3053; b) Mee, S. P. H.; Lee, V.; Baldwin, J. E., Significant Enhancement of the Stille Reaction with a New Combination of Reagents—Copper(I) Iodide with Cesium Fluoride. *Chem. Eur. J.* **2005**, *11* (11), 3294-3308; c) Yin; Liebscher, J., Carbon−Carbon Coupling Reactions Catalyzed by Heterogeneous Palladium Catalysts. *Chem. Rev.* **2007**, *107* (1), 133-173; d) Kanwal, I.; Mujahid, A.; Rasool, N.; Rizwan, K.; Malik, A.;

Ahmad, G.; Shah, S. A. A.; Rashid, U.; Nasir, N. M., Palladium and Copper Catalyzed Sonogashira Cross Coupling Has Been an Excellent Methodology for C-C Bond Formation for 17 Years: A Review. *Catalysts* **2020**, *10* (4), 443-491; e) Miyaura, N.; Suzuki, A., Palladium-Catalyzed Cross-Coupling Reactions of Organoboron Compounds. *Chem. Rev.* **1995**, *95* (7), 2457-2483; f) Negishi, E., Palladium- or Nickel-Catalyzed Cross Coupling. A New Selective Method for Carbon-Carbon Bond Formation. *Acc. Chem. Res.* **1982**, *15* (11), 340-348.

49. The Nobel Prize in Chemistry 2010. Nobel Media AB 2020 https://www.nobelprize.org/prizes/chemistry/2010/summary/ (accessed 28 Sep 2020).

50. a) Chinchilla, R.; Nájera, C., Recent Advances in Sonogashira Reactions. *Chem. Soc. Rev.* **2011**, *40* (10), 5084-5121; b) Jana, R.; Pathak, T. P.; Sigman, M. S., Advances in Transition Metal (Pd,Ni,Fe)-Catalyzed Cross-Coupling Reactions Using Alkyl-organometallics as Reaction Partners. *Chem. Rev.* **2011**, *111* (3), 1417-1492.

51. a) Crabtree, R. H., Oxidative Addition and Reductive Elimination. In *The Organometallic Chemistry of the Transition Metals*, 6 ed.; Crabtree, R. H., Ed. John Wiley & Sons, Inc.: **2014**; pp 163-184; b) Labinger, J. A., Tutorial on Oxidative Addition. *Organometallics* **2015**, *34* (20), 4784-4795.

52. a) Senn, H. M.; Ziegler, T., Oxidative Addition of Aryl Halides to Palladium(0) Complexes: A Density-Functional Study Including Solvation. *Organometallics* **2004**, *23* (12), 2980-2988; b) Fitton, P.; Rick, E. A., The Addition of Aryl Halides to Tetrakis(triphenylphosphine)palladium(0). *J. Organomet. Chem.* **1971**, *28* (2), 287-291.

53. a) Graening, T.; Schmalz, H.-G., Pd-Catalyzed Enantioselective Allylic Substitution: New Strategic Options for the Total Synthesis of Natural Products. *Angew. Chem. Int. Ed.* **2003**, *42* (23), 2580-2584; b) Graening, T.; Schmalz, H.-G., Pd-Katalysierte Enantioselektive Allylische Substitution: Neue Strategische Optionen für die Naturstoffsynthese. *Angew. Chem. Germ. Ed.* **2003**, *115* (23), 2684-2688; c) Torborg, C.; Beller, M., Recent Applications of Palladium-Catalyzed Coupling Reactions in the Pharmaceutical, Agrochemical, and Fine Chemical Industries. *Adv. Synth. Catal.* **2009**, *351* (18), 3027-3043.

54. a) Benson, S. W., III - Bond Energies. *J. Chem. Educ.* **1965**, *42* (9), 502; b) Cottrell, T. L., *The Strengths of Chemical Bonds*. 2 ed.; Butterworths: London, **1958**; p 317; c) Darwent, B. D., *NSRDS-NBS : National standard reference data 31*. Supt. of Docs., U.S. G.P.O.: Washington, D.C., **1964**; p 48.

55. Sherwood, J.; Clark, J. H.; Fairlamb, I. J. S.; Slattery, J. M., Solvent Effects in Palladium Catalysed Cross-Coupling Reactions. *Green Chem.* **2019**, *21* (9), 2164-2213.

56. Crabtree, R. H., Homogeneous Catalysis. In *The Organometallic Chemistry of the Transition Metals*, 6 ed.; Crabtree, R. H., Ed. John Wiley & Sons, Inc.: **2014**; pp 224-258.

57. Sikk, L.; Tammiku-Taul, J.; Burk, P.; Kotschy, A., Computational Study of the Sonogashira Cross-Coupling Reaction in the Gas Phase and in Dichloromethane Solution. *J. Mol. Model.* **2012**, *18* (7), 3025-3033.

58. a) Brown, J. M.; Cooley, N. A., Carbon-Carbon Bond Formation Through Organometallic Elimination Reactions. *Chem. Rev.* **1988**, *88* (7), 1031-1046; b) Ananikov, V. P.; Musaev, D. G.; Morokuma, K., Vinyl−Vinyl Coupling on Late Transition Metals through C−C Reductive Elimination Mechanism. A Computational Study. *J. Am. Chem. Soc.* **2002**, *124* (11), 2839-2852.

59. Nova, A.; Ujaque, G.; Maseras, F.; Lledós, A.; Espinet, P., A Critical Analysis of the Cyclic and Open Alternatives of the Transmetalation Step in the Stille Cross-Coupling Reaction. *J. Am. Chem. Soc.* **2006**, *128* (45), 14571-14578.

60. a) Farina, V.; Kapadia, S.; Krishnan, B.; Wang, C.; Liebeskind, L. S., On the Nature of the "Copper Effect" in the Stille Cross-Coupling. *J. Org. Chem.* **1994**, *59* (20), 5905-5911; b) Faza, R. Á. O. N.; de Lera, A. R.; Cárdenas, D. J., A Density Functional Theory Study of the Stille Cross-Coupling via Associative Transmetalation. The Role of Ligands and Coordinating Solvents. *Adv. Synth. Catal.* **2007**, *349* (6), 887-906.

61. Böhm, V. P. W.; Herrmann, W. A., A Copper-Free Procedure for the Palladium-Catalyzed Sonogashira Reaction of Aryl Bromides with Terminal Alkynes at Room Temperature. *Eur. J. Org. Chem.* **2000**, *2000* (22), 3679-3681.

62. a) Dieck, H. A.; Heck, F. R., Palladium Catalyzed Synthesis of Aryl, Heterocyclic and Vinylic Acetylene Derivatives. *J. Organomet. Chem.* **1975**, *93* (2), 259-263; b) Sonogashira, K.; Tohda, Y.; Hagihara, N., A Convenient Synthesis of Acetylenes: Catalytic Substitutions of Acetylenic Hydrogen with Bromoalkenes, Iodoarenes and Bromopyridines. *Tetrahedron Lett.* **1975**, *16* (50), 4467-4470.

63. a) Beaupérin, M.; Fayad, E.; Amardeil, R.; Cattey, H.; Richard, P.; Brandès, S.; Meunier, P.; Hierso, J.-C., First Copper(I) Ferrocenyltetraphosphine Complexes: Possible Involvement in Sonogashira Cross-Coupling Reaction? *Organometallics* **2008**, *27* (7), 1506-1513; b) Beaupérin, M.; Job, A.; Cattey, H.; Royer, S.; Meunier, P.; Hierso, J.-C., Copper(I) Iodide Polyphosphine Adducts at Low Loading for Sonogashira Alkynylation of Demanding Halide Substrates: Ligand Exchange Study between Copper and Palladium. *Organometallics* **2010**, *29* (12), 2815-2822.

64. Wallow, T. I.; Novak, B. M., Highly Efficient and Accelerated Suzuki Aryl Couplings Mediated by Phosphine-Free Palladium Sources. *J. Org. Chem.* **1994**, *59* (17), 5034-5037.

65. Norrild, J. C.; Eggert, H., Evidence for Mono- and Bisdentate Boronate Complexes of Glucose in the Furanose Form. Application of $^{1}J_{C-C}$ Coupling Constants as a Structural Probe. *J. Am. Chem. Soc.* **1995**, *117* (5), 1479-1484.

66. a) Onak, T., *Organoborane Chemistry*. 1 ed.; Elsevier Inc. : Amsterdam, **1975**; b) Negishi, E., Selective Carbon-Carbon Bond Formation via Transition Metal Catalysis: Is Nickel or Palladium Better than Copper. In *Aspects of*

*Mechanism and Organometallic Chemistry*, 1 ed.; Brewster, J. H., Ed. Springer US: New York, **1978**; pp 285 - 317.

67. a) Nicolaou, K. C.; Bulger, P. G.; Sarlah, D., Palladium-Catalyzed Cross-Coupling Reactions in Total Synthesis. *Angew. Chem. Int. Ed.* **2005**, *44* (29), 4442-4489; b) Nicolaou, K. C.; Bulger, P. G.; Sarlah, D., Palladiumkatalysierte Kreuzkupplungen in der Totalsynthese. *Angew. Chem. Germ. Ed.* **2005**, *117* (29), 4516-4563.

68. McGlacken, G. P.; Fairlamb, I. J. S., Palladium-Catalysed Cross-Coupling and Related Processes: Some Interesting Observations That Have Been Exploited in Synthetic Chemistry. *Eur. J. Org. Chem.* **2009**, *2009* (24), 4011-4029.

69. a) Hundertmark, T.; Littke, A. F.; Buchwald, S. L.; Fu, G. C., $Pd(PhCN)_2Cl_2/P(t\text{-}Bu)_3$: A Versatile Catalyst for Sonogashira Reactions of Aryl Bromides at Room Temperature. *Org. Lett.* **2000**, *2* (12), 1729-1731; b) Littke, A. F.; Schwarz, L.; Fu, G. C., $Pd/P(t\text{-}Bu)_3$: A Mild and General Catalyst for Stille Reactions of Aryl Chlorides and Aryl Bromides. *J. Am. Chem. Soc.* **2002**, *124* (22), 6343-6348.

70. King, A. O.; Yasuda, N., Palladium-Catalyzed Cross-Coupling Reactions in the Synthesis of Pharmaceuticals. In *Organometallics in Process Chemistry*, 1 ed.; Larsen, R., Ed. Springer Verlag: Berlin-Heidelberg, **2004**; Vol. 6, pp 205-245.

71. a) Littke, A. F.; Fu, G. C., A Convenient and General Method for Pd-Catalyzed Suzuki Cross-Couplings of Aryl Chlorides and Arylboronic Acids. *Angew. Chem. Int. Ed.* **1998**, *37* (24), 3387-3388; b) Littke, A. F.; Fu, G. C., Eine Bequeme und Allgemein Anwendbare Methode für Pd-Katalysierte Suzuki-Kreuzkupplungen von Arylchloriden und Arylboronsäuren. *Angew. Chem. Germ. Ed.* **1998**, *110* (24), 3586-3587; c) Stürmer, R., Take the Right Catalyst: Palladium-Catalyzed C−C, C−N, and C−O Bond Formation on Chloroarenes. *Angew. Chem. Int. Ed.* **1999**, *38* (22), 3307-3308; d) Stürmer, R., Der Richtige Katalysator Macht's: Palladiumkatalysierte Cl-Substitution an Chlorarenen Unter Bildung von C-C-, C-N- und C-O-Bindungen. *Angew. Chem. Germ. Ed.* **1999**, *111* (22), 3509-3510.

72. Littke, A. F.; Fu, G. C., Heck Reactions in the Presence of $P(t\text{-}Bu)_3$: Expanded Scope and Milder Reaction Conditions for the Coupling of Aryl Chlorides. *J. Org. Chem.* **1999**, *64* (1), 10-11.

73. a) Farina, V.; Krishnan, B., Large Rate Accelerations in the Stille Reaction with Tri-2-furylphosphine and Triphenylarsine as Palladium Ligands: Mechanistic and Synthetic Implications. *J. Am. Chem. Soc.* **1991**, *113* (25), 9585-9595; b) Casado, A. L.; Espinet, P.; Gallego, A. M., Mechanism of the Stille Reaction. 2. Couplings of Aryl Triflates with Vinyltributyltin. Observation of Intermediates. A More Comprehensive Scheme. *J. Am. Chem. Soc.* **2000**, *122* (48), 11771-11782.

74. a) Dounay, A. B.; Overman, L. E., The Asymmetric Intramolecular Heck Reaction in Natural Product Total Synthesis. *Chem. Rev.* **2003**, *103* (8), 2945-2964; b) Shibasaki, M.; Boden, C. D. J.; Kojima, A., The Asymmetric Heck Reaction. *Tetrahedron* **1997**, *53* (22), 7371-7395.

75. Tschoerner, M.; Pregosin, P. S.; Albinati, A., Contributions to the Enantioselective Heck Reaction Using MeO−Biphep Ligands. The Case Against Dibenzylidene Acetone. *Organometallics* **1999**, *18* (4), 670-678.

76. a) Layer, R. W., The Chemistry of Imines. *Chem. Rev.* **1963**, *63* (5), 489-510; b) Dalessandro, E. V.; Collin, H. P.; Guimarães, L. G. L.; Valle, M. S.; Pliego, J. R., Mechanism of the Piperidine-Catalyzed Knoevenagel Condensation Reaction in Methanol: The Role of Iminium and Enolate Ions. *J. Phys. Chem. B* **2017**, *121* (20), 5300-5307; c) Heravi, M. M.; Janati, F.; Zadsirjan, V., Applications of Knoevenagel condensation reaction in the total synthesis of natural products. *Monatsh. Chem. - Chemical Monthly* **2020**, *151* (4), 439-482.

77. a) Gray, H. B.; Winkler, J. R., Electron Tunneling Through Proteins. *Quarterly Reviews of Biophysics* **2003**, *36* (3), 341-372; b) Mikkelsen, K. V.; Ratner, M. A., Electron Tunneling in Solid-state Electron-Transfer Reactions. *Chem. Rev.* **1987**, *87* (1), 113-153; c) Oskouyi, A. B.; Sundararaj, U.; Mertiny, P., Tunneling Conductivity and Piezoresistivity of Composites Containing Randomly Dispersed Conductive Nano-Platelets. *Materials* **2014**, *7* (4), 2501-2521; d) Schrieffer, J. R., Theory of Electron Tunneling. *Rev. Mod. Phys.* **1964**, *36* (1), 200-204; e) Davis, W. B.; Svec, W. A.; Ratner, M. A.; Wasielewski, M. R., Molecular-Wire Behaviour in *p* -Phenylenevinylene Oligomers. *Nature* **1998**, *396* (6706), 60-63; f) Gilbert, M.; Albinsson, B., Photoinduced Charge and Energy Transfer in Molecular Wires. *Chem. Soc. Rev.* **2015**, *44* (4), 845-862.

78. a) Ning, Z.; Tian, H., Triarylamine: a Promising Core Unit for Efficient Photovoltaic Materials. *Chem. Commun.* **2009**, (37), 5483-5495; b) Quinton, C.; Alain-Rizzo, V.; Dumas-Verdes, C.; Clavier, G.; Vignau, L.; Audebert, P., Triphenylamine/Tetrazine Based π-Conjugated Systems as Molecular Donors for Organic Solar Cells. *New J. Chem.* **2015**, *39* (12), 9700-9713; c) Mahmood, A., Triphenylamine Based Dyes for Dye Sensitized Solar Cells: A Review. *Sol. Energy* **2016**, *123*, 127-144; d) Kumar, S.; Rajamalli, P.; Cordes, D. B.; Slawin, A. M. Z.; Zysman-Colman, E., Highly Fluorescent Emitters Based on Triphenylamine-π-Triazine (D-π-A) System: Effect of Extended Conjugation on Singlet-Triplet Energy Gap. *Asian J. Org. Chem.* **2020**, *9* (9), 1277-1285; e) Cecconi, B.; Manfredi, N.; Montini, T.; Fornasiero, P.; Abbotto, A., Dye-Sensitized Solar Hydrogen Production: The Emerging Role of Metal-Free Organic Sensitizers. *Eur. J. Org. Chem.* **2016**, *2016* (31), 5194-5215.

79. a) Ambrose, J. F.; Nelson, R. F., Anodic Oxidation Pathways of Carbazoles. *J. Electrochem. Soc.* **1968**, *115* (11), 1159-1164; b) Karon, K.; Lapkowski, M., Carbazole Electrochemistry: A Short Review. *J. Solid State Electrochem.* **2015**, *19* (9), 2601-2610.

80. Ambrose, J. F.; Carpenter, L. L.; Nelson, R. F., Electrochemical and Spectroscopic Properties of Cation Radicals: III . Reaction Pathways of Carbazolium Radical Ions. *J. Electrochem. Soc.* **1975**, *122* (7), 876-894.

81. a) Kulhánek, J.; Bureš, F.; Pytela, O.; Mikysek, T.; Ludvík, J.; Růžička, A., Push-Pull Molecules with a Systematically Extended π-Conjugated System Featuring 4,5-Dicyanoimidazole. *Dyes Pigm.* **2010**, *85* (1), 57-65; b) Kulhánek, J.; Bureš, F.; Opršal, J.; Kuznik, W.; Mikysek, T.; Růžička, A., 1,4-Phenylene and 2,5-

Thienylene π-Linkers in Charge-Transfer Chromophores. *Asian J. Org. Chem.* **2013**, *2* (5), 422-431; c) Bureš, F., Fundamental Aspects of Property Tuning in Push–Pull Molecules. *RSC Adv.* **2014**, *4* (102), 58826-58851.

82. a) Li, R.; Lv, X.; Shi, D.; Zhou, D.; Cheng, Y.; Zhang, G.; Wang, P., Dye-Sensitized Solar Cells Based on Organic Sensitizers with Different Conjugated Linkers: Furan, Bifuran, Thiophene, Bithiophene, Selenophene, and Biselenophene. *J. Phys. Chem. C* **2009**, *113* (17), 7469-7479; b) Kim, S. H.; Kim, H. W.; Sakong, C.; Namgoong, J.; Park, S. W.; Ko, M. J.; Lee, C. H.; Lee, W. I.; Kim, J. P., Effect of Five-Membered Heteroaromatic Linkers to the Performance of Phenothiazine-Based Dye-Sensitized Solar Cells. *Org. Lett.* **2011**, *13* (21), 5784-5787; c) Casanova, D., The Role of the π Linker in Donor–π–Acceptor Organic Dyes for High-Performance Sensitized Solar Cells. *ChemPhysChem* **2011**, *12* (16), 2979-2988; d) Li, P.; Wang, Z.; Song, C.; Zhang, H., Rigid Fused π-Spacers in D–π–A Type Molecules for Dye-Sensitized Solar Cells: A Computational Investigation. *J. Mater. Chem. C* **2017**, *5* (44), 11454-11465; e) Samae, R.; Surawatanawong, P.; Eiamprasert, U.; Pramjit, S.; Saengdee, L.; Tangboriboonrat, P.; Kiatisevi, S., Effect of Thiophene Spacer Position in Carbazole-Based Dye-Sensitized Solar Cells on Photophysical, Electrochemical and Photovoltaic Properties. *Eur. J. Org. Chem.* **2016**, *2016* (21), 3536-3549.

83. a) Li, Y.; Scudiero, L.; Ren, T.; Dong, W.-J., Synthesis and Characterizations of Benzothiadiazole-Based Fluorophores as Potential Wavelength-Shifting Materials. *J. Photochem. Photobiol. A* **2012**, *231* (1), 51-59; b) Neto, B. A. D.; Lapis, A. A. M.; da Silva Júnior, E. N.; Dupont, J., 2,1,3-Benzothiadiazole and Derivatives: Synthesis, Properties, Reactions, and Applications in Light Technology of Small Molecules. *Eur. J. Org. Chem.* **2013**, *2013* (2), 228-255; c) Zhu, H.; Li, W.; Wu, Y.; Liu, B.; Zhu, S.; Li, X.; Ågren, H.; Zhu, W., Insight into Benzothiadiazole Acceptor in D–A−π–A Configuration on Photovoltaic Performances of Dye-Sensitized Solar Cells. *ACS Sustain. Chem. Eng.* **2014**, *2* (4), 1026-1034; d) Pop, F.; Seifert, S.; Hankache, J.; Ding, J.; Hauser, A.; Avarvari, N., Modulation of the Charge Transfer and Photophysical Properties in Non-Fused Tetrathiafulvalene-Benzothiadiazole Derivatives. *Org. Biomol. Chem.* **2015**, *13* (4), 1040-1047; e) Elmorsy, M. R.; Su, R.; Fadda, A. A.; Etman, H. A.; Tawfik, E. H.; El-Shafei, A., Molecular Engineering and Synthesis of Novel Metal-Free Organic Sensitizers with D-π-A-π-A Architecture for DSSC Applications: The Effect of the Anchoring Group. *Dyes Pigm.* **2018**, *158*, 121-130.

84. Shen, M.; Rodríguez-López, J.; Huang, J.; Liu, Q.; Zhu, X.-H.; Bard, A. J., Electrochemistry and Electrogenerated Chemiluminescence of Dithienylbenzothiadiazole Derivative. Differential Reactivity of Donor and Acceptor Groups and Simulations of Radical Cation−Anion and Dication−Radical Anion Annihilations. *J. Am. Chem. Soc.* **2010**, *132* (38), 13453-13461.

85. a) Akimoto, H.; Yamada, S., Stereochemical Studies—VIII: Unequivocal Determination of the Absolute Configuration in Biaryl Systems. *Tetrahedron* **1971**, *27* (24), 5999-6009; b) v. Richter, V., Die Chemie auf der Vierten Russischen Naturforscherversammlung in Kasan. *Ber. Dtsch. Chem. Ges.* **1873**, *6* (2), 1249–1260.

86. a) Chen, Y.; Yekta, S.; Yudin, A. K., Modified BINOL Ligands in Asymmetric Catalysis. *Chem. Rev.* **2003**, *103* (8), 3155-3212; b) Kočovský, P.; Vyskočil, Š.; Smrčina, M., Non-Symmetrically Substituted 1,1'-Binaphthyls in Enantioselective Catalysis. *Chem. Rev.* **2003**, *103* (8), 3213-3246; c) Meca, L.; Řeha, D.; Havlas, Z., Racemization Barriers of 1,1'-Binaphthyl and 1,1'-Binaphthalene-2,2'-diol: A DFT Study. *J. Org. Chem.* **2003**, *68* (14), 5677-5680; d) Patel, D. C.; Woods, R. M.; Breitbach, Z. S.; Berthod, A.; Armstrong, D. W., Thermal Racemization of Biaryl Atropisomers. *Tetrahedron: Asymmetry* **2017**, *28* (11), 1557-1561.

87. a) Brenet, S.; Baptiste, B.; Philouze, C.; Berthiol, F.; Einhorn, J., BINOL-Fused Maleimides – A New Class of C2-Symmetric Chiral Imides. *Eur. J. Org. Chem.* **2013**, *2013* (6), 1041-1045; b) Brunel, J. M., BINOL: A Versatile Chiral Reagent. *Chem. Rev.* **2005**, *105* (3), 857-898.

88. McNaught, A. D.; Wilkinson, A.; International Union of Pure and Applied Chemistry., *Compendium of Chemical Terminology : IUPAC Recommendations*. 2nd ed.; Blackwell Science: Oxford England ; Malden, MA, USA, **1997**.

89. Cooke, A. S.; Harris, M. M., 437. Ground-State Strain and Other Factors Influencing Optical Stability in the 1,1′-Binaphthyl Series. *J. Chem. Soc.* **1963**, (0), 2365-2373.

90. Sogah, G. D. Y.; Cram, D. J., Host-Guest Complexation. 14. Host Covalently Bound to Polystyrene Resin for Chromatographic Resolution of Enantiomers of Amino Acid and Ester Salts. *J. Am. Chem. Soc.* **1979**, *101* (11), 3035-3042.

91. Nieger, M., CCDC 2010086: Experimental Crystal Structure Determination. *CSD Communication* **2020**.

92. a) Cui, Y.; Wu, Y.; Lu, X.; Zhang, X.; Zhou, G.; Miapeh, F. B.; Zhu, W.; Wang, Z.-S., Incorporating Benzotriazole Moiety to Construct D–A−π–A Organic Sensitizers for Solar Cells: Significant Enhancement of Open-Circuit Photovoltage with Long Alkyl Group. *Chem. Mater.* **2011**, *23* (19), 4394-4401; b) Wang, L.; Shen, P.; Cao, Z.; Liu, X.; Huang, Y.; Liu, C.; Chen, P.; Zhao, B.; Tan, S., Effects of the Acceptors in Triphenylamine-Based D–A′–π–A Dyes on Photophysical, Electrochemical, and Photovoltaic Properties. *J. Power Sources* **2014**, *246*, 831-839; c) Shen, Z.; Chen, J.; Li, X.; Li, X.; Zhou, Y.; Yu, Y.; Ding, H.; Li, J.; Zhu, L.; Hua, J., Synthesis and Photovoltaic Properties of Powerful Electron-Donating Indeno[1, 2-b]thiophene-Based Green D–A−π–A Sensitizers for Dye-Sensitized Solar Cells. *ACS Sustain. Chem. Eng.* **2016**, *4* (6), 3518-3525.

93. a) Wiberg, J.; Marinado, T.; Hagberg, D. P.; Sun, L.; Hagfeldt, A.; Albinsson, B., Effect of Anchoring Group on Electron Injection and Recombination Dynamics in Organic Dye-Sensitized Solar Cells. *J. Phys. Chem. C* **2009**, *113* (9), 3881-3886; b) Ambrosio, F.; Martsinovich, N.; Troisi, A., What Is the Best Anchoring Group for a Dye in a Dye-Sensitized Solar Cell? *J. Phys. Chem. Lett.* **2012**, *3* (11), 1531-1535; c) Zhang, L.; Cole, J. M., Anchoring Groups for Dye-Sensitized Solar Cells. *ACS Appl. Mater. Interfaces* **2015**, *7* (6), 3427-3455; d) Chen, Y.-C.; Lin, J. T., Multi-Anchored Sensitizers for Dye-Sensitized Solar Cells. *Sustain. Energ. Fuels* **2017**, *1* (5), 969-985; e) Hagfeldt, A.; Boschloo, G.; Sun, L.; Kloo, L.; Pettersson, H., Dye-Sensitized Solar Cells. *Chem. Rev.* **2010**, *110* (11), 6595-6663; f)

Galoppini, E., Linkers for Anchoring Sensitizers to Semiconductor Nanoparticles. *Coord. Chem. Rev.* **2004**, *248* (13), 1283-1297.

94. a) Cahen, D.; Grätzel, M.; Guillemoles, J. F.; Hodes, G., Dye-Sensitized Solar Cells: Principles of Operation. In *Electrochemistry of Nanomaterials*, Hodes, G., Ed. Wiley VCH Verlag GmbH: Weinheim, **2001**; pp 201-228; b) Wang, L.; Yang, X.; Zhao, J.; Zhang, F.; Wang, X.; Sun, L., Efficient Organic Sensitizers with Pyridine-N-oxide as an Anchor Group for Dye-Sensitized Solar Cells. *ChemSusChem* **2014**, *7* (9), 2640-2646; c) Tai, Q.; Yan, F., Emerging Semitransparent Solar Cells: Materials and Device Design. *Adv. Mater.* **2017**, *29* (34), 1700192/1700191-1700192/1700137; d) Gong, J.; Sumathy, K.; Qiao, Q.; Zhou, Z., Review on Dye-Sensitized Solar Cells (DSSCs): Advanced Techniques and Research Trends. *Renew. Sustain. Energy Rev.* **2017**, *68*, 234-246; e) Sharma, K.; Sharma, V.; Sharma, S. S., Dye-Sensitized Solar Cells: Fundamentals and Current Status. *Nanoscale Res. Lett.* **2018**, *13* (1), 381/381-381/346.

95. Barriga, S., 2,2,6,6-Tetramethylpiperidin-1-oxyl (TEMPO). *Synlett* **2001**, *2001* (4), 563-563.

96. Chernick, E. T.; Casillas, R.; Zirzlmeier, J.; Gardner, D. M.; Gruber, M.; Kropp, H.; Meyer, K.; Wasielewski, M. R.; Guldi, D. M.; Tykwinski, R. R., Pentacene Appended to a TEMPO Stable Free Radical: The Effect of Magnetic Exchange Coupling on Photoexcited Pentacene. *J. Am. Chem. Soc.* **2015**, *137* (2), 857-863.

97. Kégl, T. R.; Kollár, L.; Kégl, T., DFT Study on the Oxidative Addition of 4-Substituted Iodobenzenes on Pd(0)-Phosphine Complexes. *Adv. Phys. Chem* **2015**, *2015*, 985268.

98. Wang, L.; Ji, E.; Liu, N.; Dai, B., Site-Selective *N*-Arylation of Carbazoles with Halogenated Fluorobenzenes. *Synthesis* **2016**, *48* (5), 737-750.

99. Limberg, F. R. P.; Miasojedovas, A.; Pingel, P.; Reisbeck, F.; Janietz, S.; Monkman, A. P.; Krüger, H., Hole-Transporting Side-Chain Polystyrenes Based on TCTA with Tuned Glass Transition and Optimized Electronic Properties. *RSC Adv.* **2015**, *5* (101), 83122-83128.

100. Farina, V.; Krishnamurthy, V.; Scott, W. J., The Stille Reaction. In *Organic Reactions*, **2004**; pp 1-652.

101. Dall'Agnese, C.; Hernández Maldonado, D.; Le Borgne, D.; Moineau-Chane Ching, K. I., Dissymmetrization of Benzothiadiazole by Direct C–H Arylation: A Way to Symmetrical and Unsymmetrical Elongated π-Conjugated Molecules. *Eur. J. Org. Chem.* **2017**, *2017* (46), 6872-6877.

102. Wipf, P.; Jung, J.-K., Formal Total Synthesis of (+)-Diepoxin σ. *J. Org. Chem.* **2000**, *65* (20), 6319-6337.

103. Mosca, D.; Stopin, A.; Wouters, J.; Demitri, N.; Bonifazi, D., Stereospecific Winding of Polycyclic Aromatic Hydrocarbons Into Trinacria Propellers. *Chem. Eur. J.* **2017**, *23* (61), 15348-15354.

104. Aronovich, D. A., Modern Achievements in the Field of Cyanoacrylate Adhesives. Mechanisms of Polymerization of Cyanoacrylates and Their Application Value. *Polym. Sci. Ser. D* **2019**, *12* (3), 290-295.

105. a) Li, B.; Berliner, M.; Buzon, R.; Chiu, C. K. F.; Colgan, S. T.; Kaneko, T.; Keene, N.; Kissel, W.; Le, T.; Leeman, K. R.; Marquez, B.; Morris, R.; Newell, L.; Wunderwald, S.; Witt, M.; Weaver, J.; Zhang, Z.; Zhang, Z., Aqueous Phosphoric Acid as a Mild Reagent for Deprotection of tert-Butyl Carbamates, Esters, and Ethers. *J. Org. Chem.* **2006**, *71* (24), 9045-9050; b) Salomon, C. J.; Mata, E. G.; Mascaretti, O. A., Recent Developments in Chemical Deprotection of Ester Functional Groups. *Tetrahedron* **1993**, *49* (18), 3691-3734.

106. Chen, B.; Sun, H.-X.; Qin, J.-F.; Wang, B., DMF-Mediated Deprotection of Bulky Silyl Esters Under Neutral and Fluoride-Free Conditions. *Tetrahedron Lett.* **2016**, *57* (3), 253-255.

107. Eaton, G. R., *Quantitative EPR A Practitioners Guide*. Springer: Vienna, **2010**.

108. Matsumoto, N.; Shimosaka, T., Validation of a Quantitative Analytical Method Based on the Effective Magnetic Moment and the Curie–Weiss Law. *Accred. Qual. Assur.* **2015**, *20* (2), 115-124.

109. a) Matsumoto, N.; Itoh, N., Measuring Number of Free Radicals and Evaluating the Purity of Di(phenyl)-(2,4,6-trinitrophenyl)iminoazanium [DPPH] Reagents by Effective Magnetic Moment Method. *Anal. Sci.* **2018**, *34* (8), 965-971; b) Buchner, M.; Höfler, K.; Henne, B.; Ney, V.; Ney, A., Tutorial: Basic Principles, Limits of Detection, and Pitfalls of Highly Sensitive SQUID Magnetometry for Nanomagnetism and Spintronics. *J. Appl. Phys.* **2018**, *124* (16), 161101/161101-161101/161113; c) Garcia, M. A.; Pinel, E. F.; Venta, J. d. l.; Quesada, A.; Bouzas, V.; Fernández, J. F.; Romero, J. J.; González, M. S. M.; Costa-Krämer, J. L., Sources of Experimental Errors in the Observation of Nanoscale Magnetism. *J. Appl. Phys.* **2009**, *105* (1), 13925/13921-13925/13927.

110. Suryawanshi, S. B.; Mahajan, P. G.; Bodake, A. J.; Kolekar, G. B.; Patil, S. R., Carbazole based nanoprobe for selective recognition of $Fe^{3+}$ ion in aqueous medium: Spectroscopic insight. *Spectrochim. Acta A Mol. Biomol. Spectrosc.* **2017**, *183*, 232-238.

111. a) Chang, Y. J.; Chow, T. J., Dye-Sensitized Solar Cell Utilizing Organic Dyads Containing Triarylene Conjugates. *Tetrahedron* **2009**, *65* (24), 4726-4734; b) Feng, H.; Li, R.; Song, Y.; Li, X.; Liu, B., Novel D-π-A-π-A Coumarin Dyes for Highly Efficient Dye-Sensitized Solar Cells: Effect of π-Bridge on Optical, Electrochemical, and Photovoltaic Performance. *J. Power Sources* **2017**, *345*, 59-66; c) Rabie, U. M., A Review on Electronic Spectral Studies of Charge Transfer Complexes. *J. Mol. Struct.* **2013**, *1034*, 393-403.

112. a) Chen, H.; Huang, H.; Huang, X.; Clifford, J. N.; Forneli, A.; Palomares, E.; Zheng, X.; Zheng, L.; Wang, X.; Shen, P.; Zhao, B.; Tan, S., High Molar Extinction Coefficient Branchlike Organic Dyes Containing Di(*p*-tolyl)phenylamine Donor for Dye-Sensitized Solar Cells Applications. *J. Phys. Chem. C* **2010**, *114*

(7), 3280-3286; b) Yin, N.; Wang, L.; Lin, Y.; Yi, J.; Yan, L.; Dou, J.; Yang, H.-B.; Zhao, X.; Ma, C.-Q., Effect of the π-Conjugation Length on the Properties and Photovoltaic Performance of A-π-D-π-A Type Oligothiophenes With a 4,8-Bis(thienyl)benzo[1,2-b:4,5-b']dithiophene Core. *Beilstein J. Org. Chem.* **2016**, *12*, 1788-1797.

113. Zimdars, S.; Langhals, H.; Knochel, P., Functionalization of the Benzo[c][1,2,5]thiadiazole Scaffold via Mg-, Zn- and Mn-Intermediates. *Synthesis* **2011**, *2011* (08), 1302-1308.

114. Zhang, H.; Zeng, J.; Luo, W.; Wu, H.; Zeng, C.; Zhang, K.; Feng, W.; Wang, Z.; Zhao, Z.; Tang, B. Z., Synergistic Tuning of the Optical and Electrical Performance of AIEgens with a Hybridized Local and charge-Transfer Excited State. *J. Mater. Chem. C* **2019**, *7* (21), 6359-6368.

115. a) Lee, C.; Yang, W.; Parr, R. G., Development of the Colle-Salvetti Correlation-Energy Formula Into a Functional of the Electron Density. *Phys. Rev. B* **1988**, *37* (2), 785-789; b) Petersson, G. A.; Al-Laham, M. A., A Complete Basis Set Model Chemistry. II. Open-Shell Systems and the Total Energies of the First-Row Atoms. *J. Chem. Phys.* **1991**, *94* (9), 6081-6090; c) Petersson, G. A.; Bennett, A.; Tensfeldt, T. G.; Al-Laham, M. A.; Shirley, W. A.; Mantzaris, J., A Complete Basis Set Model Chemistry. I. The Total Energies of Closed-Shell Atoms and Hydrides of the First-Row Elements. *J. Chem. Phys.* **1988**, *89* (4), 2193-2218.

116. a) Chai, J.-D.; Head-Gordon, M., Long-Range Corrected Hybrid Density Functionals with Damped Atom–Atom Dispersion Corrections. *Phys. Chem. Chem. Phys.* **2008**, *10* (44), 6615-6620; b) Yanai, T.; Tew, D. P.; Handy, N. C., A New Hybrid Exchange–Correlation Functional Using the Coulomb-Attenuating Method (CAM-B3LYP). *Chem. Phys. Lett.* **2004**, *393* (1), 51-57.

117. a) Adamo, C.; Jacquemin, D., The Calculations of Excited-State Properties with Time-Dependent Density Functional Theory. *Chem. Soc. Rev.* **2013**, *42* (3), 845-856; b) Petersilka, M.; Gossmann, U. J.; Gross, E. K. U., Excitation Energies from Time-Dependent Density-Functional Theory. *Phys. Rev. Lett.* **1996**, *76* (8), 1212-1215; c) Runge, E.; Gross, E. K. U., Density-Functional Theory for Time-Dependent Systems. *Phys. Rev. Lett.* **1984**, *52* (12), 997-1000; d) Cramer, C. J.; Truhlar, D. G., Implicit Solvation Models: Equilibria, Structure, Spectra, and Dynamics. *Chem. Rev.* **1999**, *99* (8), 2161-2200; e) Tomasi, J.; Mennucci, B.; Cammi, R., Quantum Mechanical Continuum Solvation Models. *Chem. Rev.* **2005**, *105* (8), 2999-3094; f) Tomasi, J.; Persico, M., Molecular Interactions in Solution: An Overview of Methods Based on Continuous Distributions of the Solvent. *Chem. Rev.* **1994**, *94* (7), 2027-2094.

118. Fulmer, G. R.; Miller, A. J. M.; Sherden, N. H.; Gottlieb, H. E.; Nudelman, A.; Stoltz, B. M.; Bercaw, J. E.; Goldberg, K. I., NMR Chemical Shifts of Trace Impurities: Common Laboratory Solvents, Organics, and Gases in Deuterated Solvents Relevant to the Organometallic Chemist. *Organometallics* **2010**, *29* (9), 2176-2179.

119. Huq, M. M.; Robiur Rahman, M.; Naher, M.; Khan, M. M. R.; Masud, M. K.; Hossain, G. M. G.; Zhu, N.; Lo, Y. H.; Younus, M.; Wong, W.-Y., Synthesis,

Characterization and Catalytic Activities of Palladium(II) Nitroaryl Complexes. *J. Inorg. Organomet. Polymer. Mater.* **2016**, *26* (6), 1243-1252.

120. Guthrie, D. A.; Tovar, J. D., Conformation as a Protecting Group: A Regioselective Aromatic Bromination En Route to Complex π-Electron Systems. *Org. Lett.* **2008**, *10* (19), 4323-4326.

121. Imit, M.; Imin, P.; Adronov, A., Supramolecular Interactions of Fluorene-Based Copolymers Containing 3,4-Propylenedioxythiophene and Phenazine Units with SWNTs. *Polym. Chem.* **2016**, *7* (33), 5241-5248.

122. Parker, C. A.; Rees, W. T., Correction of Fluorescence Spectra and Measurement of Fluorescence Quantum Efficiency. *Analyst* **1960**, *85* (1013), 587-600.

123. Melhuish, W. H., Quantum Efficiencies of Fluorescence of Organic Substances: Effect of Solvent and Concentration of the Fluorescent Solute. *J. Phys. Chem.* **1961**, *65* (2), 229-235.

124. Jones, G.; Jackson, W. R.; Halpern, A. M., Medium Effects on Fluorescence Quantum Yields and Lifetimes for Coumarin Laser Dyes. *Chem. Phys. Lett.* **1980**, *72* (2), 391-395.

125. Nakamaru, K.; Nishio, K.; Nobe, H., Reexamination of the Luminescence Quantum Yields of Tris(2,2'-bipyridyl or 1,10-Phenanthroline and Their Derivatives)Ruthenium(II) ions in Aqueous Solutions at Room Temperature (25°C). *Sci. Rep. Hirosaki Univ.* **1979**, *26* (1), 57-62.

126. Frisch, M. J.; Trucks, G. W.; Schlegel, H. B.; Scuseria, G. E.; Robb, M. A.; Cheeseman, J. R.; Scalmani, G.; Barone, V.; Petersson, G. A.; Nakatsuji, H.; X. Li, M. C.; Marenich, A. V.; Bloino, J.; Janesko, B. G.; Gomperts, R.; Mennucci, B.; Hratchian, H. P.; Ortiz, J. V.; Izmaylov, A. F.; Sonnenberg, J. L.; Williams-Young, D.; Ding, F.; Lipparini, F.; Egidi, F.; Goings, J.; Peng, B.; Petrone, A.; Henderson, T.; Ranasinghe, D.; Zakrzewski, V. G.; J. Gao, N. R.; Zheng, G.; Liang, W.; Hada, M.; Ehara, M.; Toyota, K.; Fukuda, R.; Hasegawa, J.; Ishida, M.; Nakajima, T.; Honda, Y.; Kitao, O.; Nakai, H.; Vreven, T.; Throssell, K.; Montgomery Jr., J. A.; Peralta, J. E.; Ogliaro, F.; Bearpark, M. J.; Heyd, J. J.; Brothers, E. N.; Kudin, K. N.; Staroverov, V. N.; Keith, T. A.; Kobayashi, R.; Normand, J.; Raghavachari, K.; Rendell, A. P.; Burant, J. C.; Iyengar, S. S.; Tomasi, J.; Cossi, M.; Millam, J. M.; Klene, M.; Adamo, C.; Cammi, R.; Ochterski, J. W.; Martin, R. L.; Morokuma, K.; Farkas, O.; Foresman, J. B.; Fox, D. J. *Gaussian 16, Revision C.01*, Gaussian, Inc., Wallingford CT: 2019.

127. Becke, A. D., Density-Functional Thermochemistry. III. The Role of Exact Exchange. *J. Chem. Phys.* **1993**, *98* (7), 5648-5652.

128. Fluorescence measurments for this compound displayed a consistent change in intensity overtime, hence, no accurate fluorescence data can be reported for this compound.

129. Accurate SQUID measurments were not possible for this compound, due to a too small amount of compound.